Transiently Immobilised *N*-Heterocyclic Carbenes: Boomerang Organocatalysts

A Thesis Submitted by

Fu-Howe Lee

In partial fulfilment of the requirements for the degree of

DOCTOR OF PHILOSOPHY

Imperial College London
Department of Chemical Engineering
Exhibition Road
South Kensington
London
SW7 2AZ

Declaration of Originality

I, Fu-Howe Lee, hereby confirm that I solely produced the presented thesis under the supervision of Dr Andreas Kogelbauer, Dr Matthew J. Fuchter, Dr Paul D. Lickiss, and Dr Klaus Hellgardt at the Department of Chemical Engineering and the Department of Chemistry, Imperial College London, and that I did not use any other material other than that cited or known to the public domain.

London,

Fu-Howe Lee

Copyright Declaration

The copyright of this thesis rests with the author and is made available under a Creative Commons Attribution Non-Commercial No Derivative licence. Researchers are free to copy, distribute or transmit the thesis on condition that they attribute it, that they do not use it for commercial purposes and that they do not alter, transform or build upon it. For any reuse or redistribution, researchers must make clear to others the licence terms of this work.

Acknowledgements

I wish to thank my supervisors for the support and words of wisdom that they have provided throughout my time at Imperial College London. I am grateful for their guidance and advice but more importantly, I am appreciative of the opportunity to pursue the research presented here.

I also wish to thank the analytical staff: John Barton and Lisa Haigh for mass spectra, and Dick Sheppard and Pete Haycock for NMR spectra. Pete was immensely helpful in accommodating many awkward requests.

My short time at Imperial was made all the more bearable by the friends that loitered on the 7th floor in the Barrett and Fuchter groups. I must thank them all for their company, supervision, and assistance during my studies.

I bestow particular gratitude to: Dr Marko Weimar who was forced to help an “unenlightened” Chemical Engineer work amongst Chemists, and who had to endure all the trials and tribulations that ensued; Dr Brian Slafer and Dr Aniello Palma for their contributions in problem sessions which have been immensely helpful; Robert Davidson who has had to tolerate regular interrogations on rather simple subjects; Stef Reid for great help in maintaining and repairing the, at times, temperamental glovebox; Dr Paolo di Fruscia for his constant smile and positive outlook; and conversely, Dr Andreas Doepner for his unique if not distorted humour.

I also wish to mention the particular endeavours of Dr Jochen Brandt and Dr Robert Richardson at the final hurdle.

Abstract

There have been reports in the literature on *N*-Heterocyclic Carbene - Silicon (NHC·Si) interactions and their involvement in organocatalytic cycles. However, there is little experimental evidence to support this postulation. Indeed, other plausible mechanisms that do not invoke an NHC·Si interaction can be drawn. We show that there is insufficient evidence to support the postulated NHC·Si interaction in the protection of NHCs by silicones reported by Baceiredo and co-workers.

The synthesis and use of ^{13}C-labelled NHCs allowed for the clear monitoring of the carbene moiety by ^{13}C NMR spectroscopy. ^{1}H, ^{13}C and ^{29}Si NMR spectra did not indicate the formation of NHC·Si complexes at temperatures from 298K to 198K in toluene-d_8 or THF-d_8 for a range of silicones and low molecular weight silicon species of varying Lewis-acidities. DOSY spectra did not show specific or non-specific interactions between NHCs and silicon species in solution, which would have been expected for an NHC·Si interaction. *In situ* IR measurements of a model NHC-catalysed reaction of methyl 2-phenylacetate with ethanolamine also failed to provide conclusive evidence of an NHC·Si interaction which would lead to diminished rates of reaction.

Furthermore, computational studies of the above systems do not predict an NHC·Si interaction. Simulations predict that the formation of such NHC·Si interactions is thermodynamically disfavoured at room temperature based on Gibbs free energies calculated at the MP2/aug-cc-pVTZ//B3LYP/6-311+G(d,p) level.

Mass-transfer analysis, as applied to the systems described by Baceiredo and co-workers, show that retardation of decomposition can be explained by steady-state mass-transfer limited by diffusion of oxygen without the need to invoke a NHC·Si interaction. The analytical solution of transient mass-transfer shows that protection afforded by diffusion is non-linear and that the evolution of the concentration profile is proportional to $e^{-(D \cdot t/L^2)}$, where D is the diffusion coefficient, t is time, and L the non-dimensional length.

Table of Contents

Declaration of Originality 2

Copyright Declaration 3

Acknowledgements 4

Abstract 5

Abbreviations 9

Table of Figures 13

Table of Schemes 15

1. Introduction 18

1.1 An Overview of Carbenes 18

1.2 Synthetic Routes to Free NHCs 22

1.3 NHCs as Catalysts in Umpolung Reactions 24

1.4 Esterification 26

1.4.1 Activation of a Carboxylic Acid 27

1.4.2 Activation of an Alcohol 28

1.4.3 NHC-Catalysed Transesterification 29

1.5 Amidation 37

1.5.1 Activation of Carboxylic Acids 37

1.5.2 Direct Amidation - Acyloxyboron Intermediates 39

1.5.3 Metal-Catalysed Amidations 41

1.5.4 Organocatalytic Amidation 42

1.5.5 NHC-Catalysed Amidation *via* Transesterification 43

1.6 Protection of NHCs 44

1.6.1 Isolation and Reuse 46

1.6.2 Formation of Latent Adducts 47

1.6.3 Chlorination of Backbone Positions 48

1.6.4 Protection by Silicones - NHC·Si Interactions 49

1.7 NHC·Si Interactions 52

Conclusions 60

2. Attempts to Characterise an NHC·Si Interaction and its Effects on NHC Decomposition 61

2.1 Synthesis and Isolation of Free NHCs 61

2.1.1 NHC Precursors: Imidazolium Halides 61

2.1.2 Synthesis of Diazabutadienes 64

2.1.3 Ring-closing of Diazabutadienes to Form an Imidazolium Salt 65
2.1.4 Synthesis of I*t*Bu·HCl and I*t*Bu·HBF_4 67
2.1.5 Deprotonation of Imidazolium Halides 68
Conclusions 69
2.2. Synthesis of NHC·Si Adducts Reported in the Literature 70
2.2.1 NHC·$SiCl_4$ Adducts 70
2.2.2 Me_2I*t*Bu·$SiCl_4$ 72
Conclusions 75
2.3 Quantifying the Decomposition of NHCs and the Role of Silicon Species (NHC·Si Interactions) 76
2.3.1 Synthesis of a Postulated IMes Decomposition Product 76
2.3.2 Quantitative NMR 78
2.3.3 Decomposition of IMe 83
2.3.4 Decomposition/Protection of IMes – An NHC·Si Interaction? 86
2.3.5 Equilibrium Limited Formation of an NHC·Si Interaction 91
2.3.6 Variable Temperature NMR Studies 92
2.3.7 Diffusion Ordered Spectroscopy 95
Conclusions 101
2.4 Synthesis of 4,5-Disubstituted Imidazolium Salts 102
2.4.1 Synthesis of Backbone-Substituted Diazabutadienes 103
2.4.2 Backbone-Substitution *via* Ring-Lithiation of NHC·Borane Adducts 104
2.4.3 Polyakova's Route - Backbone Substitution *via* a Formamide 106
2.4.4 Methylation of a Formamide and Ring-Closing 109
2.4.5 Me_2I*t*Bu and Lewis-Acidic Si Species 110
Conclusions 115
3. Computational Modelling of an NHC·Si Interaction 116
3.1 Electronic Energy of Interactions 116
3.1.1 NHC·$SiCl_4$ - B3LYP/6-311+G(d,p) 117
3.1.2 IMe·PDMS - B3LYP/6-311+G(d,p) 119
3.1.3 NHC·$SiCl_4$ - MP2/6-311+G(d,p)//B3LYP/6-311+G(d,p) 119
3.1.4 NHC·Si - MP2/6-311+G(d,p)//B3LYP/6-311+G(d,p) 121
3.2 Gibbs Free Energy of Interaction - B3LYP/6-311+G(d,p) 121
3.2.1 MP2/aug-cc-pVTZ//B3LYP/6-311+G(d,p) 126
3.2.2 MP2/aug-cc-pVTZ//B97D/6-311+G(d,p) 127
Conclusions 130

4. Reaction Kinetics: NHC-Catalysed Reactions 132
4.1 Synthesis of Postulated Reaction Intermediates 135
4.1.1Synthesis of a Postulated Aminoester Intermediate 135
4.1.2 Synthesis of a Postulated Oxazole Intermediate 138
Conclusions 142
4.2 React-IR 143
4.2.1 *In Situ* Monitoring of the IMes-Catalysed Amidation 144
4.2.2 The Effect of M_2 on NHC-Catalysed Amidation 147
Conclusions 155
5. Physical Protection of an NHC 156
5.1 Decomposition Limited by Mass Transfer (Diffusion) 159
5.2 Steady State Mass Transfer 164
5.2.1 Homogeneous Systems 164
5.2.2 Non-Homogeneous System 166
5.3 Transient Mass Transfer 167
5.3.1 Non-Homogeneous Boundary Conditions 168
5.3.2 Steady State Solution 169
5.3.3 Solution of a Homogeneous System 170
5.3.4 Separation of Variables 171
5.3.5 Initial Value Solution as a Fourier Series 172
Conclusions 176
6. NHC·Si Interactions - Quo Vadis? 177
7. Experimental 180
8. References 201
Appendix A: Quantum Chemical Calculations 211
Appendix B: NMR Spectra 224
Appendix C: Failed Procedures 391

Abbreviations

Å	Angstrom
Ac	Acetyl
Ad	Adamantyl
aq	Aqueous
Ar	Aryl
ATR	Attenuated total (internal) reflectance
Bn	Benzyl
BSSE	Basis set superposition error
Bu	Butyl
°C	Degrees Celsius
cat.	Catalytic
$CDCl_3$	Deuterated chloroform
CDI	Carbonyldiimidazole
conc.	Concentrated
conv.	Conversion
δ	Chemical shift
d	Doublet
D_4	Octamethylcyclotetrasiloxane
DCC	*N,N*'-Dicyclohexylcarbodiimide
DCM	Dichloromethane
dd	Doublet of doublets
DDQ	2,3-Dichloro-5,6-dicyano-1,4-benzoquinone
DEAD	Diethyl azodicarboxylate
Dipp	2,6-di*iso*propylphenyl
DMAP	4-Dimethylaminopyridine
DMF	*N*,*N*-Dimethylformamide

DMSO	Dimethylsulfoxide
DMSO-d_6	Deuterated dimethylsulfoxide
DOSY	Diffusion Ordered Spectroscopy
dq	Doublet of quartets
EDCI	1-Ethyl-3-(3-dimethylaminopropyl)carbodiimide
Et	Ethyl
Et_3N	Triethylamine
Et_2O	Diethylether
EtOAc	Ethyl acetate
EtOH	Ethanol
G	Gibbs free energy
h	Hour
H	Enthalpy
HCl	Hydrochloric acid
H_2O	Water
HRMS	High resolution mass spectroscopy
Hz	Hertz
i	*Iso*
IAd	1,3-bis(adamantyl)imidazol-2-ylidene
IDipp	1,3-bis(2,6-di*iso*propylphenyl)imidazol-2-ylidene
Im.	Imidazole
IMe	1,3-bis(methyl)imidazol-2-ylidene
IMes	1,3-bis(2,4,6-trimethylphenyl)imidazol-2-ylidene
*i*PrOH	*Iso*propanol
IR	Infrared (spectroscopy)
I*t*Bu	1,3-bis(*tert*-butyl)imidazol-2-ylidene
J	Coupling constant

K	Kelvin
L	Non-dimensional length
LA	Lewis-acid
m	Multiplet
µ	Micro (10^{-6})
M	Molar
M_2	Hexamethyldisiloxane
MD_4M	Tetradecamethylhexasiloxane
$MD_4^{Ph}M$	$Me_3SiO(Me_2SiO)_{6.6}(MePhSiO)_{7.1}SiMe_3$
MDM	Octamethyltrisiloxane
Me	Methyl
Me_2IMe	1,3,4,5-Tetramethyl-imidazol-2-ylidene
Me_2I*t*Bu	1,3-bis(*tert*-butyl)-4,5-dimethyl-imidazol-2-ylidene
MeOH	Methanol
Mes	Mesityl
min	Minute
mol	Mole
m	*Meta*
NHC	*N*-Heterocyclic Carbene
NMR	Nuclear Magnetic Resonance (Spectroscopy)
o	*ortho*
p	*para*
PDMS	Poly(dimethyl)siloxane
Ph	Phenyl
PPh_3	Triphenylphosphine
ppm	Parts per million
Pr	Propyl

pt	Proton transfer
q	Quartet
qd	Quartet of doublets
ROP	Ring-Opening Polymerisation
r.t.	Room temperature
S	Entropy
sat.	Saturated
SIDipp	1,3-bis(2,6-di*iso*propylphenyl)imidazolin-2-ylidene
SIMes	1,3-bis(2,4,6-trimethylphenyl)imidazolin-2-ylidene
SNR	Signal to noise ratio
t	Triplet
t	*Tertiary*
THF	Tetrahydrofuran
THF-d_8	Deuterated Tetrahydrofuran
TLC	Thin layer chromatography
TMS	Trimethylsilyl
Tol	Toluene
Tol-d_8	Deuterated Toluene
UV	Ultraviolet
ZPVE	Zero-point valence energy

Table of Figures

Figure 1: Possible Hybridisation States of the Carbene Moiety 18
Figure 2: Electronic Configuration of the Carbene Moiety 19
Figure 3: Dimerisation of Reactive Carbenes to form an Alkene 19
Figure 4: Dimerisation of Singlet Carbenes – End-on Approach 19
Figure 5: Electronic Effects of Adjacent Heteroatoms – Stabilisation of the Singlet State 20
Figure 6: Huckel Type Aromaticity - Stabilisation of the Singlet State 20
Figure 7: Early Examples of Transition Metal-Carbene Complexes 21
Figure 8: Examples of *N*-Heterocyclic Carbenes 22
Figure 9: Common Examples of the Amide Linkage – Active Pharmaceutical Ingredients 37
Figure 10: Arylboronic Acids – Catalysts of Direct Amidation[79] 41
Figure 11: Quantifying the Decomposition of IMes in the Presence of $MD_4^{Ph}M$ – Time-resolved ^1H NMR Spectra Presented by Baceiredo and Co-workers[90] 50
Figure 12: Proposed NHC·Si (Lewis-base - Lewis-acid) Interaction[90] 51
Figure 13: Pentacoordinate Silicon Species - Silatranes with a Range of Apical Substituents 57
Figure 14: Pentacoordinate Silicon Species - NHC·$SiCl_4$ Complexes[32,111] 58
Figure 15: Geometry of Penta- and Hexacoordinate NHC·SiX_4 Complexes 58
Figure 16: ^{13}C NMR Spectrum of ^{13}C-Labelled IMes·HCl Exhibiting Increased SNR of the C2 Position 66
Figure 17: Pentacoordinate NHC·$SiCl_4$ Complexes Reported in the Literature[32,111] 70
Figure 18: ^{29}Si NMR Spectrum of IDipp·$SiCl_4$ Showing a Single Resonance at −109 ppm 72
Figure 19: ^{13}C NMR Spectrum of the Isolated Solid in C_6H_5Cl with D_2O Lock 73
Figure 20: ^{29}Si NMR Spectrum of the Isolated Solid in CD_2Cl_2 74
Figure 21: Comparison of (a) ^{13}C-Labelled and (b) Natural Abundance IMes – Increased SNR of the Carbene Moiety ca. 220 ppm 79
Figure 22: ^{13}C-Labelled IMes (*4b) Prior to Exposure (a) and 17 Hours After Exposure to Air (b) 80
Figure 23: Relative Concentration of ^{13}C-IMes in Solution - Derived from ^{13}C Quantitative NMR 81
Figure 24: Titration Curve of IDipp (4c) with Water at −35 °C in THF-d_8 by Nyulászi and Co-workers[89] 82
Figure 25: ^{13}C NMR Spectrum of IMe (4a) Formed *In Situ* – Carbene Moiety ca. 210 ppm 84
Figure 26: Silanes and Siloxanes Used for Initial Studies on NHC Decomposition 85
Figure 27: Decomposition of IMe at Time 0, 1.5, 15, 23, 42, and 63 Hours 86
Figure 28: ^{13}C NMR Spectra of IMes (a), and IMes with M_2 (1:10 Mole Ratio) (b), in C_6D_6 at Room Temperature After 8 Hours 88
Figure 29: ^{13}C NMR Spectrum of ^{13}C-Labelled IMes (*4b) with Trimethoxymethylsilane (116) (1:10 mole ratio) 90
Figure 30: ^{29}Si NMR Spectra of IMes and M_2 (1:1 mole ratio) in THF-d_8 at 298K (Red) to 198K (Purple) in 25K Steps 94
Figure 31: DOSY Spectrum – M_2 (0.1 mmol) in THF-d_8 (0.4 mL) 96
Figure 32: DOSY Spectrum – IMes (4b, 0.01 mmol) and M_2 (114, 0.02 mmol) in THF-d_8 (0.4 mL) 99
Figure 33: DOSY Spectrum – IMes (4b, 0.01 mmol) and M_2 (114, 0.02 mmol) in Toluene-d_8 (0.4 mL) 100
Figure 34: Effect of Backbone Chlorination in the ROP of Lactide - Conversion Versus Time Reported by Hedrick and Co-workers[66] 102

Figure 35: Selection of Lewis Acidic Silanes Used for NMR Experiments 110
Figure 36: ^{13}C NMR Spectrum of IMes and $(MeO)_2Si(C_6F_5)_2$ in Toluene-d_8 at Room Temperature 112
Figure 37: ^{13}C (a), and ^{29}Si (b) NMR Spectra of IMes and Me_3SiCF_3 in Toluene-d_8 at Room Temperature 114
Figure 38: NHC·Si System as Modelled by Baceiredo and Co-workers[90] 116
Figure 39: IR Spectrum of the Unstable Boc-free Aminoester 138
Figure 40: IR Spectrum of 2-Benzyloxazole 140
Figure 41: IR Spectrum *N*-(2-Hydroxyethyl)-2-phenylacetamide 141
Figure 42: Comparison of Manually and Software-Integrated Peaks for the Derivation of Concentrations of Methyl 2-phenylacetate (157) and *N*-(2-Hydroxyethyl)-2-phenylacetamide (71) 145
Figure 43: NHC-Catalysed Amidation (Equimolar Ester and Amine) 145
Figure 44: Amidation (Equimolar Ester and Amine) - Proposed 2nd Order Kinetics Overall 146
Figure 45: Concentration Profiles of Ester, Amide, and an Intermediate without (a) and with M_2 (b) in THF 148
Figure 46: Approximation of Absorbance Profiles with Lines of Best Fit 149
Figure 47: Amidation with 10 mmol Excess Ester without M_2 150
Figure 48: Stoichiometric Amidation of an Ester with Ethanolamine and without M_2 151
Figure 49: Amidation with 10 mmol Excess Ester with M_2 152
Figure 50: Stoichiometric Amidation of an Ester with Ethanolamine and with M_2 153
Figure 51: Stoichiometric Amidation of an Ester with Ethanolamine and with M_2 - Overlay 154
Figure 52: Derivation of a Power Law Relation between Viscosity of Single Molecular Weight PDMS and Molecular Weight 157
Figure 53: ^{1}H (a) and ^{29}Si (b) NMR Spectra of IMes (60 mg) and PDMS (4000 g·mol^{-1}, 600 mg) with Tol-d_8 Lock 158
Figure 54: Biphasic NMR Samples of IMes in DMSO-d_6 and Silicon Species Exposed to Air 159
Figure 55: ^{13}C NMR Spectra of IMes (30 mg) in DMSO-d_6 (0.4 mL) under Paraffin (0.3 mL) at Time 0 (a) and after 5 Days (b) 161
Figure 56: ^{13}C NMR Spectrum of IMes (30 mg) in DMSO-d_6 (0.4 mL) under Paraffin (0.3 mL) After 27 Days 162
Figure 57: ^{13}C NMR Spectrum of IMes (30 mg) in DMSO-d_6 (0.4 mL) under PDMS (770 g·mol^{-1}, 0.3 mL) After 8 Days 162
Figure 58: ^{1}H NMR Spectrum of IMes (30 mg) in DMSO-d_6 (0.4 mL) with DMF Standard Under Paraffin (19 cSt) After 27 Days 163
Figure 59: Mass-Transfer - Concentration Profiles across Interfaces 164
Figure 60: Evolution of a Concentration Profile within PDMS of 0.02m Depth 174
Figure 61: Evolution of a Concentration Profile within PDMS of 0.05m Depth 175

Table of Schemes

Scheme 1: Deprotonation of an Imidazolium Salt to form an NHC 22
Scheme 2: Alternative Methods for the Synthesis of Free NHCs 23
Scheme 3: Mechanism of the Acyloin Addition Catalysed by Cyanide 24
Scheme 4: Mechanism of an NHC-Catalysed Acyloin Addition 25
Scheme 5: Mechanism of an NHC-Catalysed Stetter Reaction 26
Scheme 6: Mechanism of Fischer Esterification of a Carboxylic Acid with an Alcohol 27
Scheme 7: Mechanism of Steglich Esterification – DMAP as a Nucleophilic Catalyst 28
Scheme 8: Side Reaction of Steglich Esterification - Formation of *N*-acylureas 28
Scheme 9: Mechanism of the Mitsunobu Reaction – Inversion of an Alcohol Stereocentre 29
Scheme 10: Proposed Mechanism of an NHC-Catalysed ROP of Cyclic Esters – Nucleophilic Attack[60] 30
Scheme 11: NHC-Catalysed Transesterification of Methyl Acetate with Benzyl Alcohol 31
Scheme 12: NHC-Catalysed Transesterification of Vinyl Acetate with Benzyl Alcohol 35
Scheme 13: Proposed Mechanism for the Formation of an Unexpected Reaction Intermediate in NHC Catalysed Transesterifications[65] 35
Scheme 14: NHC Catalysed Transesterification – Proposed Nucleophilic Activation of an Ester 36
Scheme 15: Amidation with Schotten-Baumann Conditions – Formation of Acyl Chlorides 38
Scheme 16: Amidation *via* Activation of a Carboxylic Acid with CDI – Formation of Activated Esters 38
Scheme 17: Direct Reaction of Carboxylic Acids with Amines - Ammonium Carboxylate Salt Formation 39
Scheme 18: Proposed Mechanism for the Direct Amidation of Carboxylic Acids with Aminoboranes *via* an Acyloxyboron Intermediate 40
Scheme 19: Borate Ester-Promoted Amidation *via* the Formation of Acyloxyborate Intermediates . 41
Scheme 20: Proposed Mechanism of Ru-Catalysed Amidation 42
Scheme 21: Appel-like Reaction - Activation of a Carboxylic Acid 43
Scheme 22: Amide Synthesis *via* Nucleophilic Attack of an Activated Carboxylic Acid 43
Scheme 23: NHC-Catalysed Amidation of Esters - Primary and Secondary Amines 43
Scheme 24: NHC-Catalysed Amidation of Esters - Aminoalcohols 44
Scheme 25: Proposed Decomposition Routes of NHCs by Water and Oxygen 45
Scheme 26: Proposed Decomposition Pathway of Pentafluorophenyl-Substituted Triazol-3-ylidenes 46
Scheme 27: Isolation and Reuse of an NHC[92] 47
Scheme 28: NHC·CO_2 Adducts as Latent NHCs[93] 48
Scheme 29: Synthesis of a Mildly Air-Stable NHC - Chlorination of Backbone Positions with Concomitant Formation of Chloroform 49
Scheme 30: Proposed Mechanism of NHC-Catalysed ROP of D_4 – Nucleophilic Ring-Opening of a Cyclic Siloxane[101] 52
Scheme 31: NHC-Catalysed Dehydration of Disilanol Oligomers 53
Scheme 32: Proposed Mechanism of NHC-Catalysed Cyanosilylation – Activation of a Silicon Centre and Formation of a Pentacoordinate Species[95] 54
Scheme 33: Nucleophilic Substitution at a Silicon Centre 55
Scheme 34: NHC-catalysed Hydrosilylation[106] 56

Scheme 35: Nucleophilic Attack of an NHC on a Silicon Halide – Formation of an NHC·Si Adduct and Expulsion of Chloride[109] 59
Scheme 36: Nucleophilic Attack of Chloride on a Lewis Acidic Silane – Formation of a Pentacoordinate Silicon Species[109] 59
Scheme 37: One-pot Synthesis of Imidazolium Halides as Reported by Arduengo and Co-workers[15] 62
Scheme 38: Synthesis of Methylimidazolium Iodide - Alkylation of Methylimidazole[11] 62
Scheme 39: Modular Synthesis of Imidazolium Halides *via* the Formation and Isolation of Diazabutadienes 63
Scheme 40: Synthesis of Aryl-Substituted Diazabutadienes – Condensation of Arylamines and Glyoxal[12] 64
Scheme 41: Synthesis of *N,N'*-bis(*tert*-butyl)-1,4-diazabutadiene 64
Scheme 42: Mistryukov's Synthesis of a Diazabutadiene – $CaCl_2$ as a Drying Agent[117] 65
Scheme 43: Ring-closing of a Diazabutadiene with Paraformaldehyde and TMSCl 65
Scheme 44: Synthesis of ^{13}C-Labelled IMes-HCl – ^{13}C-labelled Formaldehyde as Carbon Source 66
Scheme 45: One-pot Synthesis of I*t*Bu·HCl as Reported by Herrmann and Co-workers[118] 67
Scheme 46: Synthesis of a Free NHC – Deprotonation of an Imidazolium Halide by *t*BuOK 68
Scheme 47: Synthesis of IDipp-$SiCl_4$ – Formation of a Pentacoordinate Silicon Species 71
Scheme 48: Attempted Formation of a Me_2I*t*Bu·$SiCl_4$ Complex 72
Scheme 49: Synthesis of a *N,N'*-Disubstituted Urea with Phosgene[121] 77
Scheme 50: Attempted Ru-Catalysed Synthesis of 1,3-Disubstituted 4,5-Dihydroimidazol-2-ones[122] 77
Scheme 51: Synthesis of an Imidazol-2-one – Cu_2O Assisted Oxidation of an Imidazolium Halide[36] .. 77
Scheme 52: Deprotonation of IMe·HI in the Presence of Silicon Species to Form IMe (4a) *In Situ* 83
Scheme 53: Attempted Synthesis of 2,3-Disubstituted-1,4-diazabutadienes 103
Scheme 54: Possible Decomposition Pathway of Butan-2,3-dione Derivatives 104
Scheme 55: Reported Synthesis of NHC·Boranes[30] 104
Scheme 56: Reported Ring Lithiation of NHC·Boranes[137] 105
Scheme 57: Reported Synthesis of a Formamide Substrate for Ring-closure[88] 106
Scheme 58: Amination of a Propargylic Alcohol[88] 107
Scheme 59: Attempted Synthesis of a Mixed Anhydride[138,139] 107
Scheme 60: Literature Reported *N*-Formylations[140,141] 108
Scheme 61: Ethyl Formate as a Formylating Agent[142] 108
Scheme 62: Formyl Acetate as a Formylating Agent 109
Scheme 63: Formylation of a Propargylic Amine[88] 109
Scheme 64: Ring-Closing of a Formamide to Yield a Backbone-Substituted Imidazolium Salt[88] 109
Scheme 65: Proposed Mechanism of IMes-Catalysed Amidation of an Ester as Reported by Movassaghi and Schmidt – Activation of an Alcohol[71] 132
Scheme 66: Proposed Mechanism of IMes-Catalysed Esterification/Acylation as Reported by Nolan and Co-workers – Nucleophilic Activation of Esters[61–63] 133
Scheme 67: Attempted NHC-Catalysed Amidation of Methyl Acetate with Ethylamine 134
Scheme 68: Acylazolium Ions as Acylating Agents and the Role of IMes[72] 134
Scheme 69: Possible Mechanism for the Formation of an Oxazole Intermediate 136
Scheme 70: Boc-Protection of Ethanolamine 136
Scheme 71: Attempted IMes-Catalysed Amidation of Methyl 2-phenylacetate with *N*-Boc-ethanolamine 136
Scheme 72: CDI-Promoted Esterification of Phenylacetic Acid with an *N*-Protected Ethanolamine. 137

Scheme 73: Boc-Deprotection of an Amino-ester 137
Scheme 74: Attempted Formation of an Oxazole from a Hydroxyamide 139
Scheme 75: Attempted Synthesis of an Oxazole by the Action of $SOCl_2$ on a Hydroxyamide[182] 139
Scheme 76: Base-assisted Elimination to Yield 2-Benzyloxazole 139
Scheme 77: Proposed Mechanism of IMes-Catalysed Amidation as Reported by Movassaghi and Schmidt - Modified to Include an Oxazole and NHC·Si Interaction 144
Scheme 78: IMes-Catalysed Amidation of Methyl 2-phenylacetate with Ethanolamine 147

1. Introduction

N-Heterocyclic carbenes have been widely exploited by organic chemists in a range of chemical transformations. However, their more widespread use in industrial applications is limited by their susceptibility to irreversible degradation by water and oxygen. A valuable goal would be a process or modification which could limit the rate of degradation or make NHCs impervious to the action of oxygen and water.

1.1 An Overview of Carbenes

The carbene moiety is defined as a divalent carbon with six valence electrons. It is formally neutral bearing no formal charge but is highly reactive. Carbenes may be sp-hybridised which gives rise to a theoretical bond angle of 180 degrees (linear), or they may be sp^2-hybridised giving a theoretical bond angle of 120 degrees (trigonal planar) as shown in Figure 1.[1] Although sp^3-hybridised cases are theoretically possible, these shall not be considered here.

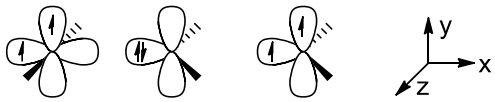


Figure 1: Possible Hybridisation States of the Carbene Moiety

In the sp-hybridised case, the electrons are unpaired (Hund's rule) in the ground state; the electrons populate degenerate and orthogonal p_x and p_y orbitals giving rise to a triplet state. In the sp^2-hybridised cases, the p_π (p_y) orbital is unchanged in energy but hybridisation of the p_x orbital lowers its energy and this gives rise to more s-character (Figure 2). As such, the ground state is expected to be the singlet state which is energetically lower-lying with both of the non-bonding electrons paired in an sp^2 orbital. The triplet state is higher in energy but the singlet-triplet energy gap may be small.[1,2] In the case of *N*-Heterocyclic carbenes (NHCs), the singlet-triplet gap is sufficiently large such that singlet-triplet transitions do not occur under ambient conditions.[1,3–5]

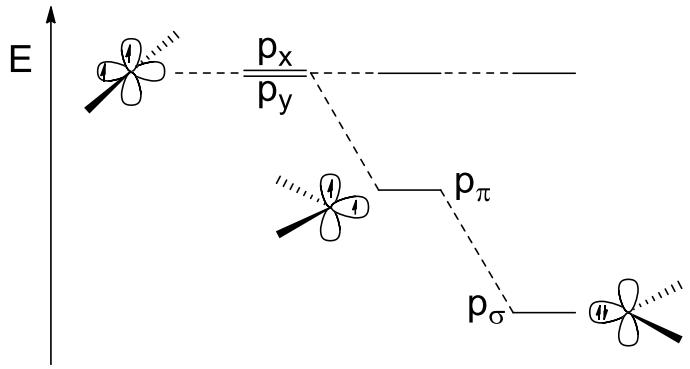


Figure 2: Electronic Configuration of the Carbene Moiety

It is the multiplicity of the carbene moiety that gives rise to its diverse chemistry. Triplet state carbenes, with unpaired electrons, have di-radical nature. Singlet state carbenes with an sp^2 lone pair are ambiphilic in nature. They are strong nucleophiles due to the lone pair but also possess electrophilic character due to the empty p_π orbital. Carbenes are thus expected to be highly reactive and able to dimerise readily giving rise to alkenes (Figure 3).

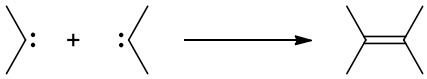


Figure 3: Dimerisation of Reactive Carbenes to form an Alkene

It should be noted that in the case of singlet carbenes, dimerisation cannot occur through end-on approach. The nucleophilic sp^2 orbital must overlap with the electrophilic empty p_π orbital which requires an orthogonal approach (Figure 4). As such, steric crowding can prevent or hinder dimerisation.

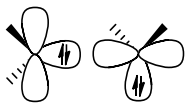


Figure 4: Dimerisation of Singlet Carbenes – End-on Approach

Theoretically, the presence of heteroatoms such as nitrogen, oxygen, or sulphur directly adjacent to the carbene moiety can stabilise the singlet state. Donation of electron density, into the empty p_π orbital is achieved by orbital overlap of a heteroatom lone pair (mesomeric effect) as shown in

Figure 5.[1,2] Although drawn for nitrogen, the same mechanism is applicable for oxygen and sulphur. This has the effect of raising the energy of the p_π orbital by donation of electron density from the heteroatom lone pair, further increasing the energy gap between the singlet and triplet states which further stabilises the lower-lying singlet state. Furthermore, this makes dimerisation less energetically favourable. Orbital overlap in the π-system has no effect on the σ system which is orthogonal.

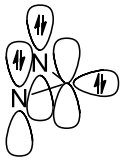


Figure 5: Electronic Effects of Adjacent Heteroatoms – Stabilisation of the Singlet State

In addition, the electronegativity of the heteroatom withdraws electron density (inductive effect) through the σ-system thus reducing the nucleophilicity of the lone pair.[1,2] This also makes dimerisation less favourable. The presence of heteroatoms adjacent to the carbene moiety has since been referred to as a push-pull system denoting the separate and orthogonal effects on electron density in the π and σ systems.

The presence of a cyclic structure would impart rigidity to the system and increase the electron donation exhibited through the π system by preventing rotation and/or maintaining orbital overlap (Figure 6).[1] Furthermore, the presence of a double bond in a 5-membered ring system gives rise to aromaticity which supplements the stability of the system. Ideally, when combined, these effects sufficiently stabilise the singlet state and allow for the synthesis, isolation, and characterisation of a free carbene.[1]

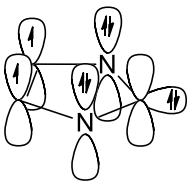
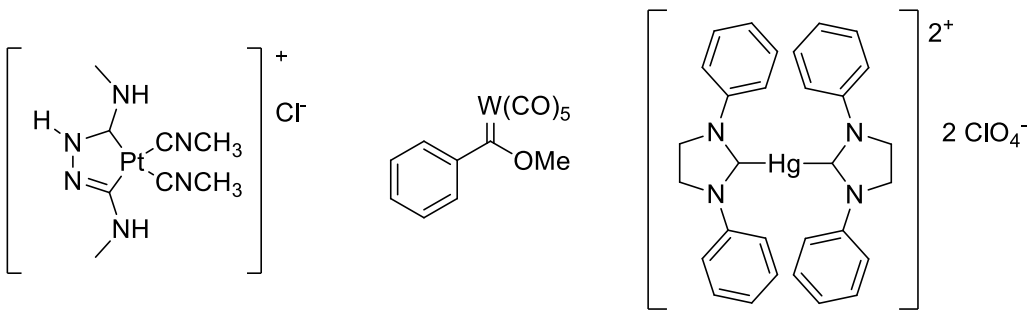


Figure 6: Huckel Type Aromaticity - Stabilisation of the Singlet State

Although the presence of bulky substituents on the adjacent heteroatoms (where possible) may prevent dimerisation by increasing steric clash and preventing the required approach for orbital overlap as shown in Figure 4, steric bulk is not necessary in the formation of stable imidazol-2-ylidenes which are thermodynamically stable.[3–6]

The history of carbenes is not without controversy, having been thought to be far too reactive to isolate, and existing only for fleeting moments as reactive intermediates. Indeed, their beginning is dominated by the isolation and characterisation of carbenoid-transition metal complexes as opposed to the free carbenes.[1] Notable examples include Chugaev's salt **1**, Fischer's tungsten-carbene complex **2**, and Wanzlick's NHC-mercury complex **3** as shown in Figure 7.[7–9]



1 **2** **3**

Figure 7: Early Examples of Transition Metal-Carbene Complexes

Although it is now recognised that Chugaev's salt **1** was the first metal-carbene complex to be synthesised and isolated, spectroscopic techniques at the time did not allow for this revelation.[10] Fischer's tungsten-carbene complex **2** was the first unambiguously characterised metal-carbene complex while Wanzlick's complex **3** was the first NHC-transition metal complex to be characterised.[8,9]

Although others had hypothesised the existence of free carbenes (and NHCs), and indeed possible methods of stabilising the carbene moiety,[1] Arduengo and co-workers were the first to isolate a stable and crystalline imidazol-2-ylidene in 1991.[6] More importantly, imidazol-2-ylidenes were shown to be thermodynamically stable.[3–6]

While there are many structures that can be labelled NHCs including but not limited to: imidazol-2-ylidenes (**4**), triazol-5-ylidenes (**5**), and cyclic alkyl amino carbenes (**6**) as shown in Figure 8. Further references to NHCs within this body of work shall refer to imidazol-2-ylidenes (**4**) exclusively.

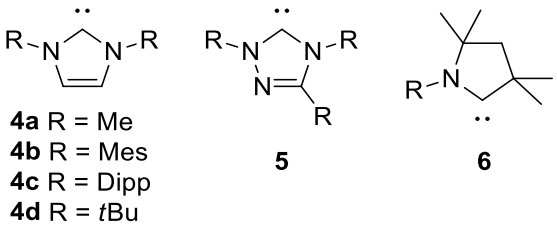
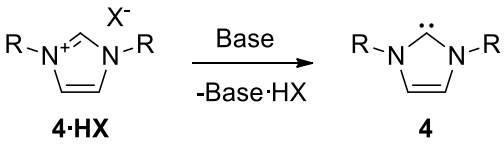


Figure 8: Examples of *N*-Heterocyclic Carbenes

1.2 Synthetic Routes to Free NHCs

Arduengo and co-workers synthesised 1,3-bis(adamantyl)imidazol-2-ylidene (**4**, R = adamantyl) by deprotonation of the corresponding imidazolium salt (**4·HX**) with a strong base under an inert atmosphere (Scheme 1): an approach that is still preferred today with the imidazolium chloride (**4·HCl**) and tetrafluoroborate salts (**4·HBF$_4$**) of a number of respective imidazol-2-ylidenes commonly available or readily synthesised.[5,6,11–18]

The deprotonation of imidazolium salts (**4·HX**) to yield imidazol-2-ylidenes (**4**) is favoured over other synthetic routes to prepare NHCs due to the commercial availability, and the stability of the starting materials, as well as the relatively mild deprotonation conditions in comparison to other procedures (*vide infra*).

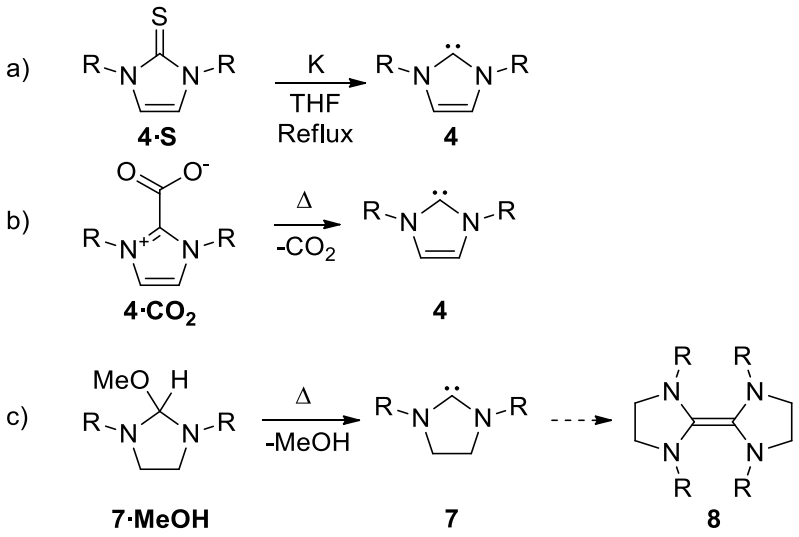


Scheme 1: Deprotonation of an Imidazolium Salt to form an NHC

It can be seen that NHCs are very basic: the NHC precursors **4·HX** are weak acids and NHCs (**4**) are strong conjugate bases. While there have been many studies of the basicity of a range of NHCs in a number of solvent systems, it is generally accepted that imidazol-2-ylidenes (**4**) in DMSO have a pKa ca. 25.[19,20]

A crystalline sample of 1,3-bis(adamantyl)imidazol-2-ylidene (**4**, R = adamantyl) was characterised by Arduengo and co-workers with the ^{13}C NMR spectrum exhibiting a distinct resonance ca. 215 ppm which is a distinguishing trait of the C2 (carbene) resonance of imidazol-2-ylidenes (**4**), with little variance due to substitution at the heteroatoms.[5,6] ^{13}C NMR spectroscopy has become a quick and reliable method of identifying the carbene moiety.

Other methods for the preparation of free NHCs exist but these are now less favoured in comparison to the ease of deprotonating an imidazolium salt (**4·HX**). These include: reduction (desulphurisation) of thioureas (**4·S**) with molten sodium/potassium in THF at reflux;[21] heating of NHC-Lewis-Acid adducts such as NHC·CO_2 (**4·CO_2**);[22–24] and vacuum pyrolysis of unsaturated NHC adducts with concomitant removal of MeOH, $CHCl_3$, etc[25–27] as shown in Scheme 2.



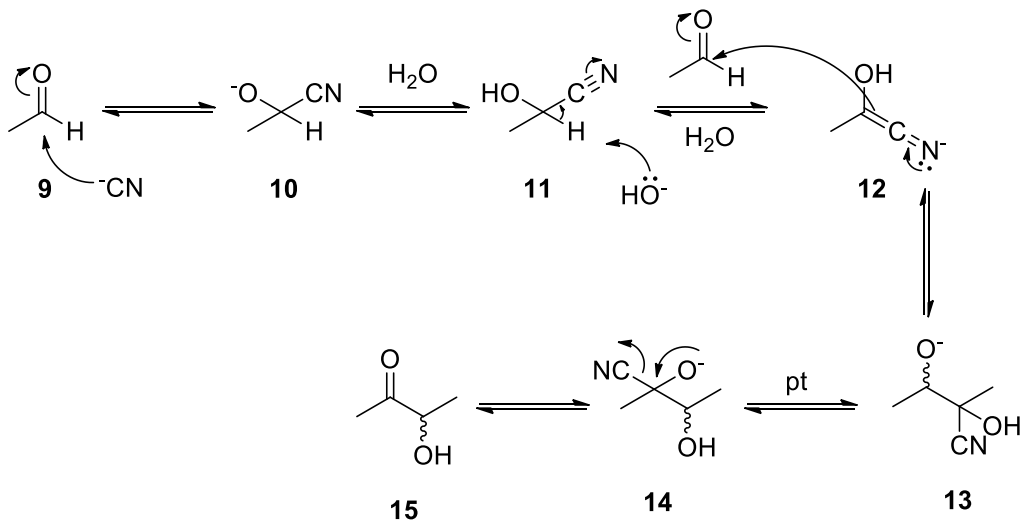
Scheme 2: Alternative Methods for the Synthesis of Free NHCs

The latter method is more suited to saturated *N*-heterocyclic imidazoline-2-ylidenes (**7**) as these are more readily able to undergo insertion reactions. However, the method is prone to dimerisation of the free carbenes under heating (Scheme 2).[28] Although NHC·Lewis-acid adducts are occasionally described as precursors to NHCs, the synthesis of these "precursors" still requires the generation of the free NHC:[21–24] the adducts would be better described as latent NHCs.

The groundbreaking report by Arduengo and co-workers led to a renewed interest in carbene chemistry, much of which was focused on NHCs (**4**) given their novelty and relative ease of preparation and isolation. They have seen wide application in main-group chemistry,[29–32] but due to their strong nucleophilic properties and increased bite angle compared to phosphines, they have also been exploited as transition metal ligands: indeed, they have come to replace the use of PPh_3 as the ligand of choice in many applications.[33–38] However, as a result of their ability as strong σ-donators, it is their use as organocatalysts which has sparked a flurry of papers.[39–44]

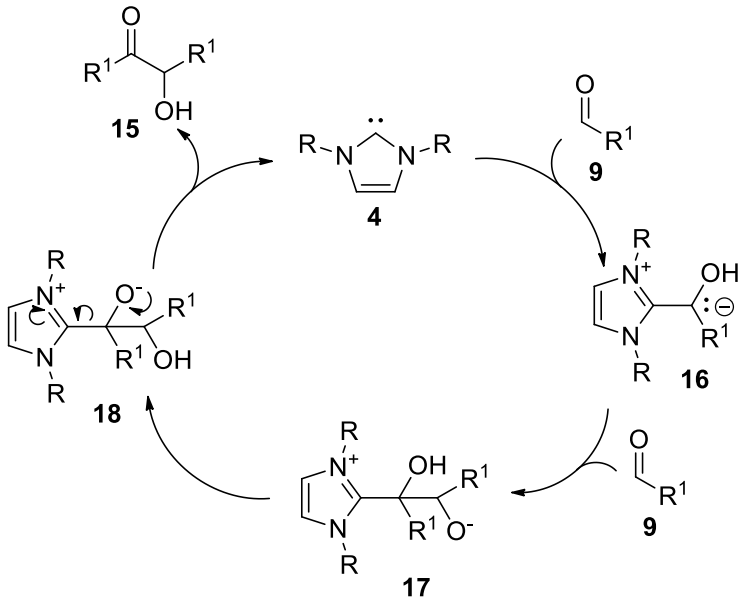
1.3 NHCs as Catalysts in Umpolung Reactions

NHCs have generally been adopted in the facilitation of umpolung reactions (polarity reversal of a functional group).[42,45] A classic example of an umpolung reaction is the acyloin addition (Scheme 3). Addition of cyanide to an aldehyde (**9**) yields a cyanohydrin (**10**) which leads to polarity reversal at the carbonyl. The electrophilic aldehyde carbon becomes nucleophilic on deprotonation of **11**. The attack of a second equivalent of an aldehyde (**9**) by **12** followed by elimination of cyanide generates an α-hydroxyketone (**15**). The reaction is frequently referred to as a condensation reaction although no water is expelled. It should be noted that NHCs do not obviate the need to use the aldehyde (**9**) in excess given that the reaction is under equilibrium control.



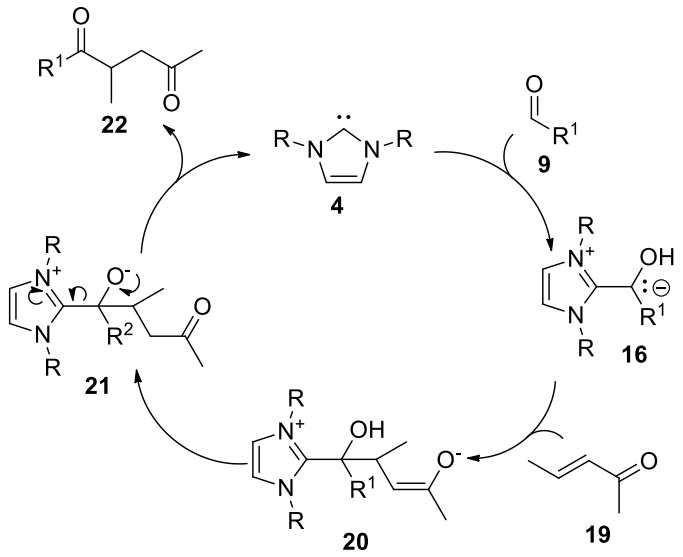
Scheme 3: Mechanism of the Acyloin Addition Catalysed by Cyanide

The reaction mechanism when an NHC (**4**) is employed is similar and proceeds *via* the Breslow intermediate (**16**).[46] Nucleophilic attack of a carbonyl (**9**) by an NHC (**4**), followed by proton transfer yields **16** as shown in Scheme 4.[46] The Breslow intermediate (**16**) is a common feature of NHC-catalysed reactions and can be thought of reacting *via* enamine chemistry or *via* a carbanion, both ultimately resulting in the same intermediate.[39–44]



Scheme 4: Mechanism of an NHC-Catalysed Acyloin Addition

A similar reaction to the acyloin addition is the Stetter reaction which allows the formation of 1,4-addition products (**22**) as shown in Scheme 5.[47] This complements the 1,2-addition products (**15**) generated from the acyloin addition (Scheme 4).

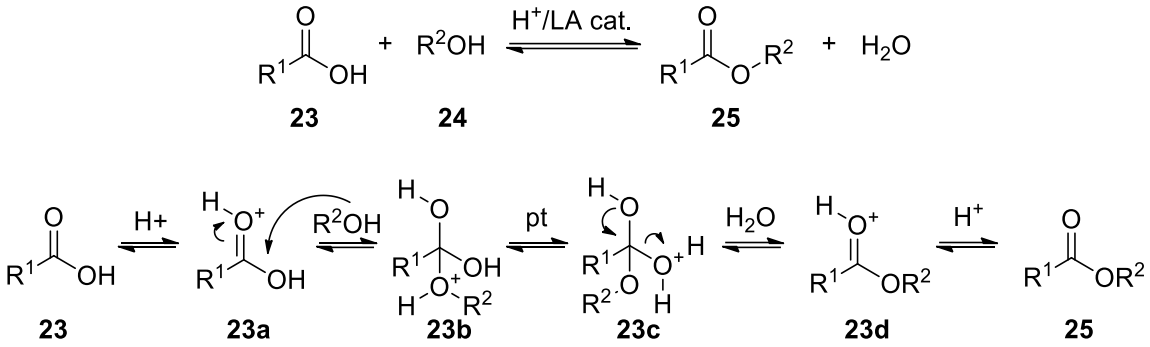


Scheme 5: Mechanism of an NHC-Catalysed Stetter Reaction

Although the Stetter reaction suffers from a reversible 1,2-addition as a side-reaction - the Breslow intermediate (**16**) is able to attack another equivalent of aldehyde (**9**) instead of the Michael acceptor (**19**) - this is of no consequence as the 1,4-addition is irreversible.

1.4 Esterification

Esters find widespread use in the fragrance and flavour industry as many possess fruity odours. Polyesters have also become commonplace in the polymer industry with notable examples including polyethylene terephthalate (PET)[48] and polylactic acid (PLA).[49] Originally, the ester linkage was prepared under Fischer conditions:[50] treating a carboxylic acid (**23**) with an alcohol (**24**), in the presence of a Lewis-or Bronsted acid catalyst. Protonation of **23** leads to the activation of the carbonyl moiety which allows the nucleophilic attack of an alcohol (**24**) on **23a**. Proton transfer and elimination of water yields the ester (**25**) as shown in Scheme 6.



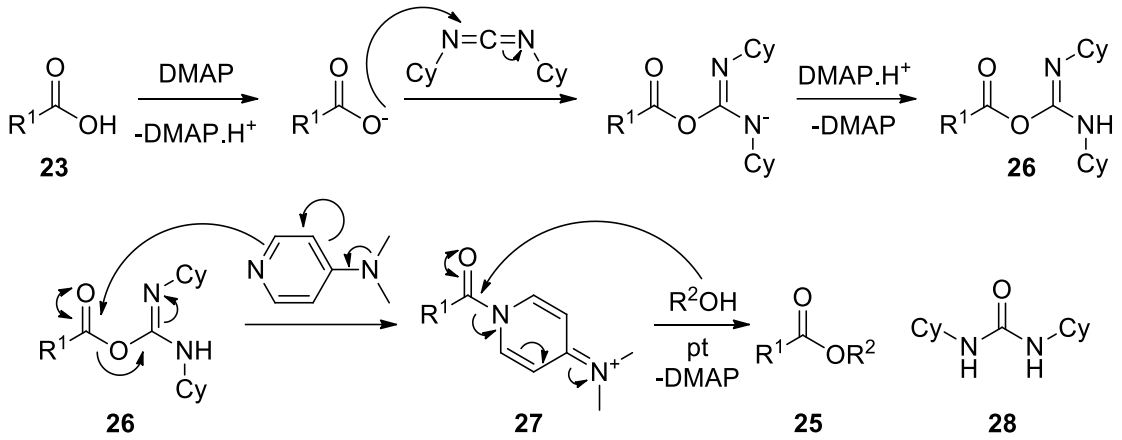
Scheme 6: Mechanism of Fischer Esterification of a Carboxylic Acid with an Alcohol

The reaction suffers from poor equilibrium though the effects can be mitigated by exploiting Le Chatelier's principle. Use of the alcohol (**24**) in excess or as solvent, or a dehydrating agent is possible. The former is usually favoured due to the relatively low cost of starting materials and the ability to recycle by distillation. H_2SO_4 may serve a dual-purpose and can act as a catalyst and a dehydrating agent. Unfortunately, this method is a poor choice for the synthesis of esters bearing sensitive functional groups. For example, *tert*-butyl esters cannot be synthesised this way as *t*BuOH is prone to expelling *iso*-butene under the strongly acidic conditions.

Other methods have been developed which are much milder such as: transesterification,[51] the use of acyl chlorides or anhydrides,[52] Steglich conditions (Scheme 7),[53] or the Mitsunobu reaction (Scheme 9).[54,55] These have the further advantage of avoiding the production of water.

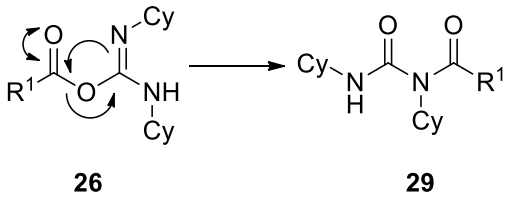
1.4.1 Activation of a Carboxylic Acid

Steglich conditions activate the carboxylic acid (**21**) with stoichiometric amounts of DCC, with DMAP commonly being used in sub-stoichiometric quantities as a nucleophilic catalyst (Scheme 7).[53] An *O*-acyl*iso*urea (**26**) is formed as an intermediate with DMAP assisting in proton transfer. The reactivity of **26** is comparable to an acid anhydride.[52] DMAP then attacks the *O*-acyl*iso*urea (**26**) forming an activated amide (**27**). The alcohol can now attack the activated amide (**27**) to form the ester (**25**) and dicyclohexylurea (**28**) as a by-product in stoichiometric quantities (Scheme 7).



Scheme 7: Mechanism of Steglich Esterification – DMAP as a Nucleophilic Catalyst

Whilst mechanistically possible for the alcohol to attack the *O*-acylisourea (**26**), there is evidence to suggest that this does not occur in the presence of DMAP.[53] DMAP is a stronger nucleophile and without its presence, a slow acyl migration is indicated by the formation of *N*-acylureas (**29**) as shown in Scheme 8.[52]

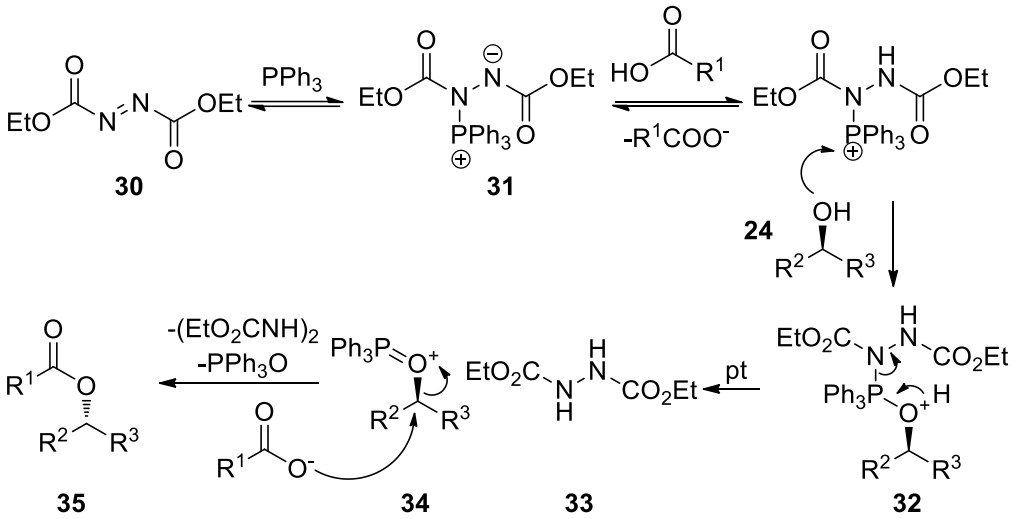


Scheme 8: Side Reaction of Steglich Esterification - Formation of *N*-acylureas

Steglich conditions can be readily applied to amidations where the use of DMAP is not required. Amines are sufficiently nucleophilic such that the side reaction (formation of *N*-acylureas) is insignificant.[52,53]

1.4.2 Activation of an Alcohol

Mitsunobu reaction conditions use stoichiometric amounts of DEAD (**30**) and PPh_3 in an effort to activate the alcohol (**24**) as shown in Scheme 9.[54,55]



Scheme 9: Mechanism of the Mitsunobu Reaction – Inversion of an Alcohol Stereocentre

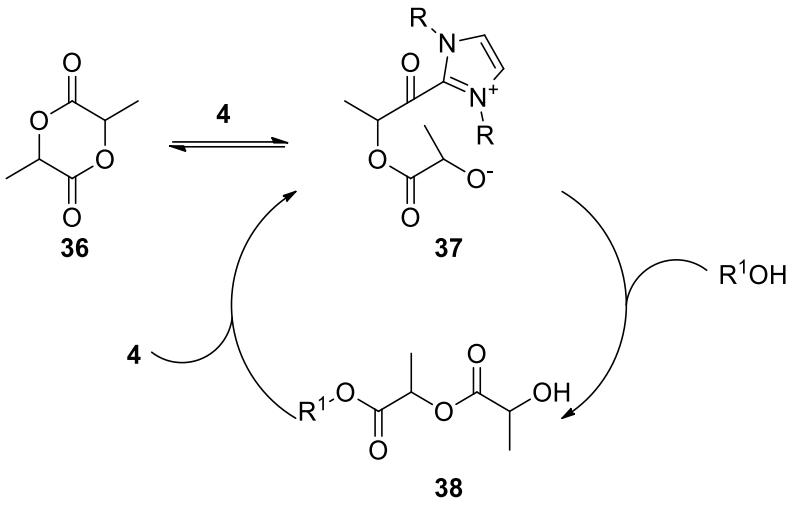
It can be seen that although Steglich[53] (Scheme 7) and Mitsunobu conditions[54,55] (Scheme 9) are useful in shifting equilibrium towards that of product formation (and in increasing yields), it comes at the cost of increased waste production and dramatically reduced atom economy.[56] Furthermore, the dicyclohexylurea (**28**) and triphenylphosphine oxide produced as by-products make product isolation more tedious.

1.4.3 NHC-Catalysed Transesterification

Transesterification is a closely related methodology, whereby a preformed ester (rather than a carboxylic acid) is transformed into another ester by way of displacing the alkoxy group with an alcohol. The only by-product is an alcohol which can be separated by mild means e.g. vacuum distillation. The process has recently come to prominence due to its applicability in the formation of fatty acid methyl esters (FAME) which are used as biodiesel,[57–59] the starting materials of which are readily available as vegetable oils (renewable) and methanol (predominantly fossil fuel sources).

In 2002, Hedrick and co-workers reported a metal-free ROP of cyclic esters (**37**) catalysed by NHCs (**4**).[60] The reaction proceeded with what appeared to be zero-order conversion and constant PDI.

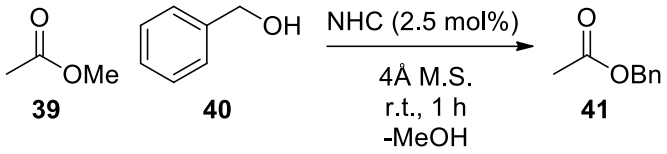
The authors proposed a catalytic cycle with the NHC (**4**) acting as a nucleophile and activating **36** with the formation of an acylazolium intermediate (**37**) as shown in Scheme 10.[60]



Scheme 10: Proposed Mechanism of an NHC-Catalysed ROP of Cyclic Esters – Nucleophilic Attack[60]

Nolan and co-workers similarly reported the use of NHCs (**4**) as nucleophilic catalysts in transesterification/acylation of methyl acetate (**39**), a specific example of which is shown in Scheme 11.[61–63] Molecular sieves were obligatory for increased yields as shown in

Table 1.



Scheme 11: NHC-Catalysed Transesterification of Methyl Acetate with Benzyl Alcohol

A range of imidazol-2-ylidenes (**4**) and their saturated counterparts imidazoline-2-ylidenes (**7**) were shown to be able catalysts with yields from the use of imidazol-2-ylidenes (Entries 1, 2, 5, and 6) exceeding that of imidazoline-2-ylidenes (Entries 3 and 4) and DMAP, and being comparable to *t*BuOK (

Table 1).

Table 1: Transesterification of Methyl Acetate with Benzyl Alcohol Catalysed by Various Nucleophiles[61]

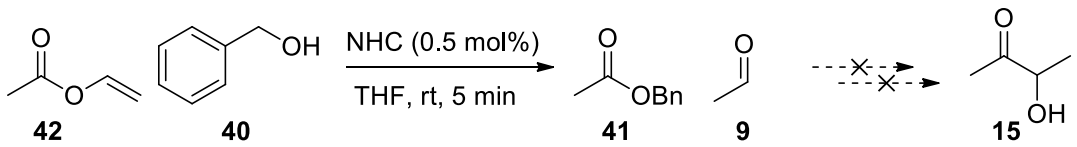
Entry	Catalyst	Yield (%)
1	IMes	93
2	IDipp	45
3	SIMes	21
4	SIDipp	21
5	IAd	100
6	I*t*Bu	100
7	DMAP	15
8	*t*BuOK	95

With saturated NHCs proving to be poor catalysts (Entries 3 and 4), it would appear that electronic effects rather than steric effects of the *N*-substituents dominate reactivity (

Table 1, Entries 1&3, and Entries 2&4). That is, the aromatic, unsaturated NHCs (**4**) led to higher yields. Nevertheless, steric effects cannot be ignored completely (

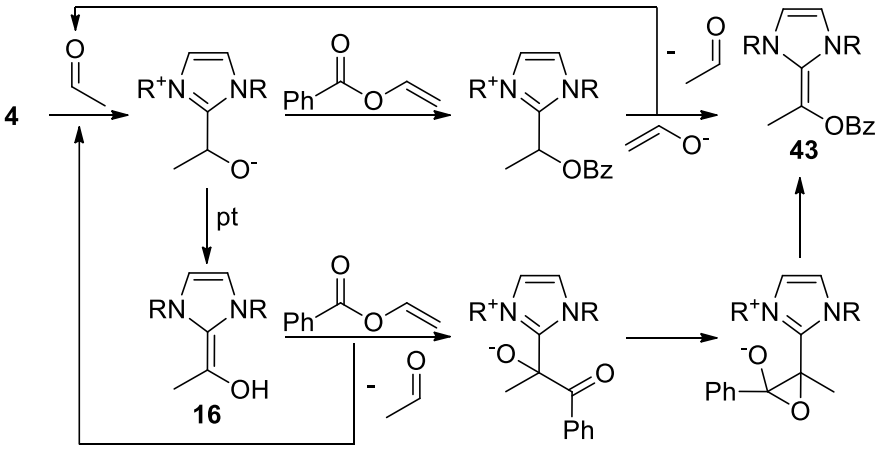
Table 1, Entries 1&2) as although IMes and IDipp have similar steric demands around the carbene centre,[5,14,64] the difference in yields between the two NHCs is prominent.

The reports by Nolan and co-workers also described the transesterification of vinyl acetate (**42**) with primary alcohols in the presence of molecular sieves.[61,62] It was interesting to note that in this case, the by-product of the transesterification was given as acetaldehyde (**9**) and not the acyloin addition product **15** (Scheme 12). This could have been expected given the ability of NHCs (**4**) to catalyse the acyloin addition (Scheme 4).



Scheme 12: NHC-Catalysed Transesterification of Vinyl Acetate with Benzyl Alcohol

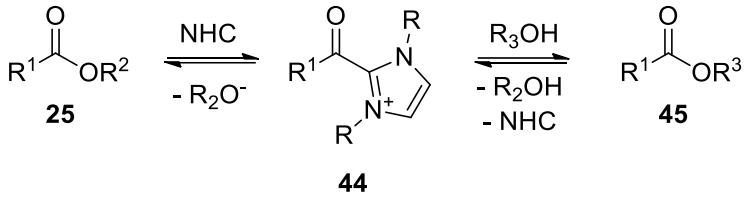
This apparent contradiction was solved by Goldup and co-workers who noticed unusual reaction intermediates in the slow transesterification of vinyl acetate (**42**) with ethanol.[65] Goldup and co-workers showed that acetaldehyde (**9**) in the presence of an ester led to the preferential formation of an unusual adduct (**43**) as shown in Scheme 13, rather than to an acyloin product.



Scheme 13: Proposed Mechanism for the Formation of an Unexpected Reaction Intermediate in NHC Catalysed Transesterifications[65]

Hedrick and co-workers extended the methodology with reports on the effect of different *N*-substituents on reactivity, and the use of a biphasic ionic liquid/THF system which allowed for simple product separation and the generation of the NHC (**4**) *in situ*.[66]

The mechanism of these reactions was disputed with the scientific community broadly divided into two groups: those that proposed NHCs (**4**) acted as nucleophiles and activated the carbonyl moiety with the formation of acylazolium species (**37** and **44**) as shown in Scheme 10 and Scheme 14;[60–63,67–69] and those that proposed NHCs (**4**) acted as bases and/or hydrogen bonded with the alcohol, which thereby increased its nucleophilicity.[70–72]



Scheme 14: NHC Catalysed Transesterification – Proposed Nucleophilic Activation of an Ester

The former was a somewhat contrarian view given the reports by Nolan and co-workers for the NHC-catalysed acylation of alcohols,[61–63] as shown in

Table 1: therein, imidazol-2-ylidenes (**4**) were observed to have comparable reactivity to other bases (*t*BuOK) rather than other nucleophiles (DMAP) which suffered from poor yields. Though not conclusive, this suggested that base catalysis was a likely mechanism.[70–72]

1.5 Amidation

Amide bonds have become ubiquitous in the polymer industry with notable examples including Kevlar[73] (**46**) and Nylon[49] (**47**). A common motif in pharmaceutical products as well, they are present in many APIs (active pharmaceutical ingredient), with important examples including penicillins (**48**) and sulphanilamide (**49**) as shown in Figure 9.

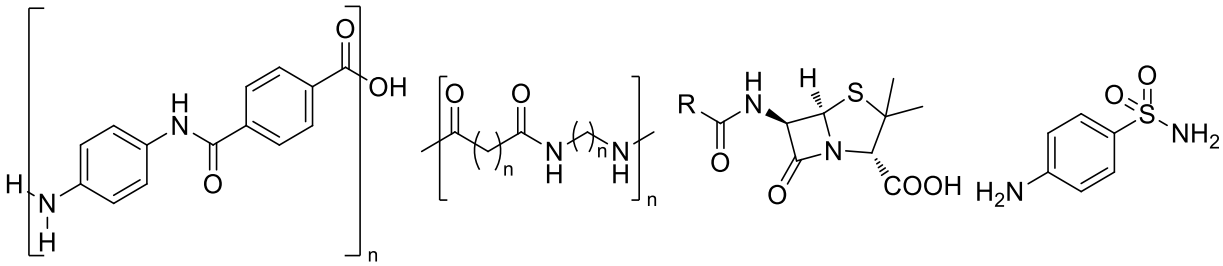


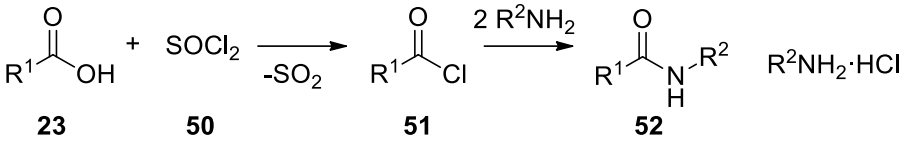
Figure 9: Common Examples of the Amide Linkage – Active Pharmaceutical Ingredients

In comparison to esterifications, generally , amidations do not suffer from poor kinetics as amines are more nucleophilic than their alcohol counterparts.[52] The increased nucleophilicity and better kinetics also have the added benefit of minimising the effect of any side-reactions that may occur depending on the chosen methodology.

1.5.1 Activation of Carboxylic Acids

Amidations are generally performed by activation of a carboxylic acid (or the use of an anhydride) rather than direct reaction of the carboxylic acid and amine as this would initially lead to formation of an ammonium carboxylate which is likely to prevent further reaction. Methods include the use of Schotten-Baumann reaction conditions[74] as shown in Scheme 15, or the use of activating agents such as EDCI, and DCC. Although such techniques are proven and popular, they suffer from poor atom

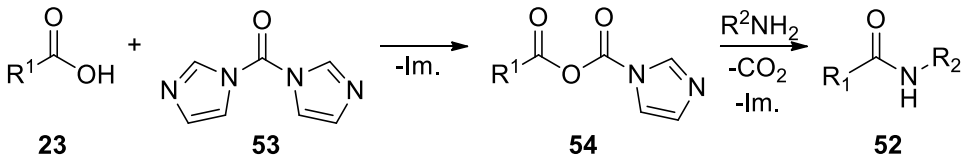
economy[56] and lead to the stoichiometric production of by-products similar to esterifications (Scheme 7).



Scheme 15: Amidation with Schotten-Baumann Conditions – Formation of Acyl Chlorides

There are many ways of generating the intermediate acyl chloride (**51**) including the use of: thionyl chloride (**50**); oxalyl chloride; PCl_3, leading to the formation of phosphorous acid; and PCl_5 leading to the formation of phosphorous oxychloride and hydrochloric acid. The generation of the soluble by-product H_3PO_3 (with use of PCl_3) may be preferable to the expulsion of SO_2 observed with the use of thionyl chloride (**50**) as shown in Scheme 15, to allow for the treatment/disposal of a liquid phase rather than scrubbing/dispersion of a gaseous phase.

Although the generation of acyl chlorides (**51**) is simple and effective, amidation in such cases also requires the use of stoichiometric amounts of base, otherwise protonation of the amine prevents nucleophilic attack of the acyl chloride (**51**). If the amine is cheap, large excesses can be used although this is not amenable for process scale up. The generation and disposal of large quantities of salts leads to a large operational and environmental cost as well as poor green metrics.[56,75] Furthermore, the industrial production of $SOCl_2$ (**50**) is regulated as a Schedule 3 precursor.[76] The use of activating agents such as CDI (**53**) also produces sizeable amounts of waste (imidazole) as shown in Scheme 16.

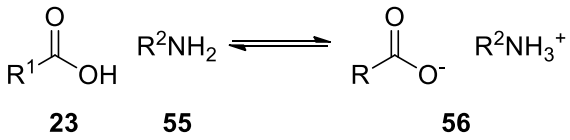


Scheme 16: Amidation *via* Activation of a Carboxylic Acid with CDI – Formation of Activated Esters

The above examples are not ideal in many respects and they lead to the production of waste streams which is not necessarily typical of all amidations. However, the methodologies have been described as they are robust and are historically important. It can be seen that alternative, greener approaches are needed.

1.5.2 Direct Amidation - Acyloxyboron Intermediates

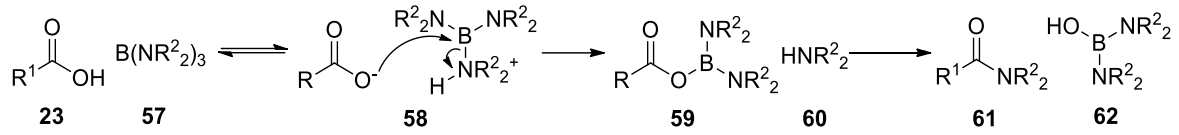
Direct amidation of a carboxylic acid and amine is the gold-standard as the only by-product would be water. It is highly desirable as it possesses sought-after metrics such as high atom economy and a reduced E-factor (defined as the mass ratio of waste to product).[56,75] However, such a transformation is not readily feasible due to the basicity of amines (**55**) leading to the deprotonation of a carboxylic acid (**23**) and the formation of ammonium(-carboxylate) salts (**56**) which are not reactive Scheme 17. Although drawn as reversible, the equilibrium will lie far (if not completely) towards the formation of an unreactive ammonium carboxylate salt (**56**).



23 **55** **56**

Scheme 17: Direct Reaction of Carboxylic Acids with Amines - Ammonium Carboxylate Salt Formation

In 1965, Nelson and Pelter reported that the reaction of carboxylic acids (**23**) with stoichiometric amounts of a trisdialkylaminoboranes (**57**) in an inert solvent yielded an exotherm (Scheme 18).[77] Although no amide was produced at this point, allowing the reaction mixture to stand (or reflux) produced an amide (**61**).[77] It was also noted that a stoichiometric amount of the trisdialkylaminoborane (**57**) was required for complete amidation.



Scheme 18: Proposed Mechanism for the Direct Amidation of Carboxylic Acids with Aminoboranes *via* an Acyloxyboron Intermediate

Given the above data, it was postulated by Nelson and Pelter that the direct amidation proceeded *via* the formation of an acyloxyboron (mixed-anhydride) intermediate **59**, after the initial formation of a carboxylate salt (**58**). Attack of the protonated trisdialkylaminoborane by the carboxylate would yield the acyloxyboron intermediate **59** and a bisdialkylaminoborane (**60**). Nucleophilic attack of the acyloxyboron (**59**) by **60** would then lead to the expected amide (**61**) as shown in Scheme 18.[77]

The observation that stoichiometric amounts of the trisdialkylaminoborane (**57**) was required, led to the conclusion that the by-product **62** is unable to further promote direct amidation. It can be seen that the use of other boron compounds that lead to the formation of acyloxyboron intermediates (**59**) may be effective in the promotion of direct amidation.

Indeed, Ganem and co-workers reported in 1978 that stoichiometric amounts of catecholborane promoted the condensation of carboxylic acids and amines at −78 °C.[78] It was reported that the condensation also proceeded *via* the formation of a reactive acyloxyboron intermediate.

In 1996, arylboronic acids such as 3,4,5-trifluorobenzeneboronic acid (**63**) and 3,5-bis(trifluoromethyl)benzene boronic acid (**64**) were reported to be effective catalysts for the direct amidation reaction of carboxylic acids with amines, requiring only 5 mol% loading, by Yamamoto and co-workers.[79]

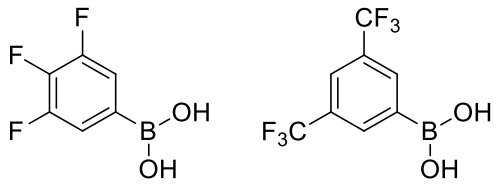
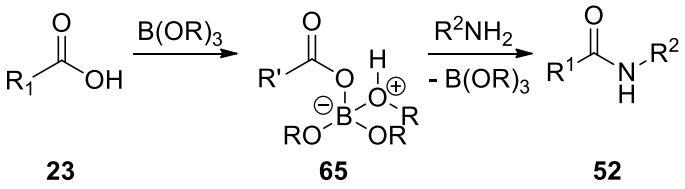


Figure 10: Arylboronic Acids – Catalysts of Direct Amidation[79]

The production of stoichiometric amounts of water does not lead to the destruction of the Lewis-acidic catalysts (**63** and **64**) as is the case with trisdialkylaminoboranes (**57**). This is said to be due to the presence of electron-withdrawing substituents on the benzene ring which afford a Lewis-acid stable to water, acids, and bases.[79] Although the reaction proceeded to completion within 1 hour, refluxing in toluene is required to achieve this.

It can be seen that the use of boron-containing compounds is a promising avenue of research for efficient direct amidations. Sheppard and Starkov reported in 2011 that borate esters promoted amidations of carboxylic acids (**23**) with amines as shown in Scheme 19, as well as facilitating transamidation of primary amides without strict anhydrous conditions.[80] Although reflux conditions were not required, the process still required elevated temperatures (80 °C) and the use of 2 equivalents of the borate ester (**65**) to enable high yields. [80]

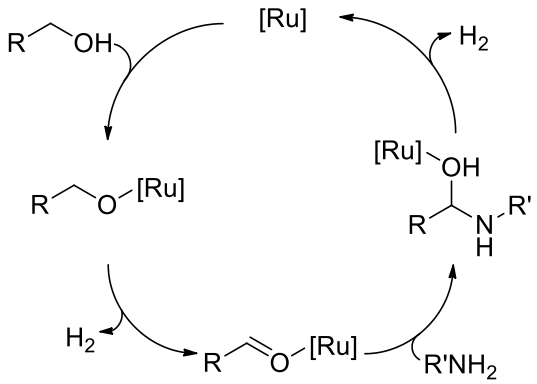


Scheme 19: Borate Ester-Promoted Amidation *via* the Formation of Acyloxyborate Intermediates

1.5.3 Metal-Catalysed Amidations

Whilst other novel catalytic examples are known, such as with triphenylstibine oxide (Ph_3SbO)/tetraphosphorous decasulfide as reported by Nomura and co-workers[81] and antimony (III) ethoxide as reported by Yamamoto and co-workers,[82] these are not amenable to industry give the use of toxic heavy-metals.

Ruthenium-catalysed approaches utilising primary alcohols and amines have been reported by Milstein and co-workers[83] but these methods pose other challenges, namely heavy-metal removal (a further unit operation). The proposed mechanism is shown in Scheme 20; although the alcohol is formally oxidised to an aldehyde during the reaction, no "oxidant" is required and indeed such examples are referred to as "hydrogen borrowing" with the only by-product of the reaction gaseous hydrogen.[83,84]

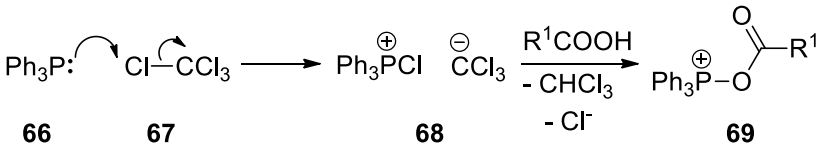


Scheme 20: Proposed Mechanism of Ru-Catalysed Amidation

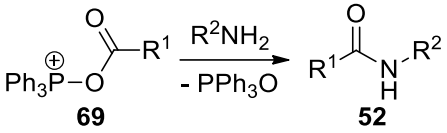
Ru-catalysed approaches are in contrast to the previously cited examples which utilised carboxylic acids rather than alcohols though this is not a criticism/disadvantage; the methods are complementary.

1.5.4 Organocatalytic Amidation

In 2014, an organocatalytic PPh_3/CCl_4 mediated amide bond formation was reported based on a simple variation of the Appel reaction (Scheme 21).[85] The intermediate (**69**) is not converted to the corresponding acyl chloride by nucleophilic attack of chloride, but to the amide by attack of the amine (Scheme 22). Triphenylphosphine oxide is reduced *in situ* using diethoxymethylsilane and bis(4-nitrophenyl)phosphate. It is of note that CCl_4 (**67**) is not widely used by process groups who have essentially taken steps to minimise or remove it from inventory due to its ability to destroy ozone (*via* the formation of chlorine radicals) and act as a greenhouse gas (a change in dipole moment of the molecule due to a stretch of a C-Cl bond yields an ability to absorb IR radiation).



Scheme 21: Appel-like Reaction - Activation of a Carboxylic Acid

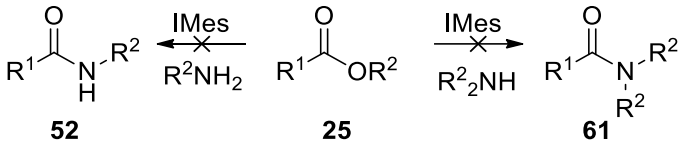


Scheme 22: Amide Synthesis *via* Nucleophilic Attack of an Activated Carboxylic Acid

This reaction had already been reported by Hodge and co-workers in 1983 who used 1% cross-linked polymers containing phosphine residues.[86] Indeed, phosphine compounds were reported by Hruby and Barstow to facilitate such reactions in 1971.[87]

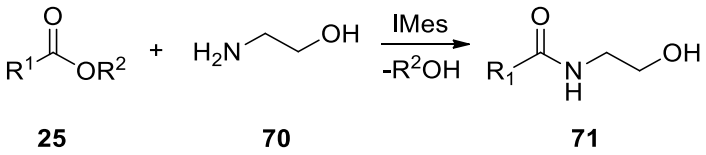
1.5.5 NHC-Catalysed Amidation *via* Transesterification

Movassaghi and Schmidt were the first to report a NHC-catalysed amidation of methyl esters with aminoalcohols.[71] In the presence of primary or secondary amines, primary amides (**52**) and secondary amides (**61**) did not form (Scheme 23).



Scheme 23: NHC-Catalysed Amidation of Esters - Primary and Secondary Amines

The presence of an internal alcohol (an alkanolamine/aminoalcohol) such as ethanolamine (**70**) was necessary (Scheme 24). Amidation could only occur when alcohol and amine groups were present on the same molecule.



Scheme 24: NHC-Catalysed Amidation of Esters - Aminoalcohols

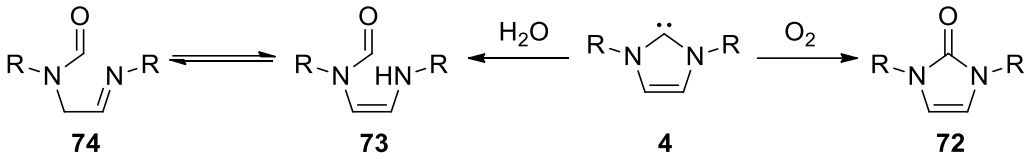
The lack of reaction with the use of primary and secondary amines with an ester (**25**) as shown in Scheme 23, in contrast to the conversion observed in the presence of aminoalcohols as shown in Scheme 24, casts doubt on the notion that nucleophilic attack of an NHC (**4**) upon an ester (**25**) leads to the formation of an activated acyl species with concomitant expulsion of an alcohol, given that amines are more nucleophilic than alcohols i.e. an activated acyl species is expected to react with an amine and yield an amide in preference to reacting with an alcohol and forming an ester.

This was in contrast to the earlier reports in the literature with nucleophilic activation of the carbonyl moiety by the NHC (**4**) as shown in Scheme 10 and Scheme 14.[60–63,67–69] Had this been the case, the NHC-catalysed amidation reported by Movassaghi and Schmidt should have proceeded without the requirement for an internal alcohol, given that amines are more nucleophilic than alcohols. This is readily seen in the cases of amidation under Steglich conditions[53] where amine nucleophiles lead to fewer side products compared to alcohol nucleophiles as shown in Scheme 7 and Scheme 8. Indeed, Movassaghi and Schmidt proposed a mechanism whereby NHCs were invoked as bases rather than nucleophiles.[71]

1.6 Protection of NHCs

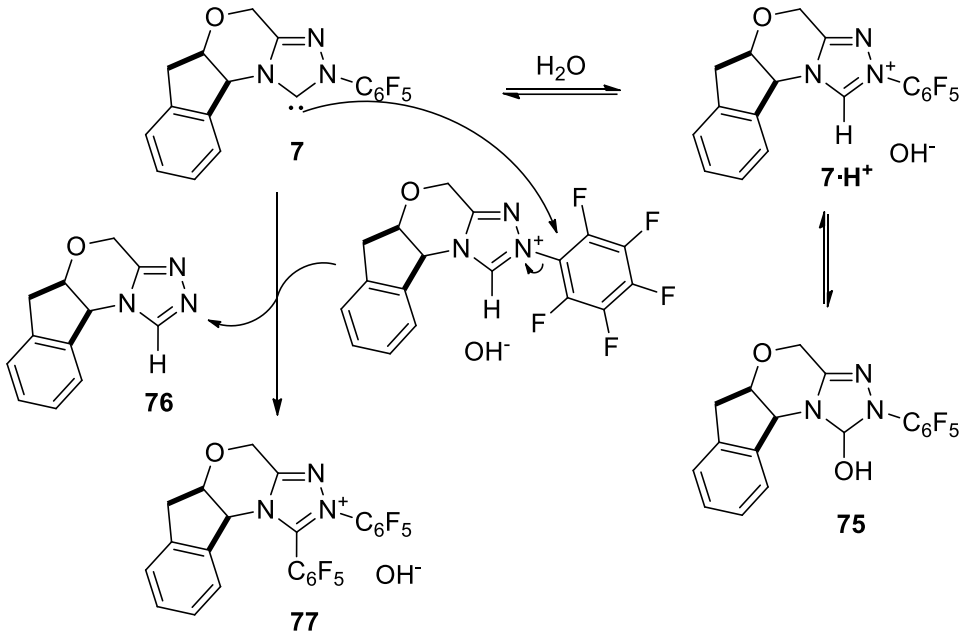
Although reports of NHCs and their wide utility are ever expanding in the literature,[39–44] their use in industry is limited by their sensitivity to both oxygen and moisture: both of which generally lead to their rapid decomposition.[5,6,16,88–90] It is postulated that the majority of the NHC (**4**) is transformed to the imidazol-2-one (**72**) by the action of oxygen and the formamides (**73** and **74**) by the action of water (Scheme 25).[16,88–90] I*t*Bu is an exception in that it does not rapidly decay in the presence of oxygen, but it is still sensitive to water i.e. the formamides **73** and **74** are favoured over the imidazol-

2-one **72**.[16,89,90] Decomposition in all cases is irreversible and unlike more robust transition metal catalysts, NHCs cannot be regenerated. Although protonation of the NHC could be possible in the presence of water, the strongly basic hydroxide counterion would lead to an equilibrium being established between the NHC and the imidazolium hydroxide. It can be seen that the irreversible decomposition pathways towards **72** and **74** would lead to little of the imidazolium hydroxide remaining.



Scheme 25: Proposed Decomposition Routes of NHCs by Water and Oxygen

However, the decomposition of NHCs (**4**) is complex and a variety of compounds are produced although these are poorly understood and/or characterised.[5,6,16,88,89] Rovis and co-workers have proposed a mechanism for a single decomposition pathway observed with pentafluorophenyl-substituted triazol-3-ylidenes (**7**) as shown in Scheme 26 with the formation of **77**.[91] Although a particular case is shown, it is obvious that *N*-substituents may play a role in decomposition which has otherwise been restricted reaction at the C2 position (Scheme 25). Indeed, the multitude of uncharacterised decomposition products of symmetrical imidazol-2-ylidenes (**4**) is testament to this.[5,6,16,88–90]

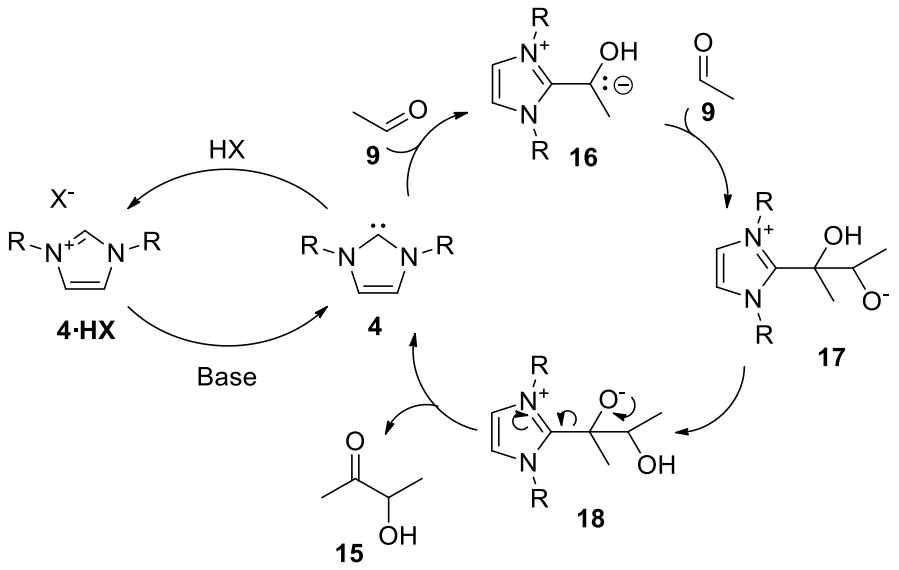


Scheme 26: Proposed Decomposition Pathway of Pentafluorophenyl-Substituted Triazol-3-ylidenes

The addition of water is shown as reversible by Rovis and co-workers[91] but in the case of imidazol-2-ylidenes (**4**), addition of water is irreversible and is reported to lead to the formation of a formamide (**73** and **74**).[16,89,90] It should be noted that all the decomposition products discussed so far are unable to participate in the catalytic cycle. The only means to "protect" an NHC during a reaction would be to prevent its decomposition from occurring from the outset.

1.6.1 Isolation and Reuse

Cowley and co-workers have described the recycling of NHCs (**4**) by protonating them once the catalytic cycle is complete.[92] The technique was coupled with an NHC-catalysed acyloin addition as shown in Scheme 27.[92] After recycling/recovery, the imidazolium salt (**4·HX**) must then be deprotonated once more to "regenerate" the NHC (**4**). The method allows the recycling of NHCs but it does not afford protection from decomposition during reaction as no modification of the NHC is performed *in situ,* nor are any changes made to the reaction conditions.

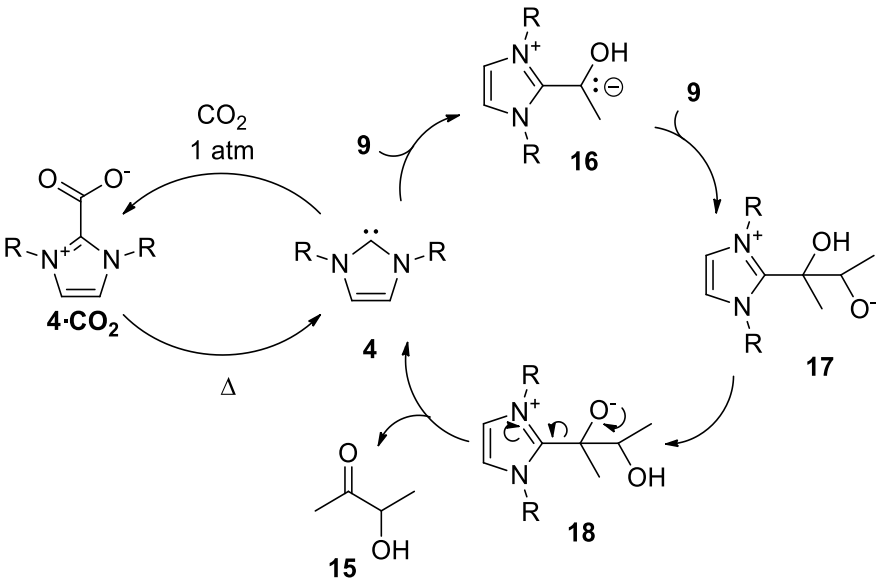


Scheme 27: Isolation and Reuse of an NHC[92]

Although technically viable, the repeated use of acid and base are: an ongoing chemical and financial demand (though less than the continued use of NHC precursors); can expose the product to harsh conditions during the isolation; and does not address the degradation of the NHCs *in situ*.[5,6,16,88,89]

1.6.2 Formation of Latent Adducts

Taton and co-workers reported the use of NHC·CO_2 adducts (**4·CO₂**) as latent NHCs and recyclable as shown in Scheme 28.[93] Adducts of NHC·CO_2 (**4·CO2**) were unfortunately described as only "mildly air-stable" though they are of some utility in protecting the carbene moiety in a similar manner as described by Cowley and co-workers[92] i.e. protection is not afforded while the NHC (**4**) is catalytically active. It should be noted that heating of the precursor (**4·CO2**) is required to release the free NHC.[93]

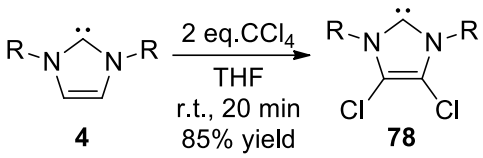


Scheme 28: NHC·CO_2 Adducts as Latent NHCs[93]

Ideally, an NHC (**4**) would be impervious or robust enough to withstand minimal quantities of moisture and oxygen, whilst being able to catalyse a range of reactions. It can be seen that the two are not mutually exclusive. It is their high reactivity as nucleophiles (and bases) that leads to their ability to act as organocatalysts,[39–44] and to their rapid decomposition.[5,6,16,88,89] The balance of the two must be met if NHCs (**4**) are to feature more widely in industrial applications where robust transition metal catalysts reign supreme.

1.6.3 Chlorination of Backbone Positions

Arduengo and co-workers described in 1997 that chlorination of the **4** gave rise to a mildly air-stable carbene (**78**) as shown in Scheme 29.[13] However, there was no indication as to its reactivity, which could be expected to be different given the markedly different electronics. Hedrick and co-workers attempted to catalyse the ROP of a cyclic ester (**36**), as previously described in Scheme 10, using the chlorinated NHC (**78**) though poor reactivity and yield was reported.[66]



Scheme 29: Synthesis of a Mildly Air-Stable NHC - Chlorination of Backbone Positions with Concomitant Formation of Chloroform

There are few other reports in the literature of NHCs (**4**) with backbone positions substituted with a halogen being used for organocatalysis. However, Nolan and co-workers have used substitution of the backbone positions with halogens as a way of tuning the electronic properties of NHC ligands in transition-metal catayasis.[94] Novel Ru-NHC complexes were synthesised and examined as catalysts in a series of metathesis reactions. However, a strong direct link between electron-donating ability of the NHC and the performance of the catalyst (yield) could not be conclusively drawn.[94] Thus, it is not conclusively shown that tuning of the electronics of a NHC (**4**) by substitution of its backbone position is a viable method to alter the reactivity of an NHC (**4**).

1.6.4 Protection by Silicones - NHC·Si Interactions

Baceiredo and co-workers reported that the decomposition of NHCs (**4**) could be severely retarded in the presence of silicon additives as shown in Table 2.[90] Furthermore, the protected NHCs were still able to catalyse a range of reactions and were unaffected by the additives.[90]

Table 2: Time-resolved Decomposition of NHCs in the Presence of Silicon Species as Reported by Baceiredo and Co-workers[90]

	Imidazol-2-one (**72**) and Formamide (**74**) (% decomposition of NHC)					
	3 h	20 h	48 h	1 w	3 w	4 w
I*t*Bu	5	9	84			
IMes	5	20	100			
I*t*Bu-PDMS	0	0	1	2	4	8
I*t*Bu-M_2	0	2	15	100		
I*t*Bu-THF	0	2	25	100		
I*t*Bu-Paraffin	0	0	7	13	87	
I*t*Bu-MD_4M	0	0	0	1	3	5
I*t*Bu-$MD_4^{Ph}M$	0	0	0	0	0	0
IMes-$MD_4^{Ph}M$	12	16	25	100		

Although Baceiredo and co-workers did not report the authentic syntheses of the decomposition products (**72-74**), they presented ^{1}H NMR spectra which they described as showing the evolution of the imidazol-2-one (**72**) and formamide (**74**) over time as reproduced from literature in Figure 11.[90]

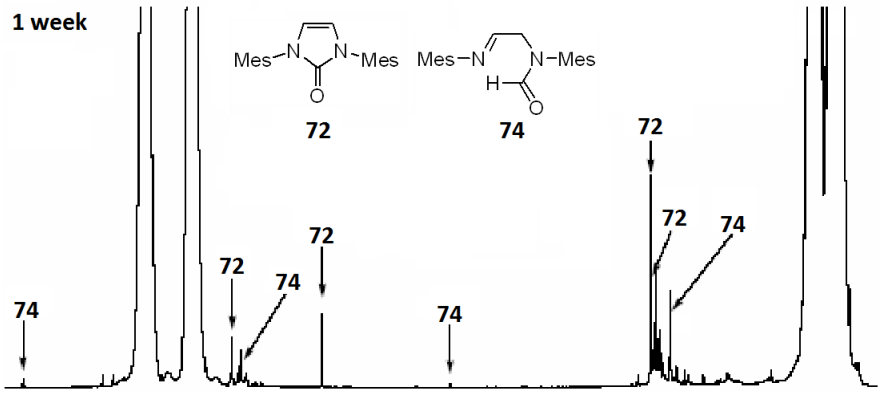
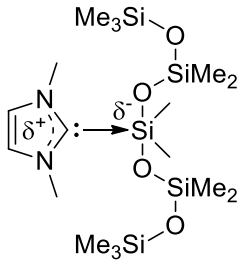


Figure 11: Quantifying the Decomposition of IMes in the Presence of $MD_4^{Ph}M$ – Time-resolved ^{1}H NMR Spectra Presented by Baceiredo and Co-workers[90]

It is widely known that silicone polymers are hydrophobic and indeed Baceiredo and co-workers highlight this, though they report that this property alone would be insufficient in protecting the carbene moiety as silicone polymers are highly permeable to gases especially oxygen.[90] Nevertheless, the decomposition of the investigated NHCs (**4**) by the action of oxygen was reported to have been impeded (Table 2). Their conclusion was that the observed protection was due to the manifestation of an NHC·Si interaction (**79**) and the reversible formation of a pentacoordinate silicon nucleus (Figure 12).[90]



79

Figure 12: Proposed NHC·Si (Lewis-base - Lewis-acid) Interaction[90]

Hyper-coordinate silicon species are well known in the literature.[95–97] However, Baceiredo and co-workers did not describe any spectroscopic data (either ^{13}C or ^{29}Si NMR spectra) to suggest the formation of such a species. However, they did provide quantum chemical calculations which estimated a weak interaction between IMe (**4a**) and a short siloxane chain (**79**) on the order of 3–5 kcal·mol^{-1} (ca. 13–21 kJ·mol^{-1}).[90]

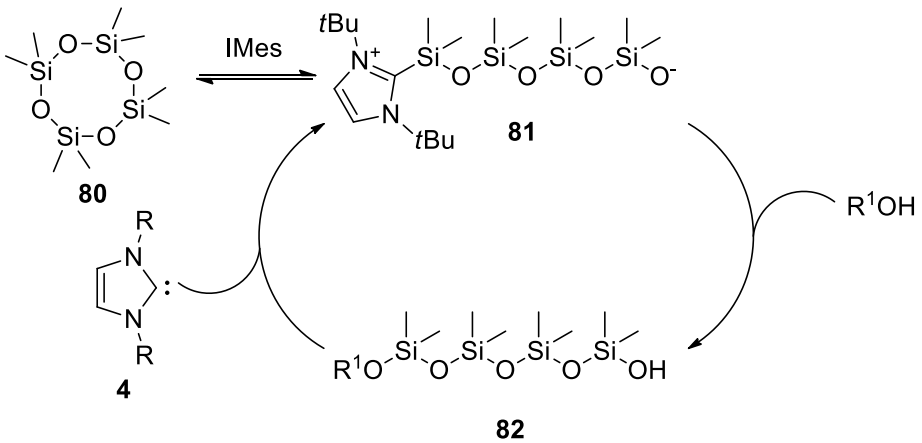
The interaction (**79**) was postulated to arise as a result of a Lewis-base-Lewis-acid interaction between the NHC and silicone polymer respectively (Figure 12). Whilst NHCs (**4**) are readily described as Lewis-bases,[19,20] silicones such as PDMS are not generally accepted to have Lewis-acidic character.[98] This could of course be tuned by careful choice of substituent(s) on silicon centres; however, the silicone of choice in the work of Baceiredo and co-workers was PDMS.

It should be noted that although computational models were based on IMe (1,3-bis(methyl)imidazol-2-ylidene), this was not the NHC used in their practical experiments nor is IMe indicative of the usual NHCs used in the literature.[33–44] Free IMe is rarely reported at ambient conditions in the literature due to its propensity to decompose:[5] even in the preparation of transition metal-ligand systems, IMe is usually prepared *in situ* rather than isolated beforehand.[99,100]

A review has clearly shown that although NHC·Si interactions and the formation of pentacoordinate Si species are invoked in many catalytic cycles, there is little, if any, experimental evidence to support this.[43] Despite this, many continue to invoke the notion of an NHC·Si interaction and dismiss other credible (and more often than not, simpler) explanations.

1.7 NHC·Si Interactions

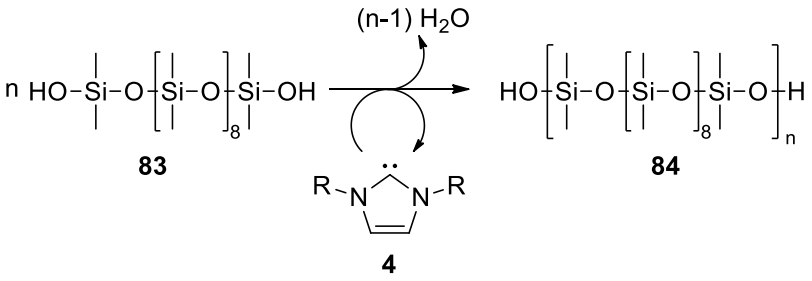
Baceiredo and co-workers also reported in 2007 an NHC-catalysed ROP of a cyclic siloxane, D_4 (**80**)[101] c.f. cyclic ester (**36**) of Hedrick and co-workers in 2003.[60] The mechanism for the ROP of **80** was said to proceed *via* nucleophilic activation of a silicon centre. The mechanism proposed by Baceiredo and co-workers as shown in Scheme 30 is cognate with the proposed mechanism of ROP of a cyclic ester (**36**) proposed by Hedrick and co-workers (Scheme 10).



Scheme 30: Proposed Mechanism of NHC-Catalysed ROP of D_4 – Nucleophilic Ring-Opening of a Cyclic Siloxane[101]

Baceiredo and co-workers reported that the nucleophilicity of the NHC (**4**) was linked to the catalytic activity, with IMes (1,3-bis(2,4,6-trimethylphenyl)imidazol-2-ylidene) being unable to catalyse the reaction. Therefore, the role of the NHC (**4**) as a Bronsted base and the reaction being catalysed by general base catalysis i.e. *via* an alkoxide after initial deprotonation of an alcohol initiator by the NHC (**4**), or indeed hydrogen bonding to the alcohol was discounted despite an NHC·D_4 (**81**) adduct not being observed by ^{29}Si NMR spectroscopy.[101]

The development of the mechanism continued with a report in 2008 by Baceiredo and co-workers on the NHC-catalysed dehydration of disilanol oligomers (**83**) i.e. condensation polymerisation as shown in Scheme 31.[102] Despite the sensitivity of NHCs to moisture, 91% yield was reported for catalyst loading as low as 2500 ppm.

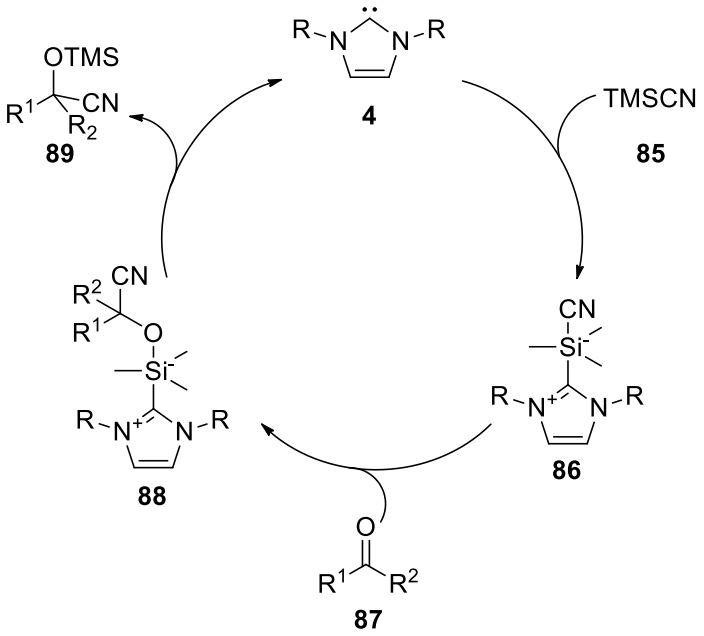


Scheme 31: NHC-Catalysed Dehydration of Disilanol Oligomers

In contrast to the NHC-catalysed ROP of cyclic siloxanes (**80**) as shown in Scheme 30,[101] the dehydration of disilanols (**83**) was explained with the NHC (**4**) invoked as a base.[102] Baceiredo and co-workers contest that in the case of general base catalysis, the size of *N*-substituents has very little effect on reactivity which is why bulky NHCs (**4**) such as IMes were effective; however, bulky NHCs were ineffective in the case of ROP of cyclic siloxanes (**80**), suggesting to them that the mode of action differed between the two cases.[102]

In 2006, Song and co-workers reported an NHC-catalysed cyanosilylation of carbonyls.[103] They assert that this proceeds *via* activation of TMSCN (**85**) by an NHC (**4**) to form a pentacoordinate silicon species (**86**) as shown in Scheme 32. Again, there was no spectroscopic evidence to corroborate this

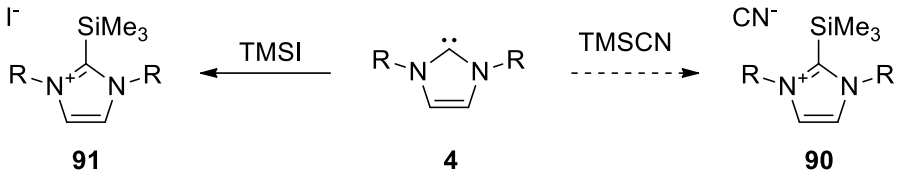
claim.[103] It is noted that pentacoordinate silicon nuclei can be examined by ^{29}Si NMR with the chemical shift providing useful insight into their electronic environment.[95]



Scheme 32: Proposed Mechanism of NHC-Catalysed Cyanosilylation – Activation of a Silicon Centre and Formation of a Pentacoordinate Species[95]

Song and co-workers also reported a rate acceleration in the presence of DMF although DMF in and of itself was not able to catalyse the reaction.[95] Kobayashi and Nishio reported in 1993 that DMF, as a neutral Lewis-base, was able to activate trichlorosilanes.[104] No ^{29}Si NMR evidence was presented by Song and co-workers to indicate that DMF activated TMSCN. However, Kobayashi and Nishio observed a significant shift upfield in ^{29}Si NMR spectra recorded in DMF-d_7 and HMPA compared to resonances in non-interacting solvents such as $CDCl_3$, CD_3CN, C_6D_6, and THF-d_8.[104] It is apparent that activation of Si centres in this case was readily observed by ^{29}Si NMR though this was not directly attributable to DMF.[104]

Soon after, Maruoka and co-workers reported that they too had observed NHC-catalysed cyanosilylation for the above systems and also for imines.[105] Although the mechanism was not investigated, the possibility of the formation of cyanide via the action of the NHC as a Lewis-base was illustrated as shown in Scheme 33.[105] This was based upon the previously reported generation of an ionic salt **91** on the addition of TMSI to IEt (1,3-bis(methyl)imidazol-2-ylidene).[105]



Scheme 33: Nucleophilic Substitution at a Silicon Centre

This is in contrast to Song and co-workers where the active catalytic species is the pentacoordinate Si species **86**.[103] The formation of cyanide is of note as it is proficient at catalysing umpolung reactions and acting as a nucleophile and base as shown in Scheme 3. It is therefore ambiguous as to which species is the true catalyst in the reported reaction.

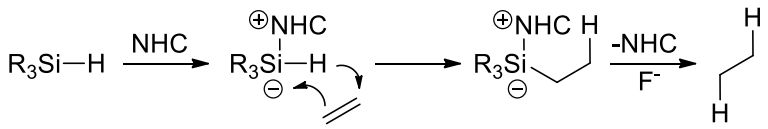
Other nucleophiles and bases were trialled including DMAP, DBU, and *t*BuOK.[105] In all cases, NHCs (ICy, I*i*Pr, and IMes) proved to be far more effective with higher yields achieved in a much smaller window of time as shown in Table 3.[105]

Table 3: Lewis-base Catalysed Cyanosilylation of Acetophenone[105]

Entry	Catalyst	Loading (mol%)	Conditions (°C, h)	Yield (%)
1	ICy	10	0, 1	97
2	*t*BuOK	10	r.t., 24	26
3	PBu_3	10	r.t., 24	0
4	DABCO	10	r.t., 24	5
5	DMAP	10	r.t., 24	0
6	DBU	10	0, 1.5	90
7	DBU	1	0, 1	12
8	ICy	1	0, 0.5	99
9	I*i*Pr	1	0, 0.5	96
10	IMes	1	0, 0.5	97

In the cases cited above, NHC·Si interactions have been invoked although robust experimental evidence is lacking i.e. there are a number of other mechanisms that can be proposed.[43] Indeed Song and co-workers themselves highlight the wide reactivity of NHCs with them acting: *via* the Breslow intermediate (**16**) in umpolung reactions including: the acyloin addition (Scheme 3); Stetter reactions (Scheme 5); through a NHC-acyl (**44**) intermediate in transesterification (Scheme 14); and as a Bronsted base in amidation (Scheme 24).[103]

Lacôte and co-workers reported in 2011 the NHC-catalysed hydrosilylation of styryl and propargylic alcohols with dihydrosilanes.[106] The proposed mechanism has been reproduced in Scheme 34 and begins with activation of the dihydrosilane by the NHC and the formation of a pentacoordinate silicon species.[106] It is of note that the reaction did not proceed without the addition of fluoride which is extensively known to activate silicon nuclei e.g. Fleming-Tamao oxidation and TBAF deprotection.



Scheme 34: NHC-catalysed Hydrosilylation[106]

Although NHC·Si interactions remain unproven in many organocatalytic cycles,[43] penta- and hexacoordinate silicon species are known in the literature.[32,95,96,107–109] Holmes and co-workers were able to synthesise a number of these and record their ^{29}Si NMR shift at T < −30 °C as shown in Table 4.[95]

Table 4: ^{29}Si NMR Shifts of Tetra- and Pentacoordinate Silicon Nuclei[95]

Silane	δ (ppm)	Silicate	δ (ppm)	Δδ (ppm)
$Si(OMe)_4$	−78.9	$Si(OMe)_5^-$	−127.5	−48.6
$Si(OEt)_4$	−82.4	$Si(OEt)_5^-$	−131.1	−48.7
$Si(i\text{-}OPr)_4$	−84.7	$Si(i\text{-}OPr)_5^-$	−133.0	−48.3
$PhSi(OMe)_3$	−55.0	$PhSi(OMe)_4^-$	−112.4	−57.4
$PhSi(OEt)_3$	−58.0	$PhSi(OEt)_4^-$	−117.3	−59.3
$Ph_2Si(OMe)_2$	−28.0	$Ph_2Si(OMe)_3^-$	−97.3	−69.3
$Ph_2Si(OEt)_2$	−30.1	$Ph_2Si(OEt)_3^-$	−101.3	−71.1

It can be seen that bulky substituents (phenyl groups) around the silicon nuclei do not preclude the formation of pentacoordinate silicon species (Table 4).[95] Although not an exhaustive list, the entries show that pentacoordinate silicon nuclei have ^{29}Si NMR resonances that are distinctly removed from those of tetracoordinate species (Table 4).[95] Though these range from −97.3 ppm to −133.0 ppm in the examples given, the change in shift (Δδ) is more limited in range (ca. 50–70 ppm).

Silatranes have also been described in literature and in 1971, Frye and co-workers reported on the synthesis of several (at the time) novel silatranes (**92-94**) with a range of substituents at silicon as shown in Figure 13.[110] In these cases, the formation of a pentacoordinate silicon species is aided by the intramolecular nature of the interaction and close proximity of the donor atom.[110]

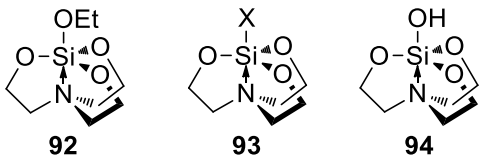
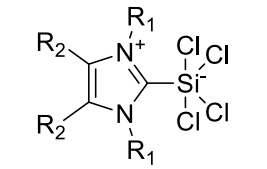


Figure 13: Pentacoordinate Silicon Species - Silatranes with a Range of Apical Substituents

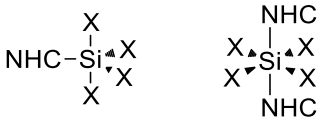
Hyper-coordinate silicon species formed by the reaction of neutral NHCs (**4**) with silicon species have also been reported and characterised. Examples include $Me_2IMe{\cdot}SiCl_4$ (**95**) and $IDipp{\cdot}SiCl_4$ (**96c**) as shown in Figure 14.[32,111]



95 R_1 = Me, R_2 = Me
96c R_1 = Dipp, R_2 = H

Figure 14: Pentacoordinate Silicon Species - NHC·$SiCl_4$ Complexes[32,111]

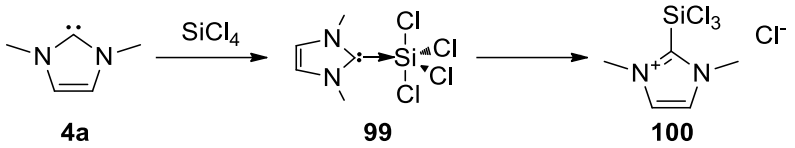
It is obvious that the presence of bulky *N*-substituents does not preclude the formation of a hyper-coordinate silicon species adopting a trigonal bipyramidal structure.[107,111] Although not shown above, SiF_4 is able to adopt both a penta- and hexacoordinate structure depending on reaction stoichiometry.[107] It is possible that the increased Lewis-acidity of SiF_4 over $SiCl_4$ and/or the smaller size of the fluorine electron density play a part in this. [107] The geometries have been confirmed by X-ray crystallography, with the NHC moiety adopting the equatorial position in the pentacoordinate species **97**, and axial positions in the hexacoordinate species **98** as shown in Figure 15. [107]



97 **98**

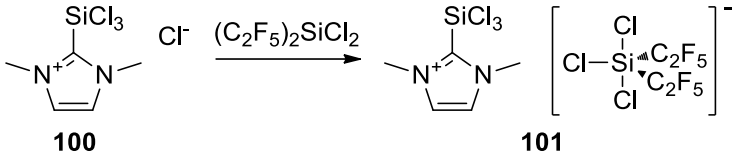
Figure 15: Geometry of Penta- and Hexacoordinate NHC·SiX_4 Complexes

Recently, Böttcher and co-workers reported several novel pentacoordinate NHC·Si complexes.[109] More interestingly, it was shown that charged species were ultimately formed, an example of which is shown in Scheme 35, rather than a neutral Si species (**99**).[109]



Scheme 35: Nucleophilic Attack of an NHC on a Silicon Halide – Formation of an NHC·Si Adduct and Expulsion of Chloride[109]

On addition of $(C_2F_5)_2SiCl_2$ (a Lewis-acidic chlorosilane) to the above, a charged pentacoordinate Si species (**101**) was formed (Scheme 36). The formation of a NHC·$(C_2F_5)_2SiCl_2$ adduct was not reported.[109]



Scheme 36: Nucleophilic Attack of Chloride on a Lewis Acidic Silane – Formation of a Pentacoordinate Silicon Species[109]

The above reactions indicate that the generation of pentacoordinate Si species from NHCs is challenging with steric and electronic properties affecting the outcome of reactions: formation of pentacoordinate Si species versus nucleophilic substitution. The use of strongly Lewis-acidic silicon species are in many cases necessary.[32,107,109,111] In the case of alkoxy-derived pentacoordinate species as analysed by Holmes and co-workers, these were generated with the use of crown ethers to remove the potassium cations.[95]

A balancing act is required: the NHC needs to have sufficient nucleophilic character to attack the Si centre to form a pentacoordinate species; too strong/bulky a nucleophile and substitution may be favoured over addition. Indeed, a good leaving group such as chloride on the silicon centre may lead to substitution over addition as is observed in Scheme 35.[109]

Conclusions

- NHCs are able to efficiently catalyse a range of reactions including transesterifications and amidations (which are of industrial importance, especially to the pharmaceutical and polymer sectors) without the need to use heavy/transition metals or harsh conditions. The methods are therefore amenable to substrates bearing sensitive groups.
- Their widespread use is limited by their sensitivity to aerobic conditions which ultimately leads to rapid decomposition. The decomposition products are numerous and uncharacterised, though the action of water and oxygen are thought to lead to the formamides and imidazol-2-one respectively.
- Whilst there is strong evidence of NHC·Si bonding for low valent and hypercoordinate silicon species, such interactions are not assured in the organocatalytic examples detailed above e.g. cyanosilylation, ROP of D_4, and trifluoromethylation. Experimental data as well as robust computational data would be useful in identifying and quantifying NHC·Si interactions.
- Baceiredo and co-workers have reported that NHCs were protected by the presence of silicones and attributed this to an NHC·Si interaction as a result of a Lewis-base/acid interaction.
- We therefore initially sought to: corroborate the notion of an NHC·Si interaction; probe its mechanism of action; tune the strength of the NHC·Si interaction such that decomposition/reactivity could be adjusted; exploit the interaction to allow for the sequestering of NHCs (**4**) in a plug-flow reactor system, thereby allowing simple product separation and purification without decomposition of the carbene moiety.

2. Attempts to Characterise an NHC·Si Interaction and its Effects on NHC Decomposition

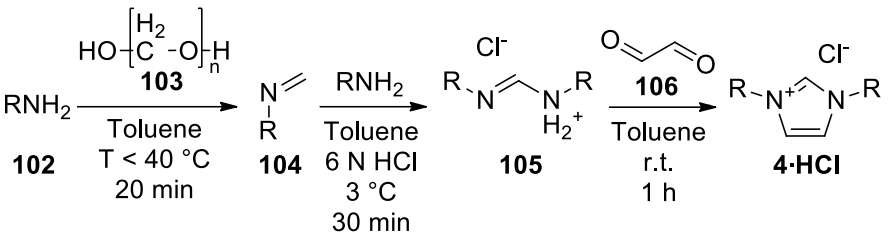
We began to probe the postulated NHC·Si interaction experimentally by way of NMR spectroscopy as the methodology would be able to provide direct data on the electronic environments of the nuclei of interest (^{13}C and ^{29}Si). Furthermore, the methodology would probe the postulated interaction in the solution phase c.f. gas phase quantum chemical calculations. Beyond this, we wished to develop an understanding of the effects of Lewis acidity/basicity on the strength of the NHC·Si interaction.

2.1 Synthesis and Isolation of Free NHCs

In order to probe the postulated NHC·Si interaction, the synthesis of NHCs and their precursors was undertaken. Although there were many methods described in the literature applicable for the synthesis of NHC precursors and NHCs bearing different *N*-substituents,[11,12,17,18,21,112] we began with the synthesis of IMes (**4b**), IDipp (**4c**), I*t*Bu (**4d**), and their precursors. These NHCs (**4**) were chosen as a representative sample of imidazol-2-ylidenes that were commonly discussed and utilised in the literature.[33–44]

2.1.1 NHC Precursors: Imidazolium Halides

Imidazolium halides were selected as the precursors of choice due to their ubiquity and relative ease of synthesis and handling.[11,12,17,18,112] Thioureas (**4·S**), for example, would have required the use of potassium metal (or sodium/potassium alloy) as shown in Scheme 2, for the generation of the free NHC (**4**).[21]

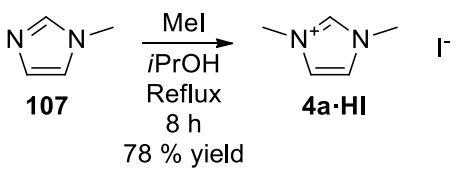


Scheme 37: One-pot Synthesis of Imidazolium Halides as Reported by Arduengo and Co-workers[15]

Early methods for the synthesis of aryl-substituted imidazolium salts were based on one-pot procedures published in the 1990s by Arduengo and co-workers in the patent literature as shown in Scheme 37.[15] Reaction of an amine (**102**) with paraformaldehyde (**103**) yielded an imine (**104**) *in situ*. Addition of a further equivalent of amine (**102**) yielded formamidines (**105**) which could be ring-closed with glyoxal (**106**). Reports indicated that the methodology led to the formation of dark oils that had to be triturated with acetonitrile to retrieve the product.[113,114] This methodology proved inadequate due to the low yields, and long reaction and isolation times.[15,113,114]

An attempt was made to prepare I*i*Pr·HCl, as shown in Scheme 37,[15] however, the crude product was a dark oil from which the title compound could not be isolated with or without trituration from MeCN. Analysis of the crude product by ^{1}H NMR spectroscopy did not indicate the formation of the product nor could reaction intermediates be identified.

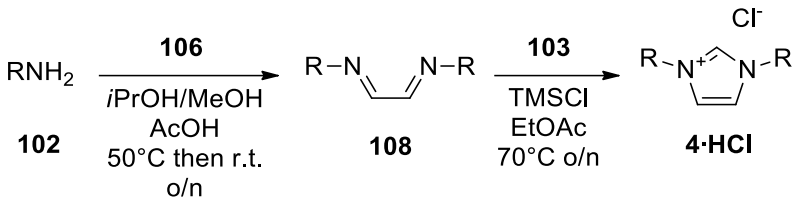
Simpler methods for the synthesis of free NHCs (**4**) and imidazolium salts (**4·HX**) have since been reported in the literature.[11,12,18,112] While alkylation of a suitable imidazole (**107**) would be a viable method to synthesise some simple imidazolium halides, this would be limited to alkyl substituents i.e. the use of alkyl iodides as alkylating agents.[11]



Scheme 38: Synthesis of Methylimidazolium Iodide - Alkylation of Methylimidazole[11]

IMe·HI (**4a·HI**) was prepared by alkylating methylimidazole (**107**)at reflux with excess methyl iodide (Scheme 38).[11] The product appeared to be hygroscopic in small quantities but little moisture was absorbed when **4a·HI** was synthesised at a larger scale (2 g). Although it was reported that the corresponding free NHC, IMe (**4a**), was highly reactive and unstable in solution at room temperature,[5] spectroscopic analysis of IMe formed *in situ* (and its interactions with silicon species) was sought. It was envisaged that experimental evidence of an NHC·Si (**79**) interaction could be gathered, based on the reports in the literature.[90,115]

For more complex *N*-substituents, a modular approach towards their synthesis has been reported for the synthesis of 1,3-disubstituted imidazolium halides (Scheme 39).[12,17,18] An imidazolium halide (**4·HX**) could be prepared by ring-closing of a diazabutadiene (**108**) with paraformaldehyde (**103**); the diazabutadiene was itself prepared by the condensation of an appropriate amine (**102**) with glyoxal (**106**). Such an approach allowed for greater overall yields as impurities were removed from the diazabutadienes during washing and isolation which was not possible for one-pot approaches.

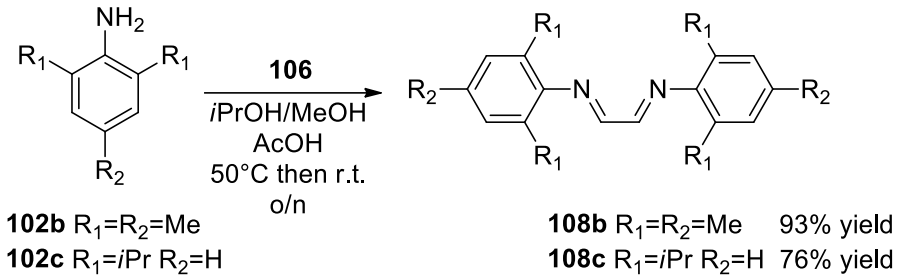


Scheme 39: Modular Synthesis of Imidazolium Halides *via* the Formation and Isolation of Diazabutadienes

Although ring-closing with chloromethyl ethylether had been reported,[14] paraformaldehyde (**103**) was selected due to its easier measurement and use as a solid. Furthermore, the procedure reported by Hintermann was reported to offer higher yields.[12] With chloromethyl ether, Arduengo and co-workers reported the yield of the ring-closing step alone as 40% and 47% for the preparation of IMes·HCl (**4b·HCl**) and IDipp·HCl (**4c·HCl**) respectively, over the course of 16 hours;[14] the method described by Hintermann was reported to produce the said compounds in 69% and 71% yield in 2 hours.[12]

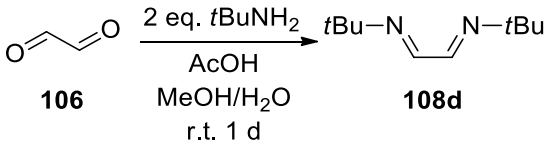
2.1.2 Synthesis of Diazabutadienes

This synthesis of diazabutadienes, as described by Hintermann, was reported to be amenable for a range of aromatic/electron poor *N*-substituents.[12] *N*,*N*'-Bis(2,4,6-trimethylphenyl)-1,4-diazabutadiene (**108b**) and *N*,*N*'-bis(2,6-di*iso*propylphenyl)-1,4-diazabutadiene (**108c**) were prepared in this fashion by condensing 2 equivalents of the relevant amine (**102b** and **102c**) with glyoxal (**106**), as shown in Scheme 40, in 93% and 76% yield respectively c.f. 87% and 90% described in literature.[12] Earlier reported methods of preparing the diazabutadienes in *n*-propanol:H_2O took up to 20 hours for a comparable yield.[14] It appeared that the precipitation of the product with the reaction conditions described by Hintermann drove production of the diazabutadienes **108b** and **108c**.[12]

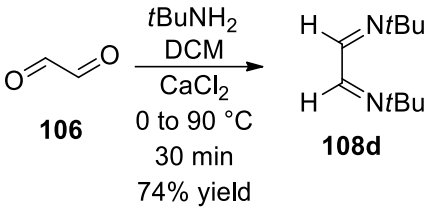


Scheme 40: Synthesis of Aryl-Substituted Diazabutadienes – Condensation of Arylamines and Glyoxal[12]

However, the methodology, was not successful for the synthesis of *N*,*N*'-bis(*tert*-butyl)-1,4-diazabutadiene (**108d**) as shown in Scheme 41. Further attempts to condense 2 equivalents of *tert*-butyl amine with an equivalent of glyoxal (**106**) at 0 °C and at room temperature in water appeared to lead to product formation with precipitation of a white solid, though isolation proved to be far more cumbersome. Crystallisation of the white solid from EtOH/H_2O (1:1) as described by West and co-workers was unsuccessful.[116]



Scheme 41: Synthesis of *N,N'*-bis(*tert*-butyl)-1,4-diazabutadiene

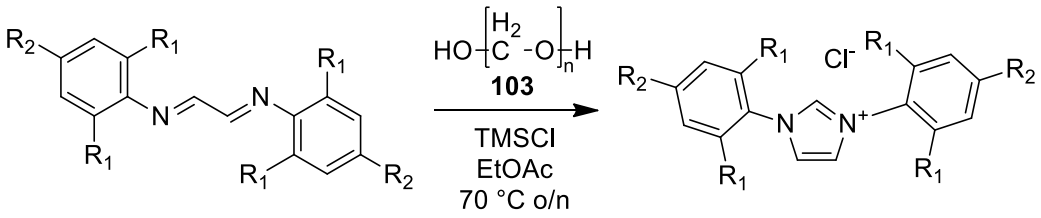


Scheme 42: Mistryukov's Synthesis of a Diazabutadiene – $CaCl_2$ as a Drying Agent[117]

Preparation of **108d** in DCM, as shown in Scheme 42, followed by crystallisation from Et_2O as described by Mistryukov proved to be effective with *N*,*N*'-bis(*tert*-butyl)-1,4-diazabutadiene (**108d**) isolated in 74% yield.[117] The presence of calcium chloride as a drying agent was crucial for the isolation of the title compound.

2.1.3 Ring-closing of Diazabutadienes to Form an Imidazolium Salt

As previously shown in Scheme 39, the aryl-substituted diazabutadienes **108b** and **108c** were transformed to the corresponding imidazolium salts by installing the C2 carbon and ring-closing using paraformaldehyde **(103)** and TMSCl as shown in Scheme 43. IMes·HCl (**4b·HCl**) and IDipp·HCl (**4c·HCl**) were synthesised in 79% and 90% yield respectively c.f. 69% and 71% yield reported in literature.[12] The slow addition of TMSCl led to higher yields in comparison to dropwise addition.



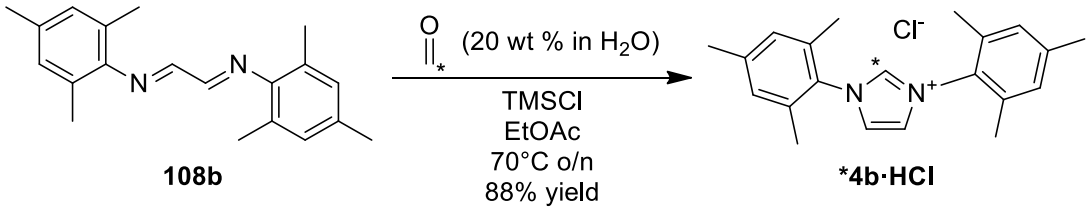
108b R_1 = Me, R_2 = Me
108c R_1 = *i*Pr, R_2 = H

4b·HCl R_1 = Me, R_2 = Me 79% yield
4c·HCl R_1 = *i*Pr, R_2 = H 90% yield

Scheme 43: Ring-closing of a Diazabutadiene with Paraformaldehyde and TMSCl

Whilst the original methodology reported by Hintermann used only dry paraformaldehyde (**103**), as shown in Scheme 43,[12] we had success in using aqueous formaldehyde solution without noticeable hydrolysis of TMSCl or reduction in yield. The availability of ^{13}C-labelled formaldehyde solution was exploited in the synthesis of ^{13}C-labelled IMes·HCl (***4b·HCl**) as shown in Scheme 44. Isolated yield of

^{13}C-labelled IMes·HCl (***4b·HCl**) was 88% compared with 79% yield of natural abundance IMes·HCl (**4b·HCl**) when dry paraformaldehyde (**103**) was used.



Scheme 44: Synthesis of ^{13}C-Labelled IMes-HCl – ^{13}C-labelled Formaldehyde as Carbon Source

^{13}C-labelling, indicated by * in Scheme 44, was observed by ^{1}H NMR spectroscopy which showed ^{1}H-^{13}C carbon coupling (a doublet at 10.76 ppm) and by ^{13}C NMR spectroscopy (which indicated significant enhancement of the C2 resonance at 139.6 ppm) as shown in Figure 16, and by high-resolution mass spectroscopy.

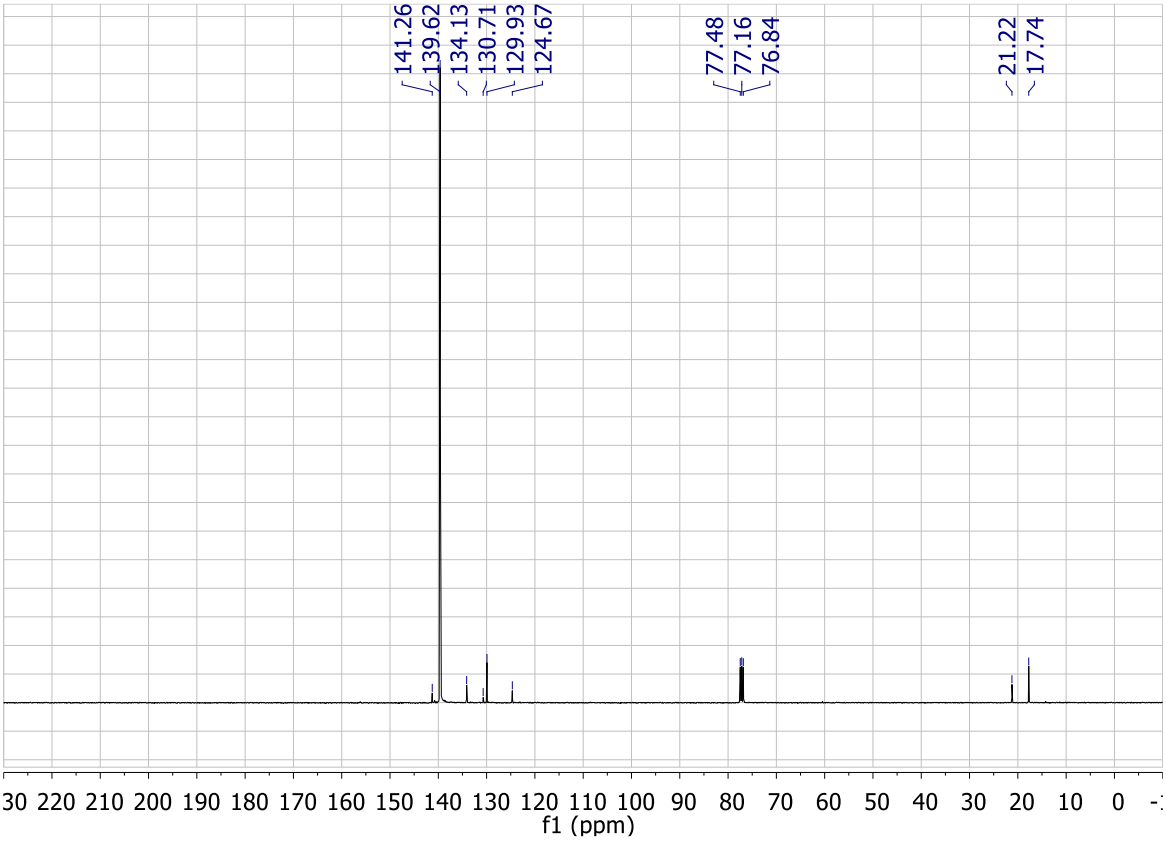


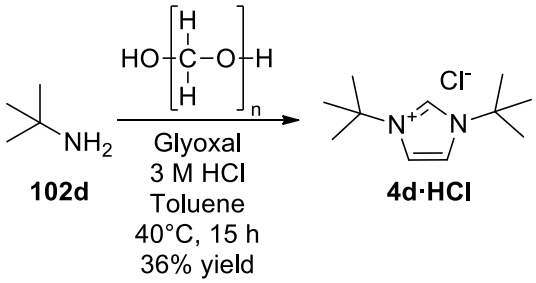
Figure 16: ^{13}C NMR Spectrum of ^{13}C-Labelled IMes·HCl Exhibiting Increased SNR of the C2 Position

In common with literature reports, the isolated salts IMes·HCl (**4b·HCl**) and IDipp·HCl (**4c·HCl**) had a yellow and pink colour respectively. However, the impurities could not be identified by ^{1}H NMR spectroscopy.[12] The discolouration was removed by recrystallising the salts from DCM/EtOAc.

Soxhlet extraction using acetone has been described in the literature but proved impractical in our hands.[114] The process required dry solvent; reflux conditions for extended periods of time; and led to a lower purity product and poorer yield when compared to recrystallisation from DCM/EtOAc.

2.1.4 Synthesis of I*t*Bu·HCl and I*t*Bu·HBF$_4$

Although *N*,*N*'-bis(*tert*-butyl)-1,4-diazabutadiene (**108d**) had been successfully synthesised, transformation to the imidazolium halide with TMSCl and paraformaldehyde (**103**) was not successful. I*t*Bu·HCl (**4d·HCl**) was instead prepared according to the one-pot method described by Herrmann and co-workers (Scheme 45).[118]



Scheme 45: One-pot Synthesis of I*t*Bu·HCl as Reported by Herrmann and Co-workers[118]

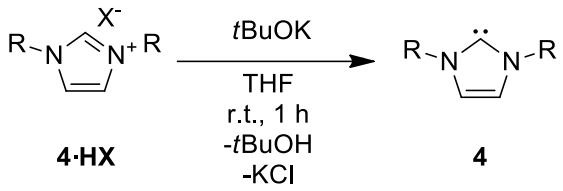
Initially, the route yielded the product **4d·HCl** as a white solid in 36% yield, but the synthesis proved capricious: further attempts of synthesis and isolation yielded brown oil. ^{1}H NMR data were in accordance with literature reports[16,118] for I*t*Bu·HCl (**4d·HCl**), but efforts to initiate crystallisation were unsuccessful. Washing the oil with $NaBF_4$ (3 M in H_2O). However, led to the formation of the tetrafluoroborate salt (**4d·HBF$_4$**) as a white solid which was isolated in 87% overall yield.

Several modifications to the original methodology (described by Herrmann and co-workers)[118] were made in an attempt to isolate further amounts of the chloride salt **4d·HCl** as a solid (including the use of aqueous formaldehyde, dry paraformaldehyde, HCl/Dioxane, and slow addition of aq. HCl)

though these were ultimately unsuccessful. It was not ascertained why the hydrochloride salt **4d·HCl** could not be reproducibly isolated as a solid.

2.1.5 Deprotonation of Imidazolium Halides

Free NHCs were synthesised by deprotonation of the corresponding imidazolium salts (**4·HX**) with *t*BuOK (Scheme 46). Although the use of a stoichiometric amount of base was commonly reported in the literature, we observed that this did not lead to complete deprotonation within the reaction times stated in literature (usually between 30 and 60 minutes).[5,6,14,63,71,119]



4·HX **4**

Scheme 46: Synthesis of a Free NHC – Deprotonation of an Imidazolium Halide by *t*BuOK

In our hands, the use of 1.5 equivalents of *t*BuOK ensured a rapid deprotonation of the imidazolium halide (**4·HX**). Literature procedures described the use of NaH as base instead of, or in unison with *t*BuOK,[5,13,14] however, the use of NaH was not pursued due to tedious removal of mineral oils from NaH dispersions and the poor solubility of the base in THF.

After deprotonation, the free NHCs (**4**) were extracted with hot toluene. KCl was removed by filtration of the extract through a fine frit. *t*BuOH was evaporated *in vacuo* along with excess toluene. Recrystallisation of IMes (**4b**) and IDipp (**4c**) from hexane led to the removal of impurities. This afforded, on cooling to room temperature, the NHCs as large colourless needles which were stored under an inert atmosphere at room temperature. IMes (**4b**), IDipp (**4c**), and I*t*Bu (**4d**) were isolated and characterised by NMR spectroscopy with ^{1}H and ^{13}C NMR data in accordance with literature reported values.[5,14,16]

Conclusions

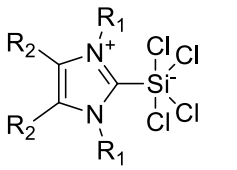
- The synthesis of imidazol-2-ylidenes (**4**) has been well studied with several methods available in the literature. Recently reported methods were high yielding and offered simpler methodologies in comparison to the seminal reports of Arduengo and co-workers.[5,6,12,14–18]
- The modular route with isolation of a diazabutadiene intermediate (**108**) prior to ring-closing as reported by Hintermann was amenable to the synthesis of imidazolium salts bearing aromatic substituents.[12] Advantages over one-pot methods included higher yields and purity, simpler purification and isolation, and comparable overall reaction times.[15,16]
- The modular route failed for the synthesis of I*t*Bu·HCl (**4d·HCl**) though ItBu·HBF_4 (**4d·HBF_4**) was successfully synthesised with a one-pot method described by Denk and co-workers.[16]
- The use of aqueous ^{13}C-labelled formaldehyde solution (rather than solid paraformaldehyde as reported), allowed for the synthesis of ^{13}C-labelled IMes·HCl (***4b·HCl**).
- Purification of the imidazolium salts was possible by recrystallising from DCM/EtOAc. This was preferred over Soxhlet extraction with dry acetone which led to poorer product yields and purity.[114]
- The isolation of free NHCs (**4**) (but not their precursors) required strict dry and anaerobic conditions with the presence of water or oxygen leading to decomposition.[5,6,13,14,16,89,90] Storage of the NHCs was only possible under an inert atmosphere.
- NHCs (**4**) were identified by their characteristic ^{13}C NMR resonance ca. 215 ppm in a range of polar and non-polar aprotic solvents including THF, C_6D_6, Tol-d_8, and DMSO.[5,13,14,17,20]

2.2. Synthesis of NHC·Si Adducts Reported in the Literature

With free NHCs (**4**) in hand, it was envisaged that evidence of an NHC·Si interaction could be inferred from ^{1}H, ^{13}C, and/or ^{29}Si NMR data given the change in shifts observed between tetra- and pentacoordinate silicon species.[32,95–97,107,111] Prior to beginning our own novel studies on NHC·Si interactions/compounds, it was appropriate to corroborate data already available in the literature with respect to known NHC·Si complexes.

2.2.1 NHC·$SiCl_4$ Adducts

NHC·$SiCl_4$ complexes, as shown in Figure 17, were of interest given that $SiCl_4$ is a Lewis acid and the postulated role of PDMS in the NHC·Si interaction was as a Lewis acid. Although NHC·$SiCl_4$ complexes are thermodynamically stable, they were not envisaged to be of interest as organocatalysts given that they were moisture sensitive compounds.[32,107,111]



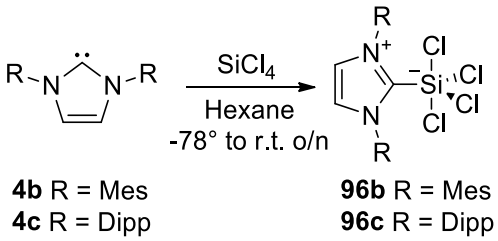
95 R_1 = Me, R_2 = Me
96c R_1 = Dipp, R_2 = H

Figure 17: Pentacoordinate NHC·$SiCl_4$ Complexes Reported in the Literature[32,111]

The presence of water would lead to the rapid hydrolysis of the Si-Cl bonds and formation of HCl which would attack the NHC (**4**) and form an imidazolium halide (**4·HX**), thus rendering the species unable to participate in organocatalytic cycles. However, NHC·$SiCl_4$ compounds provided a model system for pentacoordinate silicon species with regards to ^{1}H, ^{13}C, ^{29}Si NMR spectra. They had also been modelled computationally with the results of interest to us in our future discussion of computational results.[111,115,120]

Reports in the literature indicated that NHCs (**4**) readily formed NHC-$SiCl_4$ complexes, even with bulky *N*-substituents such as 2,4,6-trimethylphenyl (IMes) or 2,6-di*iso*propylphenyl (IDipp)

groups.[21,107,111] It was also reported that in the case of SiF_4, penta- and hexacoordinate silicon species were observed depending on reaction stoichiometry.[111] It was therefore apparent that NHCs bearing sterically demanding substituents were still able to form thermodynamically stable NHC·Si complexes. This was of great importance prior to beginning our own novel studies of NHC·Si interactions between relatively bulky NHCs (**4b-4d**) and less Lewis-acidic (in comparison to $SiCl_4$) silicon species. The synthesis of IDipp·$SiCl_4$ (**96c**) by slow addition of $SiCl_4$ to IDipp (**4c**) in dry hexane at −78 °C, as shown in Scheme 47, yielded a white solid.[111]



Scheme 47: Synthesis of IDipp-$SiCl_4$ – Formation of a Pentacoordinate Silicon Species

The ^{29}Si NMR spectra of IDipp·$SiCl_4$ (**96c**) and IMes·$SiCl_4$ (**96b**) showed a single resonance at ca. −109 ppm as reported in literature which was indicative of a penta-coordinate silicon species.[107,111] Indeed, a shift of ca. −70 ppm (w.r.t. free $SiCl_4$) was expected for a range of silicon species transitioning from tetra- to pentacoordinate based on the reports of Holmes and co-workers.[95]

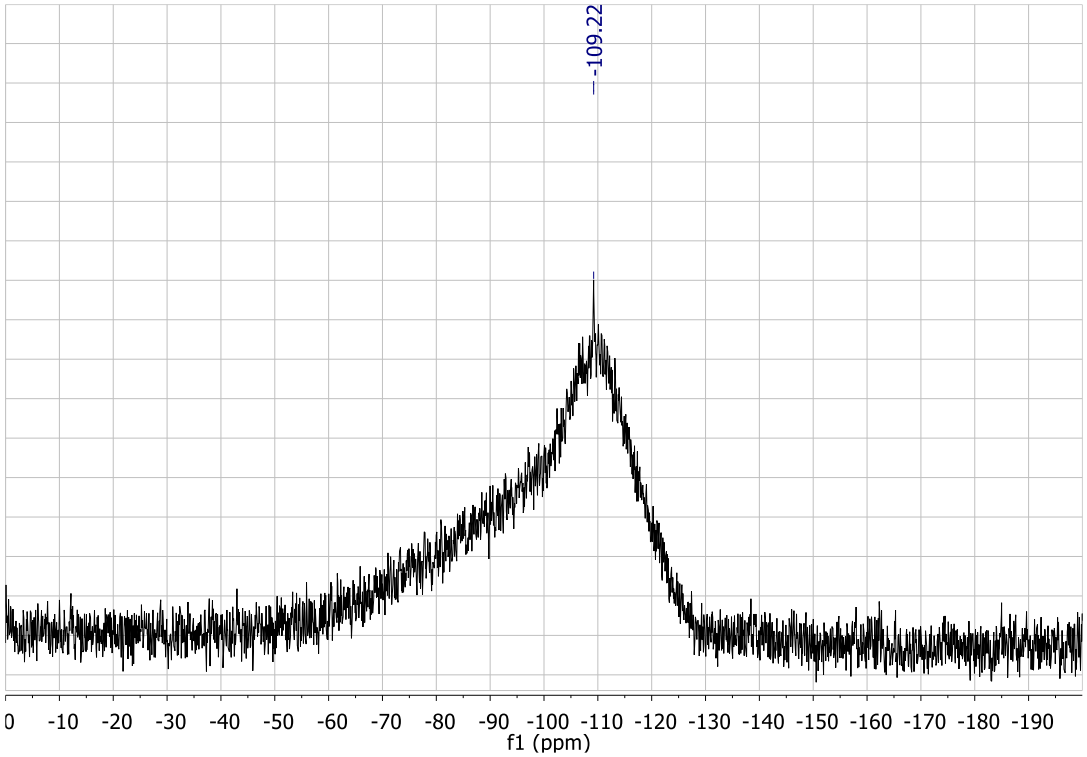
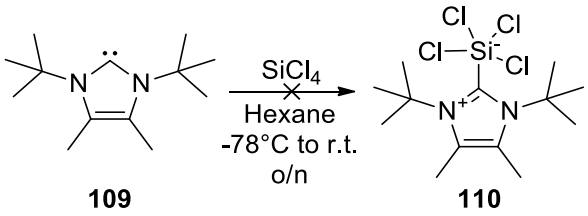


Figure 18: ^{29}Si NMR Spectrum of IDipp·$SiCl_4$ Showing a Single Resonance at −109 ppm

2.2.2 $Me_2ItBu{\cdot}SiCl_4$

It was envisaged that such NHC·$SiCl_4$ systems could be expanded upon with the formation of complexes with a more Lewis-basic NHC such as Me_2ItBu (**109**) as shown in Scheme 48**Error! Reference source not found.**. The synthesis of Me_2ItBu is discussed later in Chapter 5.



Scheme 48: Attempted Formation of a $Me_2ItBu{\cdot}SiCl_4$ Complex

Slow addition of neat $SiCl_4$ to a solution of **109** in hexane led to the formation of a white solid on warming to room temperature. However, attempts to characterise the compound by NMR spectroscopy were unsuccessful. Although IMes·$SiCl_4$ (**96b**) and IDipp·$SiCl_4$ (**96c**) were soluble in THF-d_8, DCM-d_2, or C_6D_6,[107,111] the isolated solid was poorly soluble in THF-d_8, toleune-d_8, C_6D_6, and C_6H_5Cl.

In THF-d_8, ^{29}Si NMR spectroscopy indicated the presence of free $SiCl_4$: in C_6H_5Cl with D_2O lock, the ^{13}C NMR spectrum indicated the presence of free Me_2I*t*Bu with a C2 resonance at 204 ppm (Figure 19).

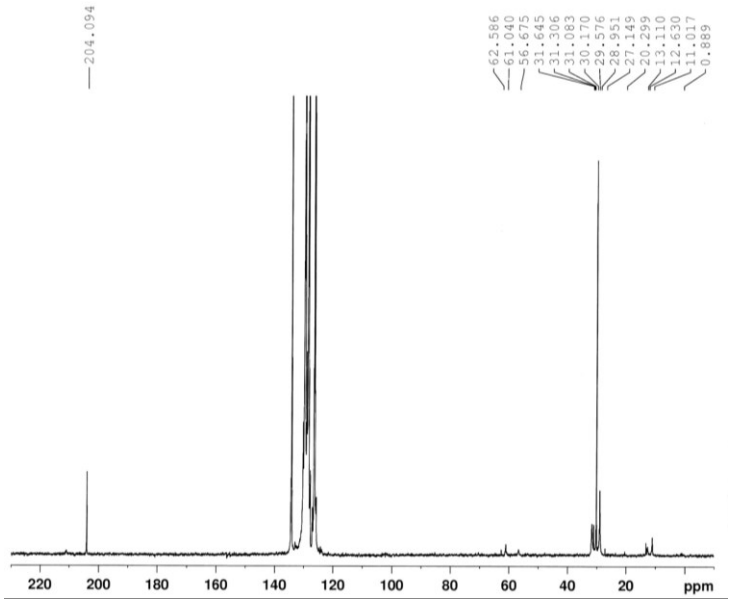


Figure 19: ^{13}C NMR Spectrum of the Isolated Solid in C_6H_5Cl with D_2O Lock

In the case of DCM-d_2, dissolution of the solid was achieved but the solution rapidly turned violet in colour. No starting materials or the desired product could be identified by ^{1}H and ^{13}C NMR spectroscopy. A ^{29}Si NMR shift was observed at −21.8 ppm which was in accordance with free $SiCl_4$ (Figure 20). The lack of a ca. −70 ppm change in ^{29}Si NMR shift indicated that a pentacoordinate silicon species had not been formed.[95]

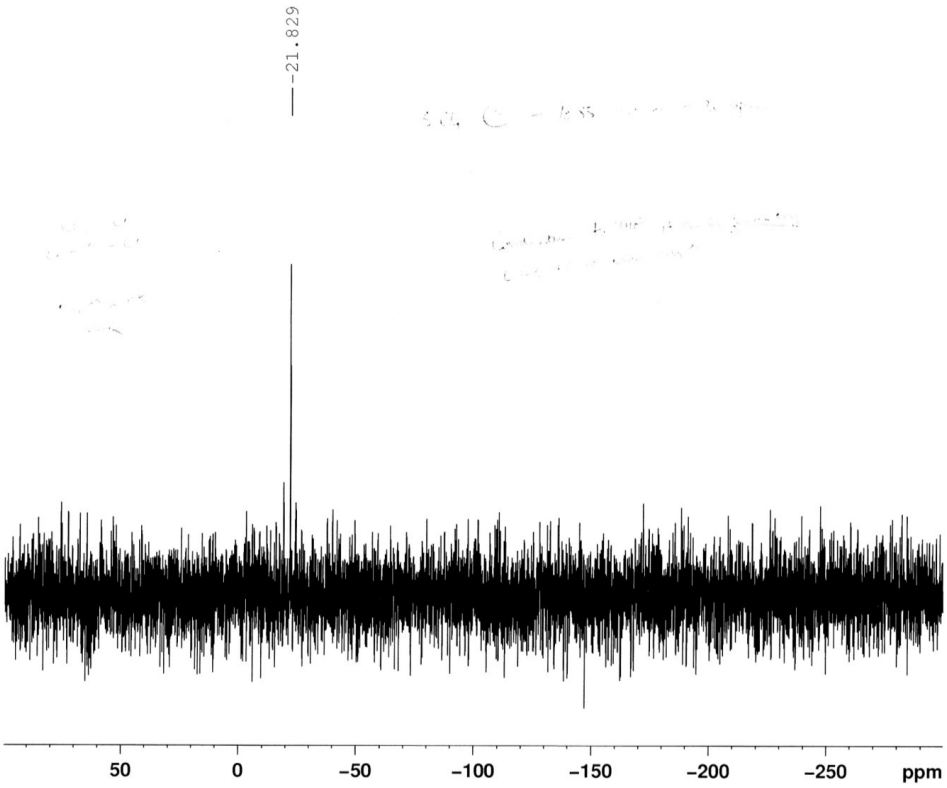


Figure 20: ^{29}Si NMR Spectrum of the Isolated Solid in CD_2Cl_2

Conclusions

- Whilst NHC·$SiCl_4$ systems were not of synthetic relevance due to their moisture sensitivity, their synthesis corroborated the data reported in the literature and the ca. −70 ppm change in ^{29}Si NMR shift provided a spectroscopic indicator of pentacoordinate Si species.[32,95,107,111]
- The synthesis of IMes·$SiCl_4$ (**96b**) and IDipp·$SiCl_4$ (**96c**) indicated that the relatively bulky 2,6-di*iso*propylphenyl and 2,4,6-trimethylphenyl groups did not prevent the formation of a pentacoordinate silicon species. However, the synthesis of **110** utilising Me_2I*t*Bu (**109**) was not successful.
- ^{29}Si NMR spectroscopy provided a rapid and reliable method for the determination of silicon co-ordination (more specifically, the transition from a tetra- to a pentacoordinate species) and therefore NMR spectroscopy was a suitable method by which to characterise the postulated interaction of low molecular weight silicon species, and silicone oligo-/polymers with NHCs.

2.3 Quantifying the Decomposition of NHCs and the Role of Silicon Species (NHC·Si Interactions)

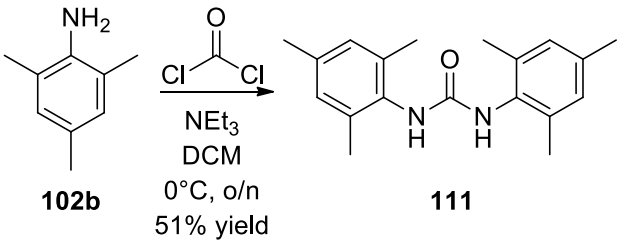
Given that we wished to exploit the NHC·Si interaction (**79**) that was reported by Baceiredo and co-workers to afford protection to NHCs as shown in Figure 12, it was appropriate to gather qualitative evidence of such an NHC·Si interaction by NMR spectroscopy as this had not been presented in the literature.[90] Although such evidence was available for NHC·$SiCl_4$ compounds, it had not yet been extended to organocatalytically relevant systems.[32,43,107,109,111]

However, it was also appropriate to gain quantitative evidence of an NHC·Si interaction to support the notion of a weak Lewis-base Lewis-acid interaction.[90] Given the postulated mechanism of interaction, and the well-known hydrophobic nature of silicone polymers, it was appropriate to probe the decomposition of NHCs (**4**) in the presence of low molecular weight silicon species. West and co-workers reported that the Lewis-acidity of silicone chains was chiefly affected by the substituents on the silicon chain, rather than chain length.[98] It was therefore expected that the same protection and weak NHC·Si interaction would be observed in low molecular weight silicon species as mimics of silicone polymers. We wished to quantify the decomposition of the NHC moiety and the corresponding formation of decomposition products.

2.3.1 Synthesis of a Postulated IMes Decomposition Product

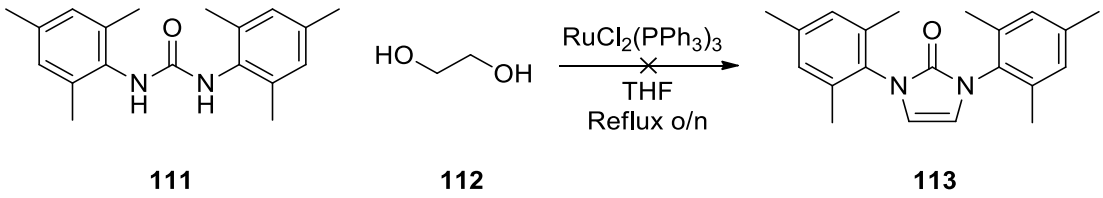
Literature reports indicated that the decomposition of NHCs (**4**) by the action of water and oxygen on the carbene moiety (C2 position) led to the formation of a number of unknown decomposition products,[5,6,16,89,90] though in the case of NHCs bearing bulkier *N*-substituents, the imidazol-2-one (**72**) and the formamides (**73-74**) were the major products.[16,89,90] In order to quantify and characterise the decomposition of NHCs (**4**), though specifically IMes (**4b**), it was necessary to prepare authentic samples of a proposed decomposition product. Given the hydrophobic nature of silicones, the expected primary decomposition product of IMes (**4b**) was the imidazol-2-one (**72**) by the action of oxygen.

In an attempt to make the expected imidazol-2-one (**72**), **111** was prepared by the reaction of 2,4,6-trimethylaniline (**102b**) with phosgene solution in 51% yield as shown in Scheme 49, c.f. 78% reported in literature by Bouteillier and co-workers.[121]



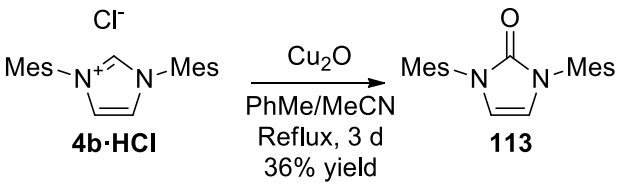
Scheme 49: Synthesis of a *N,N'*-Disubstituted Urea with Phosgene[121]

A ruthenium-catalysed reaction of **111** with ethan-1,2-diol (**112**) to form an imidazol-2-one (**113**) was attempted, as shown in Scheme 50, but did not yield the desired product.[122] Performing the reaction under argon with THF at reflux overnight in a sealed vessel was also not successful. The method was based on results published by Watanabe and co-workers who reported the synthesis of imidazol-2-ones albeit with methyl and ethyl *N*-subsituents.[122]



Scheme 50: Attempted Ru-Catalysed Synthesis of 1,3-Disubstituted 4,5-Dihydroimidazol-2-ones[122]

The expected urea from the decomposition of IMes (**4b**) was instead synthesised in 36% yield, by oxidation of **4b·HCl** with stoichiometric Cu_2O (Scheme 51).[36]



Scheme 51: Synthesis of an Imidazol-2-one – Cu_2O Assisted Oxidation of an Imidazolium Halide[36]

It was noted that the imidazol-2-one (**113**) was poorly soluble in a number of solvents.[123] Indeed, the poor solubility of **113** made identification by ^{1}H and ^{13}C NMR spectroscopy difficult in $CDCl_3$ and THF-d_8.[123] It was therefore uncertain as to how Baceiredo and co-workers were able to quantify the concentration of the imidazol-2-ones (**72**) in solution using ^{1}H NMR during their decomposition studies in THF-d_8 only.[90] Given the inability to quantitatively assess the concentration of a decomposition product (**113**) by ^{1}H NMR spectroscopy, we turned to ^{13}C NMR spectroscopy to quantify the consumption of starting material (**4b**) instead.

2.3.2 Quantitative NMR

Quantitative ^{13}C NMR spectra of toluene-d_8 solutions of ^{13}C-labelled IMes (***4b**) were collected at timed intervals both prior and after the exposure of the sample to air as this allowed the decomposition of the NHC to be followed, rather than the evolution of a decomposition product (**113**) which was poorly soluble.[123] "Standard" ^{13}C NMR spectra were not quantitative due to the short relaxation times used in the NMR pulse sequences. Therefore, unlike ^{1}H NMR spectra, the resonances of standard ^{13}C NMR spectra could not be integrated such that the ratio of areas indicated the ratio of nuclei (the empirical formula).

Quantitative ^{13}C NMR, with pulse sequence relaxation times sufficiently long to allow ^{13}C nuclei to return to thermal equilibrium, would have normally required: a high concentration of sample due to the low abundance of ^{13}C versus ^{12}C; long sampling times due to the slow relaxation time of ^{13}C nuclei; and numerous scans due to the lower SNR without polarisation transfer from adjacent ^{1}H nuclei. However, the use of ^{13}C-labelled IMes (***4b**) allowed us to address these problems. The increase in abundance of ^{13}C in the sample of IMes, as a result of ^{13}C-labelling, allowed ^{13}C NMR spectra with good resolution of the C2 peak to be recorded in a shorter time; the increase in signal-to-noise ratio compared to the natural abundance IMes (**4b**) was significant (Figure 21).

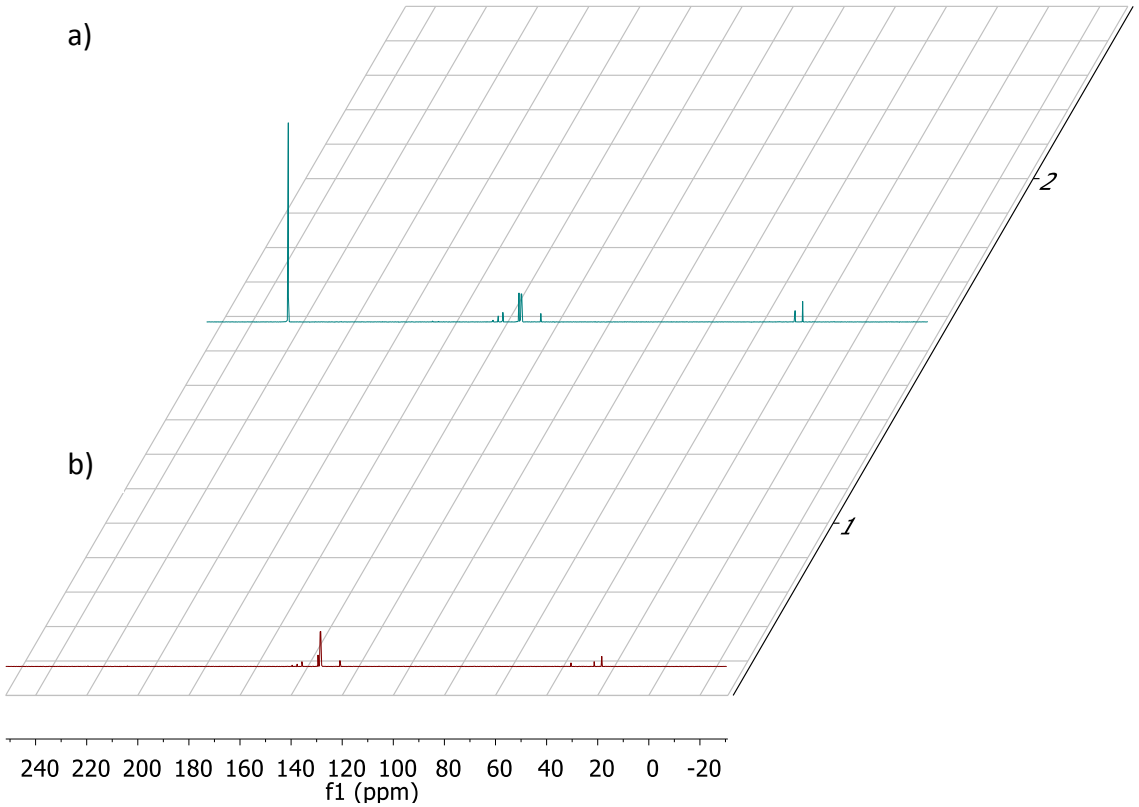
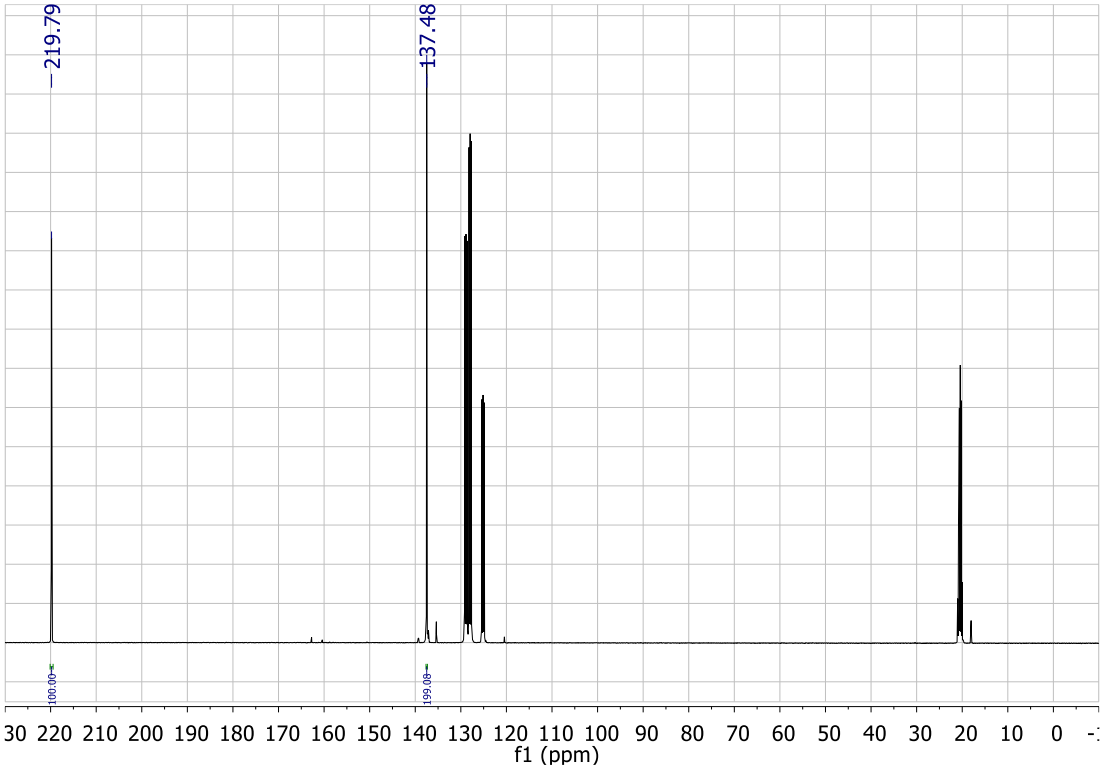


Figure 21: Comparison of (a) ^{13}C-Labelled and (b) Natural Abundance IMes – Increased SNR of the Carbene Moiety ca. 220 ppm

Quantitative ^{13}C NMR showed a clear and distinct change in the intensity of the C2 resonance at ca. 220 ppm prior to and after exposure of ^{13}C-labelled IMes (*4b) to air (Figure 22).

a)



b)

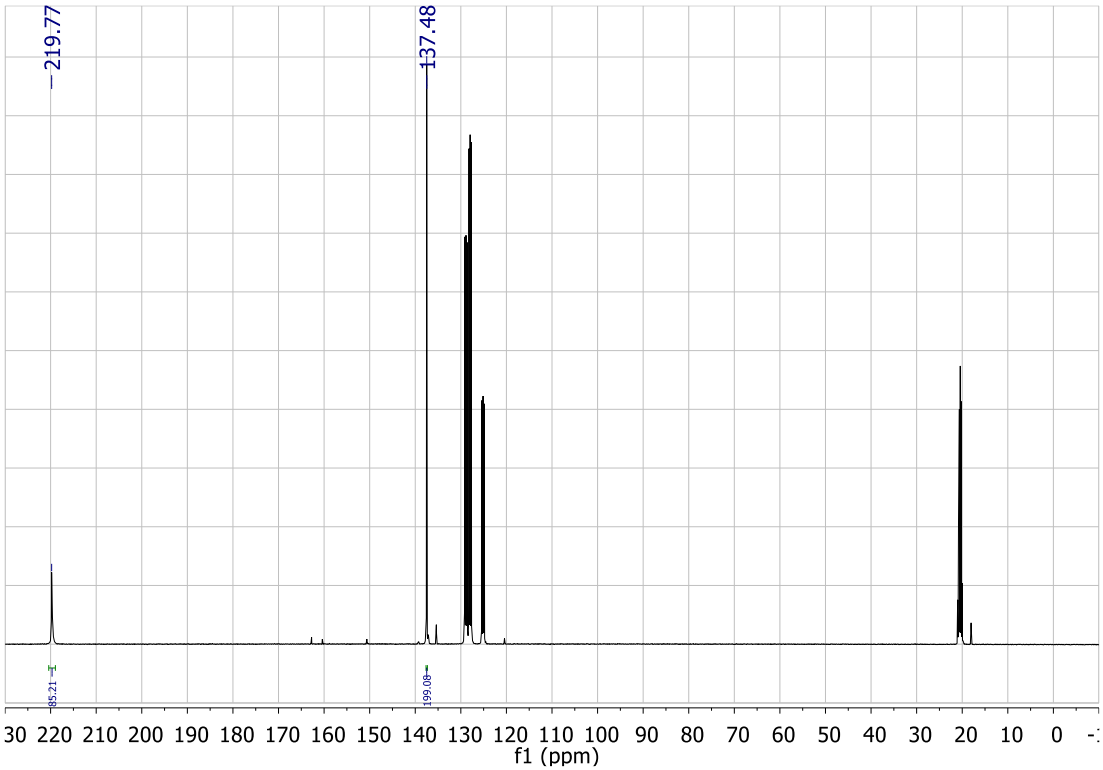


Figure 22: ^{13}C-Labelled IMes (*4b) Prior to Exposure (a) and 17 Hours After Exposure to Air (b)

Error! Reference source not found. Although ^{13}C-labelled IMes (***4b***) was used, there was no distinct rowth of a ^{13}C resonance that could have corresponded to the carbon resonance(s) of a decomposition product such as the formamide: although decomposition of IMes (**4b**) could be

qualitatively followed as a result of ^{13}C-labelling, the generation of the decomposition products could not be followed reliably. Closer inspection of the spectra indicated the formation of numerous new peaks with one at ca. 151 ppm. However, quantitative analysis of the product was not possible due to the relatively low peak height (and poor signal-to-noise ratio) in comparison to the baseline. This was counterintuitive: given the large decrease in the peak height (concentration) of the C2 resonance as shown in Figure 22, a reciprocal increase in peak height (concentration) of (a) new resonance(s) was expected given the quantitative nature of the ^{13}C NMR spectra collected.

Our attempts to quantify the decomposition of ^{13}C-labelled IMes (***4b**) yielded anomalous results. The concentration of the NHC (***4b**) was based on the ^{13}C NMR shift of the C2 peak which was referenced to a set of residual toluene peaks. It was observed that the derived concentration data appeared to show decomposition stopping after ca. 2500 minutes (Figure 23).

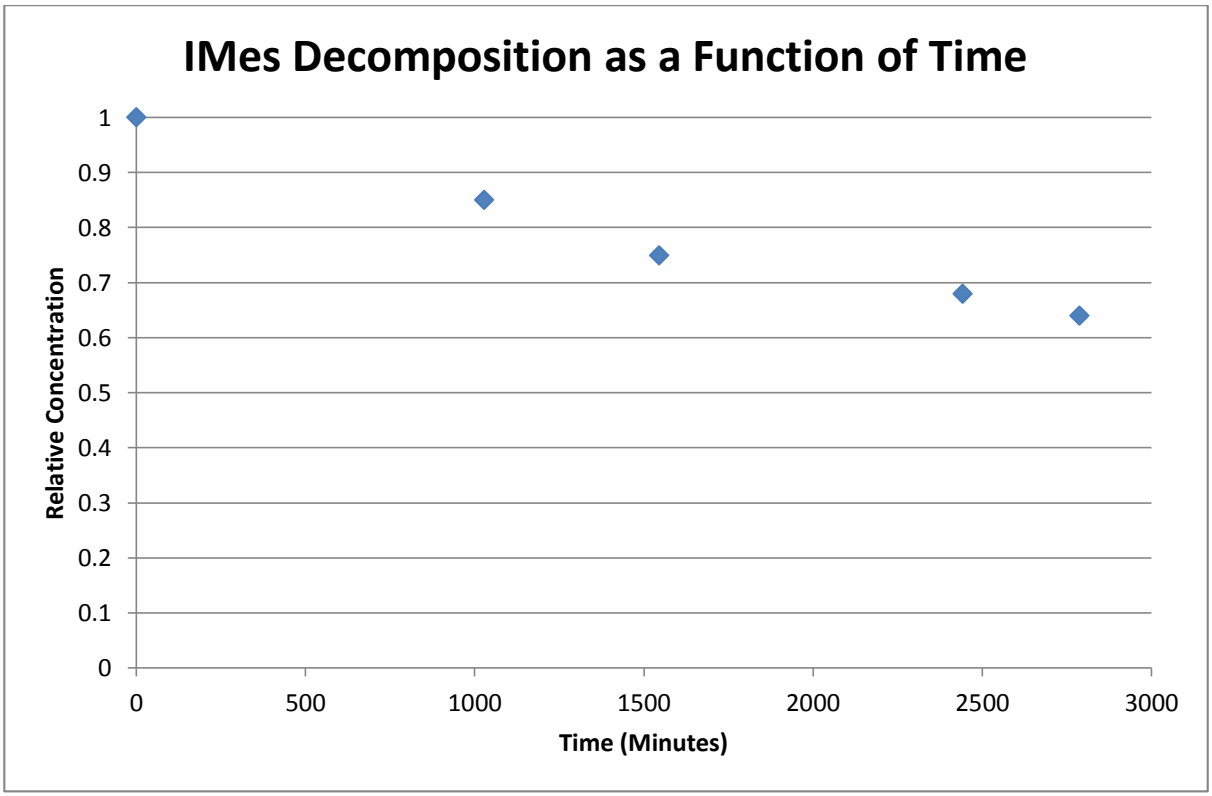


Figure 23: Relative Concentration of ^{13}C-IMes in Solution - Derived from ^{13}C Quantitative NMR

It was reported by Nyulászi and co-workers that the addition of 1 equivalent of water to IDipp (**4c**) in C_6D_6 led to a broad resonance at 217.2 c.f. 220.4 for IDipp (**4c**) in C_6D_6 without water; the addition of 2 equivalents of water added to IDipp (**4c**) in THF-d_8 led to no detectable peak ca. 220-200 ppm at room temperature.[89] That is, the addition of 2 equivalents of water were required in for decomposition of the carbene moiety to occur in THF-d_8: the addition of 1 equivalent of water in C_6D_6 was anomalous as it led to broadening of the peak.

The broad ^{13}C NMR resonance at 217.2 ppm was not attributed to the imidazol-2-one (**72**) or formamides (**73-74**) but to unknown intermediates.[89] It was therefore possible that the broadening of the characteristic carbene peak observed by us was a product of the decomposition of the carbene moiety coupled with the formation of unknown intermediates. The separation of these two effects was not possible due to the lack of characterisation data for the postulated intermediates. Therefore, the concentration datapoints shown in Figure 23Figure 22 are upper values assuming no formation of decomposition intermediates. Unfortunately, this meant that the quantitative analysis of the C2 resonance of ^{13}C-labelled IMes to yield concentration profiles of IMes (**4b**) as a function of time would not be possible.

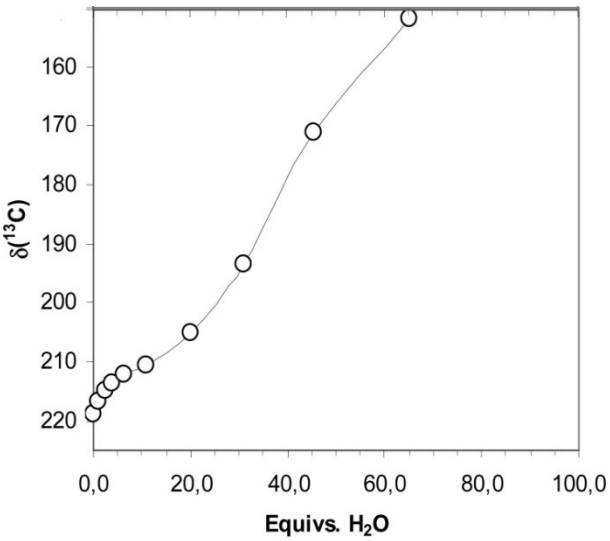


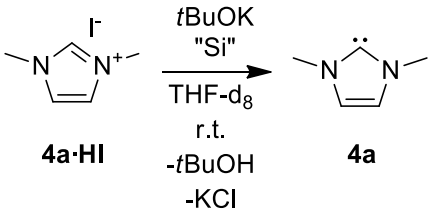
Figure 24: Titration Curve of IDipp (4c) with Water at –35 °C in THF-d_8 by Nyulászi and Co-workers[89]

Further evidence presented by Nyulászi and co-workers showed that titration of a THF-d_8 solution of IDipp with water at −35 °C exhibited changes of up to 60 ppm in the C2 resonance of IDipp in ^{13}C NMR spectra as shown in Figure 24.[89] It was now apparent that quantitative analysis of the decomposition of the NHCs (**4**) and the evolution of decomposition products (**72-74**) would not be possible given the formation of unidentified intermediates with ^{13}C NMR shifts similar to that of the free NHCs (**4**).[89]

2.3.3 Decomposition of IMe

As NHC·Si interactions were expected to change the electronic environment around the C2 carbon nuclei and the silicon nuclei, evidence of an NHC·Si interaction was sought in the form of observed changes in ^{13}C NMR shift of the C2 resonance, or changes in ^{29}Si NMR shift of silicon species in samples of NHCs containing low molecular weight silicon species. ^{1}H NMR data was not of primary interest given the inability to infer an NHC·Si (carbon-silicon) interaction.

Initial studies began with IMe (**4a**) rather than IMes given the former's propensity to decompose: indeed, the isolation of IMe (**4a**) as a free NHC was not possible in our hands due to its rapid decomposition on removal of solvent.[5] IMe (**4a**) was formed *in situ* in the presence of silicon species, as shown in Scheme 52, for the purposes of preliminary NMR studies described below. A proposed decomposition product (imidazol-2-one) of IMes was synthesised (*vide supra*) as the decomposition products of IMe are described as unknown and numerous.



Scheme 52: Deprotonation of IMe·HI in the Presence of Silicon Species to Form IMe (4a) *In Situ*

^{1}H NMR spectra indicated deprotonation of the imidazolium halide (**4a·HI**) had proceeded (disappearance of the imidazolium proton resonance) while ^{13}C NMR spectra showed a characteristic C2 (carbene) resonance ca. 215 ppm as reported in literature for IMe (**4a**) as shown in Figure 25.[5]

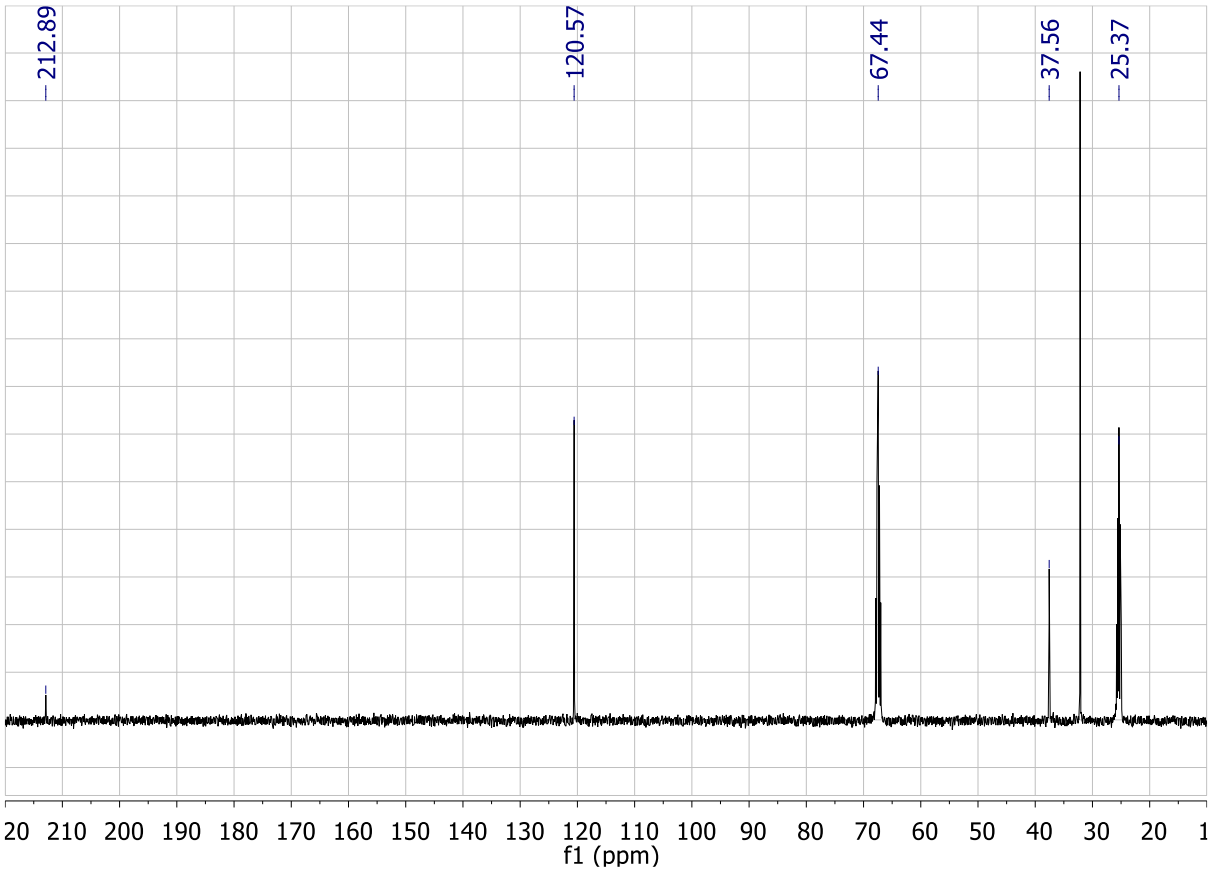


Figure 25: ^{13}C NMR Spectrum of IMe (4a) Formed *In Situ* – Carbene Moiety ca. 210 ppm

Decomposition of IMe (**4a**) at room temperature was much more rapid than that of the more bulky NHCs such as IMes (**4b**) and IDipp (**4c**) with the formation of brown oil and dark precipitates as reported by Arduengo and co-workers.[5]

It was envisaged, in light of the tendency of IMe (**4a**) to decompose even under an anaerobic and moisture-free environment,[5] that studies with IMe (**4a**) would therefore yield more rapid and distinct differences in decomposition in comparison to IMes (**4c**) which had been reported to be more stable and less prone to decomposition.[5,16,90] Indeed, the presence of bulky *N*-substituents (combined with electronic effects) were shown to stabilise the carbene moiety.[124–128]

However, the rapid decomposition of IMe (**4a**) had been underestimated. Indeed, the collection of ^{13}C NMR spectra was hindered by both the rapid decomposition of IMe (**4a**) and the lack of ^{13}C-labelling of the C2 (carbene) position which made identifying the weak resonance ca. 215 ppm difficult. Although we had intended to gain spectroscopic evidence of an NHC·Si interaction, the decomposition of IMe (**4a**) was followed visually. Given that dark oils formed during decomposition, the evolution of colour was used as a qualitative indicator of decomposition.[5] It was accepted that although the observations would not have been robust evidence of an NHC·Si interaction, the experiments could serve as a qualitative indicator of protection/NHC·Si interaction in order to guide later experiments.

A number of low molecular weight silicon species were chosen for the initial studies including: M_2 (**114**), dimethoxydimethylsilane (**115**), trimethoxymethylsilane (**116**), D_4 (**80**), MDM (**117**), and tetramethoxysilane (**118**) as shown in Figure 26.

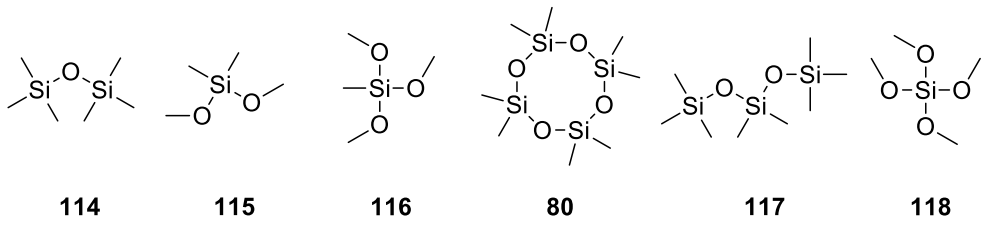


Figure 26: Silanes and Siloxanes Used for Initial Studies on NHC Decomposition

80 and **114-118** were chosen as low molecular weight mimics of silicones given that the mechanism of interaction as proposed by Baceiredo and co-workers[90] was that of a Lewis-base Lewis-acid interaction (**79**) which would be primarily affected by the substituents on the silicon chain rather than chain length.[98] D_4 (**80**) was further chosen as a cyclic siloxane as Baceiredo and co-workers had reported that NHC-catalysed ROP of D_4 proceeded *via* NHC activation of a silicon centre (Scheme 30).[101] Methoxy-substituted silanes (**115-116** and **118**) were chosen to provide a series of silicon species with differing Lewis-acidities.[98]

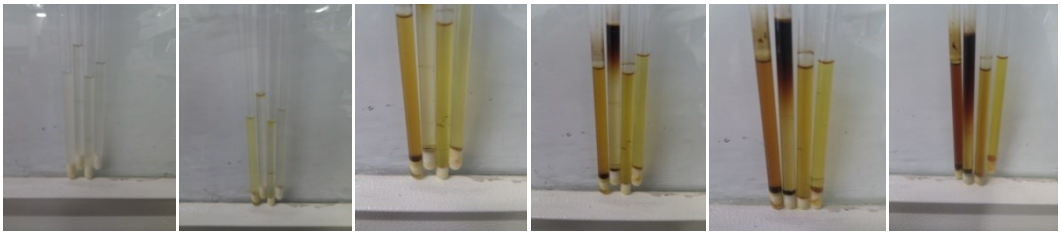


Figure 27: Decomposition of IMe at Time 0, 1.5, 15, 23, 42, and 63 Hours

Samples of IMe (**4a**) in THF-d_8 with 10 equivalents (with respect to the NHC) of: M_2 (**114**), dimethoxydimethylsilane (**115**), trimethoxymethylsilane (**116**), and D_4 (**80**) were monitored over course of 63 hours as shown in Figure 27 from left to right. Qualitatively, it was observed that silicon additives had a non-innocent effect on IMe decomposition, as shown by the differences between samples in Figure 27: given that the decomposition products imparted colour to the solution,[5] the difference in colour between the samples was attributed to either retardation of decomposition (the formation of dark oils and precipitates), or to changes in the decomposition pathways i.e. no conclusion was made to "protection" at this point.

As the decomposition of IMe (**4a**) was still rapid in the presence of low molecular weight silicon species, in comparison to the protection reported by Baceiredo and co-workers for a number of NHCs bearing bulkier *N*-substituents,[90] and because of the difficulties in characterising decomposition/interaction for the short-lived IMe (**4a**), NMR experiments were conducted with IMes (**4b**) given that the decomposition of IMes (**4b**) was reported to be slower in comparison to IMe.[5,16,129]

2.3.4 Decomposition/Protection of IMes – An NHC·Si Interaction?

Samples of IMes (**4b**) in C_6D_6 with 1 equivalent (with respect to IMes) of: M_2 (**114**), dimethoxydimethylsilane (**115**), trimethoxymethylsilane (**116**), MDM (**117**), and tetramethoxysilane (**118**), were monitored by ^1H and ^{13}C NMR spectroscopy. IMes in C_6D_6 was used as a reference/control.

Although a number of deuterated NMR solvents could have been used, C_6D_6 as a non-Lewis-basic solvent was selected given the proposed nature of the NHC-Si interaction.[90] THF-d_8 (in which NHCs are commonly characterised) may have disrupted any NHC·Si interaction due to electron-pair donation from oxygen atoms, though in preliminary studies of IMe, THF-*d8* was used given the poor solubility of *t*BuOK in C_6D_6.

NMR samples of IMes (**4b**) with silicon additives were prepared in a glovebox under a dry nitrogen or argon atmosphere and were allowed to equilibrate overnight. On removal of the NMR tubes from the glovebox such that they were exposed to an aerobic environment, it was observed that IMes (**4b**) in C_6D_6 without any silicon additives, and IMes (**4b**) in C_6D_6 with tetramethoxysilane (**118**) began to discolour after 3 hours whereas samples in the presence of M_2 (**114**), dimethoxydimethylsilane (**115**), trimethoxymethylsilane (**116**), and MDM (**117**), remained colourless after 3 hours. It was apparent that IMes (**4b**) with bulky *N*-substituents was prone to relatively rapid decomposition under aerobic conditions.

However, ^{13}C NMR spectra were successfully collected. A minor difference between the ^{13}C NMR spectra of samples of IMes (**4b**), and IMes with M_2 (**114**) was noticeable after 8 hours as shown in Figure 28. Although the spectra were not quantitative, the lower peak height and broadening of the C2 resonance appeared to indicate greater decomposition in IMes without M_2 as shown in Figure 28 (a). As described previously, quantitative analysis of the decomposition of IMes (**4b**) was not possible due to the observed formation of decomposition intermediates and broadening of the C2 shift.[89] However, the minor change in the ^{13}C NMR shift of the C2 position (< 1 ppm) in the presence of M_2 did not afford direct evidence of an NHC·Si interaction. Indeed, Nyulászi reported a change of 3 ppm for IDipp (**4c**) in the presence of 1 equivalent of water at room temperature.[89]

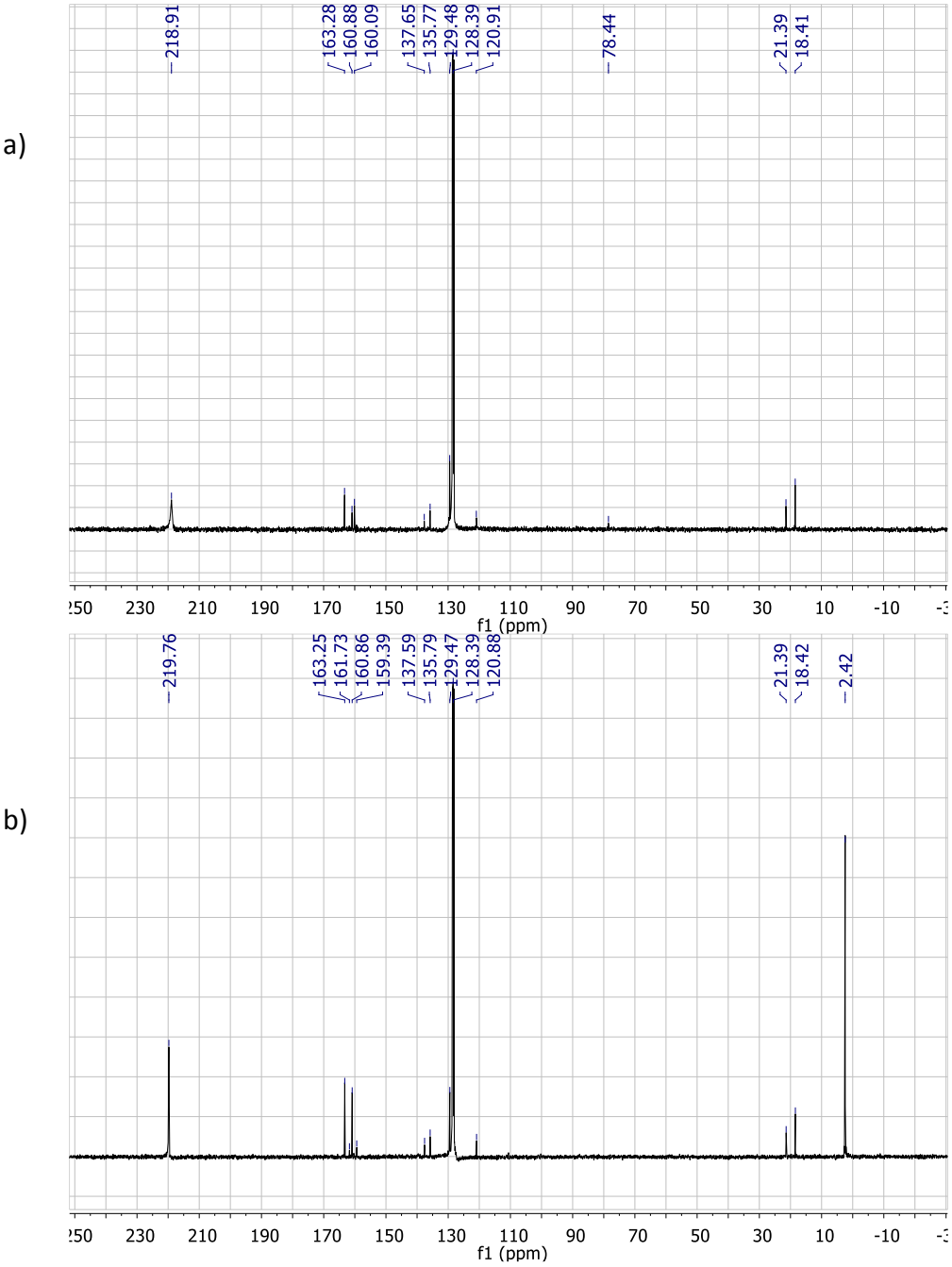


Figure 28: ^{13}C NMR Spectra of IMes (a), and IMes with M_2 (1:10 Mole Ratio) (b), in C_6D_6 at Room Temperature After 8 Hours

After 8 hours, a dark precipitate had begun to form in the control sample of IMes (**4b**) in C_6D_6 without any silicon additives. Samples containing M_2 (**114**), dimethoxydimethylsilane (**115**), and D_4 (**80**) also began to discolour: however, those containing trimethoxymethylsilane (**116**), and MDM (**117**) remained colourless with no precipitation. Although spectroscopic evidence of an NHC·Si interaction was not yet forthcoming, the presence of a single equivalent of a low molecular weight

silicon species appeared to affect the decomposition of IMes (**4b**). In all of the above cases, no changes were observed in the ^{29}Si NMR spectra.

It should be noted that the data presented above did not provide conclusive evidence of an NHC·Si interaction. However, the observations served to direct further investigations given the paucity of experimental data on NHC·Si interactions in the literature.[43] Indeed, given the lack of spectroscopic evidence, the minimal changes in decomposition could have been due to mass-transfer effects and changes in bulk properties of the solvent system due to presence of silicon additives rather than due to an NHC·Si interaction.

To further qualify the statement on mass-transfer effects: diffusion coefficients of solutes such as oxygen and water through a solvent system would be altered by the presence of any impurities. If the "protection" observed by Baceiredo and co-workers[90] was as a result of changes to the bulk solvent, the "protection" would not be due to an NHC·Si interaction but due to mass transfer effects (limited diffusion): the protection afforded by a silicon species as a result of an NHC·Si interaction would have to be over and above that afforded by diffusion alone. The preliminary ^{1}H and ^{13}C NMR data collected at room temperature as described above did not support an NHC·Si interaction.

In light of the above results using low molecular weight silicon species, the samples were prepared again with ^{13}C-labelled IMes (***4b**) and further ^{1}H, ^{13}C, and ^{29}Si NMR spectra were recorded in an effort to spectroscopically observe any potential NHC·Si interaction. The same visual observations observed with natural abundance IMes (**4b**) were made with samples containing ^{13}C-labelled IMes (***4b**). It must be noted that the "protection" observed by us was not comparable in length to that reported by Baceiredo and co-workers who reported "protection" on the scale of days and weeks as shown in Table 2,[90] as opposed to hours in our case. Furthermore, it was not apparent by ^{13}C and ^{29}Si NMR spectroscopy that an NHC·Si interaction existed at room temperature.

Indeed, the ^{13}C NMR spectrum of ^{13}C-labelled IMes (***4b**) and trimethoxymethylsilane (**116**) in C_6D_6, as shown in Figure 29, showed no conclusive evidence of an NHC·Si interaction. Although a ca. 1 ppm change in the C2 resonance was observed, this was within the ca. 3 ppm change (and broadening) that Nyulászi and co-workers reported for the decomposition of IDipp (**4c**).[89] Similar results were observed with the other silicon species.

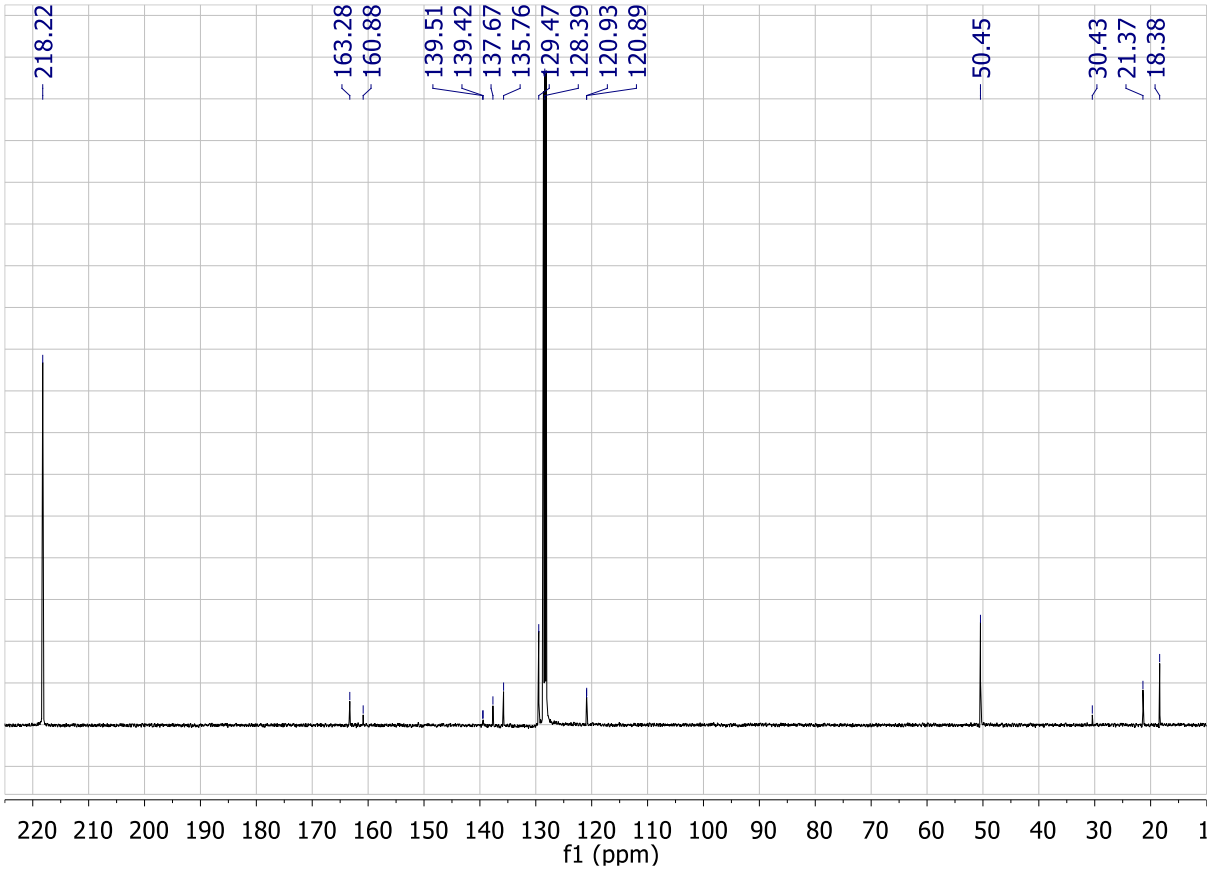


Figure 29: ^{13}C NMR Spectrum of ^{13}C-Labelled IMes (*4b) with Trimethoxymethylsilane (116) (1:10 mole ratio)

The NMR experiments were then repeated with 5 equivalents of: M_2 (**114**), dimethoxydimethylsilane (**115**), and trimethoxymethylsilane (**116**) with respect to IMes (**4b**) in C_6D_6. A small change ca. 1 ppm in the observed ^{13}C NMR shift of the C2 resonance was again observed. For comparison, the resonance of the carbene moiety for IMes in C_6D_6 without silicon additives was observed at 219.5 ppm, which was in agreement with 219.7 ppm reported by Arduengo and co-workers.[14] The spectroscopic data appeared anomalous and did not support the notion of an NHC·Si interaction.

2.3.5 Equilibrium Limited Formation of an NHC·Si Interaction

Baceiredo and co-workers had predicted a weak interaction (of the order of 3–5 kcal·mol^{-1} in magnitude, ca. 13–21 kJ·mol^{-1}), and had also reported that the protected species were able to catalyse a range of reactions.[90] It was concluded that an NHC interacting with a silicon species would not be able to catalyse a reaction given that the carbene moiety was bound (to a silicon nucleus). Therefore equilibrium-limited formation of an NHC·Si species was assumed which would be compatible with the weak interaction predicted, and with the observation that protected NHCs were still catalytically active.[90] Indeed, the equilibrium-limited formation of an NHC·Si complex may have explained the lack of spectroscopic evidence reported above.

If formation and separation of the postulated NHC·Si species were fast compared to the ^{13}C and ^{29}Si NMR timescale, this would have accounted for why single peaks in ^{13}C and ^{29}Si NMR were observed rather than two distinct peaks corresponding to the bound and unbound states. The lack of distinct change in the ^{13}C and ^{29}Si NMR shifts would also be consistent with equilibrium lying far towards that of the unbound species (as expected for the weak NHC·Si interaction predicted).[90] The NMR spectra therefore showed that although there was no spectroscopic evidence of an NHC·Si interaction, it could not preclude it.

In order to push equilibrium towards the formation of an NHC·Si complex such that conclusive ^{13}C and ^{29}Si NMR data indicative of an NHC·Si interaction could be collected, samples of IMes (**4b**) in C_6D_6 with 5, 10 and 100 equivalents of a silicon species were prepared. Increasing the concentration of a silicon species in solution with IMes (**4b**) had little cumulative effect on the C2 resonance for a range of silanes and siloxanes as shown in Table 5.

Table 5: ^{13}C Shift (ppm) of IMes-C_2 at 298K with Varying Quantities of Silanes and Siloxanes

	Equivalents			
	1	5	10	100
Dimethoxydimethylsilane	218.3	212.2	218.4	212.5
Trimethoxymethylsilane	219.3	216.0	217.8	-
Tetramethoxysilane	215.6	-	214.7	-
M_2	219.3	219.5	218.6	-
MDM	219.4	-	-	-
D_4	219.1	-	-	-

The minimal changes in the ^{13}C NMR shifts were of the order of 1–5 ppm at room temperature and were consistent with reports by Nyulászi and co-workers,[89] hence they did not provide conclusive evidence of an NHC·Si interaction.

2.3.6 Variable Temperature NMR Studies

As increasing the mole ratio of silicon additives to IMes (**4b**) did not have the desired effect of providing conclusive spectroscopic evidence of an NHC·Si interaction, NMR spectra were recorded at lower temperatures as the formation of an interacting NHC·Si species would be entropically more favoured in such cases. The formation of the said NHC·Si species was again expected to lead to a more significant shift in the ^{13}C NMR shift of the carbene moiety which would have been indicative of a change in its electronic environment. A change in the ^{29}Si NMR resonance of the silicon species of ca. −70 ppm was also expected given the difference in resonance between tetra- and pentacoordinate silicon species reported in the literature.[32,95,107,109,111]

Low temperature ^{13}C NMR spectra (298K to 198K in 25K steps) of samples of IMes (**4b**) and a number of silicon species in THF-d_8 were collected. THF-d_8 was used as the solvent for this purpose given the relatively high melting point of C_6D_6. M_2 (**114**), dimethoxydimethylsilane (**115**), and

trimethoxymethylsilane (**116**) were used as low molecular weight mimics of silicon polymers in varying ratios as shown in Table 6.

Table 6: Variable Temperature NMR Studies of IMes in the Presence of Silicon Additives – Recorded C_2 Resonances (ppm)

	Temperature											
	273K			248K			223K			198K		
	Equivalents			Equivalents			Equivalents			Equivalents		
	1	10	100	1	10	100	1	10	100	1	10	100
$Me_2Si(OMe)_2$	-	217	210	-	215	207	-	213	205	-	211	201
$MeSi(OMe)_3$	219	-	-	218	-	-	217	-	-	216	-	-
M_2	219	-	-	218	-	-	218	-	-	217	-	-

Although the data, as shown in Table 6 and Table 7, indicated changes in the C2 resonance of IMes (**4b**) in THF-d_8 increased as temperature was lowered, and as the concentration of silicon species was increased, this was not conclusive evidence of a NHC·Si interaction. Indeed, a ca. 0.5 ppm shift upfield of the C2 resonance of IMes (**4b**) per 25K reduction of temperature was observed in samples of IMes (**4b**) in THF-d_8 without any silicon additives as shown in Table 7.

Table 7: Characteristic ^{13}C NMR Shift (ppm) of IMes C2 Position as a Function of Temperature

	Temperature (K)				
	298	273	248	223	198
IMes	219.8	219.3	218.7	218.1	217.6
IMes-$Me_2Si(OMe)_2$ (1:20 mole ratio)	215.0	212.4	209.8	207.3	205.5

Although the changes in C2 resonance, as shown Table 6 and Table 7, were greater than the ca. 3 ppm observed by Nyulászi and co-workers at room temperature during the decomposition of IDipp (**4c**), they were not in excess of the ca. −60 ppm change in the C2 shift observed by Nyulászi and co-workers in the case of IDipp (**4c**) exposed to ca. 60 equivalents of water at −35 °C. The results of our low-temperature ^{13}C NMR studies also did not provide conclusive evidence of an NHC·Si interaction.

In order to probe the other species concerned in the proposed NHC·Si interaction, ^{29}Si NMR spectra of solutions of IMes (**4b**) and M_2 (**114**) (1:1 mole ratio) in THF-d_8 from 298K to 198K in 25K steps

were collected (Figure 30). As temperature was lowered, a −70 ppm change in ^{29}Si NMR shift which would have been indicative of the formation of a pentacoordinate species,[32,95,96,107,130] did not materialise.

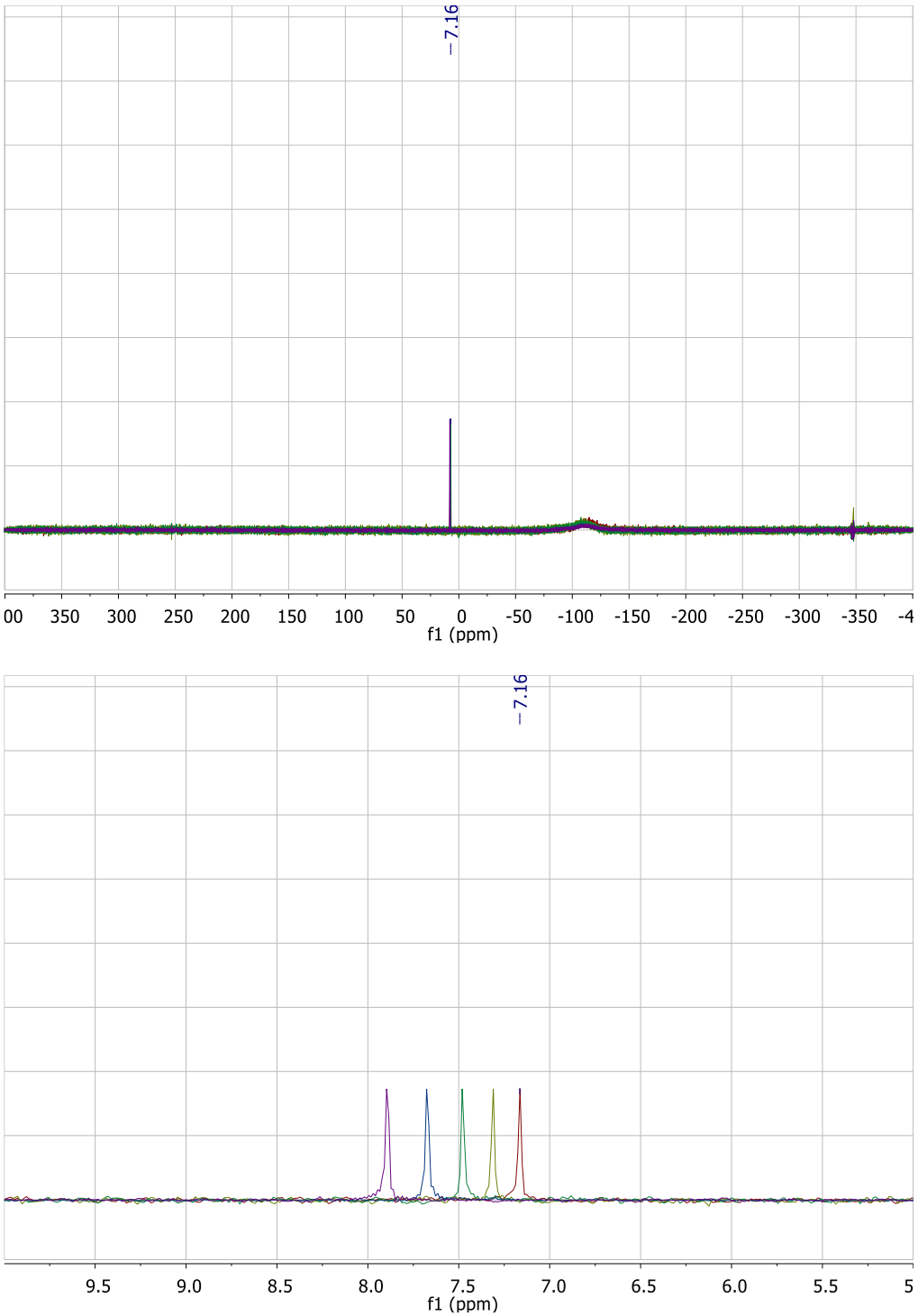


Figure 30: ^{29}Si NMR Spectra of IMes and M_2 (1:1 mole ratio) in THF-d_8 at 298K (Red) to 198K (Purple) in 25K Steps

Furthermore, a change of smaller magnitude in the ^{29}Si NMR spectra (as expected for the equilibrium limited formation of an NHC·Si species) was also not observed. Minor changes in NMR shift, as shown Figure 30, were likely to be due solely to temperature and not an NHC·Si interaction given that the shifts moved downfield as temperature decreased, whereas a ca. 70 ppm shift upfield was expected for a NHC-Si species.[32,95,107,109,111]

2.3.7 Diffusion Ordered Spectroscopy

1D ^{1}H, ^{13}C, and ^{29}Si NMR spectroscopy had so far been unable to: quantify decomposition of IMes (**4b**) (either the generation of decomposition products, or the consumption of IMes (**4b**)); or provide direct evidence of an NHC·Si interaction (in the form of changes in the ^{13}C and ^{29}Si NMR shifts) at room and reduced temperature. Diffusion ordered spectroscopy (DOSY) was therefore investigated. DOSY experiments have been reported as a method to identify and quantify intermolecular bonding in solution by measuring the difference in diffusion coefficients of bound and unbound species.[131] Rocchigiani and co-workers exploited the methodology to study the formation of frustrated Lewis-pairs which otherwise displayed no difference in their NMR resonances.[132]

Although in our cases described above, minor differences in ^{13}C NMR shifts (and ^{29}Si NMR shifts) were observed for IMes (**4b**) and silicon compounds (**80** and **114-118**) in C_6D_6 and THF-d_8 at temperatures varying from 298K to 198K, the changes in shift were inconclusive. In the case of DOSY experiments, the ^{13}C (and ^{29}Si) NMR shifts would not be important as we would not be probing the environment around the C2 (and Si) nuclei, but the diffusion coefficient(s) of the entire molecule(s).[131] In principle, an NHC·Si complex (**79**) would be a "bound state" with a lower diffusion coefficient as a result of its combined (increased) volume compared with that of a free NHC and a free silicon species.[131]

In order to validate the methodology, the diffusion coefficient of water in a number of solvents was measured and compared to literature values as shown in Table 8.

Table 8: Comparison of Measured and Reported Diffusion Coefficient of Water in Solvent

Solvent	Diffusion Coefficient of Water in Solvent (10^{-9} $m^2 \cdot s^{-1}$)	
	Reported	Measured
THF	4.18[133]	4.25
DMSO	ca. 1.00[134]	0.92
Toluene	6.19[135]	6.19

Measurements for a sample of M_2 (**114**, 0.1 mmol) in THF-d_8 (0.4 mL), as shown in Figure 31, with ^{1}H NMR resonance (ppm) along the x-axis and estimated diffusion coefficient (log $m^2 \cdot s^{-1}$) on the y-axis showed that the species had a diffusion coefficient of $1.77 \cdot 10^{-9}$ $m^2 \cdot s^{-1}$ in its free (unbound state).

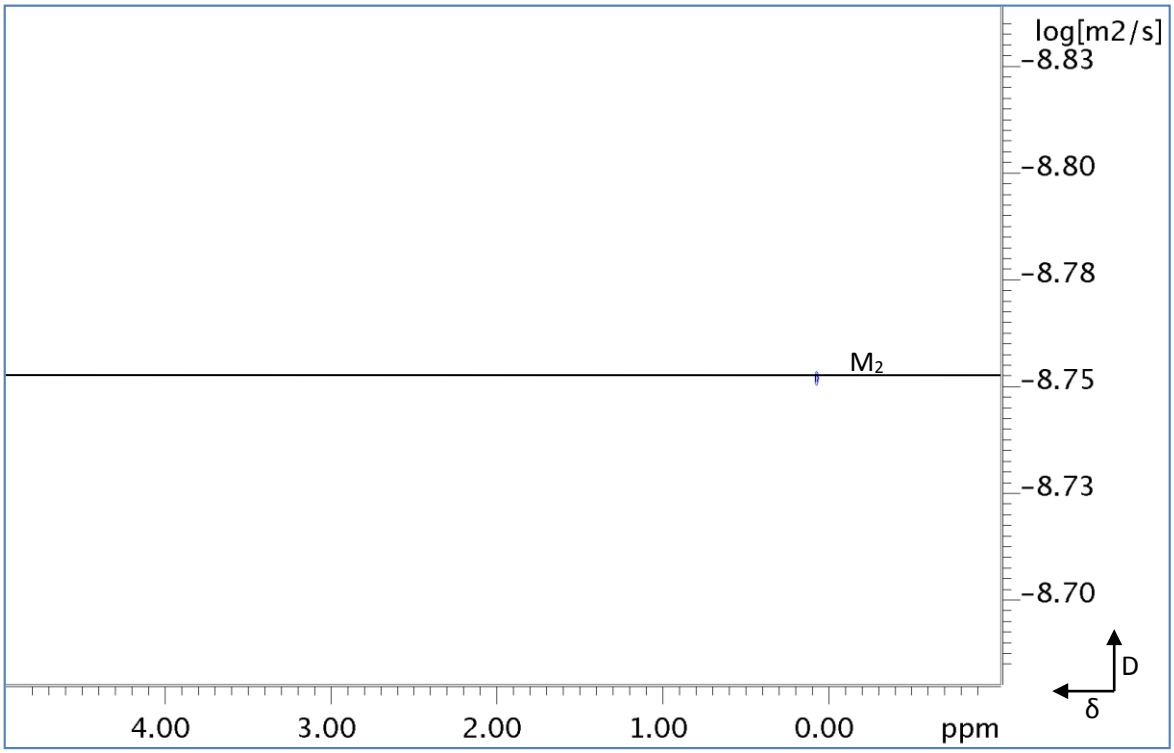


Figure 31: DOSY Spectrum – M_2 (0.1 mmol) in THF-d_8 (0.4 mL)

The diffusion coefficients for a number of other species were then measured by DOSY, as shown in Table 9.

Table 9: Diffusion Coefficient/Diffusivity of Free IMes (4b) and Silicon Species (0.1 mmol in 0.4 mL THF)

	D (10^{-9} $m^2 \cdot s^{-1}$)
IMes	1.06
M_2	1.77
MDM	1.47
D_4	1.25

An equimolar sample of IMes (**4b**, 0.1 mmol) and D_4 (**80**, 0.1 mmol) in THF-d_8 in (0.4 mL) was incubated inside a glovebox overnight and subjected to the same DOSY analysis as described above. The results, as shown in Table 10, indicated a modest reduction in the diffusion coefficients of both solutes, which could imply an interaction between the species. However, this could also have been due to the relatively high concentration of solutes in solution changing the nature of the "solvent" observed by the individual species.[131]

Table 10: Solute Diffusion Coefficients for IMes and D_4 in THF-d_8 (0.1 mmol in 0.4 mL)

	D (10^{-9} $m^2 \cdot s^{-1}$)
IMes (free)	1.06
IMes (in presence of D_4)	0.986
D_4 (free)	1.25
D_4 (in presence of IMes)	1.05

Concentrations were reduced such that the NMR samples remained dilute and to minimise any changes in the bulk solvent by the presence of solutes. IMes (**4b**, 3 mg, 0.01 mmol) and 2 equivalents of M_2 (**114**) were made up in THF-d_8 (0.4 mL), and in toluene-d_8 (0.4 mL) so that the effect of solvent could also be gauged.

M_2 (**114**) was chosen in preference over D_4 (**80**) as the diffusion coefficient of M_2 was the highest of the low molecular weight silicon species sampled, and therefore provided a large margin over the diffusion coefficient measured for free IMes (**4b**) as shown in Table 9. A change in diffusion coefficient as a result of interaction between two species could then be more easily discerned.

Table 11: Diffusion Coefficients of IMes (0.01 mmol) and M_2 (0.02 mmol) in THF-d_8 (0.4 mL)

	D (10^{-9} $m^2 \cdot s^{-1}$)
IMes (free)	1.20
IMes (in presence of M_2)	1.21
M_2 (in presence of IMes)	1.83

The results indicated that the presence of M_2 (**114**) had no effect on the diffusion coefficient of IMes (**4b**) in THF-d_8 as shown in Table 11. The diffusion coefficient of M_2 (**114**) was also significantly greater than that of IMes with no overlap of the diffusion coefficients of the two species, as shown in Figure 32, which indicated that the formation of an NHC·Si complex did not occur in solution.

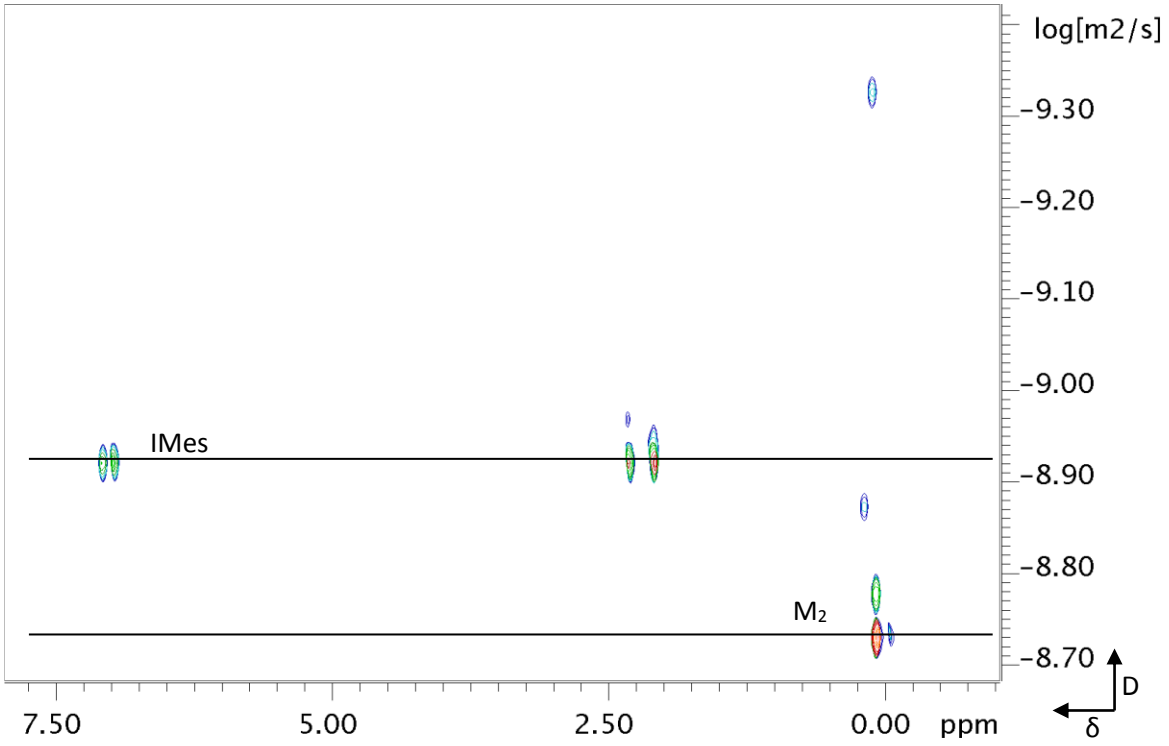


Figure 32: DOSY Spectrum – IMes (4b, 0.01 mmol) and M_2 (114, 0.02 mmol) in THF-d_8 (0.4 mL)

The results in toluene-d_8, as shown in Table 12 and Figure 33, indicated a similar trend to that observed for THF-d_8, with minimal change in the diffusion coefficient for IMes (**4b**) with and without the presence of M_2 (**114**). The spectroscopic data showed a marked difference between the diffusion coefficients of the two solutes (Figure 33).

Table 12: Diffusion Coefficients of IMes (0.01 mmol) and M_2 (0.02 mmol) in Toluene-d_8 (0.4 mL)

	D (10^{-9} $m^2 \cdot s^{-1}$)
IMes (free)	1.04
IMes (in presence of M_2)	1.05
M_2 (in presence of IMes)	1.68

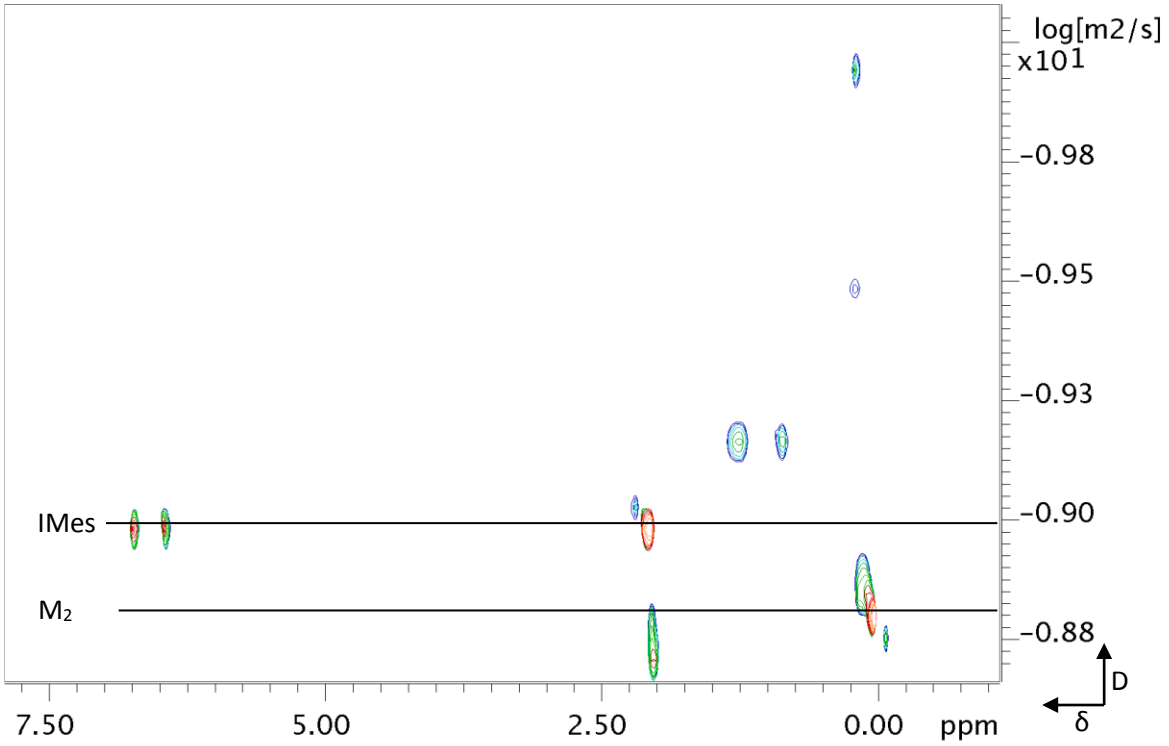


Figure 33: DOSY Spectrum – IMes (4b, 0.01 mmol) and M_2 (114, 0.02 mmol) in Toluene-d_8 (0.4 mL)

It should be noted that a number of extra and erroneous peaks were present in the data, as shown in Figure 32 and Figure 33, due to the automated peak-picking algorithm selecting low level noise within the baseline. These were not edited for the purposes of data integrity. The "true" peaks are those of high intensity which were readily identified by the red colouring.

The DOSY results presented above provided strong evidence that there was no spectroscopically observable interaction between NHCs and silicon species in solution at room temperature.

Conclusions

- Synthesis of an imidazol-2-one (**113**) from the reaction of IMes·HCl (**4·HCl**) with Cu_2O was successful, most likely proceeding *via* the formation of an oxygen-sensitive IMes·Cu intermediate. The imidazol-2-one (**113**) suffered from poor solubility in a number of solvents including THF-d_8 and C_6D_6, although the decomposition studies presented by Baceiredo and co-workers quantified the concentration of the imidazol-2-one and formamide in solution.[90]
- Quantitative analysis of the decomposition of ^{13}C-labelled IMes (***4b**) using ^{13}C NMR spectroscopy was not possible due to the generation of a number of unknown (intermediate) products.[5,16,89,90]
- IMe (**4a**) was synthesised *in situ* and the characteristic carbene resonance was observed by ^{13}C NMR spectroscopy. Although decomposition was observed to be affected by the presence of low molecular silicon species, conclusive spectroscopic evidence to corroborate an NHC·Si interaction could not be collected. This was further complicated by the rapid decomposition of IMe at ambient temperatures.
- IMes (**4b**) replaced the use of IMe (**4a**) given the increased stability of **4b** at room temperature though initial studies were limited by the poor signal-to-noise ratio of the characteristic carbene resonance ca. 220 ppm.
- The use of ^{13}C-labelled IMes (***4b**) greatly simplified the spectroscopic observation of the carbene moiety, although the use of varying mole ratios of silicon additives, and variable temperatures failed to provide conclusive evidence of a NHC·Si interaction by way of ^{13}C or ^{29}Si NMR spectroscopy. The small changes in shift observed in the ^{13}C NMR spectra could not be entirely attributed to temperature, nor could they be conclusively assigned to an NHC·Si interaction given the changes in shift observed by Nyulászi and co-workers in their titrations of IDipp with water.[89]
- Samples of IMes and a number of low molecular weight silicon species were analysed by DOSY with no conclusive evidence of an NHC·Si interaction.

2.4 Synthesis of 4,5-Disubstituted Imidazolium Salts

Given the lack of conclusive spectroscopic evidence reported in the previous chapter with the use IMes (**4b**) and a range of low molecular weight silicon species, it was apparent that the synthesis of NHCs of varying Lewis-basicity but of similar steric demand around the C2 position would be useful to probe the notion of an NHC·Si interaction based on a Lewis-base/acid interaction.[90] A more Lewis-basic NHC was expected to afford a stronger NHC·Si interaction given the proposed mechanism of interaction between an NHC and silicon species, as shown in Figure 12.[90]

Fully substituted imidazolium halides - those bearing substituents on the backbone positions - were of interest as the placement of electron-donating substituents on the backbone was reported to yield more Lewis-basic NHCs.[94] Although Arduengo and co-workers reported that chlorination of the backbone positions led to a mildly air-stable carbene in the case of IMe,[13] Hedrick and co-workers reported catalytic activity was severely reduced in the case of ROP of cyclic esters (**36**) by backbone chlorination, as shown in Figure 34.[66] While chlorine withdrew electron density through the σ-system which reduced the nucleophilicity of the carbene moiety, it donated electron density through the π-system which increases the relative energy of the carbene p_{π}-orbital and decreased electrophilic character. It was observed that "tuning" of the Lewis-basicity of an imidazol-2-ylidene would require careful balancing of the two competing effects.[66,94]

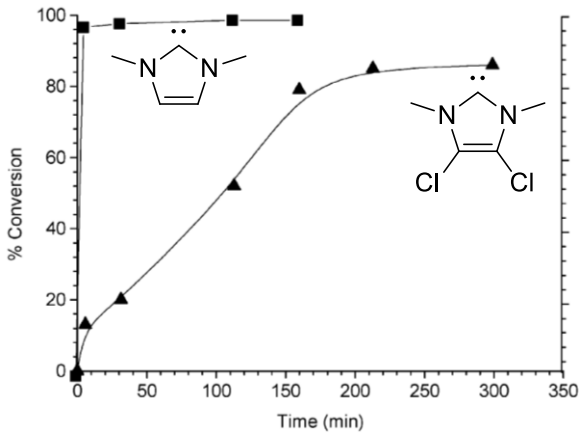
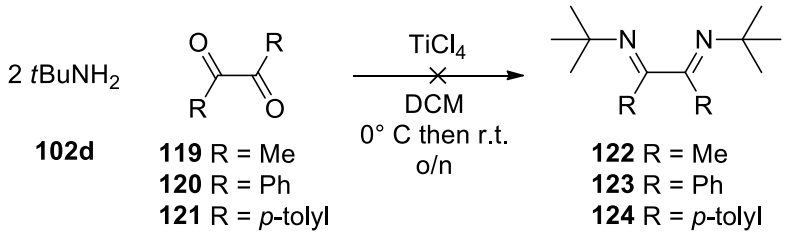


Figure 34: Effect of Backbone Chlorination in the ROP of Lactide - Conversion Versus Time Reported by Hedrick and Co-workers[66]

Initially, we wished to synthesise NHC precursors with methyl substituents on the backbone. Preliminary computational results (discussed later), indicated that backbone substitution with methyl groups could lead to a stronger NHC·Si interaction. Aryl substituents were also of interest given the possibility of "tuning" the electronics of the aryl ring by choice of ring-substituent.

2.4.1 Synthesis of Backbone-Substituted Diazabutadienes

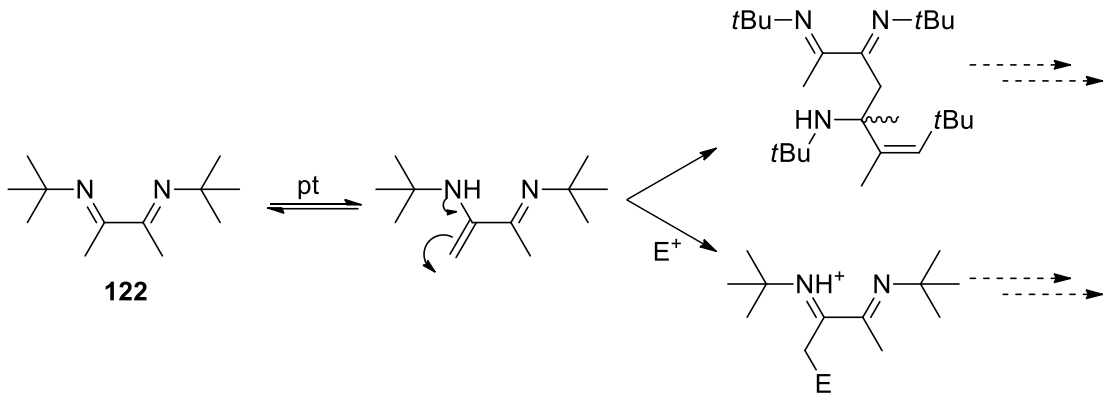
It was envisaged that a substituted I*t*Bu·HX salt could be formed by ring-closing of a diazabutadiene using paraformaldehyde (**103**) based on previous work described in Scheme 39.[12] Such a method was successful in the synthesis of IMes·HCl (**4b**), IDipp·HCl (**4c**), and ^{13}C-labelled IMes·HCl (***4b·HCl**). The construction of the diazabutadiene moiety was attempted as previously reported with reaction of 2 equivalents of *tert*-butyl amine (**102b**) with a suitable diketone (**119-121**) as shown in Scheme 53. $TiCl_4$ was used as a Lewis-acid to facilitate this reaction as described by de Kimpe and co-workers.[136] *Tert*-butyl amine (**102b**) was selected as it would have yielded *tert*-butyl *N*-substituents on the synthesised NHCs and precursors. Such substituents have been reported to lead to more Lewis-basic NHCs, in comparison to IMes (**4b**) and IDipp (**4c**).[88] Furthermore, the *tert*-butyl substituent had been shown to be more resilient to decomposition by oxygen and water.[16] It was envisaged that these properties could be exploited towards the formation of a stronger NHC·Si interaction that could therefore be characterised spectroscopically.



Scheme 53: Attempted Synthesis of 2,3-Disubstituted-1,4-diazabutadienes

Reaction of *tert*-butyl amine (**102d**) with butan-2-3-dione (**119**) yielded a dark solid on addition of $TiCl_4$ from which the expected product could not be isolated. ^{1}H NMR spectra of the crude product did not indicate the formation of the expected product (**122**). There existed the possibility that rapid

decomposition proceeded *via* enamine pathways as shown in Scheme 54, which would not have been available when **120** and **121** were used.

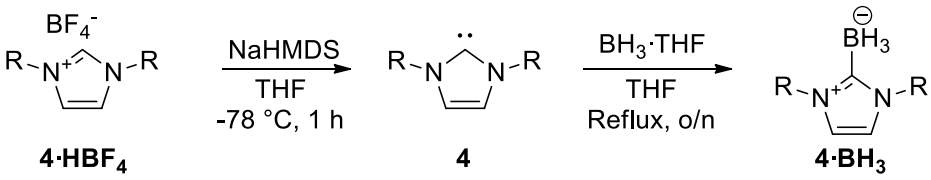


Scheme 54: Possible Decomposition Pathway of Butan-2,3-dione Derivatives

However, the reactions of *tert*-butyl amine (**102d**) with benzil (**120**), and *tert*-butyl amine (**102d**) with 1,2-di-*p*-tolylethane-1,2-dione (**121**) were also not successful with starting materials **120** and **121** recovered in 81% and 50%. ^{1}H NMR spectra of the crude product did not indicate the formation of the expected products (**123** and **124**).

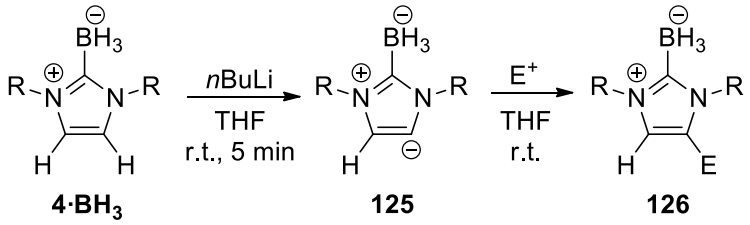
2.4.2 Backbone-Substitution *via* Ring-Lithiation of NHC·Borane Adducts

Literature procedures for the preparation of a range of NHC·Boranes starting from imidazolium salts such as **4a·HBF$_4$** as shown in Scheme 55, had been reported by Curran and co-workers.[30] The products (**4·BH$_3$**) were described as not being sensitive to air or moisture and easily handled which made purification undemanding.[30]



Scheme 55: Reported Synthesis of NHC·Boranes[30]

The isolation of the NHC·Boranes was of interest to us as Curran and co-workers had also reported that substitution of the backbone positions of an imidazolium ring was achieved by lithiation of an NHC·Borane followed by quenching with an electrophile as shown in Scheme 56.[137]



Scheme 56: Reported Ring Lithiation of NHC·Boranes[137]

Although a range of NHC·Boranes were successfully lithiated and quenched by Curran and co-workers, I*t*Bu·BH_3 (**4·BH_3**, R = *t*Bu) was not reported as one of those: the original work described only R = *i*Pr, Me, Dipp, Mes.[137]

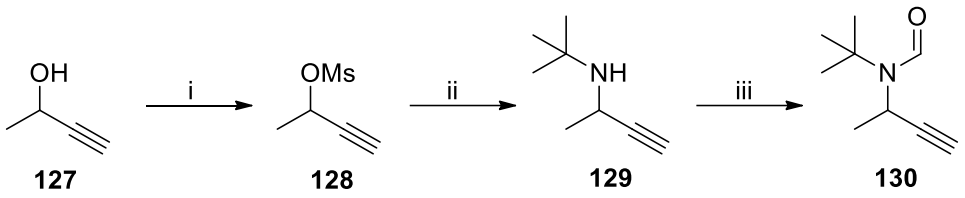
Efforts to lithiate and substitute the backbone positions of I*t*Bu·BH_3 (**4·BH_3**, R = *t*Bu) began with attempts to deuterate the backbone positions. Deprotonation of I*t*Bu·BH_3 (**4·BH_3**, R = *t*Bu) with *n*-BuLi and quenching with an electrophile (methyl iodide) was not successful with only starting material recovered (Scheme 56). Prolonging reaction times at room temperature also did not lead to the formation of the expected methyl-substituted product.

Milder deprotonation of the backbone position(s) with LDA at −78 °C followed by quenching with D_2O and MeOD were also unsuccessful; H-D and C-D couplings were not observed by ^{1}H and ^{13}C NMR spectroscopy respectively and only starting material was recovered. Prolonging reaction times and increasing reaction temperature led to decomposition of I*t*Bu·BH_3 (**4·BH_3**, R = *t*Bu). It was not ascertained why the reaction failed to yield the expected products.

2.4.3 Polyakova's Route - Backbone Substitution *via* a Formamide

César and co-workers reported that there were no published procedures for the substitution of backbone positions beginning from a substituted diazabutadiene as attempted above.[18] This was further acknowledged by Polyakova and co-workers in their synthesis of a backbone-substituted imidazolium salt *via* a formamide.[88]

Polyakova and co-workers[88] reported that but-3-yn-2-ol (**127**) was successfully transformed to the methanesulfonate (**128**). The mesylate (**128**) was then aminated with *tert*-butyl amine (**102d**) before *N*-formylation of the propargyl amine (**129**) afforded a formamide (**130**) as shown in Scheme 57.



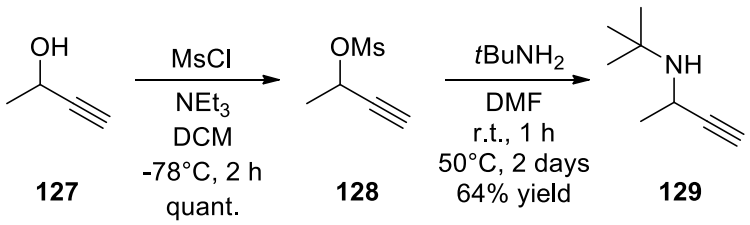
127 **128** **129** **130**

i) 1.5 eq MsCl, NEt_3, DCM ii) 3 eq *t*$BuNH_2$, DMF iii) 2 eq acetic formic anhydride, THF

Scheme 57: Reported Synthesis of a Formamide Substrate for Ring-closure[88]

It was reported that no purification was required for any of these transformations.[88] The formation of the imidazolium salt from the formamide (**130**) was conducted in a one-pot procedure but the discussion shall be left until later to allow for the analysis of *N*-formylation which proved troublesome at first.

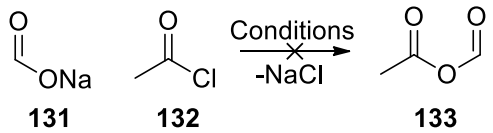
In our hands, mesylation of **127** proceeded quantitatively. Although Polyakova and co-workers reported that the product was isolated in 99% yield as yellow oil which could be used without further purification,[88] distillation of **127** yielded colourless oil. We found that distilling **127** under moderate vacuum allowed for cleaner reactions and afforded easier separations in later steps of the synthesis.



Scheme 58: Amination of a Propargylic Alcohol[88]

Amination of **128** with *tert*-butyl amine (**102d**) proceeded in 64% yield as shown in Scheme 58 c.f. 78% reported in the literature,[88] but *N*-formylation of **129** proved challenging. Polyakova and co-workers described the use of acetic formic anhydride (**133**) but did not detail the synthesis of this seemingly simple reactant.

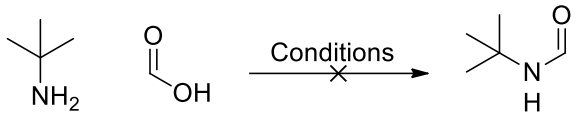
Literature syntheses of the mixed anhydride were capricious in our hands.[138,139] Many procedures relied on the reaction of sodium formate (**131**) with acetyl chloride (**132**). Typical examples, as shown in Scheme 59, differed in choice of solvent and reaction temperature. Little success was had in repeating these results.



i) Et_2O, T<27 °C, 6 h or ii) THF, 0 °C, 24 h

Scheme 59: Attempted Synthesis of a Mixed Anhydride[138,139]

Other methods to formylate **129** were sought. A report by Rao and co-workers stated that formylation could be achieved with formic acid (**134**) and $ZnCl_2$ as a Lewis-acid catalyst as shown in Scheme 60 (i).[140] Given that *tert*-butyl amine (**102d**) was reported to have been formylated by this method, an attempt was made to repeat the reported results. Even under a strictly anhydrous and inert atmosphere, with reaction overnight, the expected product (**135**) was not isolated.



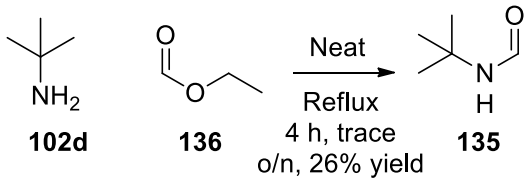
102d **134** **135**

i) $ZnCl_2$, 70 °C, 45 min or ii) Thiamine Hydrochloride, 80 °C, 40 min

Scheme 60: Literature Reported *N*-Formylations[140,141]

Thiamine hydrochloride was also reported to be an efficient catalyst by Hu and co-workers. However these results could not be repeated either (Scheme 60 (ii)).[141] In hindsight, the formation of *tert*-butyl ammonium formate on mixing of amine **102d** and formic acid **134** was unlikely to lead to any further reaction due to the formation of unreactive ammonium carboxylate salts in parallel to the direct reaction of a carboxylic acid and an amine to form an amide.

The use of ethyl formate (**136**) as a formylating agent under refluxing conditions was reported by Moffat and co-workers.[142] In our hands, heating **102d** and **136** at reflux for 4 hours led to a trace yield of the expected product (**135**) c.f. 29% yield reported in the literature.[142] Performing the reaction in a sealed tube overnight led to 26% yield (Scheme 61).

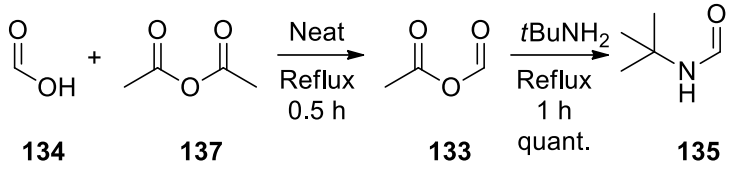


102d **136** **135**

Scheme 61: Ethyl Formate as a Formylating Agent[142]

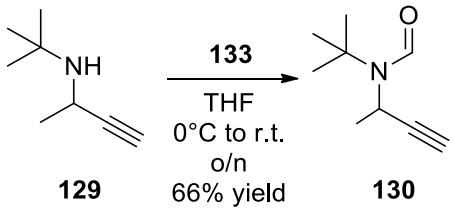
Drenth and co-workers reported that the use of 1.1 equivalents of ethyl formate (**136**) led to quantitative yields although this was not observed by us.[143] The use of additives such as *p*-TsOH and DMAP up to 20 mole% did not lead to a higher yield of product.

Preparing formyl acetate (**133**) *in situ* by heating acetic anhydride (**137**) with a slight excess of formic acid (**134**) at reflux allowed the successful formylation of *tert*-butyl amine (**102d**) (Scheme 62).[144]



Scheme 62: Formyl Acetate as a Formylating Agent

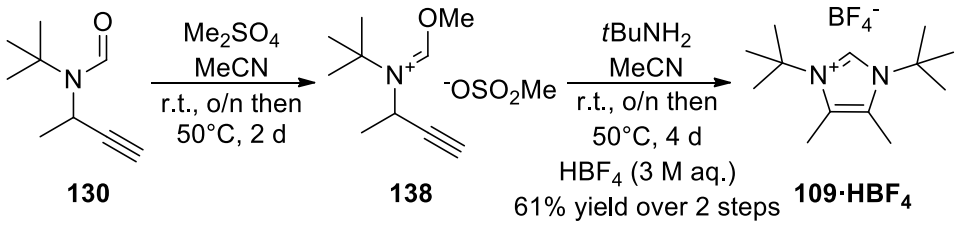
Heating of the reaction mixture was not required for conversion although elevated temperature allowed for a more rapid generation of the mixed anhydride (**133**). Furthermore, the presence of a slight excess of formic acid **134** and the by-product acetic acid did not appear to perturb the reaction as clean conversion of *tert*-butyl amine (**102d**) was observed. In common with Polyakova's method, **129** was formylated with 2 equivalents of formyl acetate (**133**) as shown in Scheme 63.



Scheme 63: Formylation of a Propargylic Amine[88]

2.4.4 Methylation of a Formamide and Ring-Closing

With the troublesome *N*-formylation completed, the ring-closing of **130** could proceed. As described by Polyakova and co-workers, the formamide (**130**) was methylated with dimethyl sulphate over the course of two days.[88] The salt **138** was not isolated but a one-pot ring-closing was instigated by the addition of an appropriate amine (Scheme 64). Off-white needles of the tetrafluoroborate salt (**109·HBF$_4$**) were isolated by washing the intermediate product with NaBF$_4$ (3 M in H$_2$O) and recrystallising the salt from DCM/EtOAc.

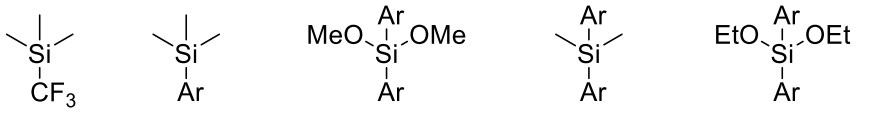


Scheme 64: Ring-Closing of a Formamide to Yield a Backbone-Substituted Imidazolium Salt[88]

Deprotonation of the imidazolium salt (**109·HBF$_4$**) with *t*BuOK (1 M in THF) in THF at −78 °C yielded the expected carbene Me$_2$I*t*Bu (**109**) as colourless oil in up to 80% yield. The characteristic carbene resonance was observed in the ^{13}C NMR spectrum at 212 ppm**Error! Reference source not found.**.

2.4.5 Me$_2$I*t*Bu and Lewis-Acidic Si Species

As NMR spectra of ^{13}C-labelled IMes (***4b**) and a variety of low molecular weight silicon species (**80** and **114-118**) measured at temperatures ranging from 298K to 198K had not provided definitive evidence of a NHC·Si interaction by ^{13}C or ^{29}Si NMR, more Lewis-acidic silicon species (e.g. those bearing pentafluorophenyl substituents) were studied (Figure 35).



139 **140** Ar = C_6F_5 **141** Ar = C_6F_5 **142** Ar = C_6F_5 **143** Ar = C_6F_5

Figure 35: Selection of Lewis Acidic Silanes Used for NMR Experiments

The NHC·Si interaction was proposed to be due to a Lewis base-Lewis acid interaction,[90] therefore increasing the Lewis-acidity of the silicon species, and/or increasing the Lewis-basicity of the NHC, should have favoured the formation of a stronger NHC·Si interaction. The commercially available silicon compounds shown in Figure 35 were chosen due to the presence of electron withdrawing substituents on silicon which were expected to increase Lewis-acidity of the silicon centre.[95,98] Me$_2$I*t*Bu (**109**) also replaced IMes (**4b**) as the NHC of study as the presence of methyl substituents on the backbone positions had been shown to increase Lewis-basicity in comparison to I*t*Bu by Polyakova and co-workers.[88]

Initial experiments with Me$_2$I*t*Bu (**109**, 0.02 mmol) and silanes **139-143** (0.10 mmol) were limited by the difficulties in accurately quantifying the mass of Me$_2$I*t*Bu (**109**) used given its low melting point and the non-cooled atmosphere of the glovebox. However, addition of **139-143** to Me$_2$I*t*Bu (**109**) in toluene-d_8 or THF-d_8 at r.t. led to the immediate formation of dark precipitates/oil. Solution phase

^{13}C NMR spectra were greatly affected by poor shimming of the samples due to the inhomogeneous solutions formed.

However, after settling of solids in toluene-d_8 samples, the free NHC was observed in the ^{13}C NMR spectra at 212 ppm and ^{29}Si NMR spectra indicated only the presence of the free silicon species. A ca. −70 ppm change in shift was not observed. Attempts to solvate the precipitates/oils by removal of toluene-d_8 under reduced pressure from NMR samples, followed by dilution with C_6H_5Cl afforded ^{13}C NMR spectra of the free NHC (**109**) at 204 ppm. A deuterium lock was afforded by a D_2O capillary: liquid D_2O was not in contact with the NMR sample. The precipitates and oils were not unambiguously identified. Furthermore, solution phase NMR spectra did not provide conclusive evidence of an NHC·Si interaction.

Given that previous experiments had been conducted with less Lewis-basic IMes (**4b**), NMR samples of IMes (**4b**, 0.01 mmol), in place of Me_2ItBu 1**09,** and **139-143** were prepared**.** Solution phase NMR data which were indicative of residual IMes (**4b**) or of IMes·Si species in solution were collected, though in some cases, a characteristic C2 NMR shift could not be observed (Table 13).

Table 13: ^{13}C and ^{29}Si NMR Shifts on Addition of Si Species (0.1 mmol unless Otherwise Stated) to IMes (0.01 mmol) in Toluene-d_8 (0.4 mL) or THF-d_8 (0.4 mL)

	^{13}C δ (ppm)		^{29}Si δ (ppm)	
	Toluene-d_8	THF-d_8	Toluene-d_8	THF-d_8
Me_3SiCF_3	220 & 223	-	33 & 30	3
$(C_6F_5)SiMe_3$	- (0.05 mmol Si)	216	33 & 30 (0.05 mmol Si)	-
$(C_6F_5)_2Si(OMe)_2$	220 (0.01 mmol Si)	-	- (0.01 mmol Si)	−89
$Ph_2Si(OEt)_2$	220	219	-	

Dark oil formed on the addition of **139** (0.1 mmol) to IMes (**4b**, 0.01 mmol) in toluene-d_8 or THF-d_8 (0.4 mL), while dark precipitates formed on addition of **140** or **141** to IMes (**4b**, 0.01 mmol) in toluene-d_8 or THF-d_8 (0.4 mL). Addition of **143** to IMes (**4b**, 0.01 mmol) in toluene-d_8 or THF-d_8 (0.4 mL) did not lead to the formation of precipitates or oil. ^{13}C and ^{29}Si NMR spectra did not provide evidence of an NHC·Si interaction (Table 13). For example, the ^{13}C NMR spectrum of **141** (0.01 mmol) and IMes (0.01 mmol) in toluene-d_8 (0.4 mL) indicated a lack of change in the C2 resonance (Figure 36).

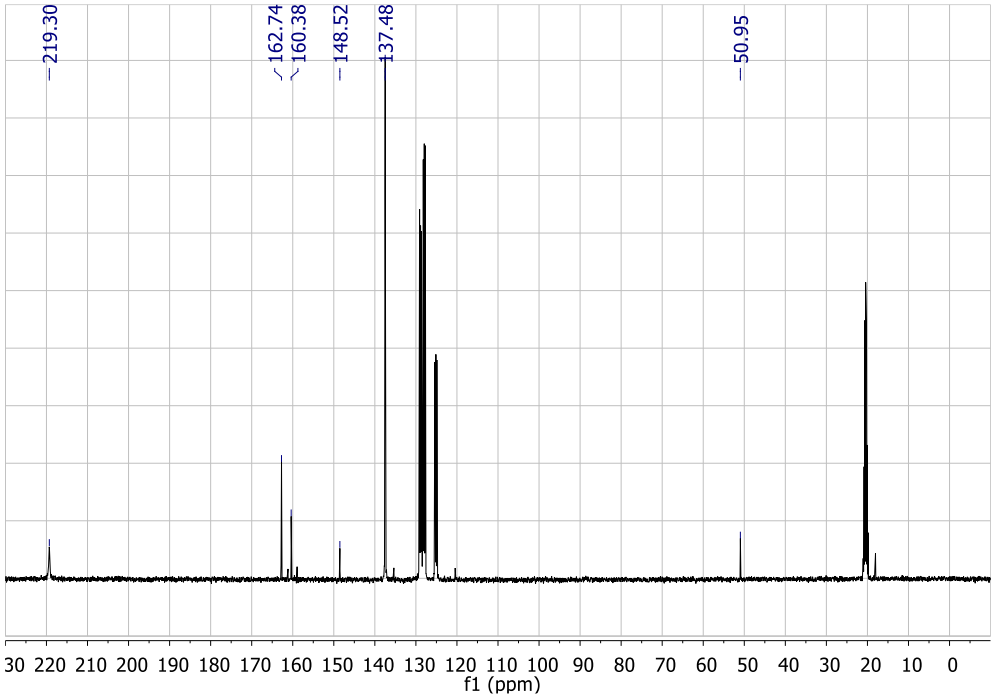
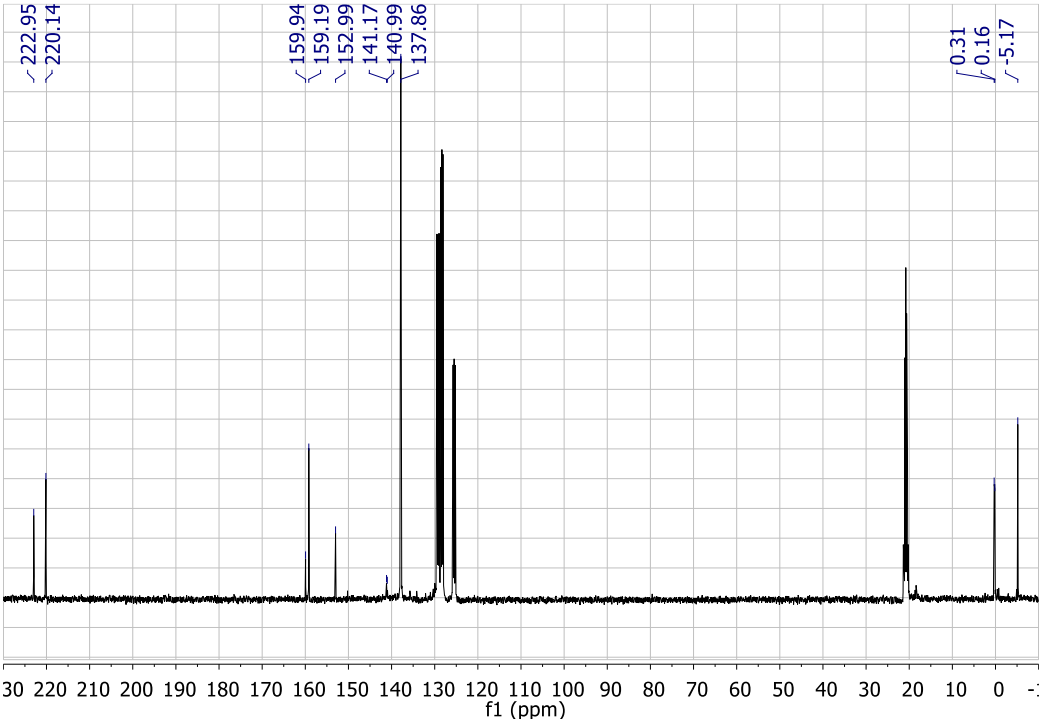


Figure 36: ^{13}C NMR Spectrum of IMes and $(MeO)_2Si(C_6F_5)_2$ in Toluene-d_8 at Room Temperature

It was observed that Me_3SiCF_3 (**139**) and $(C_6F_5)SiMe_3$ (**140**) in toluene-d_8 led to the anomalous splitting of the IMes (**4b**) C2 resonance in the ^{13}C NMR spectrum and a similar splitting was observed in the ^{29}Si spectrum as shown in Figure 37 (a) and (b). However, these resonances were not indicative of the formation of a pentacoordinate silicon species given the minimal change in shift.[32,95,107,111]

It must be stressed that the precipitates formed in these experiments were not characterised due to the inability to dissolve them in a range of solvents. In many cases, the dark precipitates formed immediately on addition of the Si species to a solution of IMes (**4b**) in THF-d_8 or toluene-d_8. Toluene-d_8 at 398 K, DCM-d_2, 1,2-difluorobenzene, and C_6H_5Cl with D_2O lock were all unable to dissolve sufficient amounts of the solids to allow for characterisation by ^1H NMR.

a)



b)

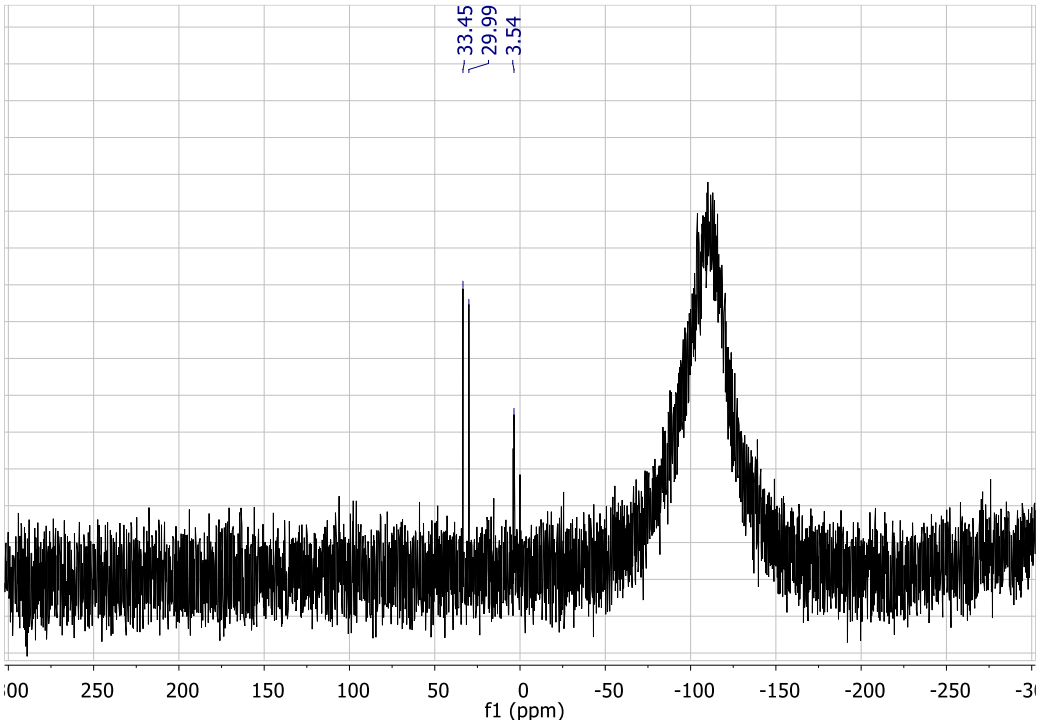


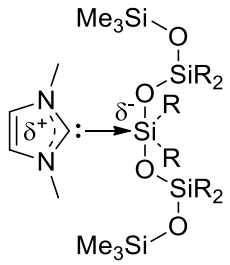
Figure 37: ^{13}C (a), and ^{29}Si (b) NMR Spectra of IMes and Me_3SiCF_3 in Toluene-d_8 at Room Temperature

Conclusions

- Substitution of NHC backbone positions with chlorine had been shown to lead to reactivity differences in NHCs, most likely due to altered electronics leading to changes in Lewis-acidity/basicity.[66,94]
- The extension of the modular routes (described previously) towards the synthesis of backbone-substituted imidazolium salts was not successful.
- I*t*Bu·BH_3 was synthesised and was readily handled under aerobic conditions. However, ring-lithiation and electrophilic substitution of the backbone positions as reported by Curran and co-workers was not successful in our hands.[137] Prolonging the reaction time, the use of LDA as well as *n*-BuLi as base, and the variation of temperature did not allow for electrophilic substitution of the backbone positions.
- The synthesis of 1,3-bis(*tert*-butyl)-4,5-disubstituted imidazol-2-ylidene (**109**) was achieved by Polyakova and co-workers.[88] *N*-Formylation using ethyl formate at elevated temperatures with or without nucleophilic catalysts,[142,143] or formic acid and catalytic $ZnCl_2$, or formic acid and catalytic thiamine hydrochloride, were unsuccessful.[140,141] Though the methodology suffered from numerous synthetic steps and long reaction, it assured the synthesis of Me_2I*t*Bu·HBF_4 (**109·HBF_4**).
- The use of more Lewis-acidic silicon species with Me_2I*t*Bu, a more Lewis-basic NHC, led to the formation of dark precipitates/oils that were poorly soluble in a range of solvents. The precipitates/oils were not successfully characterised. NMR spectra of the remaining solutions indicated only the presence of free Me_2I*t*Bu and or free silicon species with no apparent change in the ^{13}C or ^{29}Si NMR shifts indicative of an NHC·Si interaction.
- A less Lewis-basic NHC, IMes (**4b**), was used with the more Lewis-acidic silicon species but ^{13}C and ^{21}Si NMR spectra again yielded no evidence of an NHC·Si interaction.
- Spectroscopic techniques have so far been unable to prove the existence of NHC·Si interactions for a number of NHCs and silicon species and room and reduced temperatures.

3. Computational Modelling of an NHC·Si Interaction

Given that extensive use of NMR spectroscopy had failed to provide conclusive evidence of an NHC-Si interaction for a number of low molecular weight silicon species (Figure 26), it was appropriate to further analyse the computational work of Baceiredo and co-workers.[90] The original work of Baceiredo and co-workers limited the computational modelling to a single NHC, IMe (**4a**) interacting with 2 silicone oligomers as shown in Figure 38 (where R was methyl or phenyl).[90] Silicones with further/different substitution, and low molecular weight silicon species of varying Lewis-acidity were not modelled despite the postulated nature of the interaction.[90] Furthermore, the chosen NHC, IMe (**4a**) was reported to be unstable at room temperature even under an inert atmosphere.[5]



79

Figure 38: NHC·Si System as Modelled by Baceiredo and Co-workers[90]

IMe (**4a**) was commonly used as a simple model of an imidazol-2-ylidene in the computational literature surrounding NHCs,[90,115,120] however, IMes (**4b**), IDipp (**4c**), and I*t*Bu (**4d**) were more realistic (sterically demanding) models of NHCs used in organocatalysis.[39–44]

3.1 Electronic Energy of Interactions

Given that computational results for NHC·$SiCl_4$ compounds were available in the literature,[111,115,120] these simulations were revisited to first validate our methodology, prior to expanding on the work of Baceiredo and co-workers.[90] The interaction energies were calculated as the electronic energy of the bound NHC·$SiCl_4$ species less that of the unbound NHC and $SiCl_4$ with corrections made for zero-point valence energy as shown in Equation 1.

$$E_{\text{int}} = E(NHC \cdot Si) + ZPVE(NHC \cdot Si) - \{E(NHC) + E(Si)\} - \{ZPVE(NHC) + ZPVE(Si)\}$$

Equation 1: Calculation of Electronic Energy of Interaction

3.1.1 NHC·$SiCl_4$ - B3LYP/6-311+G(d,p)

A number of theories and basis sets were evaluated by us in order to judge their suitability in modelling NHC·Si interactions. To begin with, the structures of several NHCs were optimised at the B3LYP/6-311+G(d,p) level[145–150] in analogy to Baceiredo and co-workers[90] at the B3LYP/6-31+G(d) level.[151–155] The choice of a larger basis set was to minimise the possibility of poor estimates of interaction energy due to basis-set superposition error.[156,157]

By conducting counterpoise calculations,[156,157] corrections for basis-set superposition error (BSSE) were made (Table 14). Use of the counterpoise method, in which the basis of the other fragment (without nuclei or electrons i.e. ghost atoms), allowed BSSE to be estimated by permitting a fragment's electrons to occupy the orbitals of the other fragment. Calculated BSSE would then be an indication of how suitable (sufficiently large) a basis-set was. Indeed, our results at the B3LYP/6-311+G(d,p) level indicated that BSSE accounted for up to 40% of the interaction energy of IMe·$SiCl_4$, as shown in Table 14.

Table 14: BSSE-Corrected Interaction Energies of NHC·$SiCl_4$ Complexes (kcal·mol^{-1})

	E(·10^{-3} kcal·mol^{-1})	ZPVE	E_{Int}	BSSE	E_{Corr}
IMe·$SiCl_4$	−1528.3	+85.6	−10.6	+4.4	−6.3
IMes·$SiCl_4$	−1916.7	+257.6	+56.6	+11.4	+68.1
IDipp·$SiCl_4$	−2064.7	+368.4	+84.8	+12.1	+96.9
I*t*Bu·$SiCl_4$	−1676.3	+191.0	+17.5	+5.6	+23.1
Me_2IMe·$SiCl_4$	−1577.7	+120.3	−12.3	+4.6	−7.7
Me_2ItBu·$SiCl_4$	−1725.7	+225.9	+15.5	+6.3	+21.8

The uncorrected (for BSSE) result for IMe·$SiCl_4$, as shown in Table 14, matched the value reported by Robinson and co-workers[111] at −10.6 kcal·mol^{-1} (ca. −44 kJ·mol^{-1}). Although the result for Me_2IMe, which differed only by substitution of the backbone positions with methyl groups, appeared to indicate a more thermodynamically favoured interaction of −7.7 kcal·mol^{-1} (−32 kJ·mol^{-1}) versus −6.3 kcal·mol^{-1} (−26 kJ·mol^{-1}),such small energy differences are within the errors of DFT.[158–162] A similar result was observed between I*t*Bu·$SiCl_4$ and Me_2I*t*Bu·$SiCl_4$ as shown in Table 14. Robinson and co-workers did not comment on or account for BSSE which our calculations predicted would dominate ca. 40% of the interaction energy as shown in Table 14.

Correcting for BSSE led to a reduction of the predicted interaction energy to −6.3 kcal·mol^{-1} (−26 kJ·mol^{-1}) which called into question the validity of the uncorrected results: empirically, results should be treated with caution if BSSE exceeds ca. 15% of the uncorrected energy. The magnitude of the error therefore posed uncertainty over the suitability of the level of theory/size of basis-set used.

In comparison with our result of −6.3 kcal·mol^{-1} (−26 kJ·mol^{-1}), the BSSE-corrected value reported by Hollóczki and Nyulászi was −8.2 kcal·mol^{-1} (−34 kJ·mol^{-1}).[115] The minor difference between the two predicted values could be due to small differences in the optimised structures: Hollóczki and Nyulászi calculated the energies using structures optimised at the B3LYP/6-31G(d) level,[115] whereas our results were based on structures optimised at the B3LYP/6-311+G(d,p) level.[145–150]

The interaction energies for larger and more sterically demanding systems such as IMes (**4b**) and IDipp (**4c**), as shown in Table 14, appeared to indicate that such complexes were not thermodynamically favoured in the gas phase. However, IMes·$SiCl_4$ and IDipp·$SiCl_4$ were isolated as solids and characterised in solution by ^{1}H, ^{13}C, and ^{29}Si NMR spectroscopy:[111] B3LYP/6-311+G(d,p) was therefore unable to accurately calculate the interaction energies for NHCs bearing bulky *N*-substituents.

3.1.2 IMe·PDMS - B3LYP/6-311+G(d,p)

Given the poor results at the B3LYP/6-311+G(d,p) level for NHC·$SiCl_4$ complexes when BSSE were accounted for, the NHC·Si interaction reported by Baceiredo and co-workers, with respect to silicone oligomers,[90] was further investigated.

Calculations showed that the interaction energy of IMe·PDMS (**79**) as shown in Figure 38, where R = methyl, was +16 kcal·mol^{-1} (+67 kJ·mol^{-1}) at the B3LYP/6-311+G(d,p) level i.e. the proposed NHC·Si interaction between an NHC and a silicone oligomer was not predicted to be favoured which was in contrast to the conclusions of Baceiredo and co-workers at the MP2/6-31+G(d)//B3LYP/6-31+G(d) level.[90] The modelling of larger more sterically demanding NHCs such as IMes (**4b**) and IDipp (**4c**) with silicone oligomers was not undertaken given the above result.

3.1.3 NHC·$SiCl_4$ - MP2/6-311+G(d,p)//B3LYP/6-311+G(d,p)

Given that B3LYP-optimised geometries were generally considered good estimates of structure,[161] the single-point energies of NHC·$SiCl_4$ complexes were re-evaluated at the MP2/6-311+G(d,p)//B3LYP/6-311+G(d,p)+ZPVE level to ascertain the suitability of this approach in calculating NHC·Si interactions of NHCs with silicone oligomers. An *ab-initio* method, MP2 has been reported to be more accurate in accounting for electron correlation (and dispersion effects), and exchange. However, it was computationally more expensive.[163–166] Although dispersive effects could have affected large complexes such as NHC·PDMS, where intermolecular interactions were predicted to be weak, this was not initially considered given the reports in literature that were based upon results at B3LYP.[90,115]

Table 15: Energies of NHC·$SiCl_4$ Complexes at the MP2/6-311+G(d,p)//B3LYP/6-311+G(d,p) Level (kcal·mol^{-1})

	$E_{electronic}$	ZPVE	$E_{interaction}$
IMe·$SiCl_4$	−1525986.86	85.57	−23.0
IMes·$SiCl_4$	−1913560.14	257.61	−21.9
IDipp·$SiCl_4$	−2061105.36	368.36	−1.9

The results, as shown in

Table 15, indicated that single-point energies at the MP2/6-311+G(d,p)//B3LYP/6-311+G(d,p) level corrected the apparent flaws in the evaluation of electronic energy at the B3LYP/6-311+G(d,p) (even before corrections for BSSE): the formation of the sterically demanding IMes·$SiCl_4$ and IDipp·$SiCl_4$ complexes published in the literature were predicted to be favoured.[107,111]

3.1.4 NHC·Si - MP2/6-311+G(d,p)//B3LYP/6-311+G(d,p)

Given the qualitatively correct results predicted for the NHC·$SiCl_4$ complexes presented above, the methodology was expanded to include the silicone oligomers reported by Baceiredo and co-workers.[90]

Table 16: MP2 Single-Point Energies of NHC·Si Compounds with Structures Optimised at B3LYP (kcal·mol^{-1})

	$E_{electronic}$	ZPVE	$E_{Interaction}$
IMe·PDMS	−1123254.08	279.73	0.0
Me_2IMe·PDMS	−1172456.66	314.38	−3.6

The original result reported by Baceiredo and co-workers for IMe·PDMS at the MP2/6-311+G(d)//B3LYP/6-31+G(d) level indicated an interaction energy of roughly −(3–5) kcal·mol^{-1} (ca. 13–21 kJ·mol^{-1}), but our results indicated a weaker interaction, as shown in Table 16. Indeed, the result for IMe·PDMS called into question the notion of an NHC·Si interaction. More sterically demanding NHCs were not modelled given the poor results with IMe (**4a**).

It should be noted that electronic energies with zero-point valence energies were presented above to allow a direct comparison to data available in the literature.[90,111,115,120] However, the above complexes would only form if calculated Gibbs free energy of the reaction was less than 0.

3.2 Gibbs Free Energy of Interaction - B3LYP/6-311+G(d,p)

Therefore, the above results were extended by consideration of Gibbs free energies rather than electronic energies (and zero-point valence energy). Initially, interaction energies were estimated at

the B3LYP/6-311+G(d,p) level as a first approximation. The interaction energies of NHC·Si complexes were calculated as the difference in the Gibbs free energies of the final and initial species. BSSEs were calculated using the counterpoise method and corrected interaction energies were calculated as shown in Equation 2 c.f. Equation 1 for the calculation of electronic energies.

$$E_{\text{int}} = E_G(NHC \cdot Si) - \{E_G(NHC) + E_G(Si)\}$$

Equation 2: Calculation of Gibbs Energy of Interaction

The use of Gibbs free energy was considered to be more meaningful, given the entropic effects of forming an NHC·Si complex, especially for the sterically more demanding IMes (**4b**) and IDipp (**4c**) systems.

$$\Delta G = \Delta H - T\Delta S$$

Equation 3: Definition of Gibbs Energy in Terms of Enthalpy and Entropy

From the definition of Gibbs free energy, as shown in Equation 3, it was observed that tuning of the NHC·Si interaction strength (ΔG) by manipulation of the entropic term through temperature was possible. Indeed, attempts to exploit this were described in Chapter 2.3.6

It was already established in the literature that B3LYP was unable to account for dispersion interactions,[167–172] though theories such as B97D[173] were able to add empirical corrections for dispersion while treatment of electron correlation at the MP2 level was able to capture dispersion effects.[163–166] Given the computational expense of MP2, geometry optimisations were not conducted at this level of theory. Instead, Gibbs free energies of the unbound NHCs and of the free silicon species in the gas-phase were calculated at the B3LYP/6-311+G(d,p) level, as shown in Table 17.

Table 17: Energies of Free NHCs and Silicon Species at B3LYP/6-311+G(d,p) (Hartree)

	Gibbs Free Energy
IH	−226.2

IMe	−304.8
I*t*Bu	−540.6
IMes	−924.1
IDipp	−1160
Me_2IMe	−383.4
Me_2I*t*Bu	−619.2
$SiCl_4$	−2131
PDMS	−1489

The Gibbs free energies of interaction (corrected for BSSE) for a number of NHC·$SiCl_4$ complexes were calculated and it was shown that structures and energies evaluated at the B3LYP/6-311+G(d,p) level were greater than 0, as shown in

Table 18. The implication was that although electronic energies were favourable, the Gibbs free energy predicted that the formation of NHC·$SiCl_4$ complexes was not favoured at room temperature. This contradicted experimental data though was not surprising given the poor results described above with respect to electronic energies. It was therefore likely that structures and Gibbs free energies calculated at the B3LYP/6-311+G(d,p) level would be inaccurate in the description of the NHC·Si systems described by Baceiredo and co-workers.[90]

Table 18: Interaction Energies of NHCs and $SiCl_4$ at the B3LYP/6-311+G(d,p) Level (kcal·mol^{-1})

	E_G	E_{int}	E_{corr}
IH·$SiCl_4$	−2356.84	−1.59	+2.34
IMe·$SiCl_4$	−2435.42	+4.07	+8.45
I*t*Bu·$SiCl_4$	−2671.17	+34.6	+40.3
IMes·$SiCl_4$	−3054.69	+339	+350
IDipp·$SiCl_4$	−3289.73	+444	+457
Me_2IMe·$SiCl_4$	−2514.03	+2.14	+6.71
Me_2I*t*Bu·$SiCl_4$	−2749.76	+32.4	+38.7

NHC·Si interaction energies were recalculated and predicted that the interactions were strongly disfavoured, as shown in Table 19. Furthermore, the substitution of backbone positions with methyl groups had little effect on the interaction energy (c.f. IMe·PDMS and Me_2IMe·PDMS).

Table 19: Interaction Energies of NHCs and PDMS at the B3LYP/6-311+G(d,p) Level (kcal·mol^{-1})

	E_G	E_{int}	E_{corr}
IMe·PDMS	−1793.79	+31.9	+33.8
I*t*Bu·PDMS	−2029.54	+63.0	+65.8
Me_2IMe·PDMS	−1872.40	+30.2	+32.3

It was observed that BSSE was of a smaller magnitude for NHC·PDMS systems, as shown in Table 19, than in the case of NHC·$SiCl_4$ systems, as shown in

Table 18. I.e. the "artificial" stabilisation of a complex would have been greater in modelled NHC·$SiCl_4$ systems than in the NHC·PDMS systems. It was now apparent that there was a failure of the method and/or basis set to correctly predict interaction energies of the systems we were investigating, or that the proposed NHC·Si interaction was not favoured. Results for IMes and IDipp were not sought for Table 19 in light of the data which already precluded an interaction for small NHCs (IMe and Me_2IMe).

3.2.1 MP2/aug-cc-pVTZ//B3LYP/6-311+G(d,p)

Given that results now indicated that an NHC·Si interaction was not predicted to occur, which was in contrast with the conclusions of Baceiredo and co-workers,[90] and because B3LYP was unable to capture the effects of dispersion,[167–172] single-point energies were calculated at MP2 with the aug-cc-pVTZ basis set[174–176] such that an improved estimate of E_{int} could be calculated. Although electronic energies predicted the favourable formation of NHC·$SiCl_4$ complexes at the MP2/6-311+G(d,p)//B3LYP/6-311+G(d,p) level, estimates of Gibbs free energies at the MP2/6-311+G(d,p)//B3LYP/6-311+G(d,p) level were quantitatively incorrect as they predicted that formation of NHC·$SiCl_4$ complexes was not favoured at room temperature whereas experimental data proved otherwise.[111]

Table 20: Comparison of E_{corr} and E_{int} of NHCs and $SiCl_4$ Structures Optimised at the B3LYP/6-311+G(d,p) Level (kcal·mol^{-1})

	B3LYP/6-311+G(d,p)	MP2/aug-cc-pVTZ
IH·$SiCl_4$	+2.34	−24.2
IMe·$SiCl_4$	+8.45	−23.0
I*t*Bu·$SiCl_4$	+40.3	−2.05
IMes·$SiCl_4$	+21.4	−18.0
IDipp·$SiCl_4$	+457	+3.57
Me_2IMe·$SiCl_4$	+6.71	−25.8

$Me_2ItBu{\cdot}SiCl_4$	+38.7	−10.6

Although the energies calculated at the MP2/aug-cc-pVTZ//B3LYP/6-311+G(d,p) level were not corrected for BSSE, the results differed greatly to energies calculated at the B3LYP/6-311+G(d,p) level, as shown in Table 20. Single-point energies calculated at MP2/aug-cc-pVTZ//B3LYP/6-311+G(d,p) correctly predicted the formation of NHC·$SiCl_4$ complexes except for the case of IDipp·$SiCl_4$.

Table 21: Comparison of E_{corr} and E_{int} of NHCs and PDMS Structures Optimised at the B3LYP/6-311+G(d,p) Level

	B3LYP/6-311+G(d,p)	MP2/aug-cc-pVTZ
IMe·PDMS	+33.8	−0.03
I*t*Bu·PDMS	+65.8	+18.4
Me_2IMe·PDMS	+32.3	−3.56

Extending these calculations to include NHC·PDMS models indicated that although Gibbs free energies calculated at MP2/aug-cc-pVTZ//B3LYP/6-311+G(d,p) predicted a more favourable interaction compared to energies calculated B3LYP/6-311+G(d,p), as shown in Table 21, an NHC·Si interaction between I*t*Bu and PDMS was not favoured at +18.4 kcal·mol^{-1} (+77.0 kJ·mol^{-1}). This was in contrast to the report of Baceiredo and co-workers which stated that the protection of NHCs from decomposition were due to such an NHC·Si interaction.[90]

3.2.2 MP2/aug-cc-pVTZ//B97D/6-311+G(d,p)

It was therefore considered of utmost importance to ascertain whether the structures of NHC·Si complexes were affected by dispersion effects which had so far been ignored. Although energies were calculated at the MP2 level which was better able to account for dispersion effects than B3LYP due to its better handling of electron correlation,[163–166] the structures were optimised at B3LYP and dispersion effects would have been ignored in calculating geometry. While geometry optimisations

could have been performed at MP2, this would have been computationally expensive. Therefore, structures were optimised at the B97D level which has been reported as a DFT method able to empirically account for dispersion.[173]

Gibbs free energies corrected for BSSE at the B97D/6-311+G(d,p) level and at the MP2/aug-cc-pVTZ//B97D/6-311+G(d,p) level were calculated, as shown in Table 22, with the results of previous calculations using B3LYP structures included for comparison. NHC·$SiCl_4$ systems were again used as a benchmark given that their formation has been reported.[107,111]

Table 22: Comparison of Structural Differences Between B3LYP and B97D

	B3LYP Structures		B97D Structures	
	B3LYP/6-311+G(d,p)	MP2/aug-cc-pVTZ	B97D/6-311+G(d,p)	MP2/aug-cc-pVTZ
IH·$SiCl_4$	+2.34	−24.2	−0.371	−27.8
IMe·$SiCl_4$	+8.45	−23.0	+2.24	−24.4
I*t*Bu·$SiCl_4$	+40.3	−2.05	+29.1	-
IMes·$SiCl_4$	+21.4	−18.0	+4.40	-
IDipp·$SiCl_4$	+457	+3.57	+28.6	-
Me_2IMe$SiCl_4$	+6.71	−25.8	+0.01	−26.3
Me_2I*t*Bu·$SiCl_4$	+38.7	−10.6	+23.8	-

Results, as shown in Table 22, indicated that although B97D geometries and energies (Column 4) were an improvement upon B3LYP geometries and energies (Column 2), they were still inadequate in predicting the change in Gibbs free energy for NHC·$SiCl_4$ complexes. The latter point is apparent in the difference between data in columns 4 and 5 which showed that significant improvements could be made by accounting for electron correlation (dispersion) using an *ab-initio* method (MP2) compared with empirical methods (B97D).

Table 23: Comparison of E_{corr} and E_{int} of NHCs and PDMS Structures Optimised at B97D/6-311+G(d,p)

	B3LYP Structures		B97D Structures	
	B3LYP/6-311+G(d,p)	MP2/aug-cc-pVTZ	B97D/6-311+G(d,p)	MP2/aug-cc-pVTZ
IMe·PDMS	+33.8	-0.03	+0.02	+0.02

Extending these calculations to include IMe·PDMS indicated that the proposed NHC·Si interaction based on Gibbs free energies calculated at MP2/aug-cc-pVTZ//B97D/6-311+G(d,p) was not favoured, as shown in Table 23. This was again in contrast to the computational results presented by Baceiredo and co-workers.[90] Calculations of IMes·PDMS and I*t*Bu·PDMS failed to converge at the MP2/aug-cc-pVTZ//B97D/6-311+G(d,p) level although given our results reported above, and the increased steric bulk of IMes (**4b**) and IDipp (**4c**), the Gibbs free energies of the sterically more demanding NHCs were unlikely to be more favourable than that for the IMe·PDMS model.

Conclusions

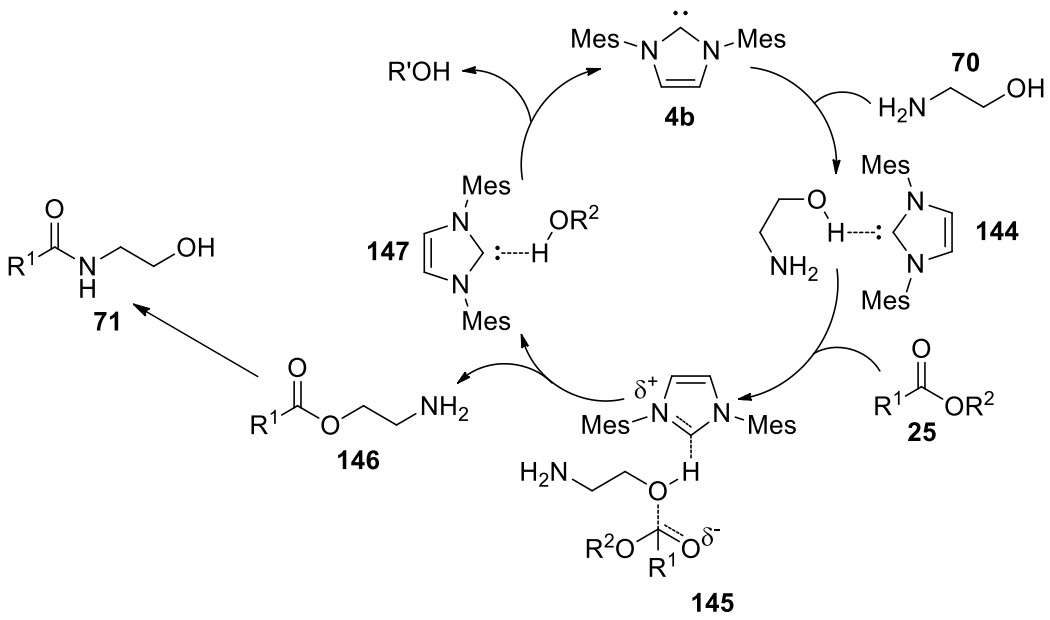
- The data presented by Baceiredo and co-workers were based upon electronic energies rather than Gibbs free energies.[90] Gibbs free energy corrections would have been available to Baceiredo and co-workers as a result of frequency calculations undertaken by themselves, yet electronic energies were used. Electronic energies gave no indication as to whether the formation of the complexes at room temperature was thermodynamically favoured.
- B3LYP/6-31+G(d) was unsuitable for the calculation of energies for the systems under investigation as dispersion greatly affected the calculated energies. Dispersion had a lesser effect on the optimised geometries of the compounds modelled.
- B3LYP (or B97D) provided good estimates of geometry for single-point energy calculations at MP2.
- Geometries and electronic energies calculated at B3LYP/6-311+G(d,p) did not correctly predict the favourable formation of NHC·$SiCl_4$ complexes at room temperature. Furthermore, the use of a larger basis-set in estimating NHC·PDMS interaction energies predicted an unfavourable interaction in contrast to the results of Baceiredo and co-workers.[90]
- Single-point energies calculated at MP2/6-311+G(d,p) using the above B3LYP/6-311+G(d,p) geometries led to the prediction of the formation of NHC·$SiCl_4$ complexes at room temperature but did not predict a favourable NHC·Si interaction for IMe·PDMS.
- Given that the above calculations did not account for entropic effects, Gibbs free energies were calculated at B3LYP/6-311+G(d,p). The formation of NHC·$SiCl_4$ complexes and IMe·PDMS were not predicted to be favoured. Calculation of single-point energies at MP2/aug-cc-pVTZ indicated that the formation of NHC·$SiCl_4$ complexes was predicted to be thermodynamically favoured, though an I*t*Bu·PDMS interaction was estimated at ca. +18 kcal·mol^{-1} (+75 kJ·mol^{-1}). Although earlier calculations at MP2 utilised a Pople basis-set (6-311+G(d,p), this was to allow comparison of our results to literature reports.[90,107,111,115,120]

Dunning (Huzinaga) basis-sets such as aug-cc-pVTZ[174–176] are considered more appropriate for post-HF methods such as MP2.[163–166]

- Optimisation structures and calculations of Gibbs free energies at B97D (which empirically corrects dispersion) 6-311+G(d,p)predicted the formation of NHC·$SiCl_4$ complexes but did not favour the formation of IMe·PDMS. Similar results were observed with single-point energies calculated at MP2/aug-cc-pVTZ using the above structures.
- Electronic energies at MP2/6-311+G(d,p)//B3LYP/6-311+G(d,p) along with Gibbs free energies at MP2/aug-cc-pVTZ//B3LYP/6-311+G(d,p), B97D/6-311+G(d,p), and MP2/aug-cc-pVTZ//B97D/6-311+G(d,p) correctly predict the formation of NHC·$SiCl_4$ complexes but do not predict the formation of NHC·PDMS complexes in the gas phase. The role of solvation had not been considered in the literature or by us.[90,115,120]

4. Reaction Kinetics: NHC-Catalysed Reactions

Given the lack of ^{1}H, ^{13}C, and ^{29}Si NMR data at variable temperature, and DOSY NMR data at room temperature, and a lack of computational evidence to support an NHC·Si interaction, analysis of reaction kinetics was undertaken as it was reasoned that an NHC·Si interaction would lead to diminished rates in an NHC-catalysed reaction. Prior to the use of React-IR to gather kinetic data *in situ*, several small scale NHC-catalysed reactions were carried out with measurements made *ex situ* in order to probe the mechanism of NHC-catalysed reactions given that the role of NHCs (as bases or as nucleophiles, for example) was disputed.[61–63,67–72]



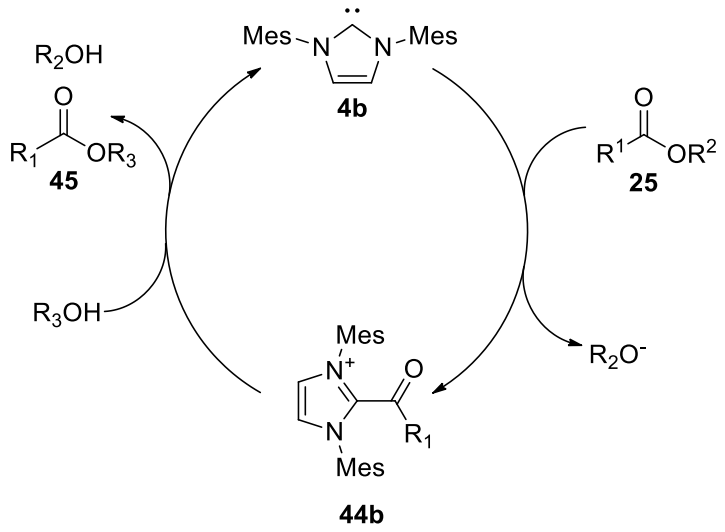
Scheme 65: Proposed Mechanism of IMes-Catalysed Amidation of an Ester as Reported by Movassaghi and Schmidt – Activation of an Alcohol[71]

In 2005, Movassaghi and Schmidt reported an NHC-catalysed amidation of an unactivated ester (**25**) and an aminoalcohol such as ethanolamine (**70**) at room temperature, as shown in Scheme 65.[71] The reaction was postulated to proceed *via* an initial transesterification based on React-IR data which indicated an absorbance at 1736 cm^{-1}, in the amidation of γ-lactone with ethanolamine (**70**). This was attributed to an intermediate ester.[71] Although the intermediate ester was not isolated, the

mechanism was plausible given previously published work on NHC-catalysed transesterifications by Nolan and co-workers.[61–63]

However, it was proposed by Movassaghi and Schmidt that NHCs acted as Bronsted bases/hydrogen-bonded to the alcohol and increased their nucleophilicity, as shown in Scheme 65.[71] Such a postulate was supported by the isolation of an IMes-methanol complex.[71] ^{1}H NMR of the complex in THF-d_8 showed the residual OH resonance at 5.33 ppm c.f. 3.02 reported for free and dilute MeOH in THF-d_8.[177]

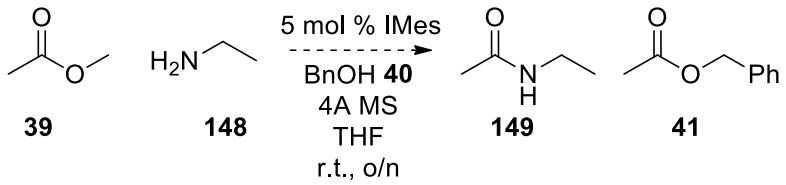
On the other hand, Nolan and co-workers suggested that NHCs activated esters *via* acylation, as shown in Scheme 66.[61–63] Had IMes (**4b**) led to the formation of an acylazolium species *via* nucleophilic attack of the ester, it would have been expected that an amine would have attacked in favour over an alcohol, given the increased nucleophilicity of an amine over the latter.



Scheme 66: Proposed Mechanism of IMes-Catalysed Esterification/Acylation as Reported by Nolan and Co-workers – Nucleophilic Activation of Esters[61–63]

To probe these assertions, an NHC-catalysed reaction of methyl acetate (**39**) with ethylamine (**148**) in the presence (and absence) of stoichiometric amounts of benzyl alcohol was conducted, as shown in Scheme 67. Without benzyl alcohol, only starting materials were recovered with no amide product

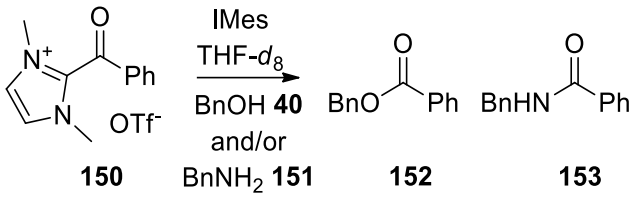
detected. The presence of benzyl alcohol led to the exclusive formation of methyl benzoate (**41**) and no amide product.



Scheme 67: Attempted NHC-Catalysed Amidation of Methyl Acetate with Ethylamine

The difference in reactivity between an amine and alcohol nucleophile led us to question whether the role of IMes (**4b**) was *via* nucleophilic activation of an ester.

Studer and co-workers reported on the reactivity of acylazolium ions (**150**) as stoichiometric acylating agents, as shown in Scheme 68.[72] Their results with benzyl alcohol (**40**) and/or benzyl amine (**151**) with or without IMes (**4b**) in stoichiometric quantities (or 20 mole%) provided strong evidence that IMes promoted esterification by activation of the alcohol by hydrogen-bonding.[71,72]



Scheme 68: Acylazolium Ions as Acylating Agents and the Role of IMes[72]

In reactions without IMes (**4b**), no reaction with BnOH (**40**) was observed. However the addition of IMes (**4b**) led to full conversion to the ester **152**.[72] It was therefore apparent that IMes (**4b**) promoted the esterification reaction. It was also shown that IMes (**4b**) did not react with the acylazolium ion **150**.[72] Reaction of $BnNH_2$ (**151**) with the acylazolium ion **150** led to the formation of the amide **153** without the need for IMes (**4b**).[72] This last result indicated that amines were indeed more nucleophilic than their alcohol counterparts, and that in the presence of an acylazolium species **150**, direct amidation could occur.

In contrast, we observed no amide product in the NHC-catalysed reaction of methyl acetate with ethylamine. This suggested that IMes (**4b**) did not form an intermediate acylazolium species by nucleophilic attack of an ester (methyl acetate). Indeed, had an acylazolium species been formed, it was expected that the more nucleophilic amine (rather than the alcohol) would attack, leading to the amide. This was in accordance with the results of Studer and co-workers.[72]

Studer and co-workers further reported that **150** in the presence of BnOH (**40**), together with $BnNH_2$ (**151**) and stoichiometric amounts of IMes (**4b**), only the ester **152** was formed.[72] It was therefore apparent from the lack of formation of the amide **153** that IMes (**4b**) promoted the reaction by activation of the alcohol rather than the formation of an acylazolium intermediate which would have favoured the formation of an amide rather than an ester product.[72] Indeed, Studer and co-workers[72] also presented computational evidence of hydrogen-bonding for NHC-methanol of ca. 11 $kcal \cdot mol^{-1}$.

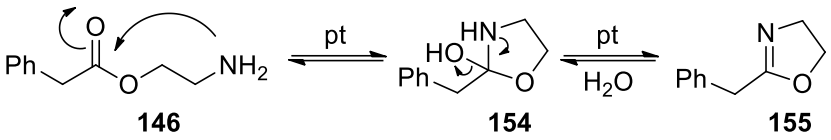
4.1 Synthesis of Postulated Reaction Intermediates

In order to probe the kinetics of the reaction, it was prudent to prepare authentic samples of the postulated intermediates. Previous reports in the literature had not isolated the intermediates or synthesised the proposed compounds.[71] The structures were suggested based on *in situ* IR spectra .

4.1.1 Synthesis of a Postulated Aminoester Intermediate

Although evidence pointed towards hydrogen-bonding between an NHC and an alcohol, which led to initial transesterification in NHC-catalysed amidations as reported by Movassaghi and Schmidt, the intermediate ester had not been isolated.[71] In order to gain spectroscopic data (React-IR) to support this, authentic samples of the proposed ester were synthesised.

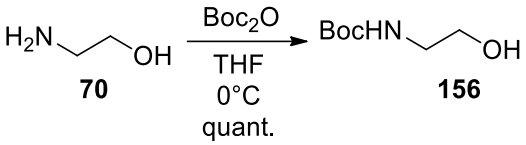
Efforts were also made to synthesise an oxazole (**155**) in light of React-IR data that suggested the formation of a further intermediate species (*vide infra*). A possible mechanism for the formation of the intermediate during NHC-catalysed amidations began with the postulated intermediate ester undergoing intermolecular attack with expulsion of water, as shown in Scheme 69.



146 **154** **155**

Scheme 69: Possible Mechanism for the Formation of an Oxazole Intermediate

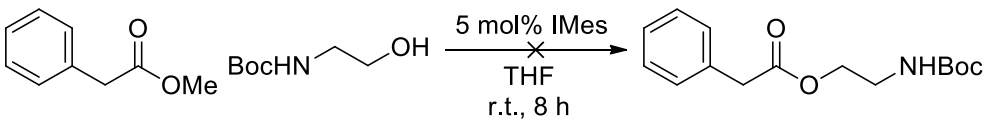
Initial attempts to synthesise the aminoester (**146**) were not successful, with intramolecular O-N acyl transfer occurring readily. Boc-protection of the amine group was therefore undertaken as it was hoped that this would sterically hinder intramolecular O-N acyl transfer amidation, and reduce the nucleophilicity of the amine. Boc-protection of ethanolamine was successful and proceeded with quantitative yield in THF or DCM, as shown in Scheme 70.



70 **156**

Scheme 70: Boc-Protection of Ethanolamine

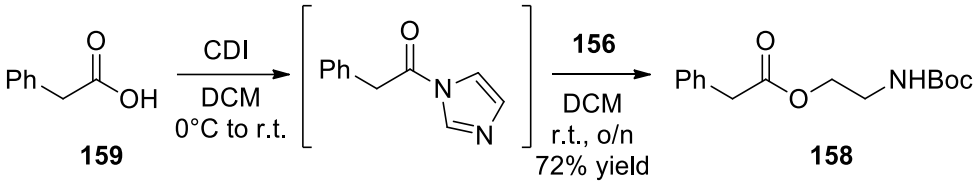
Transesterification of methyl 2-phenylacetate (**157**) with the Boc-protected ethanolamine (**156**) catalysed by IMes (**4b**) was attempted, as shown in Scheme 71, but returned only starting material i.e. no conversion to the ester or the amide was observed. The underlying cause for the failure of the reaction to proceed was not found, but it was possible that the presence of an electrophilic Boc group (competing carbonyl group), or hydrogen bonding between IMes and the secondary amine interfered with the NHC-catalysed transesterification.



157 **156** **158**

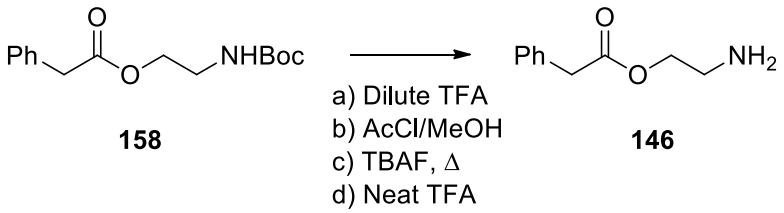
Scheme 71: Attempted IMes-Catalysed Amidation of Methyl 2-phenylacetate with *N*-Boc-ethanolamine

A more conventional reaction was attempted with CDI-promoted esterification of Boc-protected ethanolamine (**156**), with phenylacetic acid (**159**) as shown in Scheme 72.



Scheme 72: CDI-Promoted Esterification of Phenylacetic Acid with an *N*-Protected Ethanolamine

The reaction initially proved capricious but eventually afforded 2-Boc-aminoethyl-2-phenylacetate (**158**) in 72% yield overall. Unfortunately, the removal of the Boc-protecting group, to yield the hypothesised intermediate ester, proved to be reasonably challenging. Standard techniques, as shown in Scheme 73, such as dilute TFA, and HCl generated *in situ* from AcCl and MeOH failed to afford the aminoester **146**. TBAF promoted deprotection, which was reported by Coudert and co-workers to be a mild methodology,[178] was also unsuccessful. The use of neat TFA allowed the isolation of a Boc-free ester, though **146** was prone to decomposition.



Scheme 73: Boc-Deprotection of an Amino-ester

Identification of the decomposition product(s) by ^{1}H NMR spectroscopy was not successful with decomposition proving rapid. However, it did not appear that the amide **71** had formed *via* intramolecular O-N acyl transfer, or hydrolysis of the ester linkage had occurred. Although decomposition was rapid, which did not allow full characterisation of the proposed intermediate ester by ^{1}H and ^{13}C NMR spectroscopy, an IR spectrum, as shown in Figure 39, was however collected of the product which indicated a carbonyl resonance at 1672 cm^{-1} which was comparable to 1670 cm^{-1} reported by Sinisterra and co-workers.[179] Characterisation of the compound by *ex situ*

IR spectroscopy was nonetheless necessary in order to ascertain the accuracy of ReactIR in distinguishing between the carbonyl compounds with similar wavenumbers for their C=O stretch.

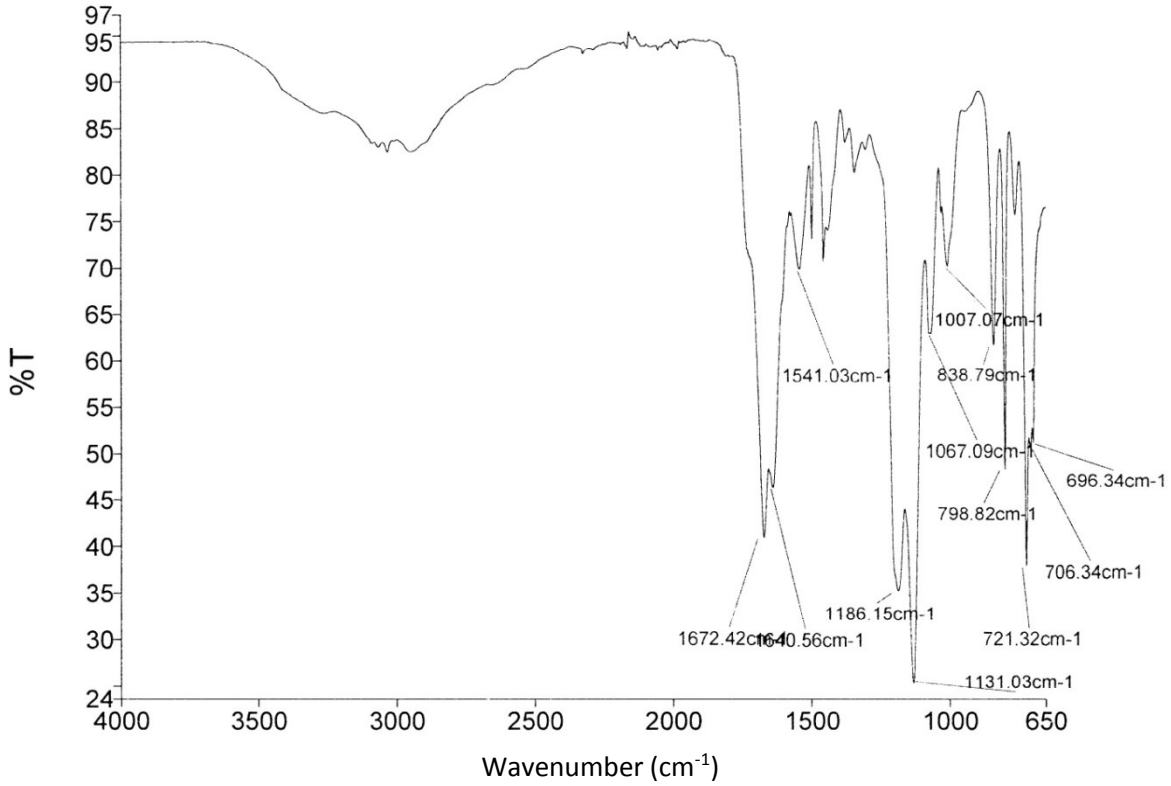


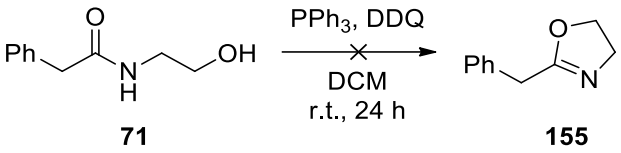
Figure 39: IR Spectrum of the Unstable Boc-free Aminoester

Given the instability of the ester, it was concluded that isolation of the free ester from the reaction mixture of the NHC-catalysed reaction of methyl 2-pheynlacetate (**157**) with ethanolamine (**70**) would not be successful. It was also apparent that we would be unable to directly manipulate the concentration of the intermediate ester during reactions in order to further probe kinetic data.

4.1.2 Synthesis of a Postulated Oxazole Intermediate

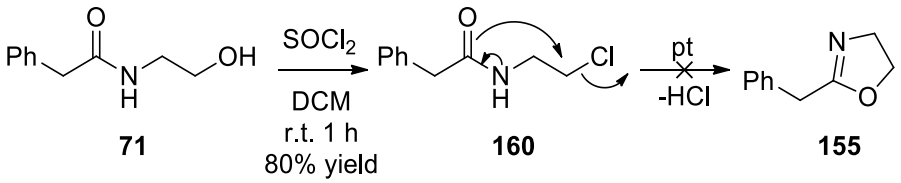
However, we proposed that the NHC-catalysed reaction of methyl 2-phenylacetate with ethanolamine also led to the formation of an intermediate oxazole (**155**). Attempts to prepare the oxazole (**155**) proved to reasonably challenging. It had been reported that **155** could be prepared from the *N*-(2-hydroxyethyl)-2-phenylacetamide (**71**) in the presence of PPh_3/DDQ,[180,181] as shown in

Scheme 74, though this could not be repeated by us. No conversion to the oxazole was observed with only starting material recovered.



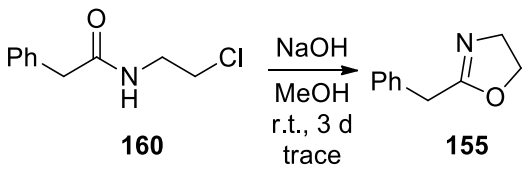
Scheme 74: Attempted Formation of an Oxazole from a Hydroxyamide

It was also reported that the oxazole could be prepared from **71** in the presence of excess $SOCl_2$,[182] as shown in Scheme 75. However, only the intermediate *N*-(2-chloroethyl)-2-phenylacetamide (**160**) was isolated in 80% yield in our hands. The chlorination of *N*-(2-hydroxyethyl)-2-phenylacetamide (**71**) with $SOCl_2$ was reported to proceed in 99% yield by Kubiczek and Smahel.[183]



Scheme 75: Attempted Synthesis of an Oxazole by the Action of $SOCl_2$ on a Hydroxyamide[182]

However, base assisted elimination, as shown in Scheme 76,[182,184] yielded the desired **155** though only in trace yield (16 mg).



Scheme 76: Base-assisted Elimination to Yield 2-Benzyloxazole

The IR spectrum for 2-benyloxazole (**155**) was also recorded and indicated the imine absorbance to be at 1665 cm^{-1} as shown in Figure 40. Li and Xu reported the IR absorbance corresponding to the imine stretch at 1676 cm^{-1},[181] while Li and co-workers attributed the imine stretch to 1642 cm^{-1}.[180]

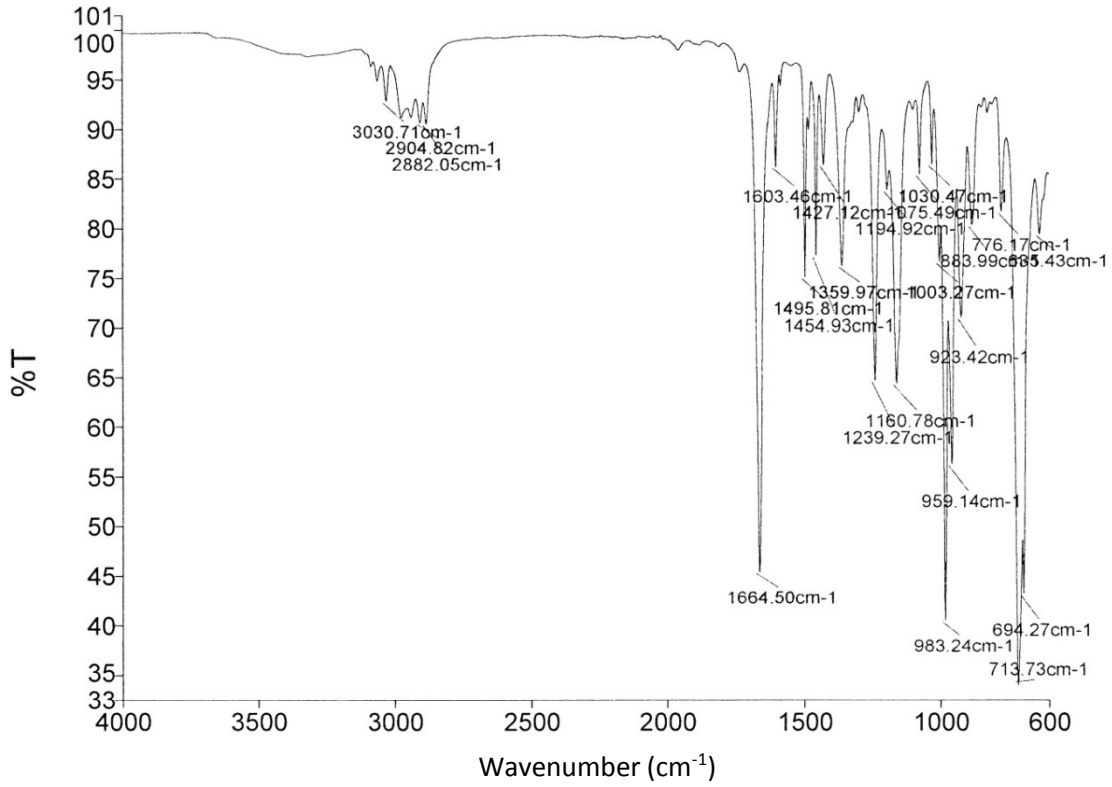


Figure 40: IR Spectrum of 2-Benzyloxazole

We observed the carbonyl stretch of the amide at 1624 cm^{-1}, as shown in Figure 41, in comparison to 1624 cm^{-1} reported by Jamieson and co-workers,[185] 1635 cm^{-1} reported by Sheppard and Starkov,[80] and 1645 cm^{-1} reported by Movassaghi and Schmidt.[71]

From the data cited above, and the spectra shown in Figure 39, Figure 40, and Figure 41, it was observed that the carbonyl and imine absorbances for the postulated aminoester and oxazole intermediates, and the amide product overlapped and that discriminating between them during *in situ* React-IR measurements would be somewhat challenging.

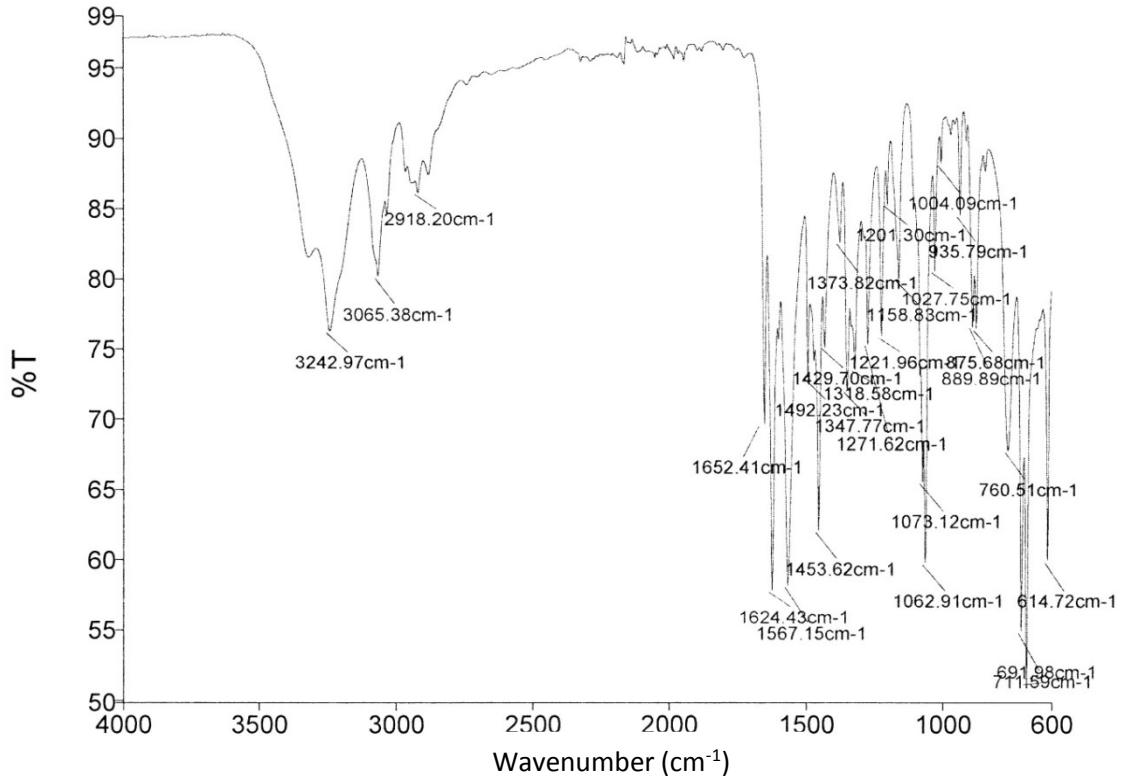


Figure 41: IR Spectrum *N*-(2-Hydroxyethyl)-2-phenylacetamide

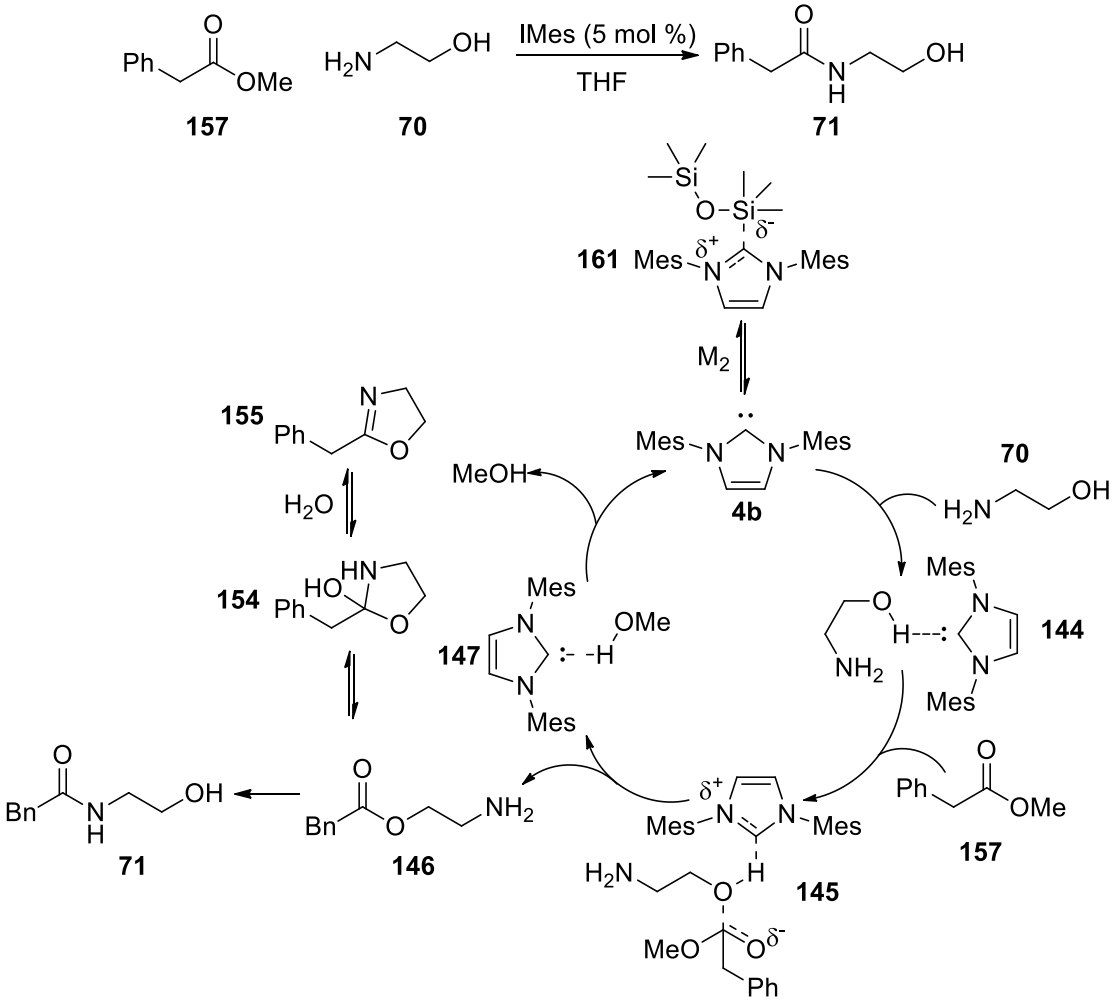
Conclusions

- Movassaghi and Schmidt emphasised that the reported amidation proceeded *via* an initial transesterification based on React-IR data that showed an absorbance at 1736 cm^{-1} which was attributed to the presence of an intermediate ester.[71]
- The postulated intermediate ester could not be isolated in our hands given its propensity to decompose. However, an IR spectrum was successfully recorded which matched literature data.[179]
- The synthesis of the postulated oxazole was also successful although IR data was not in accordance with those published in the literature.[180,181]
- The IR carbonyl absorbances of the intermediate ester, amide product, and the imine absorbance of the postulated oxazole, lie in close proximity and make distinguishing between the species in solution under reaction conditions difficult.
- The mechanism of the reaction is unlikely to be resolved by React-IR (alone) given the inability to track all intermediate(s). Closing a mass balance in order to derive intermediate concentrations is not possible given the inability to follow the concentrations of (N-1) intermediates.

4.2 React-IR

Given the expected difficulties in discriminating between the proposed intermediates in the NHC-catalysed reaction of methyl 2-phenylacetate (**157**) with ethanolamine (**70**) as a result of overlapping IR absorbances, we wished to derive qualitative kinetic data that could support the notion of an NHC·Si interaction. Our proposed mechanism of reaction, as shown in Scheme 77, included the postulated formation of 2-benyloxazole, and interaction of IMes with a silicon species, M_2 (**114**), which was chosen as a low molecular weight mimic of PDMS. Baceiredo and co-workers had proposed that the NHC·Si interaction was a Lewis-base/acid interaction, in which case, similar results between M_2 and PDMS should have been observed given the similar Lewis-acidities.[98] PDMS was not used in our experiments as its hydrophobic nature would have also contributed to the "protection" of the NHC from decomposition by water. We sought to eliminate this contribution in the search for evidence of an NHC·Si interaction.

Should an NHC·Si interaction have existed, our proposed mechanism indicated that this would have led to a quantity of IMes (**4b**) being taken out of the catalytic cycle, as shown in Scheme 77. This would have led to a diminished rate of reaction. The inclusion of an intermediate oxazole was based on initial IR data which indicated an absorbance at 1680 cm^{-1} which was not attributed to an intermediate ester (*vide infra*).



Scheme 77: Proposed Mechanism of IMes-Catalysed Amidation as Reported by Movassaghi and Schmidt - Modified to Include an Oxazole and NHC·Si Interaction

4.2.1 *In Situ* Monitoring of the IMes-Catalysed Amidation

To validate the use of React-IR to monitor the IMes-catalysed reaction of methyl 2-phenylacetate (**157**) with ethanolamine (**70**), reactions of the ester and amine in equimolar concentrations were conducted in order to probe the ability to follow the decrease in concentration of starting materials, and the generation of the amide product. From the raw IR data, two concentration profiles were derived for the starting ester, as shown in Figure 42: the first, labelled "IRT", was the result of automated software analysis whereas the second, labelled "1742/cm" was a manually selected peak. The overlapping concentration profiles of the ester indicated that the integration of area under a single peak at 1742 cm^{-1} adequately resolved the concentration of the starting ester. The

concentrations of the amide were calibrated against *ex situ* measurements and errors were less than 5 mol%.

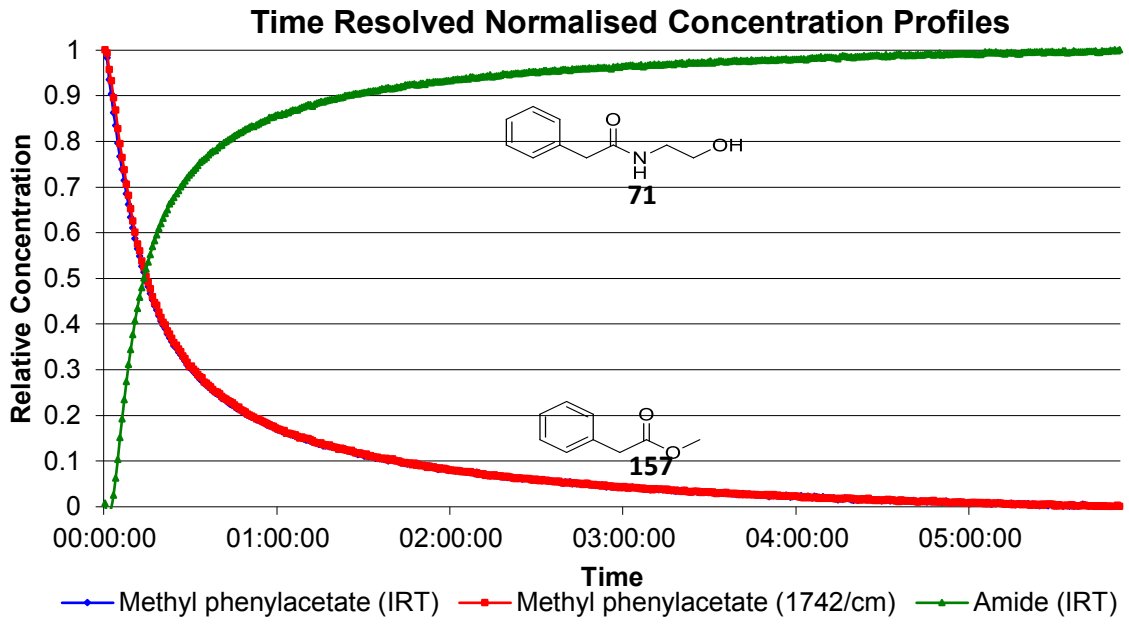


Figure 42: Comparison of Manually and Software-Integrated Peaks for the Derivation of Concentrations of Methyl 2-phenylacetate (157) and *N*-(2-Hydroxyethyl)-2-phenylacetamide (71)

Rate of reaction, which was derived from the change in concentration with respect to time, was plot as a function of concentration as shown in Figure 43.

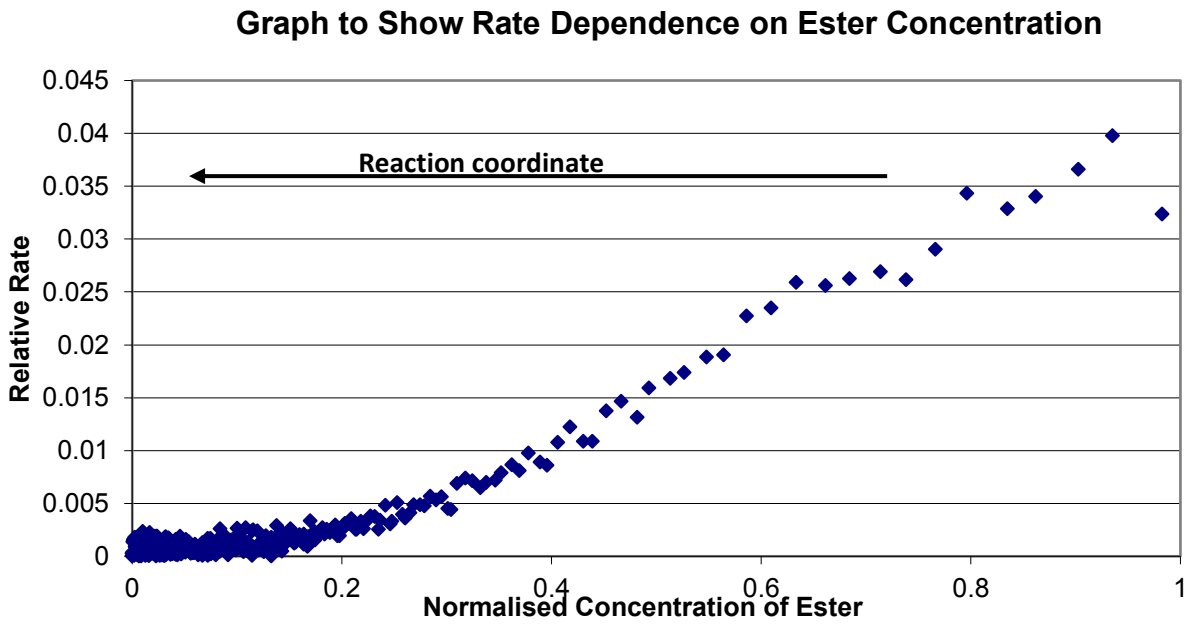


Figure 43: NHC-Catalysed Amidation (Equimolar Ester and Amine)

It should be noted that the reaction coordinate proceeds from right to left in graphs of rate versus concentration rather than the conventional left to right that is apparent on graphs of concentration versus time. A simple aide-mémoire is that concentration of the reactant decreases as the reaction progresses.

A convincing linear trend line could be fit to the majority of data in Figure 43 when normalised ester concentration exceeded 0.3 and indeed it was tempting to assume a first order rate of reaction with minor catalyst deactivation towards the end of reaction. However, plotting rate as a function of the square of ester concentration allowed an overall second order rate of reaction to be concluded, as shown in Figure 44.

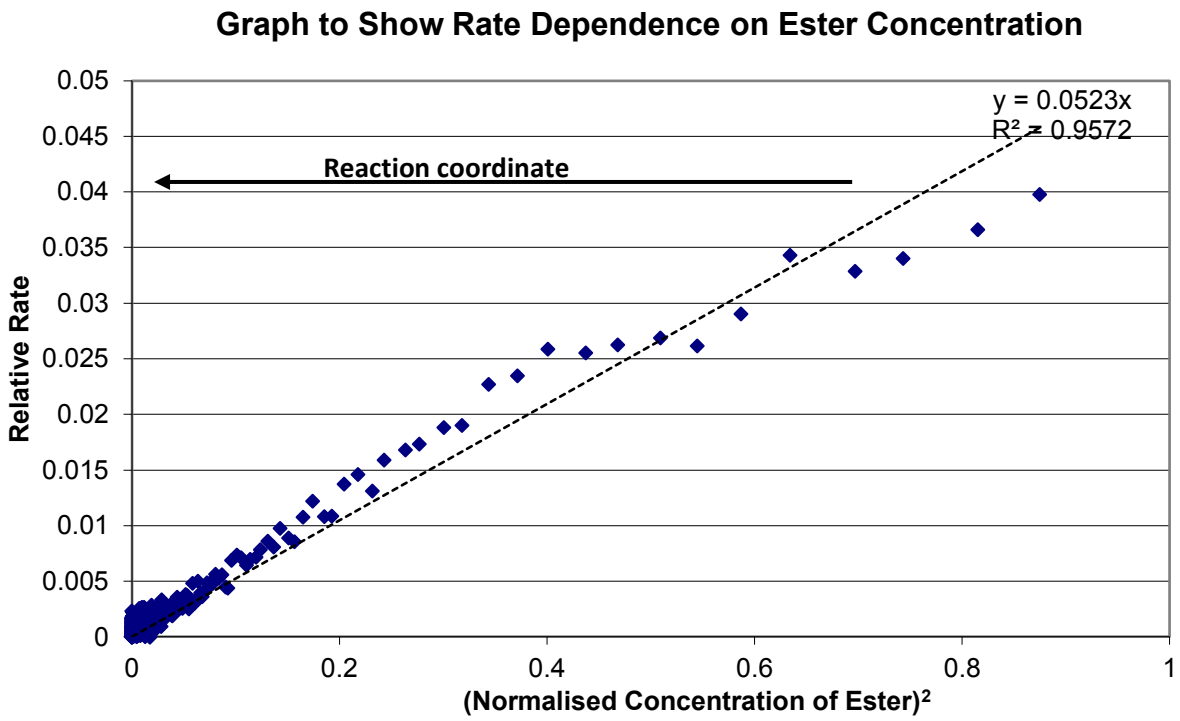


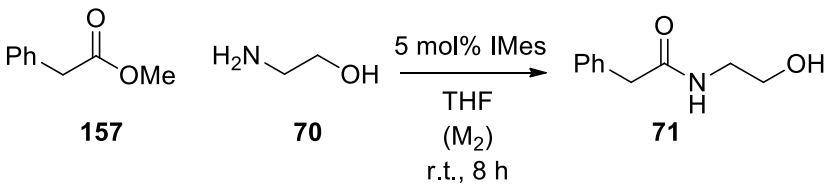
Figure 44: Amidation (Equimolar Ester and Amine) - Proposed 2nd Order Kinetics Overall

Although the overall rate order could be estimated, individual reaction rate orders (i.e. order with respect to ethanolamine (**70**) and order with respect to methyl 2-phenylacetate (**157**)) could not be estimated due to the inability to independently follow the amine concentration. A suitable NH IR absorbance was not found. Although React-IR was able to acquire IR spectra from 4800 - 450 cm^{-1},

peaks towards the higher wavenumbers suffered from low peak height and resolution as a result of diminished depth-of-penetration of the evanescent wave.[186]

4.2.2 The Effect of M_2 on NHC-Catalysed Amidation

The IMes-catalysed reaction of methyl 2-phenylacetate (**157**), with ethanolamine (**70**) in the presence and absence of M_2 (**114**), as shown in Scheme 78, was monitored by React-IR.



Scheme 78: IMes-Catalysed Amidation of Methyl 2-phenylacetate with Ethanolamine

Raw concentration profiles, as shown in Figure 45, displayed little discernible difference between reactions in the absence of M_2 (left-hand chart), and in the presence of M_2 (right-hand chart). The initial reactions (before ca. 4 hours) were conducted with a 10 mmol excess of ester in both cases, and were followed by an additional 10 mmol aliquot of amine at ca. 4 hours such that the reactants were now equimolar. Overall, the reactions yielded 1.568g (87%) and 1.688g (94%) of the expected amide with and without M_2 (**114**) respectively. The difference in isolated yield alone was not sufficient evidence of an NHC·Si interaction.

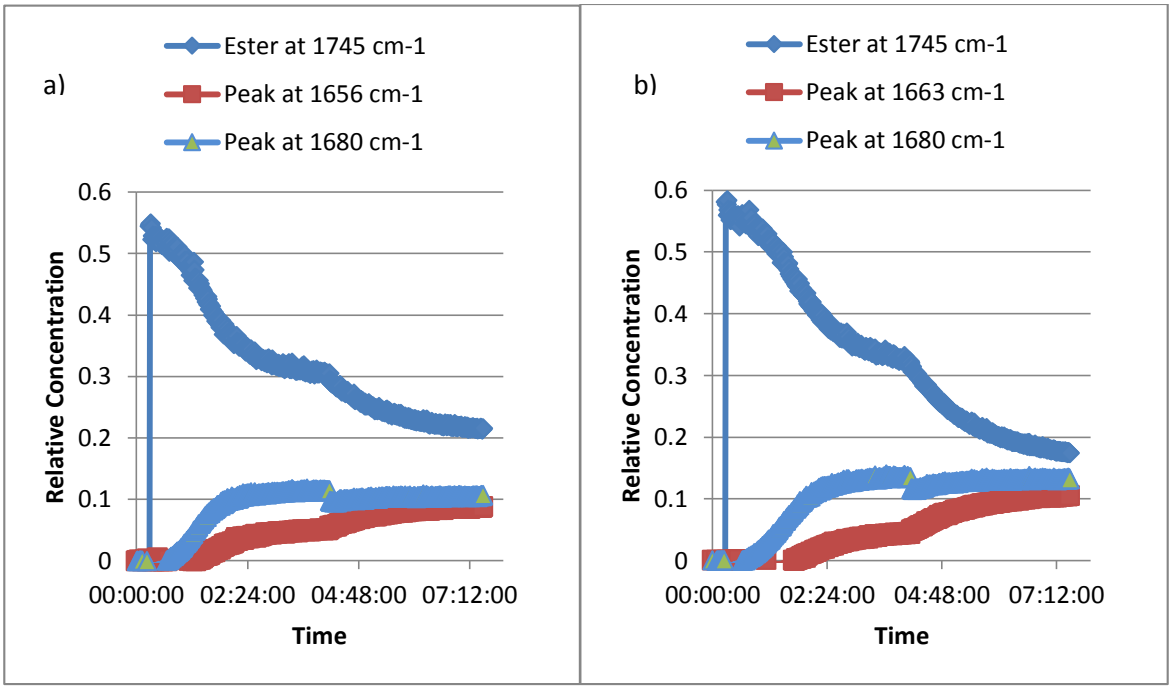


Figure 45: Concentration Profiles of Ester, Amide, and an Intermediate without (a) and with M_2 (b) in THF

On closer inspection, it was observed that the spectra derived from React-IR measurements suffered from a number of effects: the absorbance of the amide product *in situ* was not identical to that recorded of the solid sample; the datapoints were also not smooth but suffered from jitter, most likely due to the relatively dilute concentration of reactants. Of the former, the difference in the wavenumber was most likely due to the assumption of a linear absorption coefficient by the software which could not be corrected by hand.[186] *In situ* measurements showed the IR absorbance of the amide at 1656 - 1663 cm^{-1}, as shown in Figure 45, whereas *ex situ* measurements of the amide showed the carbonyl absorbance to be at 1624 cm^{-1}, as shown in Figure 41Figure 44. This made the identification of the proposed intermediates rather difficult given that the absorbances measured *ex situ* were already similar. It was therefore ambiguous as to whether the absorbance observed at 1680 cm^{-1} *in situ* was that of the postulated aminoester (1672 cm^{-1} measured *ex situ*, as shown in Figure 39), that of the postulated oxazole (1664 cm^{-1} measured *ex situ*, as shown in Figure 40), or a further unknown intermediate.

Of the latter, kinetic data could not be directly derived from these data as they were not smooth functions against time, as shown in Figure 45. Smoothed lines of best fit were used to estimate the absorbance profiles with concentration and rate derived from these instead, as shown in Figure 46. It was seen from the R^2 value that the trend lines showed little deviation from the raw data. It also demonstrated that the concentration profiles were not flawed *per se* but suffered from a poor signal-to-noise ratio which could be due to instrument capability (or lack of).

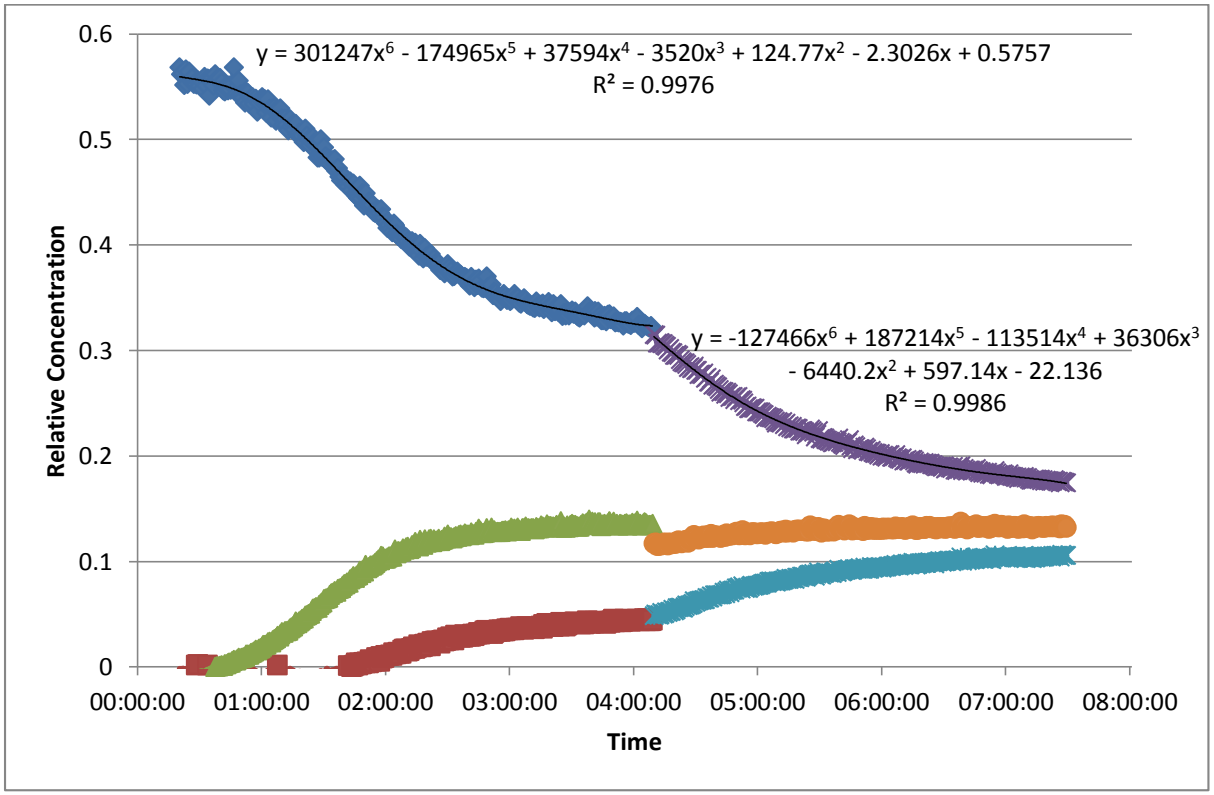


Figure 46: Approximation of Absorbance Profiles with Lines of Best Fit

The same treatment was afforded to both experiments depicted in Figure 45. Using concentrations and rates derived from the above trend lines, rate versus concentration to the power n graphs were obtained.

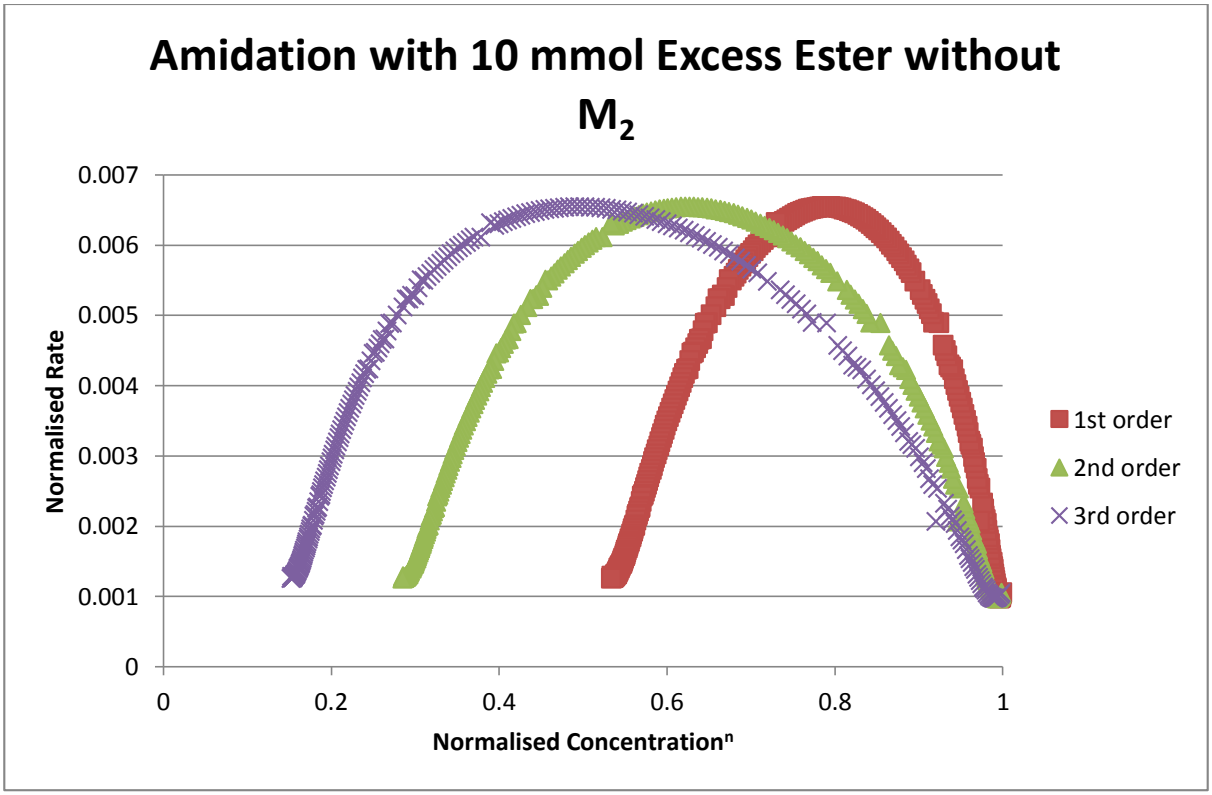


Figure 47: Amidation with 10 mmol Excess Ester without M_2

A most remarkable effect was seen in the kinetic data when the ester was used in 10 mmol excess to the amine, as shown in Figure 47. The initial gradient of the normalised rate versus concentration to the power n graphs indicated that the reaction was initially of a negative order i.e. rate inhibition was present. The reaction returned to positive order kinetics prior to an equimolar situation (when the additional 10 mmol aliquot of ethanolamine was injected). Although the negative order kinetics could be an indication of poor mixing, this was unlikely given that the stirrers were operating at 800 rpm and in light of further data discussed below.

On addition of 10 mmol ethanolamine such that the reaction was now equimolar, the following rates and concentrations were derived, as shown in Figure 48.

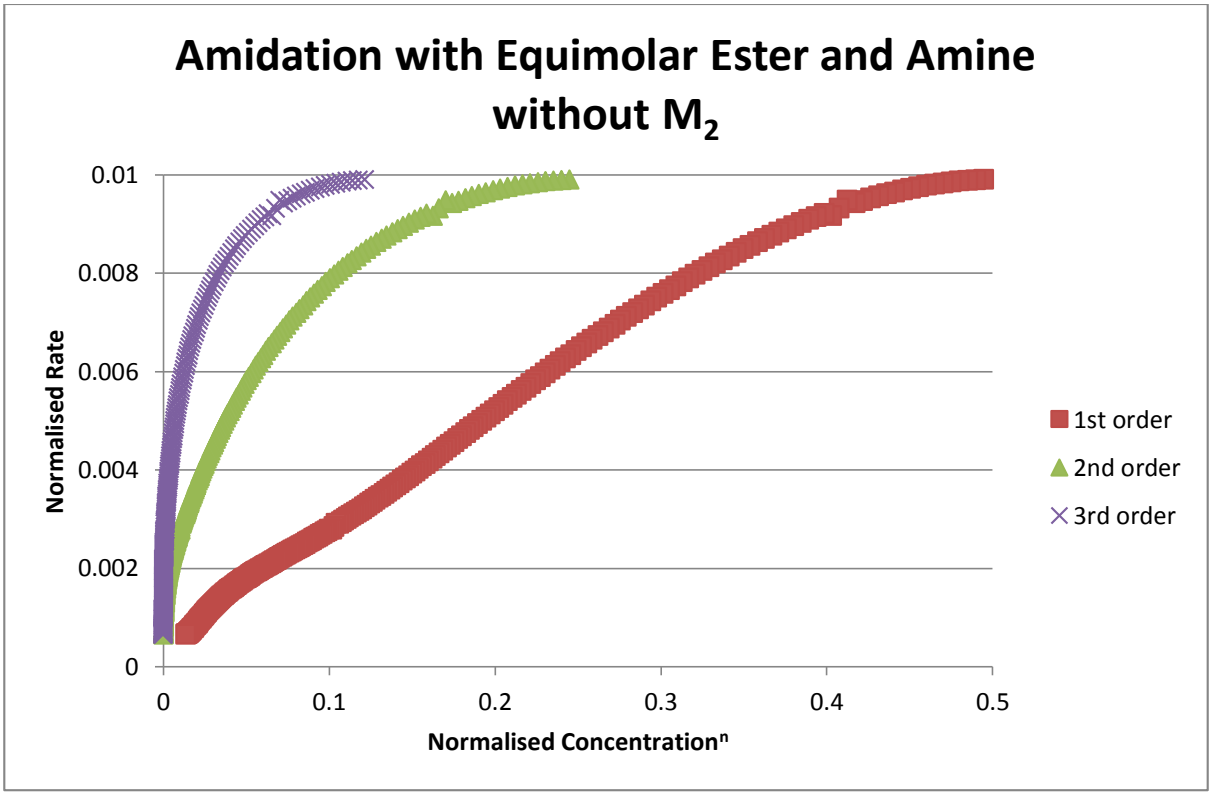


Figure 48: Stoichiometric Amidation of an Ester with Ethanolamine and without M_2

It was seen that the reaction was positive order and most likely 1st order overall in contrast to earlier data which showed 2nd order kinetics overall. The data also suggested that poor mixing (and therefore an initially poor rate of reaction) was not the cause for earlier negative reaction kinetics. If poor mixing were the case, the same inhibitory kinetics should have been observed in Figure 48 on the addition of the 10 mmol aliquot of amine.

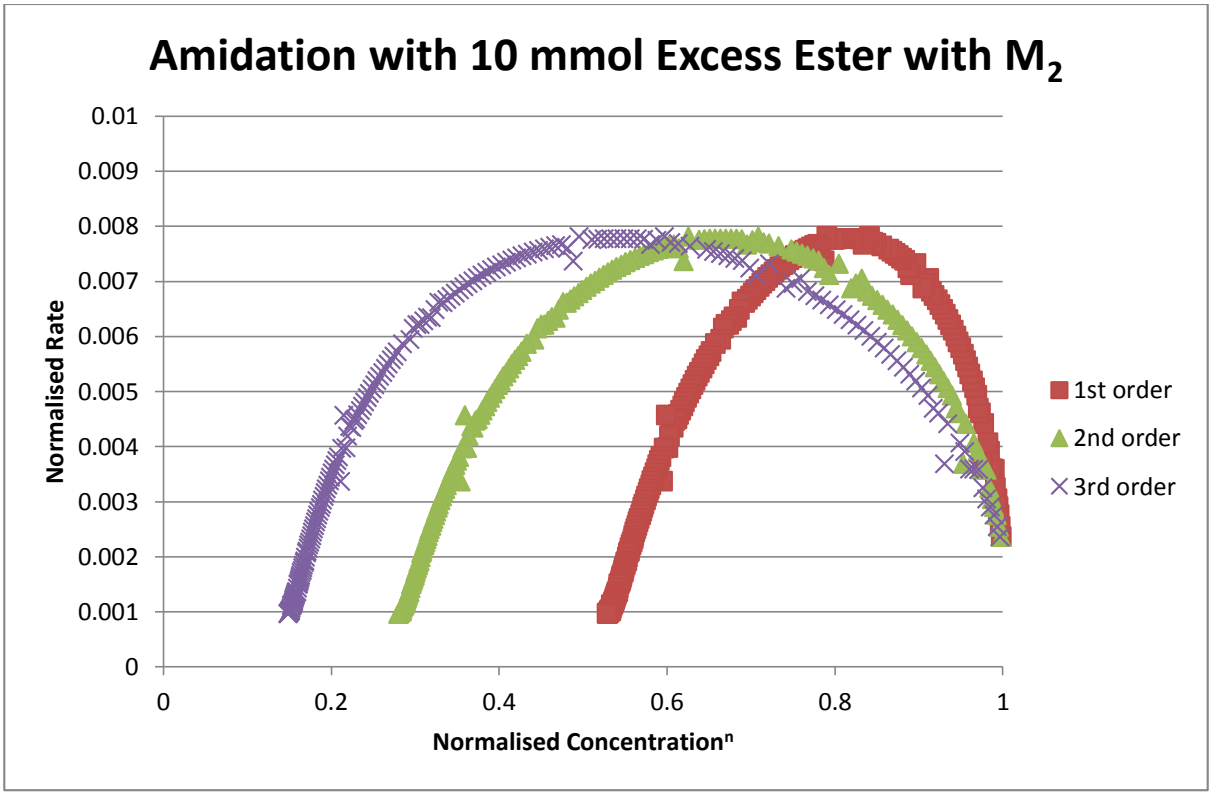


Figure 49: Amidation with 10 mmol Excess Ester with M_2

Negative order kinetics were also evident in the case of the reaction in the presence of M_2 (**114**) which was conducted in parallel, as shown in Figure 49. An initial phase of inhibitory kinetics was observed, followed by positive order kinetics in the case of the ester in 10 mmol excess in the presence of M_2 (**114**), as shown in Figure 50. The return to positive order kinetics also occurred at a similar concentration of ester (within 2%) as previously discussed for the case without M_2 (**114**).

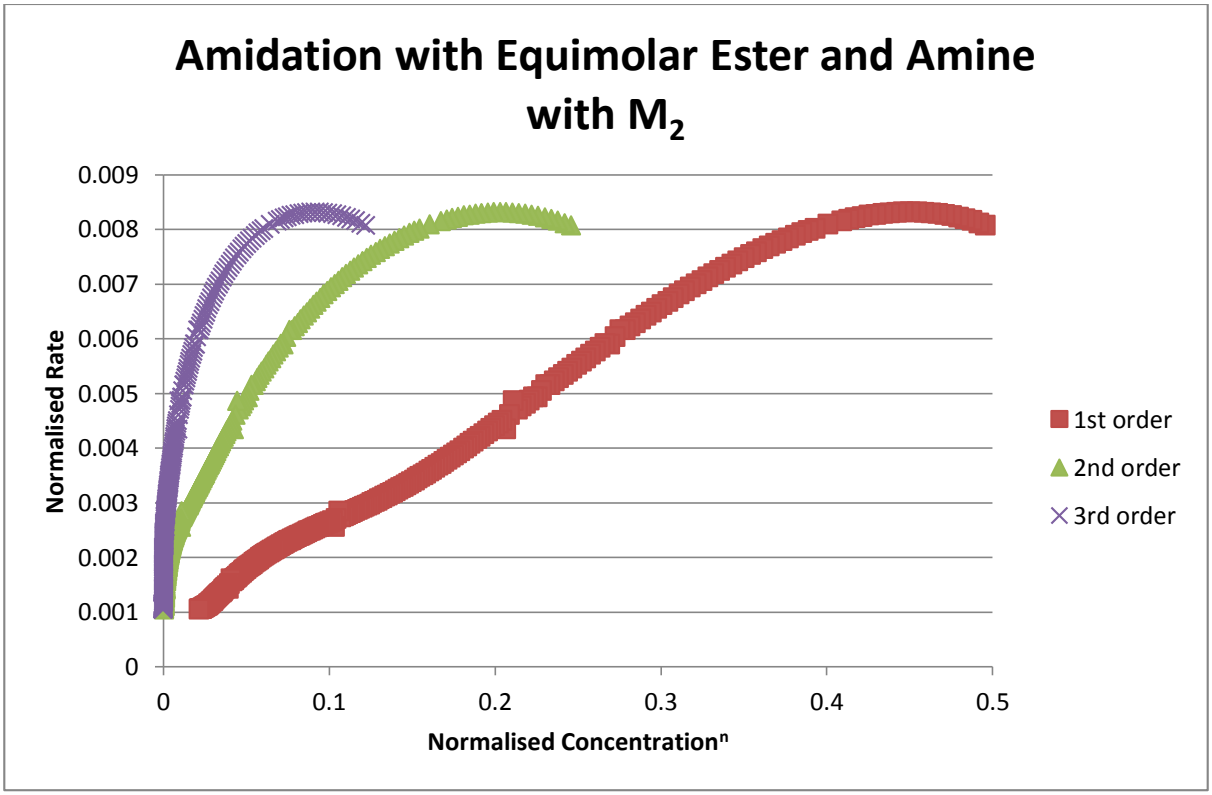


Figure 50: Stoichiometric Amidation of an Ester with Ethanolamine and with M_2

Given that our proposed mechanism which incorporated an NHC·Si interaction, as shown in Scheme 77, would have led to diminished rates of reaction, no discernible differences in rate could be detected. Indeed, similar kinetic data was observed for the NHC-catalysed reaction of methyl 2-phenylacetate with ethanolamine with and without the presence of M_2.

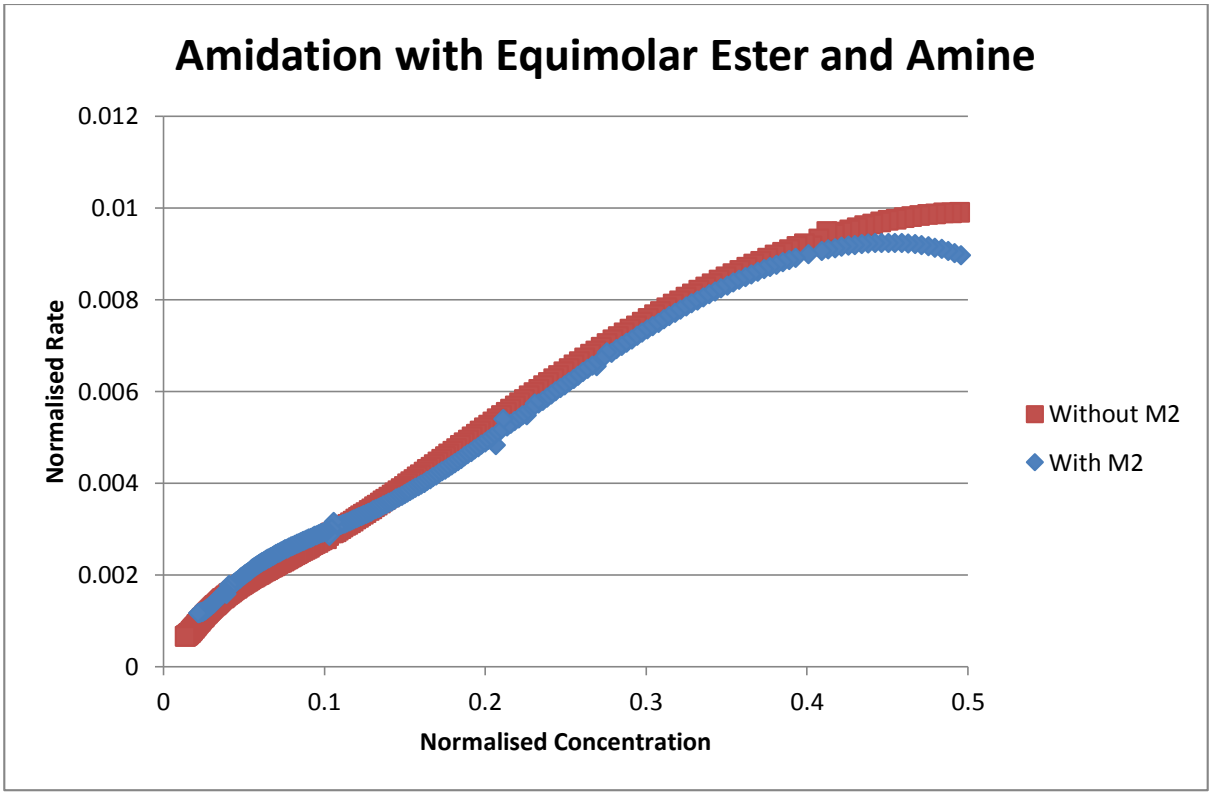


Figure 51: Stoichiometric Amidation of an Ester with Ethanolamine and with M_2 - Overlay

Overlaying the two kinetic data for the reactions with and without M_2 respectively, indicated similar reaction kinetics as shown in Figure 51. The strong correlation suggested that M_2 had no significant impact on the NHC-catalysed reaction and that there was unlikely to be a NHC·Si interaction in this case. Furthermore, an NHC·Si interaction should have been more favourable at lower concentrations of methyl 2-phenylacetate (**157**) and ethanolamine (**70**), given that the latter can no longer hydrogen bond with IMes, as shown in Scheme 77. This should have resulted in the increased formation of an IMes·M_2 complex (**161**) (should NHC·Si interactions exist) which would have diminished reaction rates at low reactant concentrations. This was not observed, as shown in Figure 46.

Conclusions

- Kinetic data has not provided conclusive evidence of an NHC·Si interaction. Indeed, results of the NHC-catalysed amidation show that M_2 (**114**) did not lead to different reaction kinetics compared to reactions without the presence of M_2.
- The ester intermediate proposed by Movassaghi and Schmidt could not be isolated as the amide rapidly formed *via* suspected O-N acyl transfer although an ATR IR spectrum of the proposed intermediate ester was recorded. It is possible that the NHC merely catalyses the transesterification reaction which is already known, and that the O-N acyl transfer that leads to the amide product is spontaneous.[61–63,71]
- The formation of an oxazole as an intermediate was investigated based on an observed absorbance at 1680 cm^{-1} which was not expected to be of an ester. However, authentic samples of 2-benzyloxazole indicated an absorbance at 1665 cm^{-1}. A lack of spectral resolution prevented the resolution of reaction intermediates and *N*-(2-hydroxyethyl)-2-phenylacetamide product.

5. Physical Protection of an NHC

Having exhausted a number of methodologies to derive experimental evidence of an NHC·Si interaction, the original report by Baceiredo and co-workers was revisited. It was asserted that protected NHCs were able to catalyse a range of reactions, and that the recorded yields or activity were unchanged when compared to that of unprotected NHCs. However, it did not comment on whether the NHCs remained protected in solution i.e. whether decomposition of the NHCs occurred under reaction conditions.[90] It was therefore of interest as to whether protection was due to mass transfer effects as it was ambiguous as to whether protection was only assured during storage of NHCs in/under silicones.[90]

We therefore wished to compare protection by silicones with protection by high molecular weight hydrocarbons which would not be able to exhibit an NHC·Si interaction. Given that diffusion coefficients for oxygen and water in single molecular weight PDMS and paraffin (a mixture) were not readily available, viscosity was used as a crude indicator of the diffusion coefficients of small molecules (oxygen and water). It had been shown that for spherical particles of radius r (m), the diffusion coefficient D ($m^2 \cdot s^{-1}$) of the particles was inversely proportional to the viscosity μ ($kg \cdot m^{-1} \cdot s^{-1}$), as shown in Equation 4.[187,188]

$$D = \frac{k_B T}{6\pi\mu r}$$

Equation 4: Stokes-Einstein Equation - Diffusion Coefficient as a Function of Viscosity

As there was no description of the molecular weight distribution or viscosity of the paraffin oil that was used by Baceiredo and co-workers,[90] paraffin oil with viscosity of 19 cSt was selected for use in our studies. For comparison, the viscosity of PDMS (1850 $g \cdot mol^{-1}$) was estimated to be 19 cSt, using a power law relation as shown in Equation 5, based on literature data.[189] The power law was derived by a line of best fit, as shown in Figure 52, with strong correlation to the datapoints ($R^2 > 0.99$).

$$\text{Viscosity} = 238.79 \cdot \text{MW}^{0.6955}$$

Equation 5: Power Law Relation Between Viscosity of Single Molecular Weight (MW) PDMS and Molecular Weight

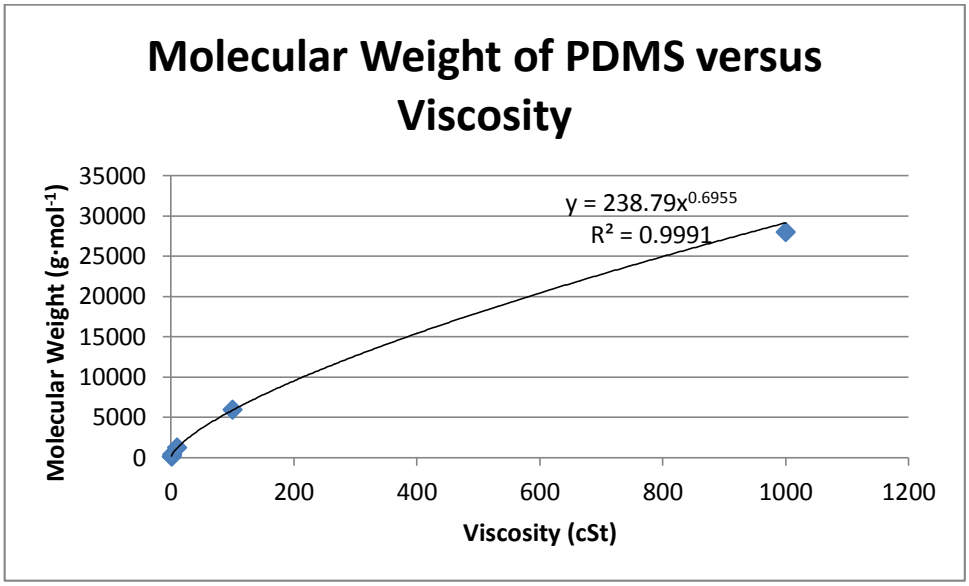
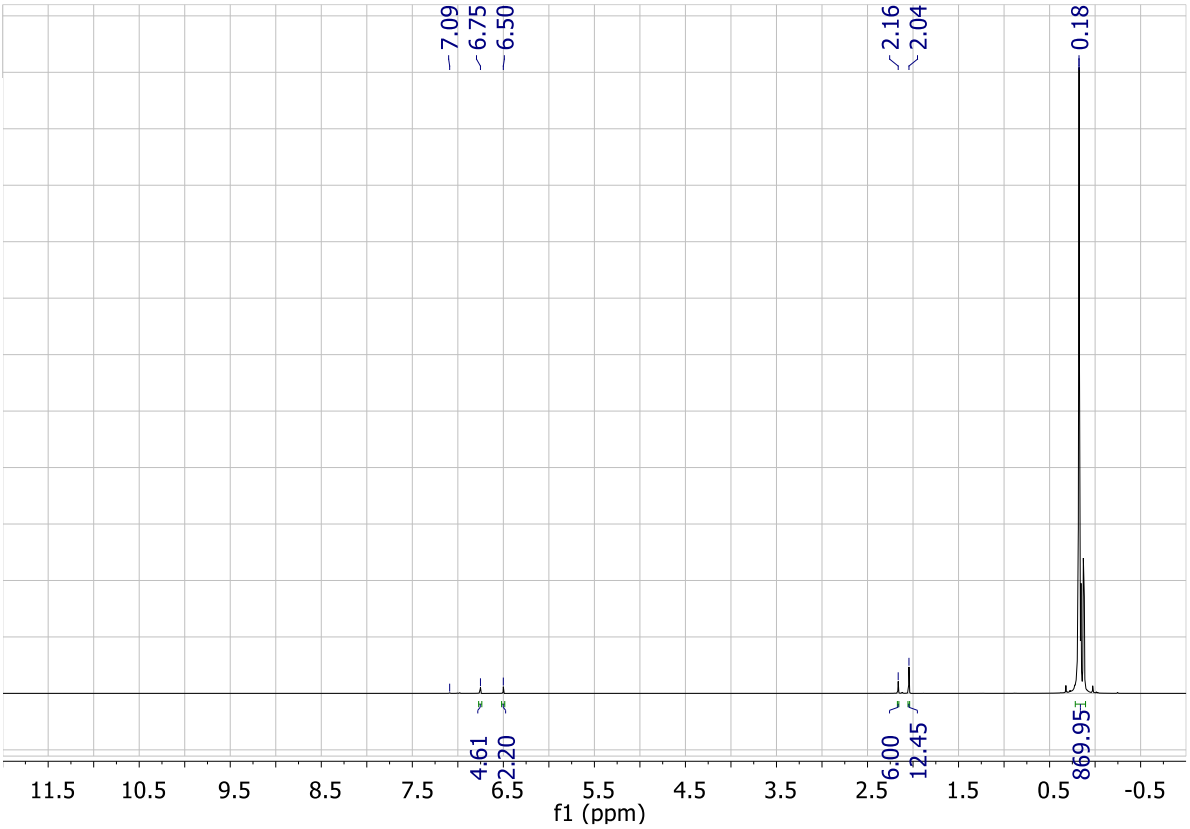


Figure 52: Derivation of a Power Law Relation between Viscosity of Single Molecular Weight PDMS and Molecular Weight

Samples of IMes (**4b**) in neat PDMS, of molecular weights varying from 770 g·mol^{-1} to 4,000 g·mol^{-1} were prepared as described by Baceiredo and co-workers.[90] However, it was observed that IMes was very poorly soluble in PDMS. Moreover, IMes remained poorly soluble in small molecular weight silicon species such as D_4, MDM, and M_2. Heating and vigorous shaking of the samples did not increase solubility. It was apparent that in these cases, IMes and PDMS therefore occupied separate phases. It must be borne in mind that protection was reported to be due to an NHC·Si interaction i.e. such an interaction would strictly require a solution.

The poor solubility of IMes in PDMS (4,000 g·mol^{-1}) was apparent as shown in the ^{1}H NMR spectrum of Figure 53 (a). Furthermore, ^{29}Si-^{13}C couplings, and a ca. −70 ppm change in the ^{29}Si resonances, were not observed by ^{29}Si NMR as shown in Figure 53 (b). A ca. −70 ppm shift had been reported between tetra- and pentacoordinate silicon species.[95,109,111,115] Toluene-d_8 in a sealed capillary was used to provide a deuterium lock but was not in contact with IMes or PDMS.

a)



b)

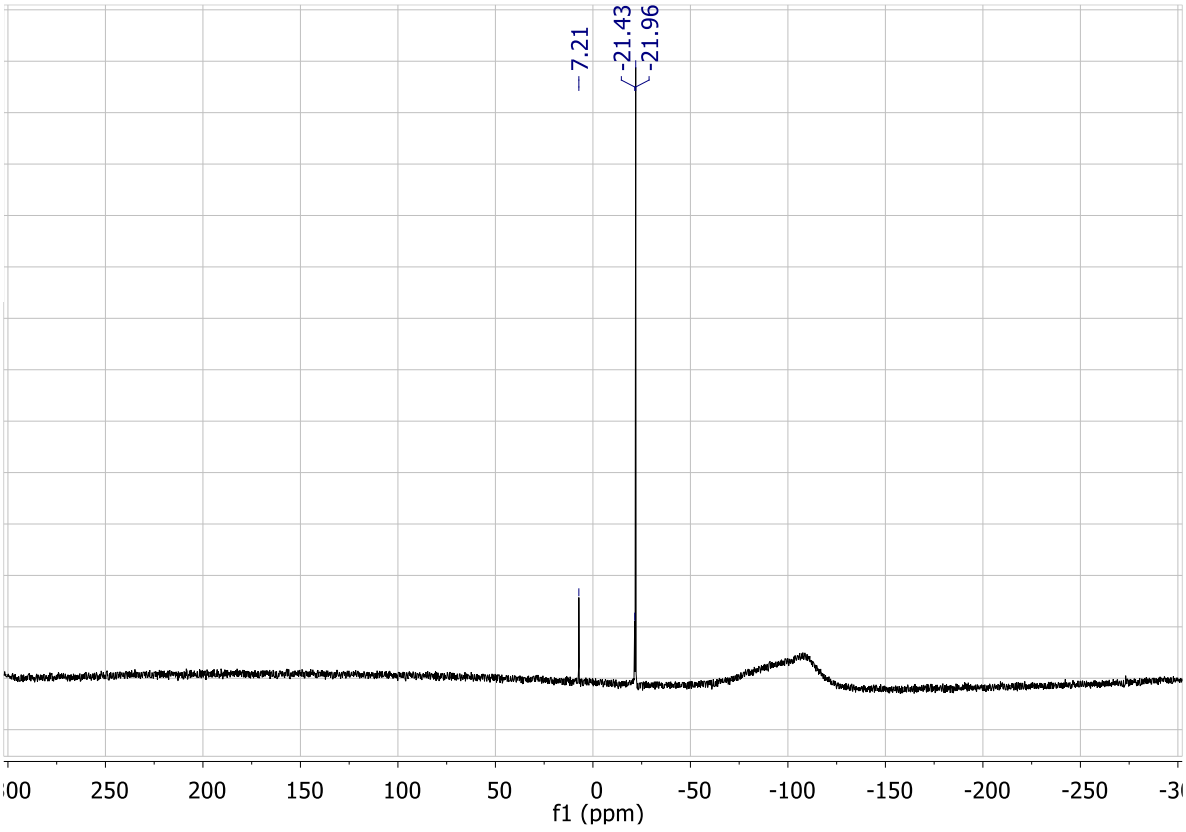


Figure 53: ^{1}H (a) and ^{29}Si (b) NMR Spectra of IMes (60 mg) and PDMS (4000 g·mol^{-1}, 600 mg) with Tol-d_8 Lock

On the addition of a small amount of toluene-d_8 in order to form a homogeneous (single-phase) solution, no protection was observed with decomposition of IMes observed overnight by ^{13}C NMR spectroscopy (disappearance of the characteristic C2 resonance). Even with PDMS present in excess (10:1 mass ratio), decomposition was not retarded when the NHC and PDMS were in the same phase. Similarly, no changes in NMR shifts were observed in the ^{13}C or ^{29}Si NMR spectra further indicating a lack of interaction. ^{13}C NMR shifts were in accordance with free IMes in solution, and ^{29}Si NMR spectra did not show a ca. −70 ppm change in shift expected between tetra- and pentacoordinate silicon species.[95,109,111,115]

5.1 Decomposition Limited by Mass Transfer (Diffusion)

In order to probe whether the protection was afforded by mass-transfer effects rather than an NHC·Si interaction, biphasic NMR samples, as shown in Figure 54, were prepared. In such cases, a layer of PDMS (or other silicon species) sat upon a layer of IMes in DMSO-d_6. An extensive list of solvents including triethylamine, pyridine, acetonitrile, diethyl ether, THF, EtOAc, DMF, toluene, benzene, acetone, chlorobenzene, *iso*propanol, ethanol, methanol, and cyclohexane were trialled for this purpose but the majority were miscible with PDMS or formed emulsions. DMSO-d_6 was chosen due to immiscibility with PDMS or paraffin and the availability of deuterated samples for NMR experiments. It was observed that in such systems, an NHC·Si interaction could not manifest itself as the NHC and silicon species occupied separate phases.

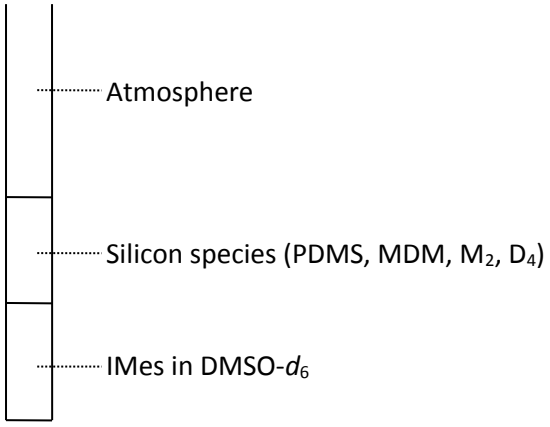


Figure 54: Biphasic NMR Samples of IMes in DMSO-d_6 and Silicon Species Exposed to Air

Indeed, IMes (**4b**, 30 mg) in DMSO-d_6 (0.4 mL) covered by a layer of paraffin of viscosity 19 cSt (0.3 mL) showed a similar protection to that reported by Baceiredo and co-workers for PDMS systems.[90] Little decay of the characteristic carbene resonance ca. 215 ppm was visible between the sample being exposed to air and after 5 days was seen, as shown in the ^{13}C NMR spectra of Figure 55 (a) and Figure 55 (b). Although Baceiredo and co-workers quantified decomposition by ^{1}H NMR spectroscopy (the evolution of decomposition products), we used ^{13}C NMR spectroscopy. Although ^{13}C NMR would not allow us accurately quantify decomposition of the carbene moiety due to the formation of unknown reaction intermediates, it had also been shown by Nyulászi and co-workers that the loss and/or broadening of the characteristic C2 resonance, occurred prior to the formation of the formamides (**73-74**) and imidazol-2-one (**72**) that would have been quantified by Baceiredo and co-workers.[90]

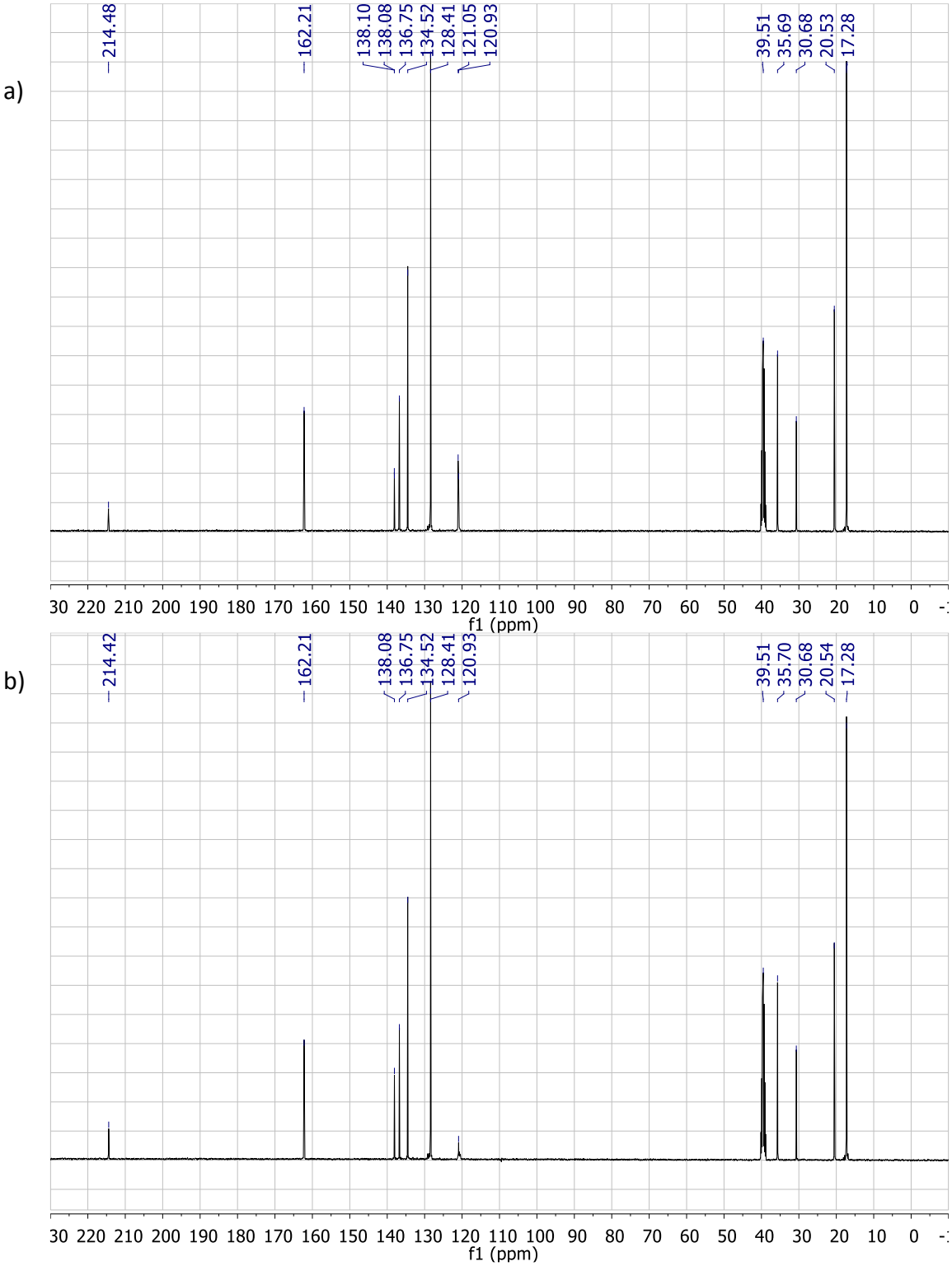


Figure 55: ^{13}C NMR Spectra of IMes (30 mg) in DMSO-d_6 (0.4 mL) under Paraffin (0.3 mL) at Time 0 (a) and after 5 Days (b)

Indeed, the decomposition of IMes (**4b**) was hindered by the presence of paraffin such that the characteristic C2 resonance was still apparent by ^{13}C NMR after 27 days, as shown in Figure 56.

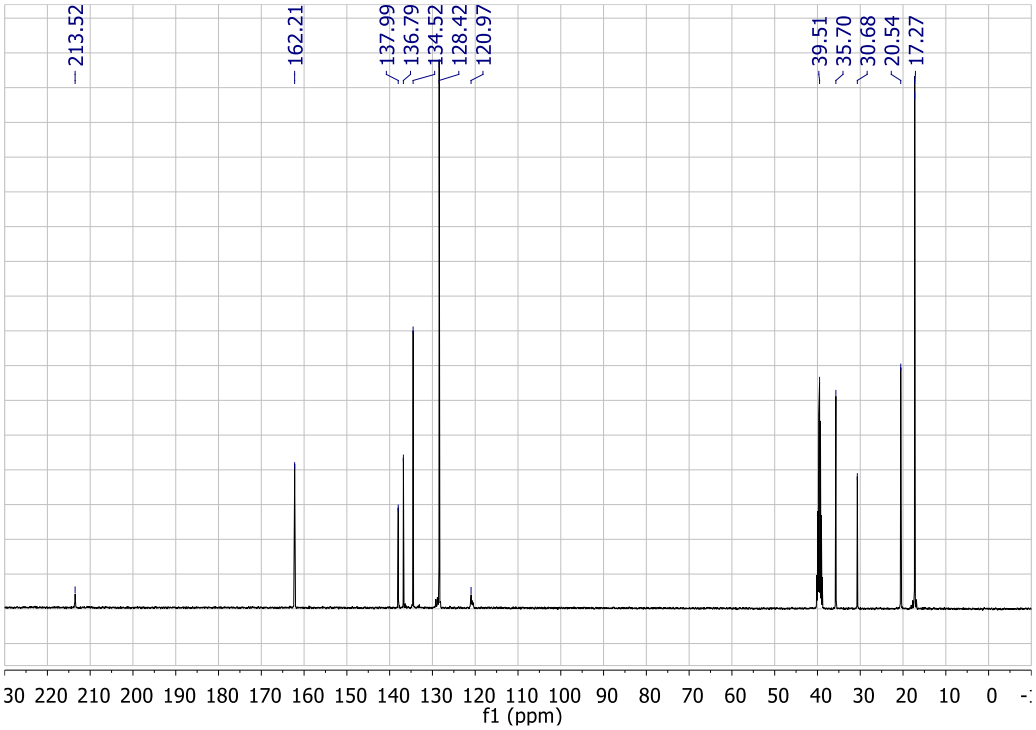


Figure 56: ^{13}C NMR Spectrum of IMes (30 mg) in DMSO-d_6 (0.4 mL) under Paraffin (0.3 mL) After 27 Days

In the case of PDMS (770 g·mol^{-1}), the C2 resonance diminished over the course of 8 days as shown in Figure 57.

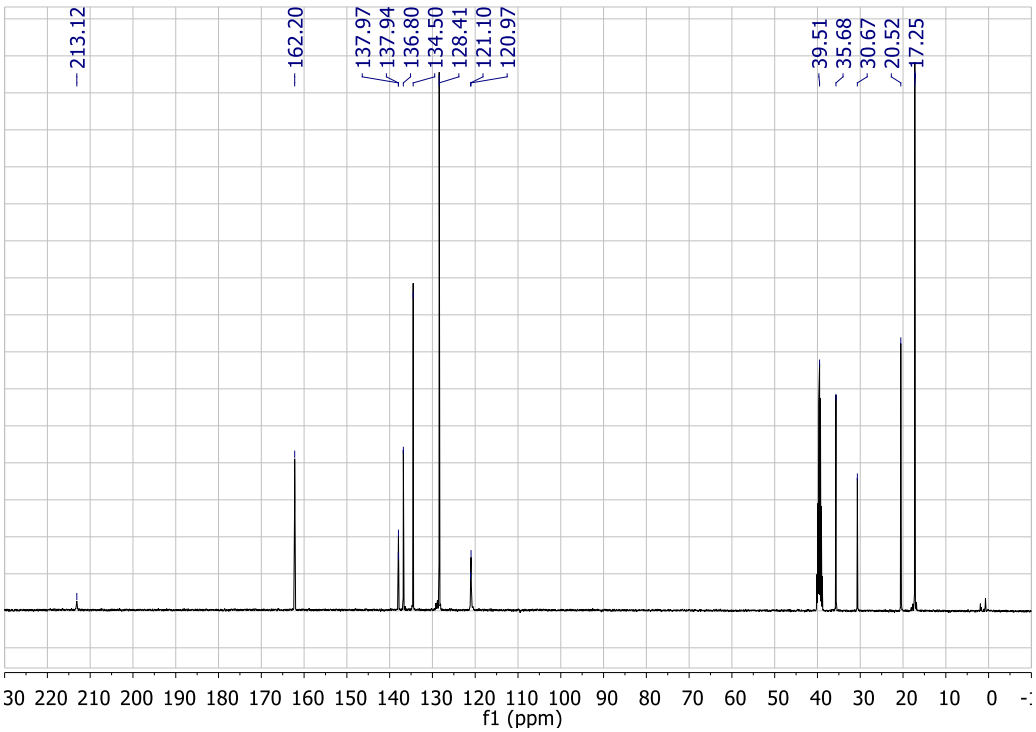


Figure 57: ^{13}C NMR Spectrum of IMes (30 mg) in DMSO-d_6 (0.4 mL) under PDMS (770 g·mol^{-1}, 0.3 mL) After 8 Days

In comparison, under PDMS (2,000, 4,000, 6,000, and 9,000 g·mol^{-1}), the characteristic C2 NMR shift of IMes (**4b**) diminished over the course of 14 days. Although we had initially assumed similar diffusion coefficients for oxygen and water in PDMS and paraffin oil, the above results indicated that this was not strictly true given the differences in decomposition observed. However, our results for paraffin were in contrast to the results reported by Baceiredo and co-workers.[90] For example, Baceiredo and co-workers reported that in the case of I*t*Bu under paraffin, decomposition of 87% of the NHC as assessed by ^{1}H NMR spectroscopy had occurred. The ^{1}H NMR spectrum of a sample in DMSO-d_6 under paraffin showed significantly less decomposition, as shown in Figure 58.

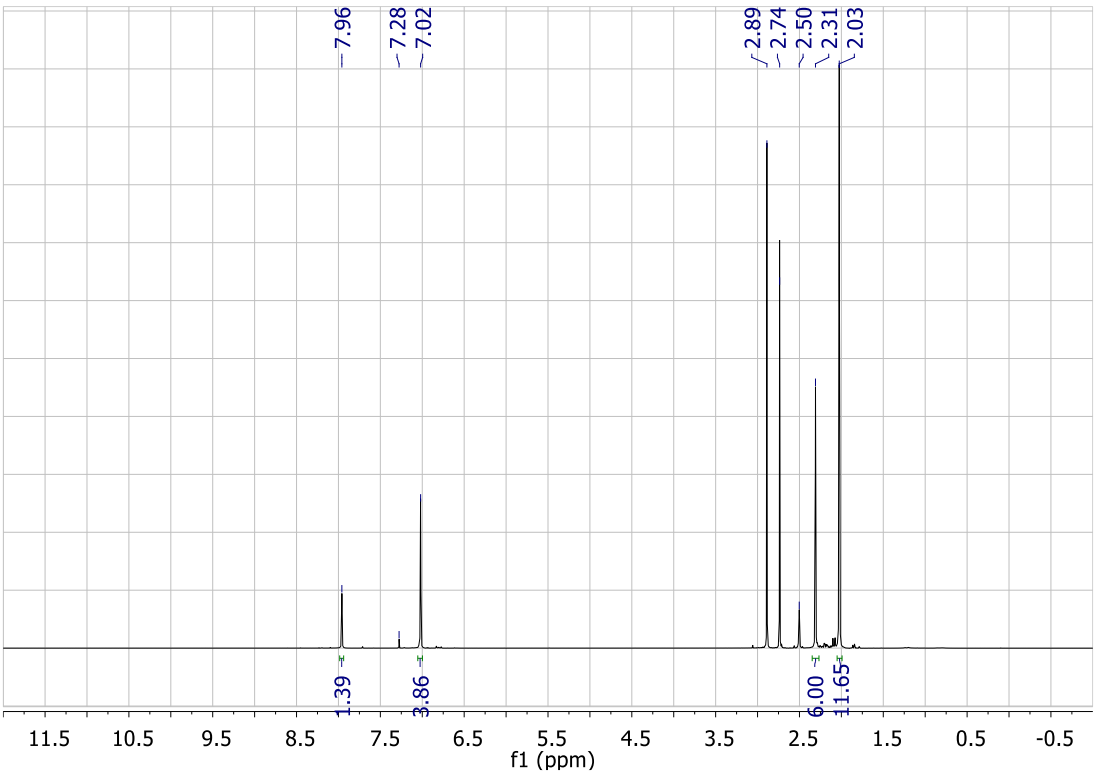


Figure 58: ^{1}H NMR Spectrum of IMes (30 mg) in DMSO-d_6 (0.4 mL) with DMF Standard Under Paraffin (19 cSt) After 27 Days

Given that the NHC and silicon species occupied separate phases, it appeared that protection could be the result of poor diffusion and not due to an NHC·Si interaction. Indeed, the protection afforded by paraffin oil (viscosity 19 cSt) was significantly better than PDMS (9000 g·mol^{-1}).

5.2 Steady State Mass Transfer

The systems described above could be divided into two: those of a single homogeneous liquid phase which we had probed with ^{1}H, ^{13}C, ^{29}Si NMR spectroscopy, 2D NMR spectroscopy, and DOSY; and those of two immiscible liquid phases which we had probed with ^{1}H and ^{13}C NMR spectroscopy in the preceding chapter. In both cases, no evidence of a NHC·Si interaction could be inferred. It was therefore of interest as to whether the observations of protection could be explained by mass-transfer.

In the biphasic systems, oxygen or water had to diffuse through a protective PDMS layer, whereas in homogeneous systems, oxygen or water species only had to diffuse across the gas-liquid interface, as shown in Figure 59.

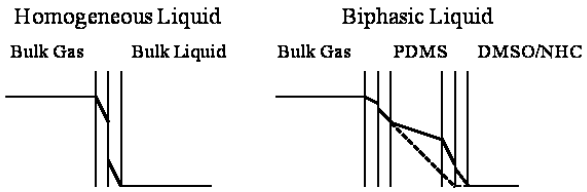


Figure 59: Mass-Transfer - Concentration Profiles across Interfaces

5.2.1 Homogeneous Systems

Although the diffusion coefficients for oxygen and water in a number of solvents were reported in literature,[190–193] quantitative data regarding the diffusive flux of the species across a stagnant air/solvent interface was not available. The diffusion coefficients of oxygen and water were in the range 1.00 - $6.19 \cdot 10^{-9}$ $m^2 \cdot s^{-1}$, as shown in Table 24.[190–193]

Table 24: Diffusion Coefficients of Oxygen and Water in a Range of Solvents

Solvent	Diffusion Coefficient of Solutes (10^{-9} $m^2 \cdot s^{-1}$)	
	Oxygen	Water
Toluene	4.38[194]	6.19[135]
THF	-	4.18[133]
DMSO	3.23[195]	ca. 1.00[134]
PDMS	2.00[190] 3.25[191]	1.45[192] 2.00[193]
Benzene	3.46[194]	-

Our assumptions in this analysis were:

- decomposition reactions were fast compared to mass-transfer and therefore mass-transfer limited;
    - this was supported by literature reports that decomposition of NHCs was fast under non-inert conditions.[5,13,90,125]
- decomposition occurred immediately at the interface with no diffusion into the bulk solvent;
    - given the fast decomposition in comparison to mass-transfer assumed above, little diffusion into the solvent would be possible prior to decomposition.
- materials were dry and degassed such that bulk concentrations of O_2 and H_2O were nil at time 0;
    - samples were prepared in a glovebox in dry and oxygen-free conditions
- decomposition and mass-transfer were at steady state such that bulk concentrations of O_2 or H_2O were invariant with time;
- a Nernst diffusion layer thicknesses of 10^{-3} and 10^{-4} m for gas and liquid films respectively;

- diffusion coefficients of 10^{-5} and 10^{-8} $m^2 \cdot s^{-1}$ for solutes in the gas and liquid phases respectively;[133,190–193]
    - This was supported by literature reported values, as shown in Table 24.

As an example, an air/toluene system was modelled. As oxygen and water were not readily soluble in toluene,[196] we initially assumed liquid-side mass-transfer control. Using the Nernst diffusion model, the overall mass-transfer coefficient was estimated using Equation 6 as $k_L = 10^{-4}$ $m \cdot s^{-1}$, where k_L was the effective mass transfer coefficient ($m \cdot s^{-1}$), D_L was the diffusion coefficient ($m^2 \cdot s^{-1}$), and δ_{Nl} was the Nernst diffusion layer thickness (m).

$$k_L = \frac{D_L}{\delta_{Nl}}$$

Equation 6: Overall Mass Transfer Coefficient (Liquid Side) - Nernst Approximation

We also assumed that: oxygen accounted for 21 mol% of air; the density of air was 1.225 $kg \cdot m^{-3}$; the molar mass of air was 0.02896 $kg \cdot mol^{-1}$. This resulted in the estimated molar concentration of oxygen to be 8.9 $mol \cdot m^{-3}$. This allowed us to estimate flux as $8.9 \cdot 10^{-4}$ $mol \cdot m^{-2} \cdot s^{-1}$ for oxygen.

However, such an analysis on an air/THF system would not be valid due to the volatility of THF which would have led to an ever moving boundary position. The assumption of a stagnant film would also not have been valid at the interface due to counter-diffusion. Air/DMSO was not modelled given the poorer diffusion coefficients in DMSO compared with toluene as shown in Table 24. Indeed, the results for toluene were a worst case scenario for the solvent systems considered.

5.2.2 Non-Homogeneous System

For the biphasic systems, as shown in Figure 59, poor solubility of oxygen and water in PDMS was assumed. Indeed, literature data corroborated this with nil solubility of water in PDMS and an equilibrium concentration of oxygen in PDMS of $1 \cdot 10^{-3}$ M reported.[190] Given that the diffusion

coefficients for oxygen and water were similar, as shown in Table 24, and given oxygen's greater concentration in air compared to water, analysis of mass transfer was conducted with oxygen.

For simplicity, and to estimate a maximum flux, it was assumed that there was no resistance to mass transfer at the PDMS/DMSO interfaces with immediate decomposition of the NHC. The mass-transfer coefficient for the air/PDMS boundary was also taken to be $k_L = 10^{-4}$ m·s^{-1} i.e. the same as that of an air/toluene system. The Nernst diffusion length in the PDMS phase was assumed to be 0.02 m. The overall mass-transfer coefficient, was estimated using Equation 7 as $1 \cdot 10^{-7}$ m·s^{-1} which gave rise to an estimated flux of $8.9 \cdot 10^{-7}$ mol·m^{-2}·s^{-1} for O_2.

$$k_o = \frac{1}{\frac{1}{k_L} + \frac{x}{D_{H_2O/PDMS}}}$$

Equation 7: Overall Mass Transfer Coefficient

Equation 7 could be viewed in terms of mass-transfer resistances where x is the diffusion length in metres. It was seen that k_o was dominated (99%) by resistance in the PDMS layer given the significantly increased path length in PDMS compared with the Nernst diffusion layer thickness of the air/toluene systems (10^{-4} m). A 0.02 m layer was estimated to reduce mass-transfer by an order of 1,000 at steady state. The analysis above could explain the observed protection without the need to invoke an NHC·Si interaction. Indeed, an NHC·Si interaction would require degradation to be minimised further than that offered by limited mass-transfer alone.

5.3 Transient Mass Transfer

It should be noted that the time to reach steady state was of utmost importance in the systems described above. Our previous assumption of fast equilibrium applied to the two-film/Nernst diffusion layer model was no longer valid due to the thickness of the diffusion layer (0.02 m). During the time taken to reach steady-state, there would have been a lower flux than that estimated at steady-state. However, such a system could still be modelled by Fick's Second Law, as shown in

Equation 8, where C was concentration (mol·m^{-3}), t was time (s), x was position (m), and D was the diffusion coefficient (m^2·s^{-1}).

$$\frac{\partial C}{\partial t} = D\frac{\partial^2 C}{\partial x^2}$$

Equation 8: Fick's Second Law

For the transient system, it was assumed:

- At time=0, PDMS of thickness L was dry and free of water.
- At time=0, the concentration at the air/PDMS interface was instantaneously increased to unit concentration and remained invariant with time.
- The concentration (of oxygen or water) at the PDMS/DMSO interface was held constant at 0 and was invariant with time due to rapid consumption of oxygen or water in the decomposition reactions.
- There was no reaction (consumption or generation of species) within the bulk.

5.3.1 Non-Homogeneous Boundary Conditions

$$D\frac{\partial^2 C}{\partial x^2} = \frac{\partial C}{\partial t} \qquad 0 < \mathrm{x} < \mathrm{L},\ \mathrm{t} > 0$$

Equation 9: Fick's Second Law for a Finite 1D Slab

Fick's Second Law was now restricted to the following conditions for position and time with the boundary and initial conditions as shown in Equation 9 and Equation 10.

$$\begin{aligned} C &= C_i & 0 < \mathrm{x} < \mathrm{L},\ \mathrm{t} = 0 \\ C &= C_i & \mathrm{x} = \mathrm{L} \\ C &= C_0 & \mathrm{x} = 0 \end{aligned}$$

Equation 10: Initial and Boundary Conditions

A non-dimensional system using substitutions for excess concentration, non-dimensional length, and the mass-transfer equivalent of the Fourier number were made as shown in Equation 11. The

solution of a non-dimensionalised system allowed for easier integration. It was seen that non-dimensional concentration and length were fixed between 0 and 1. The mass-transfer equivalent of the Fourier number was strictly ≥0.

$$\theta = \frac{C - C_i}{C_0 - C_i} \qquad X = \frac{x}{L} \qquad F = \frac{Dt}{L^2}$$

Equation 11: Substitutions to Form a Non-Dimensional Problem

The substitutions were chosen such that substitution into Equation 9 afforded the non-dimensionalised Equation 12 which was a function of new variables θ, X, and F.

$$\frac{\partial^2 \theta}{\partial X^2} = \frac{\partial \theta}{\partial F} \qquad 0 < \mathrm{X} < 1, \mathrm{F} > 0$$

Equation 12: Fick's Second Law with Non-Dimensional Terms

The initial and boundary conditions in Equation 10 were now restated as shown in Equation 13. It was seen that the boundary condition at X=0 was still non-zero (and hence non-homogeneous boundary conditions existed).

$$\begin{aligned} &\theta = 1 \quad X = 0 \\ &\theta = 0 \quad X = 1 \\ &\theta = 0 \qquad\quad 0 < \mathrm{X} < 1, \mathrm{F} = 0 \end{aligned}$$

Equation 13: Boundary Conditions and Initial Condition for the Non-Dimensional System

5.3.2 Steady State Solution

A solution of the system was not possible by separation of variables given the non-homogeneous boundary conditions. However, it was observed that as time tended to infinity, a steady state system was reached when the concentration profile would become linear and invariant with time, the flux being dependent on the concentrations, length, and diffusion coefficient alone.

At steady state, Equation 9 could be reduced to Equation 14 as the change of concentration with respect to time (or θ with respect to F) would become 0. We no longer had a PDE as a function of

two variables but an ODE as a function of non-dimensionalised position (X) which could be solved by inspection (or direct integration).

$$\frac{\partial^2 \theta_{SS}}{\partial X^2} = 0 \qquad 0 < \mathrm{X} < 1$$

Equation 14: Fick's Second Law for the System at Steady State

The steady state boundary conditions along with the steady state solution were as shown in Equation 15. It was seen that non-dimensionalising the problem afforded a simple and elegant solution.

$$\theta_{SS} = 1,\ X = 0$$
$$\theta_{SS} = 0,\ X = 1$$
$$\theta_{SS} = 1 - X$$

Equation 15: Boundary Conditions for the System at Steady State

We now assumed that the solution of the non-homogeneous problem (Equation 12 and Equation 13) could be described as the sum of a homogeneous (transient) and non-homogeneous (steady state) problem as shown in Equation 16.

$$\theta(X, F) = \theta_{SS}(X) + \theta_H(X, F)$$

Equation 16: Solution of a Non-Homogeneous Problem

5.3.3 Solution of a Homogeneous System

We again restated Fick's Second Law for the homogeneous system as shown in Equation 17

$$\frac{\partial^2 \theta_H}{\partial X^2} = \frac{\partial \theta_H}{\partial F} \qquad 0 < \mathrm{X} < 1,\ \mathrm{F} > 0$$

Equation 17: Fick's Second Law

Homogeneous boundary conditions were then applied. Our initial value, as shown in Equation 18, for the homogeneous system, was bound by the overall initial value condition as shown in Equation 13, and the steady state solution which was invariant with time as shown in Equation 15.

$$\theta_H = 0 \quad X = 0$$
$$\theta_H = 0 \quad X = 1$$
$$\theta_H = X - 1 \qquad\qquad 0 < \mathrm{X} < 1,\ \mathrm{F} = 0$$

Equation 18: Initial and Boundary Values for the Homogeneous System

5.3.4 Separation of Variables

It was assumed that solution of the homogeneous system was possible by separation of variables and that the solution was of the form as shown in Equation 19.

$$\theta_H(X,F) = \Theta(X)\Gamma(F)$$

Equation 19: General Form for the Solution of a PDE by Separation of Variables

Fick's Second Law was restated using the substitution in Equation 19 which yielded Equation 20. Given that the equations were independent of each other, we assumed an equivalence to some constant denoted by $-\eta^2$.

$$\frac{\Theta''(X)}{\Theta(X)} = \frac{\Gamma'(F)}{\Gamma(F)} = -\eta^2$$

Equation 20: Fick's Second Law after Separation of Variables

Separation of variables yielded the following two sets of independent and homogeneous ODEs.

$$\Theta''(X) + \eta^2\Theta(X) = 0$$
$$\Gamma'(F) + \eta^2\Gamma(F) = 0$$

Equation 21: Fick's Second Law as a Set of ODEs

Analysis of the auxiliary equation (characteristic equation) for the former, and inspection of the latter, showed that the solutions of the two systems were of the form as shown Equation 22.

$$\Theta = C_1\cos(\eta X) + C_2\sin(\eta X)$$
$$\Gamma = C_3 e^{-\eta^2 F}$$

Equation 22: Trial Solutions for Fick's Second Law

To satisfy Equation 19, our solution was restricted to the product of the solutions to the two ODEs and had the form shown in Equation 23. The constants in Equation 22 were restated as A, B, and C in Equation 23 for simplicity, and were constants to be found.

$$\theta_H(X,F) = Ae^{-\eta^2 F}(B\cos(\eta X) + C\sin(\eta X))$$

Equation 23: General Solution for the Homogeneous System

The constants in Equation 23 were constrained by boundary and initial values as shown in Equation 18. It was seen that η was strictly positive: were η negative, the exponential term would increase with time (in F), whereas steady state at infinite time had been previously imposed; should η be 0, the solution would be invariant with time which was physically incorrect.

It was observed that at time 0 (F=0), Equation 23 could be restated as Equation 24 which allowed boundary conditions for X (C) while ignoring F (t) to be fit.

$$\theta_H(X,0) = B\cos(\eta X) + C\sin(\eta X)$$

Equation 24: Initial Value Problem for the Homogeneous System

5.3.5 Initial Value Solution as a Fourier Series

It was seen that the solution of the initial value could be satisfied with a Fourier series. Homogeneous boundary conditions stipulated that θ_H was 0 at X=0 and at X=1. From the former, coefficient B must be 0 as the cosine function was defined as 1 at X=0.

It was now apparent that the initial value could be satisfied by a Fourier series consisting only of sine functions. Furthermore, η was restricted to the form "nπ" to satisfy the value (θ between 0 and 1) and periodicity of the function (X between 0 and 1). Note that by convention, the coefficients of the sine Fourier series were denoted Bn, as shown in Equation 25 and correspond to C in Equation 24.

$$\theta_H(X,0) = \sum_{n=1}^{\infty} B_n \sin(\frac{n\pi X}{L'})$$

Equation 25: Initial Value Problem for the Homogeneous System - Sine Fourier Series

The coefficients for Bn for a half-series were derived from Equation 26.

$$B_n = \frac{2}{L'}\int_0^{L'} (X-1)\sin(\frac{n\pi X}{L'})dX$$

Equation 26: Deriving Fourier Coefficients

Integration of Equation 26 by parts gave Equation 27. By inspection, it was seen that the coefficient B_n was of the form "2/nπ".

$$B_n = \frac{2}{L}\left[-\frac{LX}{n\pi}\cos(\frac{n\pi X}{L}) + \frac{L}{n\pi}\sin(\frac{n\pi X}{L})\right]_0^L$$

Equation 27: Fourier Coefficients for an Infinite Sum of Sine Functions

This yielded a homogeneous solution as shown in Equation 28.

$$\theta_H = -\frac{2}{\pi}\sum_{n=1}^{\infty}\frac{1}{n}\sin(n\pi X)\cdot e^{-(n\pi)^2 F}$$

Equation 28: Solution of Fick's Second Law for the Homogeneous System

The complete solution for the original problem as described in Equation 16 could then be completed as shown in Equation 29.

$$1 - X - \frac{2}{\pi}\sum_{n=1}^{\infty}\frac{1}{n}\sin(n\pi X)\cdot e^{-(n\pi)^2 F}$$

Equation 29: Solution for Transient Mass Transfer with Constant Flux

With this single equation, the evolution of concentration in terms of position and time could be modelled in unison.

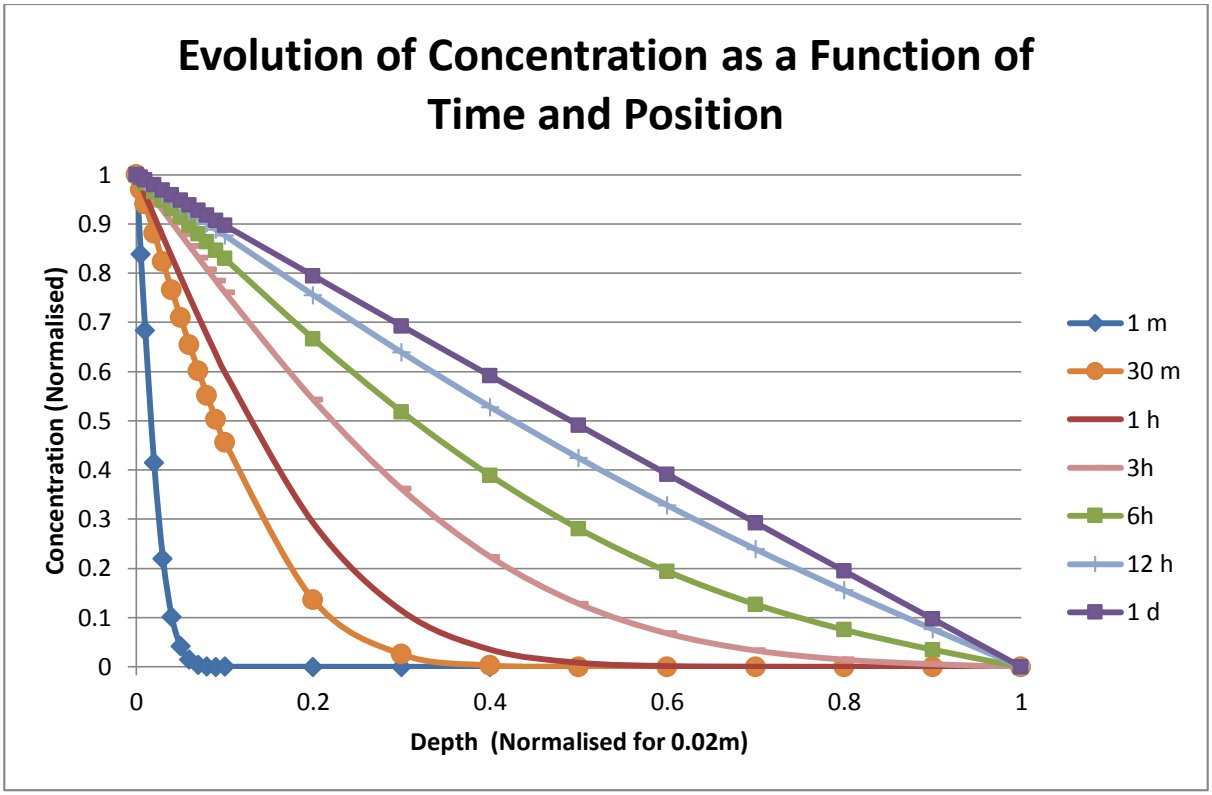


Figure 60: Evolution of a Concentration Profile within PDMS of 0.02m Depth

For example, a system with a PDMS layer of thickness 0.02 m would therefore not approach steady state until after ca. 24 h, as shown in Figure 60. Only then would the flux reach steady state. Although the problem was stated in non-dimensional terms, the solution was specific to a system of 0.02 m thickness due to the non-linear exponential term. Empirically, the concentration at the PDMS/DMSO layer would be nil until F ~ 0.2 which would occur ca. t = 40,000 s (ca. 11 h).

For a system of thickness 0.05 m, steady state would not be reached until >4 days and concentration at the PDMS/DMSO boundary would remain nil until ca. 3 days as shown in Figure 61. Although calculated for a single species, given that the diffusion coefficients of oxygen and water in PDMS were similar, as shown in Table 24, both species would yield similar results in PDMS.

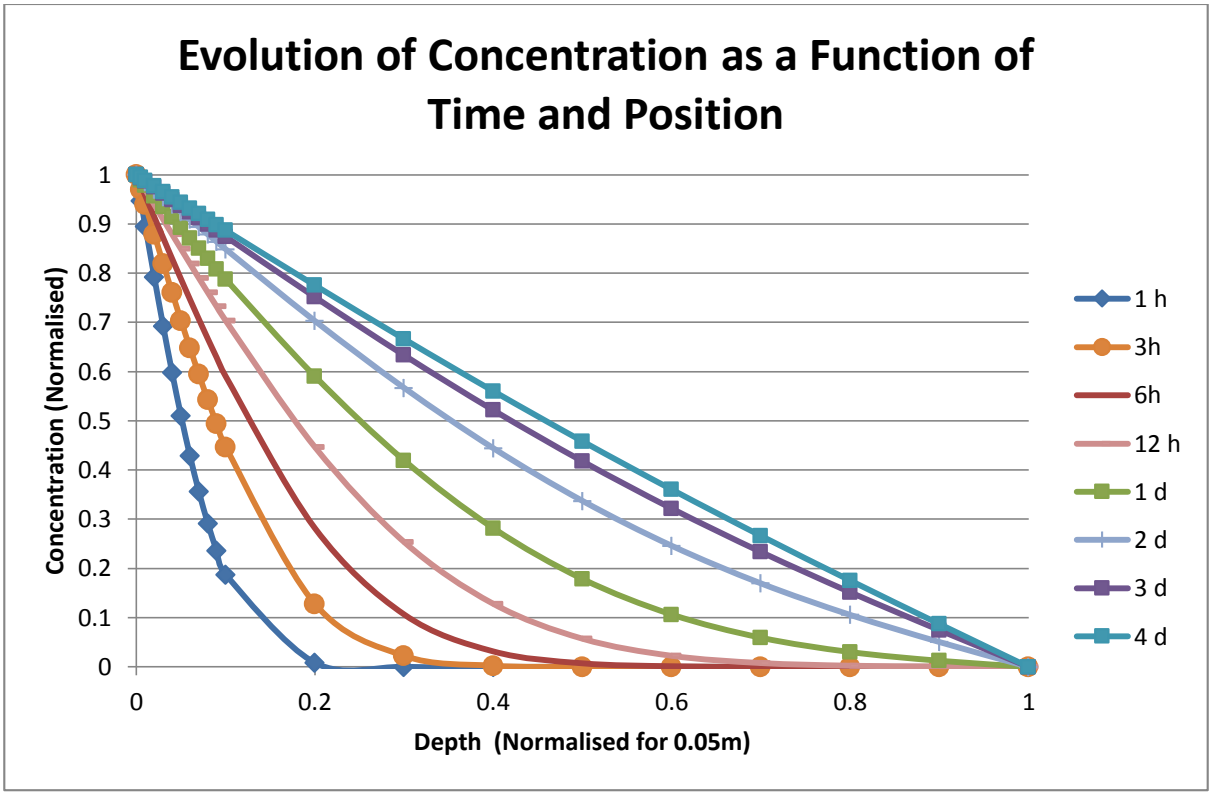


Figure 61: Evolution of a Concentration Profile within PDMS of 0.05m Depth

Conclusions

- NHCs in homogeneous solutions underwent rapid decomposition due to the action of oxygen and moisture in the atmosphere, limited only by mass-transfer effects across the air-solvent interface. Indeed, in the case of homogeneous solutions containing PDMS, decomposition was observed to be rapid. Protection of the NHC was not observed in the case of homogeneous solutions whether silicones were present or not.
- In the case of biphasic systems, protection by PDMS was apparent but an NHC·Si interaction could not be proposed given that the NHC was partitioned in DMSO: the PDMS phase was immiscible. The same protective effect was also evident with paraffin oil in place of PDMS. Paraffin oil been reported by Baceiredo and co-workers to be poorly able to protect a number of NHCs.
- It was therefore possible that the protection reported by Baceiredo and co-workers was due to mass-transfer effects arising from the layer of PDMS/paraffin oil between the NHC solution and the atmosphere. In these cases, decomposition was limited by mass-transfer effects across the air-PDMS interface, diffusion through the PDMS layer, followed by mass-transfer effects across the PDMS-solvent interface.
- Although mass-transfer effects across the PDMS-solvent interface were ignored, solution of Fick's Law for a steady-state system showed that diffusion alone could explain the protection observed by Baceiredo and co-workers without imposing an NHC·Si interaction. Furthermore, the solution of Fick's Second Law for transient systems showed that the layer of PDMS also afforded another "protection" by increasing the time required for the system to reach steady-state mass-transfer.
- Samples of IMes (**4b**) under paraffin oil remained "protected" for over 3 weeks without noticeable degradation of the carbene moiety (assessed by ^{13}C NMR spectroscopy) in contrast to samples under PDMS (770–9000 $g \cdot mol^{-1}$) which began to degrade within 14 days.

6. NHC·Si Interactions - Quo Vadis?

The initial goals of the project were the identification/quantification, tuning, and exploitation of NHC·Si interactions in boomerang catalysis. The objective was a proof of concept for the sequestration of an NHC within a plug-flow reactor by careful choice of the silicon species (most likely an appropriately substituted silicone polymer) and flow and reaction parameters. Such a system would have been of great value not only for the protection of NHCs from aerobic degradation under reaction conditions, but also for the separation of reactants and products in a single process unit concomitant with reaction.

There exists evidence of NHC·Si bonding and hypercoordinate silicon species in the form of ^{29}Si NMR spectroscopic data and crystal structures widely available in the literature:[32,107,109,111] these are not disputed. However, NHC·Si interactions invoked in many organocatalytic cycles and in the protection of NHCs by silicones has not been proven. Indeed, spectroscopic data to corroborate a number of these proposed mechanisms or interactions has not been reported in literature.[43]

^{13}C and ^{29}Si NMR spectroscopy was used to analyse samples of IMes with a range of low molecular weight silicon species in up to 100 equivalents at 298–198K and failed to afford evidence of an NHC·Si interaction. A significant change in NMR shifts for the carbene moiety and the silicon nuclei was not observed. DOSY was also unable to provide evidence for the formation of specific or non-specific NHC·Si interactions. The use of the more Lewis-basic NHC Me_2I*t*Bu and the use of more Lewis-acidic silicon species failed to yield spectroscopic evidence of an NHC·Si interaction. Inferring an interaction with *in situ* monitoring of reaction kinetics was also unsuccessful with no significant changes in reaction rates observed in an NHC-catalysed amidation. Numerous spectroscopic techniques had been unable to prove an NHC·Si interaction.

Modelling of the NHC·Si interaction proposed by Baceiredo and co-workers[90] with: a larger basis-set; BSSE corrections; the use of *ab-initio* methods able to account for dispersion; and evaluation of Gibbs free energies rather electronic energies led to the conclusion that quantum chemical

calculations did not predict a favourable NHC·Si interaction in the gas phase. Although such calculations could be extended to include a solvent model, it is unlikely that these would predict a favourable interaction for the systems described above. Indeed, such predictions would be of little value given our experimental data presented.

These results therefore preclude the development of boomerang catalysis systems that attempt to exploit NHC·Si interactions between NHCs and silicones (or indeed low molecular weight silicon species). However, given the range of reactivities for NHCs (*vide supra*), other "interactions" could still be open to exploitation for example the NHC·CO2 adducts as latent NHCs.[93]

Furthermore, the protection of NHCs by silicone polymers reported by Baceiredo and co-workers[90] could be explained by mass-transfer effects without the need to invoke NHC·Si interactions. Indeed, paraffin oil was shown to be better able to protect NHCs than silicones. In light of the lack of evidence of NHC·Si interactions in the cases investigated above, simpler mechanistic cycles invoking NHCs as bases or nucleophiles without activation of silicon nuclei should be proposed and examined.

In hindsight, a thorough study of the computational data presented in literature prior to our experimental studies with NMR spectroscopy would have allowed us to question the veracity of NHC·Si interactions sooner. However, our experimental data provided further evidence of the lack of an NHC·Si interaction in the systems proposed thus far. Indeed, our experimental data (NMR and reaction kinetics) have allowed us to develop a possible explanation (mass transfer/diffusion) which was then modelled mathematically. Qualitative results show that a modest 2 cm layer of PDMS or paraffin oil is sufficient to diminish the flux of oxygen and water by 2-3 orders of magnitude which is sufficient to explain the protection observed without having to invoke an NHC·Si interaction.

Future experiments could be exploited to not only probe our assumptions of fast decomposition with respect to mass transfer (and the implied reaction at the PDMS/solvent interface), but to also measure the diffusive fluxes of oxygen and water (and diffusion coefficients of the species) in PDMS

of varying molecular weight. Such values are not readily available in literature: where data is available, little attention is paid to the specific molecular weight of the silicone polymers used. Given the now ready availability of PDMS with narrow size distribution as used in our own studies, this should be possible.

7. Experimental

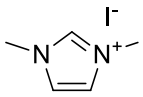
Reagents and solvents were supplied from commercial sources and used as received unless otherwise stated. C_6D_6, THF-d_8, and Tol-d_8 were dried by heating at reflux over potassium metal under a N_2 atmosphere, and degassed with 3 cycles of freeze-pump-thawing. DMSO-d_6 was dried over CaH_2. Deuterated solvents were stored over 4Å M.S. in a Saffron glovebox under a N_2 atmosphere. Silicon species were purified by distillation at reduced pressure and stored over 4Å M.S. in the glovebox.

Reactions were carried out under dry N_2 or Ar unless otherwise indicated. Reactions were monitored by analytical thin-layer chromatography (TLC) performed on Merck silica gel 60 F254 plates. TLC plates were visualised using UV light (254 nm) and/or by staining in basic $KMnO_4$, vanillin, or ninhydrin followed by heating. Solvents were removed *via* rotary evaporation under 40 °C and compounds further dried *in vacuo* unless otherwise stated. Compounds were purified by flash column chromatography using Merck Kieselgel 60 (230-400 mesh).

Infrared spectra were recorded on a Perkin Elmer FT-IR Spectrum-100 with ATR technique and are reported: [frequency of absorption (cm^{-1})]. Samples were directly coated onto the diamond window of the spectrometer; solid samples were pressed onto the diamond (120 Nm). Reported absorbances are strong or medium strength unless otherwise stated and are given in wavenumbers (cm^{-1}). React-IR experiments were performed on a React-IR 4000 and Multimax RB04-50. NMR spectra were recorded with Bruker DRX 400, AV400, and AV500 spectrometers, and referenced from residual protons (or carbon) in the NMR solvent ($CDCl_3$: 7.26, C_6D_6: 7.16, DMSO-d_6: 2.50, THF-d_8:3.58 CD_2Cl_2: 5.32, Tol-d_8: 7.09, DMF-d_7: 8.03) and ($CDCl_3$: 77.16, C_6D_6: 128.06, DMSO-d_6: 39.51, THF-d_8: 67.21, CD_2Cl_2: 53.84, Tol-d_8: 137.48, DMF-d_7: 163.15).[177,197,198] Data are reported: chemical shift [multiplicity (s = singlet, d = doublet, t =triplet, q = quartet, quint = quintet, sext =sextet, sept = septet, m =multiplet), coupling constant(s) in Hertz, (assignment)]. Low and high resolution mass spectroscopy

(EI, CI, ESI) were recorded by the Imperial College London Department of Chemistry Mass Spectroscopy Service using a Micromass Platform II and Micromass AutoSpec-Q spectrometer.

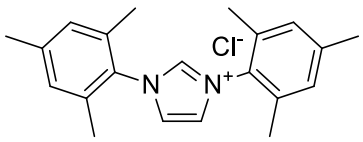
***N,N'*-Bis(methyl)imidazolium Iodide (IMe·HI):**[11]



4a·HI

To a stirred solution of 1-methylimidazole (0.80 mL, 10 mmol) in *i*PrOH (5.50 mL), iodomethane (0.65 mL, 10.5 mmol) was added dropwise. The reaction mixture was then heated at reflux for 8 hours. On cooling in an ice-bath, white solid precipitated. The suspension was filtered and the solid washed with Et_2O and THF. The title compound was isolated as white solid (1.75 g, 78% yield): ^{1}H NMR (400 MHz, $CDCl_3$): δ = 10.01 (s, 1H, NCHN), 7.40 (d, J = 1.6 Hz, 2H, NCH), 4.09 (s, 6H, CH_3); ^{13}C NMR (100 MHz, $CDCl_3$): δ = 137.8, 123.5, 37.2; HRMS (ES-TOF) m/z: $[M - I]^+$ calc for $C_5H_9N_2$ 97.0763, found: 97.0766. The ^{1}H and ^{13}C NMR data were in accordance with literature reports.[11]

***N,N'*-Bis(2,4,6-trimethylphenyl)imidazolium Chloride (IMes·HCl):**[12]

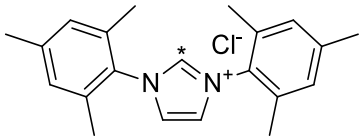


4b·HCl

N,*N*'-Bis(2,4,6-trimethylphenyl)-1,4-diazabutadiene (14.6 g, 50 mmol) and paraformaldehyde (1.50 g, 50 mmol) in EtOAc (400 mL) were stirred at 70 °C. The walls of the flask were washed with EtOAc (42 mL). A solution of TMSCl (6.35 mL, 50 mmol) in EtOAc (8 mL) was added in a slow stream with vigorous stirring. The resulting yellow-brown suspension was stirred at 70 °C overnight. The suspension was then cooled to 10°C in an ice-bath and filtered. The remaining solid was washed with copious amounts of EtOAc and Et_2O. The crude product was twice recrystallised from DCM/EtOAc. The solid was pre-dried by suction filtration followed by drying to constant weight *in vacuo* yielding a white solid (13.4 g, 79% yield): ^{1}H NMR (400 MHz, $CDCl_3$): δ 10.89 (t, J = 1.5 Hz, 1H, NCHN), 7.62 (d, J

= 1.5 Hz, 2H, NCH), 7.00 (s, 4H, Ar-H), 2.32 (s, 6H, *p*-CH_3), 2.16 (s, 12H, *o*-CH_3); ^{13}C NMR (100 MHz, $CDCl_3$): δ 141.4, 139.9, 134.2, 130.7, 130.0, 124.5, 21.3, 17.8; ^{1}H NMR (400 MHz, DMSO-d_6): δ 9.74 (s, 1H, NCHN), 8.28, (s, 2H, NCH), 7.19 (s, 4H, Ar-H), 2.46 (s, 6H, *p*-CH_3), 2.11 (s, 12H, *o*-CH_3); ^{1}H NMR (400 MHz, CD_2Cl_2): δ 11.05 (s, 1H, NCHN), 7.61 (s, 2H, NCH), 7.08 (s, 4H, Ar-H), 2.37 (s, 6H, *p*-CH_3), 2.17 (s, 12H, *o*-CH_3). The ^{1}H and ^{13}C NMR data were in accordance with literature reports.[12]

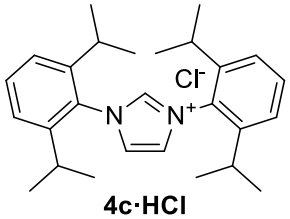
^{13}C-Labelled *N,N'*-Bis(2,4,6-trimethylphenyl)imidazolium Chloride (IMes·HCl):



***4b·HCl**

N,*N*'-Bis(2,4,6-trimethylphenyl)-1,4-diazabutadiene (1.95 g, 6.7 mmol) and ^{13}C-labelled formaldehyde (20 wt% in water, 1 mL, 6.4 mmol) in EtOAc (50 mL) were stirred at 70 °C. The walls of the flask were washed with EtOAc (5 mL). A solution of TMSCl (0.82 mL, 6.4 mmol) in EtOAc (1 mL) was added in a slow stream with vigorous stirring. The resulting orange suspension was stirred at 70 °C overnight. The suspension was then cooled to 10 °C in an ice-bath and filtered. The remaining solid was washed with copious amounts of EtOAc and Et_2O. The crude product was twice recrystallised from DCM/EtOAc. The solid was pre-dried by suction filtration followed by drying to constant weight *in vacuo* yielding a white solid (1.92 g, 88% yield): ^{1}H NMR (400 MHz, $CDCl_3$): δ 10.76 (d, J = 225 Hz, 1H, NCHN), 7.63 (dd, J = 4.7, 1.4 Hz, 2H, NCH), 7.00 (s, 4H, Ar-H), 2.32 (s, 6H, *p*-CH_3), 2.15 (s, 12H, *o*-CH_3); ^{13}C NMR (100 MHz, $CDCl_3$): δ 141.3, 139.7, 134.2, 130.8, 130.0, 124.7, 21.3, 17.8.

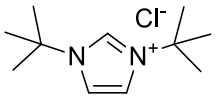
***N,N'*-Bis(2,6-di*iso*propylphenyl)imidazolium Chloride (IDipp·HCl):**[12]



4c·HCl

N,*N*'-Bis(2,6-di*iso*propylphenyl)-1,4-diazabutadiene (2.5 g, 6.6 mmol) and paraformaldehyde (196 mg, 6.5 mmol) in EtOAc (60 mL) were stirred at 70 °C. A solution of TMSCl (0.85 mL, 6.8 mmol) in EtOAc (1 mL) was added in a slow stream with vigorous stirring. The resulting orange suspension was stirred for 2 h at 70 °C. The suspension was then cooled to 10 °C in an ice-bath and filtered. The remaining solid was washed with copious amounts of EtOAc. The crude product was recrystallised from DCM/EtOAc twice. The solid was pre-dried by suction filtration followed by drying to constant weight *in vacuo* yielding a white solid (2.48 g, 90% yield): ^{1}H NMR (400 MHz, DMSO-d_6): δ 10.24 (app. t, J = 1.5 Hz, 1H, NCHN), 8.58 (d, J = 1.5 Hz, 2H, NCH), 7.69 (t, J = 7.9 Hz, 2H, *p*-Ar-H), 7.53 (d, J = 7.8 Hz, 4H, *m*-Ar-H), 2.34 (sept, J = 6.7 Hz, 4H, CH), 1.26 (d, J = 6.8 Hz, 12H, CH_3), 1.16 (d, J = 6.9 Hz, 12H, CH_3); ^{13}C NMR (100 MHz, DMSO-d_6): δ 144.8, 139.3, 131.8, 130.0, 126.2, 124.6, 28.6, 24.1, 23.1. The ^{1}H and ^{13}C NMR data were in accordance with literature reports.[12]

***N,N'*-Bis(*tert*-butyl)imidazolium Chloride (I*t*Bu·HCl):**[118]

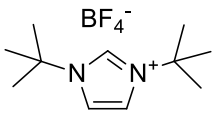


4d·HCl

To a stirred solution of paraformaldehyde (300 mg, 10 mmol) in toluene (10 mL), *tert*-butyl amine (1.06 mL, 10 mmol) was added dropwise. The mixture was heated until a clear solution formed. After cooling to 0 °C, another equivalent of *tert*-butyl amine (1.06 mL, 10 mmol) was added dropwise, followed by HCl (37 wt% in H_2O, 0.82 mL, 10 mmol) in water (2.5 mL). The solution was allowed to warm to r.t. and glyoxal (40 wt% in H_2O, 1.14 mL, 10 mmol) was added dropwise. The reaction

mixture was then stirred at 40 °C for 15 hours. After dilution with aq. $NaHCO_3$, the aqueous phase was extracted with Et_2O (2 x 10 mL). The water of the aqueous phase was then removed *in vacuo* and the residue was extracted with DCM (3 x 5 mL). The title compound was recrystallised from DCM/EtOAc (0.97 g, 36% yield): ^{1}H NMR (400 MHz, DMSO-d_6): δ 9.16 (s, 1H, NCHN), 8.10 (d, J = 1.7 Hz, 2H, NCH), 1.61 (s, 18H, CH_3); ^{13}C NMR (100 MHz, DMSO-d_6): δ 132.3, 120.5, 59.6, 29.1. The ^{1}H and ^{13}C NMR data were in accordance with literature reports.[118]

***N,N'*-Bis(*tert*-butyl)imidazolium Tetrafluoroborate (I*t*Bu·HBF$_4$):**[118]



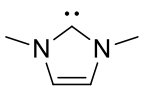
4d·HBF$_4$

To a stirred solution of paraformaldehyde (300 mg, 10 mmol) in toluene (10 mL), *tert*-butyl amine (1.06 mL, 10 mmol) was added dropwise. The reaction mixture was heated until a clear solution formed. The solution was cooled to 0 °C in an ice-bath and another equivalent of *tert*-butyl amine (1.06 mL, 10 mmol) was added dropwise, followed by HBF_4 (48 wt% in H_2O, 1.31 mL 10 mmol) and glyoxal (40 wt% in H_2O, 1.14 mL, 10mmol). The solution was then heated to 40 °C. A white precipitate began to form. After 16 h, the slurry was cooled to r.t. and filtered. The solid was washed with a minimal amount of deionised water and Et_2O, and was dried to constant weight *in vacuo*. The product was isolated as a white solid (2.32 g, 87% yield): ^{1}H NMR (400 MHz, DMSO-d_6) δ 8.99 (s, 1H, NCHN), 8.05 (d, J = 1.6 Hz, 2H, NCH), 1.60 (s, 18H, CH_3); ^{13}C NMR (100 MHz, DMSO-d_6): δ 132.1, 120.4, 59.6, 29.0. The ^{1}H and ^{13}C NMR data were in accordance with literature reports.[118]

General Procedure for the Deprotonation of an Imidazolium Salt to Yield a Free NHC:

An imidazolium salt (1 mmol) and *t*BuOK (168 mg, 1.5 mmol) in THF (5-10 mL) were stirred at r.t. for 1.5 h. Excess solvent was removed *in vacuo* leaving a white solid. The NHC was extracted into hot, dry toluene (ca. 20 mL) and the solution filtered through a frit aided by a partial vacuum. The colourless to pale yellow solution was concentrated to dryness *in vacuo* yielding an off-white solid. The NHC was recrystallised from dry hexane which yielded colourless needles on gradual cooling to room temperature.

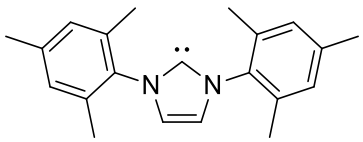
1,3-Bis(methyl)imidaol-2-ylidene (IMe):[5]



4a

The title compound was prepared *in situ* by the addition of THF-d_8 (0.7 mL) to *N,N'*-bis(methyl)imidazolium iodide (45 mg, 0.2 mmol) and tBuOK (16.8 mg, 0.15 mmol) in a NMR tube. Attempts to isolate the free NHC by removal of solvent under reduced pressure led to decomposition: ^{13}C NMR (100 MHz, THF-d_8): δ 212.9, 120.6, 37.6. The ^{13}C NMR data were in accordance with literature reports.[5]

1,3-Bis(2,4,6-trimethylphenyl)-imidazol-2-ylidene (IMes):

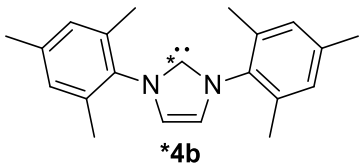


4b

The title compound was prepared according to the General Procedure from 1,3-bis(2,4,6-trimethylphenyl)imidazolium chloride and isolated as white needles in up to 76% yield: ^{1}H NMR (400 MHz, THF-d_8): δ 7.06 (s, 2H, NCH), 6.96 (s, 4H, *m*-Ar-H), 2.31 (s, 6H, *p*-CH_3), 2.08 (s, 12H, *o*-CH_3); ^{13}C

NMR (100 MHz, THF-d_8): δ 219.7, 139.7, 137.5, 135.7, 129.1, 121.2, 20.9, 17.9; ^{1}H NMR (400 MHz, C_6D_6): δ 6.81 (s, 4H, *m*-Ar-H), 6.49 (s, 2H, NCH), 2.16 (s, 6H, *p*-CH_3), 2.15 (s, 12H, *o*-CH_3); ^{13}C NMR (100 MHz, C_6D_6): δ 219.2, 139.3, 137.3, 135.5, 129.1, 120.6, 21.1, 18.1; ^{1}H NMR (400 MHz, Tol-d_8): δ 6.78 (s, 4H, *m*-Ar-H), 6.50 (s, 2H, NCH), 2.17 (s, 6H, *p*-CH_3), 2.12 (s, 12H, *o*-CH_3); ^{13}C NMR (100 MHz, Tol-d_8): δ 218.8, 139.5, 137.6, 135.7, 129.5, 120.9, 21.4, 18.8, 18.4; ^{1}H NMR (400 MHz, DMSO-d_6): δ 7.27 (s, 2H, NCH), 7.02 (s, 4H, *m*-Ar-H), 2.30 (s, 6H, *p*-CH_3), 2.02 (s, 12H, *o*-CH_3); ^{13}C NMR (100 MHz, DMSO-d_6): δ 214.3, 138.1, 136.8, 134.5, 128.4, 121.1, 20.6, 17.3. The ^{1}H and ^{13}C NMR data were in accordance with literature reports.[14]

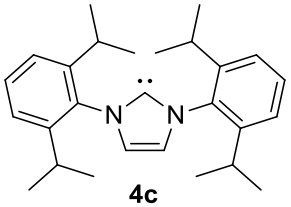
^{13}C-Labelled 1,3-Bis(2,4,6-trimethylphenyl)-imidazol-2-ylidene (IMes):



***4b**

The title compound was prepared according to the General Procedure from ^{13}C-labelled 1,3-Bis(2,4,6-trimethylphenyl)imidazolium chloride and isolated as white needles in up to 71% yield: ^{1}H NMR (400 MHz, C_6D_6): δ 6.81 (s, 4H, *m*-Ar-H), 6.51 (s, 2H, NCH), 2.16 (br s, 18H, CH_3); ^{13}C NMR (100 MHz, C_6D_6): δ 219.4, 139.4, 139.3, 137.2, 135.5, 129.1, 120.6, 21.1, 18.1. The ^{1}H and ^{13}C NMR data were in accordance with literature reports.[14]

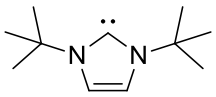
1,3-Bis(2,6-di*iso*propylphenyl)-imidazol-2-ylidene (IDipp):



4c

The title compound was prepared according to the General Procedure from 1,3-bis(2,6-di*iso*propylphenyl)imidazolium chloride and isolated as white needles in up to 67% yield: ^{1}H NMR (400 MHz, C_6D_6): δ 7.33–7.27 (m, 2H, *p*-Ar-H), 7.22–7.17 (m, 4H, *m*-Ar-H), 6.62 (s, 2H, NCH), 2.97 (sept, J = 6.9 Hz, 4H, CH), 1.29 (d, J= 6.9 Hz, 12H, CH_3), 1.19 (d, J = 7.0 Hz, 12H, CH_3); ^{13}C NMR (100 MHz, C_6D_6): δ 219.7, 146.3, 138.9, 129.1, 123.7, 121.6, 28.8, 24.8, 23.7. The ^{1}H and ^{13}C NMR data were in accordance with literature reports.[14]

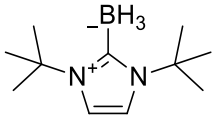
1,3-Bis(*tert*-butyl)-imidazol-2-ylidene (I*t*Bu):



4d

The title compound was prepared according to the General Procedure from and 1,3-bis(*tert*-butyl)imidazolium chloride or 1,3-bis(*tert*-butyl)imidazolium tetrafluoroborate but was not recrystallised from hexane. The title compound was isolated as a white crystalline solid in up to 60% yield: ^{1}H NMR (400 MHz, C_6D_6): δ 6.78 (s, 2H, NCH), 1.51 (s, 18H, CH_3); ^{13}C NMR (100 MHz, C_6D_6): δ 212.8, 115.1, 55.8, 31.5. The ^{1}H and ^{13}C NMR data were in accordance with literature reports.[16]

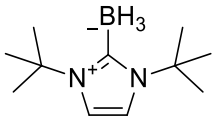
I*t*Bu·BH_3 from I*t*Bu·HBF_4:



4d·BH_3

Based on a literature procedure reported by Curran and co-workers,[30] NaHMDS (1 M in THF, 1.1 mL, 1.1 mmol) was added dropwise to a stirred solution of I*t*Bu·HBF_4 (250 mg, 0.932 mmol) in THF (5 mL) at −78 °C. After 1 hour, BH_3·THF (1 M in THF, 1 mL, 1 mmol) was added dropwise. The solution was stirred and warmed to r.t. overnight. Volatiles were removed under reduced pressure and the remaining solid purified by flash column chromatography with DCM as eluent. The title compound was recovered as an off-white solid (20.3 mg, 11% yield): ^{1}H NMR ($CDCl_3$, 400 MHz): δ 6.99 (s, 2H, NCH), 1.78 (s, 18H, CH_3); ^{11}B NMR ($CDCl_3$, 128 MHz): δ -31.8; ^{13}C NMR ($CDCl_3$, 100 MHz): δ = 115.7, 90.9, 60.0, 30.3.

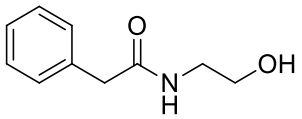
I*t*Bu·BH_3 from I*t*Bu:[30]



4d·BH_3

Based on a literature procedure reported by Curran and co-workers,[30] BH_3·THF (1 M in THF, 2.4 mL, 2.4 mmol) was added dropwise to a stirred solution of I*t*Bu (360 mg, 2 mmol) in THF (5 mL) at −78 °C. The solution was warmed to r.t. overnight. Volatiles were removed under reduced pressure and the remaining solid purified by flash column chromatography with DCM as eluent. The title compound was recovered as a white solid (366 mg, 82% yield). The spectroscopic data was identical to the data of the compound obtained from I*t*Bu·HBF_4.

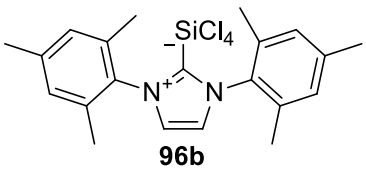
***N*-(2-Hydroxyethyl)-2-phenylacetamide:**[71]



71

To a solution of IMes (30 mg, 0.10 mmol) in THF (1.95 mL), methyl phenylacetate (280 µL, 2 mmol) and ethanolamine (120 µL, 2 mmol) were added sequentially. The reaction mixture was stirred for 8 h at room temperature. The volatiles were removed under reduced pressure and the residue purified by flash column chromatography (5% MeOH/DCM) to afford the amide as a white solid (336 mg, 94% yield): ^{1}H NMR (400 MHz, $CDCl_3$): δ 7.26–7.13 (m, 5H, Ar-H), 5.77 (br s, 1H, NH), 3.69 (app. q, J = 4.8 Hz, 2H, CH_2OH), 3.47 (s, 2H, Ph-CH_2), 3.37 (q, J = 4.6 Hz, 2H, NCH_2), 2.55 (t, J = 4.9 Hz, 1H, OH); ^{13}C NMR (100 MHz, $CDCl_3$): δ 172.3, 134.8, 128.9, 128.4, 126.7, 60.8, 42.8, 42.0; HRMS (ES-TOF) m/z: $[M + H]^+$ calc for $C_{10}H_{14}NO_2$ 180.1025, found: 180.1025. The ^{1}H and ^{13}C NMR data were in accordance with literature reports.[71]

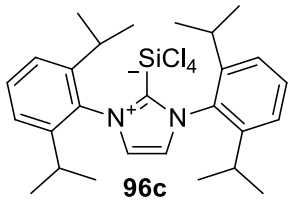
IMes·$SiCl_4$:



96b

To a stirred solution of IMes (30 mg, 0.1 mmol) in hexane (2 mL), $SiCl_4$ (0.1 mmol) was added. A white precipitate formed immediately. The slurry was stirred under an inert atmosphere for 48 h. The solid was washed with hexane through a syringe filter. NMR samples were prepared by passing deuterated solvents through the syringe filter and collecting the filtrate: ^{1}H NMR (400MHz, CD_2Cl_2): δ 7.61 (s, 2H, NCH), 7.09 (s, 4H, Ar-H), 2.38 (s, 6H, *p*-CH_3), 2.17 (s, 6H, *o*-CH_3); ^{13}C NMR (100 MHz, CD_2Cl_2): δ 141.9, 139.4, 134.6, 131.0, 130.2, 125.0, 21.3, 17.8; ^{29}Si NMR (75 MHz, C_6D_6): δ -110.

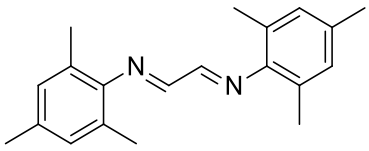
IDipp·$SiCl_4$:



96c

To a stirred solution of IDipp (39 mg, 0.1 mmol) in hexane (2 mL), $SiCl_4$ (0.1 mmol) was added. A white precipitate formed immediately. The slurry was stirred under an inert atmosphere for 48 h. The solid was washed with hexane through a syringe filter. NMR samples were prepared by passing deuterated solvents through the syringe filter and collecting the filtrate: ^{1}H NMR (400MHz, CD_2Cl_2): δ 7.42 (d, J = 7.8 Hz, 6H, Ar-H), 7.29 (s, 2H, NCH), 2.99 (sept, J = 6.7 Hz, 4H, CH), 1.44 (d, J = 6.6 Hz, 12H, CH_3), 1.17 (d, J = 6.9 Hz, 12H, CH_3); ^{13}C NMR (100 MHz, C_6D_6): δ 147.1, 132.1, 124.6, 123.1, 29.4, 26.6, 22.3; ^{29}Si NMR (75 MHz, C_6D_6): δ -109. The ^{1}H, ^{13}C, and ^{29}Si NMR data were in accordance with literature reports.[111]

***N*,*N*'-Bis(2,4,6-trimethylphenyl)-1,4-diazabutadiene:**[12]

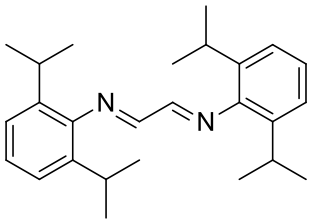


108b

Glyoxal (40 wt% in H_2O, 23 mL, 200 mmol) in *i*PrOH (100 mL) was added under stirring to 2,4,6-trimethylaniline (56 mL, 400 mmol) and AcOH (1 mL) in *i*PrOH (100 mL) at 50 °C. A mild exothermic reaction ensued and the formation of a suspension was observed within 15 minutes. The mixture was cooled to r.t. and stirred overnight. The suspension was filtered and the solid product was washed with *i*PrOH until the initially dark orange/brown filtrate turned bright yellow. The product was pre-dried by suction filtration then dried to constant weight *in vacuo*. The filtrate and washings were set aside and concentrated to a volume ca. 50 mL by rotary evaporation to allow for a second crystallisation. The product was isolated as bright yellow needles (54.4 g, 93% yield): ^{1}H NMR (400

MHz, $CDCl_3$): δ 8.10 (s, 2H, NCH), 6.91 (s, 4H, Ar-H), 2.29 (s, 6H, *p*-CH_3), 2.16 (s, 12H, *m*-CH_3); ^{13}C NMR (100 MHz, $CDCl_3$): δ 163.6, 147.6, 134.4, 129.1, 126.7, 20.9, 18.4. The ^{1}H and ^{13}C NMR data were in accordance with literature reports.[12]

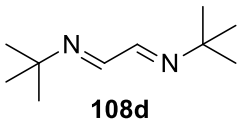
***N*,*N*'-Bis(2,6-di*iso*propylphenyl)-1,4-diazabutadiene:**[12]



108c

Glyoxal (40 wt% in H_2O, 5.30 mL, 50 mmol) in MeOH (25 mL) was added under stirring to 2,6-di*iso*propylaniline (18.9 mL, 100 mmol) and AcOH (0.10 mL) in MeOH (25 mL) at 50 °C. A mild exothermic reaction ensued and the formation of a suspension was observed within 15 minutes. The mixture was cooled to r.t. and stirred overnight. The suspension was filtered and the solid product was washed with MeOH until the initially dark orange/brown filtrate turned bright yellow. The product was pre-dried by suction filtration then dried to constant weight *in vacuo*. The filtrate and washings were set aside and concentrated to a volume ca. 50 mL by rotary evaporation to allow for a second crystallisation. The product was isolated as bright yellow needles (14.3 g, 76% yield): ^{1}H NMR (400 MHz, $CDCl_3$): δ 8.10 (s, 2H, NCH), 7.22–7.15 (m, 6H, Ar-H), 2.94 (sept, J = 6.9 Hz, 4H, CH), 1.21 (d, J = 6.9 Hz, 24H, CH_3); ^{13}C NMR (100 MHz, $CDCl_3$): δ 163.2, 148.2, 136.9, 125.3, 123.3, 28.2, 23.5. The ^{1}H and ^{13}C NMR data were in accordance with literature reports.[12]

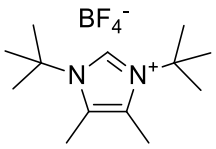
***N*,*N*'-Bis(*tert*-butyl)-1,4-diazabutadiene:**[117]



108d

Glyoxal (40 wt% in H_2O, 2.50 mL, 22 mmol) was added dropwise to a stirred solution of *tert*-butyl amine (4.6 mL, 44 mmol) in DCM (6 mL) at 0 °C. Anhydrous $CaCl_2$ (2 g) was added in a single portion. After 30 min, the reaction mixture was heated until phase separation occurred. The organic layer was decanted and concentrated under reduced pressure. The title compound was isolated as a crystalline solid (2.75 g, 74% yield) by adding Et_2O to the oily residue and letting it stand overnight: ^{1}H NMR (400 MHz, $CDCl_3$): δ 7.93 (s, 2H, NCH), 1.25 (s, 18H, CH_3); ^{13}C NMR (100 MHz, $CDCl_3$): δ 158.0, 58.4, 29.5; HRMS (CI+) m/z: $[M + H]^+$ calc for $C_{10}H_{21}N_2$ 169.1705, found: 169.1702. The ^{1}H and ^{13}C NMR data were in accordance with literature reports.[117]

1,3-Bis(*tert*-butyl)-4,5-dimethylimidazolium Tetrafluoroborate (Me_2I*t*$Bu\cdot HBF_4$):[88]

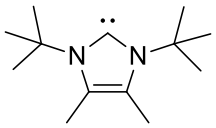


109·HBF_4

To a vigorously stirred solution of *N*-(but-3-yn-2yl)-*N*-*tert*-butylformamide (5.79 g, 37.8 mmol) in MeCN (11 mL), dimethyl sulphate (4.29 mL, 45.4 mmol) was added dropwise at room temperature. The reaction mixture was stirred overnight followed by 24 h at 50 °C. The reaction mixture was then cooled to -20 °C and *tert*-butyl amine (6.35 mL, 60.5 mmol) was added dropwise. The resulting mixture was then warmed to r.t. and stirred overnight followed by a further 48 h at 50 °C. Volatiles were removed *in vacuo* and the crude residue taken up in $CHCl_3$ (100 mL). The solution was washed with $NaBF_4$ (3 M in H_2O, 3 x 25 mL) and the organic layer dried over $MgSO_4$. The solvent was removed in vacuo and the residue recrystallised from $CHCl_3$/EtOAc to yield the title compound as a white solid (6.85 g, 61% yield): ^{1}H NMR (400 MHz, $CDCl_3$): δ 8.37 (s, 1H, NCHN), 2.42 (s, 6H, CH_3), 1.75

(s, 18H, CH_3); ^{13}C NMR (100 MHz, $CDCl_3$): δ 130.5, 128.3, 61.0, 29.0, 11.3. The ^{1}H and ^{13}C NMR data were in accordance with literature reports.[88]

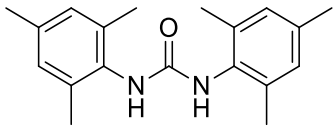
1,3-Bis(*tert*-butyl)-4,5-dimethyl-imidazol-2-ylidene (Me_2ItBu):[88]



109

The title compound was prepared according to the General Procedure from 1,3-bis(*tert*-butyl)-4,5-dimethylimidazolium tetrafluoroborate, with the exception that *t*BuOK was delivered as a 1M THF solution at −78 °C. The reaction mixture was slowly warmed to r.t. and stirred for an additional 1.5 hours prior to workup. The title compound was isolated as colourless oil in up to 64% yield: ^{1}H NMR (400 MHz, THF-d_8): δ 2.21 (s, 6H), 1.55 (s, 18H); ^{13}C NMR (100 MHz, THF-d_8): δ 212.2, 124.3, 57.2, 33.9, 13.0; ^{1}H NMR (400 MHz, CD_2Cl_2): δ 2.39 (s, 6H), 1.79 (s, 18H); ^{1}H NMR (400 MHz, Tol-d_8): δ 2.00 (s, 6H), 1.58 (s, 18H). The ^{1}H and ^{13}C NMR data were in accordance with literature reports.[88]

***N,N'*-Bis(2,4,6-trimethylphenyl)urea:**

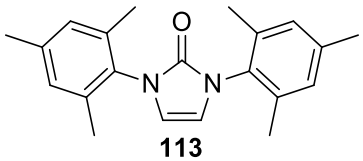


111

To a stirred solution of 2,4,6-trimethylaniline (4.2 mL, 30 mmol) and NEt_3 (4.5 mL, 32 mmol) in DCM (50 mL), phosgene (20% toluene solution, 2.7 mL, 5.4 mmol) was added slowly at 0 °C. The solution was warmed to r.t. and an exothermic reaction ensued. A white precipitate formed. The reaction mixture was stirred overnight at room temperature. The reaction mixture was diluted with 0.1 N HCl (60 mL) and the organic phase decanted. The organic layer was washed with aq. $NaHCO_3$ until the aqueous layer was neutral pH. The organic layer was then dried over $MgSO_4$ and volatiles were

removed under reduced pressure. Recrystallising from EtOH yielded a colourless solid (1.02 g, 64% yield). The isolated solid was very poorly soluble in Tol-d_8, C_6D_6, $CDCl_3$, DMSO-d_6, and D_2O at room and elevated temperatures. No suitable solvent for NMR analysis was identified.[121,199] HRMS (ES-TOF) m/z: $[M + H]^+$ calc for $C_{19}H_{25}NO_2$ 297.1967, found: 297.1963.

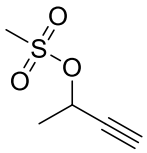
1,3-Bis(2,4,6-trimethylphenyl)-imidazol-2-one:



113

Based on a literature procedure reported by Owen and co-workers,[36] a flask was charged with copper(I)oxide (143 mg, 1 mmol) and IMes·HCl (341 mg, 1 mmol). Toluene (100 mL) and acetonitrile (25 mL) were subsequently added to the mixture. The mixture was heated to reflux for 3 d to provide a colourless solution with a small amount of red-brown precipitate. After removing the solid material by filtration, all volatiles were removed under reduced pressure. The residue was subsequently extracted with DCM (3 x 10 mL), filtered through Celite, and layered with an equal volume of hexane. A colourless solid precipitated and was isolated by filtration (136 mg). The sample contained acetone, thus product purity was 85% and a revised yield of 36% was calculated: ^{1}H NMR ($CDCl_3$, 400 MHz): δ 7.05 (s, 2H, NCH), 7.00 (s, 4H, *m*-Ar-H), 2.17 (s, 6H, *p*-CH_3), 2.10 (s, 12H, *o*-CH_3); ^{1}H NMR (DMSO-d_6, 400 MHz): Major: δ 7.70 (s, 2H, NCH), 7.12 (s, 4H, *m*-Ar-H), 2.33 (s, 6H, *p*-CH_3), 2.07 (s, 12H, *o*-CH_3); Minor: δ 7.59 (s, 2H, NCH), 7.00 (s, 4H, *m*-Ar-H), 2.40 (s, 6H, *p*-CH_3), 1.63 (s, 12H, *o*-CH_3); ^{13}C NMR ($CDCl_3$, 100 MHz): δ 139.7, 135.2, 134.7, 129.7, 122.4, 21.3, 17.9. Due to the poor solubility of the product, the ^{13}C NMR signal for the carbonyl carbon could not be observed. Otherwise, the ^{1}H and ^{13}C NMR data were in accordance with literature reported values.[123]

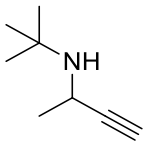
But-3-yn-2-yl methanesulfonate:[88]



128

To a stirred solution of 3-butyn-2-ol (5.6 mL, 71.3 mmol) in DCM (100 mL) at −78 °C, Et_3N (20 mL, 142.7 mmol) was added slowly followed by dropwise addition of methanesulfonyl chloride (8.3 mL, 107.0 mmol). The solution quickly became turbid with formation of a colourless precipitate. The reaction mixture was stirred for 2 h and then quenched with Et_2O/H_2O (100 mL, 1:1 v/v). The organic layer was separated, washed with brine (2 x 25 mL), and dried over $MgSO_4$. The organic phases were combined, filtered and concentrated *in vacuo* to afford the title compound as colourless oil in quantitative yield (21 g): ^{1}H NMR (400 MHz, $CDCl_3$): δ 5.28 (qd, J = 6.7, 2.1 Hz, 1H, CH, CH_3CH), 3.12 (s, 3H, CH_3, OSO_2CH_3), 2.71 (d, J = 2.2 Hz, 1H, C≡CH), 1.65 (d, J = 6.8 Hz, 3H, CH_3); ^{13}C NMR ($CDCl_3$, 100 MHz): δ 80.0, 76.3, 67.4, 39.0, 22.3. The ^{1}H and ^{13}C NMR data were in accordance with literature reports.[88]

***N*-(*tert*-butyl)-but-3-yn-2-amine:**[88]

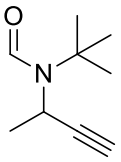


129

To a stirred solution of *tert*-butyl amine (22.5 mL, 214.0 mmol) in DMF (18 mL), but-3-yn-2-yl methanesulfonate (11.4 g, 71.3 mmol) was added dropwise. The flask was sealed and the reaction mixture was stirred at r.t. for 1 h followed by 50 °C for 3 days. The reaction mixture was then poured onto KOH (85% KOH, 14.1g, 214 mmol) in ice-cold water (70 mL), and extracted with pentane (2 x 70 mL). The organic layers were combined, dried over $MgSO_4$ followed by KOH, and evaporated under reduced pressure. Purification by flash column chromatography (50% EtOAc/Hexanes) afforded the

product as brown oil (7.48g, 84% yield): ^{1}H NMR (400 MHz, $CDCl_3$): δ 3.51 (qd, J = 6.8, 2.1 Hz, 1H, CH), 2.19 (d, J = 2.1 Hz, 1H, C≡CH), 1.31 (d, J = 6.9 Hz, 3H, CH_3), 1.16 (s, 9H, CH_3); ^{13}C NMR (100 MHz, $CDCl_3$): δ 89.6, 69.5, 51.3, 38.9, 29.7, 25.3. The ^{1}H and ^{13}C NMR data were in accordance with literature reports.[88]

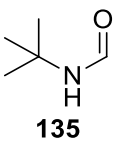
***N*-(but-3-yn-2-yl)-*N*-*tert*-butylformamide:**[88]



130

To a stirred solution of *N*-(*tert*-butyl)-but-3-yn-2-amine (8.35g, 66.7 mmol) in THF (30 mL), formyl acetate (11.75 g, 133.4 mmol) was added dropwise at -10 °C. The reaction mixture turned yellow in colour. The reaction was warmed to r.t. and stirred for an additional 3 h at 50 °C. The reaction mixture was poured into ice-cold water (70 mL) and extracted with EtOAc (3 x 70 mL). The organic layers were combined, dried over $MgSO_4$, and evaporated under reduced pressure. The title compound was recovered as an off-white solid (6.72 g, 66% yield): ^{1}H NMR (400 MHz, $CDCl_3$): Major rotamer: δ 8.42 (s, 1H, CHO), 4.39 (qd, J = 6.9, 2.4 Hz, 1H, CH_3CH), 2.29 (d, J = 2.5 Hz, 1H, C≡CH), 1.63 (d, J = 7.0 Hz, 3H, CH_3), 1.41 (s, 9H, CMe_3); ^{13}C NMR (100 MHz, $CDCl_3$): δ 160.7, 83.4, 70.0, 56.7, 40.3, 29.4, 20.3. The ^{1}H and ^{13}C NMR data were in accordance with literature reports.[88]

***N*-(*tert*-butyl)formamide from Ethyl Formate:**[142]

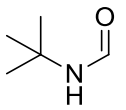


135

Ethyl formate (2.01 mL, 25 mmol) and *tert*-butyl amine (2.65 mL, 25 mmol) were heated at reflux for the appropriate time in a sealed tube. Volatiles were removed under reduced pressure. *Tert*-butyl

formamide was recovered as colourless oil in trace yield after 4 h, or 26% yield after refluxing overnight: ^{1}H NMR (400 MHz, $CDCl_3$): δ 8.16 (d, J = 12.3 Hz, 1H, *trans*-CHO), 7.91 (d, J = 2.0 Hz, 1H, *cis*-CHO), 6.96 (br s, 1H, *trans*-NH), 6.04 (br s, 1H, *cis*-NH), 1.27 (s, 9H, *trans*-CH_3), 1.23 (s, 9H, *cis*-CH_3); ^{13}C NMR (100 MHz, $CDCl_3$): δ 163.3, 160.8, 51.1, 50.2, 30.7, 28.8. The ^{1}H and ^{13}C NMR data were in accordance with literature reports.[143]

***N*-(*tert*-butyl)formamide from Formyl Acetate:**



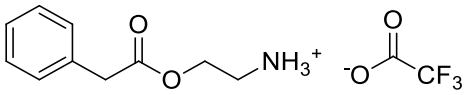
135

tert-Butyl amine (2.65 mL, 25 mmol) was added dropwise to a stirred solution of formic acid (1.90 mL, 50 mmol) and acetic anhydride (4.70 mL, 50 mmol) at room temperature. The reaction mixture was refluxed for 1 h in a sealed tube followed by removal of volatiles under reduced pressure. *Tert*-butyl formamide was isolated as colourless oil (2.57 g, quantitative yield). The spectroscopic data was identical to the data of the compound obtained from the ethyl formate reaction.

General Procedure for Kinetic Studies of IMes-Catalysed Transesterification and Amidation:

To a mixture of IMes (30 mg, 0.10 mmol) and 4Å M.S. (1.0 g) in THF (1 mL), methyl acetate (160 µL, 2 mmol) and/or benzyl alcohol (0.21 mL, 2 mmol) and/or ethylamine (1mL, 2 mmol) and/or ethanolamine (120 µL, 2 mmol) were added sequentially. The reaction mixture was stirred for 1 h at room temperature. The volatiles were removed under reduced pressure and the residue purified by flash column chromatography (10% EtOAc/Hexanes followed by 5% MeOH/DCM).

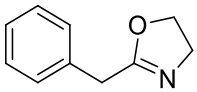
2-Aminoethyl 2-phenylacetate:



146

N-Boc-aminoethyl 2-phenylacetate (17 mg, 0.09 mmol) was added to neat TFA (0.2 mL) under stirring. Starting material was consumed within 10 minutes. Excess TFA was removed *in vacuo* to leave colourless oil. The oil readily decomposed before full characterisation could be completed: IR (ATR) ν 1672, 1641, 1541, 1186, 1131, 1067, 839, 799, 721.

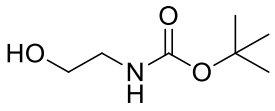
2-Benzyloxazole:[182,184]



155

N-(2-chloroethyl)-2-phenylacetamide (1 mmol, 0.2 g) in MeOH (5 mL) was stirred with NaOH (1 mmol, 40.5 mg) over 3 days. Removal of volatiles under reduced pressure and purification of the crude product by flash column chromatography (30% EtOAc/Hexanes) yielded the oxazoline in trace amount (16 mg): ^{1}H NMR (400 MHz, $CDCl_3$): δ 7.35–7.24 (m, 5H, Ar-H), 4.24 (t, J = 9.5 Hz, 2H, CH_2), 3.84 (t, J = 9.5 Hz, 2H, CH_2), 3.62 (s, 2H, Ph-CH_2); ^{13}C NMR (100 MHz, $CDCl_3$): δ 167.1, 135.3, 129.1, 128.7, 127.1, 67.8, 54.6, 34.9; HRMS (CI) m/z: $[M + H]^+$ calc for $C_{10}H_{12}NO$ 162.0919, found: 162.0916. The ^{1}H and ^{13}C NMR data were in accordance with literature reports.[182,184]

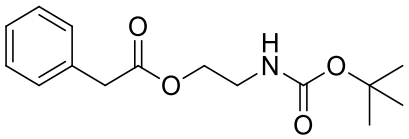
***tert*-Butyl (2-hydroxyethyl)carbamate:**[200]



156

Boc-anhydride (5 g, 23 mmol) was stirred in THF (20 mL) cooled to 0 °C. Ethanolamine (1.4 mL, 23 mmol) in THF (10 mL) was added dropwise. A mildly exothermic reaction with gas evolution ensued. The reaction was followed by TLC (10% MeOH/DCM). On complete consumption of starting material, excess solvent was removed under reduced pressure. Flash column chromatography (10% MeOH/DCM) yielded the title compound as yellow oil (3.80 g, 90% yield): ^{1}H NMR (400 MHz, $CDCl_3$): δ 4.91 (br s, 1H, NH), 3.71 (app. q, J = 5.1 Hz, 2H, CH_2), 3.29 (app. q, J = 5.4 Hz, 2H, CH_2), 2.25 (br s, 1H, OH), 1.45 (s, 9H, CH_3); HRMS (EI+) m/z: $[M]^+$ calc for $C_7H_{15}NO_3$ 161.1052, found: 161.1054. The ^{1}H NMR data were in accordance with literature reports.[200]

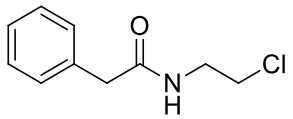
***N*-Boc-acminoethyl-2-phenylacetate:**



158

Phenylacetic acid (681 mg, 5 mmol) was added in a single portion to a stirred solution of CDI (892 mg, 5.5 mmol) in DCM (5 mL) at 0 °C. A yellow solution formed on warming to r.t. with gas evolution. On conclusion of gas evolution, *N*-Boc-ethanolamine (806 mg, 5.5 mmol) was added and the reaction stirred overnight. Purification by flash column chromatography (50% EtOAc/Hexanes) afforded the title compound as a white solid (1 g, 72% yield): ^{1}H NMR (400 MHz, $CDCl_3$): δ 7.37–7.27 (m, 5H, Ar-H), 4.75 (br s, 1H, NH), 4.16 (t, J = 5.4 Hz, 2H, OCH_2), 3.65 (s, 2H, Ph-CH_2), 3.38 (app. q, J = 5.6 Hz, 2H, $NHCH_2$), 1.46 (s, 9H, CH_3); ^{13}C NMR (100 MHz, $CDCl_3$): δ 171.6, 155.8, 133.9, 129.3, 128.7, 127.3, 79.6, 64.1, 41.3, 39.7, 28.5; HRMS (ES-TOF) m/z: $[M + Na]^+$ calc for $C_{15}H_{21}NO_4Na$ 302.1368, found: 302.1370.

***N*-(2-chloroethyl)-2-phenylacetamide:**[182,183]



160

$SOCl_2$ (0.5 mL, 0.8 g, 6.7 mmol) was added dropwise to a stirred solution of *N*-(2-hydroxyethyl)-2-phenylacetamide (0.5 g, 2.8 mmol) in $CHCl_3$ (10 mL) at room temperature. A mildly exothermic reaction ensued with gas evolution. Stirring was continued until gas evolution ceased. Volatiles were removed *in vacuo* and the crude purified by flash column chromatography (5% MeOH/DCM). The title compound was isolated as an off-white solid (0.44 g, 80% yield): ^{1}H NMR (400 MHz, $CDCl_3$): δ 7.39–7.26 (m, 5H, Ar-H), 5.79 (br s, 1H, NH), 3.62-3.51 (m, 6H, CH_2); ^{13}C NMR (100 MHz, $CDCl_3$): δ 172.5, 134.8, 129.5, 129.2, 127.5, 62.4, 43.8. 42.8; HRMS (ES-TOF) m/z: $[M + H]^+$ calc for $C_{10}H_{13}NOCl$ 198.0686, found: 198.0693.

8. References

(1) Herrmann, W. A.; Köcher, C. *Angew. Chemie Int. Ed. English* **1997**, *36*, 2162.

(2) Carter, E. A.; Goddard, W. A. *J. Phys. Chem.* **1986**, *90*, 998.

(3) Dixon, D. A.; Arduengo, A. J. *J. Phys. Chem.* **1991**, *95*, 4180.

(4) Arduengo, A. J.; Bock, H.; Chen, H.; Denk, M.; Dixon, D. A.; Green, J. C.; Herrmann, W. A.; Jones, N. L.; Wagner, M.; West, R. *J. Am. Chem. Soc.* **1994**, *116*, 6641.

(5) Arduengo, A. J.; Dias, H. V. R.; Harlow, R. L.; Kline, M. *J. Am. Chem. Soc.* **1992**, *114*, 5530.

(6) Arduengo, A. J.; Harlow, R. L.; Kline, M. *J. Am. Chem. Soc.* **1991**, *113*, 361.

(7) Tschugajeff, L.; Skanawy-Grigorjewa, M.; Posnjak, A. *Zeitschrift fuer Anorg. und Allg. Chemie* **1925**, *148*, 37.

(8) Fischer, E. O.; Maasböl, A. *Angew. Chemie Int. Ed. English* **1964**, *3*, 580.

(9) Wanzlick, H.-W.; Schönherr, H.-J. *Angew. Chemie Int. Ed. English* **1968**, *7*, 141.

(10) Rouschias, G.; Shaw, B. L. *J. Chem. Soc. D Chem. Commun.* **1970**, 183.

(11) Herrmann, W. A.; Köcher, C.; Gooßen, L. J.; Artus, G. R. J. *Chem. - A Eur. J.* **1996**, *2*, 1627.

(12) Hintermann, L. *Beilstein J. Org. Chem.* **2007**, *3*, 22.

(13) Arduengo, A. J.; Davidson, F.; Dias, H. V. R.; Goerlich, J. R.; Khasnis, D.; Marshall, W. J.; Prakasha, T. K. *J. Am. Chem. Soc.* **1997**, *119*, 12742.

(14) Arduengo, A. J.; Krafczyk, R.; Schmutzler, R.; Craig, H. A.; Goerlich, J. R.; Marshall, W. J.; Unverzagt, M. *Tetrahedron* **1999**, *55*, 14523.

(15) III, A. A. *US Pat. 5,077,414* **1991**.

(16) Denk, M. K.; Rodezno, M.; Gupta, S.; Lough, A. J. *J. Organomet. Chem.* **2001**, *617-618*, 242.

(17) De Frémont, P.; Marion, N.; Nolan, S. P. *Coord. Chem. Rev.* **2009**, *253*, 862.

(18) Benhamou, L.; Chardon, E.; Lavigne, G.; Bellemin-Laponnaz, S.; César, V. *Chem. Rev.* **2011**, *111*, 2705.

(19) Alder, R. W.; Allen, P. R.; Williams, S. J. *J. Chem. Soc. Chem. Commun.* **1995**, 1267.

(20) Nelson, D. J.; Nolan, S. P. *Chem. Soc. Rev.* **2013**, *42*, 6723.

(21) Kuhn, N.; Kratz, T. *Synthesis (Stuttg).* **1993**, *1993*, 561.

(22) Voutchkova, A. M.; Appelhans, L. N.; Chianese, A. R.; Crabtree, R. H. *J. Am. Chem. Soc.* **2005**, *127*, 17624.

(23) Fèvre, M.; Vignolle, J.; Taton, D. *Polym. Chem.* **2013**, *4*, 1995.

(24) Duong, H. A.; Tekavec, T. N.; Arif, A. M.; Louie, J. *Chem. Commun. (Camb).* **2004**, 112.

(25) Wanzlick, H.-W.; Schikora, E. *Chem. Ber.* **1961**, *94*, 2389.

(26) Enders, D.; Breuer, K.; Raabe, G.; Runsink, J.; Teles, J. H.; Melder, J.-P.; Ebel, K.; Brode, S. *Angew. Chemie Int. Ed. English* **1995**, *34*, 1021.

(27) Scholl, M.; Ding, S.; Lee, C. W.; Grubbs, R. H. *Org. Lett.* **1999**, *1*, 953.

(28) Bourissou, D.; Guerret, O.; Gabbaï, F. P.; Bertrand, G. *Chem. Rev.* **2000**, *100*, 39.

(29) Kronig, S.; Theuergarten, E.; Holschumacher, D.; Bannenberg, T.; Daniliuc, C. G.; Jones, P. G.; Tamm, M. *Inorg. Chem.* **2011**, *50*, 7344.

(30) Curran, D. P.; Solovyev, A.; Makhlouf Brahmi, M.; Fensterbank, L.; Malacria, M.; Lacôte, E. *Angew. Chemie Int. Ed.* **2011**, *50*, 10294.

(31) Asay, M.; Jones, C.; Driess, M. *Chem. Rev.* **2011**, *111*, 354.

(32) Kuhn, N.; Kratz, T.; Bläser, D.; Boese, R. *Chem. Ber.* **1995**, *128*, 245.

(33) Crabtree, R. H. *J. Organomet. Chem.* **2005**, *690*, 5451.

(34) Díez-González, S.; Marion, N.; Nolan, S. P. *Chem. Rev.* **2009**, *109*, 3612.

(35) Würtz, S.; Lohre, C.; Fröhlich, R.; Bergander, K.; Glorius, F. *J. Am. Chem. Soc.* **2009**, *131*, 8344.

(36) Slivarichova, M.; Ahmad, R.; Kuo, Y.-Y.; Nunn, J.; Haddow, M. F.; Othman, H.; Owen, G. R. *Organometallics* **2011**, *30*, 4779.

(37) Fortman, G. C.; Nolan, S. P. *Chem. Soc. Rev.* **2011**, *40*, 5151.

(38) Urban, S.; Ortega, N.; Glorius, F. *Angew. Chemie Int. Ed.* **2011**, *50*, 3803.

(39) Douglas, J.; Churchill, G.; Smith, A. *Synthesis (Stuttg).* **2012**, *44*, 2295.

(40) Marion, N.; Díez-González, S.; Nolan, S. P. *Angew. Chemie Int. Ed.* **2007**, *46*, 2988.

(41) Fèvre, M.; Pinaud, J.; Gnanou, Y.; Vignolle, J.; Taton, D. *Chem. Soc. Rev.* **2013**, *42*, 2142.

(42) Bugaut, X.; Glorius, F. *Chem. Soc. Rev.* **2012**, *41*, 3511.

(43) Fuchter, M. J. *Chem. - A Eur. J.* **2010**, *16*, 12286.

(44) Enders, D.; Niemeier, O.; Henseler, A. *Chem. Rev.* **2007**, *107*, 5606.

(45) Seebach, D. *Angew. Chemie Int. Ed. English* **1979**, *18*, 239.

(46) Breslow, R. *J. Am. Chem. Soc.* **1958**, *80*, 3719.

(47) Stetter, H.; Schreckenberg, M. *Angew. Chemie Int. Ed. English* **1973**, *12*, 81.

(48) Whinfield, J. R.; Dickson, J. T. Polymeric linear terephthalic esters, March 22, 1949.

(49) Palmer, R. J. *Encyclopedia of Polymer Science and Technology*; John Wiley & Sons, Inc.: Hoboken, NJ, USA, 2002.

(50) Fischer, E.; Speier, A. *Berichte der Dtsch. Chem. Gesellschaft* **1895**, *28*, 3252.

(51) Köpnick, H.; Schmidt, M.; Brügging, W.; Rüter, J.; Kaminsky, W. *Ullmann's Encyclopedia of Industrial Chemistry*; Wiley-VCH Verlag GmbH & Co. KGaA: Weinheim, Germany, 2000.

(52) Clayden, J.; Greeves, N.; Warren, S.; Wothers, P. *Organic Chemistry*; Oxford University Press, 2001.

(53) Neises, B.; Steglich, W. *Angew. Chemie Int. Ed. English* **1978**, *17*, 522.

(54) Mitsunobu, O.; Yamada, M. *Bull. Chem. Soc. Jpn.* **1967**, *40*, 2380.

(55) Swamy, K. C. K.; Kumar, N. N. B.; Balaraman, E.; Kumar, K. V. P. P. *Chem. Rev.* **2009**, *109*, 2551.

(56) Trost, B. M. *Angew. Chemie Int. Ed. English* **1995**, *34*, 259.

(57) MEHER, L.; VIDYASAGAR, D.; NAIK, S. *Renew. Sustain. Energy Rev.* **2006**, *10*, 248.

(58) Leung, D. Y. C.; Wu, X.; Leung, M. K. H. *Appl. Energy* **2010**, *87*, 1083.

(59) Lee, A. F.; Bennett, J. A.; Manayil, J. C.; Wilson, K. *Chem. Soc. Rev.* **2014**.

(60) Connor, E. F.; Nyce, G. W.; Myers, M.; Möck, A.; Hedrick, J. L. *J. Am. Chem. Soc.* **2002**, *124*, 914.

(61) Grasa, G. A.; Kissling, R. M.; Nolan, S. P. *Org. Lett.* **2002**, *4*, 3583.

(62) Grasa, G. a; Güveli, T.; Singh, R.; Nolan, S. P. *J. Org. Chem.* **2003**, *68*, 2812.

(63) Singh, R.; Kissling, R. M.; Letellier, M.-A.; Nolan, S. P. *J. Org. Chem.* **2004**, *69*, 209.

(64) Clavier, H.; Nolan, S. P. *Chem. Commun. (Camb).* **2010**, *46*, 841.

(65) Pignataro, L.; Papalia, T.; Slawin, A. M. Z.; Goldup, S. M. *Org. Lett.* **2009**, *11*, 1643.

(66) Nyce, G. W.; Glauser, T.; Connor, E. F.; Möck, A.; Waymouth, R. M.; Hedrick, J. L. *J. Am. Chem. Soc.* **2003**, *125*, 3046.

(67) Kamber, N. E.; Jeong, W.; Gonzalez, S.; Hedrick, J. L.; Waymouth, R. M. *Macromolecules* **2009**, *42*, 1634.

(68) Scholten, M. D.; Hedrick, J. L.; Waymouth, R. M. *Macromolecules* **2008**, *41*, 7399.

(69) Csihony, S.; Culkin, D. A.; Sentman, A. C.; Dove, A. P.; Waymouth, R. M.; Hedrick, J. L. *J. Am. Chem. Soc.* **2005**, *127*, 9079.

(70) Lai, C.-L.; Lee, H. M.; Hu, C.-H. *Tetrahedron Lett.* **2005**, *46*, 6265.

(71) Movassaghi, M.; Schmidt, M. A. *Org. Lett.* **2005**, *7*, 2453.

(72) Samanta, R. C.; De Sarkar, S.; Fröhlich, R.; Grimme, S.; Studer, A. *Chem. Sci.* **2013**, *4*, 2177.

(73) Kwoleck, S. Wholly aromatic carbocyclic polycarbonamide fiber having orientation angle of less than about 45{20, June 25, 1974.

(74) Baumann, E. *Berichte der Dtsch. Chem. Gesellschaft* **1886**, *19*, 3218.

(75) Sheldon, R. A. *Green Chem.* **2007**, *9*, 1273.

(76) *Chemical Weapons Act 1996*; United Kingdom of Great Britain and Northern Ireland, 1996.

(77) Nelson, P.; Pelter, A. *J. Chem. Soc.* **1965**, 5142.

(78) Collum, D. B.; Chen, S.-C.; Ganem, B. *J. Org. Chem.* **1978**, *43*, 4393.

(79) Ishihara, K.; Ohara, S.; Yamamoto, H. *J. Org. Chem.* **1996**, *61*, 4196.

(80) Starkov, P.; Sheppard, T. D. *Org. Biomol. Chem.* **2011**, *9*, 1320.

(81) Nomura, R.; Nakano, T.; Yamada, Y.; Matsuda, H. *J. Org. Chem.* **1991**, *56*, 4076.

(82) Ishihara, K.; Kuroki, Y.; Hanaki, N.; Ohara, S.; Yamamoto, H. *J. Am. Chem. Soc.* **1996**, *118*, 1569.

(83) Gunanathan, C.; Ben-David, Y.; Milstein, D. *Science* **2007**, *317*, 790.

(84) Nordstrøm, L. U.; Vogt, H.; Madsen, R. *J. Am. Chem. Soc.* **2008**, *130*, 17672.

(85) Lenstra, D. C.; Rutjes, F. P.; Mecinović, J. *Chem. Commun.* **2014**.

(86) Harrison, C. R.; Hodge, P.; Hunt, B. J.; Khoshdel, E.; Richardson, G. *J. Org. Chem.* **1983**, *48*, 3721.

(87) Barstow, L. E.; Hruby, V. J. *J. Org. Chem.* **1971**, *36*, 1305.

(88) Grishina, A. A.; Polyakova, S. M.; Kunetskiy, R. A.; Císařová, I.; Lyapkalo, I. M. *Chem. - A Eur. J.* **2011**, *17*, 96.

(89) Hollóczki, O.; Terleczky, P.; Szieberth, D.; Mourgas, G.; Gudat, D.; Nyulászi, L. *J. Am. Chem. Soc.* **2011**, *133*, 780.

(90) Bonnette, F.; Kato, T.; Destarac, M.; Mignani, G.; Cossío, F. P.; Baceiredo, A. *Angew. Chemie Int. Ed.* **2007**, *46*, 8632.

(91) Zhao, X.; Glover, G.; Oberg, K.; Dalton, D.; Rovis, T. *Synlett* **2013**, *24*, 1229.

(92) Powell, A. B.; Suzuki, Y.; Ueda, M.; Bielawski, C. W.; Cowley, A. H. *J. Am. Chem. Soc.* **2011**, *133*, 5218.

(93) Pinaud, J.; Vignolle, J.; Gnanou, Y.; Taton, D. *Macromolecules* **2011**, *44*, 1900.

(94) Urbina-Blanco, C. A.; Bantreil, X.; Clavier, H.; Slawin, A. M. Z.; Nolan, S. P. *Beilstein J. Org. Chem.* **2010**, *6*, 1120.

(95) Swamy, K. C. K.; Chandrasekhar, V.; Harland, J. J.; Holmes, J. M.; Day, R. O.; Holmes, R. R. *J. Am. Chem. Soc.* **1990**, *112*, 2341.

(96) Chuit, C.; Corriu, R. J. P.; Reye, C.; Young, J. C. *Chem. Rev.* **1993**, *93*, 1371.

(97) Holmes, R. R. *Chem. Rev.* **1996**, *96*, 927.

(98) West, R.; Whatley, L. S.; Lake, K. J. *J. Am. Chem. Soc.* **1961**, *83*, 761.

(99) Herrmann, W. A. *Angew. Chemie Int. Ed.* **2002**, *41*, 1290.

(100) Schaper, L.; Hock, S. J.; Herrmann, W. A.; Kühn, F. E. *Angew. Chemie Int. Ed.* **2013**, *52*, 270.

(101) Rodriguez, M.; Marrot, S.; Kato, T.; Stérin, S.; Fleury, E.; Baceiredo, A. *J. Organomet. Chem.* **2007**, *692*, 705.

(102) Marrot, S.; Bonnette, F.; Kato, T.; Saint-Jalmes, L.; Fleury, E.; Baceiredo, A. *J. Organomet. Chem.* **2008**, *693*, 1729.

(103) Song, J. J.; Gallou, F.; Reeves, J. T.; Tan, Z.; Yee, N. K.; Senanayake, C. H. *J. Org. Chem.* **2006**, *71*, 1273.

(104) Kobayashi, S.; Nishio, K. *Tetrahedron Lett.* **1993**, *34*, 3453.

(105) Kano, T.; Sasaki, K.; Konishi, T.; Mii, H.; Maruoka, K. *Tetrahedron Lett.* **2006**, *47*, 4615.

(106) Zhao, Q.; Curran, D. P.; Malacria, M.; Fensterbank, L.; Goddard, J.-P.; Lacôte, E. *Chem. - A Eur. J.* **2011**, *17*, 9911.

(107) Ghadwal, R. S.; Sen, S. S.; Roesky, H. W.; Tavcar, G.; Merkel, S.; Stalke, D. *Organometallics* **2009**, *28*, 6374.

(108) Sakaguchi, Y.; Iwade, Y.; Sekikawa, T.; Minami, T.; Hatanaka, Y. *Chem. Commun. (Camb).* **2013**, *49*, 11173.

(109) Böttcher, T.; Steinhauer, S.; Neumann, B.; Stammler, G.; Röschenthaler, G.-V.; Hoge, B. *Chem. Commun.* **2014**.

(110) Frye, C. L.; Vincent, G. A.; Finzel, W. A. *J. Am. Chem. Soc.* **1971**, *93*, 6805.

(111) Wang, Y.; Xie, Y.; Wei, P.; King, R. B.; Schaefer, H. F.; von R Schleyer, P.; Robinson, G. H. *Science (80-.).* **2008**, *321*, 1069.

(112) Hirano, K.; Urban, S.; Wang, C.; Glorius, F. *Org. Lett.* **2009**, *11*, 1019.

(113) Voges, M. H.; Rømming, C.; Tilset, M. *Organometallics* **1999**, *18*, 529.

(114) Cole, M. L.; Junk, P. C. *CrystEngComm* **2004**, *6*, 173.

(115) Hollóczki, O.; Nyulászi, L. *Organometallics* **2009**, *28*, 4159.

(116) Haaf, M.; Schmiedl, A.; Schmedake, T. A.; Powell, D. R.; Millevolte, A. J.; Denk, M.; West, R. *J. Am. Chem. Soc.* **1998**, *120*, 12714.

(117) Mistryukov, E. A. *Mendeleev Commun.* **2006**, *16*, 258.

(118) Herrmann, W. A.; Böhm, V. P. .; Gstöttmayr, C. W. .; Grosche, M.; Reisinger, C.-P.; Weskamp, T. *J. Organomet. Chem.* **2001**, *617-618*, 616.

(119) Fukuda, Y.; Maeda, Y.; Ishii, S.; Kondo, K.; Aoyama, T. *Synthesis (Stuttg).* **2006**, *2006*, 589.

(120) Liu, Z. *J. Phys. Chem. A* **2009**, *113*, 6410.

(121) Lortie, F.; Boileau, S.; Bouteiller, L. *Chemistry* **2003**, *9*, 3008.

(122) Kondo, T.; Kotachi, S.; Watanabe, Y. *J. Chem. Soc. Chem. Commun.* **1992**, 1318.

(123) Zeng, W.; Wang, E.; Qiu, R.; Sohail, M.; Wu, S.; Chen, F.-X. *J. Organomet. Chem.* **2013**, *743*, 44.

(124) Arduengo, A. J.; Goerlich, J. R.; Marshall, W. J. *J. Am. Chem. Soc.* **1995**, *117*, 11027.

(125) Denk, M. K.; Thadani, A.; Hatano, K.; Lough, A. J. *Angew. Chemie Int. Ed. English* **1997**, *36*, 2607.

(126) Arduengo, A. J.; Davidson, F.; Krafczyk, R.; Marshall, W. J.; Tamm, M. *Organometallics* **1998**, *17*, 3375.

(127) Alder, R. W.; Allen, P. R.; Murray, M.; Orpen, A. G. *Angew. Chemie Int. Ed. English* **1996**, *35*, 1121.

(128) Alder, R. W.; Blake, M. E. *Chem. Commun.* **1997**, 1513.

(129) Woodcock, H. L.; Moran, D.; Brooks, B. R.; Schleyer, P. V. R.; Schaefer, H. F. *J. Am. Chem. Soc.* **2007**, *129*, 3763.

(130) Wang, Y.; Robinson, G. H. *Inorg. Chem.* **2011**, *50*, 12326.

(131) Macchioni, A.; Ciancaleoni, G.; Zuccaccia, C.; Zuccaccia, D. *Supramolecular Chemistry*; Gale, P. A., Steed, J. W., Eds.; John Wiley & Sons, Ltd: Chichester, UK, 2012.

(132) Rocchigiani, L.; Ciancaleoni, G.; Zuccaccia, C.; Macchioni, A. *J. Am. Chem. Soc.* **2014**, *136*, 112.

(133) Leaist, D. G.; MacEwan, K.; Stefan, A.; Zamari, M. *J. Chem. Eng. Data* **2000**, *45*, 815.

(134) Packer, K. J.; Tomlinson, D. J. *Trans. Faraday Soc.* **1971**, *67*, 1302.

(135) Lees, F. P.; Sarram, P. *J. Chem. Eng. Data* **1971**, *16*, 41.

(136) De Kimpe, N.; D'Hondt, L.; Stanoeva, E. *Tetrahedron Lett.* **1991**, *32*, 3879.

(137) Solovyev, A.; Lacôte, E.; Curran, D. P. *Org. Lett.* **2011**, *13*, 6042.

(138) Cai, H.; Guengerich, F. P. *Chem. Res. Toxicol.* **2000**, *13*, 327.

(139) Picquet-Varrault, B.; Doussin, J.-F.; Durand-Jolibois, R.; Carlier, P. *Phys. Chem. Chem. Phys.* **2001**, *3*, 2595.

(140) Chandra Shekhar, A.; Ravi Kumar, A.; Sathaiah, G.; Luke Paul, V.; Sridhar, M.; Shanthan Rao, P. *Tetrahedron Lett.* **2009**, *50*, 7099.

(141) Lei, M.; Ma, L.; Hu, L. *Tetrahedron Lett.* **2010**, *51*, 4186.

(142) Moffat, J.; Newton, M. V.; Papenmeier, G. J. *J. Org. Chem.* **1962**, *27*, 4058.

(143) Kamer, P. C. J.; Nolte, R. J. M.; Drenth, W. *J. Am. Chem. Soc.* **1988**, *110*, 6818.

(144) Edwards, W. R.; Sibille, E. C. *J. Org. Chem.* **1963**, *28*, 674.

(145) Stephens, P. J.; Devlin, F. J.; Chabalowski, C. F.; Frisch, M. J. *J. Phys. Chem.* **1994**, *98*, 11623.

(146) Vosko, S. H.; Wilk, L.; Nusair, M. *Can. J. Phys.* **1980**, *58*, 1200.

(147) Lee, C.; Yang, W.; Parr, R. G. *Phys. Rev. B* **1988**, *37*, 785.

(148) Becke, A. D. *J. Chem. Phys.* **1993**, *98*, 5648.

(149) Krishnan, R.; Binkley, J. S.; Seeger, R.; Pople, J. A. *J. Chem. Phys.* **1980**, *72*, 650.

(150) McLean, A. D.; Chandler, G. S. *J. Chem. Phys.* **1980**, *72*, 5639.

(151) Francl, M. M. *J. Chem. Phys.* **1982**, *77*, 3654.

(152) Hehre, W. J. *J. Chem. Phys.* **1972**, *56*, 2257.

(153) Ditchfield, R. *J. Chem. Phys.* **1971**, *54*, 724.

(154) Petersson, G. A.; Bennett, A.; Tensfeldt, T. G.; Al-Laham, M. A.; Shirley, W. A.; Mantzaris, J. *J. Chem. Phys.* **1988**, *89*, 2193.

(155) Clark, T.; Chandrasekhar, J.; Spitznagel, G. W.; Schleyer, P. V. R. *J. Comput. Chem.* **1983**, *4*, 294.

(156) Paizs, B.; Suhai, S. *J. Comput. Chem.* **1998**, *19*, 575.

(157) Van Duijneveldt, F. B.; van Duijneveldt-van de Rijdt, J. G. C. M.; van Lenthe, J. H. *Chem. Rev.* **1994**, *94*, 1873.

(158) Wodrich, M. D.; Corminboeuf, C.; von Ragué Schleyer, P. *Org. Lett.* **2006**, *8*, 3631.

(159) Grimme, S. *Angew. Chemie Int. Ed.* **2006**, *45*, 4460.

(160) Wodrich, M. D.; Corminboeuf, C.; Schreiner, P. R.; Fokin, A. A.; von Ragué Schleyer, P. *Org. Lett.* **2007**, *9*, 1851.

(161) Schreiner, P. R.; Fokin, A. A.; Pascal, R. A.; de Meijere, A. *Org. Lett.* **2006**, *8*, 3635.

(162) Orio, M.; Pantazis, D. A.; Neese, F. *Photosynth. Res. 102*, 443.

(163) Frisch, M. J.; Head-Gordon, M.; Pople, J. A. *Chem. Phys. Lett.* **1990**, *166*, 281.

(164) Frisch, M. J.; Head-Gordon, M.; Pople, J. A. *Chem. Phys. Lett.* **1990**, *166*, 275.

(165) Sæbø, S.; Almlöf, J. *Chem. Phys. Lett.* **1989**, *154*, 83.

(166) Head-Gordon, M.; Pople, J. A.; Frisch, M. J. *Chem. Phys. Lett.* **1988**, *153*, 503.

(167) Hobza, P.; ?poner, J.; Reschel, T. *J. Comput. Chem.* **1995**, *16*, 1315.

(168) Dabkowska, I.; Jurecka, P.; Hobza, P. *J. Chem. Phys.* **2005**, *122*, 204322.

(169) Kristyán, S.; Pulay, P. *Chem. Phys. Lett.* **1994**, *229*, 175.

(170) Mourik, T. van. *Chem. Phys.* **2004**, *304*, 317.

(171) Van Mourik, T.; Gdanitz, R. J. *J. Chem. Phys.* **2002**, *116*, 9620.

(172) Tuma, C.; Daniel Boese, A.; Handy, N. C. *Phys. Chem. Chem. Phys.* **1999**, *1*, 3939.

(173) Grimme, S. *J. Comput. Chem.* **2006**, *27*, 1787.

(174) Dunning, T. H. *J. Chem. Phys.* **1989**, *90*, 1007.

(175) Woon, D. E.; Dunning, T. H. *J. Chem. Phys.* **1994**, *100*, 2975.

(176) Woon, D. E.; Dunning, T. H. *J. Chem. Phys.* **1993**, *98*, 1358.

(177) Fulmer, G. R.; Miller, A. J. M.; Sherden, N. H.; Gottlieb, H. E.; Nudelman, A.; Stoltz, B. M.; Bercaw, J. E.; Goldberg, K. I. *Organometallics* **2010**, *29*, 2176.

(178) Jacquemard, U.; Bénéteau, V.; Lefoix, M.; Routier, S.; Mérour, J.-Y.; Coudert, G. *Tetrahedron* **2004**, *60*, 10039.

(179) Dominguez, A.; Cabezas, N.; Sánchez - Montero, J. M.; Sinisterra, J. V. *Tetrahedron* **1995**, *51*, 1827.

(180) Xu, Q.; Li, Z.; Chen, H. *Chinese J. Chem.* **2011**, *29*, 925.

(181) Xu, Q.; Li, Z. *Tetrahedron Lett.* **2009**, *50*, 6838.

(182) Cassebaum, H.; Uhlig, K. *J. f**r Prakt. Chemie* **1973**, *315*, 1057.

(183) Kubiczek, G.; Smahel, A. *Monatshefte fuer Chemie* **1949**, *80*, 389.

(184) Poindexter, G. S. *J. Heterocycl. Chem.* **1983**, *20*, 1431.

(185) Caldwell, N.; Jamieson, C.; Simpson, I.; Tuttle, T. *Org. Lett.* **2013**, *15*, 2506.

(186) Griffiths, P. R.; Haseth, J. A. De. *Fourier Transform Infrared Spectrometry*; John Wiley & Sons, 2007.

(187) Einstein, A. *Ann. Phys.* **1905**, *322*, 549.

(188) Von Smoluchowski, M. *Ann. Phys.* **1906**, *326*, 756.

(189) Mark, J. E. *The Polymer Data Handbook*, 2nd Editio.; Oxford University Press.

(190) Jayarajah, C. N.; Yekta, A.; Manners, I.; Winnik, M. A. *Macromolecules* **2000**, *33*, 5693.

(191) Markov, D. A.; Lillie, E. M.; Garbett, S. P.; McCawley, L. J. *Biomed. Microdevices* **2014**, *16*, 91.

(192) Tamai, Y.; Tanaka, H.; Nakanishi, K. *Macromolecules* **1994**, *27*, 4498.

(193) Watson, J. M.; Baron, M. G. *J. Memb. Sci.* **1996**, *110*, 47.

(194) Schumpe, A.; Luehring, P. *J. Chem. Eng. Data* **1990**, *35*, 24.

(195) Ossowski, T.; Pipka, P.; Liwo, A.; Jeziorek, D. *Electrochim. Acta* **2000**, *45*, 3581.

(196) Fischer, K. *J. Chem. Thermodyn.* **2001**, *33*, 1285.

(197) Gottlieb, H. E.; Kotlyar, V.; Nudelman, A. *J. Org. Chem.* **1997**, *62*, 7512.

(198) Budavari, S. *The Merck Index: An Encyclopedia of Chemicals, Drugs, and Biologicals*, 11th ed.; Merck & Co: Rahway, N.J., 1989.

(199) Knölker, H.-J.; Braxmeier, T.; Schlechtingen, G. *Synlett* **1996**, *1996*, 502.

(200) Mayor, M.; Scheffold, R.; Walder, L. *Helv. Chim. Acta* **1997**, *80*, 1183.

(201) Gaussian 09, Revision C.01, Frisch, M. J.; Trucks, G. W.; Schlegel, H. B.; Scuseria, G. E.; Robb, M. A.; Cheeseman, J. R.; Scalmani, G.; Barone, V.; Mennucci, B.; Petersson, G. A.; Nakatsuji, H.; Caricato, M.; Li, X.; Hratchian, H. P.; Izmaylov, A. F.; Bloino, J.; Zheng, G.; Sonnenberg, J. L.; Hada, M.; Ehara, M.; Toyota, K.; Fukuda, R.; Hasegawa, J.; Ishida, M.; Nakajima, T.; Honda, Y.; Kitao, O.; Nakai, H.; Vreven, T.; Montgomery, J. A., Jr.; Peralta, J. E.; Ogliaro, F.; Bearpark, M.; Heyd, J. J.; Brothers, E.; Kudin, K. N.; Staroverov, V. N.; Kobayashi, R.; Normand, J.; Raghavachari, K.; Rendell, A.; Burant, J. C.; Iyengar, S. S.; Tomasi, J.; Cossi, M.; Rega, N.; Millam, N. J.; Klene, M.; Knox, J. E.; Cross, J. B.; Bakken, V.; Adamo, C.; Jaramillo, J.; Gomperts, R.; Stratmann, R. E.; Yazyev, O.; Austin, A. J.; Cammi, R.; Pomelli, C.; Ochterski, J. W.; Martin, R. L.; Morokuma, K.; Zakrzewski, V. G.; Voth, G. A.; Salvador, P.; Dannenberg, J. J.; Dapprich, S.; Daniels, A. D.; Farkas, Ö.; Foresman, J. B.; Ortiz, J. V.; Cioslowski, J.; Fox, D. J. Gaussian, Inc., Wallingford CT, 2009.

Appendix A: Quantum Chemical Calculations

Calculations were conducted using the Gaussian 09 suite of programmes.[201] Local energy minima were identified as stationary points with no imaginary frequencies. Frequency calculations were also utilised to afford thermal corrections for Gibbs energy (G), enthalpy (H), and zero-point valence energy (ZPVE) at 298.15K. Energies are given in Hartree unless otherwise indicated. 1 Hartree was taken to be equivalent to 627.509469 kcal·mol^{-1}.

Poly(dimethyl)siloxane was approximated as a short-chain oligomer terminated with -OMe or –TMS.

A summary of the calculated electronic energies and thermal corrections of all structures at different levels of theory with varying size of basis set (as indicated) are provided below. For reasons of brevity, stationary point geometries are provided separately and the results of frequency calculations can be inspected from the raw outputs. Unless otherwise stated, calculations were run with tight convergence criteria and an ultrafine integration grid.

IMe

B3LYP/6-311+G(d,p)

E(RB3LYP) =	-304.880659457
Zero-point correction=	0.125986 (Hartree/Particle)
Thermal correction to Energy=	0.133045
Thermal correction to Enthalpy=	0.133990
Thermal correction to Gibbs Free Energy=	0.094870
Sum of electronic and zero-point Energies=	-304.754673
Sum of electronic and thermal Energies=	-304.747614
Sum of electronic and thermal Enthalpies=	-304.746670
Sum of electronic and thermal Free Energies=	-304.785789

MP2/6-311+G(d,p)//B3LYP/6-311+G(d,p)

EUMP2 =	-0.30397432403890D+03

B97D/6-311+G(d,p)

E(RB97D) =	-304.658580187
Zero-point correction=	0.122509 (Hartree/Particle)
Thermal correction to Energy=	0.129759
Thermal correction to Enthalpy=	0.130703
Thermal correction to Gibbs Free Energy=	0.091102
Sum of electronic and zero-point Energies=	-304.536071
Sum of electronic and thermal Energies=	-304.528822
Sum of electronic and thermal Enthalpies=	-304.527877
Sum of electronic and thermal Free Energies=	-304.567478

MP2/aug-cc-pVTZ//B97D/6-311+G(d,p)

EUMP2 =	-0.30418702909779D+03

IMe·PDMS

B3LYP/6-311+G(d,p)

E(RB3LYP) =	-1794.16767336
Zero-point correction=	0.445782 (Hartree/Particle)
Thermal correction to Energy=	0.479863
Thermal correction to Enthalpy=	0.480808
Thermal correction to Gibbs Free Energy=	0.377043
Sum of electronic and zero-point Energies=	-1793.721892
Sum of electronic and thermal Energies=	-1793.687810
Sum of electronic and thermal Enthalpies=	-1793.686866
Sum of electronic and thermal Free Energies=	-1793.790631

Counterpoise: corrected energy =	-1794.164576820123
Counterpoise: BSSE energy =	0.003096536121

MP2/6-311+G(d,p)//B3LYP/6-311+G(d,p)

EUMP2 =	-0.17900193277840D+04

B97D/6-311+G(d,p)

E(RB97D) =	-1793.47489505
Zero-point correction=	0.435348 (Hartree/Particle)

Thermal correction to Energy=	0.469304
Thermal correction to Enthalpy=	0.470248
Thermal correction to Gibbs Free Energy=	0.369592
Sum of electronic and zero-point Energies=	-1793.039547
Sum of electronic and thermal Energies=	-1793.005591
Sum of electronic and thermal Enthalpies=	-1793.004647
Sum of electronic and thermal Free Energies=	-1793.105303

Counterpoise: corrected energy =	-1794.154817002306
Counterpoise: BSSE energy =	0.004552089865

MP2/aug-cc-pVTZ//B97D/6-311+G(d,p)
EUMP2 = -0.17908102558259D+04

IMe·$SiCl_4$

B3LYP/6-311+G(d,p)

E(RB3LYP) =	-2435.51221321
Zero-point correction=	0.136359 (Hartree/Particle)
Thermal correction to Energy=	0.151278
Thermal correction to Enthalpy=	0.152222
Thermal correction to Gibbs Free Energy=	0.092922
Sum of electronic and zero-point Energies=	-2435.375855
Sum of electronic and thermal Energies=	-2435.360935
Sum of electronic and thermal Enthalpies=	-2435.359991
Sum of electronic and thermal Free Energies=	-2435.419291

Counterpoise: corrected energy =	-2435.505208702835
Counterpoise: BSSE energy =	0.006976632055

MP2/6-311+G(d,p)//B3LYP/6-311+G(d,p)
EUMP2 = -0.24318148660821D+04

B97D/6-311+G(d,p)

E(RB97D) =	-2435.31612439
Zero-point correction=	0.133363 (Hartree/Particle)
Thermal correction to Energy=	0.148230
Thermal correction to Enthalpy=	0.149174
Thermal correction to Gibbs Free Energy=	0.090529
Sum of electronic and zero-point Energies=	-2435.182762
Sum of electronic and thermal Energies=	-2435.167895
Sum of electronic and thermal Enthalpies=	-2435.166951
Sum of electronic and thermal Free Energies=	-2435.225595

Counterpoise: corrected energy =	-2435.309349727558
Counterpoise: BSSE energy =	0.006774666645

MP2/aug-cc-pVTZ//B97D/6-311+G(d,p)
EUMP2 = -0.24323528289012D+04

IMes

B3LYP/6-311+G(d,p)	
E(RB3LYP) =	-924.404603558
Zero-point correction=	0.394304 (Hartree/Particle)
Thermal correction to Energy=	0.418198
Thermal correction to Enthalpy=	0.419142
Thermal correction to Gibbs Free Energy=	0.336859
Sum of electronic and zero-point Energies=	-924.010300
Sum of electronic and thermal Energies=	-923.986406
Sum of electronic and thermal Enthalpies=	-923.985462
Sum of electronic and thermal Free Energies=	-924.067744
MP2/6-311+G(d,p)//B3LYP/6-311+G(d,p)	
EUMP2 =	-0.92161456547431D+03
B97D/6-311+G(d,p)	
E(RB97D) =	-923.722661121
Zero-point correction=	0.383970 (Hartree/Particle)
Thermal correction to Energy=	0.408461
Thermal correction to Enthalpy=	0.409405
Thermal correction to Gibbs Free Energy=	0.325992
Sum of electronic and zero-point Energies=	-923.338691
Sum of electronic and thermal Energies=	-923.314200
Sum of electronic and thermal Enthalpies=	-923.313256
Sum of electronic and thermal Free Energies=	-923.396669
IMes MP2/aug-cc-pVTZ//B97D/6-311+G(d,p)	
EUMP2 =	-0.92225365974755D+03

IMes·PDMS

B3LYP/6-311+G(d,p)	
E(RB3LYP) =	-2413.68281619
Zero-point correction=	0.716039 (Hartree/Particle)
Thermal correction to Energy=	0.765839
Thermal correction to Enthalpy=	0.766783
Thermal correction to Gibbs Free Energy=	0.631068
Sum of electronic and zero-point Energies=	-2412.966777
Sum of electronic and thermal Energies=	-2412.916977
Sum of electronic and thermal Enthalpies=	-2412.916033
Sum of electronic and thermal Free Energies=	-2413.051749
Counterpoise: corrected energy =	-2413.676667220000
Counterpoise: BSSE energy =	0.005708574296
MP2/6-311+G(d,p)//B3LYP/6-311+G(d,p)	
EUMP2 =	-0.24076782433966D+04
B97D/6-311+G(d,p)	

E(RB97D) =	-226.077588432
Zero-point correction=	0.069298 (Hartree/Particle)
Thermal correction to Energy=	0.073206
Thermal correction to Enthalpy=	0.074151
Thermal correction to Gibbs Free Energy=	0.042961
Sum of electronic and zero-point Energies=	-226.008290
Sum of electronic and thermal Energies=	-226.004382
Sum of electronic and thermal Enthalpies=	-226.003438
Sum of electronic and thermal Free Energies=	-226.034627
Counterpoise: corrected energy =	-2412.545657905154
Counterpoise: BSSE energy =	0.006628649996

IMes·$SiCl_4$

B3LYP/6-311+G(d,p)

E(RB3LYP) =	-3055.03151747
Zero-point correction=	0.404613 (Hartree/Particle)
Thermal correction to Energy=	0.436217
Thermal correction to Enthalpy=	0.437161
Thermal correction to Gibbs Free Energy=	0.339787
Sum of electronic and zero-point Energies=	-3054.626905
Sum of electronic and thermal Energies=	-3054.595301
Sum of electronic and thermal Enthalpies=	-3054.594357
Sum of electronic and thermal Free Energies=	-3054.691730
Counterpoise: corrected energy =	-3054.501018183304
Counterpoise: BSSE energy =	0.018203133227

MP2/6-311+G(d,p)//B3LYP/6-311+G(d,p)

EUMP2 =	-0.30494522147747D+04

B97D/6-311+G(d,p)

E(RB97D) =	-3054.38657341
Zero-point correction=	0.395056 (Hartree/Particle)
Thermal correction to Energy=	0.426953
Thermal correction to Enthalpy=	0.427897
Thermal correction to Gibbs Free Energy=	0.330577
Sum of electronic and zero-point Energies=	-3053.991517
Sum of electronic and thermal Energies=	-3053.959620
Sum of electronic and thermal Enthalpies=	-3053.958676
Sum of electronic and thermal Free Energies=	-3054.055997
Counterpoise: corrected energy =	-3054.375369787104
Counterpoise: BSSE energy =	0.011203624033

MP2/aug-cc-pVTZ//B97D/6-311+G(d,p)

EUMP2 =	-0.30504304409950D+04

IDipp

B3LYP/6-311+G(d,p)

E(RB3LYP) =	-1160.29639482
Zero-point correction=	0.568505 (Hartree/Particle)
Thermal correction to Energy=	0.598140
Thermal correction to Enthalpy=	0.599084
Thermal correction to Gibbs Free Energy=	0.510508
Sum of electronic and zero-point Energies=	-1159.727890
Sum of electronic and thermal Energies=	-1159.698255
Sum of electronic and thermal Enthalpies=	-1159.697311
Sum of electronic and thermal Free Energies=	-1159.785886

MP2/6-311+G(d,p)//B3LYP/6-311+G(d,p)

EUMP2 =	-0.11567740955295D+04

B97D/6-311+G(d,p)

E(RB97D) =	-1159.47853405
Zero-point correction=	0.556576 (Hartree/Particle)
Thermal correction to Energy=	0.586045
Thermal correction to Enthalpy=	0.586990
Thermal correction to Gibbs Free Energy=	0.499890
Sum of electronic and zero-point Energies=	-1158.921958
Sum of electronic and thermal Energies=	-1158.892489
Sum of electronic and thermal Enthalpies=	-1158.891544
Sum of electronic and thermal Free Energies=	-1158.978644

IDipp·$SiCl_4$

B3LYP/6-311+G(d,p)

E(RB3LYP) =	-3290.88249873
Zero-point correction=	0.578696 (Hartree/Particle)
Thermal correction to Energy=	0.615848
Thermal correction to Enthalpy=	0.616793
Thermal correction to Gibbs Free Energy=	0.512156
Sum of electronic and zero-point Energies=	-3290.303904
Sum of electronic and thermal Energies=	-3290.266751
Sum of electronic and thermal Enthalpies=	-3290.265807
Sum of electronic and thermal Free Energies=	-3290.370443
Counterpoise: corrected energy =	-3290.226618773388
Counterpoise: BSSE energy =	0.019268520517

MP2/6-311+G(d,p)//B3LYP/6-311+G(d,p)

EUMP2 =	-0.32845804834873D+04

I*t*Bu

B3LYP/6-311+G(d,p)

E(RB3LYP) =	-540.831288303
Zero-point correction=	0.293244 (Hartree/Particle)
Thermal correction to Energy=	0.308061
Thermal correction to Enthalpy=	0.309005
Thermal correction to Gibbs Free Energy=	0.251818
Sum of electronic and zero-point Energies=	-540.538045
Sum of electronic and thermal Energies=	-540.523228
Sum of electronic and thermal Enthalpies=	-540.522283
Sum of electronic and thermal Free Energies=	-540.579470

MP2/6-311+G(d,p)//B3LYP/6-311+G(d,p)

EUMP2 =	-0.53917427323544D+03

B97D/6-311+G(d,p)

E(RB97D) =	-540.449140621
Zero-point correction=	0.285859 (Hartree/Particle)
Thermal correction to Energy=	0.300948
Thermal correction to Enthalpy=	0.301892
Thermal correction to Gibbs Free Energy=	0.244164
Sum of electronic and zero-point Energies=	-540.163281
Sum of electronic and thermal Energies=	-540.148193
Sum of electronic and thermal Enthalpies=	-540.147248
Sum of electronic and thermal Free Energies=	-540.204976

MP2/aug-cc-pVTZ//B97D/6-311+G(d,p)

EUMP2 =	-0.53956186630289D+03

I*t*Bu·PDMS

B3LYP/6-311+G(d,p)

E(RB3LYP) =	-2030.07653643
Zero-point correction=	0.614892 (Hartree/Particle)
Thermal correction to Energy=	0.655915
Thermal correction to Enthalpy=	0.656859
Thermal correction to Gibbs Free Energy=	0.539991
Sum of electronic and zero-point Energies=	-2029.461645
Sum of electronic and thermal Energies=	-2029.420622

Counterpoise: corrected energy =	-2030.072035651337
Counterpoise: BSSE energy =	0.004500779479

MP2/6-311+G(d,p)//B3LYP/6-311+G(d,p)

EUMP2 =	-0.20251916841522D+04

B97D/6-311+G(d,p)

E(RB97D) =	-2029.23951381
Zero-point correction=	0.602070 (Hartree/Particle)
Thermal correction to Energy=	0.642854

Thermal correction to Enthalpy=	0.643798
Thermal correction to Gibbs Free Energy=	0.529508
Sum of electronic and zero-point Energies=	-2028.637443
Sum of electronic and thermal Energies=	-2028.596660
Sum of electronic and thermal Enthalpies=	-2028.595716
Sum of electronic and thermal Free Energies=	-2028.710006

Counterpoise: corrected energy =	-2030.062447917328
Counterpoise: BSSE energy =	0.005543616344

I*t*Bu·SiCl$_4$

B3LYP/6-311+G(d,p)

E(RB3LYP) =	-2671.41883053
Zero-point correction=	0.304387 (Hartree/Particle)
Thermal correction to Energy=	0.326705
Thermal correction to Enthalpy=	0.327649
Thermal correction to Gibbs Free Energy=	0.253781
Sum of electronic and zero-point Energies=	-2671.114443
Sum of electronic and thermal Energies=	-2671.092126
Sum of electronic and thermal Enthalpies=	-2671.091181
Sum of electronic and thermal Free Energies=	-2671.165049

Counterpoise: corrected energy =	-2671.409888042595
Counterpoise: BSSE energy =	0.008980306751

MP2/6-311+G(d,p)//B3LYP/6-311+G(d,p)

EUMP2 =	-0.26669822344373D+04

B97D/6-311+G(d,p)

E(RB97D) =	-2671.07203408
Zero-point correction=	0.298078 (Hartree/Particle)
Thermal correction to Energy=	0.320374
Thermal correction to Enthalpy=	0.321318
Thermal correction to Gibbs Free Energy=	0.248357
Sum of electronic and zero-point Energies=	-2670.773956
Sum of electronic and thermal Energies=	-2670.751660
Sum of electronic and thermal Enthalpies=	-2670.750716
Sum of electronic and thermal Free Energies=	-2670.823677

Counterpoise: corrected energy =	-2671.063309492953
Counterpoise: BSSE energy =	0.008724583703

MP2/aug-cc-pVTZ//B97D/6-311+G(d,p)

EUMP2 =	-0.26676922363698D+04

Me$_2$IMe

B3LYP/6-311+G(d,p)

E(RB3LYP) =	-383.539083292
Zero-point correction=	0.181342 (Hartree/Particle)
Thermal correction to Energy=	0.191645
Thermal correction to Enthalpy=	0.192590
Thermal correction to Gibbs Free Energy=	0.146448
Sum of electronic and zero-point Energies=	-383.357742
Sum of electronic and thermal Energies=	-383.347438
Sum of electronic and thermal Enthalpies=	-383.346494
Sum of electronic and thermal Free Energies=	-383.392635

MP2/6-311+G(d,p)//B3LYP/6-311+G(d,p)

EUMP2 =	-0.38237813093159D+03

B97D/6-311+G(d,p)

E(RB97D) =	-383.262282506
Zero-point correction=	0.176328 (Hartree/Particle)
Thermal correction to Energy=	0.186920
Thermal correction to Enthalpy=	0.187864
Thermal correction to Gibbs Free Energy=	0.141028
Sum of electronic and zero-point Energies=	-383.085955
Sum of electronic and thermal Energies=	-383.075362
Sum of electronic and thermal Enthalpies=	-383.074418
Sum of electronic and thermal Free Energies=	-383.121254

MP2/aug-cc-pVTZ//B97D/6-311+G(d,p)

EUMP2 =	-0.38265017482799D+03

Me_2IMe·PDMS

B3LYP/6-311+G(d,p)

E(RB3LYP) =	-1872.82808688
Zero-point correction=	0.501001 (Hartree/Particle)
Thermal correction to Energy=	0.538469
Thermal correction to Enthalpy=	0.539413
Thermal correction to Gibbs Free Energy=	0.428012
Sum of electronic and zero-point Energies=	-1872.327086
Sum of electronic and thermal Energies=	-1872.289618
Sum of electronic and thermal Enthalpies=	-1872.288674
Sum of electronic and thermal Free Energies=	-1872.400075

Counterpoise: corrected energy =	-1872.824617588608
Counterpoise: BSSE energy =	0.003469293091

MP2/6-311+G(d,p)//B3LYP/6-311+G(d,p)

EUMP2 =	-0.18684286302251D+04

$Me_2IMe{\cdot}SiCl_4$

B3LYP/6-311+G(d,p)

E(RB3LYP) =	-2514.17322509
Zero-point correction=	0.191668 (Hartree/Particle)
Thermal correction to Energy=	0.210039
Thermal correction to Enthalpy=	0.210983
Thermal correction to Gibbs Free Energy=	0.144050
Sum of electronic and zero-point Energies=	-2513.981557
Sum of electronic and thermal Energies=	-2513.963186
Sum of electronic and thermal Enthalpies=	-2513.962242
Sum of electronic and thermal Free Energies=	-2514.029175

Counterpoise: corrected energy =	-2514.165903187941
Counterpoise: BSSE energy =	0.007277109147

MP2/6-311+G(d,p)//B3LYP/6-311+G(d,p)

EUMP2 =	-0.25102230459021D+04

B97D/6-311+G(d,p)

E(RB97D) =	-2513.92340636
Zero-point correction=	0.187184 (Hartree/Particle)
Thermal correction to Energy=	0.205641
Thermal correction to Enthalpy=	0.206586
Thermal correction to Gibbs Free Energy=	0.140201
Sum of electronic and zero-point Energies=	-2513.736222
Sum of electronic and thermal Energies=	-2513.717765
Sum of electronic and thermal Enthalpies=	-2513.716821
Sum of electronic and thermal Free Energies=	-2513.783206

Counterpoise: corrected energy =	-2513.916362586956
Counterpoise: BSSE energy =	0.007043774640

MP2/aug-cc-pVTZ//B97D/6-311+G(d,p)

EUMP2 =	-0.25108190357223D+04

Me_2I*t*Bu

B3LYP/6-311+G(d,p)

E(RB3LYP) =	-619.475344706
Zero-point correction=	0.349366 (Hartree/Particle)
Thermal correction to Energy=	0.367206
Thermal correction to Enthalpy=	0.368150
Thermal correction to Gibbs Free Energy=	0.305961
Sum of electronic and zero-point Energies=	-619.125979
Sum of electronic and thermal Energies=	-619.108139
Sum of electronic and thermal Enthalpies=	-619.107195
Sum of electronic and thermal Free Energies=	-619.169384

MP2/6-311+G(d,p)//B3LYP/6-311+G(d,p)

EUMP2 =	-0.61756684861317D+03

B97D/6-311+G(d,p)

E(RB97D) =	-619.043362313
Zero-point correction=	0.341702 (Hartree/Particle)
Thermal correction to Energy=	0.359485
Thermal correction to Enthalpy=	0.360429
Thermal correction to Gibbs Free Energy=	0.298693
Sum of electronic and zero-point Energies=	-618.701661
Sum of electronic and thermal Energies=	-618.683877
Sum of electronic and thermal Enthalpies=	-618.682933
Sum of electronic and thermal Free Energies=	-618.744670

MP2/aug-cc-pVTZ//B97D/6-311+G(d,p)

EUMP2 =	-0.61801424259095D+03

Me$_2$*It*Bu·PDMS

B3LYP/6-311+G(d,p)

E(RB3LYP) =	-2847.67031257
Zero-point correction=	0.816473 (Hartree/Particle)
Thermal correction to Energy=	0.873329
Thermal correction to Enthalpy=	0.874273
Thermal correction to Gibbs Free Energy=	0.720541
Sum of electronic and zero-point Energies=	-2846.853840
Sum of electronic and thermal Energies=	-2846.796983
Sum of electronic and thermal Enthalpies=	-2846.796039
Sum of electronic and thermal Free Energies=	-2846.949771

Counterpoise: corrected energy =	-2847.665703734697
Counterpoise: BSSE energy =	0.004608832256

MP2/6-311+G(d,p)//B3LYP/6-311+G(d,p)

EUMP2 =	-0.28409991766273D+04

Me$_2$*It*Bu·SiCl$_4$

B3LYP/6-311+G(d,p)

E(RB3LYP) =	-2750.06562710
Zero-point correction=	0.360073 (Hartree/Particle)
Thermal correction to Energy=	0.385601
Thermal correction to Enthalpy=	0.386545
Thermal correction to Gibbs Free Energy=	0.307501
Sum of electronic and zero-point Energies=	-2749.705554
Sum of electronic and thermal Energies=	-2749.680026
Sum of electronic and thermal Enthalpies=	-2749.679082
Sum of electronic and thermal Free Energies=	-2749.758126

Counterpoise: corrected energy =	-2750.055632308533
Counterpoise: BSSE energy =	0.010078156619

MP2/6-311+G(d,p)//B3LYP/6-311+G(d,p)
EUMP2 = -0.27453880328994D+04

B97D/6-311+G(d,p)
E(RB97D) = -2749.67183270
Zero-point correction= 0.352789 (Hartree/Particle)
Thermal correction to Energy= 0.378385
Thermal correction to Enthalpy= 0.379329
Thermal correction to Gibbs Free Energy= 0.300152
Sum of electronic and zero-point Energies= -2749.319044
Sum of electronic and thermal Energies= -2749.293448
Sum of electronic and thermal Enthalpies= -2749.292504
Sum of electronic and thermal Free Energies= -2749.371680

Counterpoise: corrected energy = -2749.662070553887
Counterpoise: BSSE energy = 0.009762145257

MP2/aug-cc-pVTZ//B97D/6-311+G(d,p)
EUMP2 = -0.27461534674753D+04

PDMS

B3LYP/6-311+G(d,p)
E(RB3LYP) = -1489.31107898
Zero-point correction= 0.317142 (Hartree/Particle)
Thermal correction to Energy= 0.343229
Thermal correction to Enthalpy= 0.344174
Thermal correction to Gibbs Free Energy= 0.258077
Sum of electronic and zero-point Energies= -1488.993937
Sum of electronic and thermal Energies= -1488.967850
Sum of electronic and thermal Enthalpies= -1488.966905
Sum of electronic and thermal Free Energies= -1489.053002

MP2/6-311+G(d,p)//B3LYP/6-311+G(d,p)
EUMP2 = -0.14860423046882D+04

MP2/aug-cc-pVTZ// B3LYP/6-311+G(d,p)
EUMP2 = -0.14866131425979D+04

B97D/6-311+G(d,p)
E(RB97D) = -1488.81443767
Zero-point correction= 0.309655 (Hartree/Particle)
Thermal correction to Energy= 0.335676
Thermal correction to Enthalpy= 0.336620
Thermal correction to Gibbs Free Energy= 0.252585
Sum of electronic and zero-point Energies= -1488.504783
Sum of electronic and thermal Energies= -1488.478762
Sum of electronic and thermal Enthalpies= -1488.477818
Sum of electronic and thermal Free Energies= -1488.561852

MP2/aug-cc-pVTZ //B97D/6-311+G(d,p)
EUMP2 = -0.14866131848547D+04

$SiCl_4$

B3LYP/6-311+G(d,p)
E(RB3LYP) = -2130.61140244
Zero-point correction= 0.007176 (Hartree/Particle)
Thermal correction to Energy= 0.013686
Thermal correction to Enthalpy= 0.014630
Thermal correction to Gibbs Free Energy= -0.025398
Sum of electronic and zero-point Energies= -2130.604226
Sum of electronic and thermal Energies= -2130.597716
Sum of electronic and thermal Enthalpies= -2130.596772
Sum of electronic and thermal Free Energies= -2130.636800

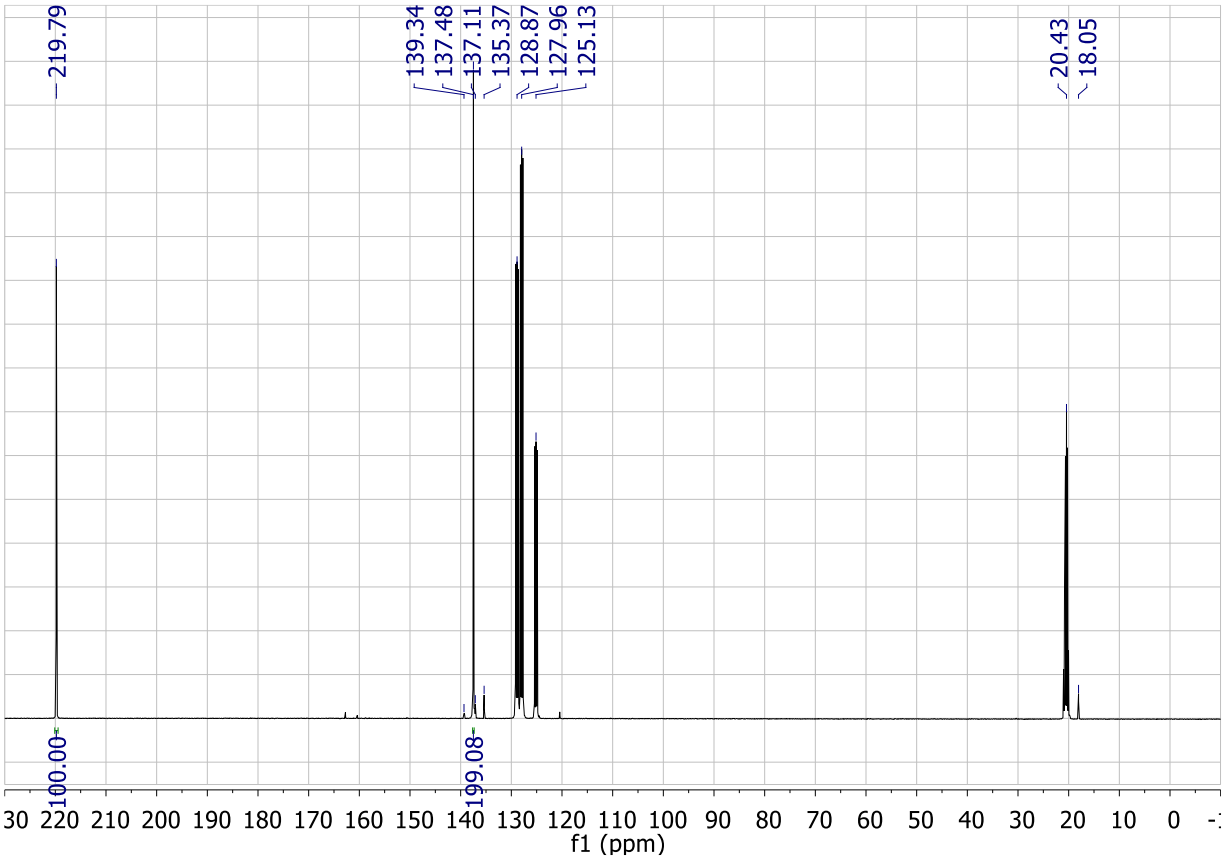
MP2/6-311+G(d,p)//B3LYP/6-311+G(d,p)
EUMP2 = -0.21278007282046D+04

B97D/6-311+G(d,p)
E(RB97D) = -2130.62549566
Zero-point correction= 0.007006 (Hartree/Particle)
Thermal correction to Energy= 0.013550
Thermal correction to Enthalpy= 0.014494
Thermal correction to Gibbs Free Energy= -0.025573
Sum of electronic and zero-point Energies= -2130.618490
Sum of electronic and thermal Energies= -2130.611946
Sum of electronic and thermal Enthalpies= -2130.611002
Sum of electronic and thermal Free Energies= -2130.651069

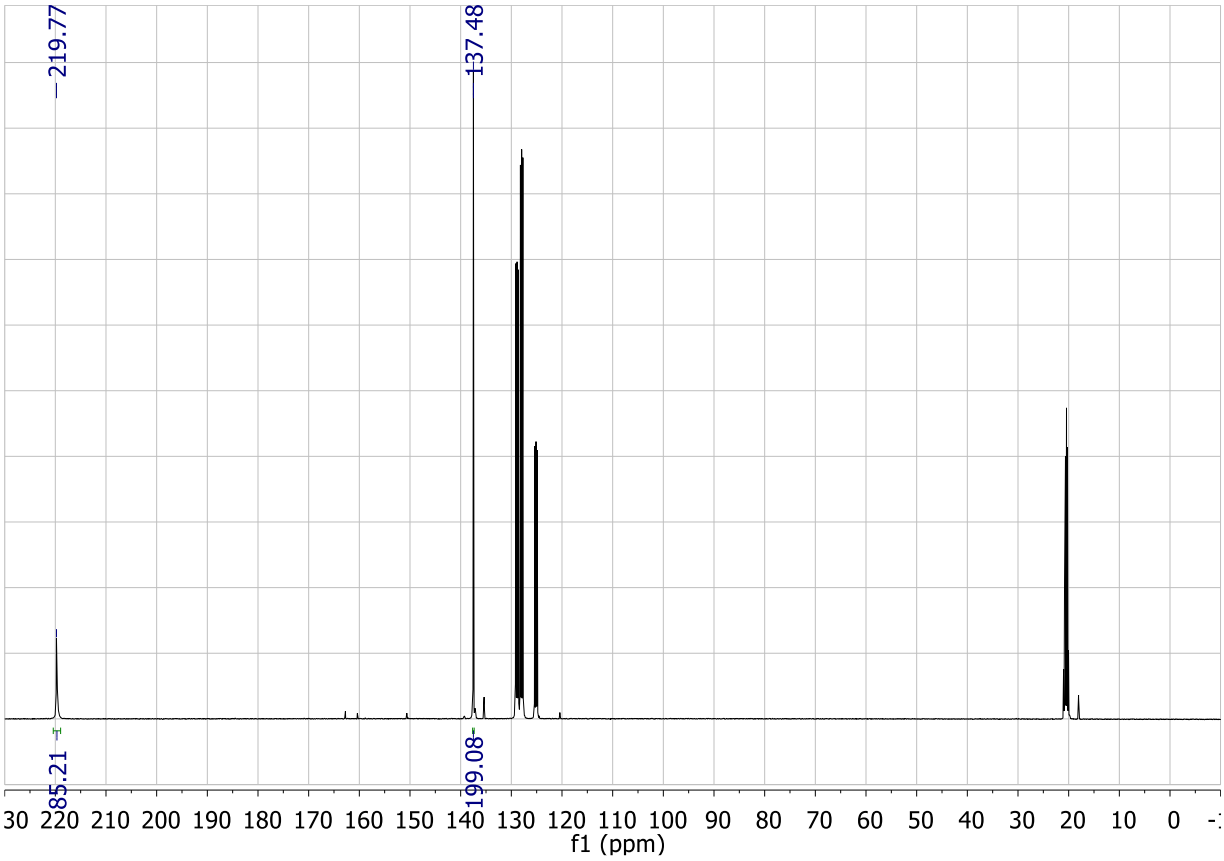
MP2/aug-cc-pVTZ//B97D/6-311+G(d,p)
EUMP2 = -0.21281230550683D+04

Appendix B: NMR Spectra

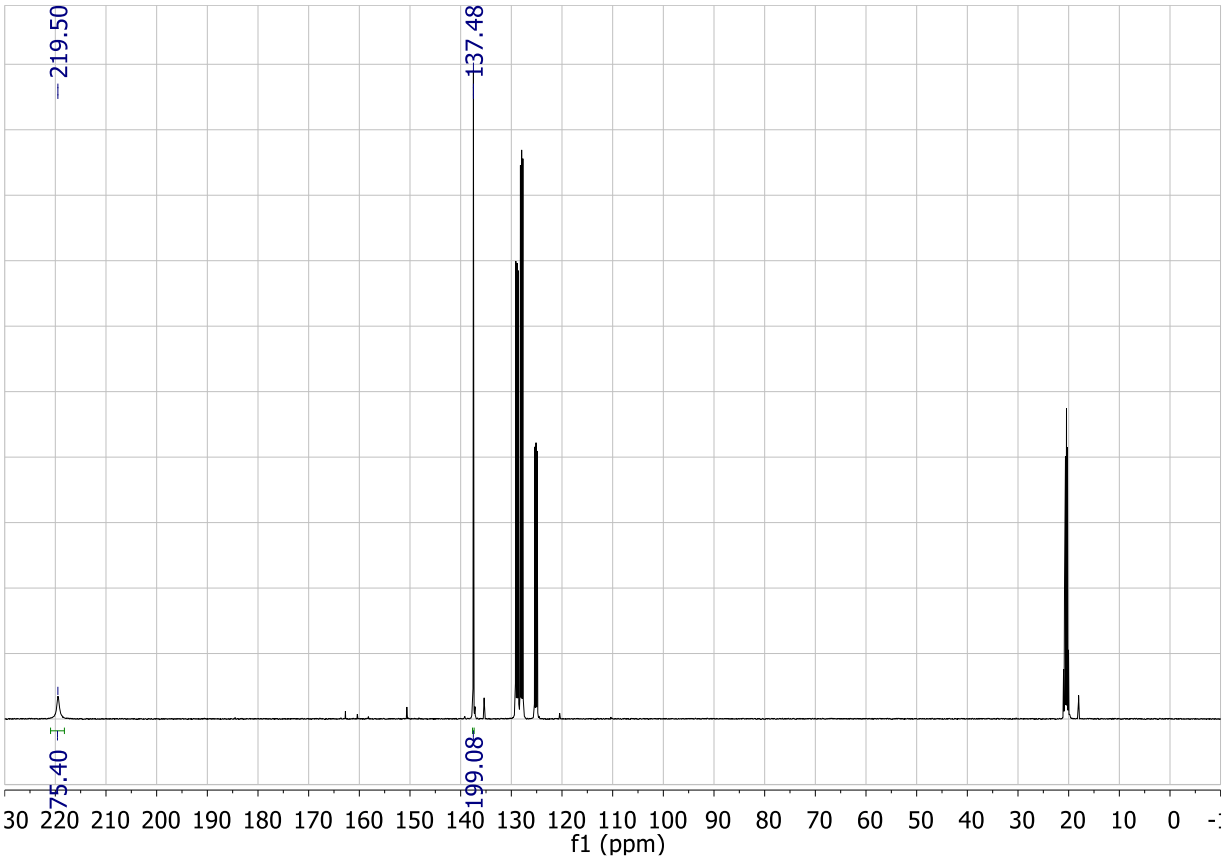
^{13}C-Labelled IMes at Time 0 - (Quantitative ^{13}C Toluene-d_8)



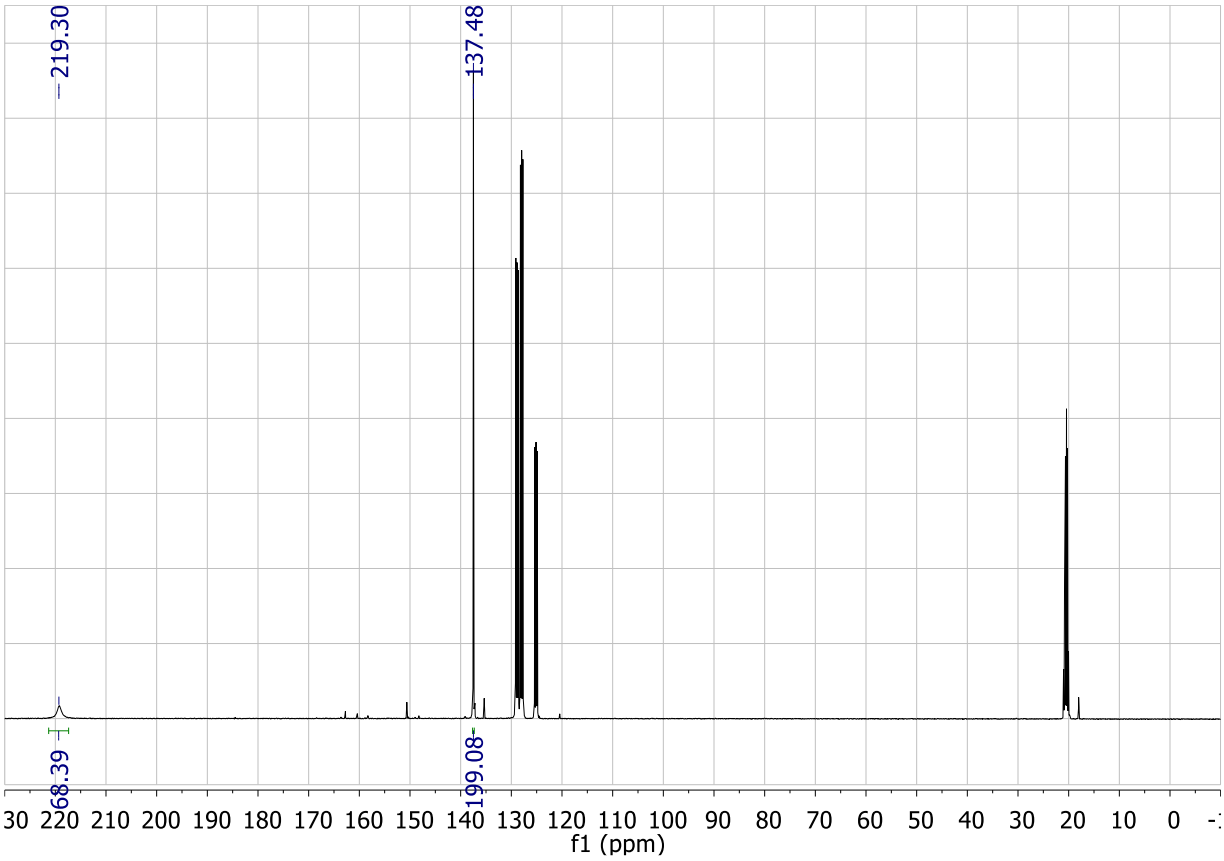
^{13}C-Labelled IMes After 17 Hours - (Quantitative ^{13}C Toluene-d_8)



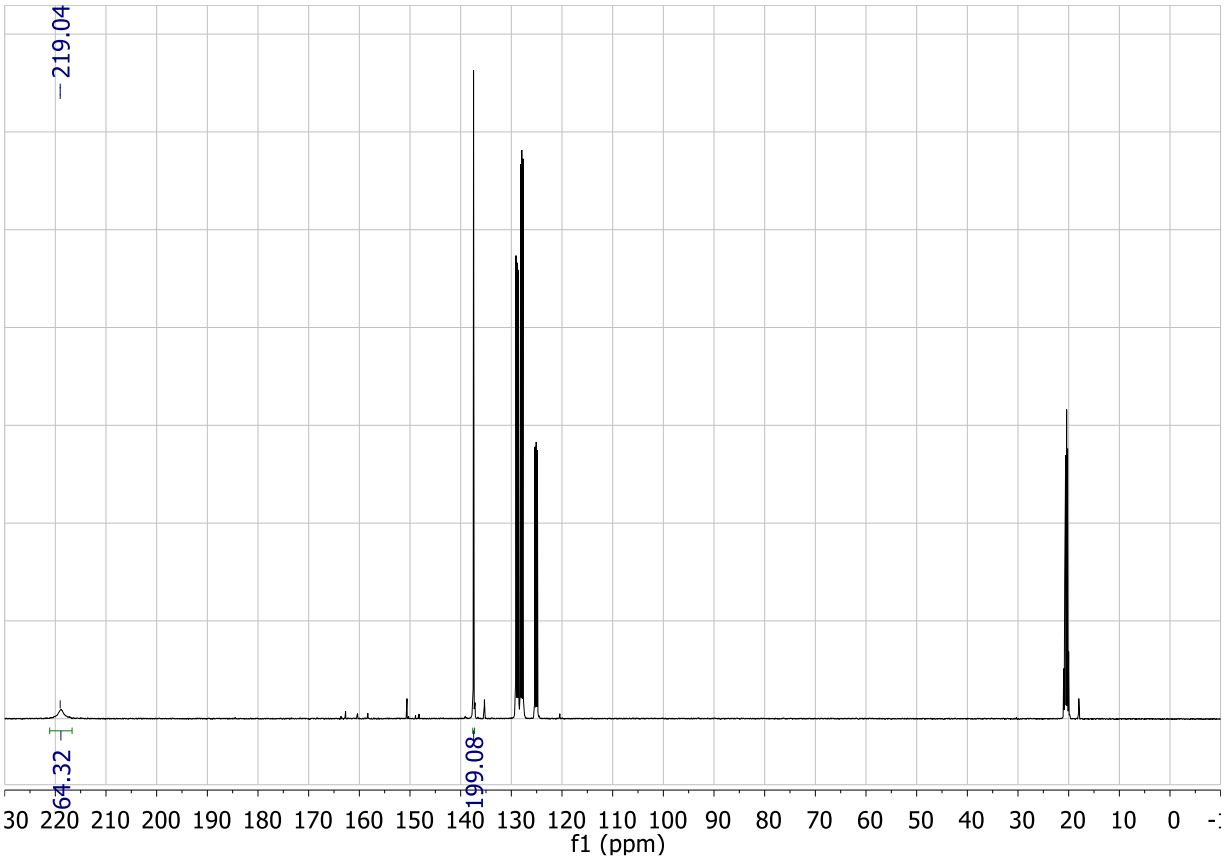
^{13}C-Labelled IMes After 26 Hours - (Quantitative ^{13}C Toluene-d_8)



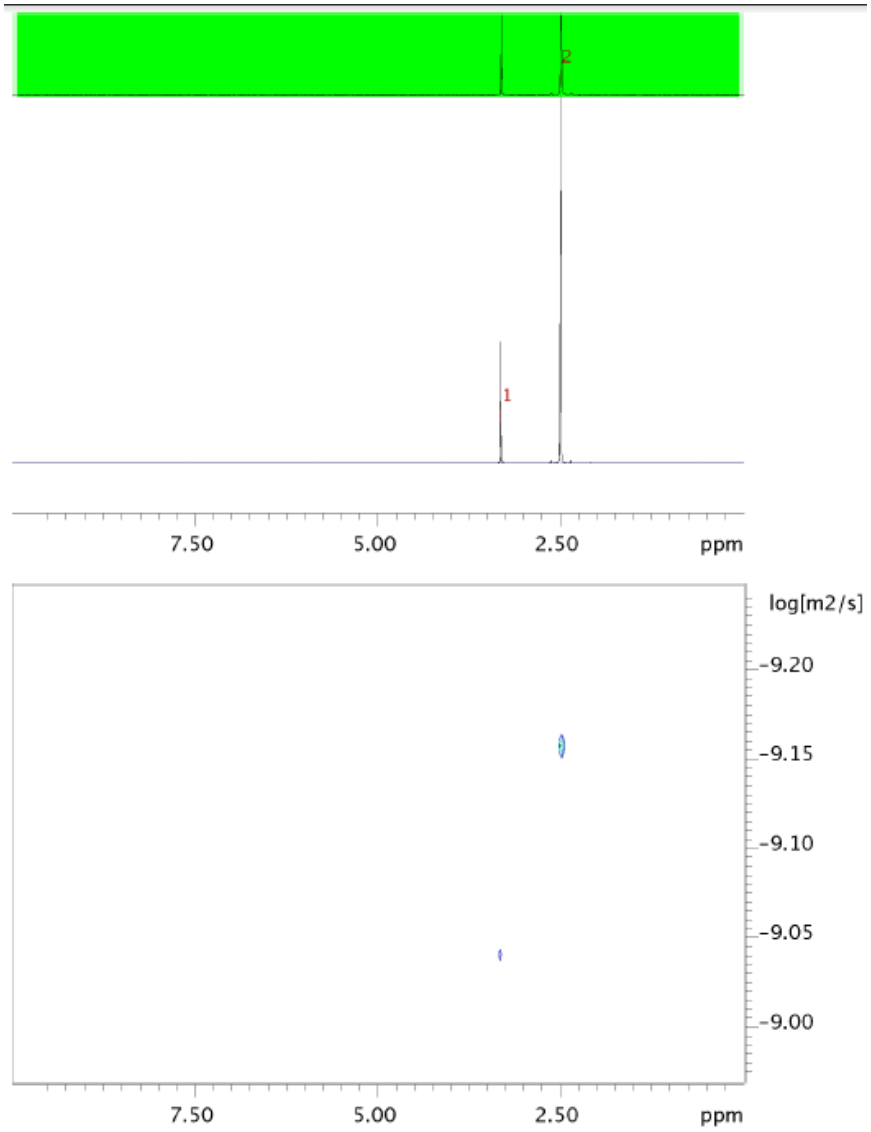
^{13}C-Labelled IMes After 41 Hours - (Quantitative ^{13}C Toluene-d_8)



^{13}C-Labelled IMes After 46 Hours - (Quantitative ^{13}C Toluene-d_8)



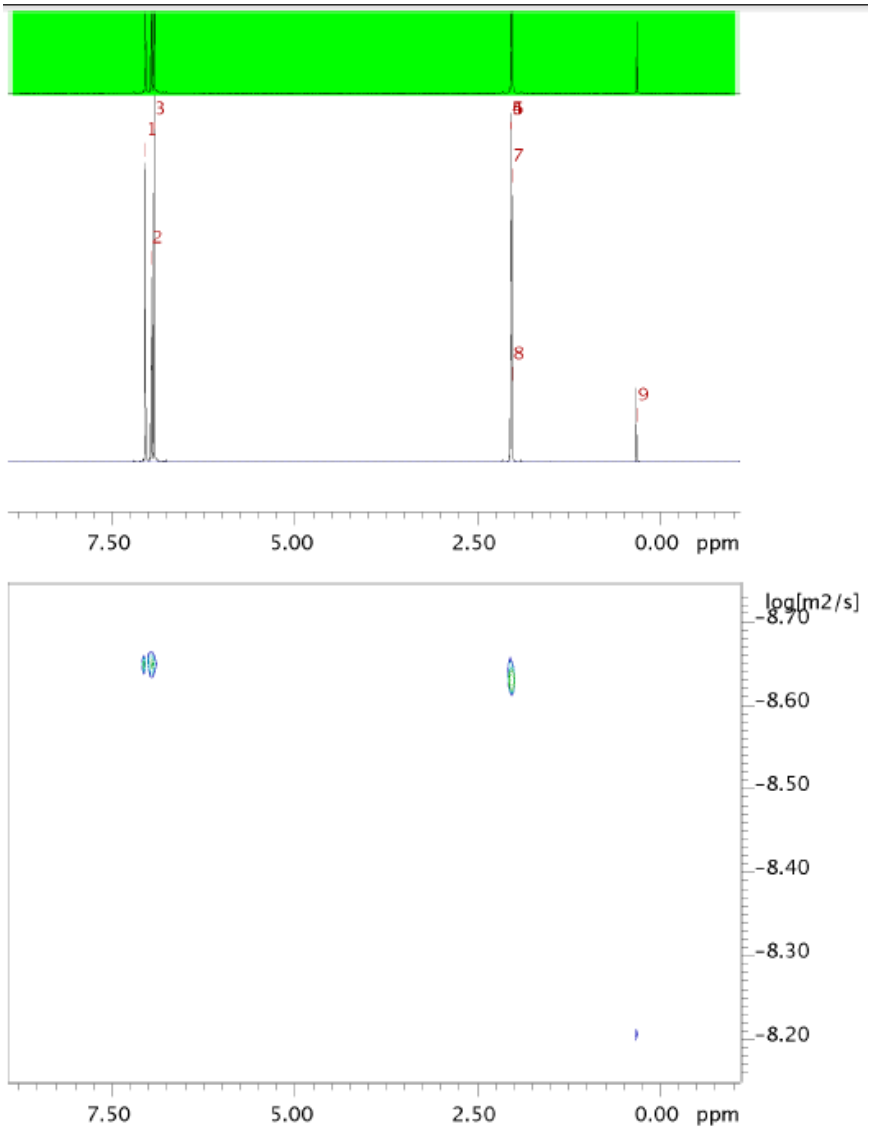
DMSO-d_6 DOSY



Fitted function:	f (x) = A * exp (-D * x^2 * gamma^2 * littleDelta^2 (bigDelta-littleDelta/3)* 10^4
used gamma:	26752 rad/(s*Gauss)
used little delta:	0.0024000 s
used big delta:	0.049900 s
used gradient strength:	variable
Random error estimation of data:	RMS per spectrum (or trace/plane)
Systematic error estimation of data:	worst case per peak scenario
Fit parameter Error estimation method:	from Monte Carlo simulations
Confidence level:	95%
Used peaks:	
Used integrals:	peak intensities
Used Gradient strength:	all values (including replicates) used

Peak name	F2 [ppm]	D [m2/s]	error
1	3.310	9.15e-10	8.565e-13
2	2.490	6.93e-10	2.311e-13

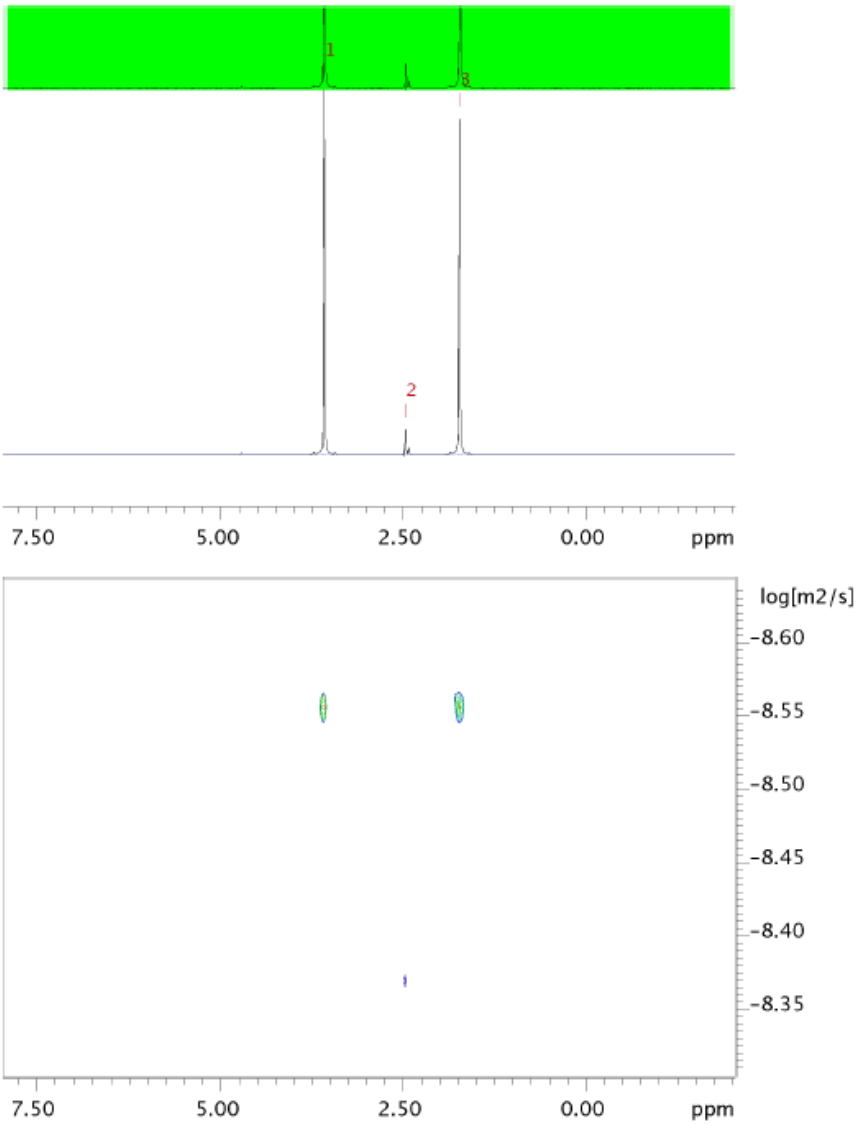
Toluene-d_8 DOSY



Fitted function:	f (x) = A * exp (-D * x^2 * gamma^2 * littleDelta^2 (bigDelta-littleDelta/3)* 10^4
used gamma:	26752 rad/(s*Gauss)
used little delta:	0.0024000 s
used big delta:	0.019900 s
used gradient strength:	variable
Random error estimation of data:	RMS per spectrum (or trace/plane)
Systematic error estimation of data:	worst case per peak scenario
Fit parameter Error estimation method:	from Monte Carlo simulations
Confidence level:	95%
Used peaks:	
Used integrals:	peak intensities
Used Gradient strength:	all values (including replicates) used

Peak name	F2 [ppm]	D [m2/s]	error
1	7.040	2.26e-09	6.828e-13
2	6.959	2.27e-09	1.118e-12
3	6.918	2.28e-09	5.475e-13
4	2.040	2.29e-09	1.673e-12
5	2.035	2.30e-09	8.661e-13
6	2.031	2.30e-09	6.150e-13
7	2.027	2.30e-09	7.875e-13
8	2.023	2.31e-09	1.360e-12
9	0.319	6.19e-09	9.083e-12

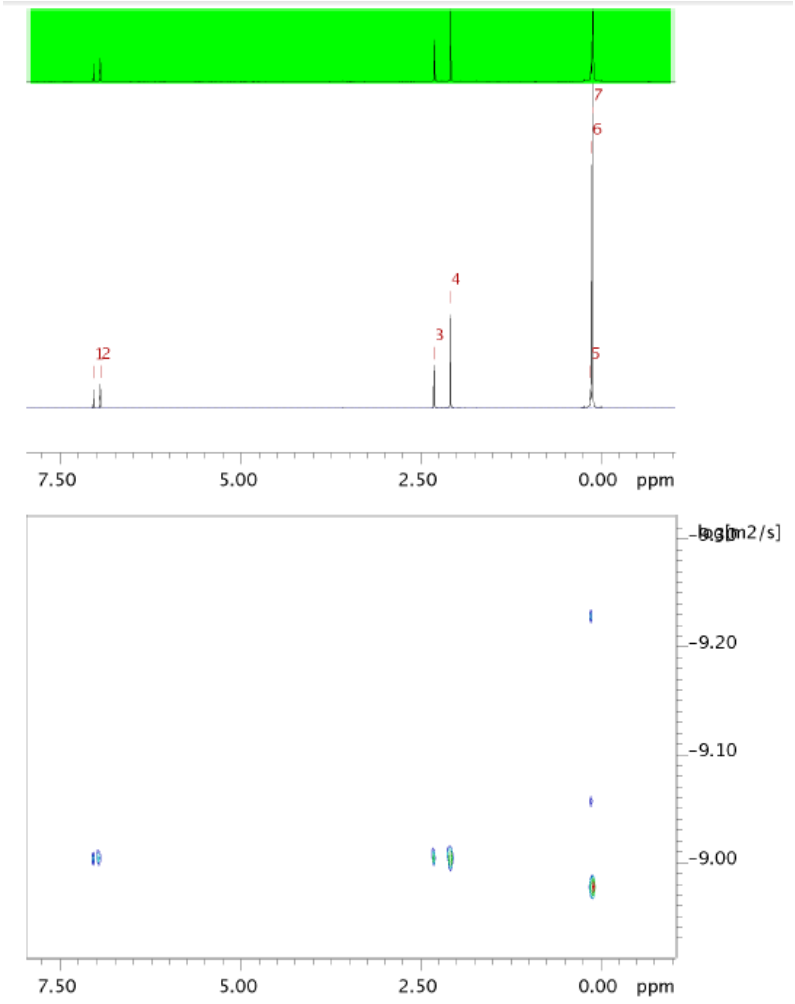
THF-d_8 DOSY



Fitted function:	f (x) = A * exp (-D * x^2 * gamma^2 * littleDelta^2 (bigDelta-littleDelta/3)* 10^4
used gamma:	26752 rad/(s*Gauss)
used little delta:	0.0024000 s
used big delta:	0.019900 s
used gradient strength:	variable
Random error estimation of data:	RMS per spectrum (or trace/plane)
Systematic error estimation of data:	worst case per peak scenario
Fit parameter Error estimation method:	from Monte Carlo simulations
Confidence level:	95%
Used peaks:	
Used integrals:	peak intensities
Used Gradient strength:	all values (including replicates) used

Peak name	F2 [ppm]	D [m2/s]	error
1	3.585	2.79e-09	5.194e-13
2	2.472	4.25e-09	1.246e-11
3	1.733	2.80e-09	5.286e-13

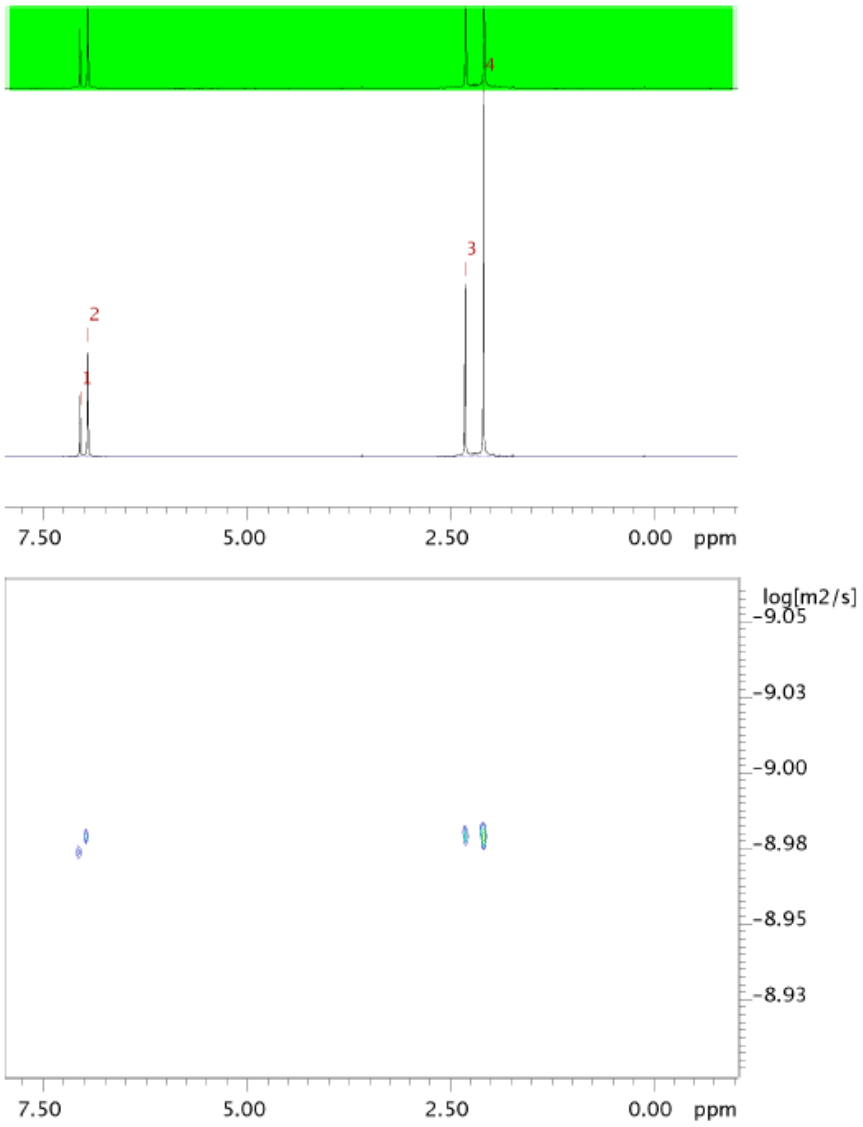
IMes (0.1 mmol) and D_4 (0.1 mmol) in THF-d_8 (0.4 mL) DOSY



Fitted function:	f (x) = A * exp (-D * x^2 * gamma^2 * littleDelta^2 (bigDelta-littleDelta/3)* 10^4
used gamma:	26752 rad/(s*Gauss)
used little delta:	0.0044000 s
used big delta:	0.049900 s
used gradient strength:	variable
Random error estimation of data:	RMS per spectrum (or trace/plane)
Systematic error estimation of data:	worst case per peak scenario
Fit parameter Error estimation method:	from Monte Carlo simulations
Confidence level:	95%
Used peaks:	
Used integrals:	peak intensities
Used Gradient strength:	all values (including replicates) used

Peak name	F2 [ppm]	D [m2/s]	error
1	7.046	9.87e-10	3.585e-13
2	6.956	9.78e-10	2.875e-13
3	2.314	9.86e-10	1.542e-13
4	2.087	9.83e-10	7.041e-14
5	0.137	5.90e-10	1.283e-13
6	0.127	8.78e-10	5.971e-13
7	0.113	1.05e-09	2.350e-14

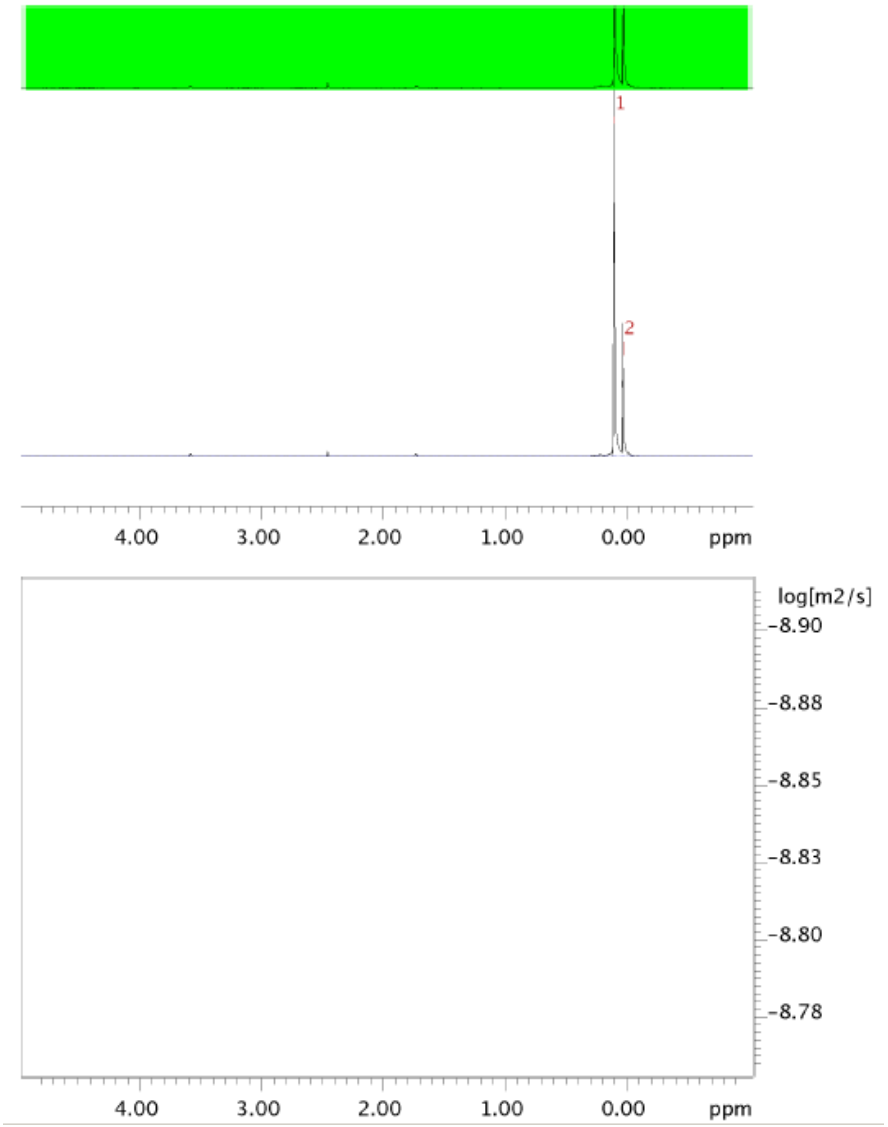
IMes (0.1 mmol) in THF-d_8 (0.4 mL) DOSY



Fitted function:	f (x) = A * exp (-D * x^2 * gamma^2 * littleDelta^2 (bigDelta-littleDelta/3)* 10^4
used gamma:	26752 rad/(s*Gauss)
used little delta:	0.0030000 s
used big delta:	0.039900 s
used gradient strength:	variable
Random error estimation of data:	RMS per spectrum (or trace/plane)
Systematic error estimation of data:	worst case per peak scenario
Fit parameter Error estimation method:	from Monte Carlo simulations
Confidence level:	95%
Used peaks:	
Used integrals:	peak intensities
Used Gradient strength:	all values (including replicates) used

Peak name	F2 [ppm]	D [m2/s]	error
1	7.056	1.06e-09	3.606e-13
2	6.960	1.05e-09	2.054e-13
3	2.313	1.05e-09	1.339e-13
4	2.088	1.05e-09	6.176e-14

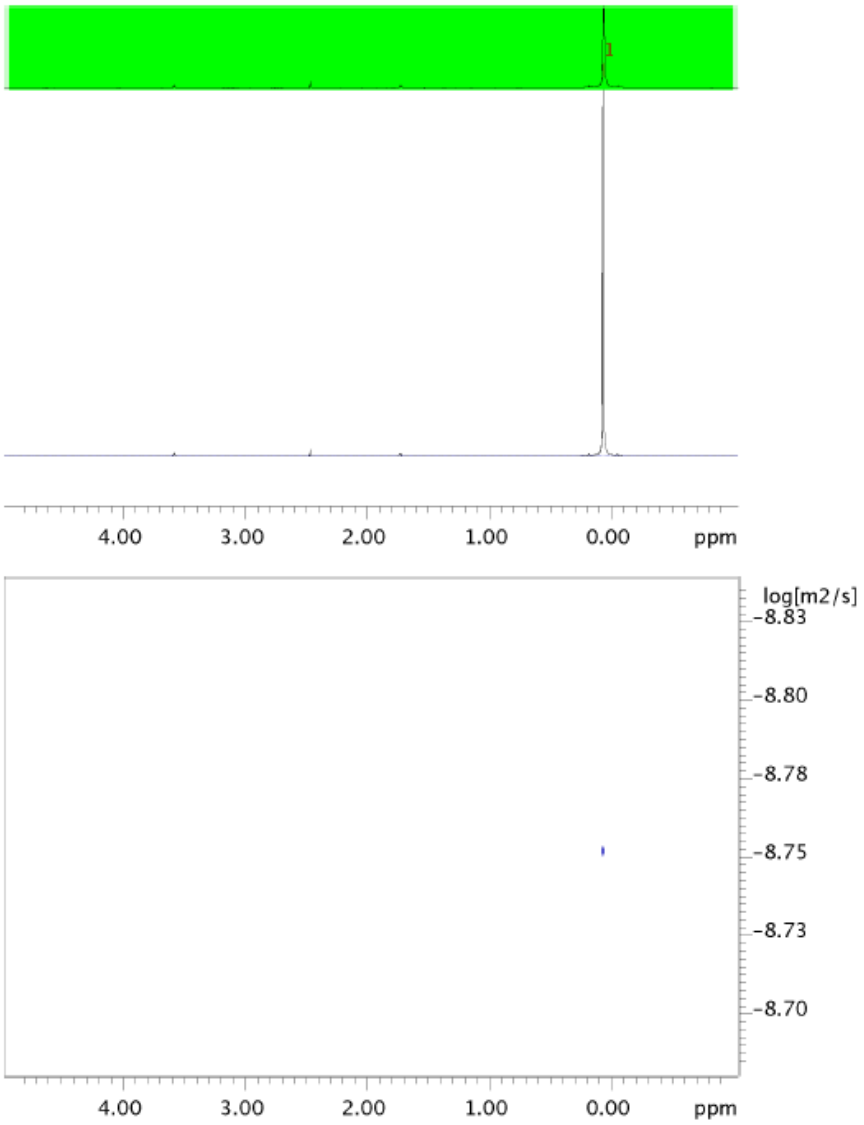
MDM (0.1 mmol) in THF-d_8 (0.4 mL) DOSY



Fitted function:	f (x) = A * exp (-D * x^2 * gamma^2 * littleDelta^2 (bigDelta-littleDelta/3)* 10^4
used gamma:	26752 rad/(s*Gauss)
used little delta:	0.0030000 s
used big delta:	0.039900 s
used gradient strength:	variable
Random error estimation of data:	RMS per spectrum (or trace/plane)
Systematic error estimation of data:	worst case per peak scenario
Fit parameter Error estimation method:	from Monte Carlo simulations
Confidence level:	95%
Used peaks:	
Used integrals:	peak intensities
Used Gradient strength:	all values (including replicates) used

Peak name	F2 [ppm]	D [m2/s]	error
1	0.101	1.47e-09	5.496e-14
2	0.030	1.48e-09	1.503e-13

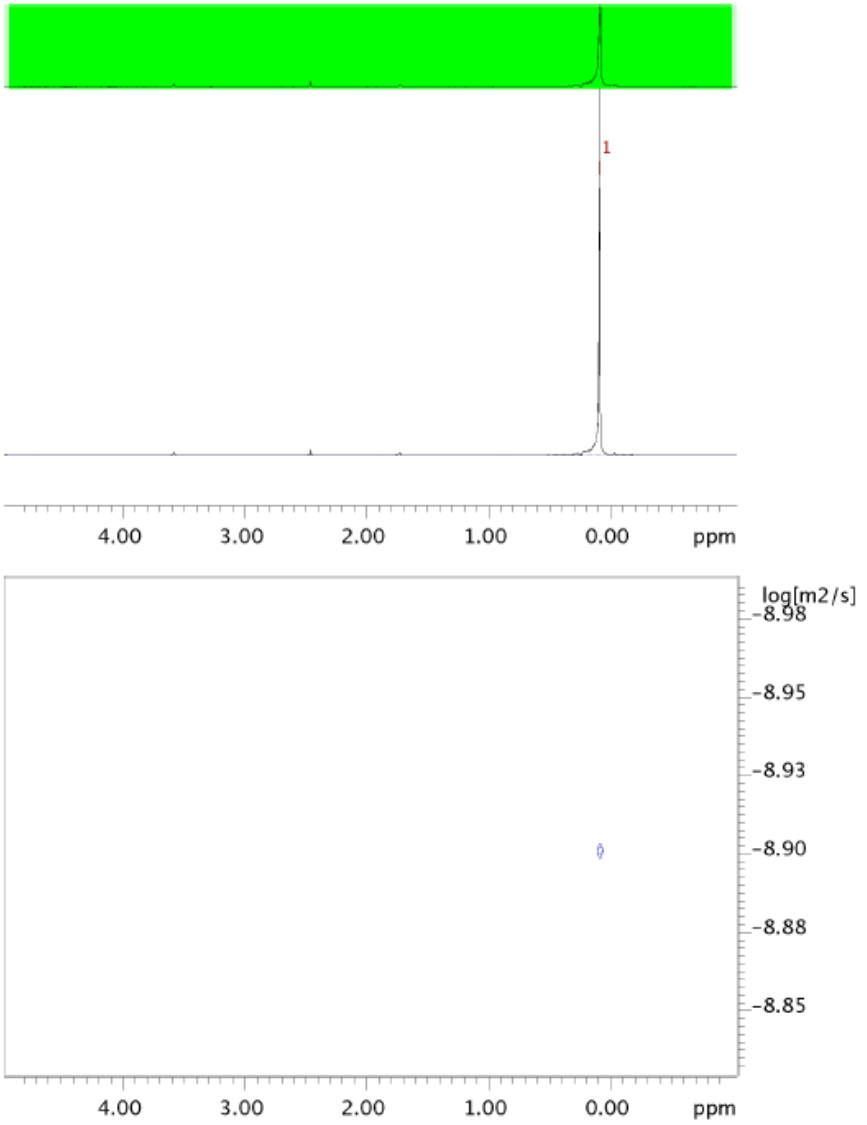
M_2 (0.1 mmol) in THF-d_8 (0.4 mL) DOSY



Fitted function:	f (x) = A * exp (-D * x^2 * gamma^2 * littleDelta^2 (bigDelta-littleDelta/3)* 10^4
used gamma:	26752 rad/(s*Gauss)
used little delta:	0.0030000 s
used big delta:	0.039900 s
used gradient strength:	variable
Random error estimation of data:	RMS per spectrum (or trace/plane)
Systematic error estimation of data:	worst case per peak scenario
Fit parameter Error estimation method:	from Monte Carlo simulations
Confidence level:	95%
Used peaks:	
Used integrals:	peak intensities
Used Gradient strength:	all values (including replicates) used

Peak name	F2 [ppm]	D [m2/s]	error
1	0.071	1.76e-09	1.565e-14

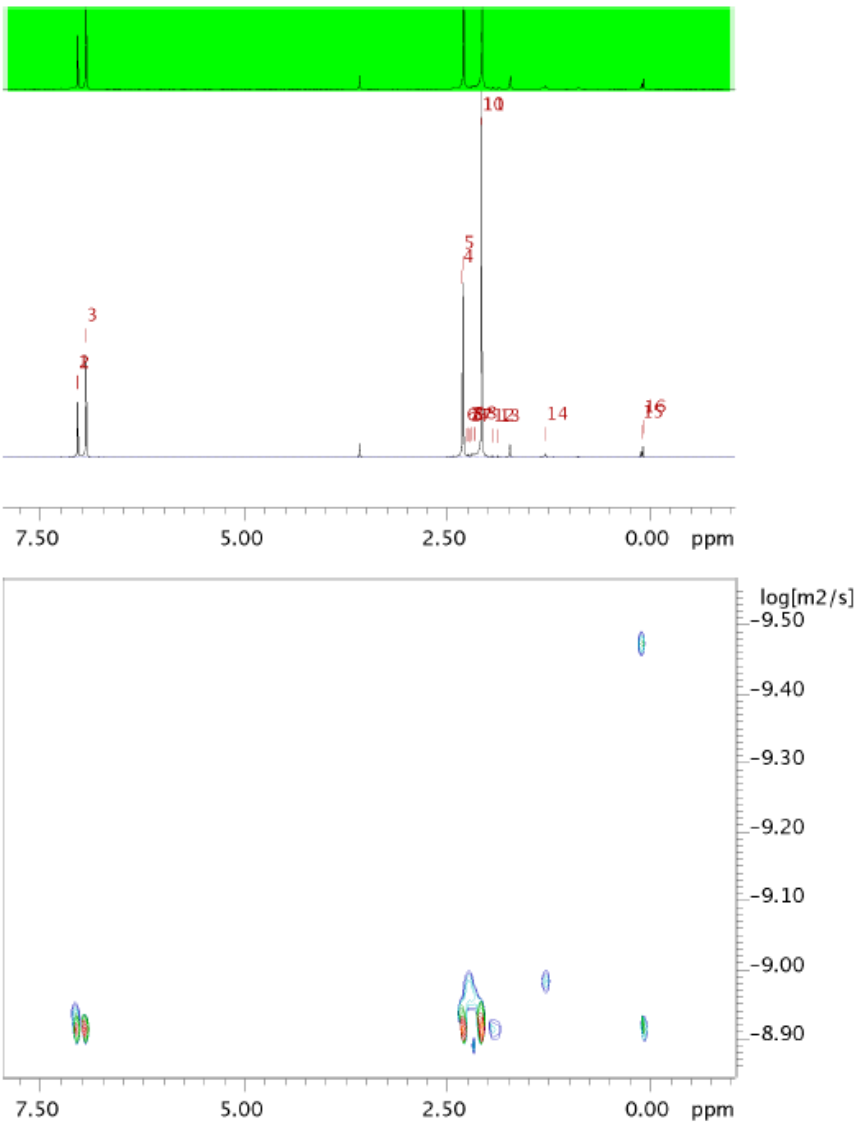
D_4 (0.1 mmol) in THF-d_8 (0.4 mL) DOSY



Fitted function:	f (x) = A * exp (-D * x^2 * gamma^2 * littleDelta^2 (bigDelta-littleDelta/3)* 10^4
used gamma:	26752 rad/(s*Gauss)
used little delta:	0.0030000 s
used big delta:	0.039900 s
used gradient strength:	variable
Random error estimation of data:	RMS per spectrum (or trace/plane)
Systematic error estimation of data:	worst case per peak scenario
Fit parameter Error estimation method:	from Monte Carlo simulations
Confidence level:	95%
Used peaks:	
Used integrals:	peak intensities
Used Gradient strength:	all values (including replicates) used

Peak name	F2 [ppm]	D [m2/s]	error
1	0.089	1.25e-09	2.248e-14

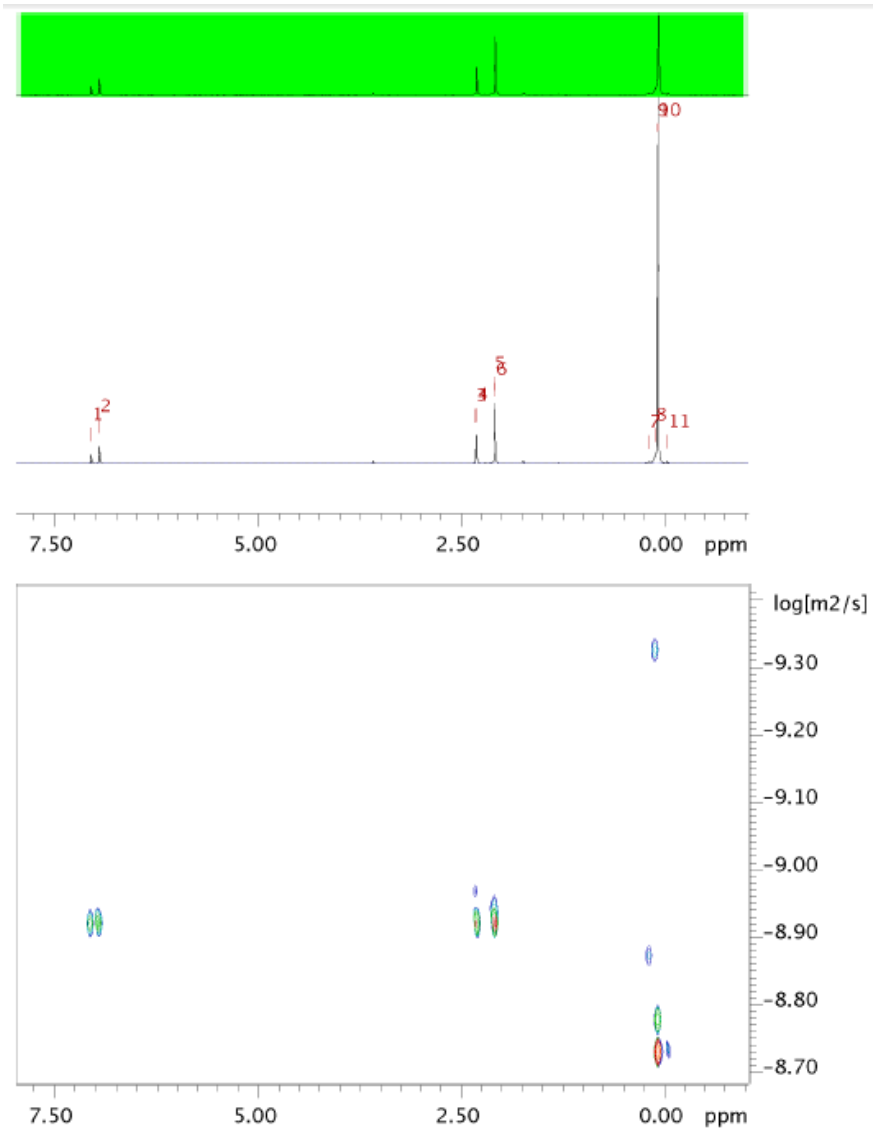
IMes (0.01 mmol) in THF-d_8 (0.4 mL) DOSY



Fitted function:	f (x) = A * exp (-D * x^2 * gamma^2 * littleDelta^2 (bigDelta-littleDelta/3)* 10^4
used gamma:	26752 rad/(s*Gauss)
used little delta:	0.0030000 s
used big delta:	0.039900 s
used gradient strength:	variable
Random error estimation of data:	RMS per spectrum (or trace/plane)
Systematic error estimation of data:	worst case per peak scenario
Fit parameter Error estimation method:	from Monte Carlo simulations
Confidence level:	95%
Used peaks:	automatically picked peaks
Used integrals:	peak intensities
Used Gradient strength:	all values (including replicates) used

Peak name	F2 [ppm]	D [m2/s]	error
1	7.070	1.17e-09	1.337e-11
2	7.058	1.20e-09	1.162e-12
3	6.956	1.20e-09	6.349e-13
4	2.322	1.14e-09	5.181e-12
5	2.309	1.20e-09	3.767e-13
6	2.272	1.12e-09	2.103e-11
7	2.241	1.05e-09	1.735e-11
8	2.205	1.07e-09	1.499e-11
9	2.167	1.07e-09	2.163e-11
10	2.092	1.17e-09	2.694e-12
11	2.080	1.20e-09	1.798e-13
12	1.951	1.22e-09	2.780e-11
13	1.878	1.19e-09	3.892e-11
14	1.295	1.04e-09	1.429e-11
15	0.113	3.43e-10	2.589e-12
16	0.092	1.25e-09	6.280e-12
17	2.232	1.12e-09	2.339e-11
18	2.179	1.26e-09	1.864e-11

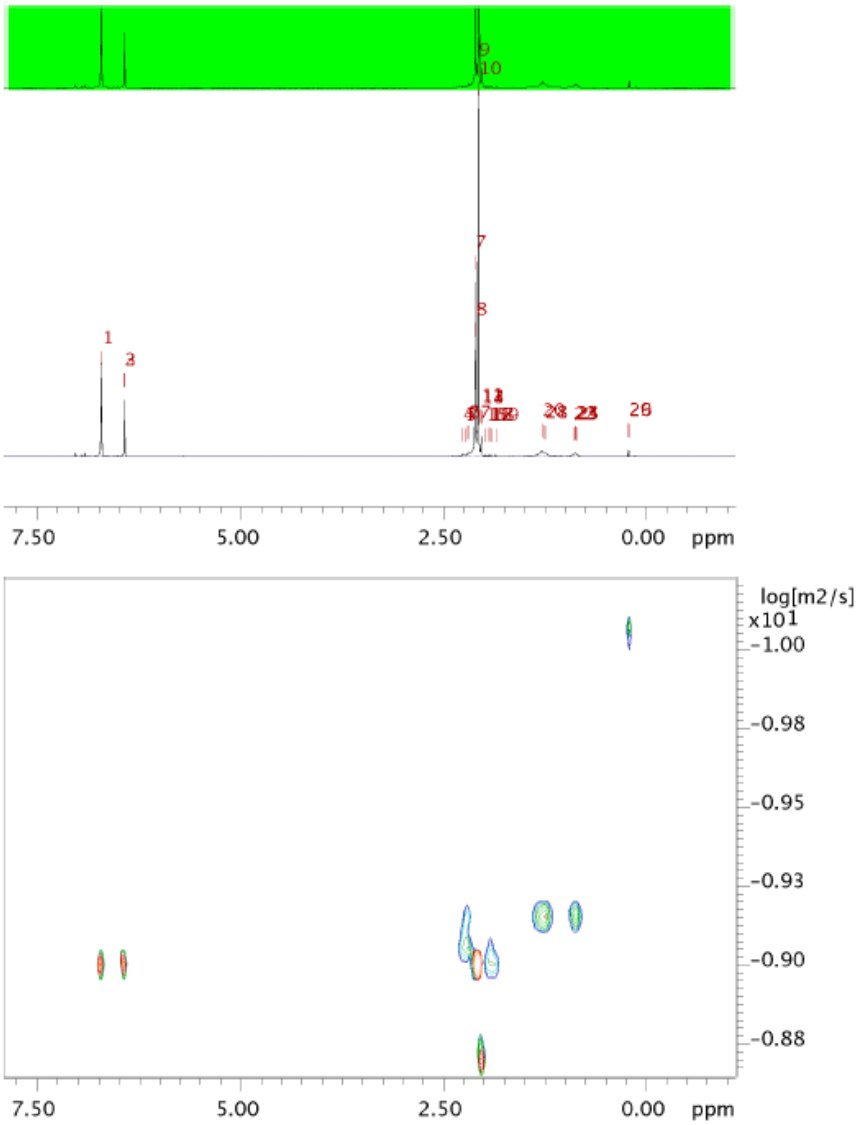
IMes (0.01 mmol) and M_2 (0.02 mmol) in THF-d_8 (0.4 mL) DOSY



Fitted function:	f (x) = A * exp (-D * x^2 * gamma^2 * littleDelta^2 (bigDelta-littleDelta/3)* 10^4
used gamma:	26752 rad/(s*Gauss)
used little delta:	0.0030000 s
used big delta:	0.039900 s
used gradient strength:	variable
Random error estimation of data:	RMS per spectrum (or trace/plane)
Systematic error estimation of data:	worst case per peak scenario
Fit parameter Error estimation method:	from Monte Carlo simulations
Confidence level:	95%
Used peaks:	automatically picked peaks
Used integrals:	peak intensities
Used Gradient strength:	all values (including replicates) used

Peak name	F2 [ppm]	D [m2/s]	error
1	7.058	1.22e-09	2.065e-12
2	6.958	1.21e-09	1.055e-12
3	2.323	1.07e-09	1.008e-11
4	2.312	1.21e-09	6.456e-13
5	2.094	1.14e-09	5.765e-12
6	2.082	1.22e-09	3.144e-13
7	0.191	1.31e-09	1.099e-11
8	0.114	4.80e-10	1.462e-12
9	0.086	1.69e-09	2.033e-12
10	0.075	1.83e-09	1.163e-13
11	-0.044	1.83e-09	1.917e-11

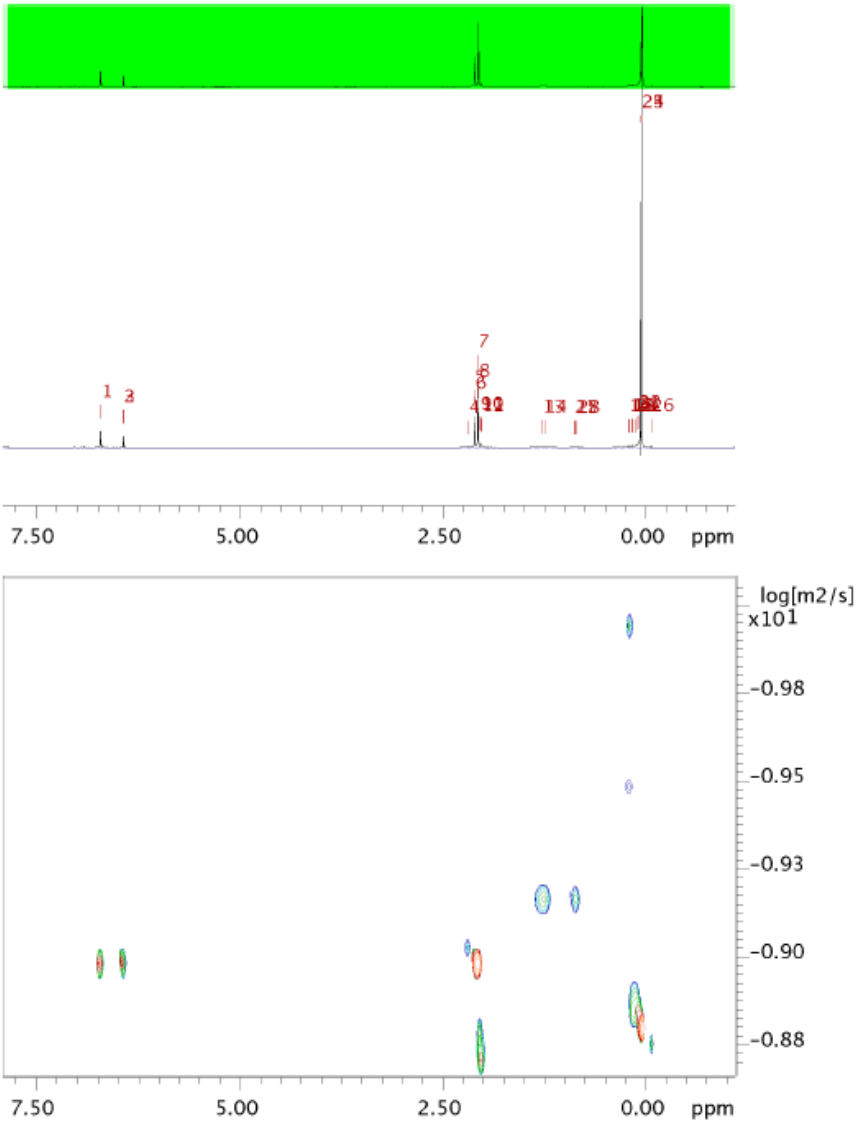
IMes (0.01 mmol) in Toluene-d_8 (0.4 mL) DOSY



Fitted function:	f (x) = A * exp (-D * x^2 * gamma^2 * littleDelta^2 (bigDelta-littleDelta/3)* 10^4
used gamma:	26752 rad/(s*Gauss)
used little delta:	0.0030000 s
used big delta:	0.039900 s
used gradient strength:	variable
Random error estimation of data:	RMS per spectrum (or trace/plane)
Systematic error estimation of data:	worst case per peak scenario
Fit parameter Error estimation method:	from Monte Carlo simulations
Confidence level:	95%
Used peaks:	automatically picked peaks
Used integrals:	peak intensities
Used Gradient strength:	all values (including replicates) used

Peak name	F2 [ppm]	D [m2/s]	error
1	6.718	1.04e-09	5.421e-13
2	6.439	1.03e-09	7.818e-12
3	6.433	1.04e-09	8.360e-13
4	2.269	8.59e-10	1.648e-11
5	2.234	8.07e-10	1.567e-11
6	2.195	9.11e-10	9.204e-12
7	2.116	1.03e-09	2.028e-12
8	2.109	1.04e-09	2.560e-13
9	2.077	1.04e-09	1.258e-12
10	2.069	1.04e-09	1.261e-13
11	2.041	1.70e-09	1.218e-11
12	2.036	2.02e-09	1.078e-11
13	2.032	2.12e-09	8.168e-12
14	2.028	2.12e-09	9.457e-12
15	1.980	1.01e-09	2.356e-11
16	1.941	1.01e-09	1.896e-11
17	1.922	9.12e-10	2.790e-11
18	1.914	9.83e-10	1.867e-11
19	1.858	9.59e-10	1.732e-11
20	1.286	6.97e-10	3.768e-12
21	1.251	7.09e-10	6.116e-12
22	0.901	6.70e-10	1.054e-11
23	0.879	6.99e-10	7.907e-12
24	0.867	7.11e-10	6.606e-12
25	0.852	7.18e-10	9.259e-12
26	0.215	8.02e-11	3.494e-25
27	2.201	7.41e-10	1.355e-11
28	1.253	7.09e-10	6.219e-12
29	0.222	9.20e-11	7.752e-12

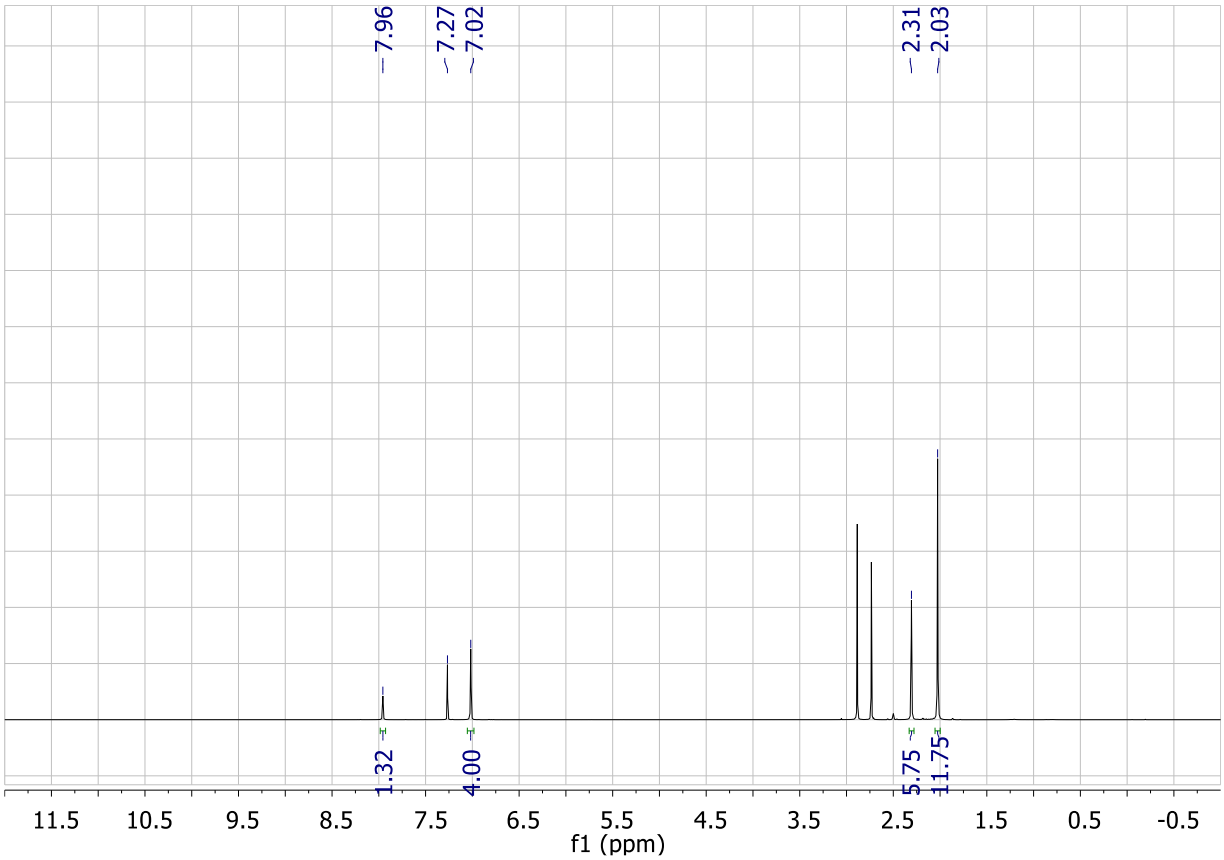
IMes (0.01 mmol) and M_2 (0.2 mmol) in Toluene-d_8 (0.4 mL) DOSY



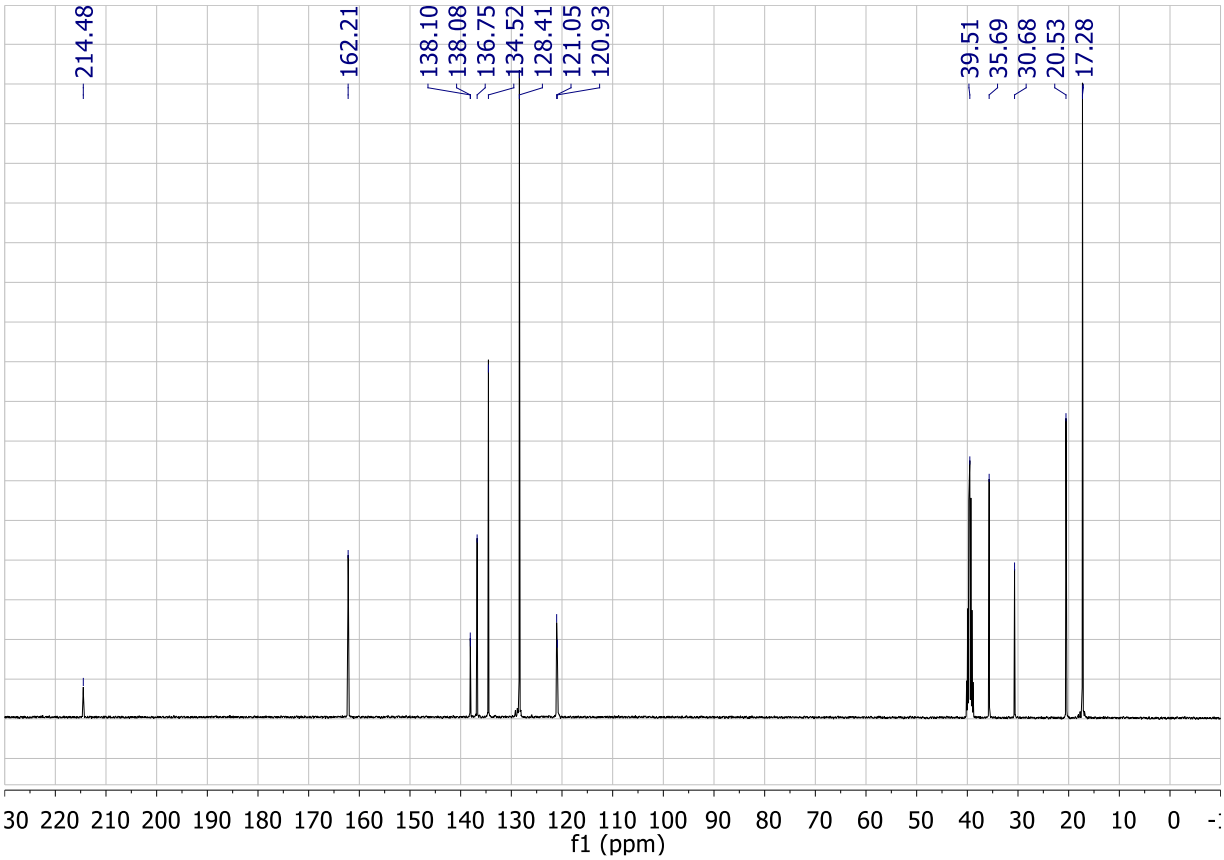
Fitted function:	f (x) = A * exp (-D * x^2 * gamma^2 * littleDelta^2 (bigDelta-littleDelta/3)* 10^4
used gamma:	26752 rad/(s*Gauss)
used little delta:	0.0030000 s
used big delta:	0.039900 s
used gradient strength:	variable
Random error estimation of data:	RMS per spectrum (or trace/plane)
Systematic error estimation of data:	worst case per peak scenario
Fit parameter Error estimation method:	from Monte Carlo simulations
Confidence level:	95%
Used peaks:	automatically picked peaks
Used integrals:	peak intensities
Used Gradient strength:	all values (including replicates) used

Peak name	F2 [ppm]	D [m2/s]	error
1	6.716	1.06e-09	7.392e-13
2	6.440	1.06e-09	1.455e-11
3	6.434	1.05e-09	1.057e-12
4	2.190	9.69e-10	1.532e-11
5	2.115	1.04e-09	3.373e-12
6	2.108	1.05e-09	3.706e-13
7	2.072	1.05e-09	2.088e-12
8	2.065	1.05e-09	1.761e-13
9	2.040	1.54e-09	1.457e-11
10	2.036	1.83e-09	1.386e-11
11	2.032	2.02e-09	1.207e-11
12	2.028	2.00e-09	1.483e-11
13	1.282	6.97e-10	6.221e-12
14	1.246	7.16e-10	9.189e-12
15	0.864	6.91e-10	9.544e-12
16	0.215	3.31e-10	8.566e-12
17	0.210	1.11e-10	1.258e-12
18	0.173	1.31e-09	1.813e-11
19	0.167	1.50e-09	9.370e-12
20	0.132	1.33e-09	1.210e-11
21	0.097	1.47e-09	8.371e-12
22	0.092	1.45e-09	5.456e-12
23	0.057	1.67e-09	9.432e-13
24	0.055	0.00	0.000
25	0.051	1.67e-09	8.913e-14
26	-0.068	1.68e-09	1.851e-11
27	0.876	6.93e-10	1.267e-11
28	0.850	6.77e-10	1.369e-11

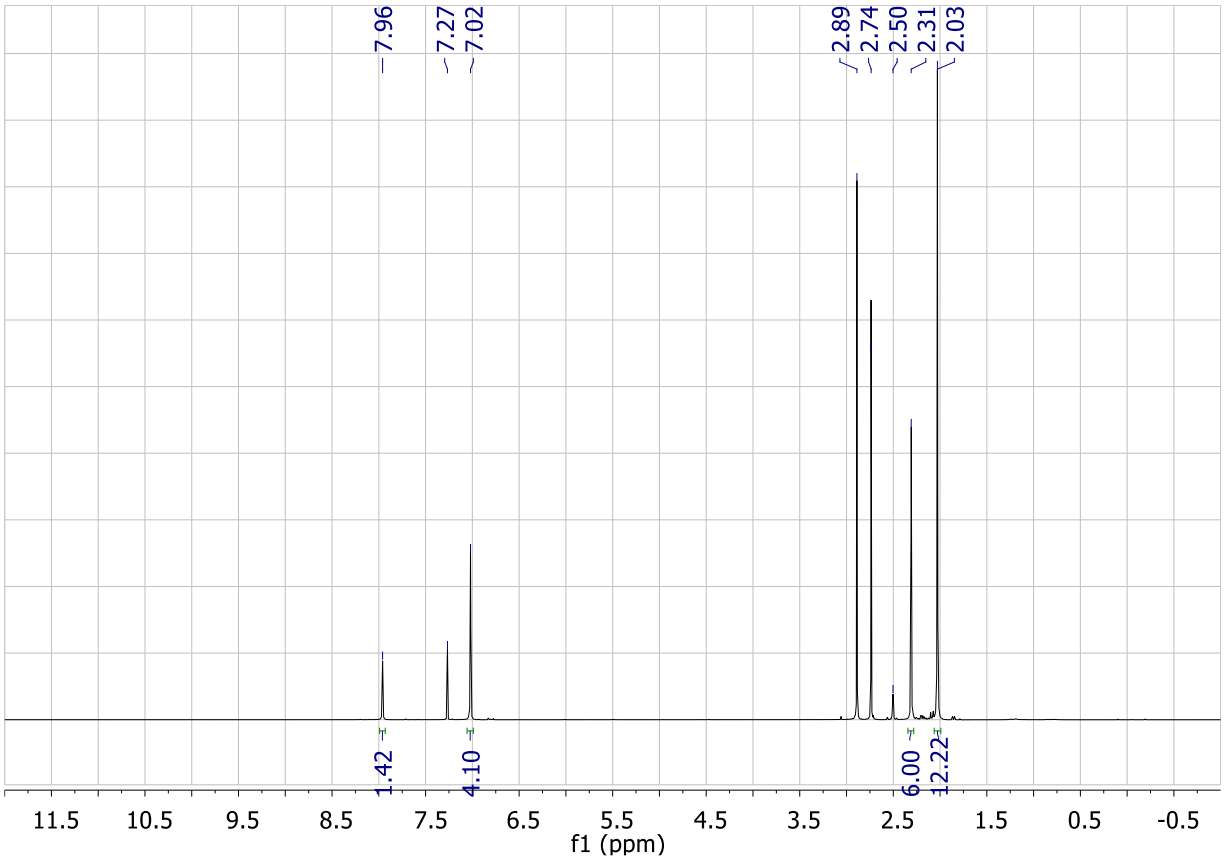
IMes (30 mg) in DMSO-d_6 (0.4 mL) Under Paraffin Oil (0.3 mL) (DMF Standard) at Time 0 (^{1}H DMSO-d_6)



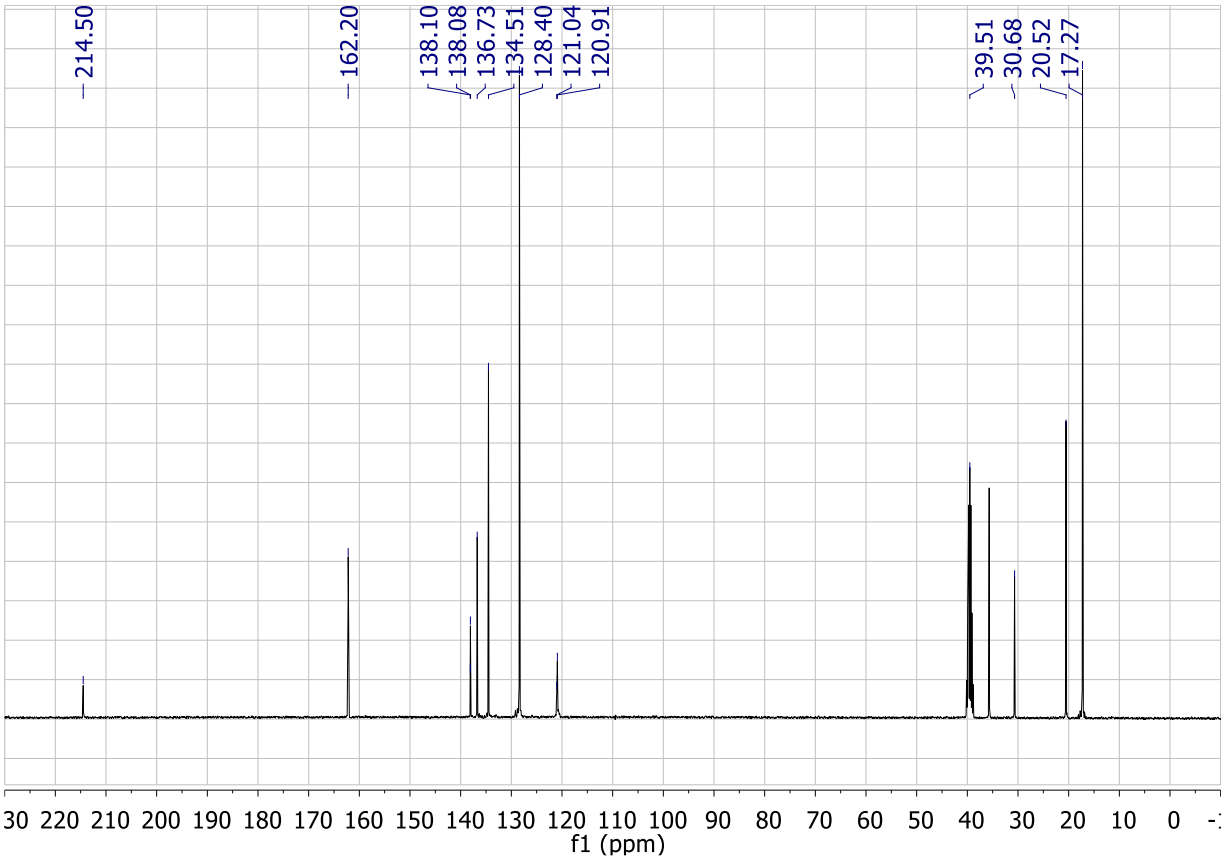
IMes (30 mg) in DMSO-d_6 (0.4 mL) Under Paraffin Oil (0.3 mL) (DMF Standard) at Time 0 (^{13}C DMSO-d_6)



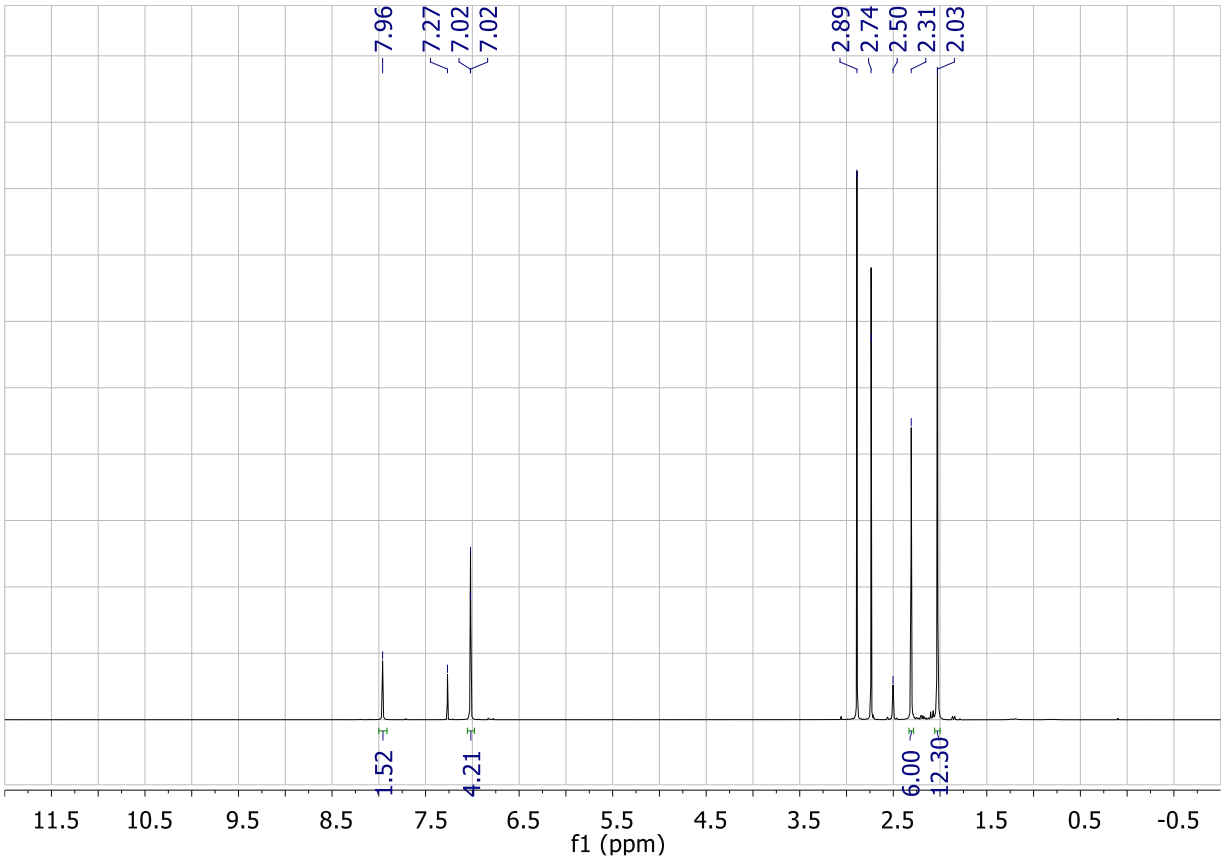
IMes (30 mg) in DMSO-d_6 (0.4 mL) Under Paraffin Oil (0.3 mL) (DMF Standard) After 1 Day (^{1}H DMSO-d_6)



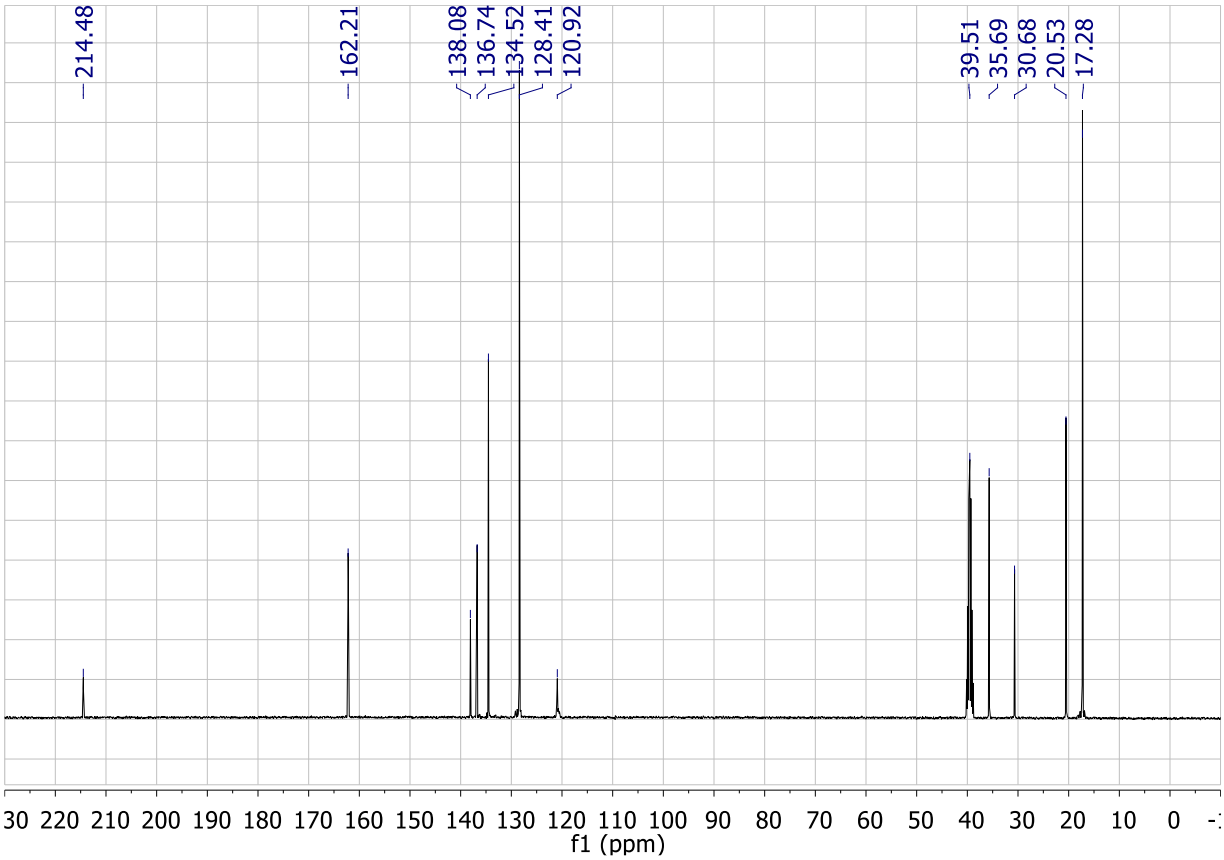
IMes (30 mg) in DMSO-d_6 (0.4 mL) Under Paraffin Oil (0.3 mL) (DMF Standard) After 1 Day (^{13}C DMSO-d_6)



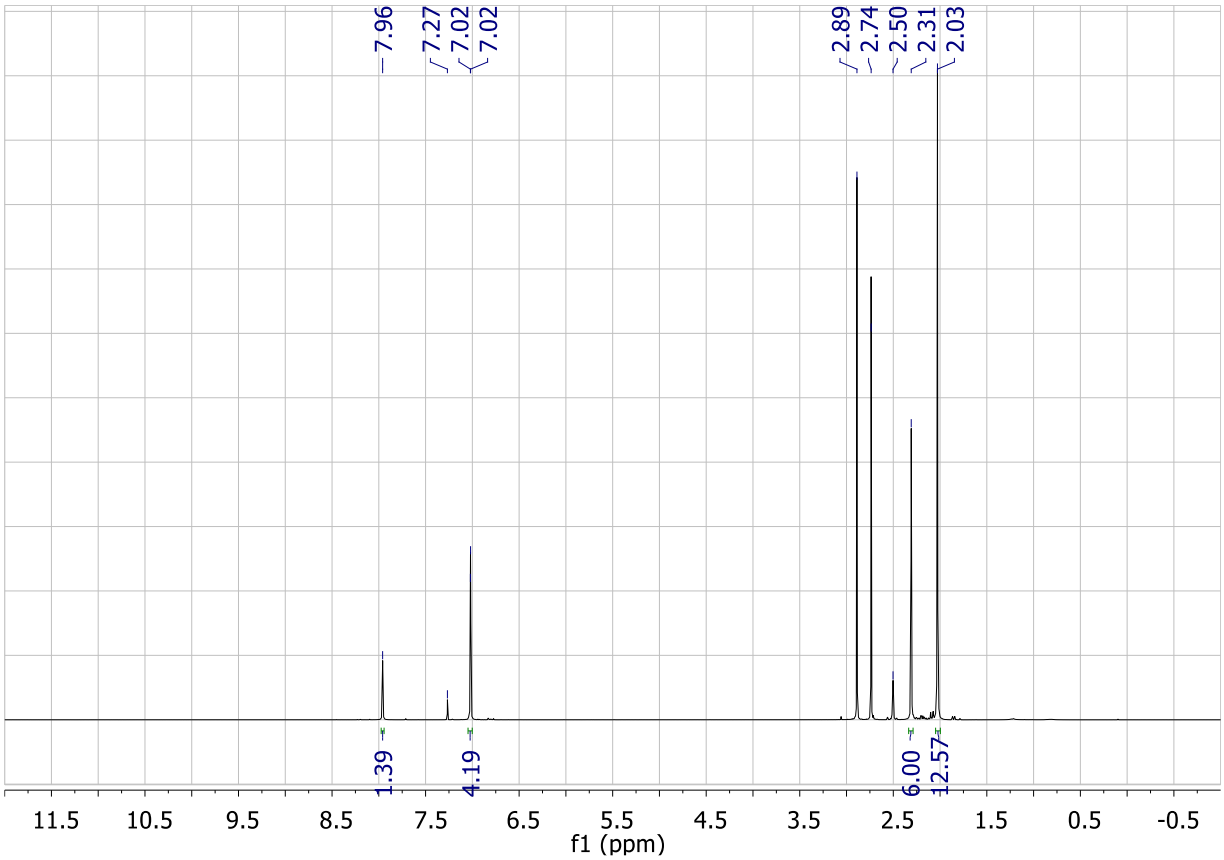
IMes (30 mg) in DMSO-d_6 (0.4 mL) Under Paraffin Oil (0.3 mL) (DMF Standard) After 2 Days (^{1}H DMSO-d_6)



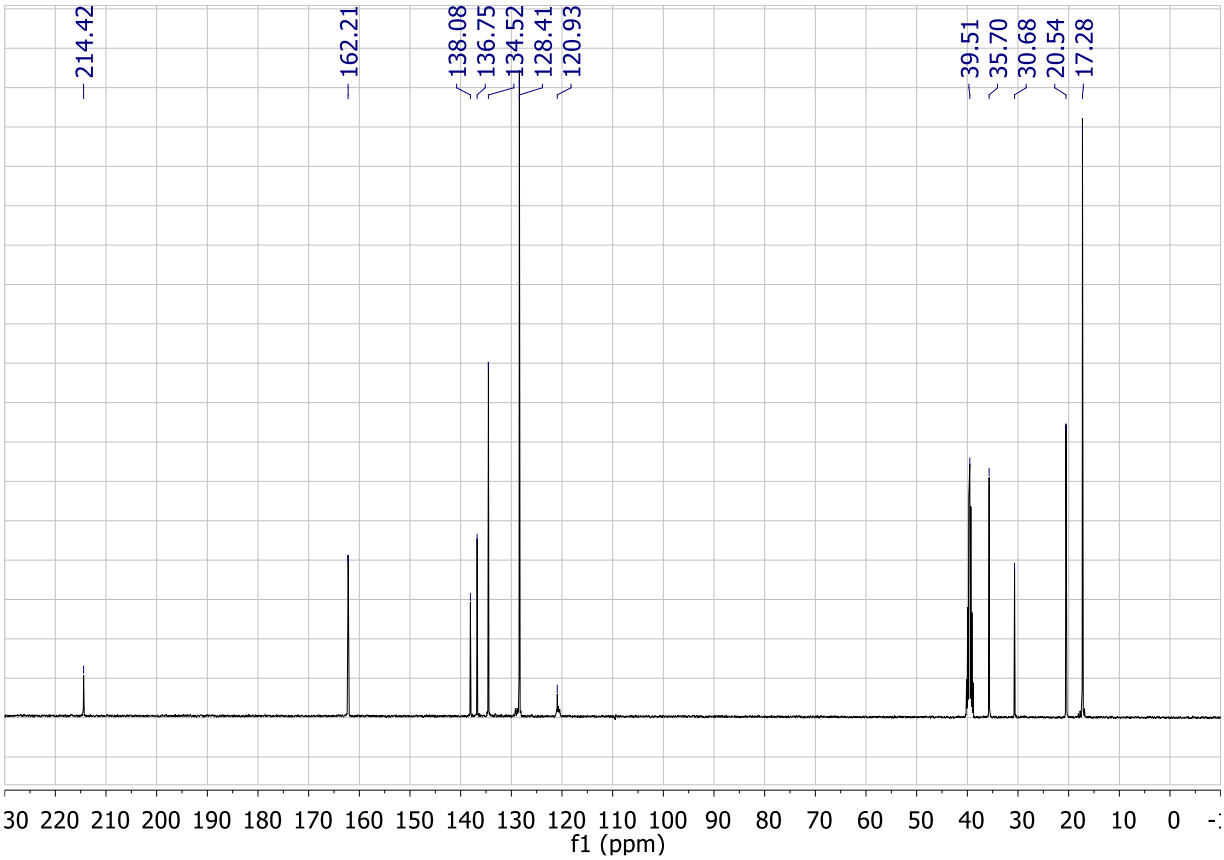
IMes (30 mg) in DMSO-d_6 (0.4 mL) Under Paraffin Oil (0.3 mL) (DMF Standard) After 2 Days (^{13}C DMSO-d_6)



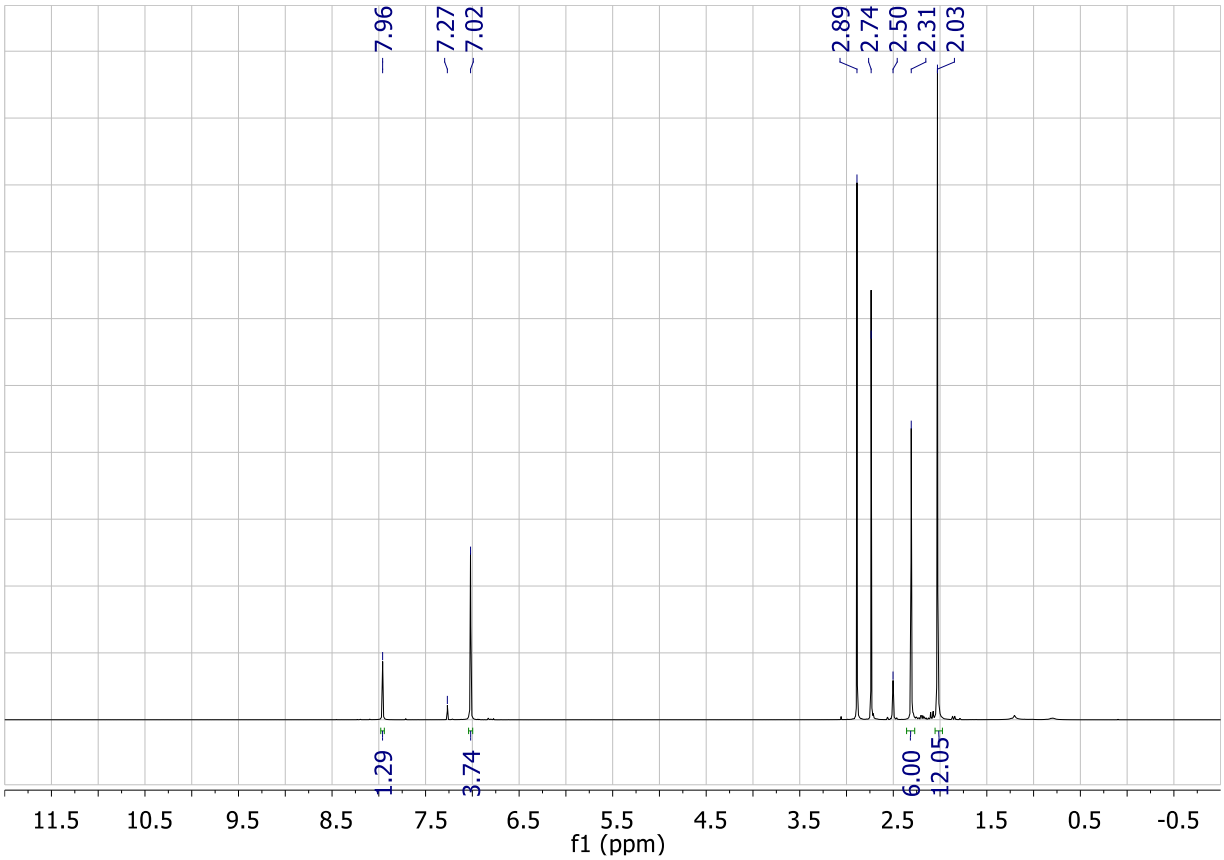
IMes (30 mg) in DMSO-d_6 (0.4 mL) Under Paraffin Oil (0.3 mL) (DMF Standard) After 5 Days (^{1}H DMSO-d_6)



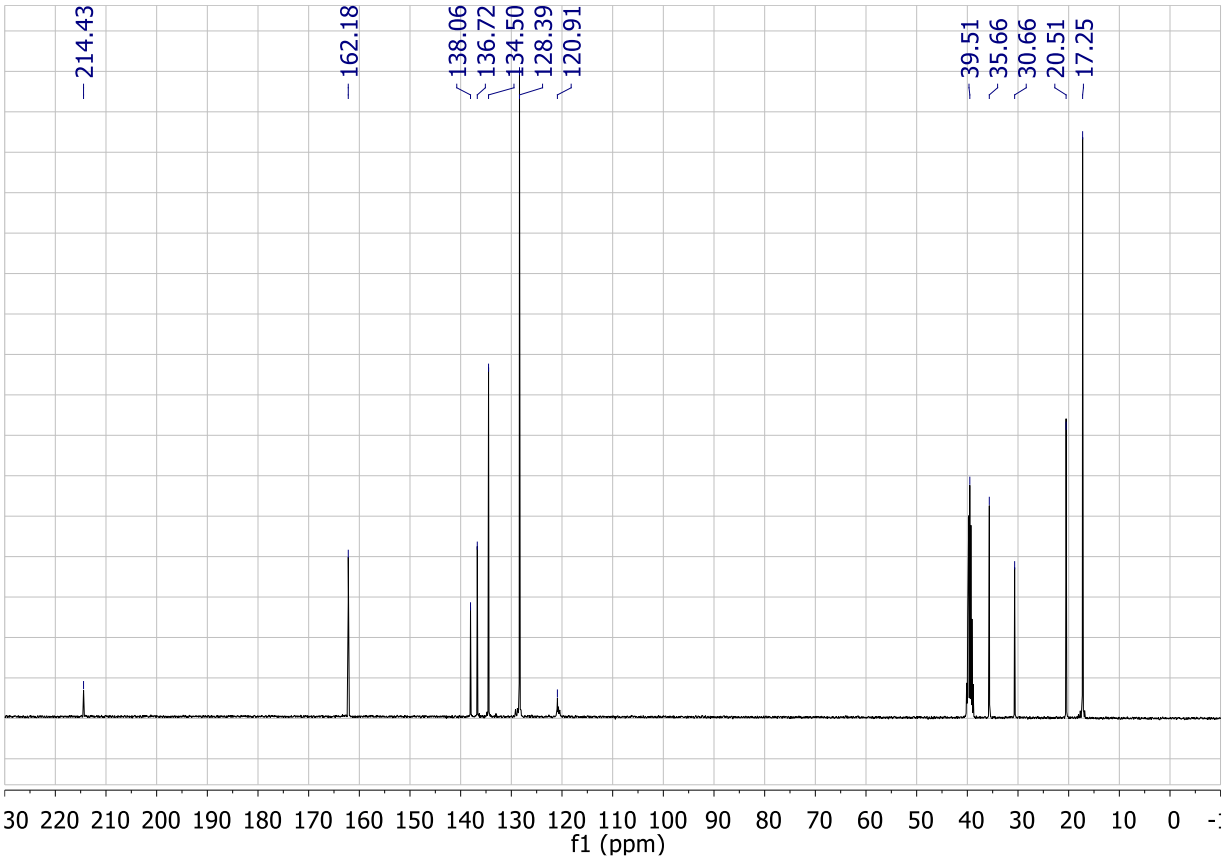
IMes (30 mg) in DMSO-d_6 (0.4 mL) Under Paraffin Oil (0.3 mL) (DMF Standard) After 5 Days (^{13}C DMSO-d_6)



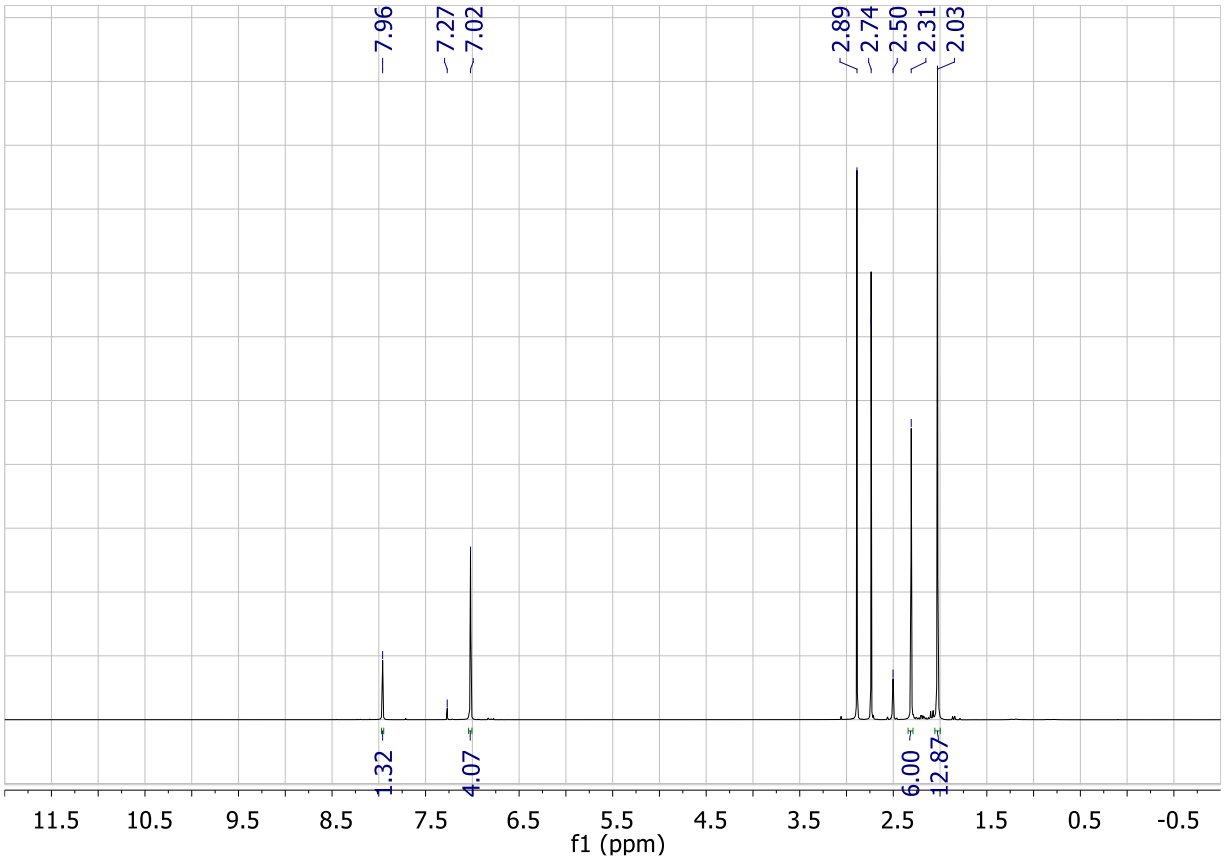
IMes (30 mg) in DMSO-d_6 (0.4 mL) Under Paraffin Oil (0.3 mL) (DMF Standard) After 8 Days (^{1}H DMSO-d_6)



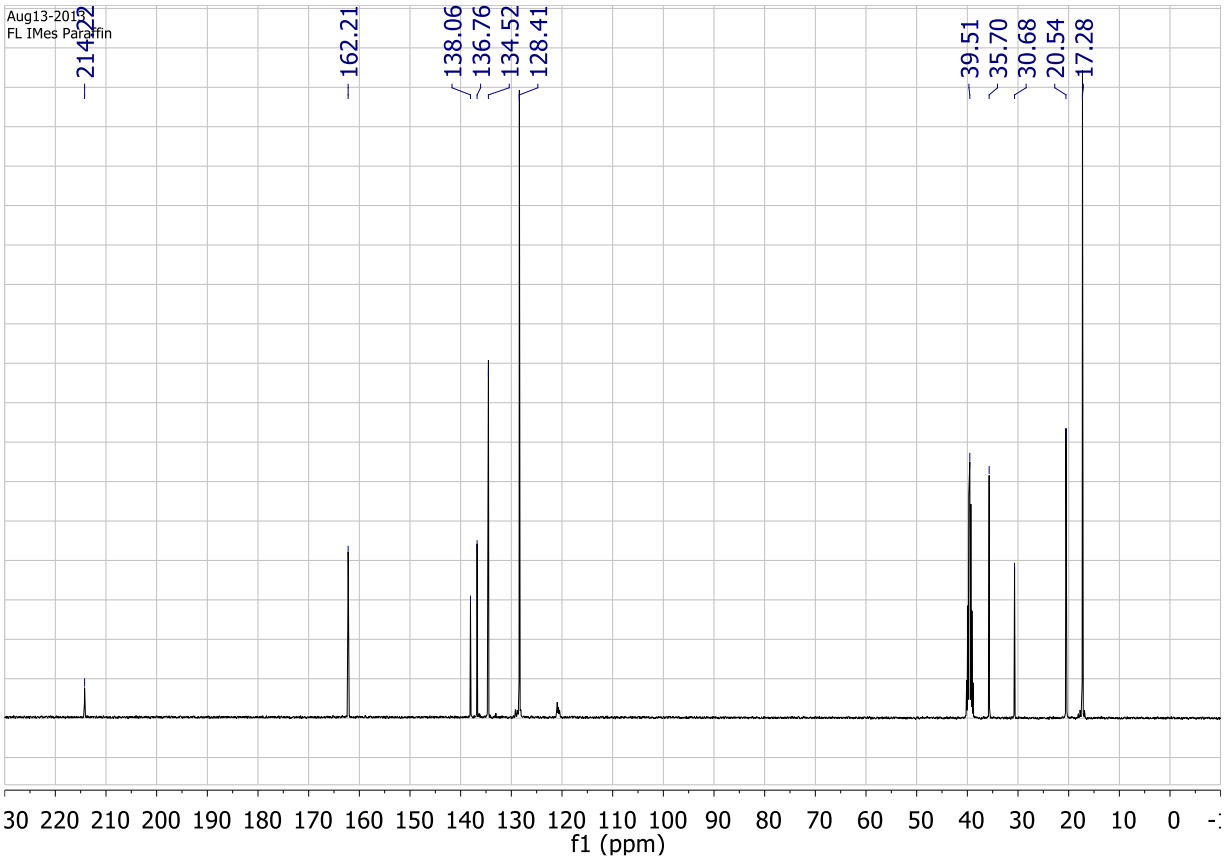
IMes (30 mg) in DMSO-d_6 (0.4 mL) Under Paraffin Oil (0.3 mL) (DMF Standard) After 8 Days (^{13}C DMSO-d_6)



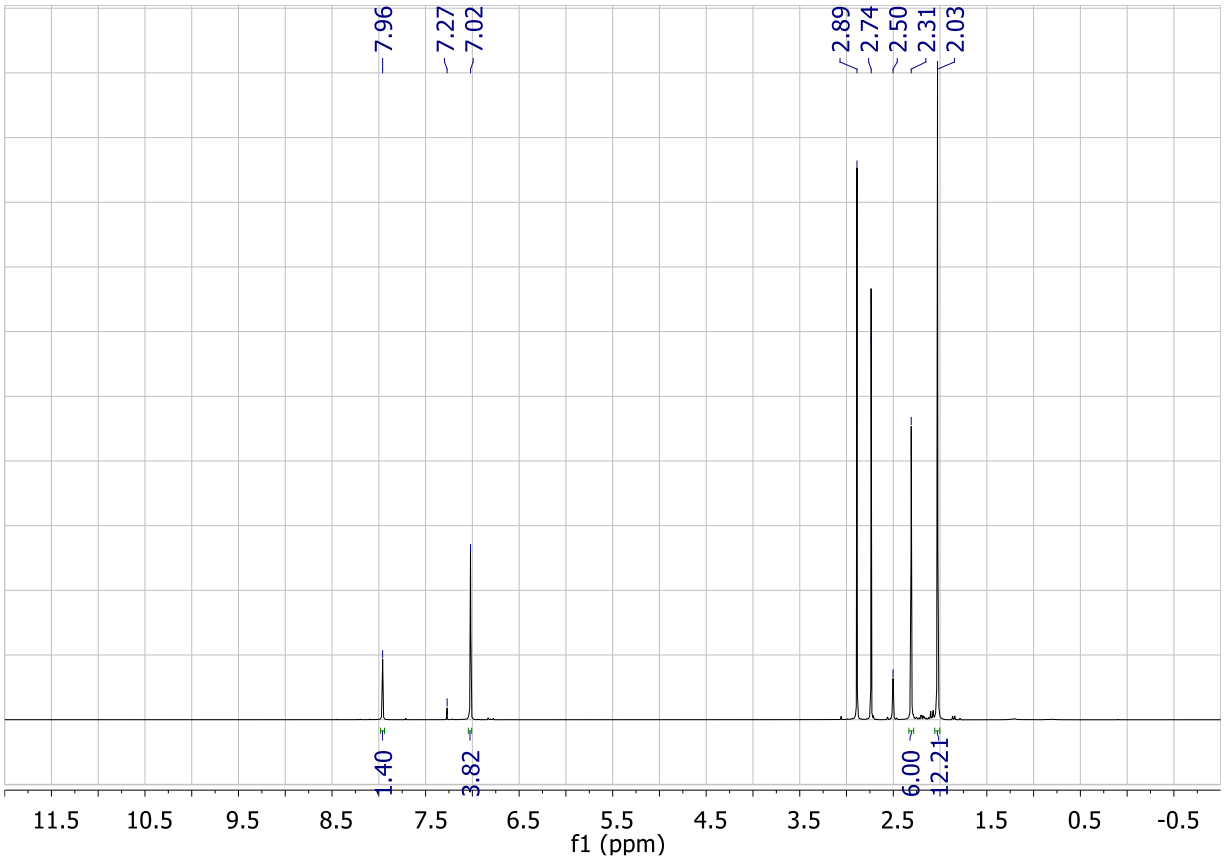
IMes (30 mg) in DMSO-d_6 (0.4 mL) Under Paraffin Oil (0.3 mL) (DMF Standard) After 13 Days (^{1}H DMSO-d_6)



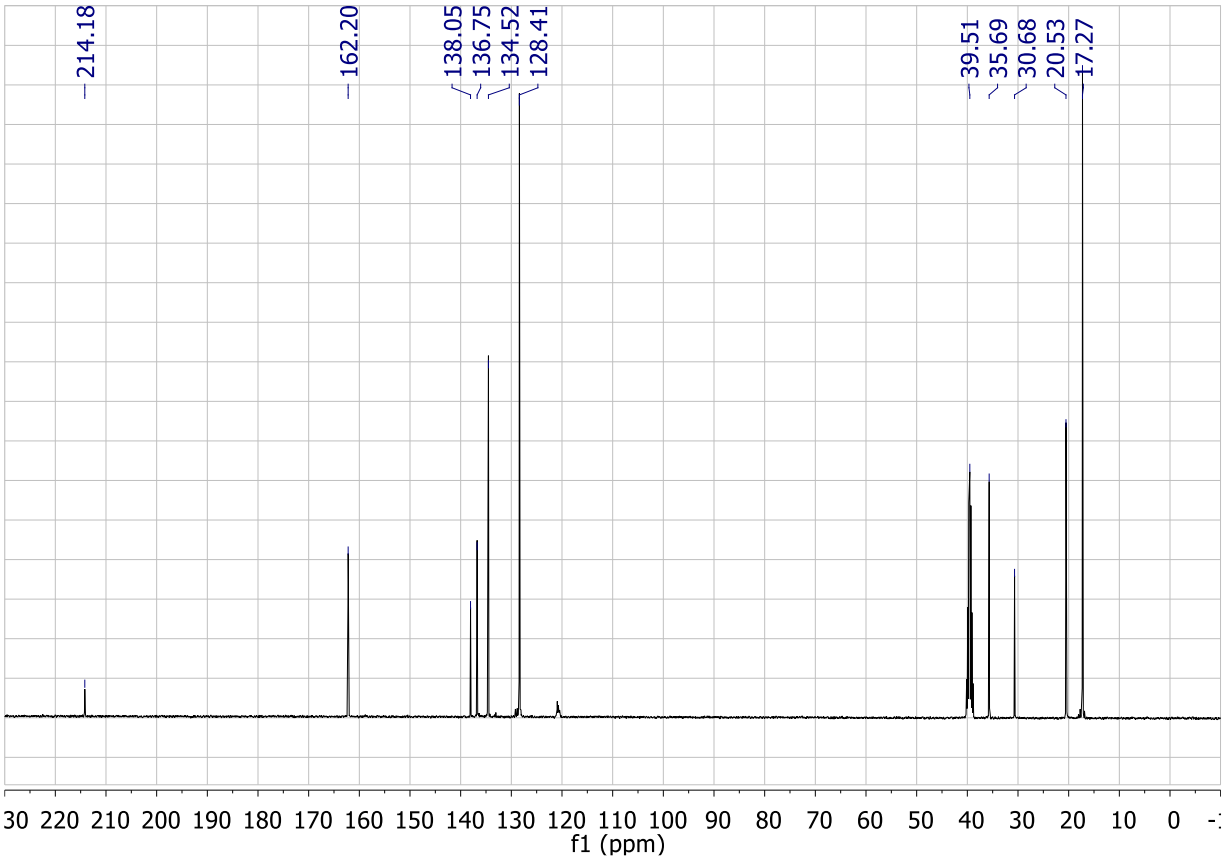
IMes (30 mg) in DMSO-d_6 (0.4 mL) Under Paraffin Oil (0.3 mL) (DMF Standard) After 13 Days (^{13}C DMSO-d_6)



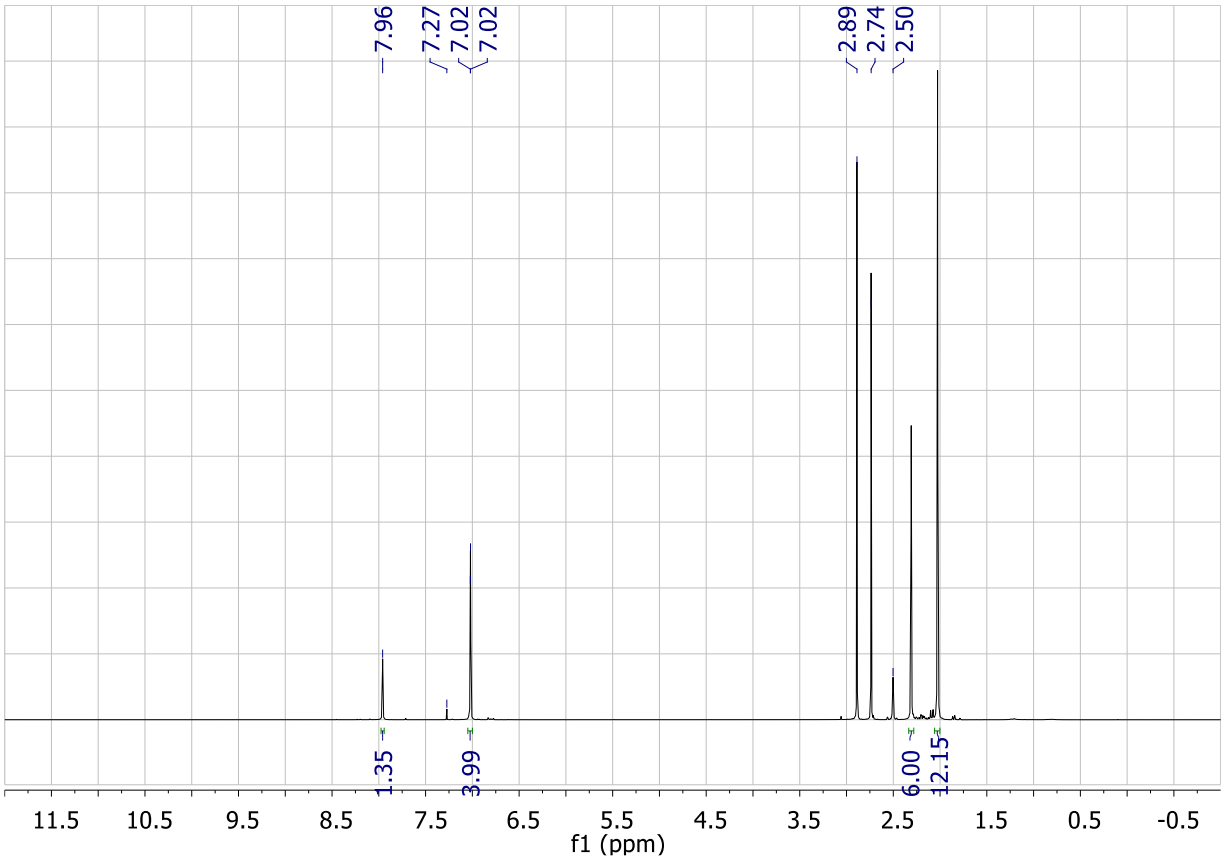
IMes (30 mg) in DMSO-d_6 (0.4 mL) Under Paraffin Oil (0.3 mL) (DMF Standard) After 14 Days (^{1}H DMSO-d_6)



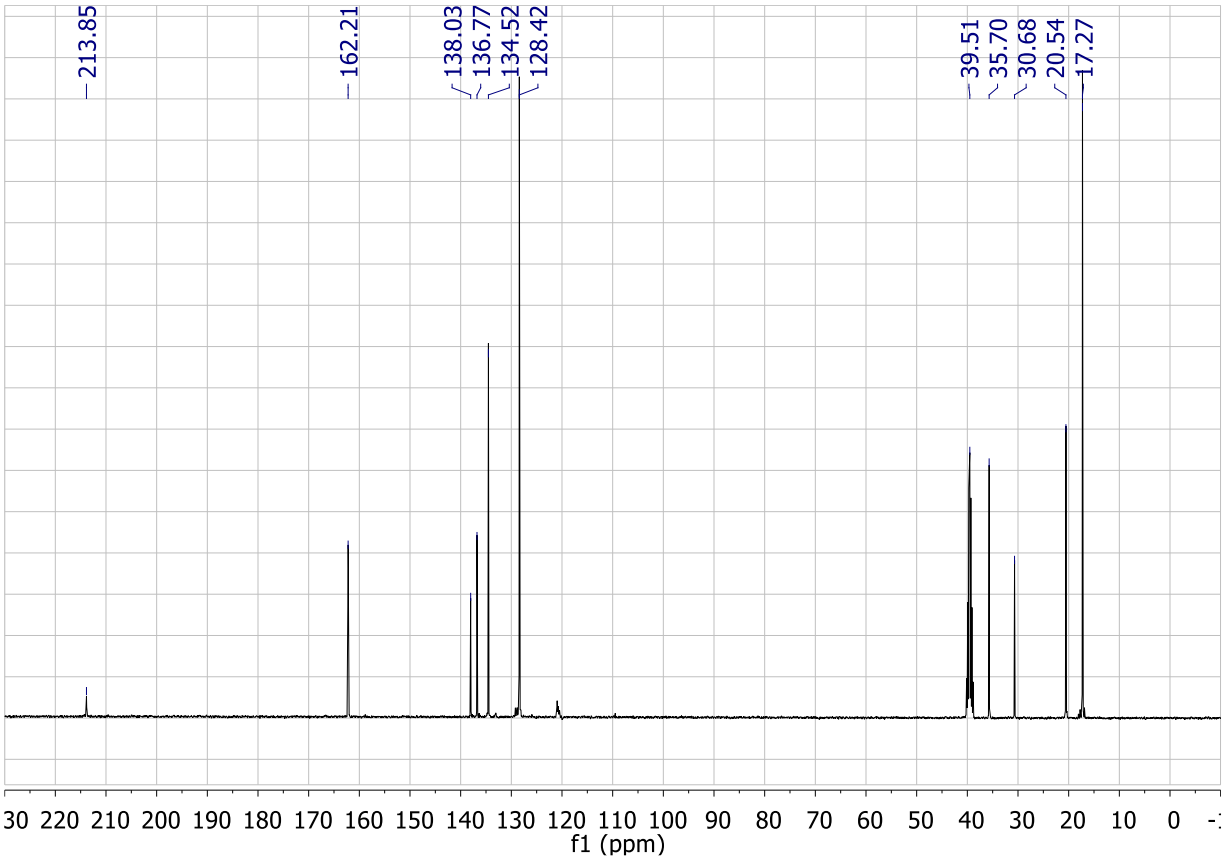
IMes (30 mg) in DMSO-d_6 (0.4 mL) Under Paraffin Oil (0.3 mL) (DMF Standard) After 14 Days (^{13}C DMSO-d_6)



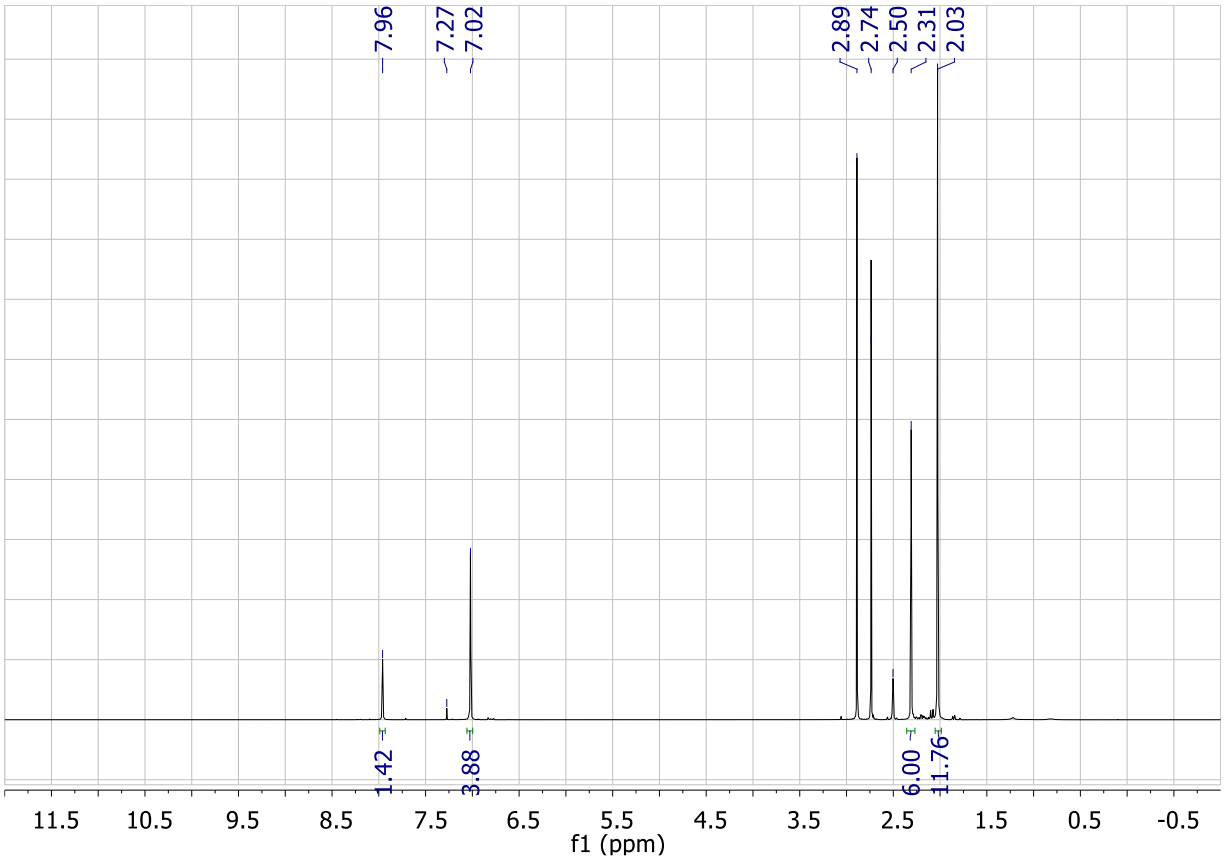
IMes (30 mg) in DMSO-d_6 (0.4 mL) Under Paraffin Oil (0.3 mL) (DMF Standard) After 20 Days (^{1}H DMSO-d_6)



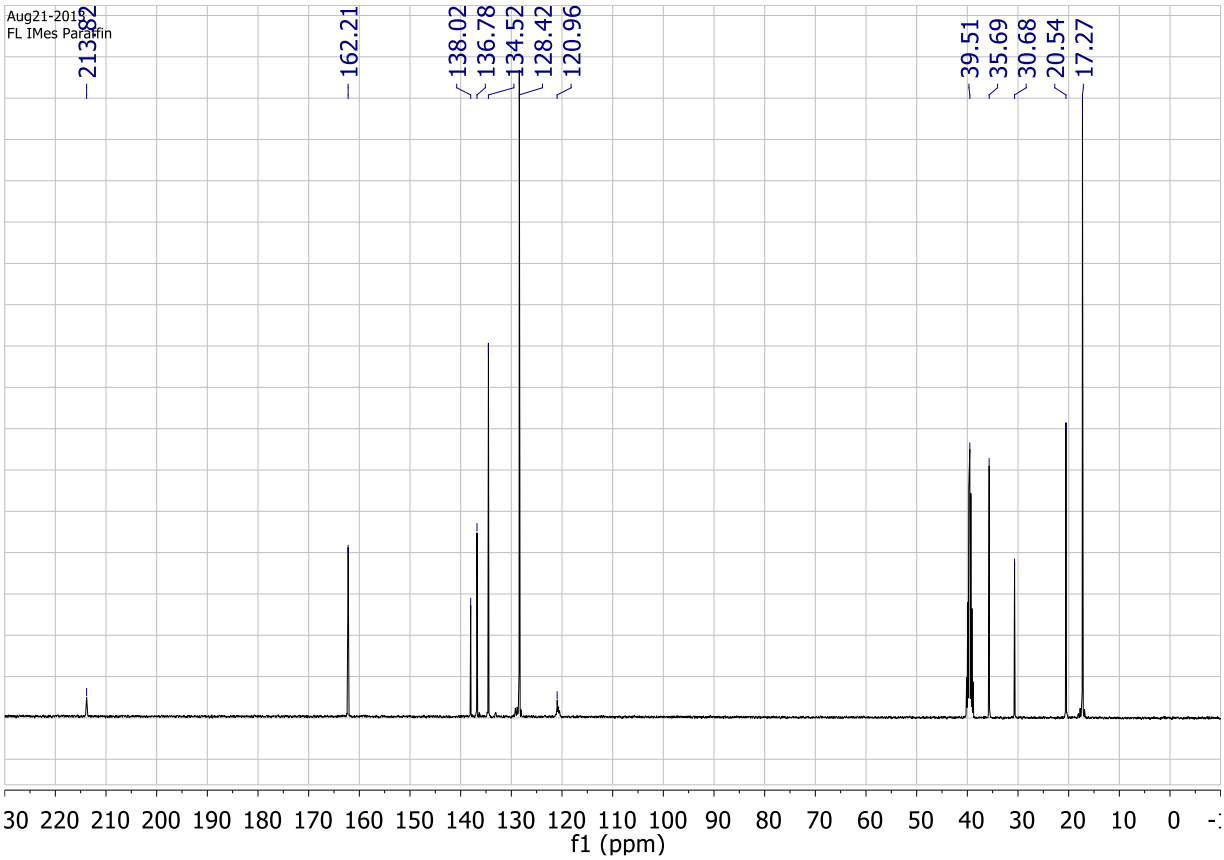
IMes (30 mg) in DMSO-d_6 (0.4 mL) Under Paraffin Oil (0.3 mL) (DMF Standard) After 20 Days (^{13}C DMSO-d_6)



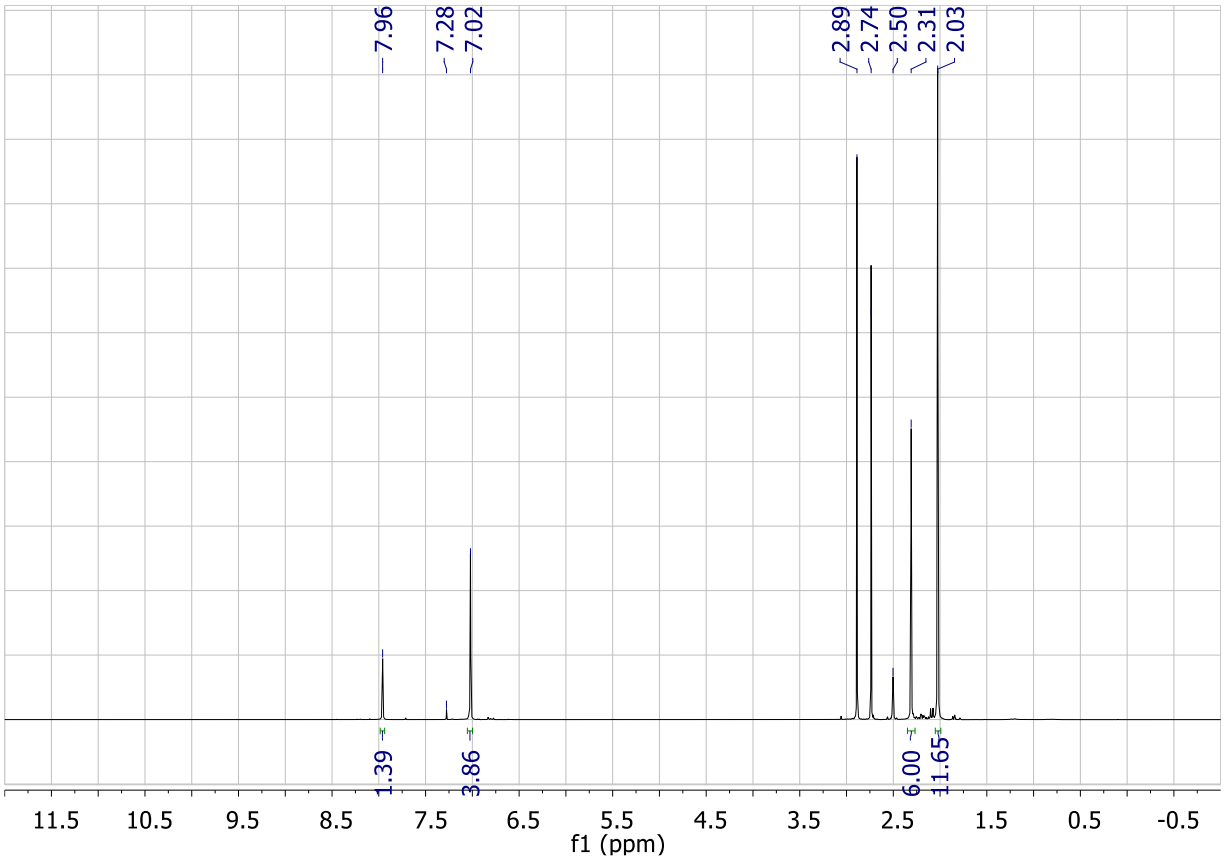
IMes (30 mg) in DMSO-d_6 (0.4 mL) Under Paraffin Oil (0.3 mL) (DMF Standard) After 21 Days (^{1}H DMSO-d_6)



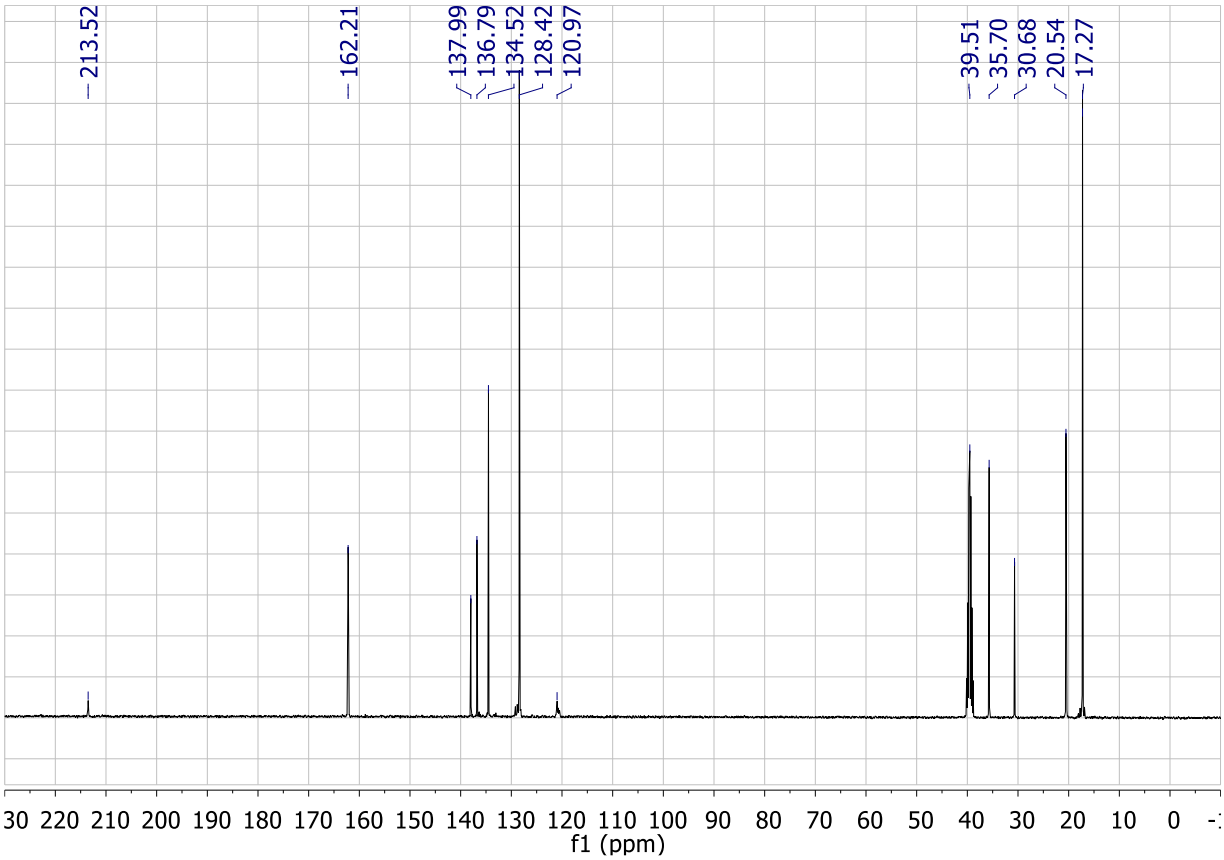
IMes (30 mg) in DMSO-d_6 (0.4 mL) Under Paraffin Oil (0.3 mL) (DMF Standard) After 21 Days (^{13}C DMSO-d_6)



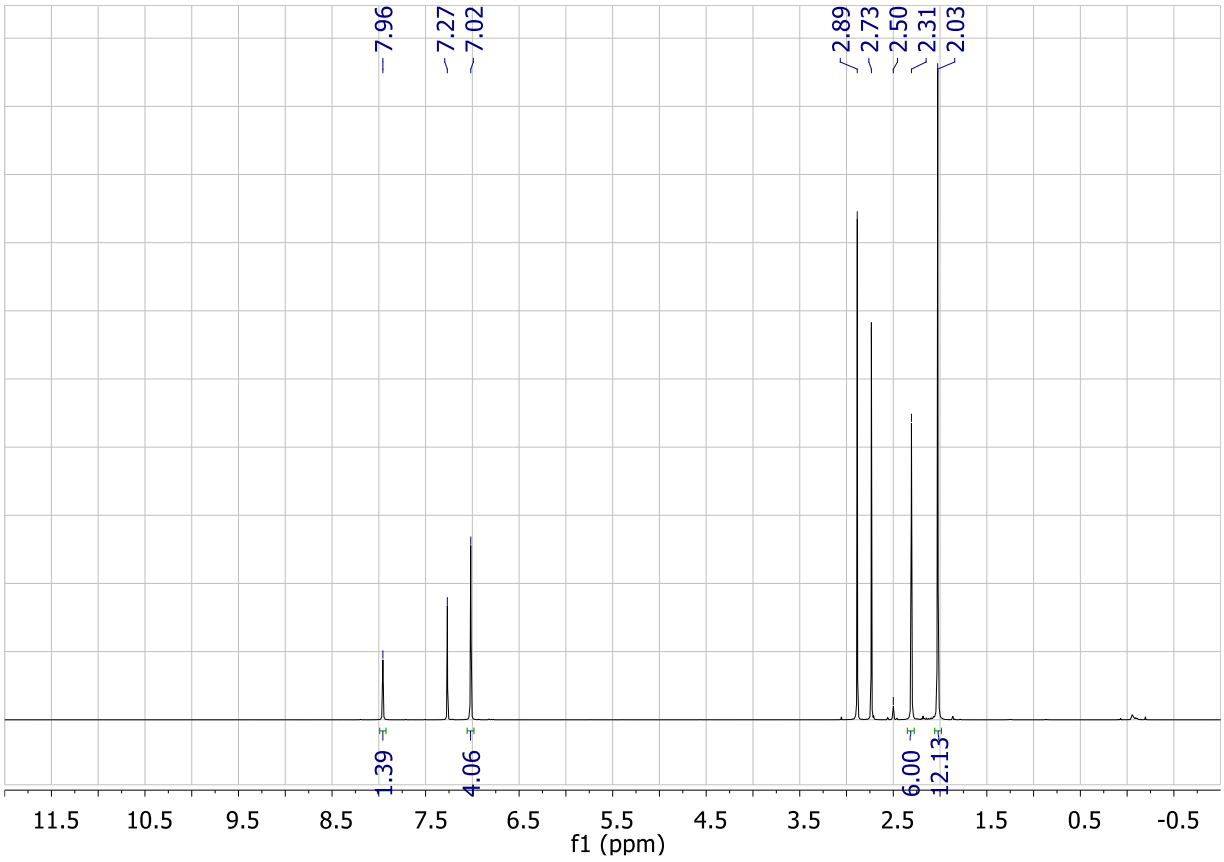
IMes (30 mg) in DMSO-d_6 (0.4 mL) Under Paraffin Oil (0.3 mL) (DMF Standard) After 27 Days (^{1}H DMSO-d_6)



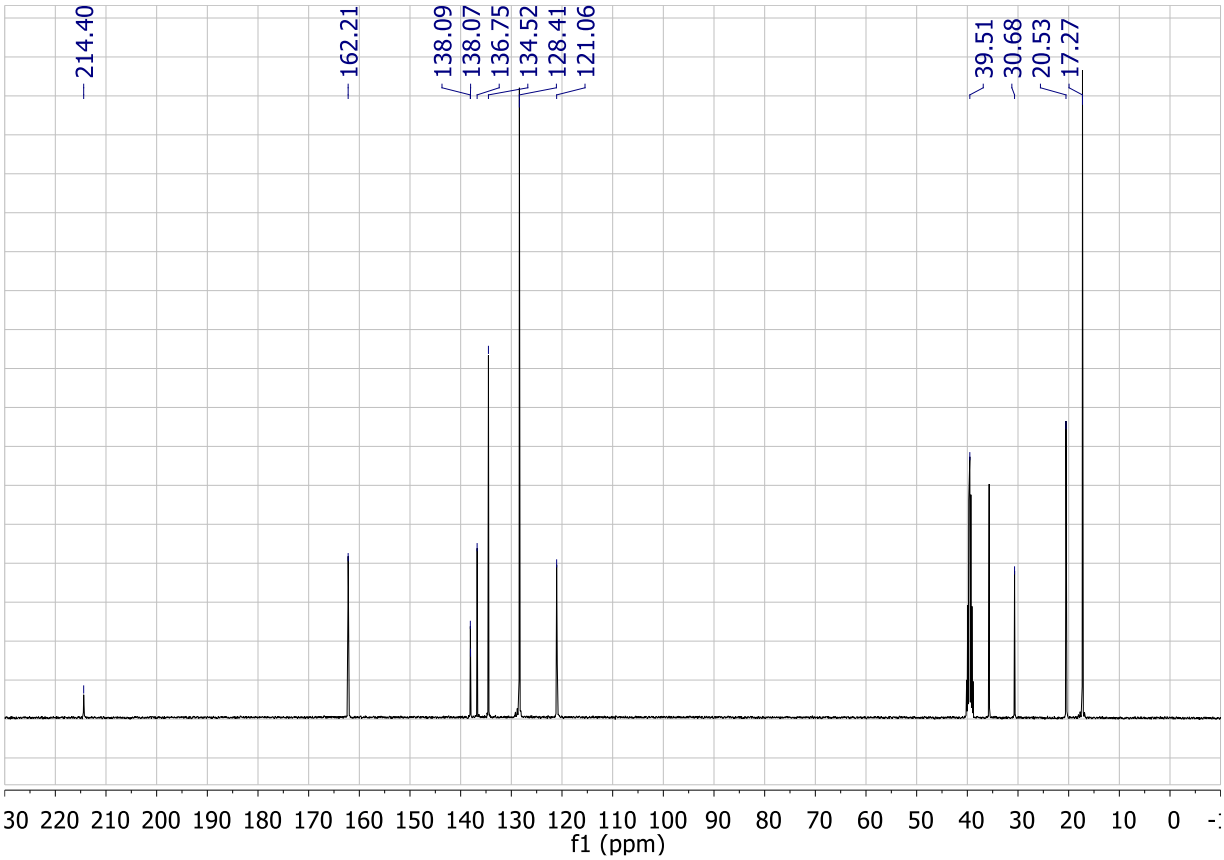
IMes (30 mg) in DMSO-d_6 (0.4 mL) Under Paraffin Oil (0.3 mL) (DMF Standard) After 27 Days (^{13}C DMSO-d_6)



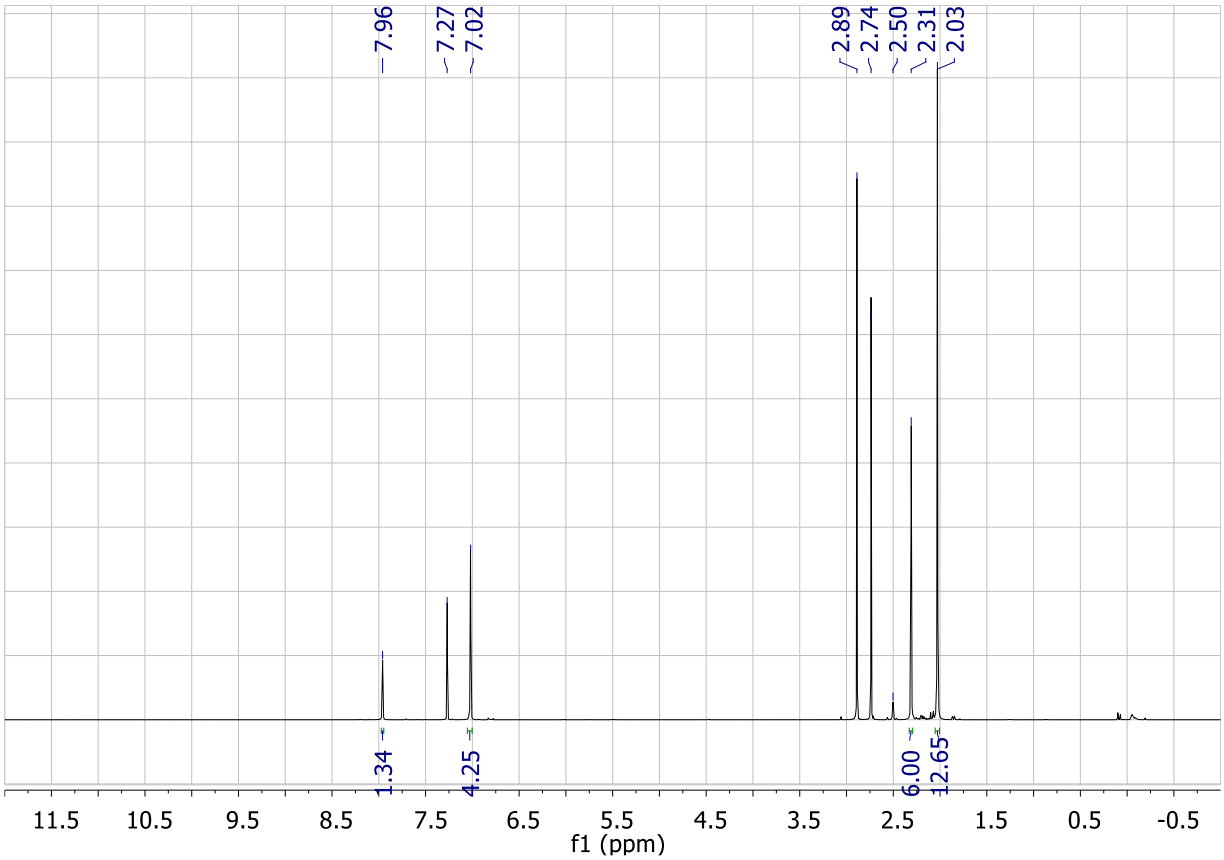
IMes (30 mg) in DMSO-d_6 (0.4 mL) Under PDMS (770 g·mol^{-1}, 0.3 mL) (DMF Standard) at Time 0 (^{1}H DMSO-d_6)



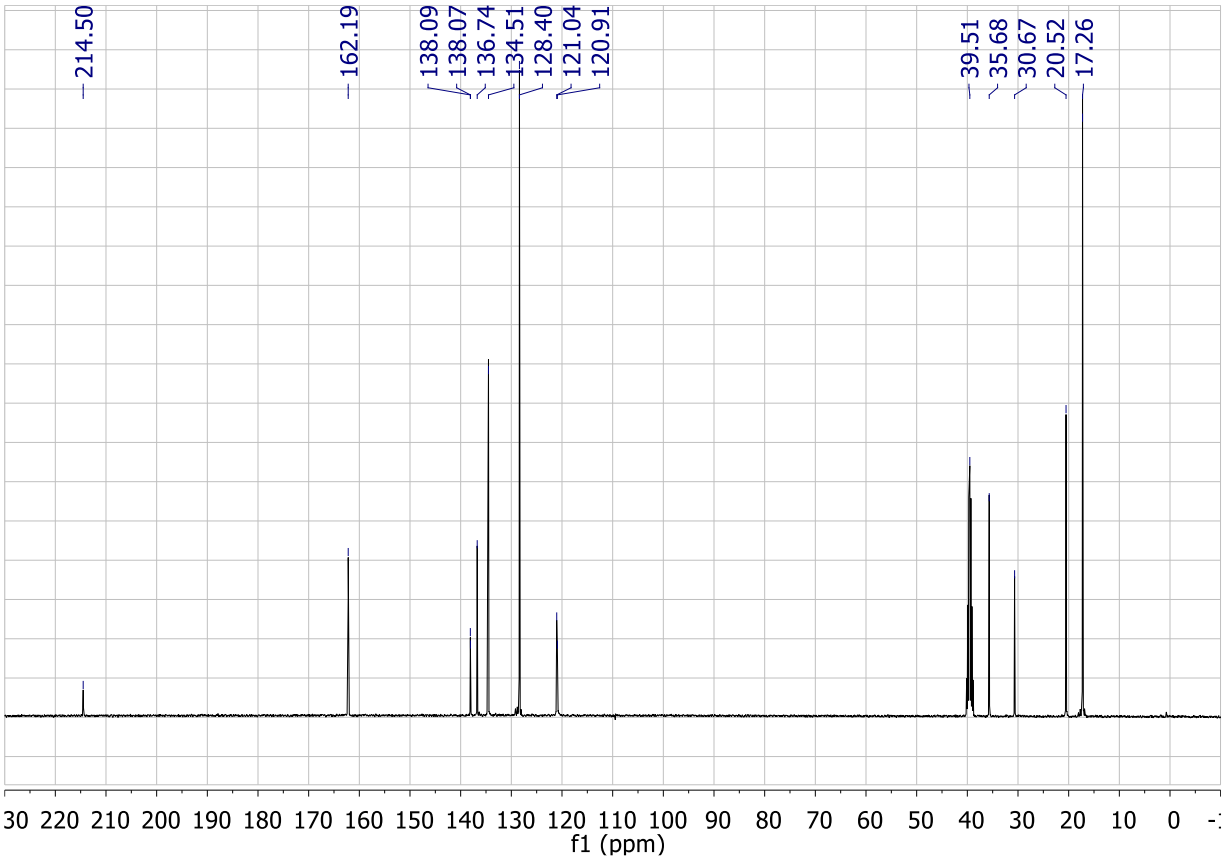
IMes (30 mg) in DMSO-d_6 (0.4 mL) Under PDMS (770 g·mol^{-1}, 0.3 mL) (DMF Standard) at Time 0 (^{13}C DMSO-d_6)



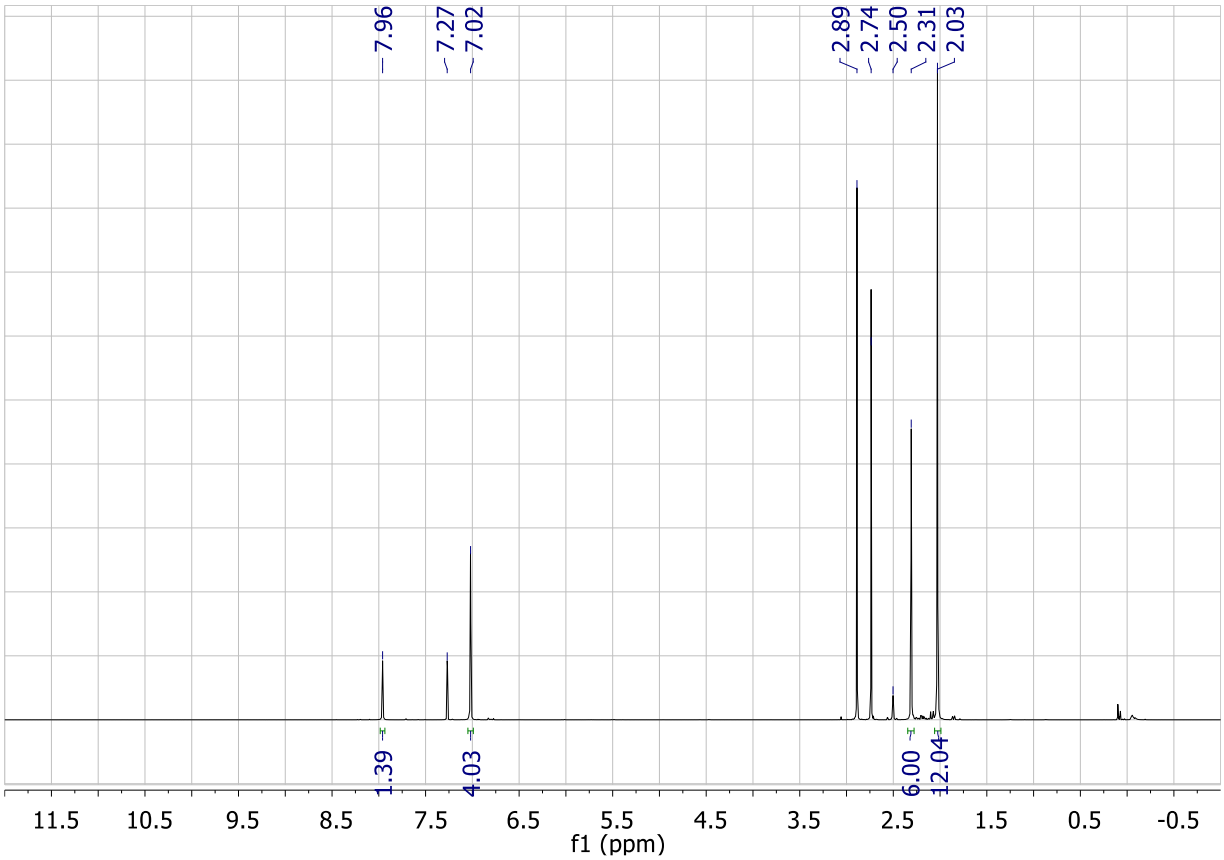
IMes (30 mg) in DMSO-d_6 (0.4 mL) Under PDMS (770 g·mol^{-1}, 0.3 mL) (DMF Standard) After 1 Day (^{1}H DMSO-d_6)



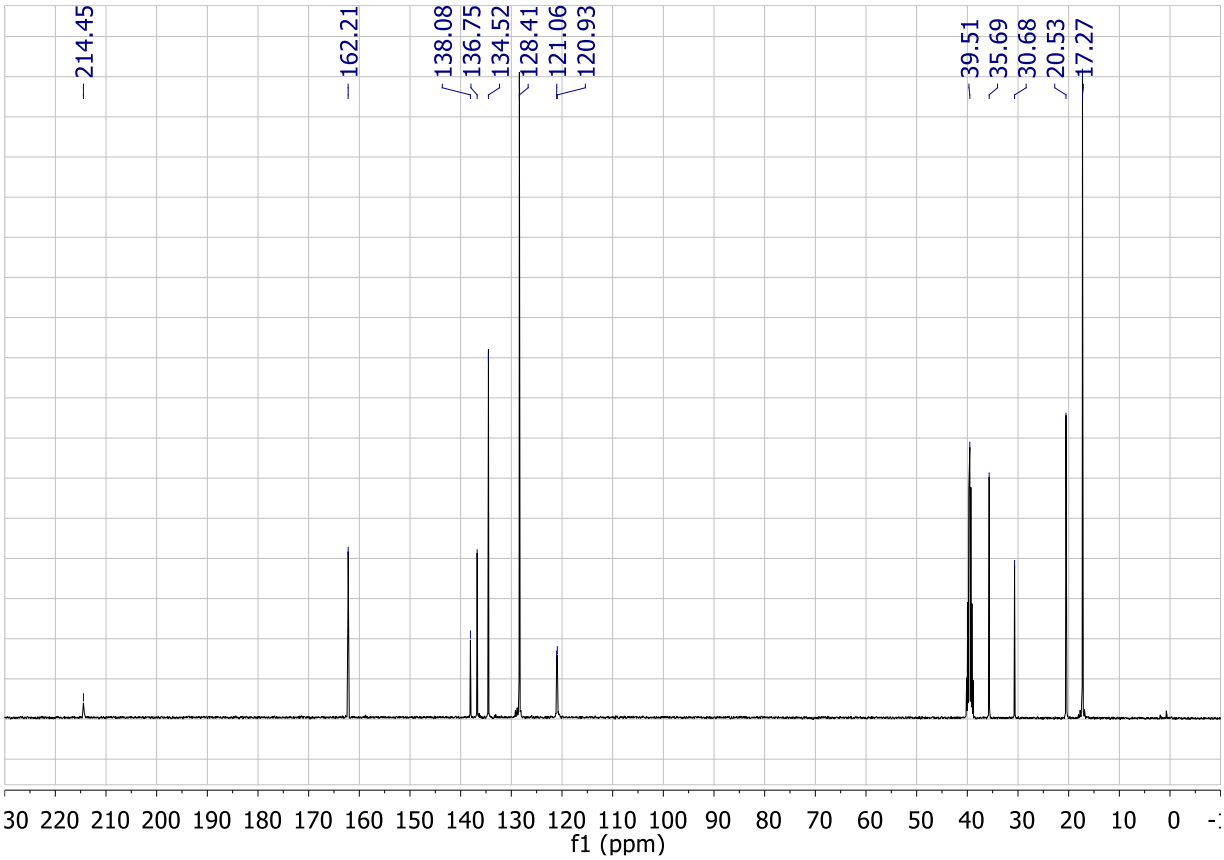
IMes (30 mg) in DMSO-d_6 (0.4 mL) Under PDMS (770 g·mol^{-1}, 0.3 mL) (DMF Standard) After 1 Day (^{13}C DMSO-d_6)



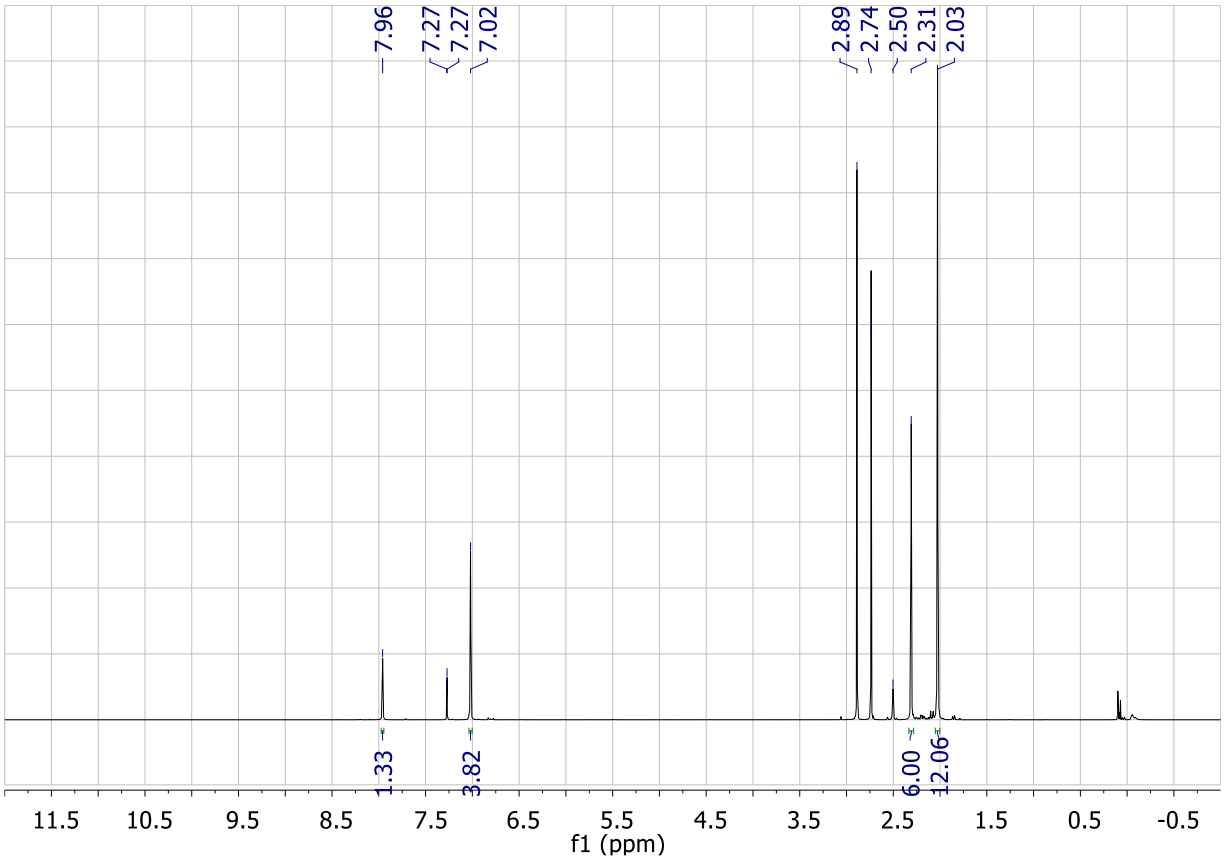
IMes (30 mg) in DMSO-d_6 (0.4 mL) Under PDMS (770 g·mol^{-1}, 0.3 mL) (DMF Standard) After 2 Day (^{1}H DMSO-d_6)



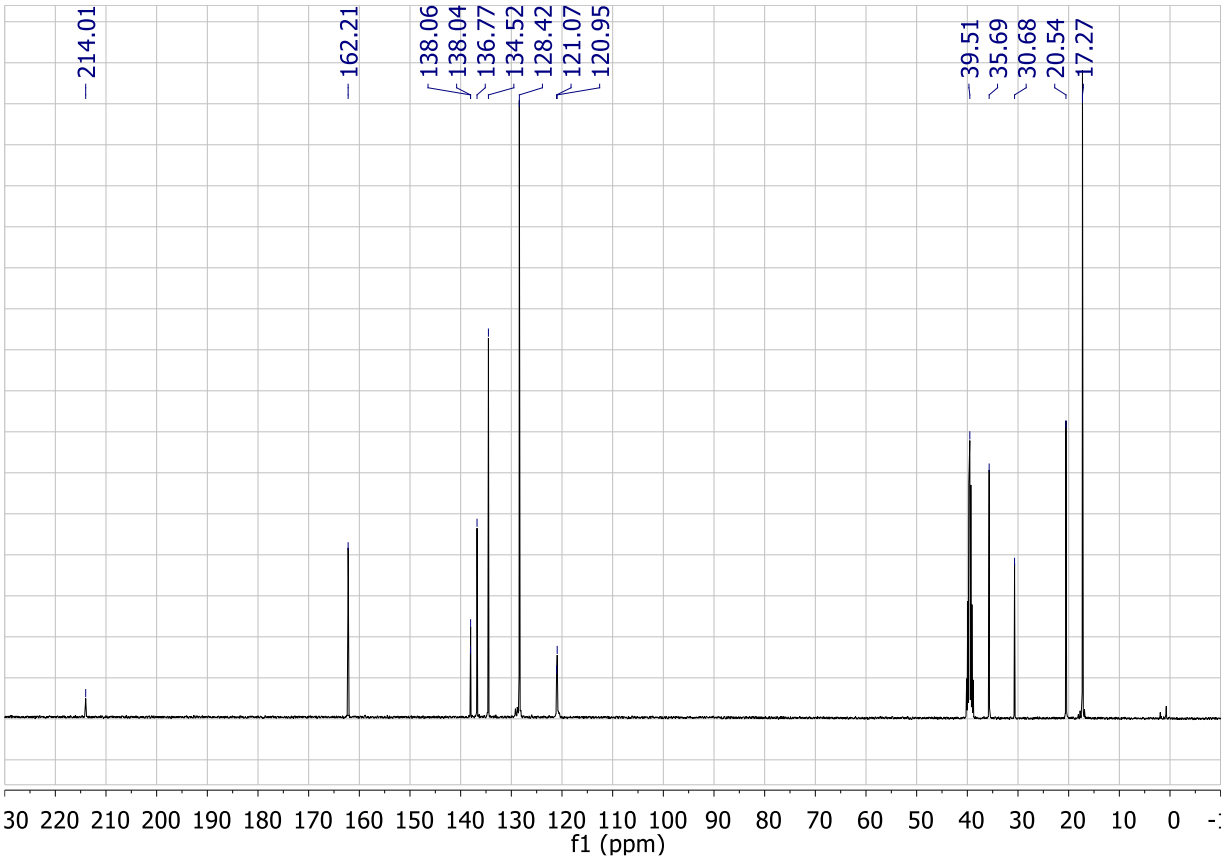
IMes (30 mg) in DMSO-d_6 (0.4 mL) Under PDMS (770 g·mol^{-1}, 0.3 mL) (DMF Standard) After 2 Days (^{13}C DMSO-d_6)



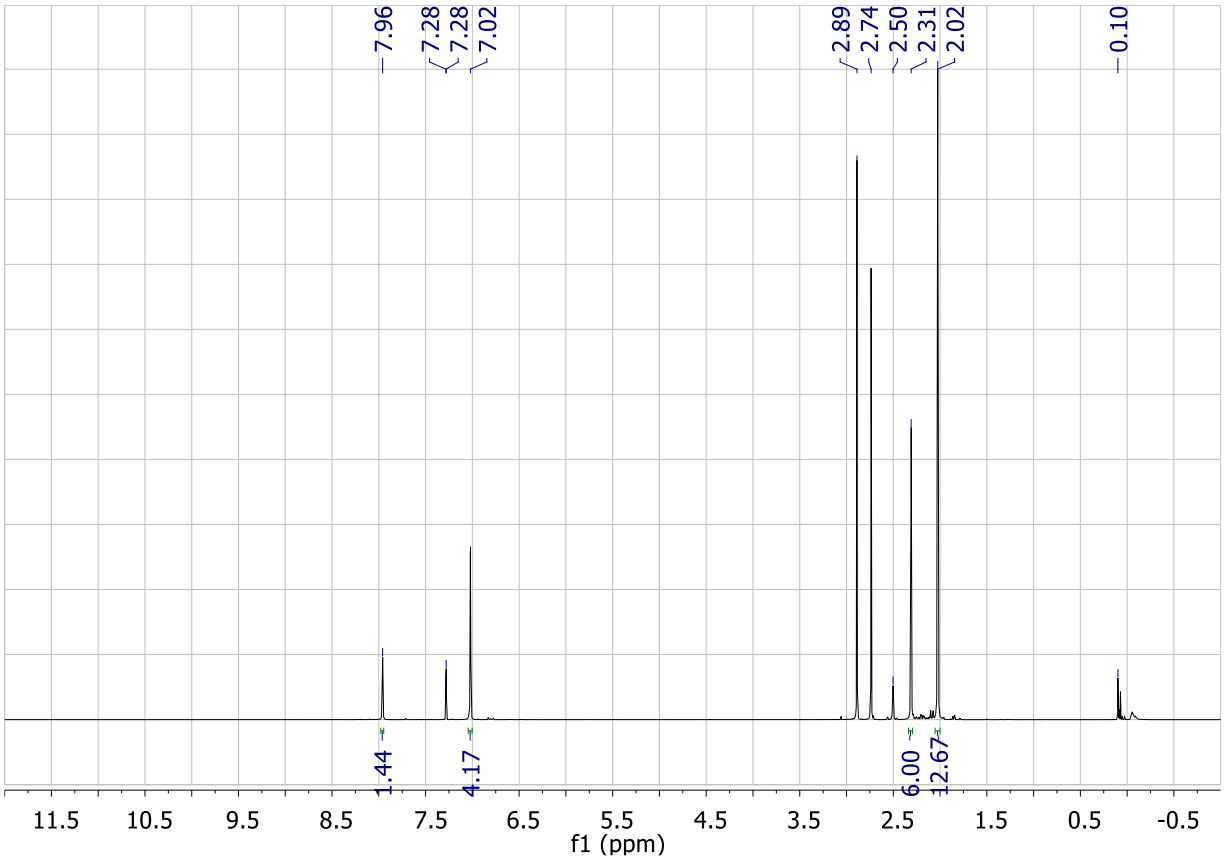
IMes (30 mg) in DMSO-d_6 (0.4 mL) Under PDMS (770 g·mol^{-1}, 0.3 mL) (DMF Standard) After 5 Days (^{1}H DMSO-d_6)



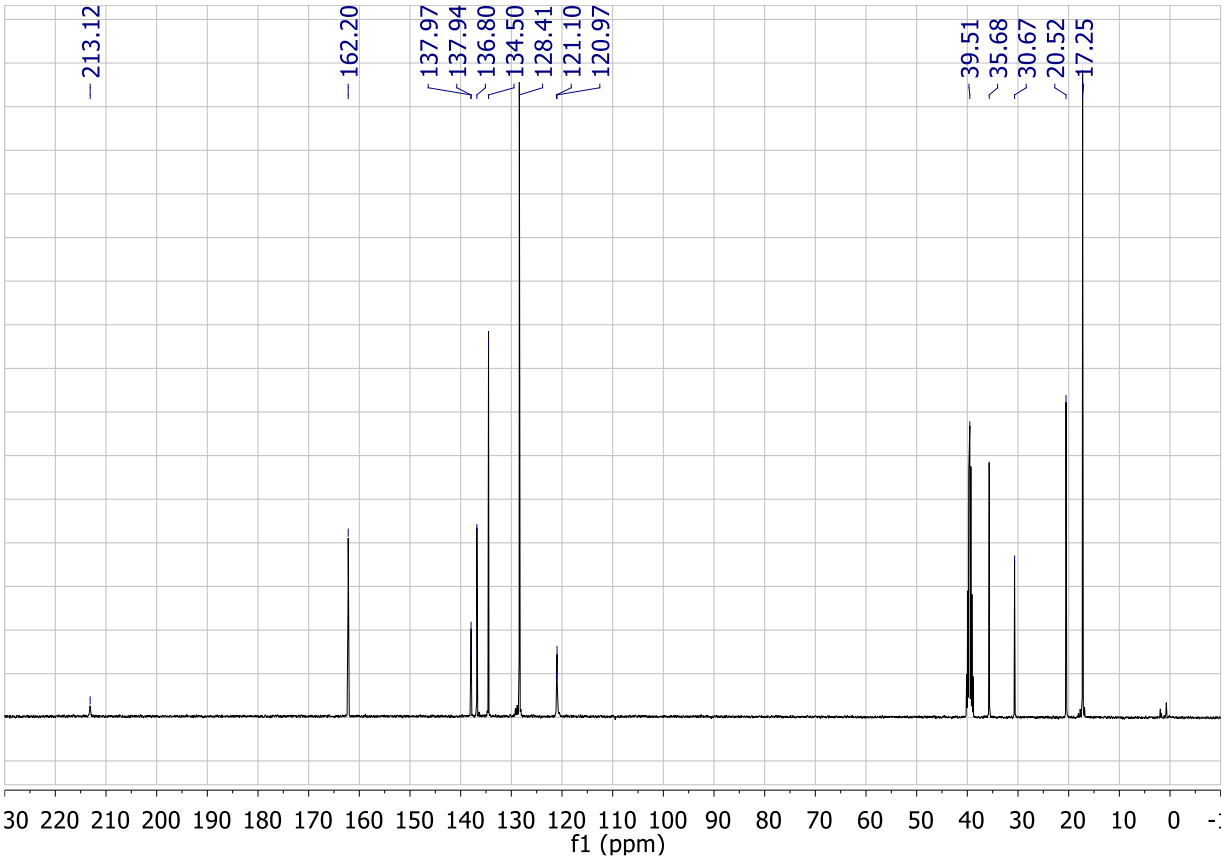
IMes (30 mg) in DMSO-d_6 (0.4 mL) Under PDMS (770 g·mol^{-1}, 0.3 mL) (DMF Standard) After 5 Days (^{13}C DMSO-d_6)



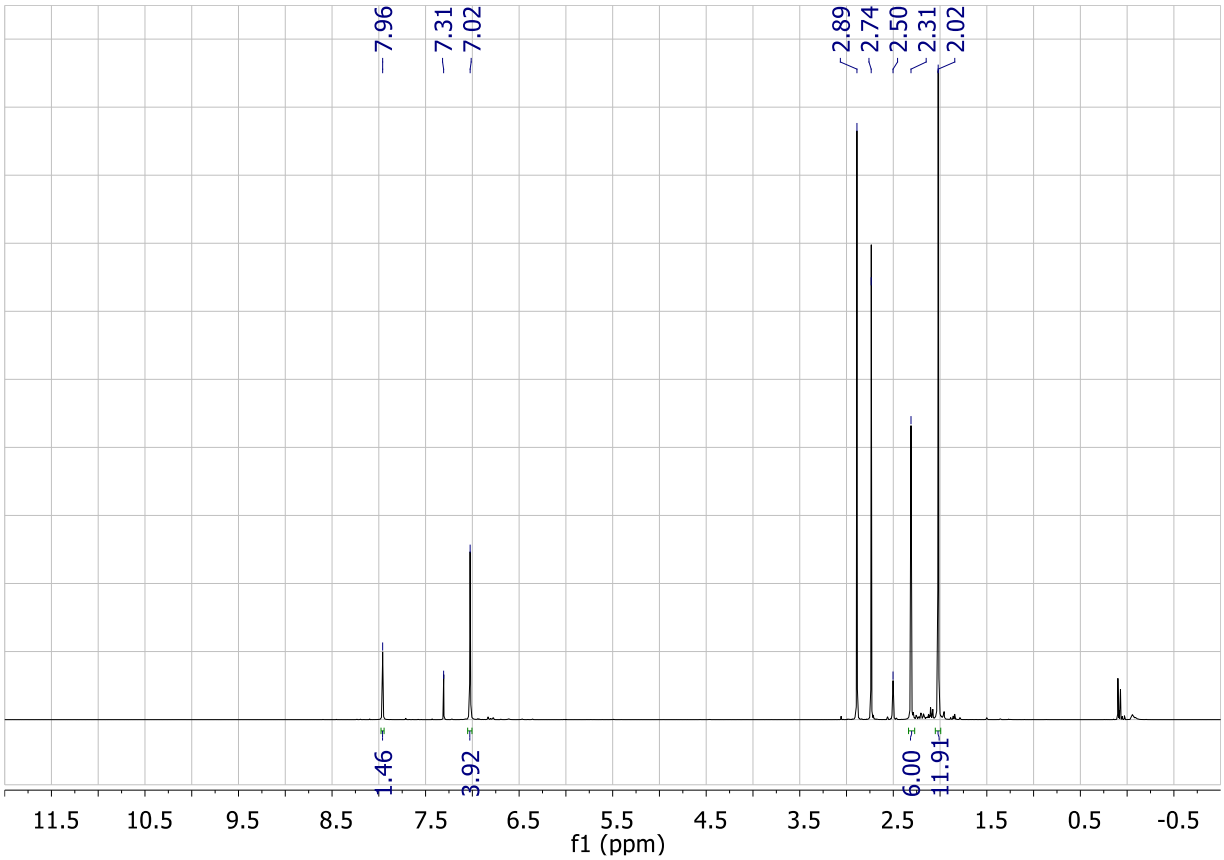
IMes (30 mg) in DMSO-d_6 (0.4 mL) Under PDMS (770 g·mol^{-1}, 0.3 mL) (DMF Standard) After 8 Days (^{1}H DMSO-d_6)



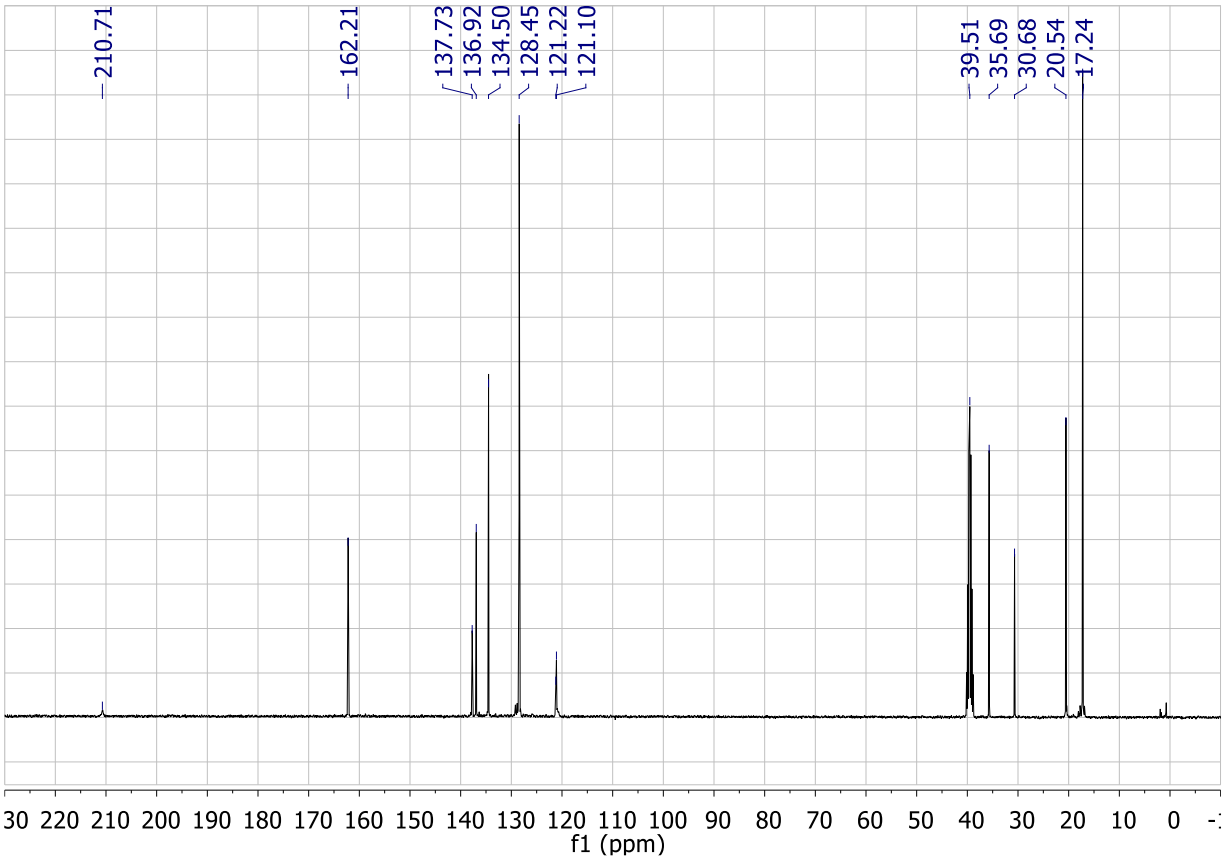
IMes (30 mg) in DMSO-d_6 (0.4 mL) Under PDMS (770 g·mol^{-1}, 0.3 mL) (DMF Standard) After 8 Days (^{13}C DMSO-d_6)



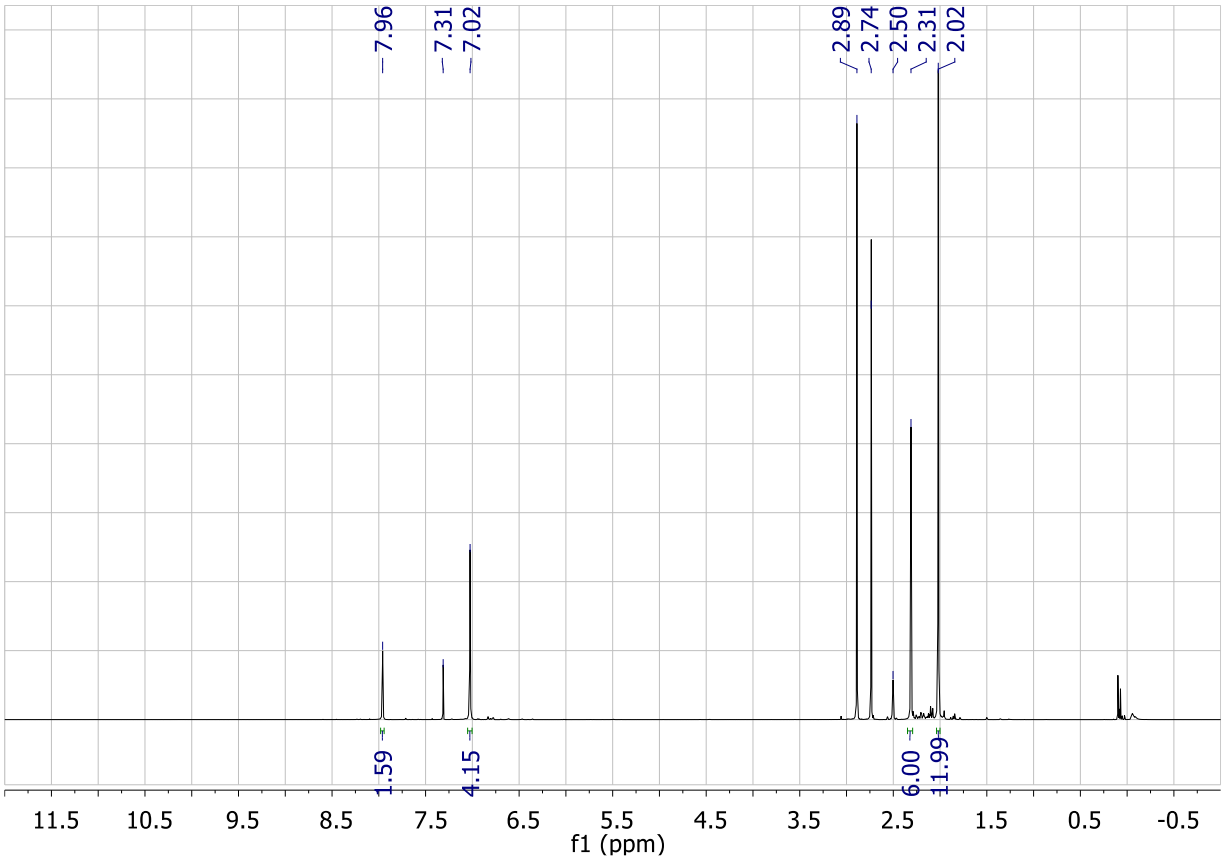
IMes (30 mg) in DMSO-d_6 (0.4 mL) Under PDMS (770 g·mol^{-1}, 0.3 mL) (DMF Standard) After 13 Days (^{1}H DMSO-d_6)



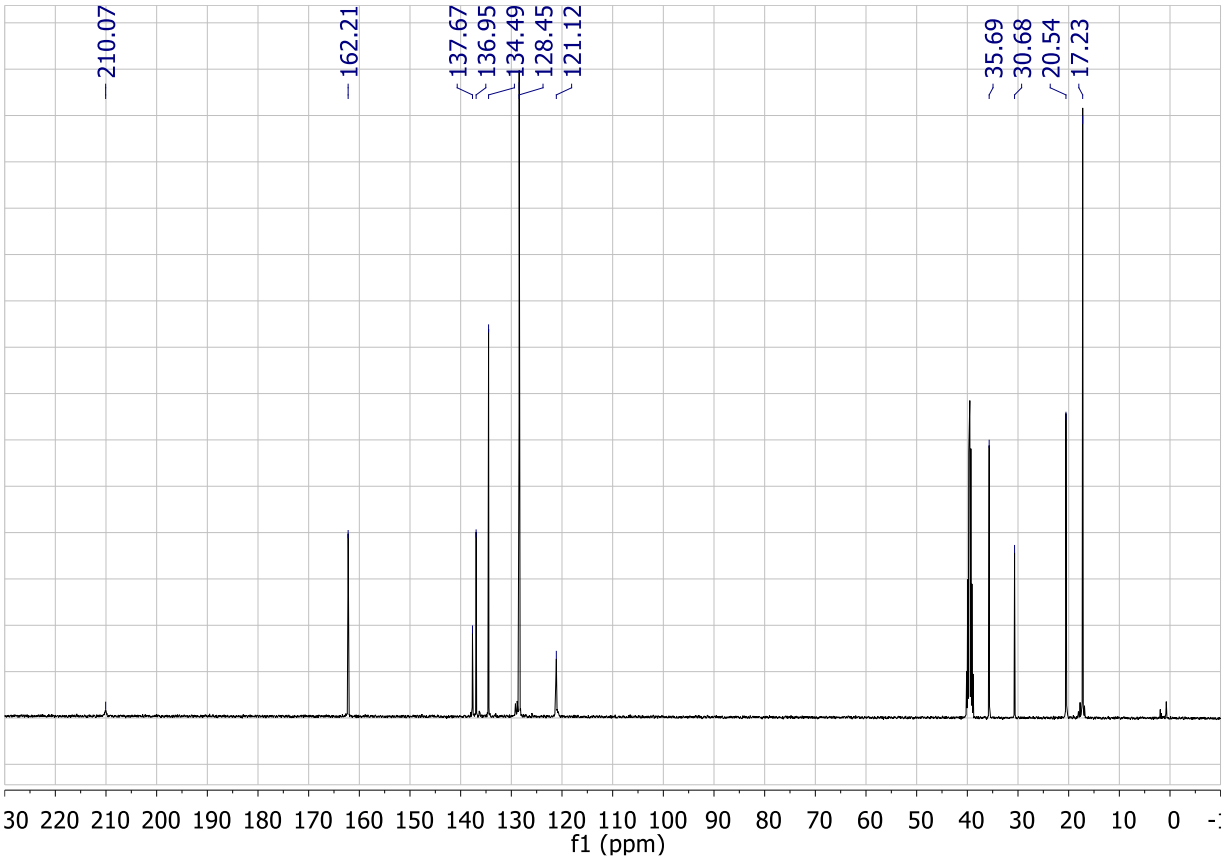
IMes (30 mg) in DMSO-d_6 (0.4 mL) Under PDMS (770 g·mol^{-1}, 0.3 mL) (DMF Standard) After 13 Days (^{13}C DMSO-d_6)



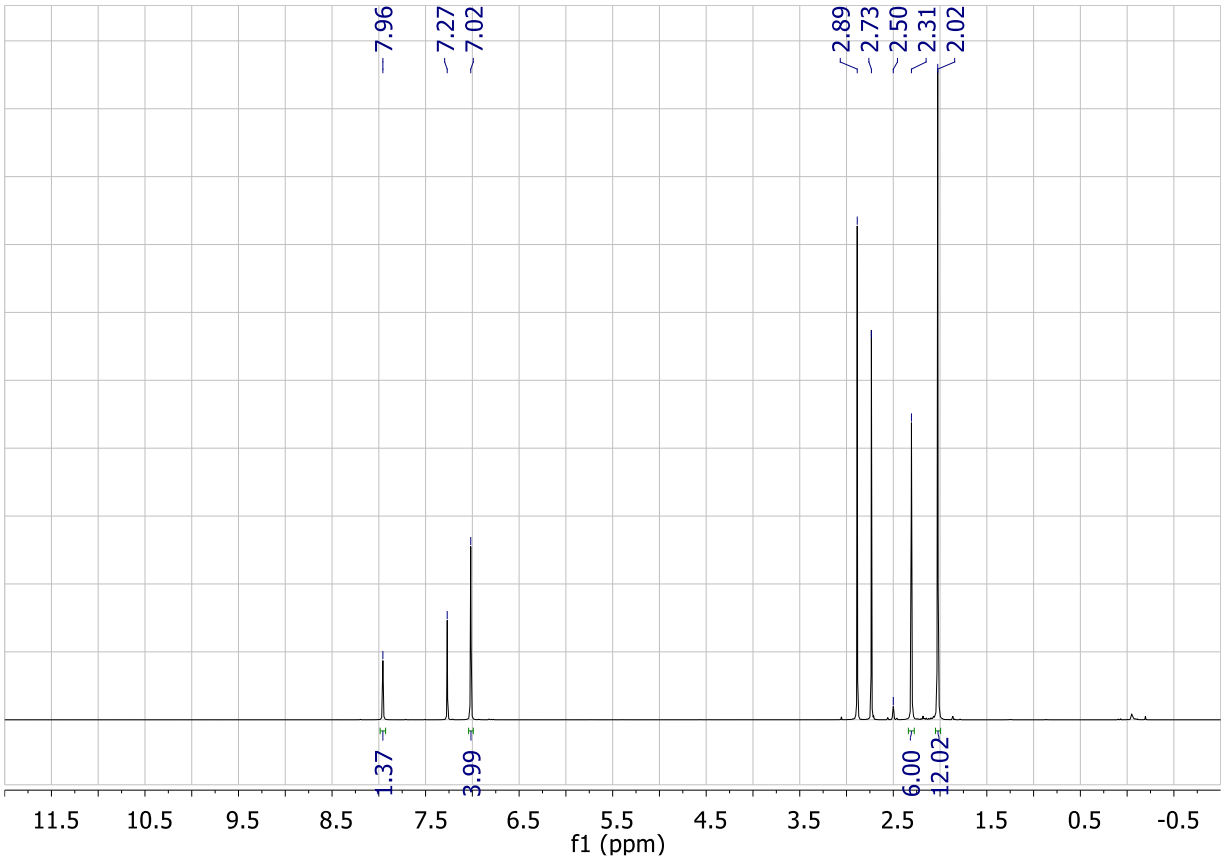
IMes (30 mg) in DMSO-d_6 (0.4 mL) Under PDMS (770 g·mol^{-1}, 0.3 mL) (DMF Standard) After 14 Days (^{1}H DMSO-d_6)



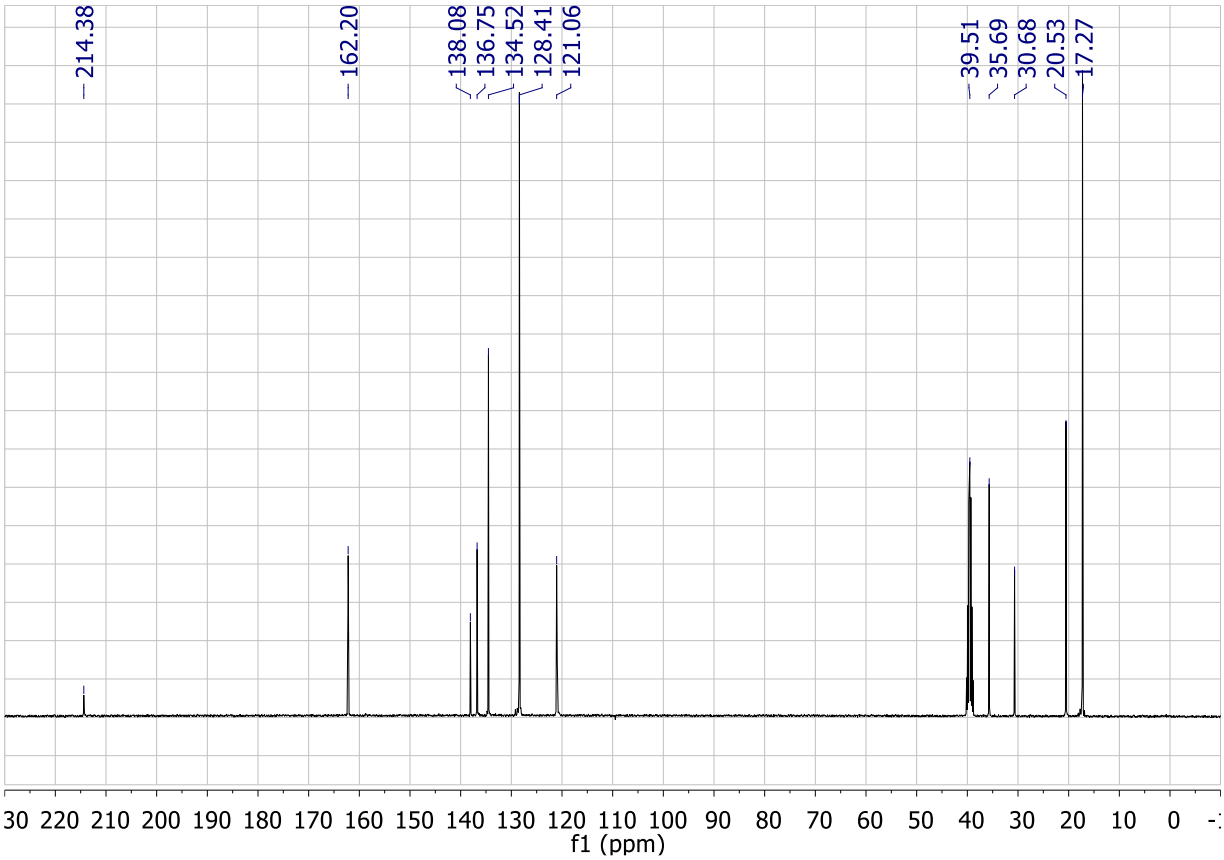
IMes (30 mg) in DMSO-d_6 (0.4 mL) Under PDMS (770 g·mol^{-1}, 0.3 mL) (DMF Standard) After 14 Days (^{13}C DMSO-d_6)



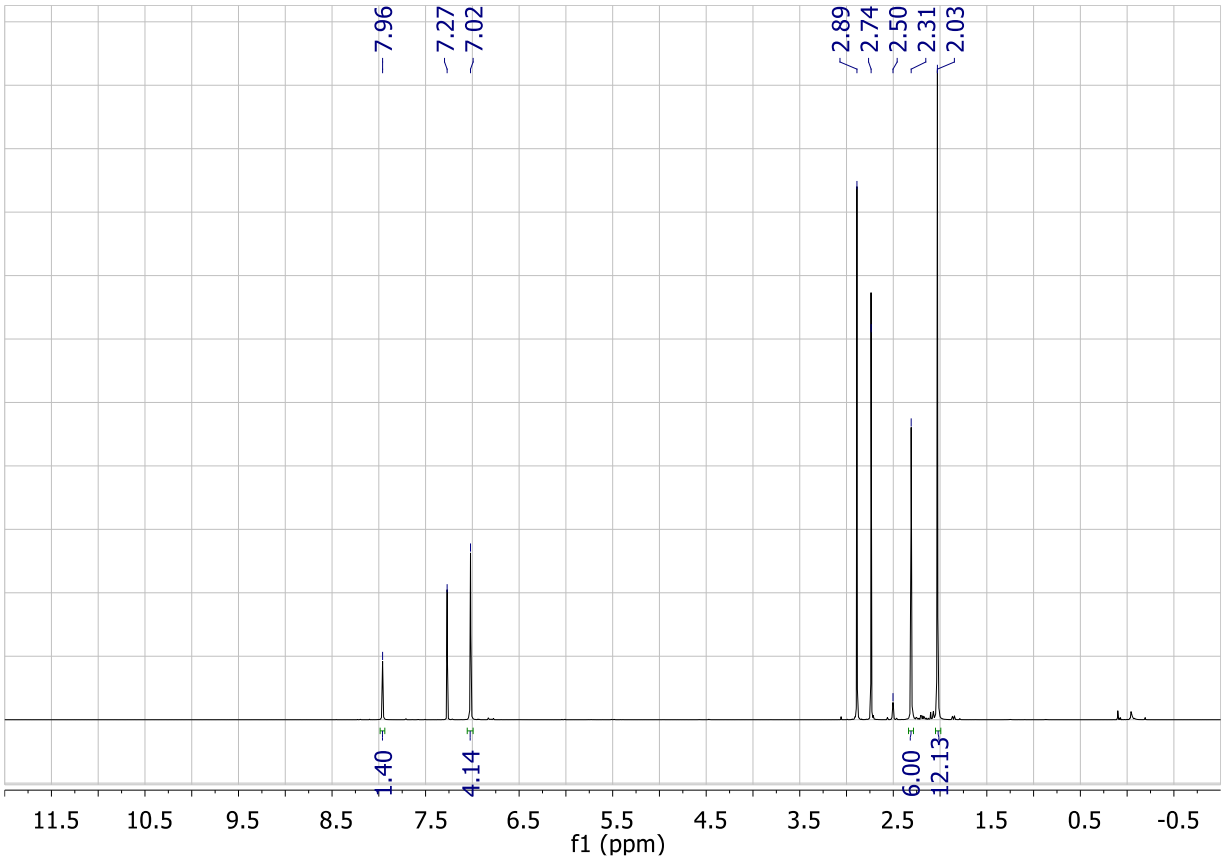
IMes (30 mg) in DMSO-d_6 (0.4 mL) Under PDMS (2,000 g·mol^{-1}, 0.3 mL) (DMF Standard) at Time 0 (^{1}H DMSO-d_6)



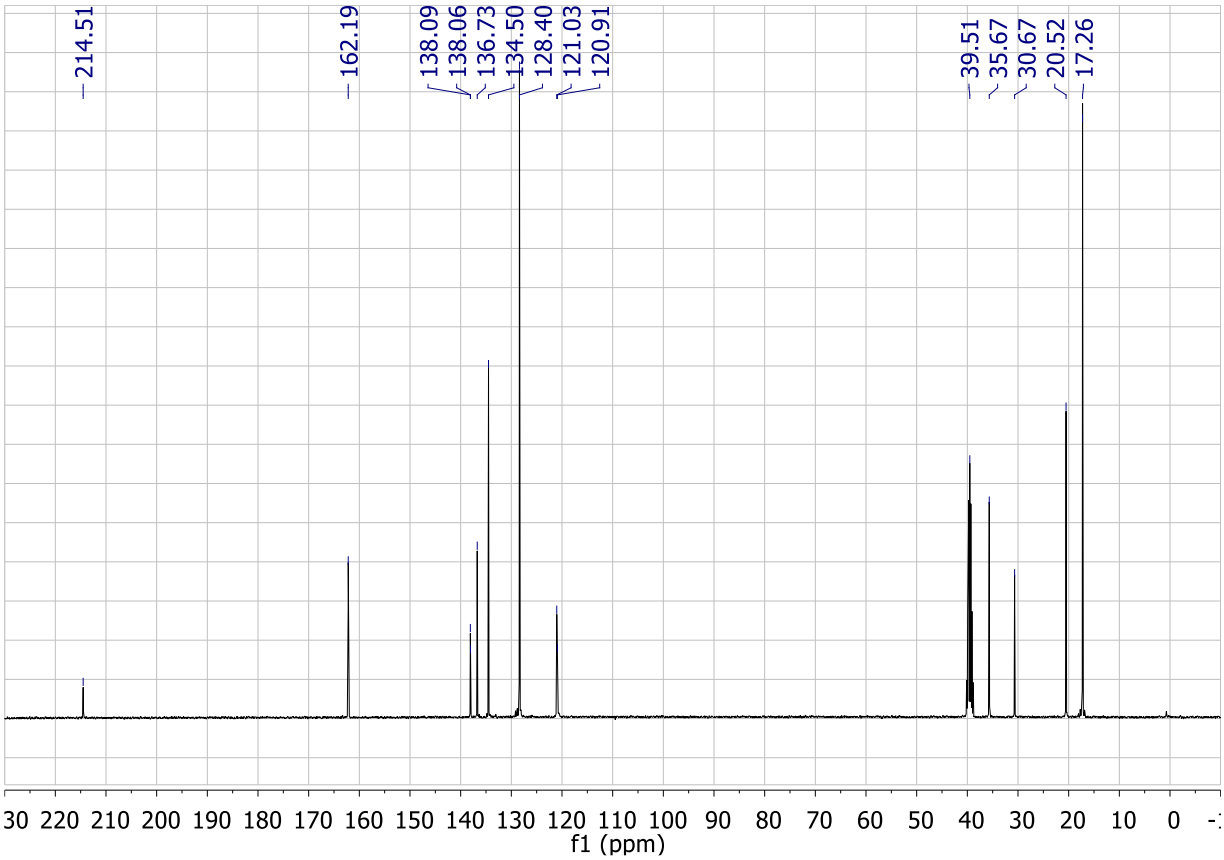
IMes (30 mg) in DMSO-d_6 (0.4 mL) Under PDMS (2,000 g·mol^{-1}, 0.3 mL) (DMF Standard) at Time 0 (^{13}C DMSO-d_6)



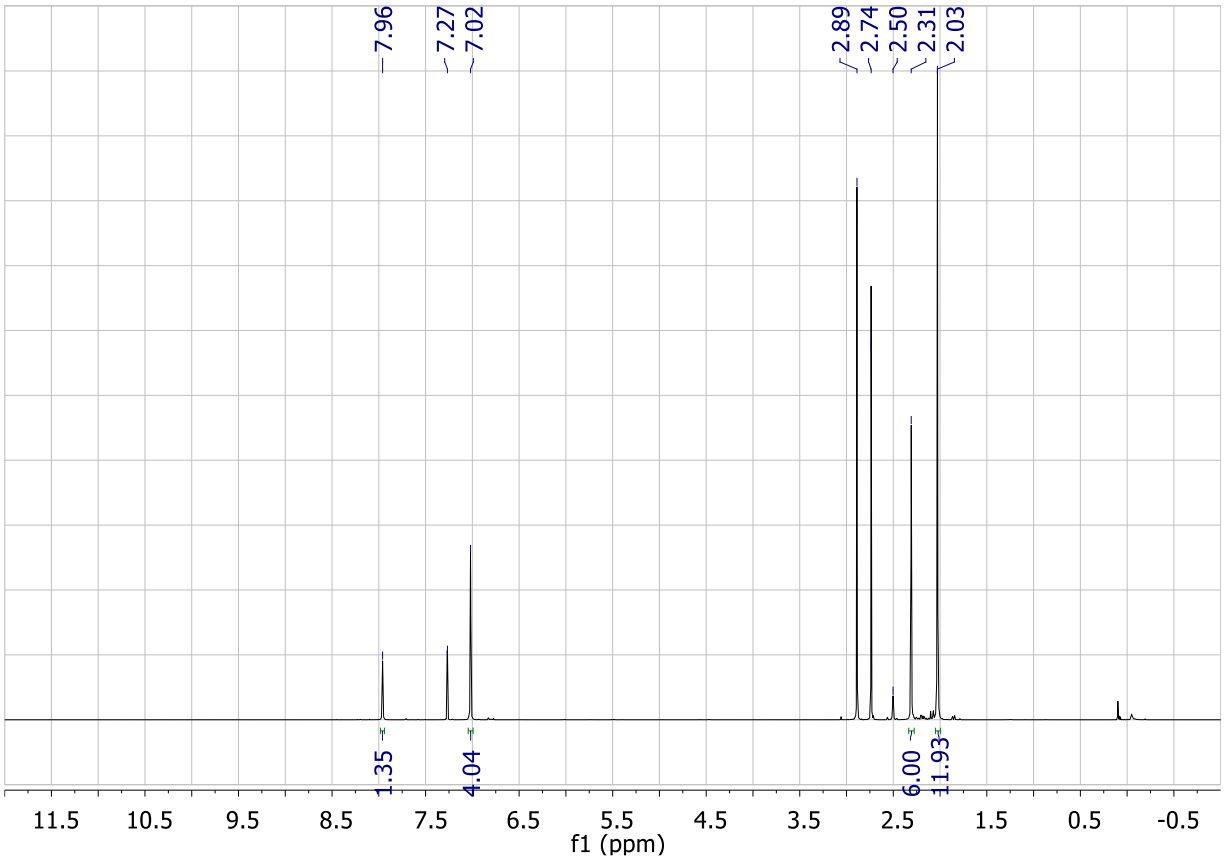
IMes (30 mg) in DMSO-d_6 (0.4 mL) Under PDMS (2,000 g·mol^{-1}, 0.3 mL) (DMF Standard) After 1 Day (^{1}H DMSO-d_6)



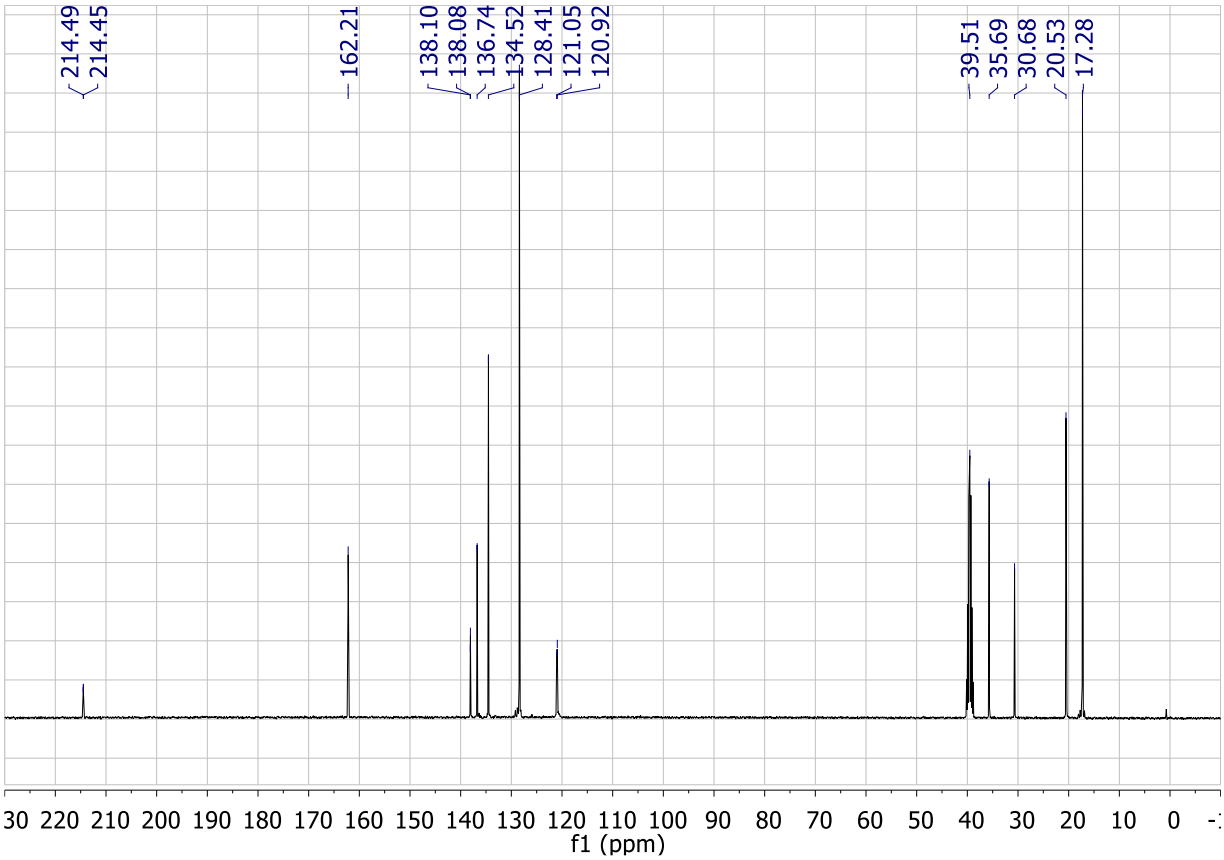
IMes (30 mg) in DMSO-d_6 (0.4 mL) Under PDMS (2,000 g·mol^{-1}, 0.3 mL) (DMF Standard) After 1 Day (^{13}C DMSO-d_6)



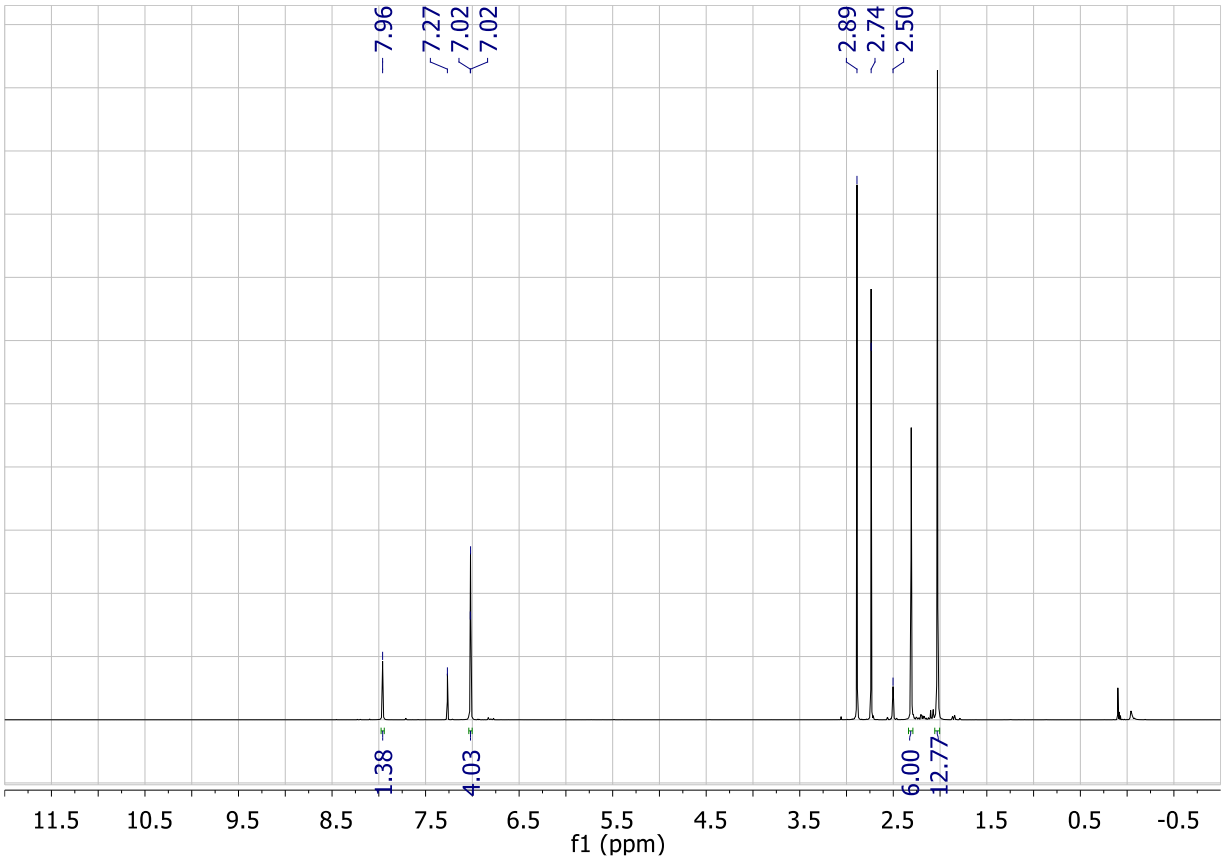
IMes (30 mg) in DMSO-d_6 (0.4 mL) Under PDMS (2,000 g·mol^{-1}, 0.3 mL) (DMF Standard) After 2 Days (^{1}H DMSO-d_6)



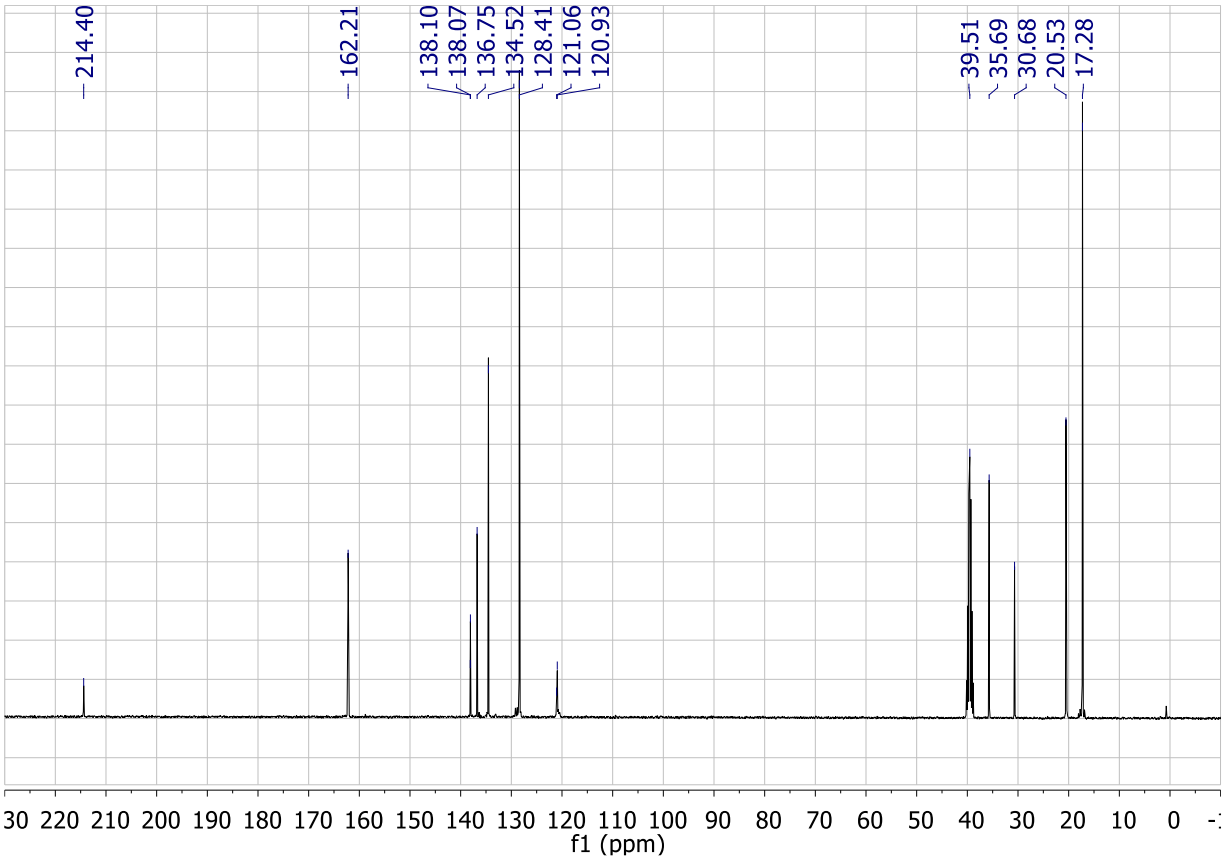
IMes (30 mg) in DMSO-d_6 (0.4 mL) Under PDMS (2,000 g·mol^{-1}, 0.3 mL) (DMF Standard) After 2 Days (^{13}C DMSO-d_6)



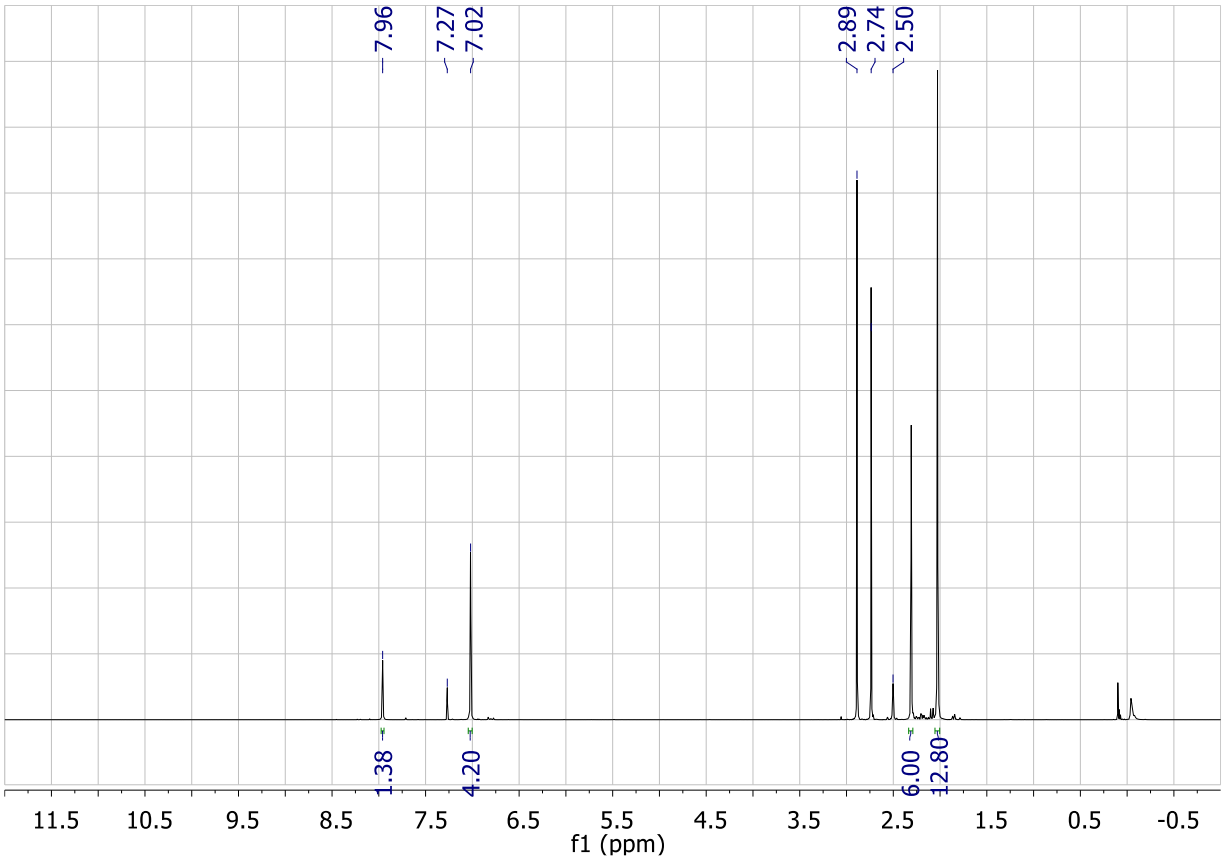
IMes (30 mg) in DMSO-d_6 (0.4 mL) Under PDMS (2,000 g·mol^{-1}, 0.3 mL) (DMF Standard) After 5 Days (^{1}H DMSO-d_6)



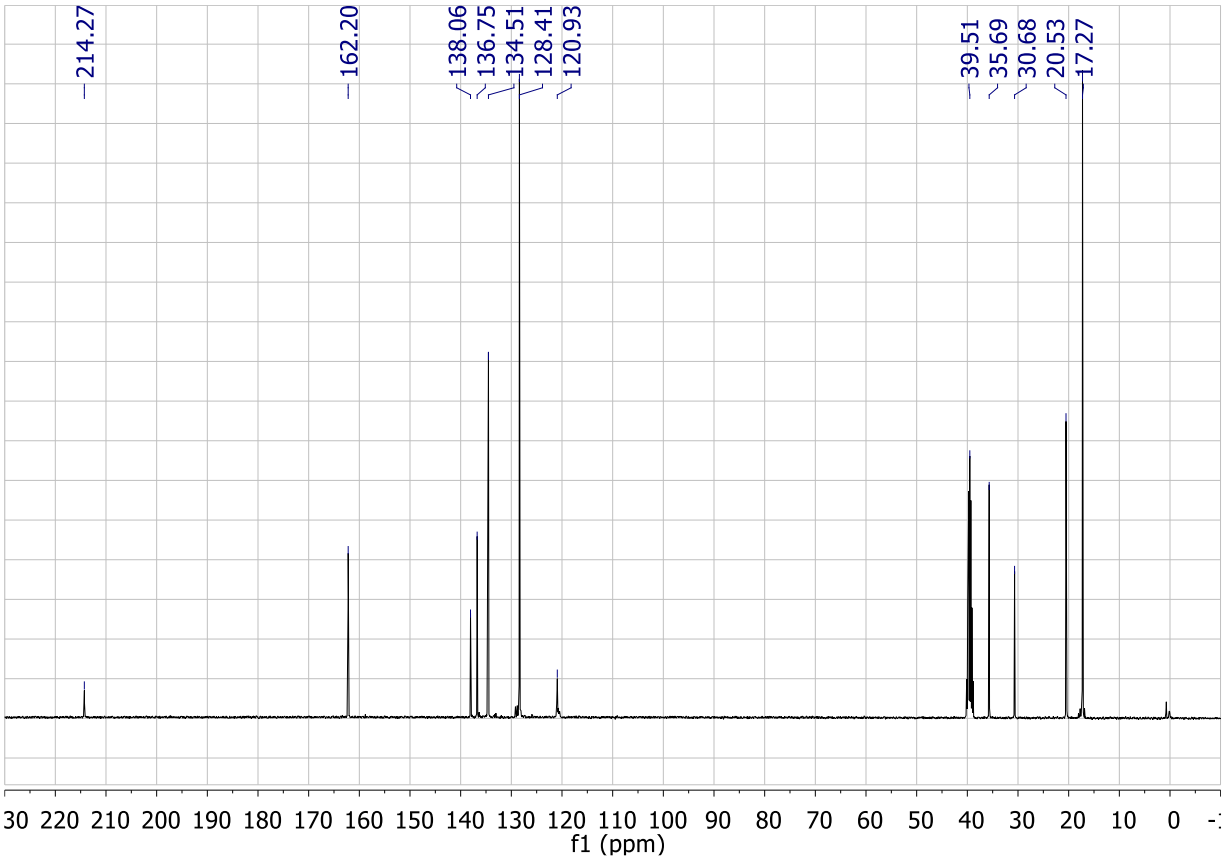
IMes (30 mg) in DMSO-d_6 (0.4 mL) Under PDMS (2,000 g·mol^{-1}, 0.3 mL) (DMF Standard) After 5 Days (^{13}C DMSO-d_6)



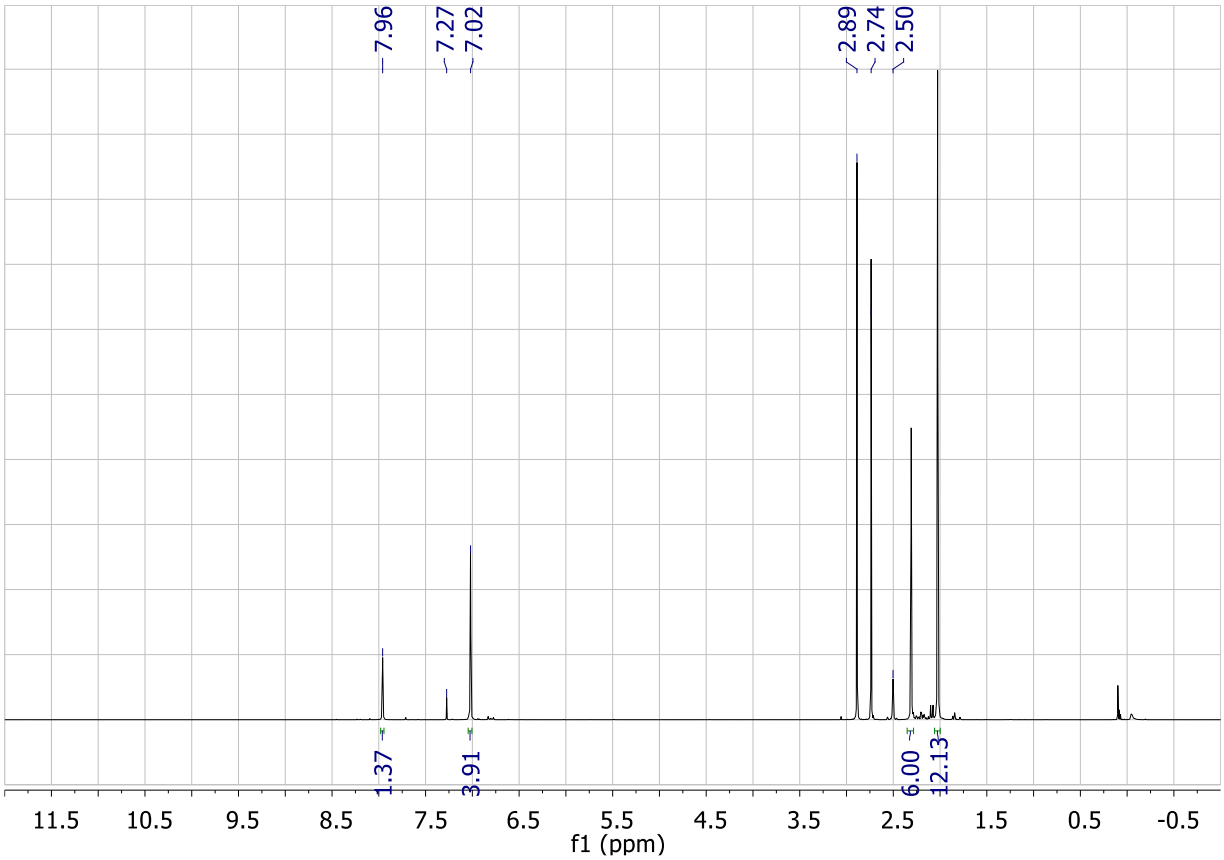
IMes (30 mg) in DMSO-d_6 (0.4 mL) Under PDMS (2,000 g·mol^{-1}, 0.3 mL) (DMF Standard) After 8 Days (^{1}H DMSO-d_6)



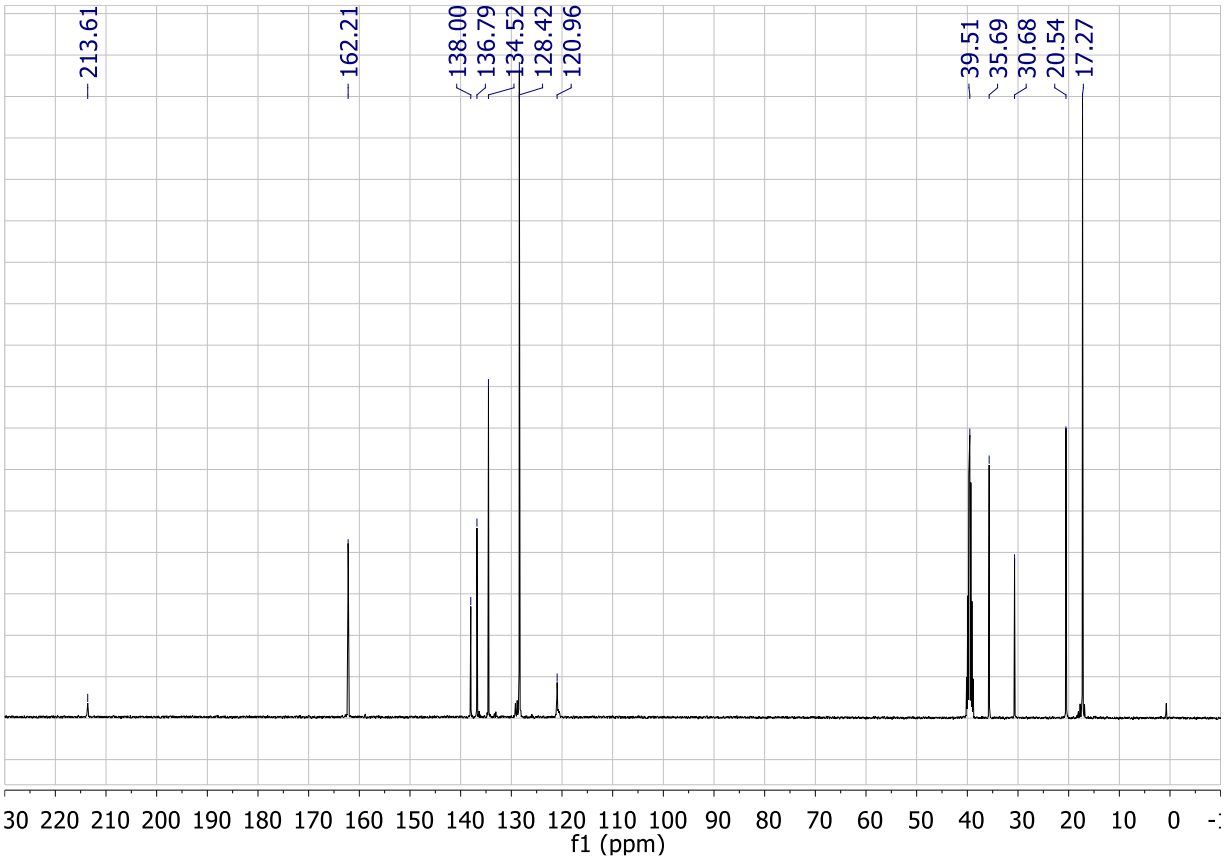
IMes (30 mg) in DMSO-d_6 (0.4 mL) Under PDMS (2,000 g·mol^{-1}, 0.3 mL) (DMF Standard) After 8 Days (^{13}C DMSO-d_6)



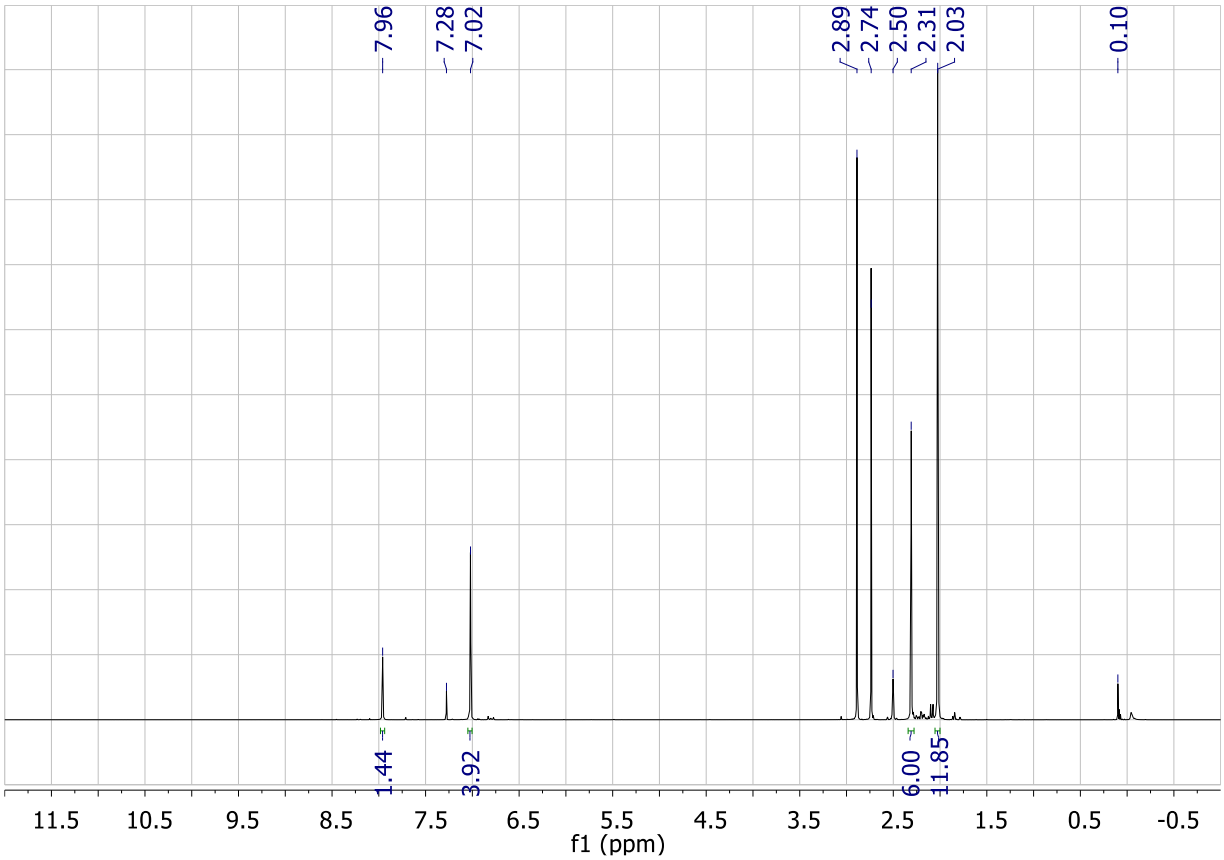
IMes (30 mg) in DMSO-d_6 (0.4 mL) Under PDMS (2,000 g·mol^{-1}, 0.3 mL) (DMF Standard) After 13 Days (^{1}H DMSO-d_6)



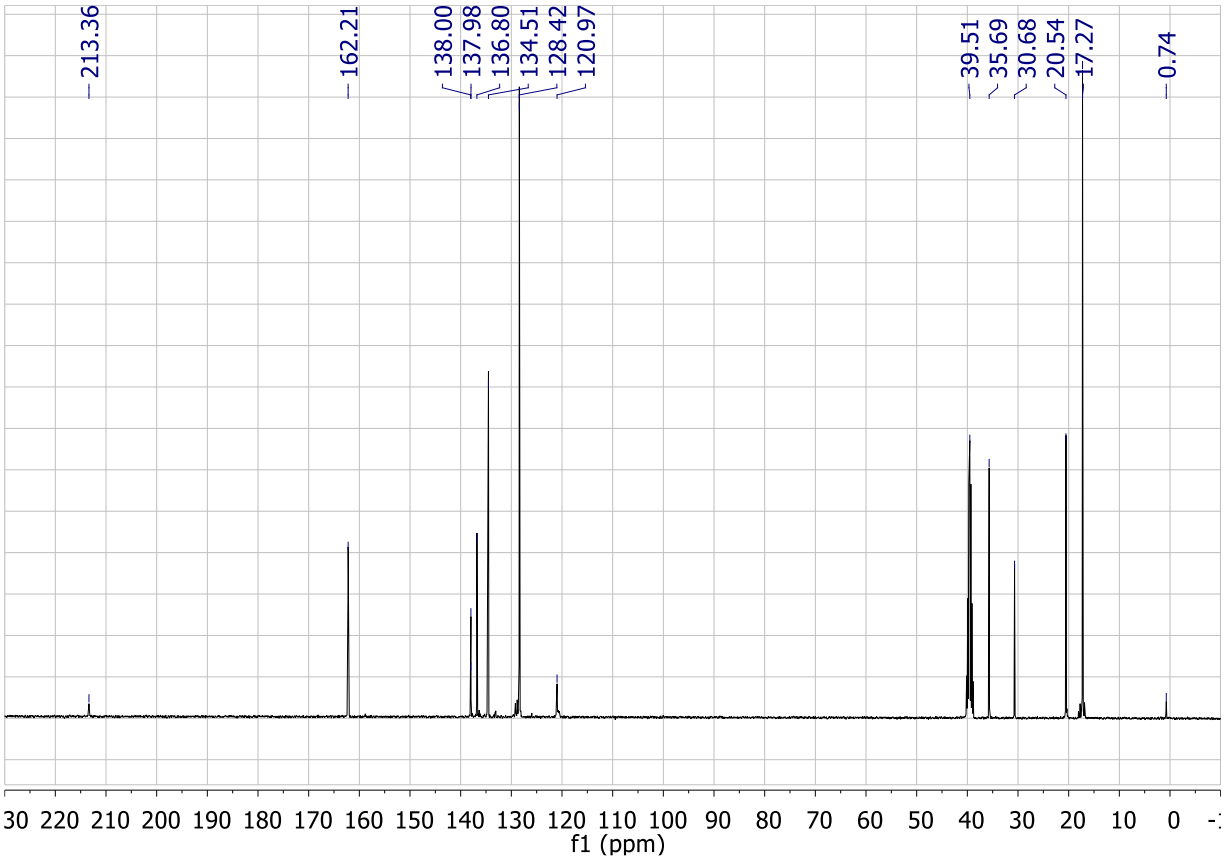
IMes (30 mg) in DMSO-d_6 (0.4 mL) Under PDMS (2,000 g·mol^{-1}, 0.3 mL) (DMF Standard) After 13 Days (^{13}C DMSO-d_6)



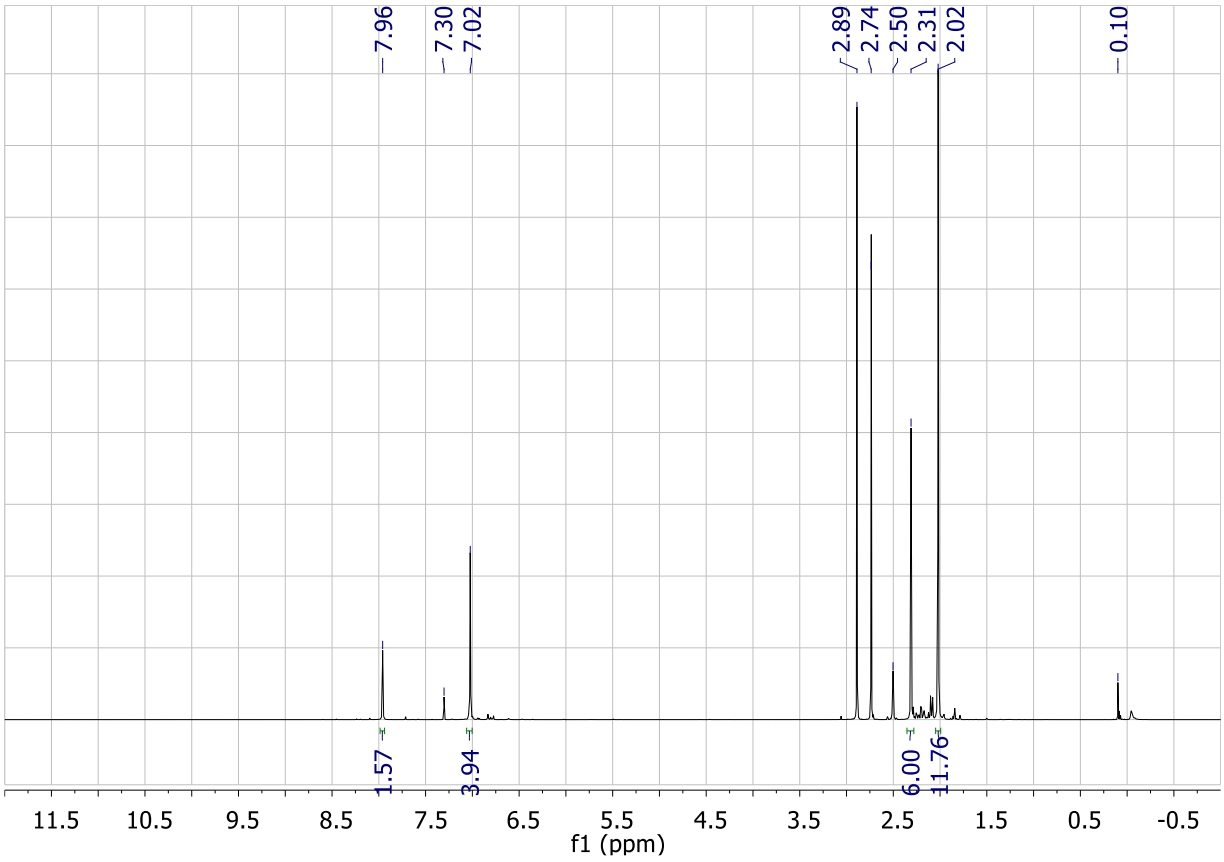
IMes (30 mg) in DMSO-d_6 (0.4 mL) Under PDMS (2,000 g·mol^{-1}, 0.3 mL) (DMF Standard) After 14 Days (^{1}H DMSO-d_6)



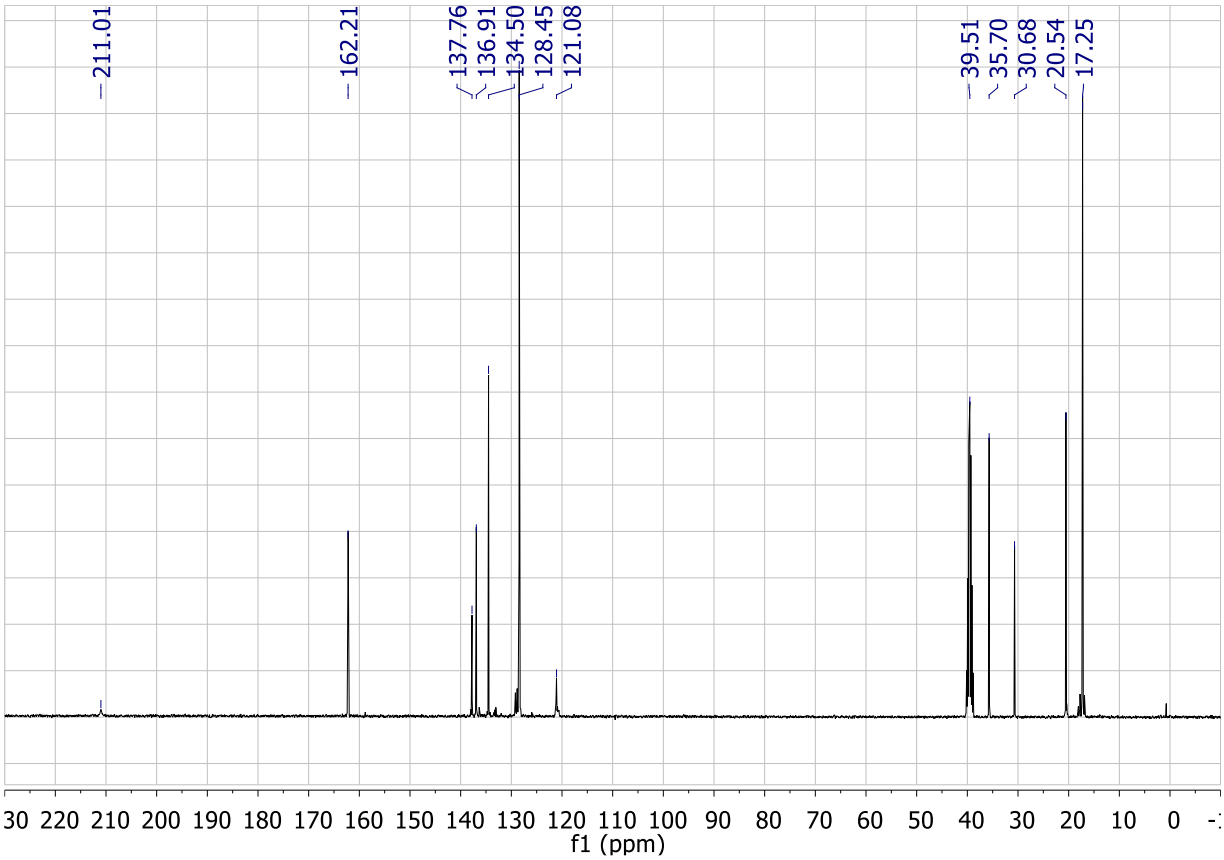
IMes (30 mg) in DMSO-d_6 (0.4 mL) Under PDMS (2,000 g·mol^{-1}, 0.3 mL) (DMF Standard) After 14 Days (^{13}C DMSO-d_6)



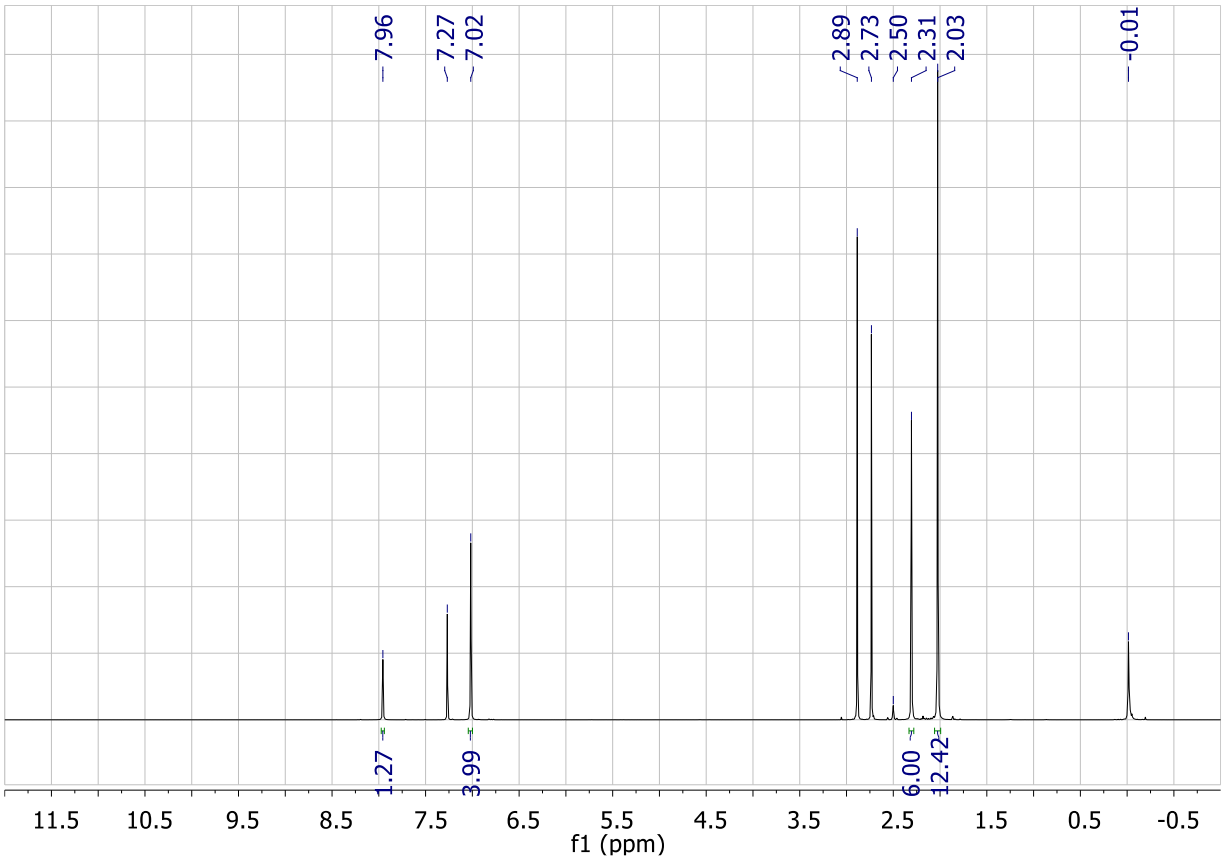
IMes (30 mg) in DMSO-d_6 (0.4 mL) Under PDMS (2,000 g·mol^{-1}, 0.3 mL) (DMF Standard) After 20 Days (^{1}H DMSO-d_6)



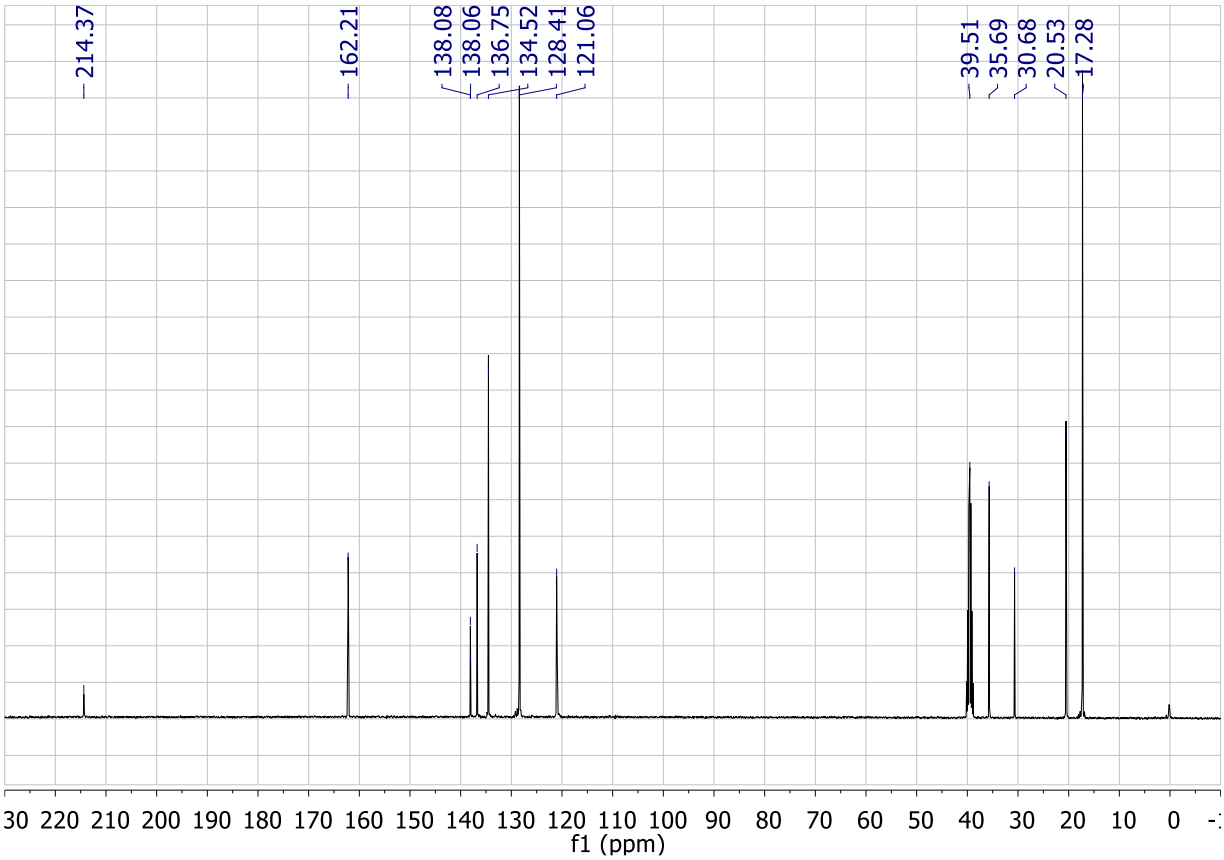
IMes (30 mg) in DMSO-d_6 (0.4 mL) Under PDMS (2,000 g·mol^{-1}, 0.3 mL) (DMF Standard) After 20 Days (^{13}C DMSO-d_6)



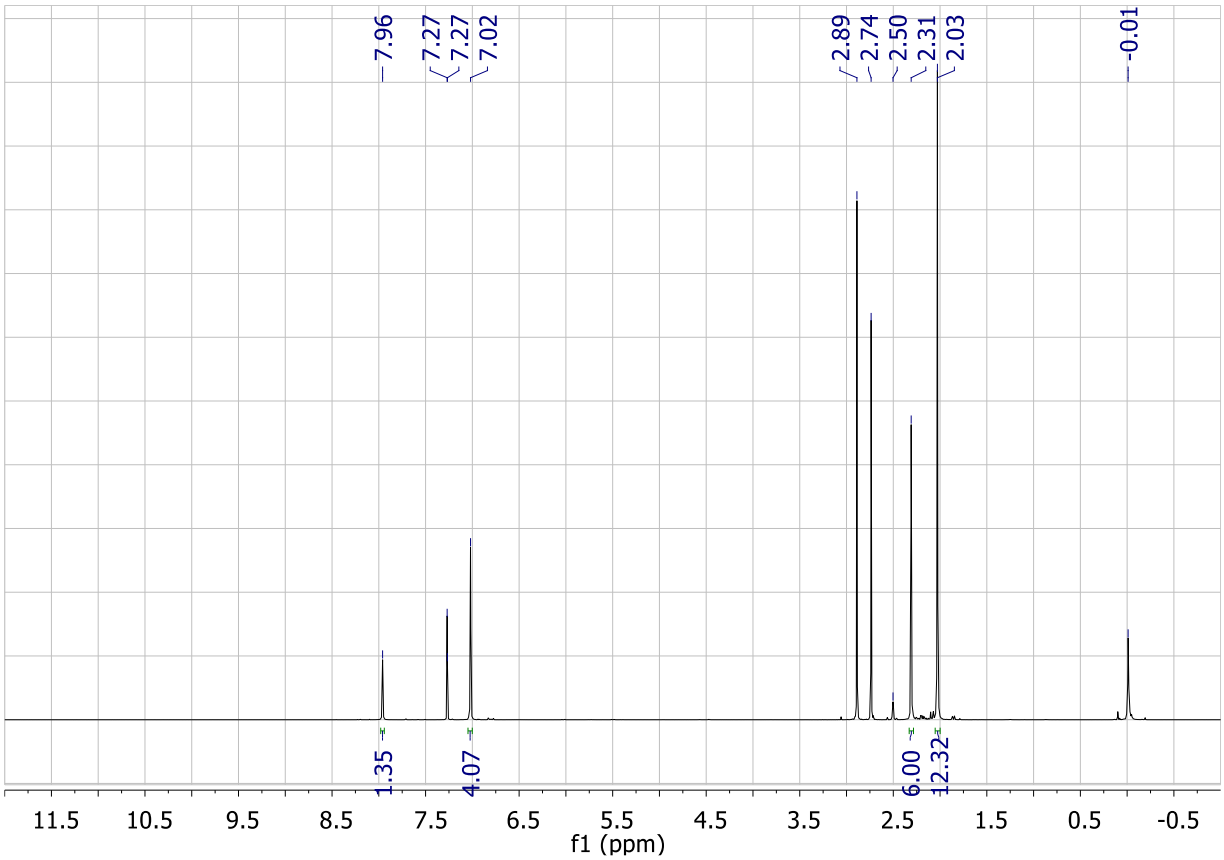
IMes (30 mg) in DMSO-d_6 (0.4 mL) Under PDMS (4,000 g·mol^{-1}, 0.3 mL) (DMF Standard) at Time 0 (^{1}H DMSO-d_6)



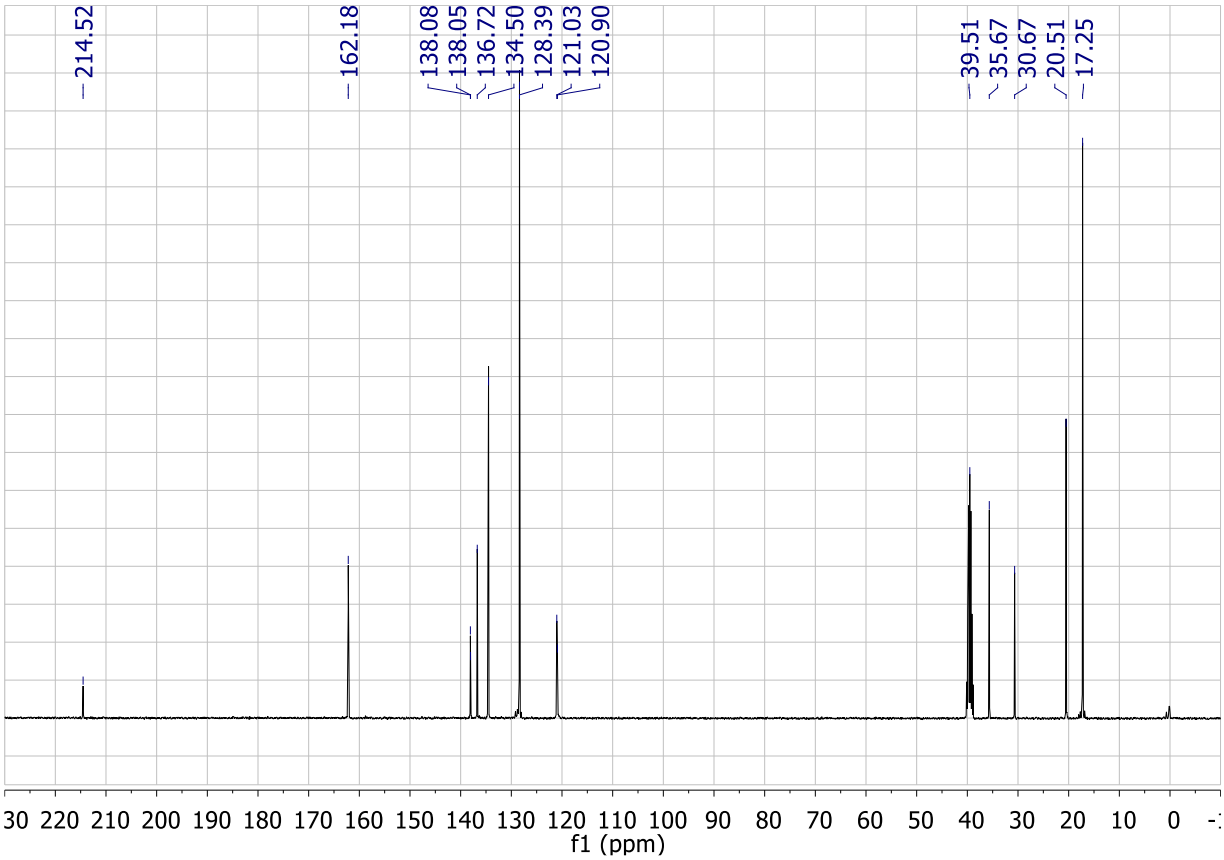
IMes (30 mg) in DMSO-d_6 (0.4 mL) Under PDMS (4,000 g·mol^{-1}, 0.3 mL) (DMF Standard) at Time 0 (^{13}C DMSO-d_6)



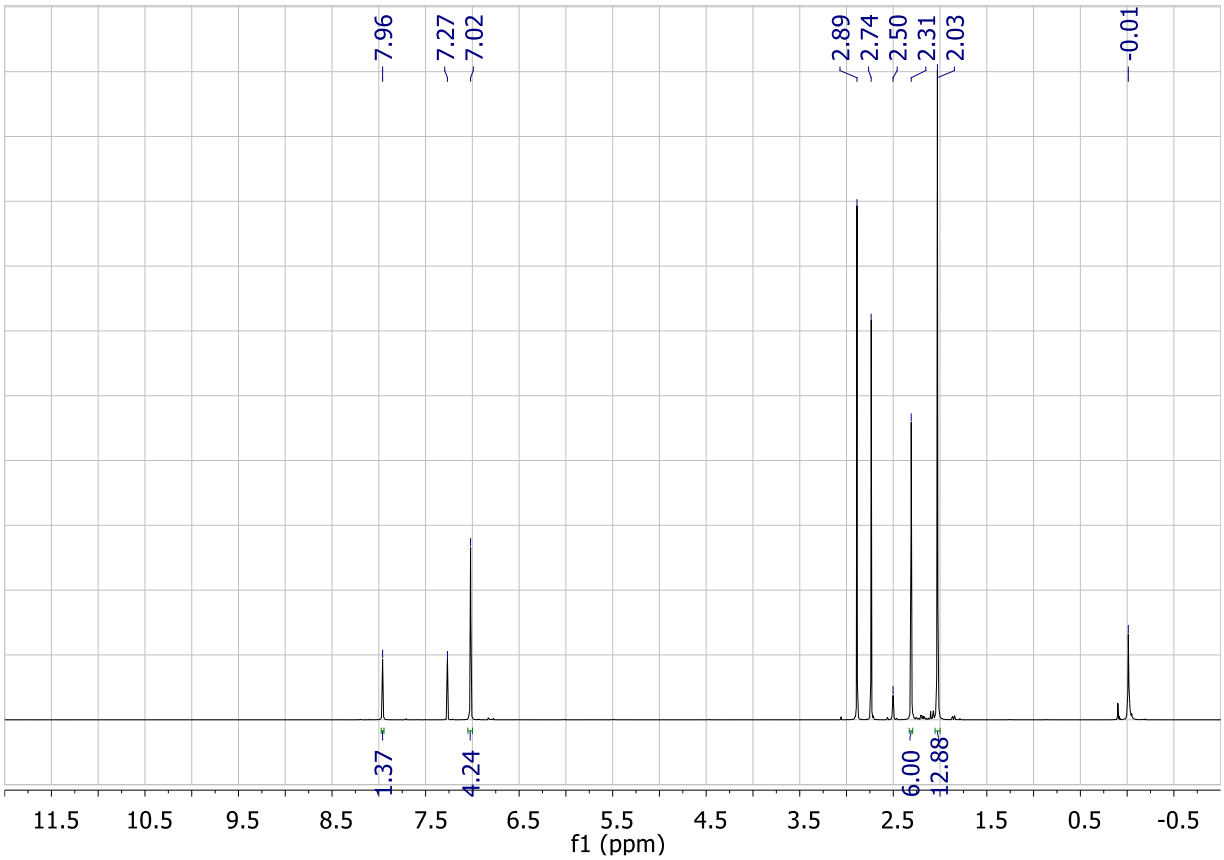
IMes (30 mg) in DMSO-d_6 (0.4 mL) Under PDMS (4,000 g·mol^{-1}, 0.3 mL) (DMF Standard) After 1 Day (^{1}H DMSO-d_6)



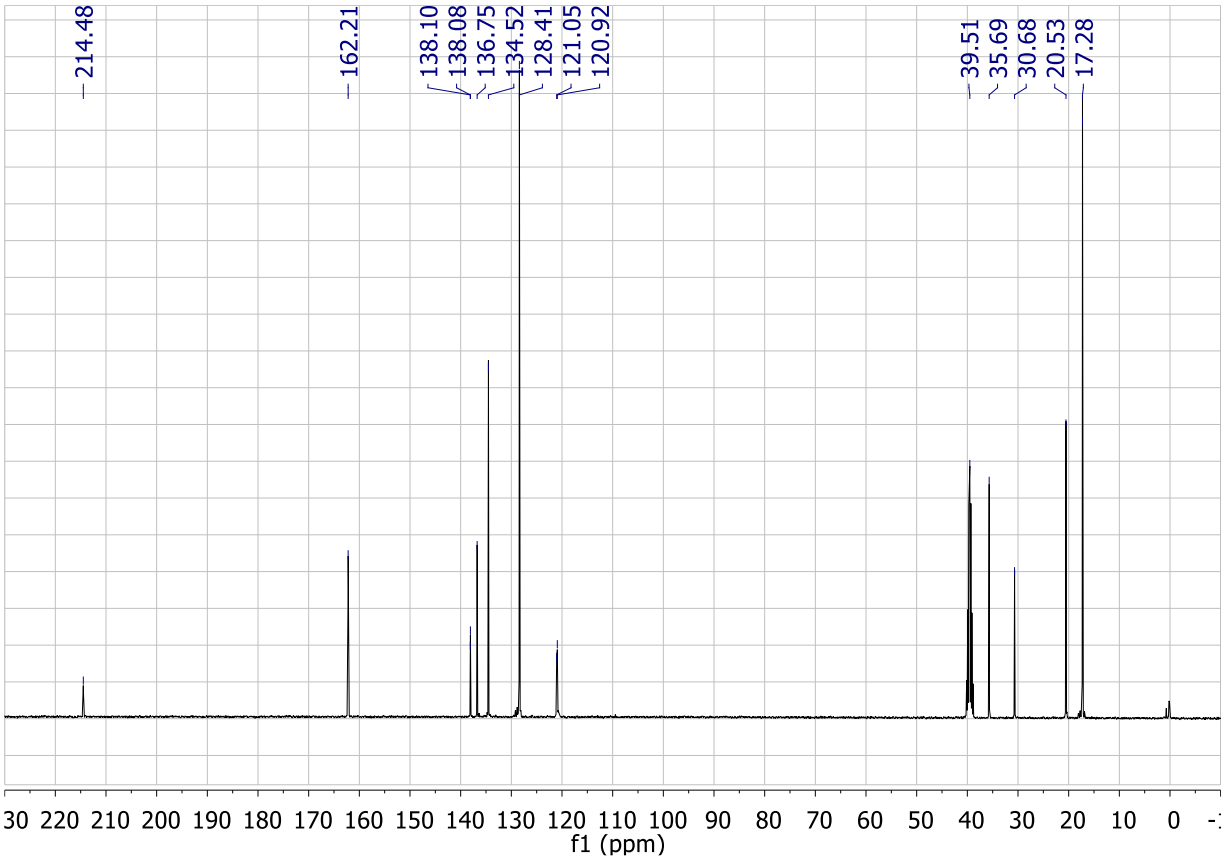
IMes (30 mg) in DMSO-d_6 (0.4 mL) Under PDMS (4,000 g·mol^{-1}, 0.3 mL) (DMF Standard) After 1 Day (^{13}C DMSO-d_6)



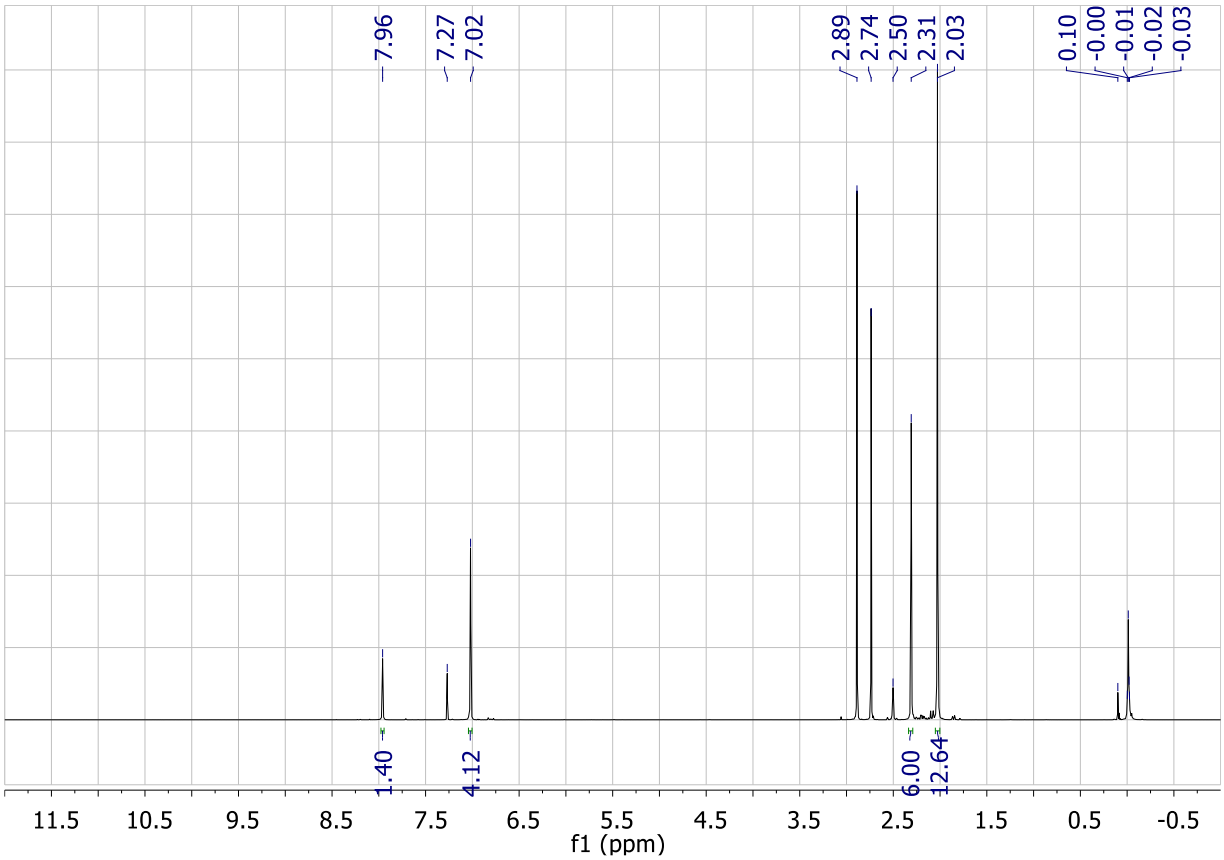
IMes (30 mg) in DMSO-d_6 (0.4 mL) Under PDMS (4,000 g·mol^{-1}, 0.3 mL) (DMF Standard) After 2 Days (^{1}H DMSO-d_6)



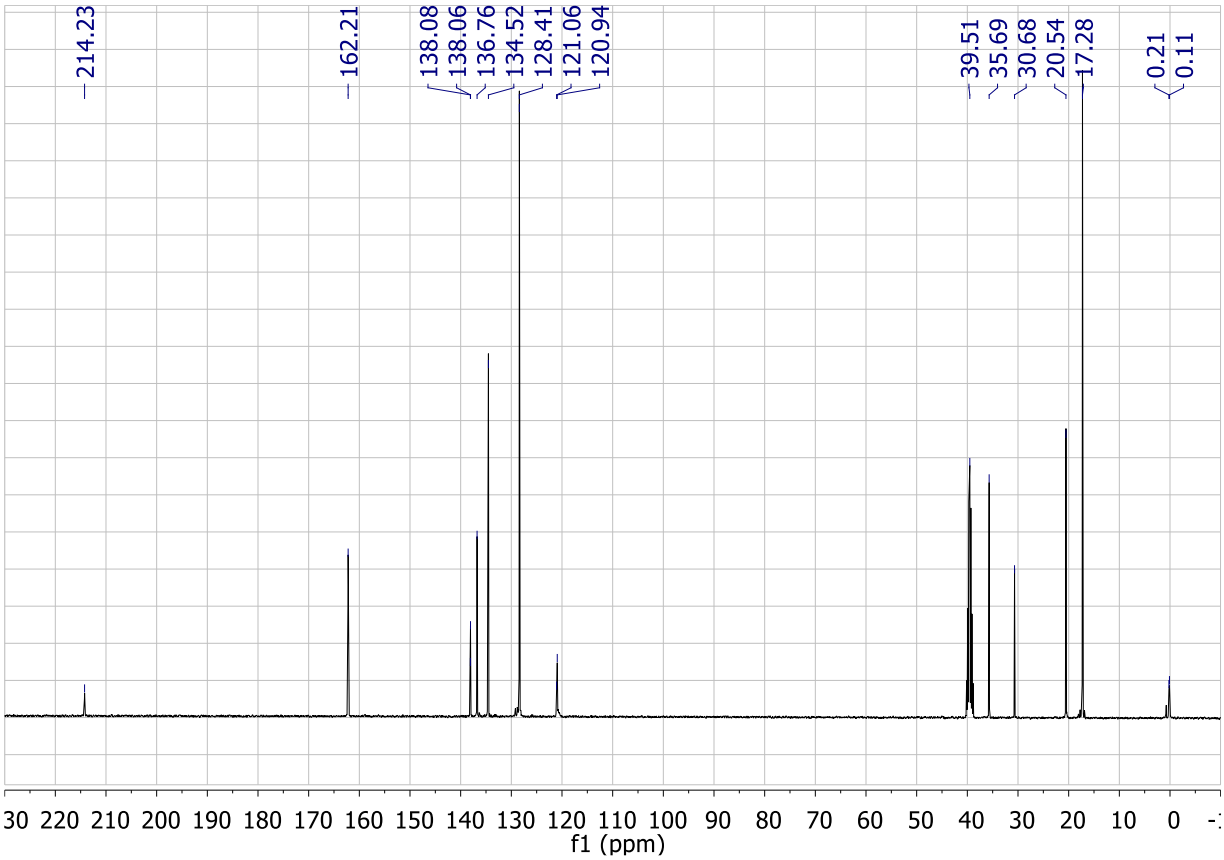
IMes (30 mg) in DMSO-d_6 (0.4 mL) Under PDMS (4,000 g·mol^{-1}, 0.3 mL) (DMF Standard) After 2 Days (^{13}C DMSO-d_6)



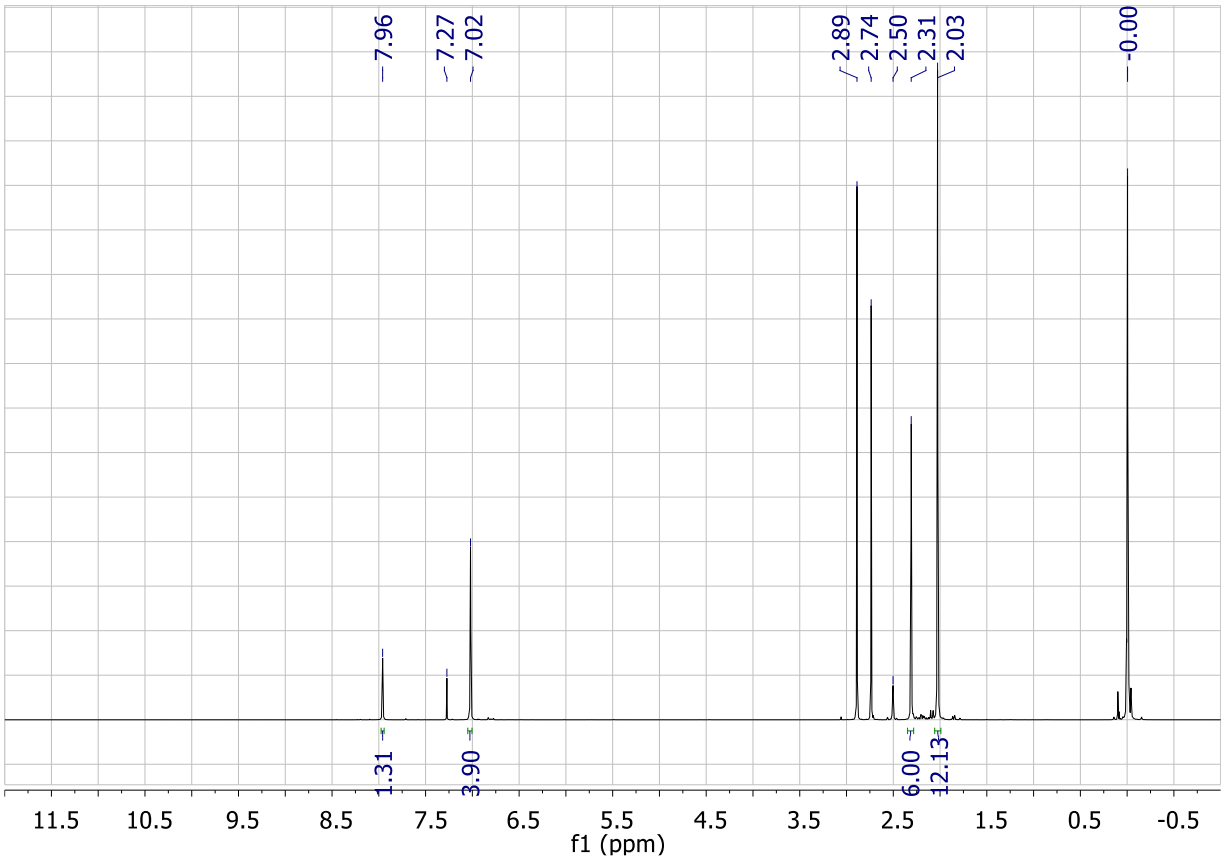
IMes (30 mg) in DMSO-d_6 (0.4 mL) Under PDMS (4,000 g·mol^{-1}, 0.3 mL) (DMF Standard) After 5 Days (^{1}H DMSO-d_6)



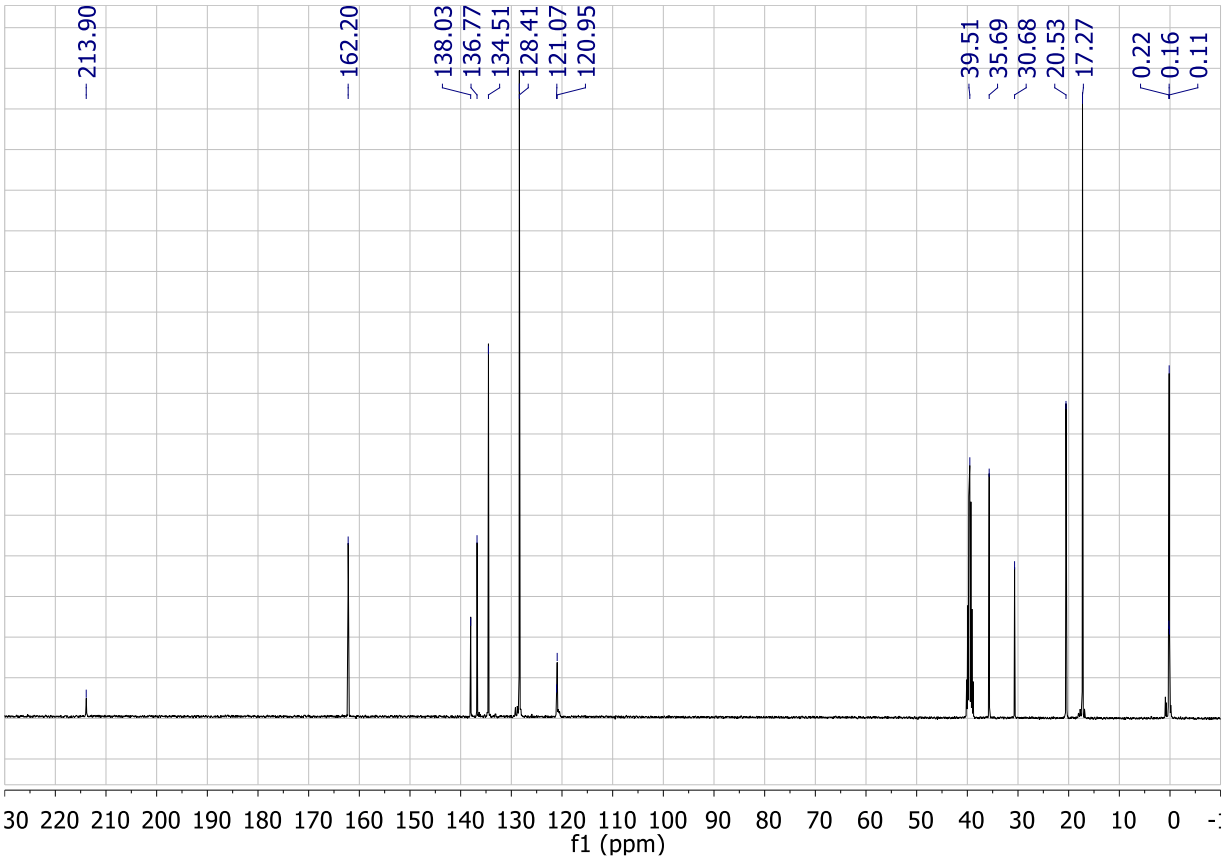
IMes (30 mg) in DMSO-d_6 (0.4 mL) Under PDMS (4,000 g·mol^{-1}, 0.3 mL) (DMF Standard) After 5 Days (^{13}C DMSO-d_6)



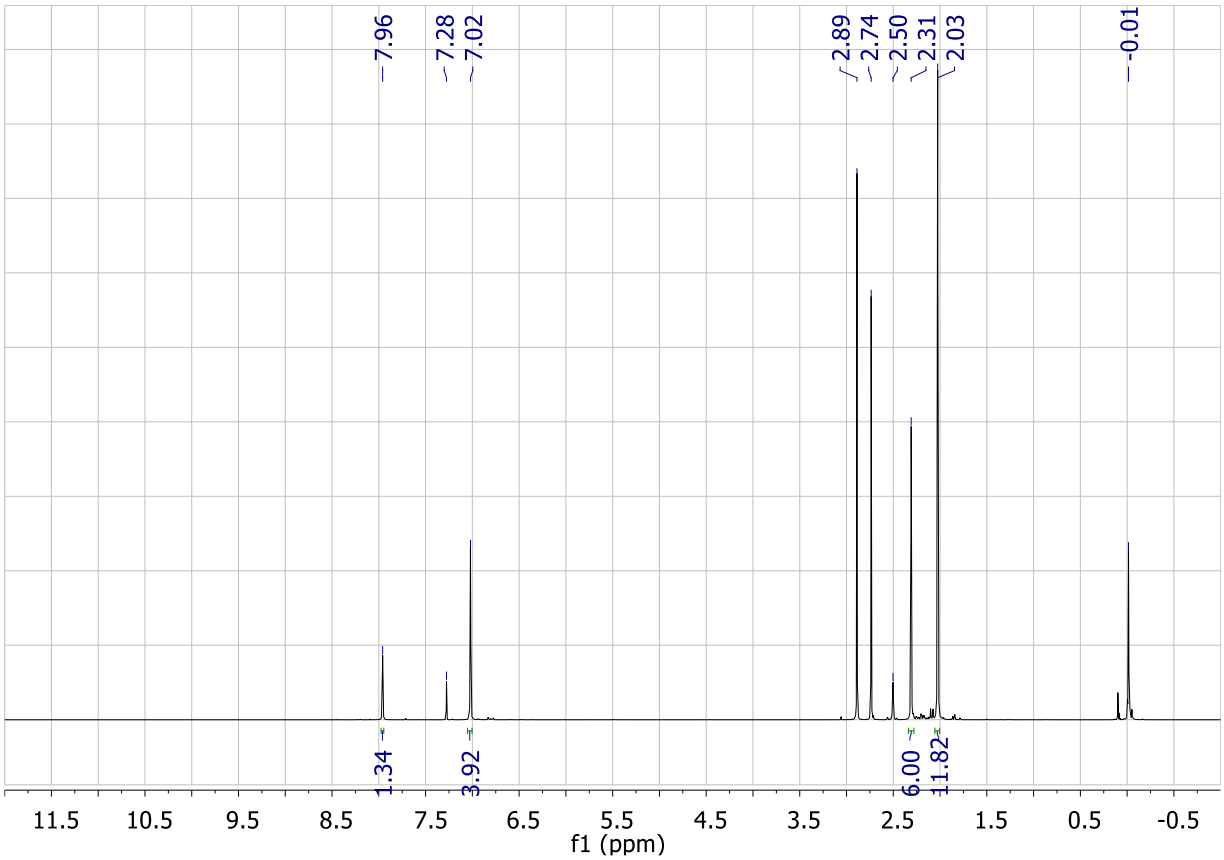
IMes (30 mg) in DMSO-d_6 (0.4 mL) Under PDMS (4,000 g·mol^{-1}, 0.3 mL) (DMF Standard) After 8 Days (^{1}H DMSO-d_6)



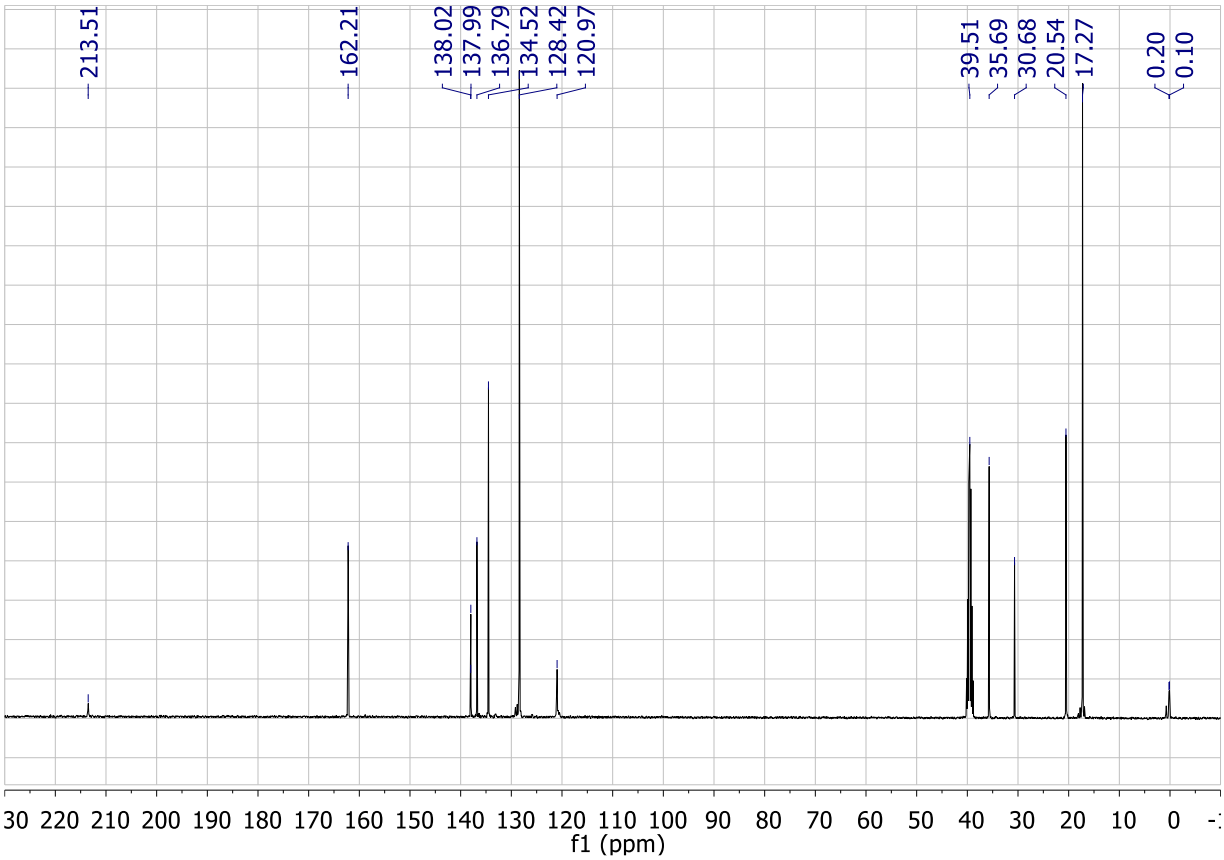
IMes (30 mg) in DMSO-d_6 (0.4 mL) Under PDMS (4,000 g·mol^{-1}, 0.3 mL) (DMF Standard) After 8 Days (^{13}C DMSO-d_6)



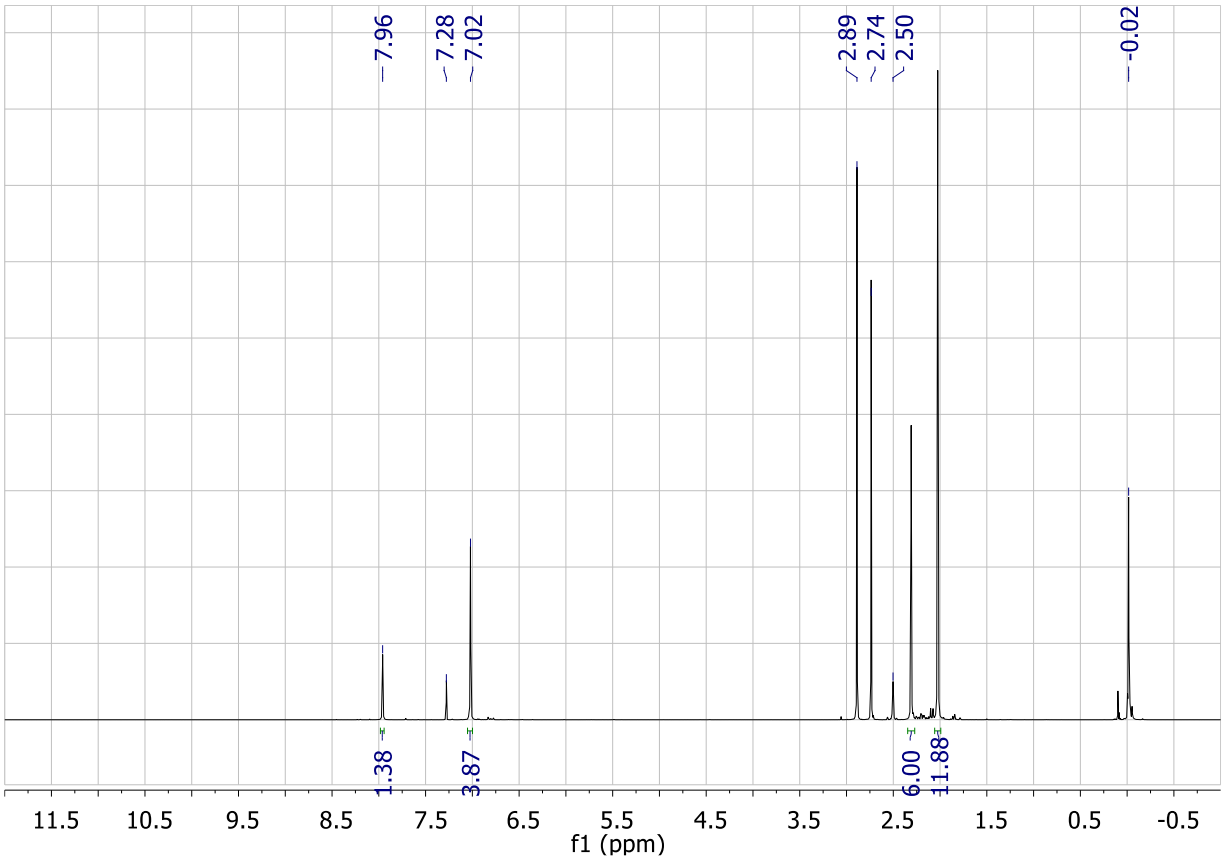
IMes (30 mg) in DMSO-d_6 (0.4 mL) Under PDMS (4,000 g·mol^{-1}, 0.3 mL) (DMF Standard) After 13 Days (^{1}H DMSO-d_6)



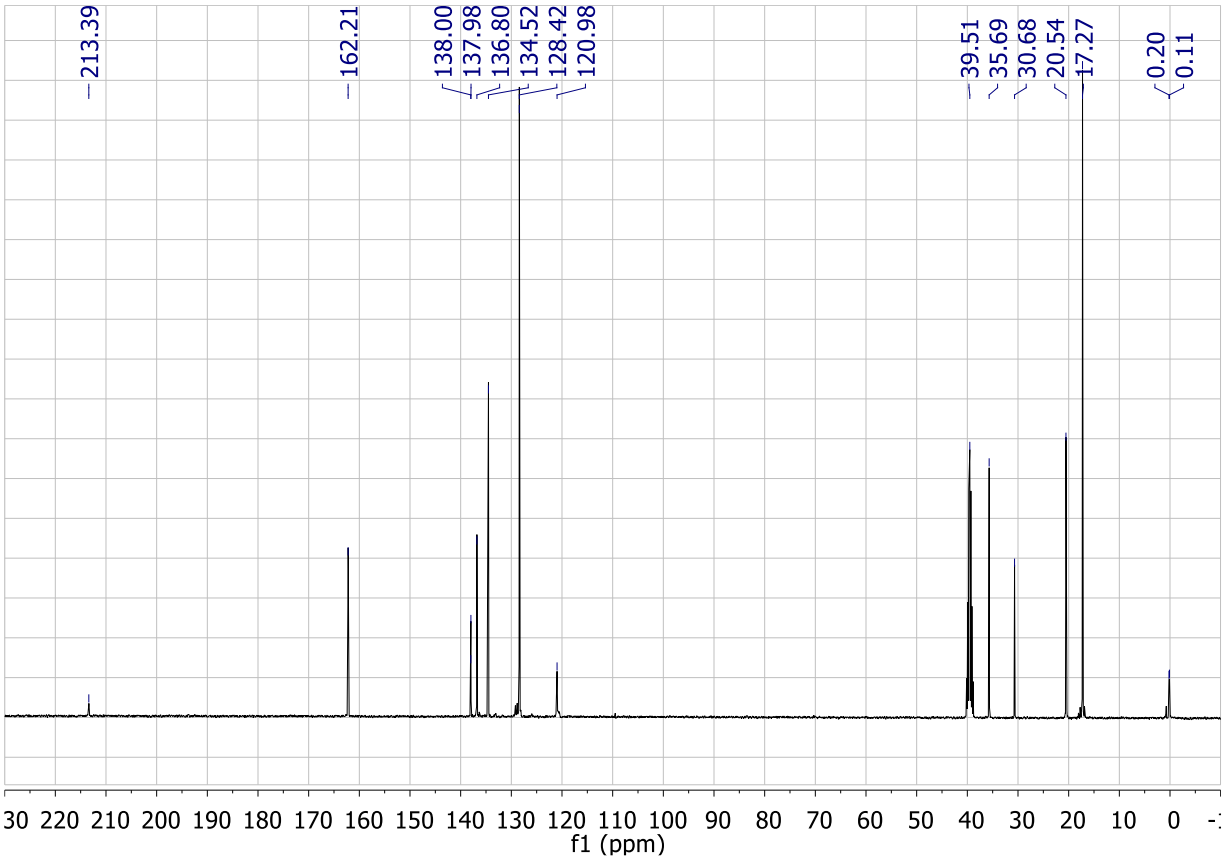
IMes (30 mg) in DMSO-d_6 (0.4 mL) Under PDMS (4,000 g·mol^{-1}, 0.3 mL) (DMF Standard) After 13 Days (^{13}C DMSO-d_6)



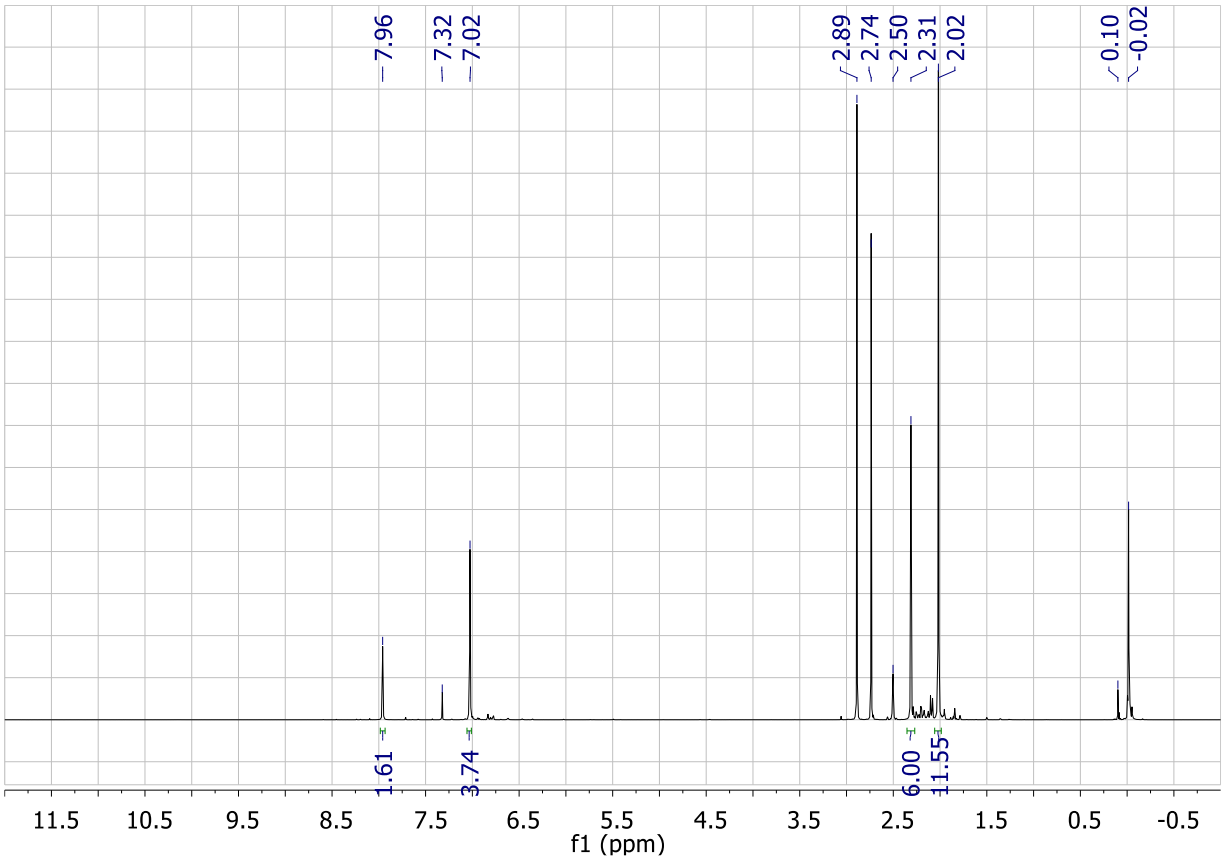
IMes (30 mg) in DMSO-d_6 (0.4 mL) Under PDMS (4,000 g·mol^{-1}, 0.3 mL) (DMF Standard) After 14 Days (^{1}H DMSO-d_6)



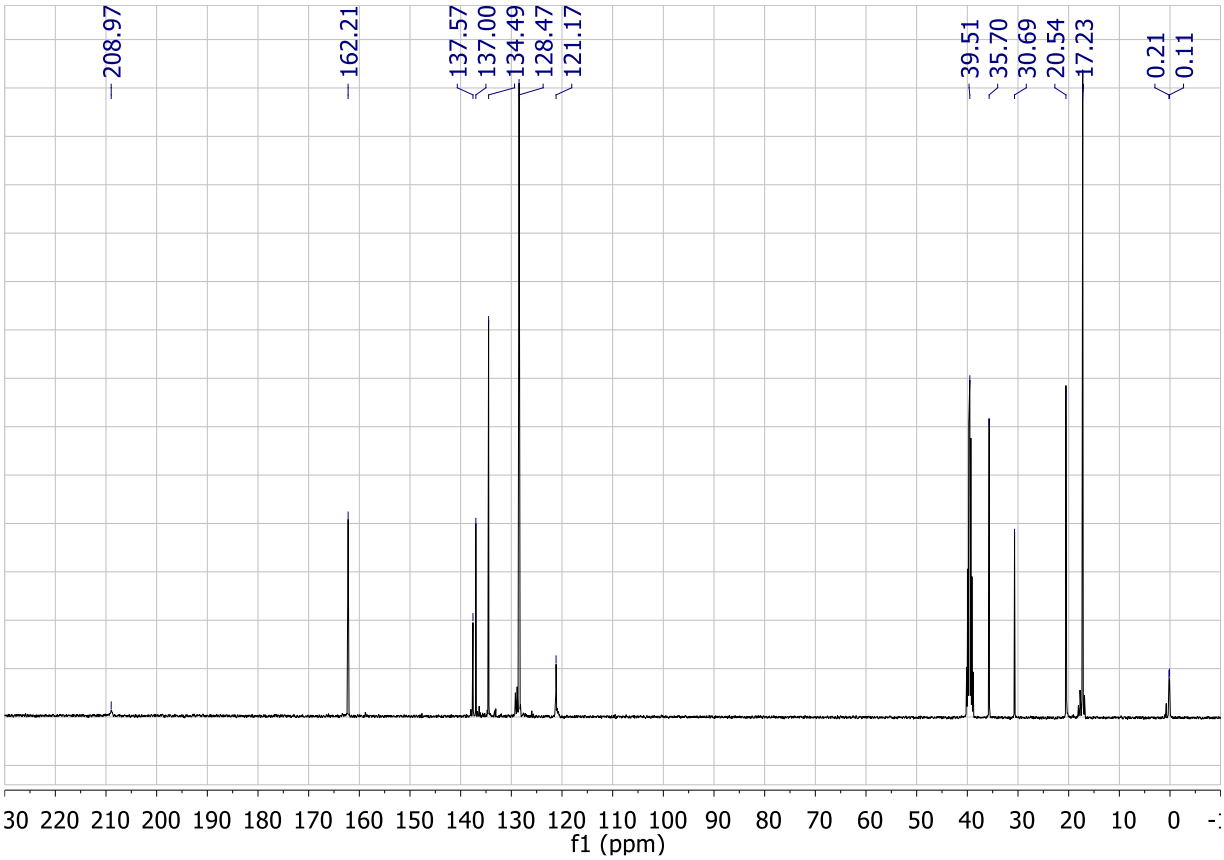
IMes (30 mg) in DMSO-d_6 (0.4 mL) Under PDMS (4,000 g·mol^{-1}, 0.3 mL) (DMF Standard) After 14 Days (^{13}C DMSO-d_6)



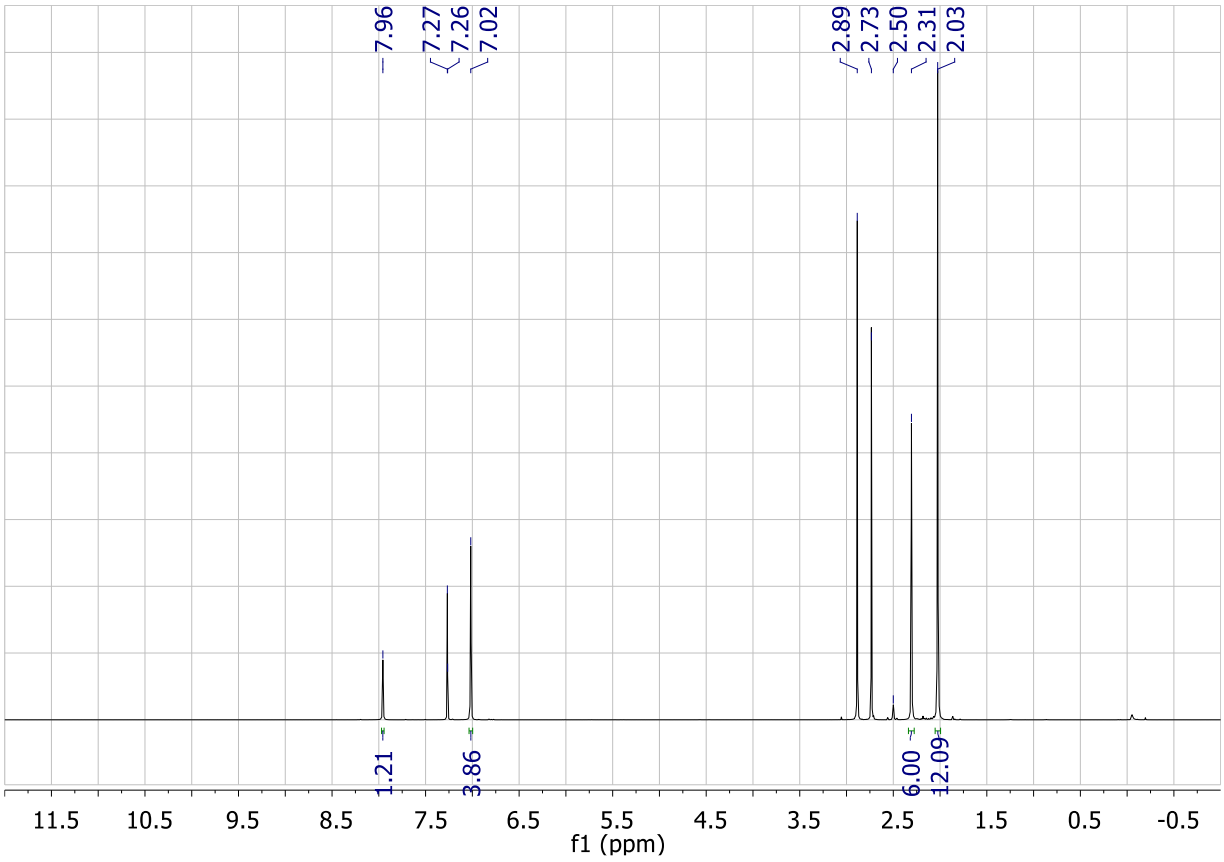
IMes (30 mg) in DMSO-d_6 (0.4 mL) Under PDMS (4,000 g·mol^{-1}, 0.3 mL) (DMF Standard) After 20 Days (^{1}H DMSO-d_6)



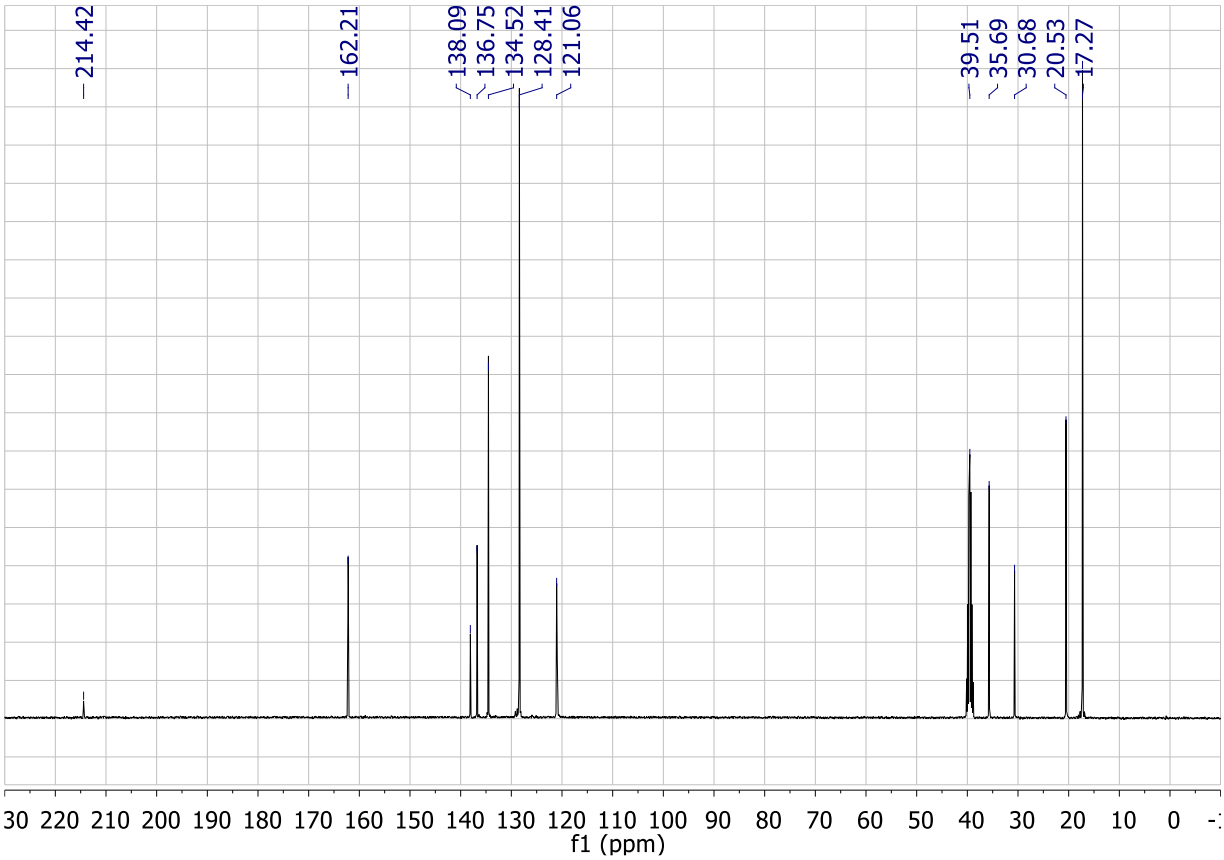
IMes (30 mg) in DMSO-d_6 (0.4 mL) Under PDMS (4,000 g·mol^{-1}, 0.3 mL) (DMF Standard) After 20 Days (^{13}C DMSO-d_6)



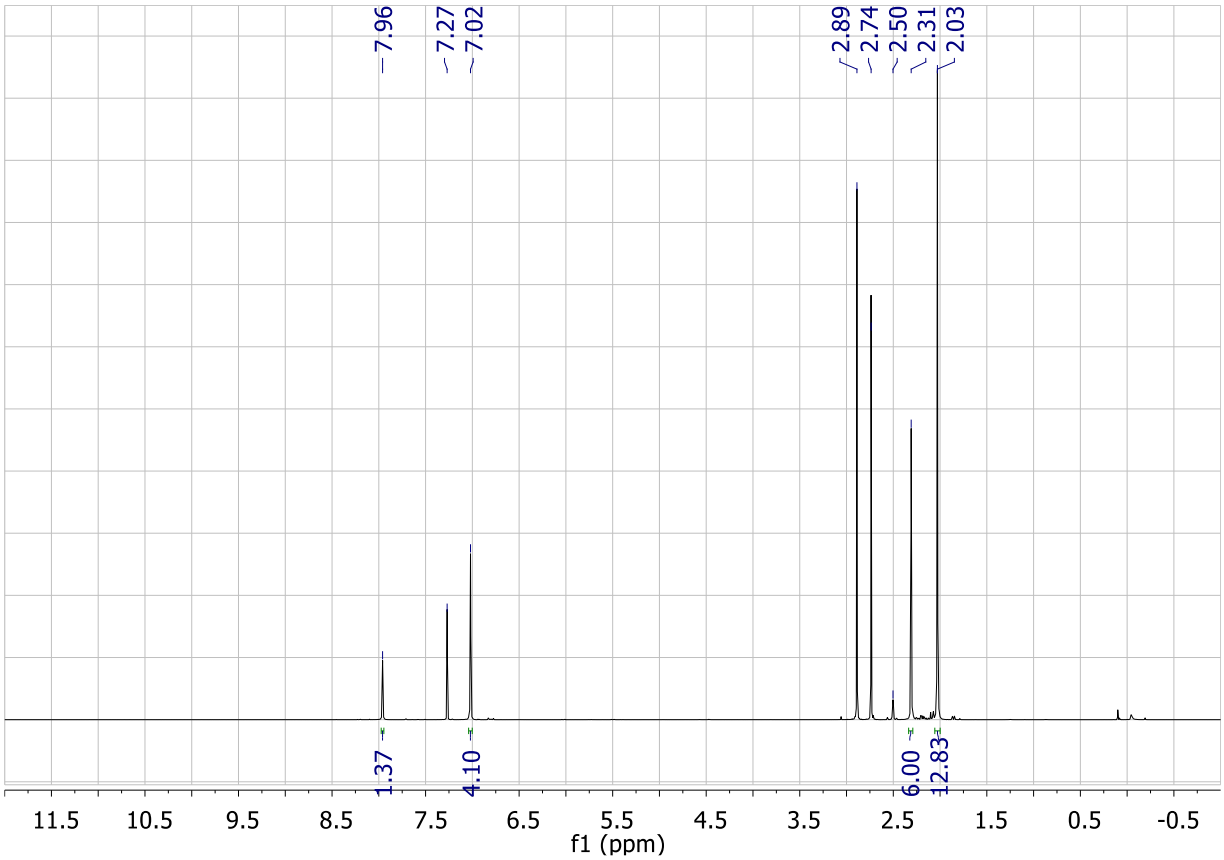
IMes (30 mg) in DMSO-d_6 (0.4 mL) Under PDMS (6,000 g·mol^{-1}, 0.3 mL) (DMF Standard) at Time 0 (^{1}H DMSO-d_6)



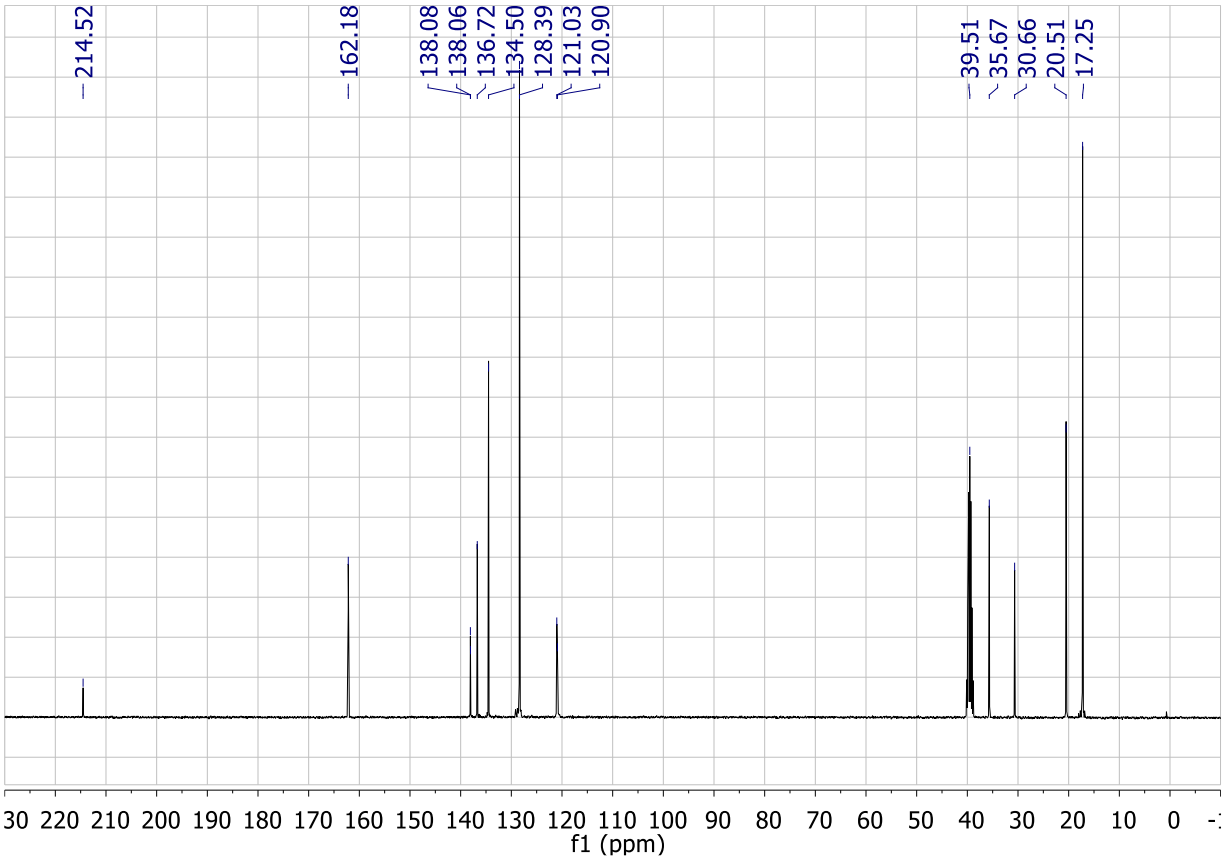
IMes (30 mg) in DMSO-d_6 (0.4 mL) Under PDMS (6,000 g·mol^{-1}, 0.3 mL) (DMF Standard) at Time 0 (^{13}C DMSO-d_6)



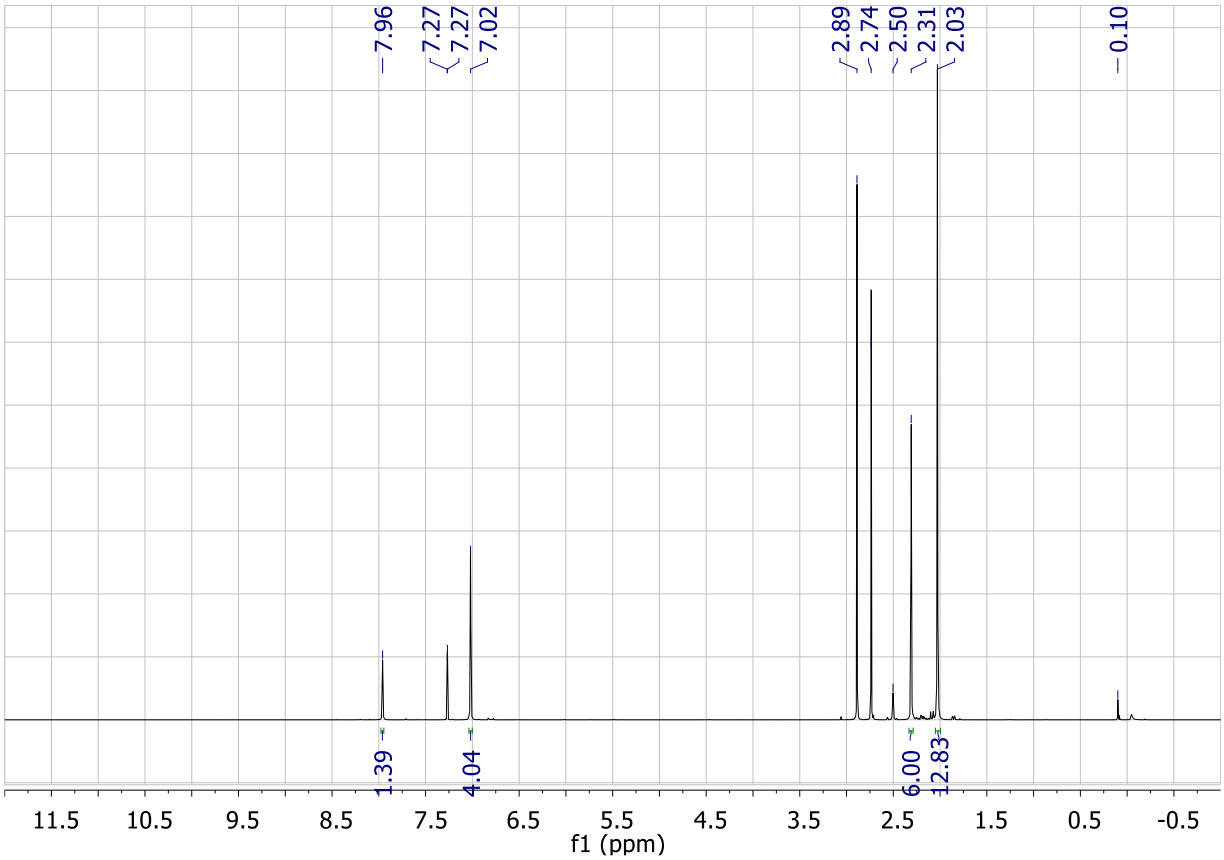
IMes (30 mg) in DMSO-d_6 (0.4 mL) Under PDMS (6,000 g·mol^{-1}, 0.3 mL) (DMF Standard) After 1 Day (^{1}H DMSO-d_6)



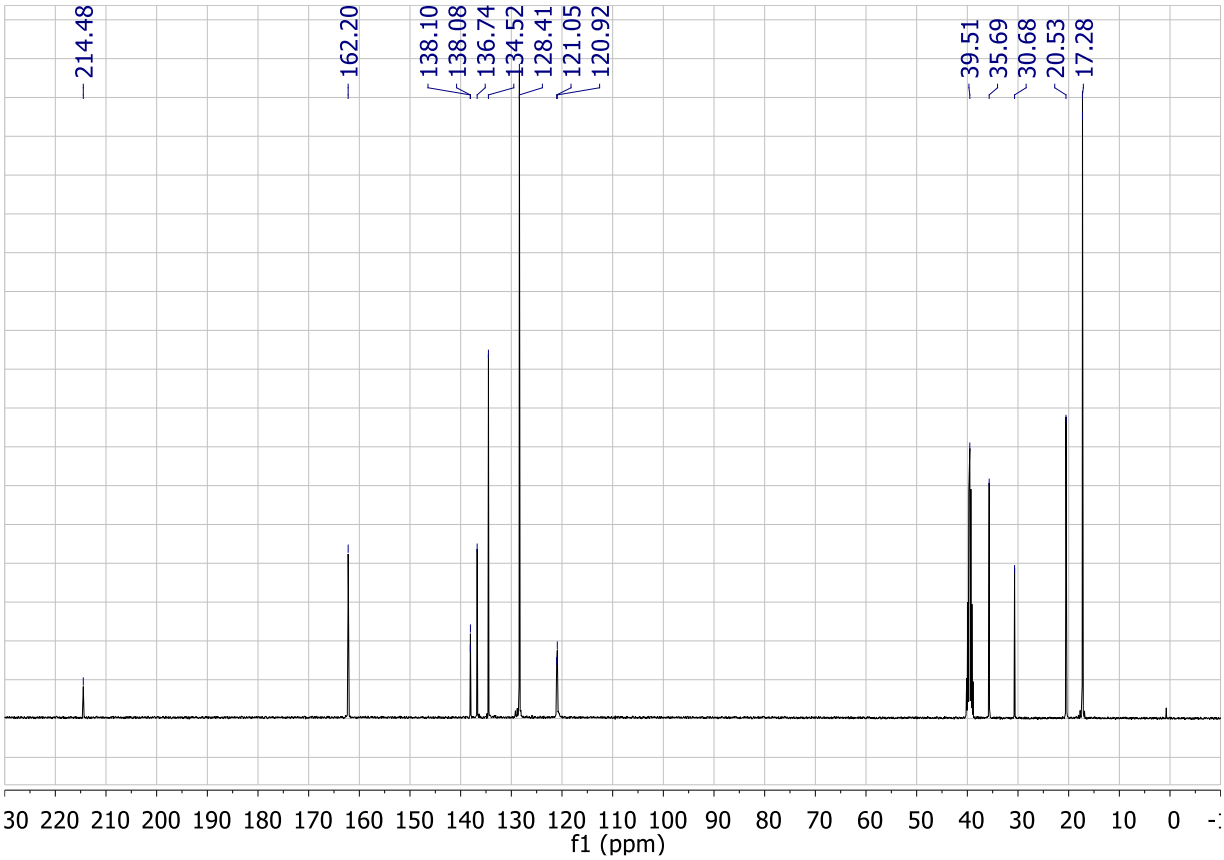
IMes (30 mg) in DMSO-d_6 (0.4 mL) Under PDMS (6,000 g·mol^{-1}, 0.3 mL) (DMF Standard) After 1 Day (^{13}C DMSO-d_6)



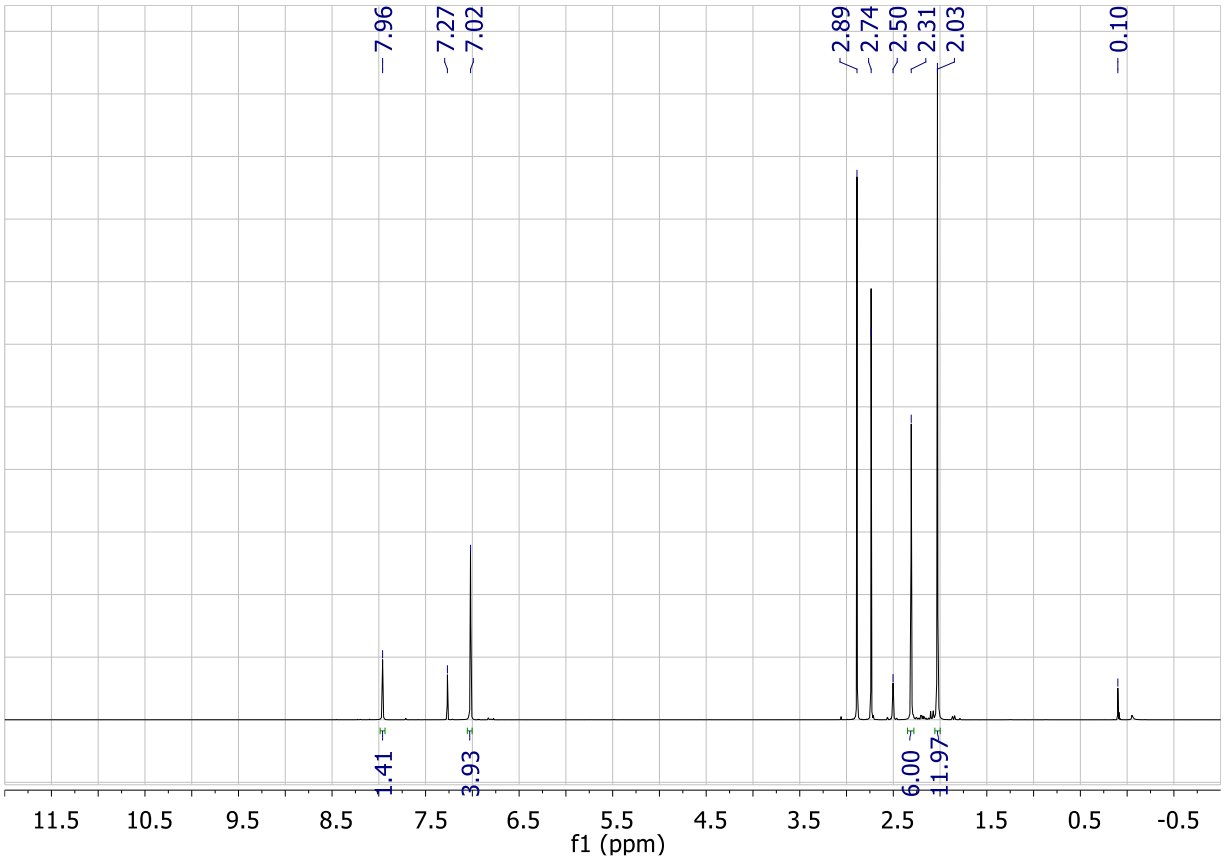
IMes (30 mg) in DMSO-d_6 (0.4 mL) Under PDMS (6,000 g·mol^{-1}, 0.3 mL) (DMF Standard) After 2 Days (^{1}H DMSO-d_6)



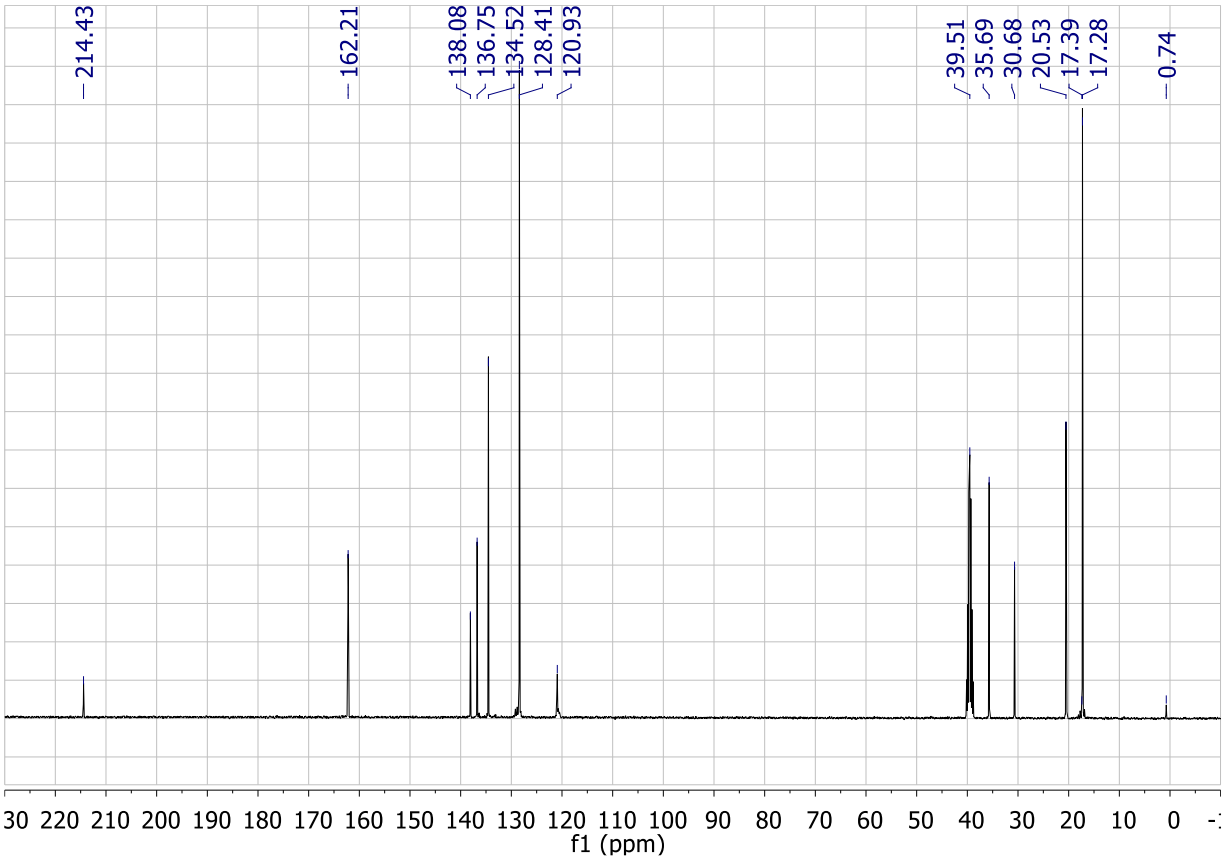
IMes (30 mg) in DMSO-d_6 (0.4 mL) Under PDMS (6,000 g·mol^{-1}, 0.3 mL) (DMF Standard) After 2 Days (^{13}C DMSO-d_6)



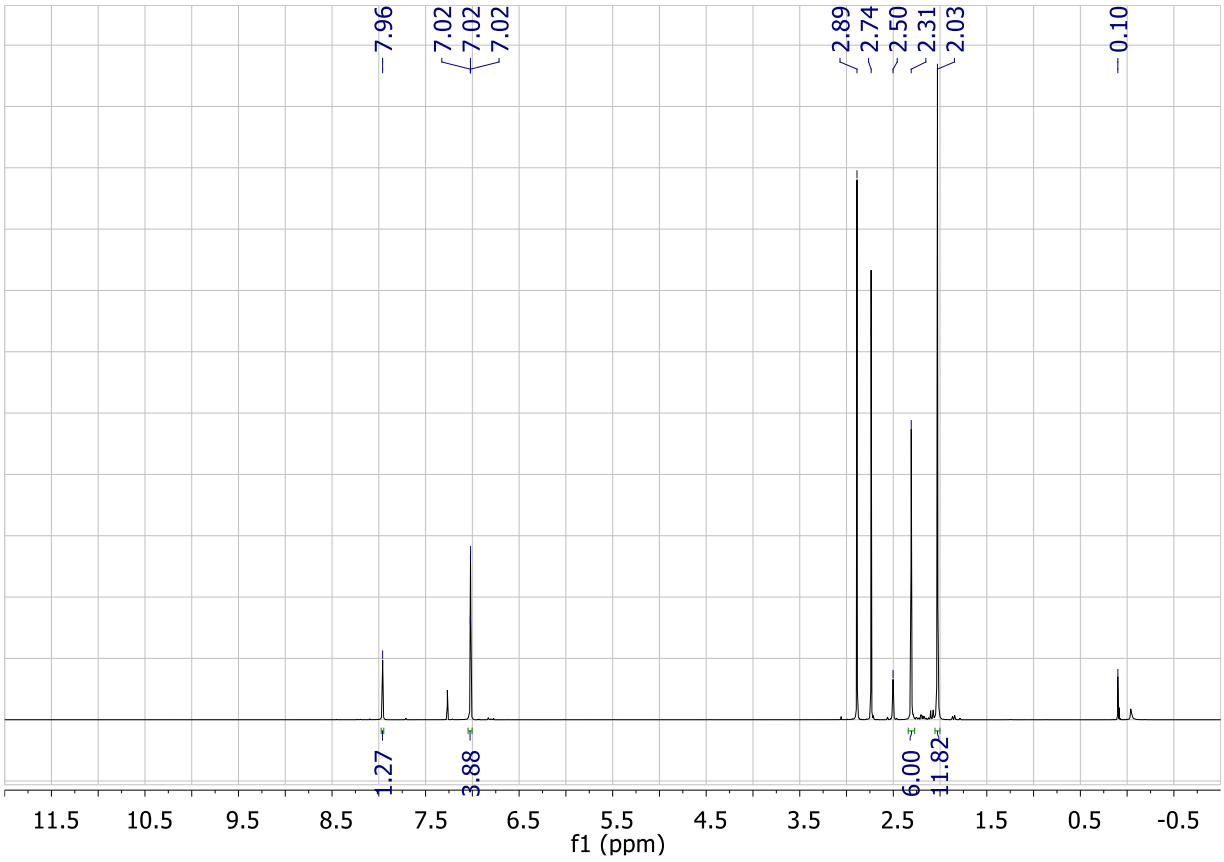
IMes (30 mg) in DMSO-d_6 (0.4 mL) Under PDMS (6,000 g·mol^{-1}, 0.3 mL) (DMF Standard) After 5 Days (^{1}H DMSO-d_6)



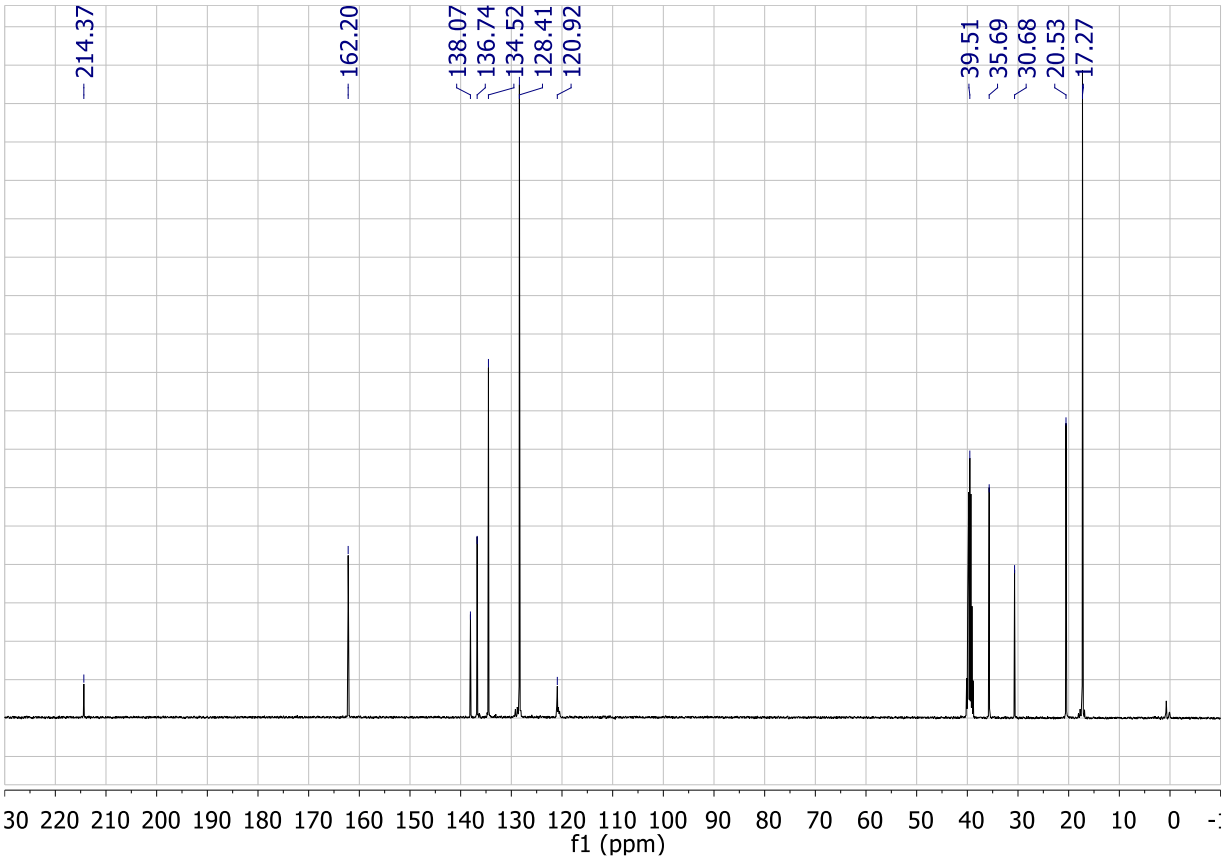
IMes (30 mg) in DMSO-d_6 (0.4 mL) Under PDMS (6,000 g·mol^{-1}, 0.3 mL) (DMF Standard) After 5 Days (^{13}C DMSO-d_6)



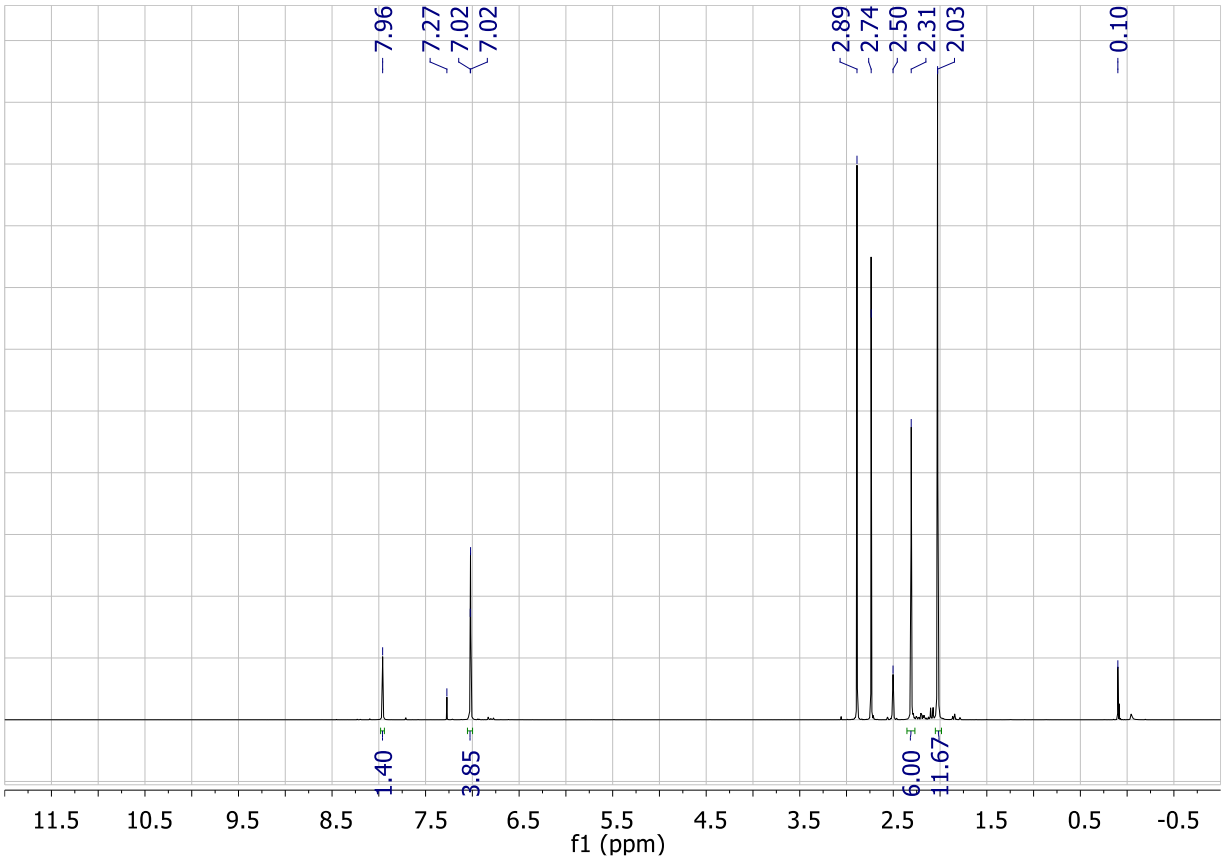
IMes (30 mg) in DMSO-d_6 (0.4 mL) Under PDMS (6,000 g·mol^{-1}, 0.3 mL) (DMF Standard) After 8 Days (^{1}H DMSO-d_6)



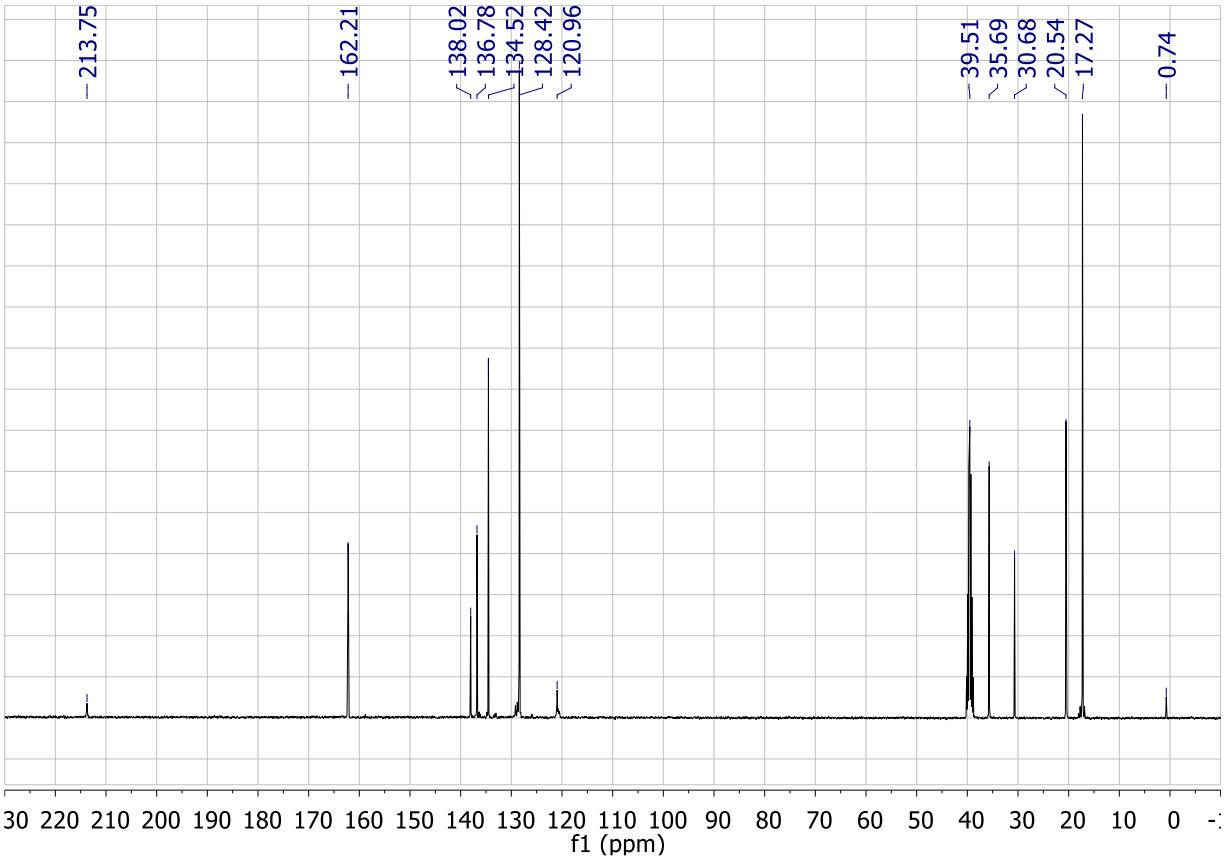
IMes (30 mg) in DMSO-d_6 (0.4 mL) Under PDMS (6,000 g·mol^{-1}, 0.3 mL) (DMF Standard) After 8 Days (^{13}C DMSO-d_6)



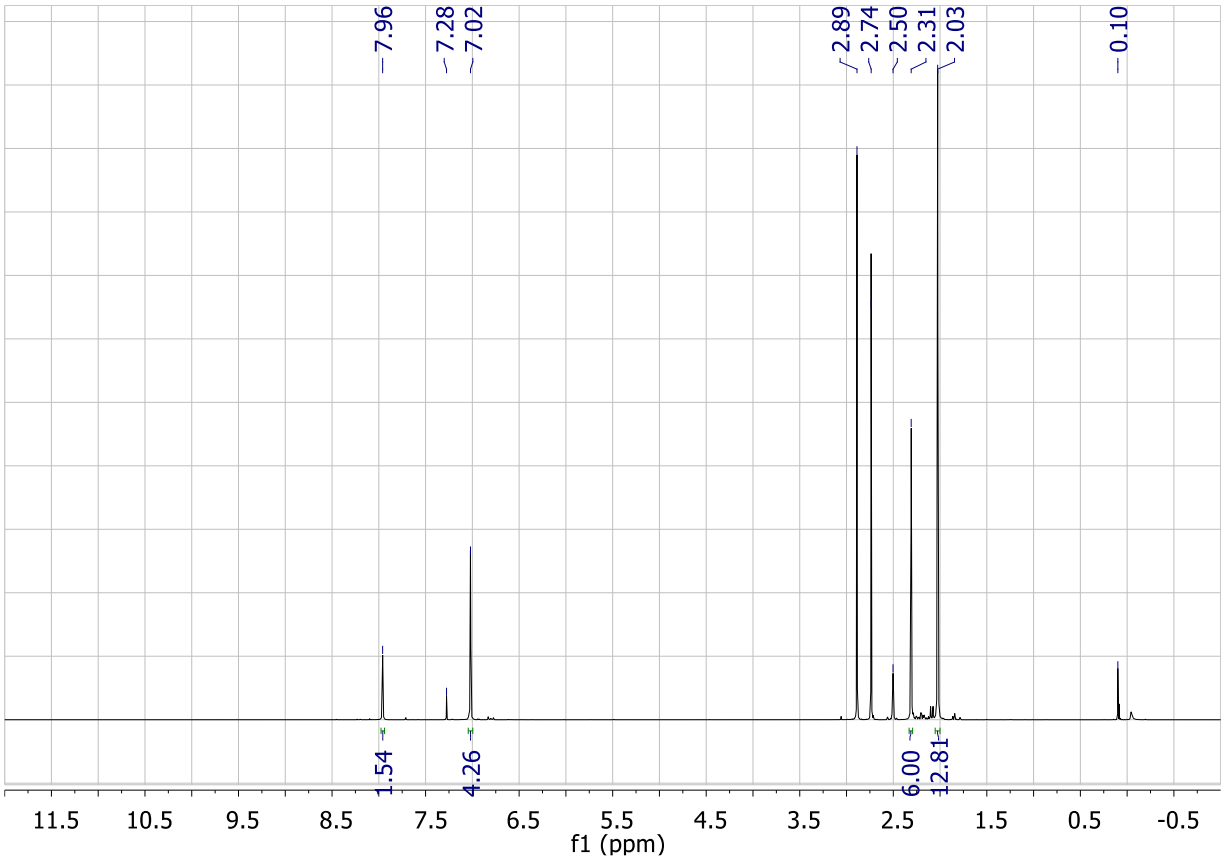
IMes (30 mg) in DMSO-d_6 (0.4 mL) Under PDMS (6,000 g·mol^{-1}, 0.3 mL) (DMF Standard) After 13 Days (^{1}H DMSO-d_6)



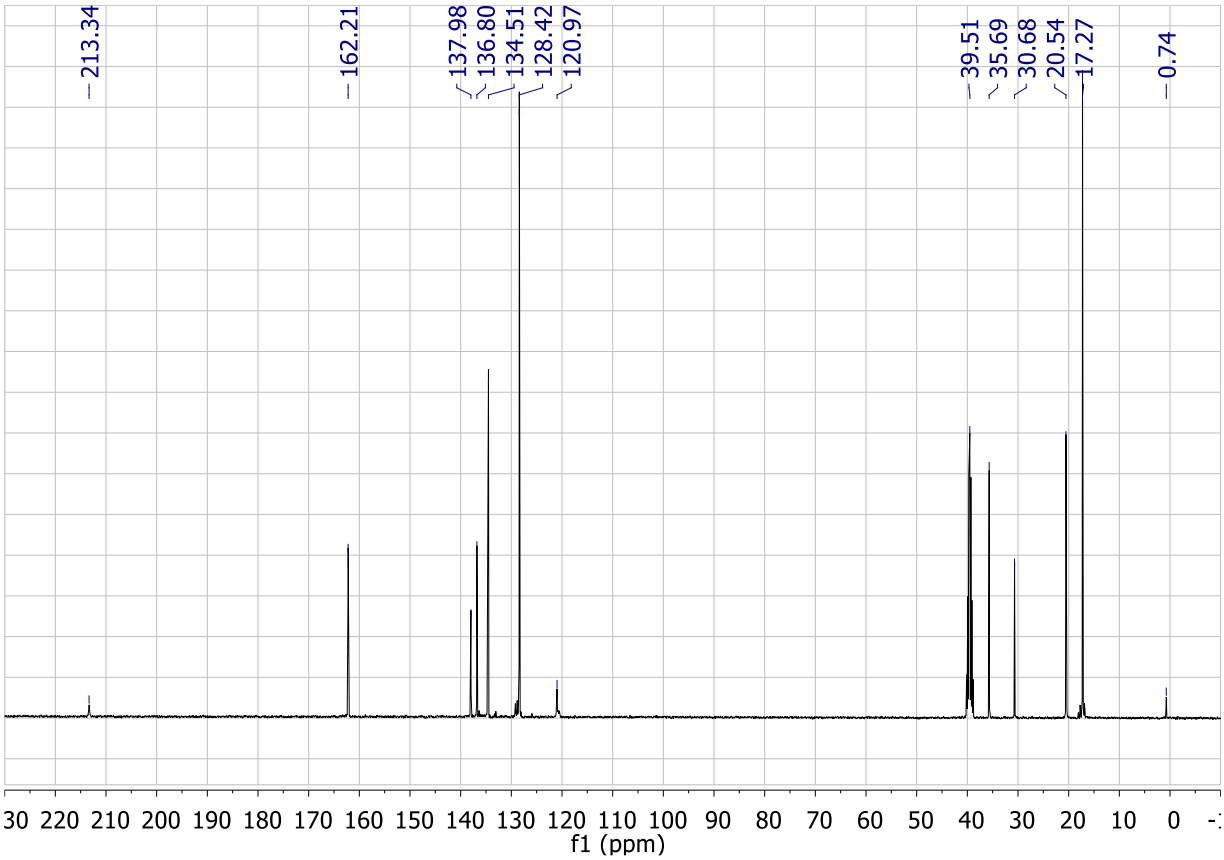
IMes (30 mg) in DMSO-d_6 (0.4 mL) Under PDMS (6,000 g·mol^{-1}, 0.3 mL) (DMF Standard) After 13 Days (^{13}C DMSO-d_6)



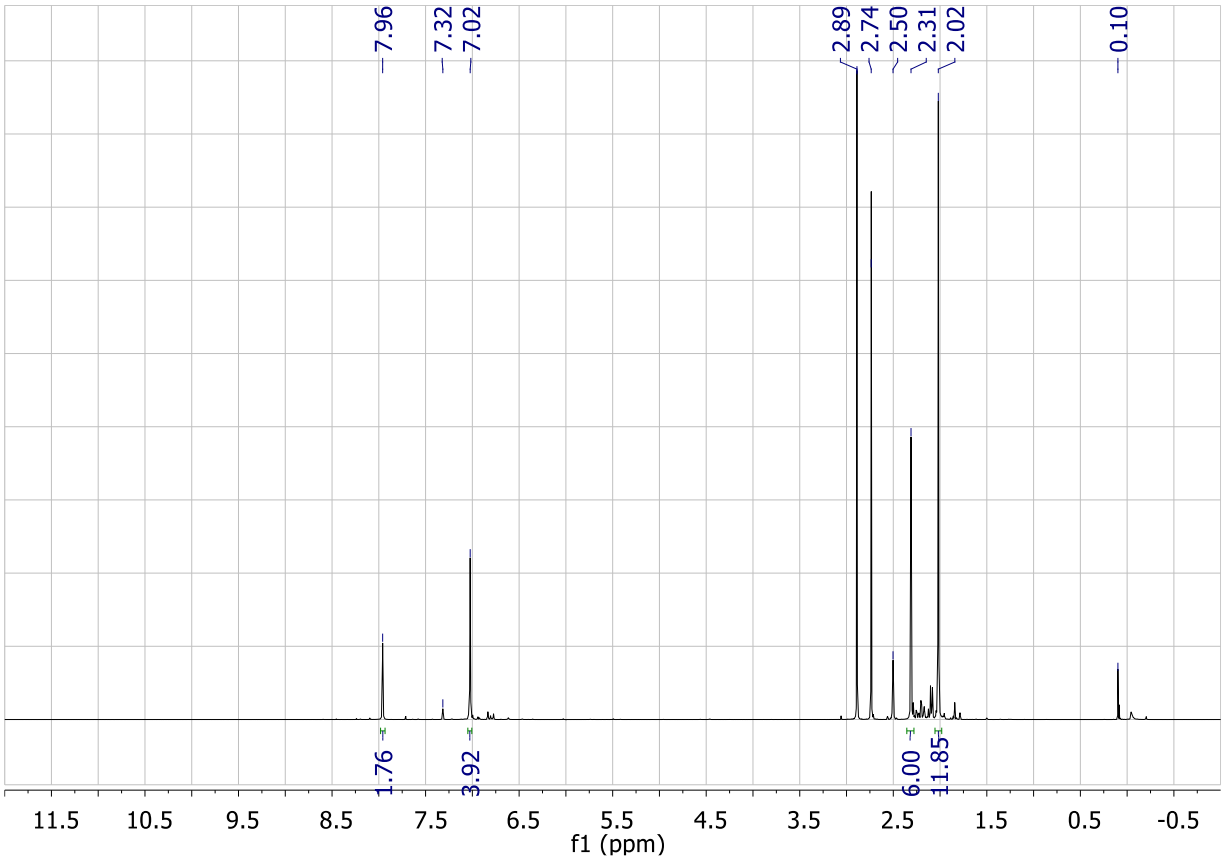
IMes (30 mg) in DMSO-d_6 (0.4 mL) Under PDMS (6,000 g·mol^{-1}, 0.3 mL) (DMF Standard) After 14 Days (^{1}H DMSO-d_6)



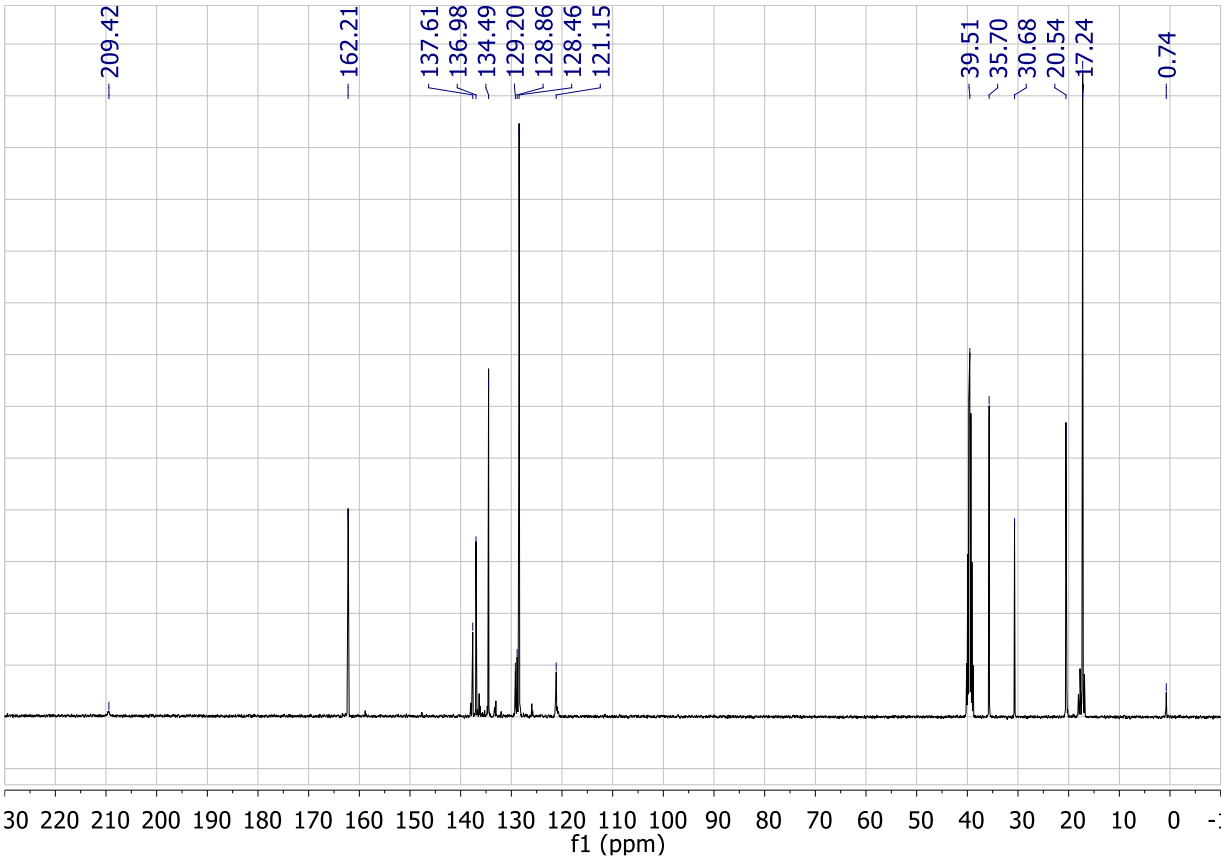
IMes (30 mg) in DMSO-d_6 (0.4 mL) Under PDMS (6,000 g·mol^{-1}, 0.3 mL) (DMF Standard) After 14 Days (^{13}C DMSO-d_6)



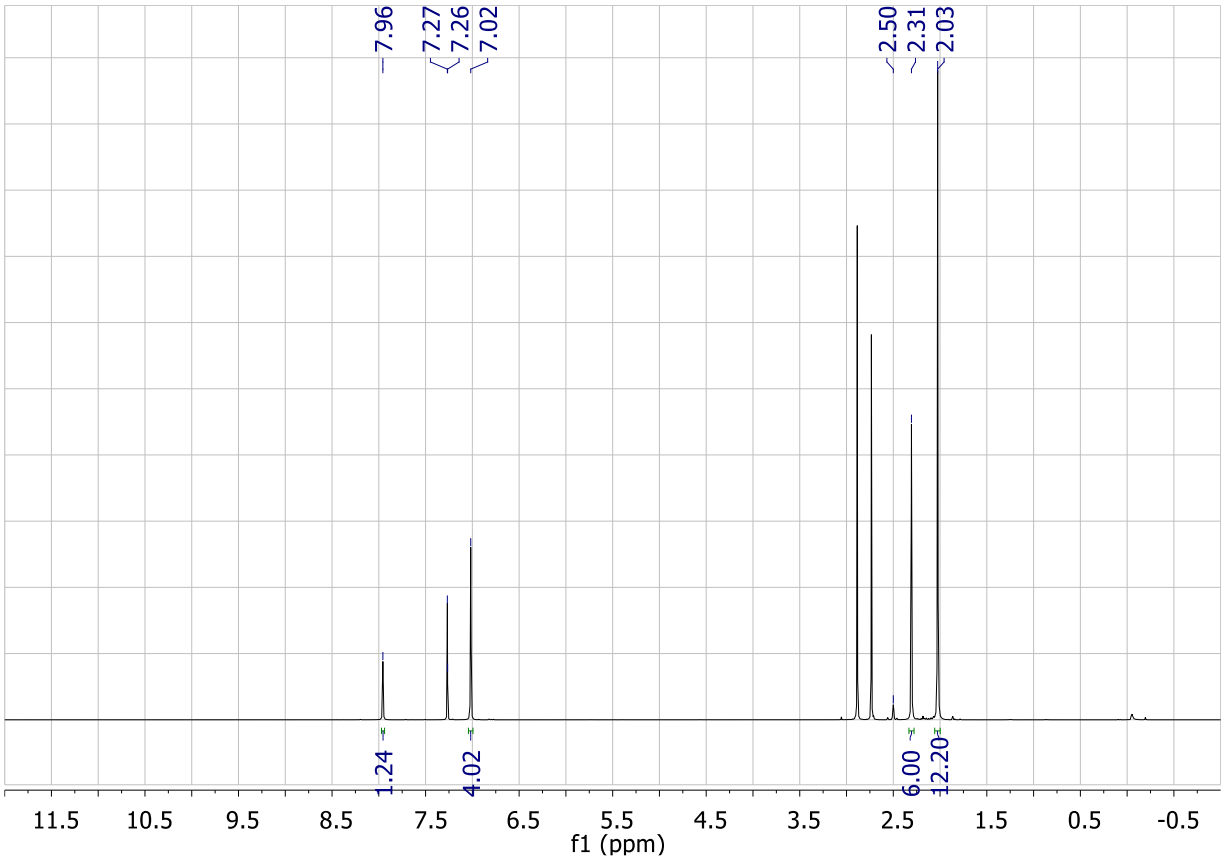
IMes (30 mg) in DMSO-d_6 (0.4 mL) Under PDMS (6,000 g·mol^{-1}, 0.3 mL) (DMF Standard) After 20 Days (^{1}H DMSO-d_6)



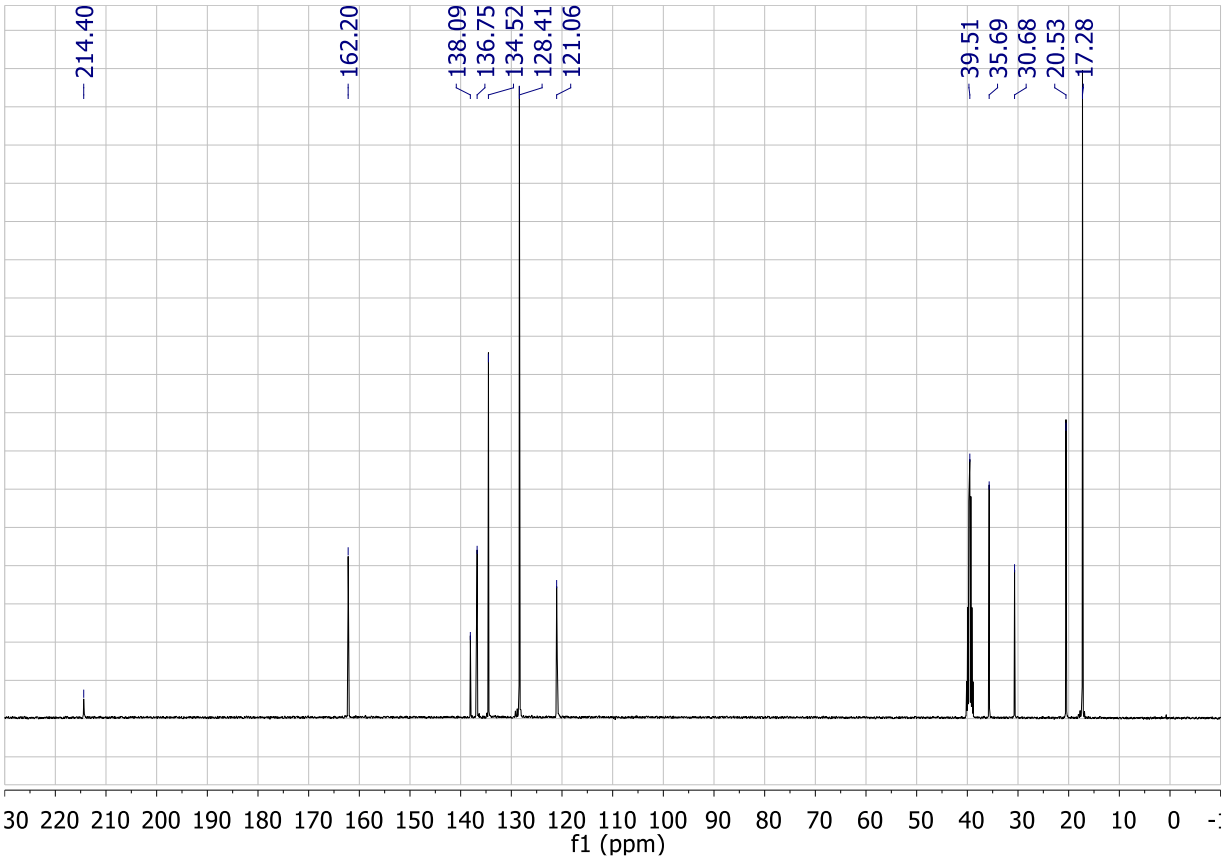
IMes (30 mg) in DMSO-d_6 (0.4 mL) Under PDMS (6,000 g·mol^{-1}, 0.3 mL) (DMF Standard) After 20 Days (^{13}C DMSO-d_6)



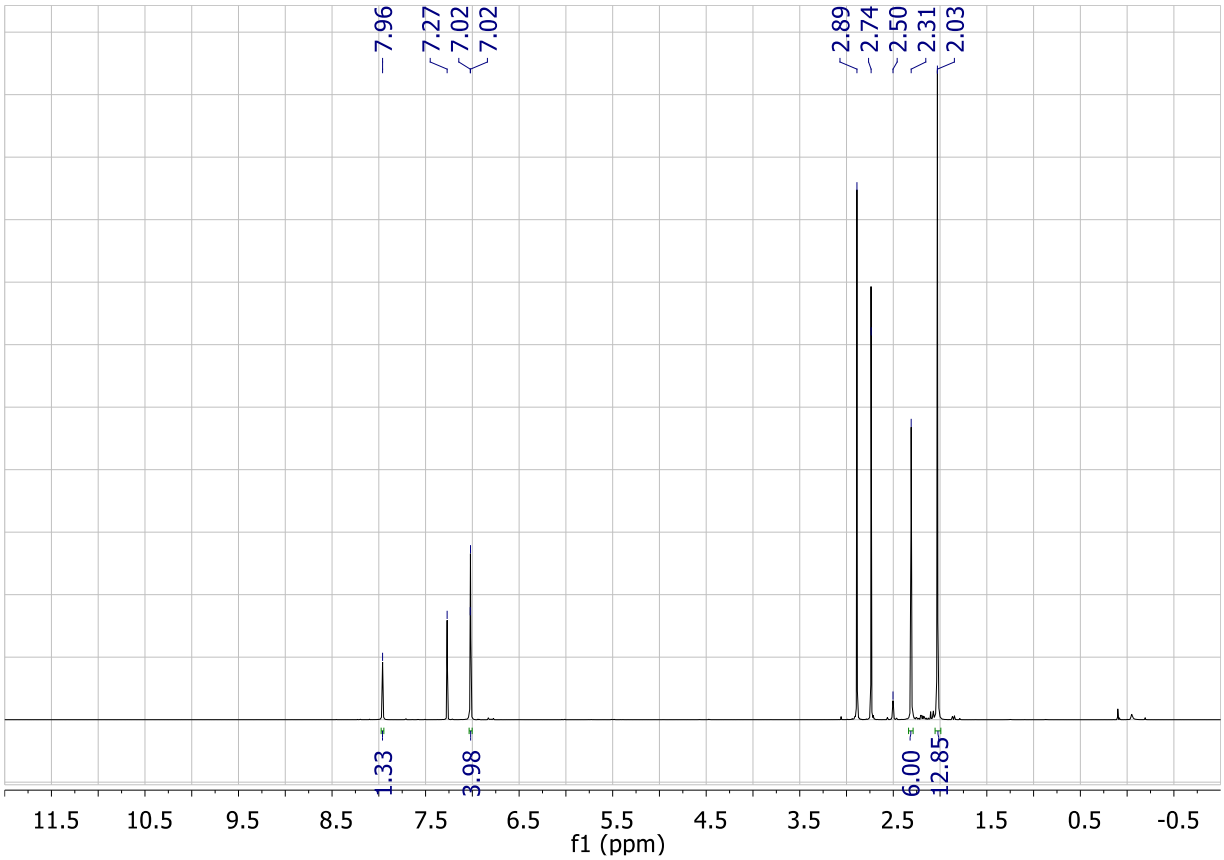
IMes (30 mg) in DMSO-d_6 (0.4 mL) Under PDMS (9,000 g·mol^{-1}, 0.3 mL) (DMF Standard) at Time 0 (^{1}H DMSO-d_6)



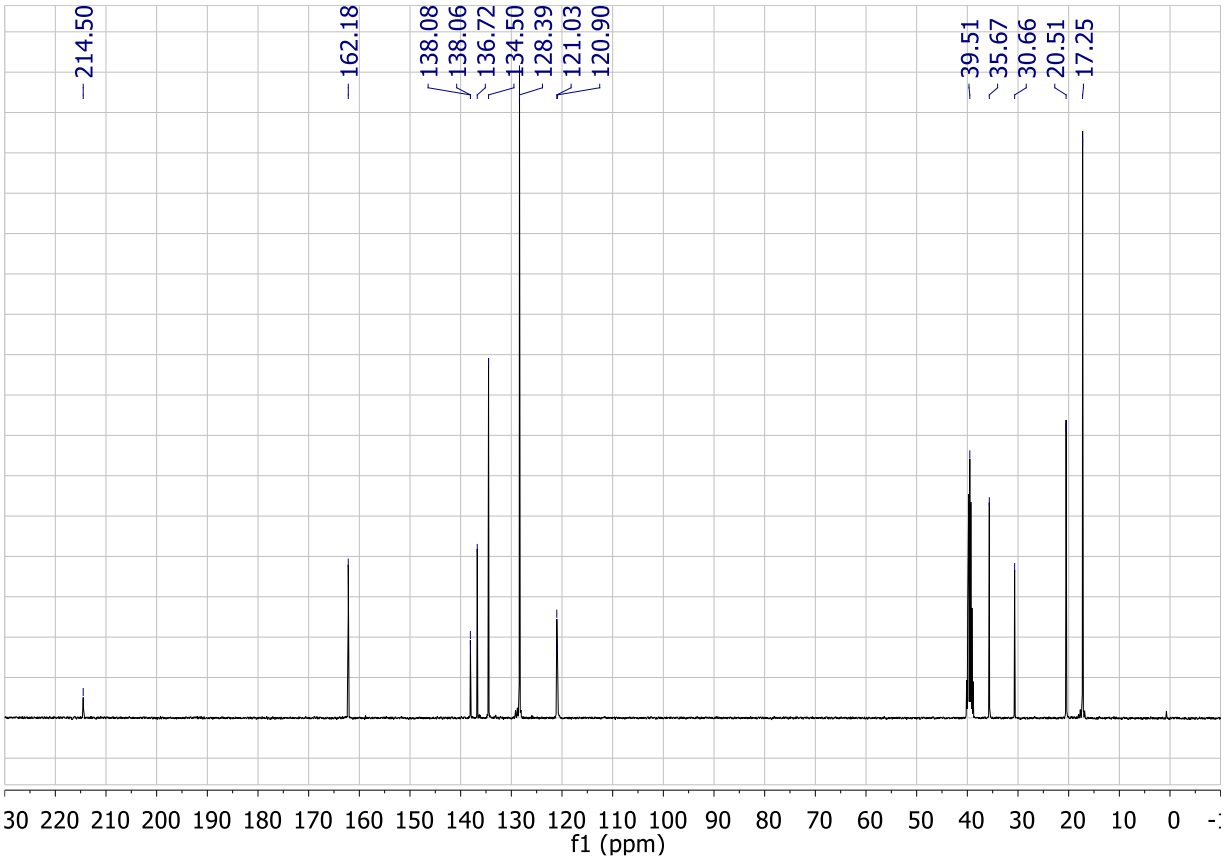
IMes (30 mg) in DMSO-d_6 (0.4 mL) Under PDMS (9,000 g·mol^{-1}, 0.3 mL) (DMF Standard) at Time 0 (^{13}C DMSO-d_6)



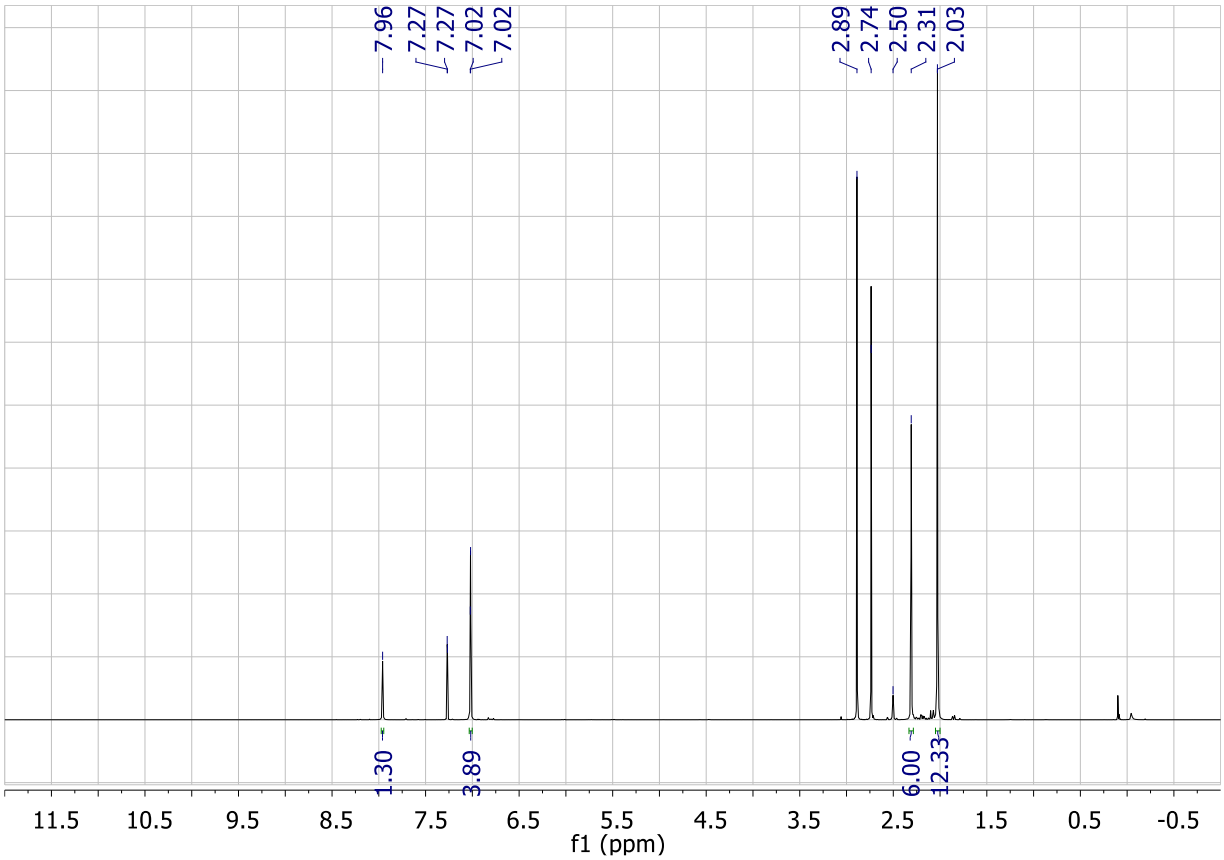
IMes (30 mg) in DMSO-d_6 (0.4 mL) Under PDMS (9,000 g·mol^{-1}, 0.3 mL) (DMF Standard) After 1 Day (^{1}H DMSO-d_6)



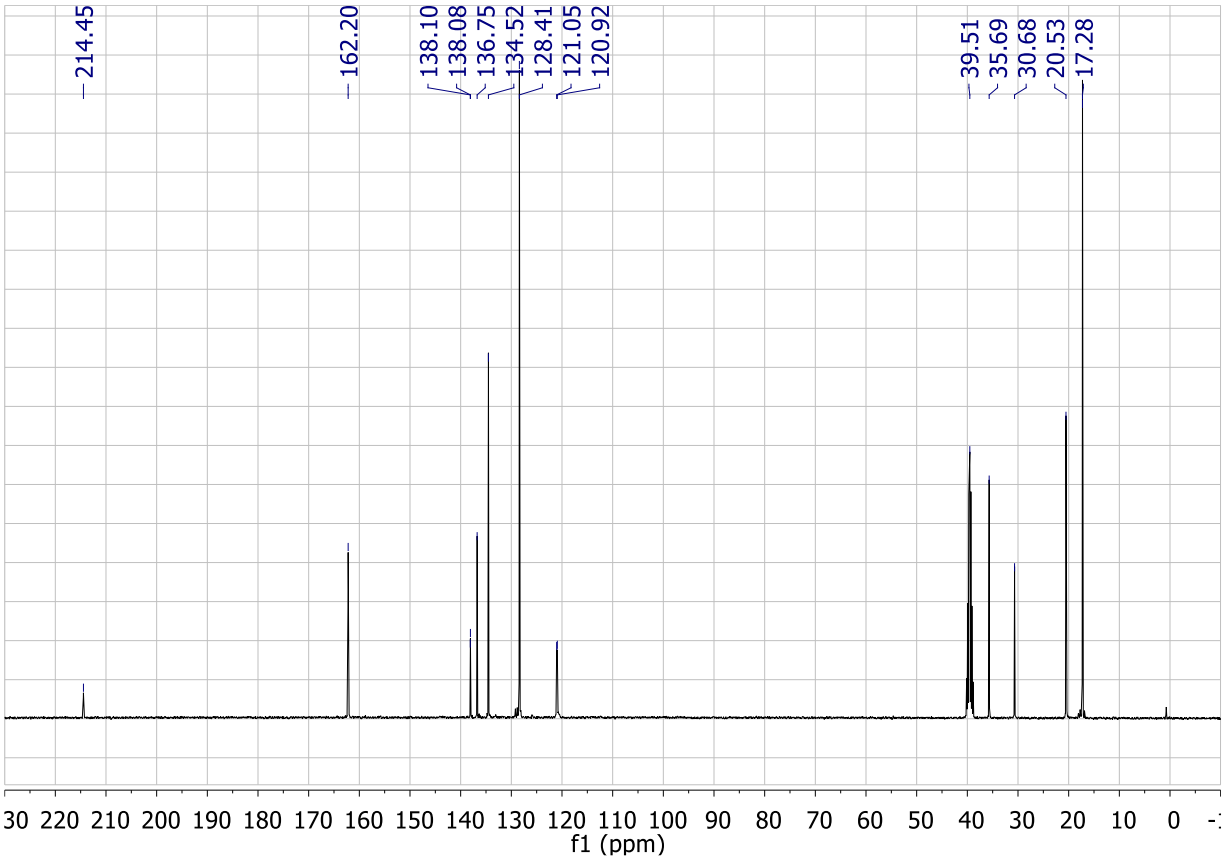
IMes (30 mg) in DMSO-d_6 (0.4 mL) Under PDMS (9,000 g·mol^{-1}, 0.3 mL) (DMF Standard) After 1 Day (^{13}C DMSO-d_6)



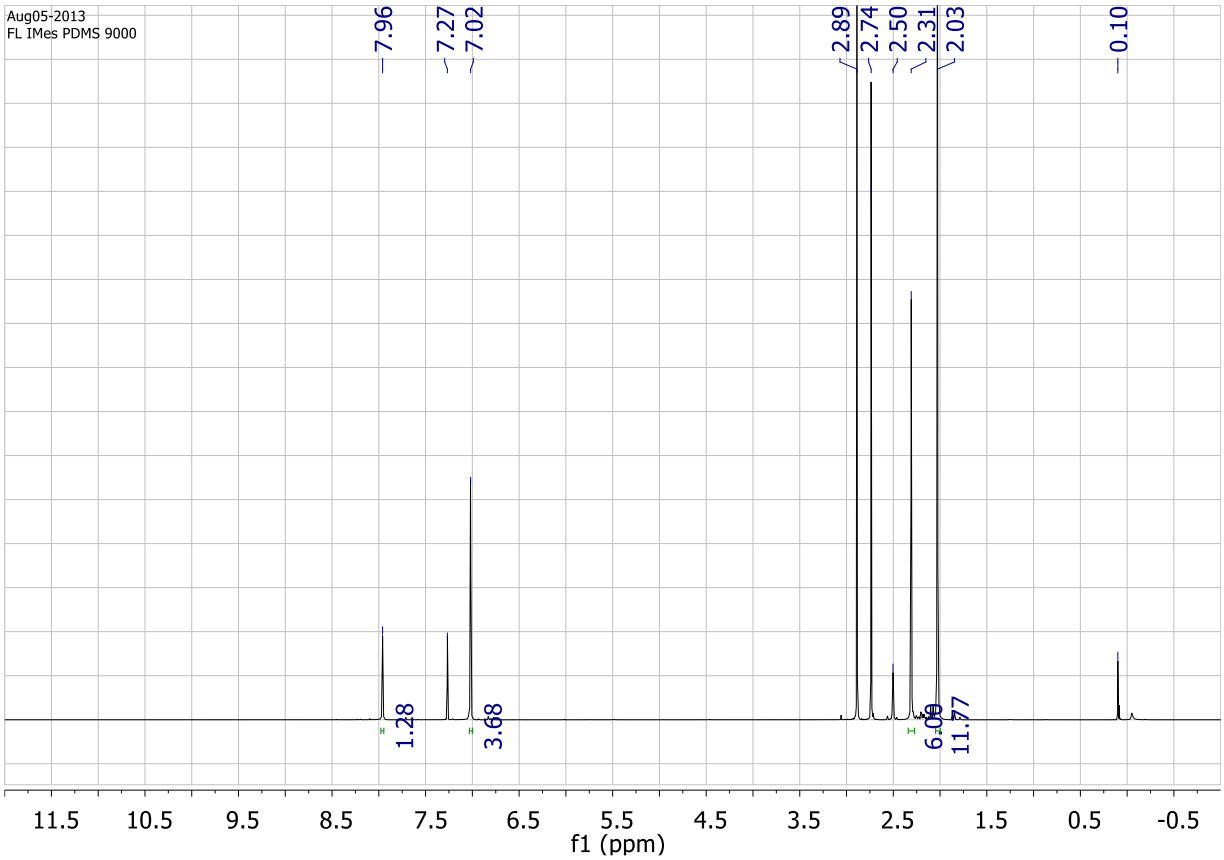
IMes (30 mg) in DMSO-d_6 (0.4 mL) Under PDMS (9,000 g·mol^{-1}, 0.3 mL) (DMF Standard) After 2 Days (^{1}H DMSO-d_6)



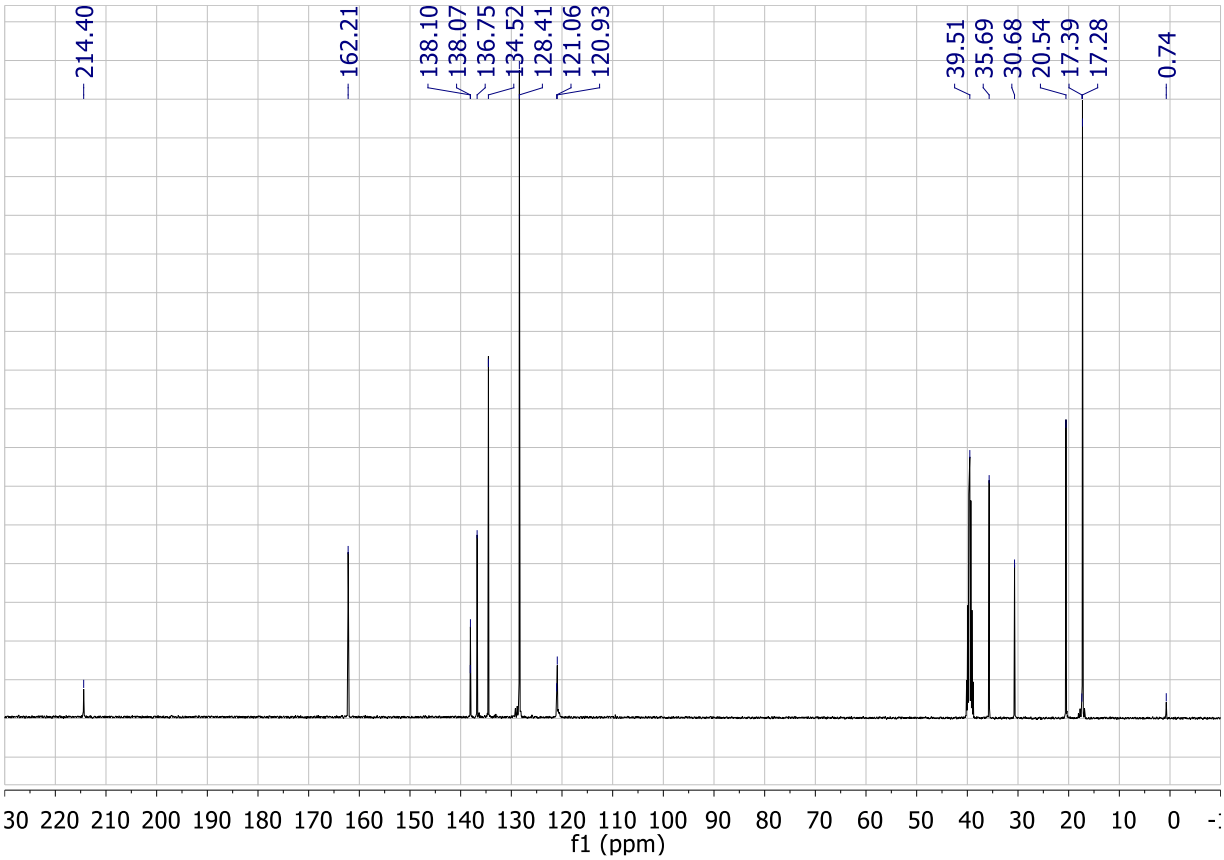
IMes (30 mg) in DMSO-d_6 (0.4 mL) Under PDMS (9,000 g·mol^{-1}, 0.3 mL) (DMF Standard) After 2 Days (^{13}C DMSO-d_6)



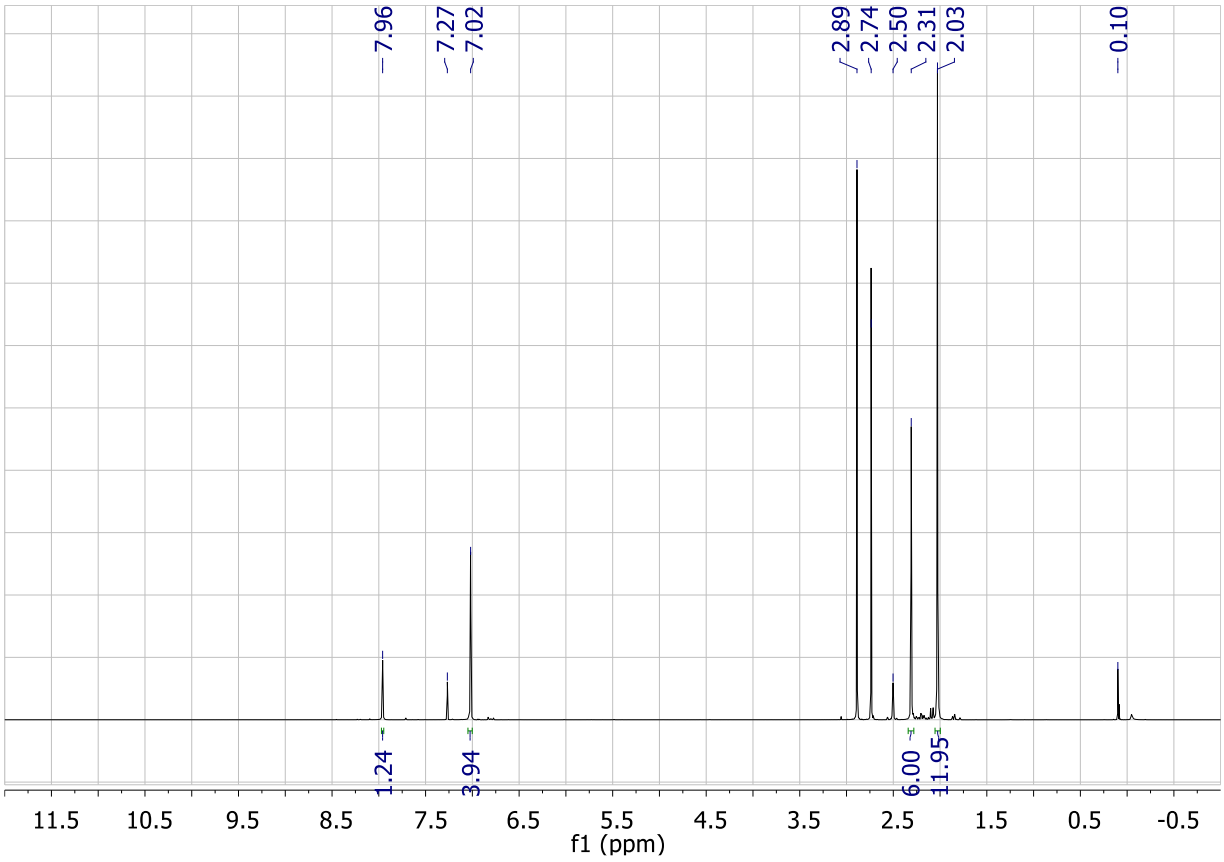
IMes (30 mg) in DMSO-d_6 (0.4 mL) Under PDMS (9,000 g·mol^{-1}, 0.3 mL) (DMF Standard) After 5 Days (^{1}H DMSO-d_6)



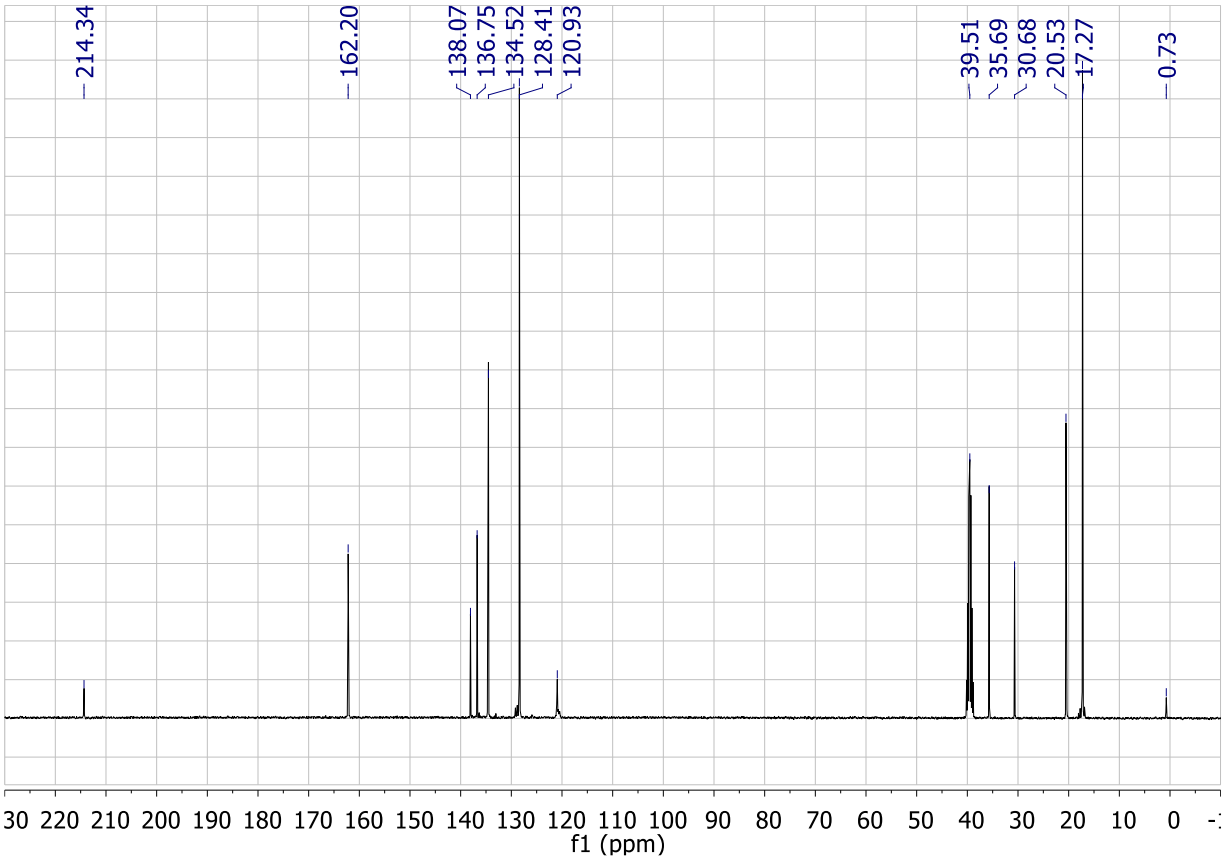
IMes (30 mg) in DMSO-d_6 (0.4 mL) Under PDMS (9,000 g·mol^{-1}, 0.3 mL) (DMF Standard) After 5 Days (^{13}C DMSO-d_6)



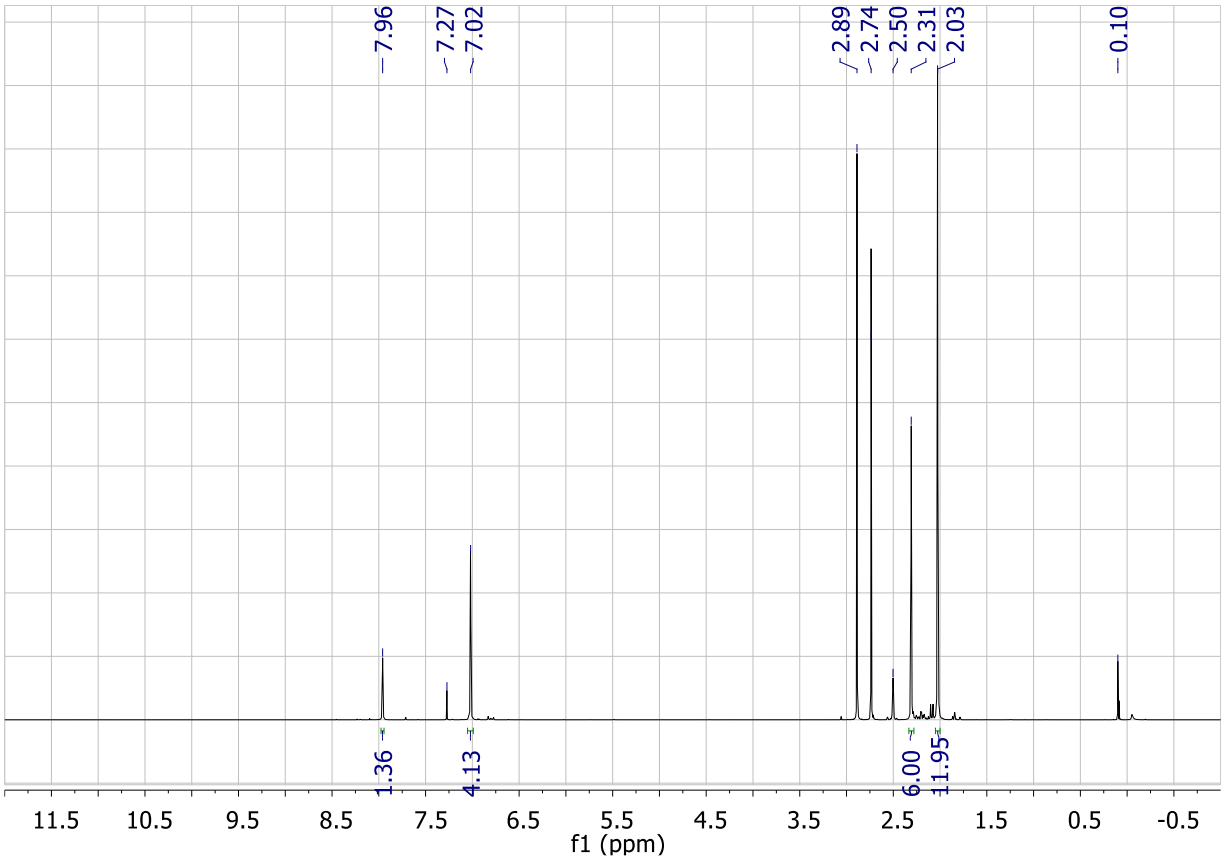
IMes (30 mg) in DMSO-d_6 (0.4 mL) Under PDMS (9,000 g·mol^{-1}, 0.3 mL) (DMF Standard) After 8 Days (^{1}H DMSO-d_6)



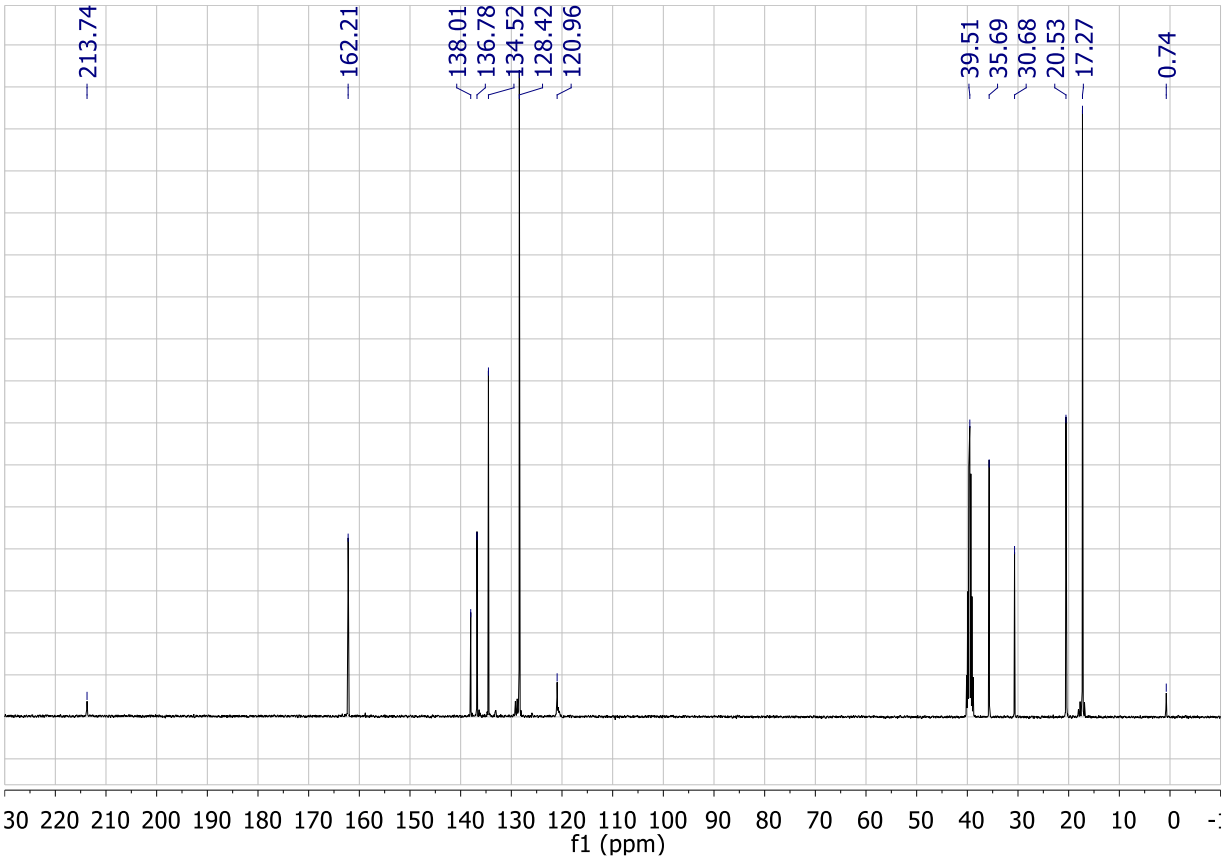
IMes (30 mg) in DMSO-d_6 (0.4 mL) Under PDMS (9,000 g·mol^{-1}, 0.3 mL) (DMF Standard) After 8 Days (^{13}C DMSO-d_6)



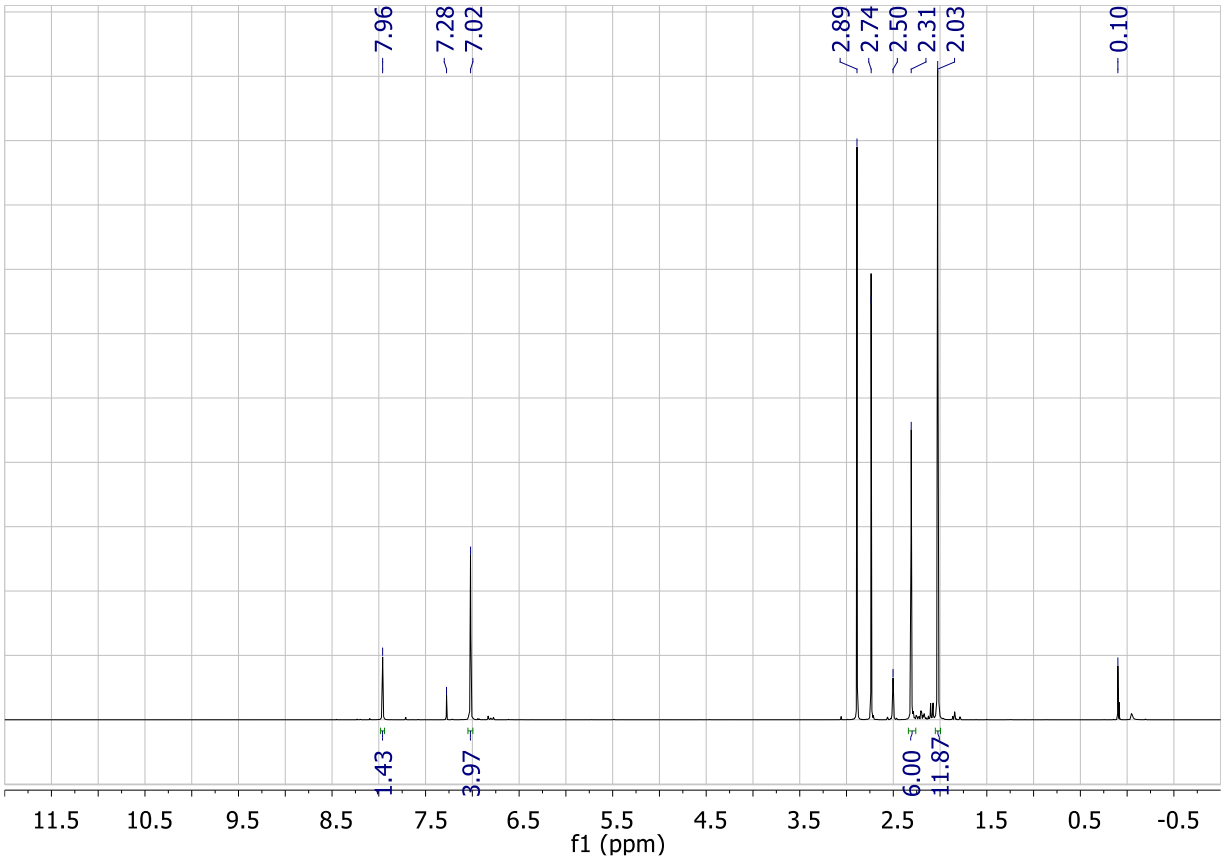
IMes (30 mg) in DMSO-d_6 (0.4 mL) Under PDMS (9,000 g·mol^{-1}, 0.3 mL) (DMF Standard) After 13 Days (^{1}H DMSO-d_6)



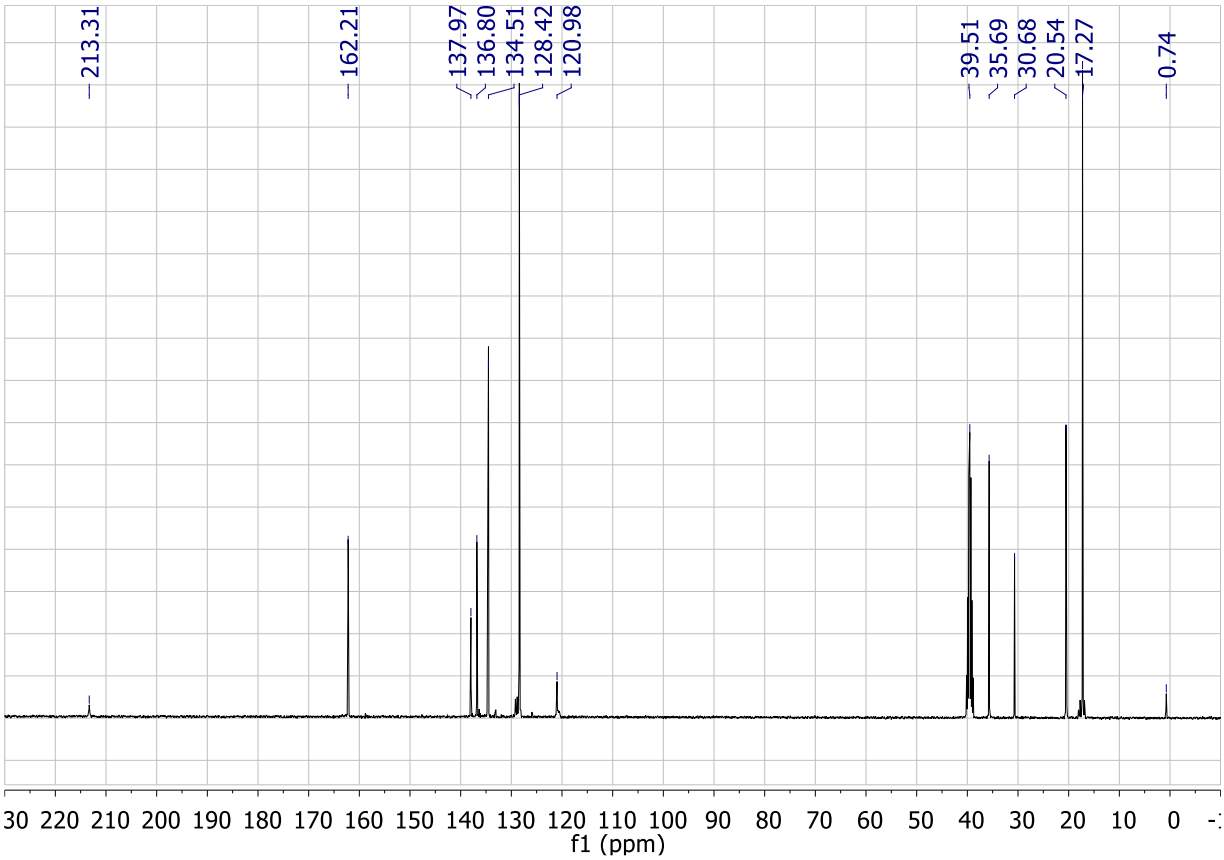
IMes (30 mg) in DMSO-d_6 (0.4 mL) Under PDMS (9,000 g·mol^{-1}, 0.3 mL) (DMF Standard) After 13 Days (^{13}C DMSO-d_6)



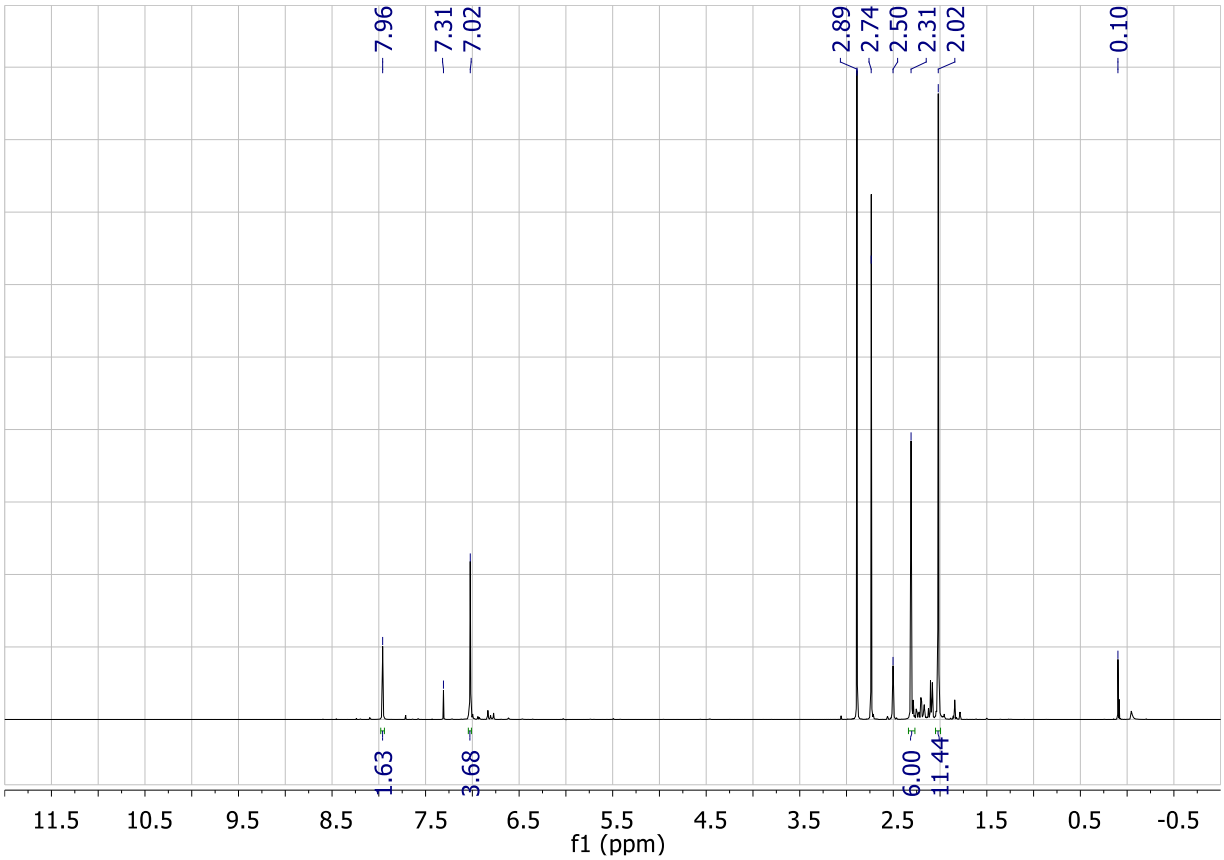
IMes (30 mg) in DMSO-d_6 (0.4 mL) Under PDMS (9,000 g·mol^{-1}, 0.3 mL) (DMF Standard) After 14 Days (^{1}H DMSO-d_6)



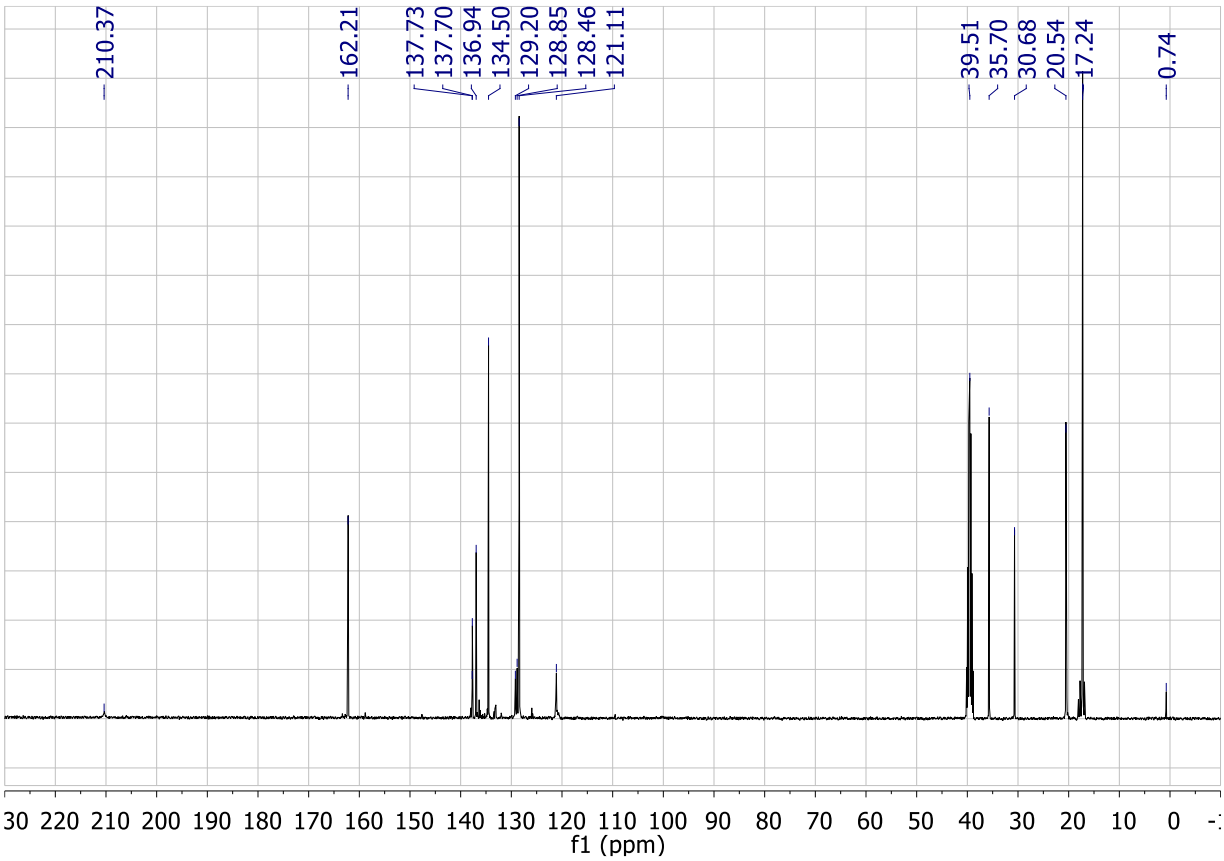
IMes (30 mg) in DMSO-d_6 (0.4 mL) Under PDMS (9,000 g·mol^{-1}, 0.3 mL) (DMF Standard) After 14 Days (^{13}C DMSO-d_6)



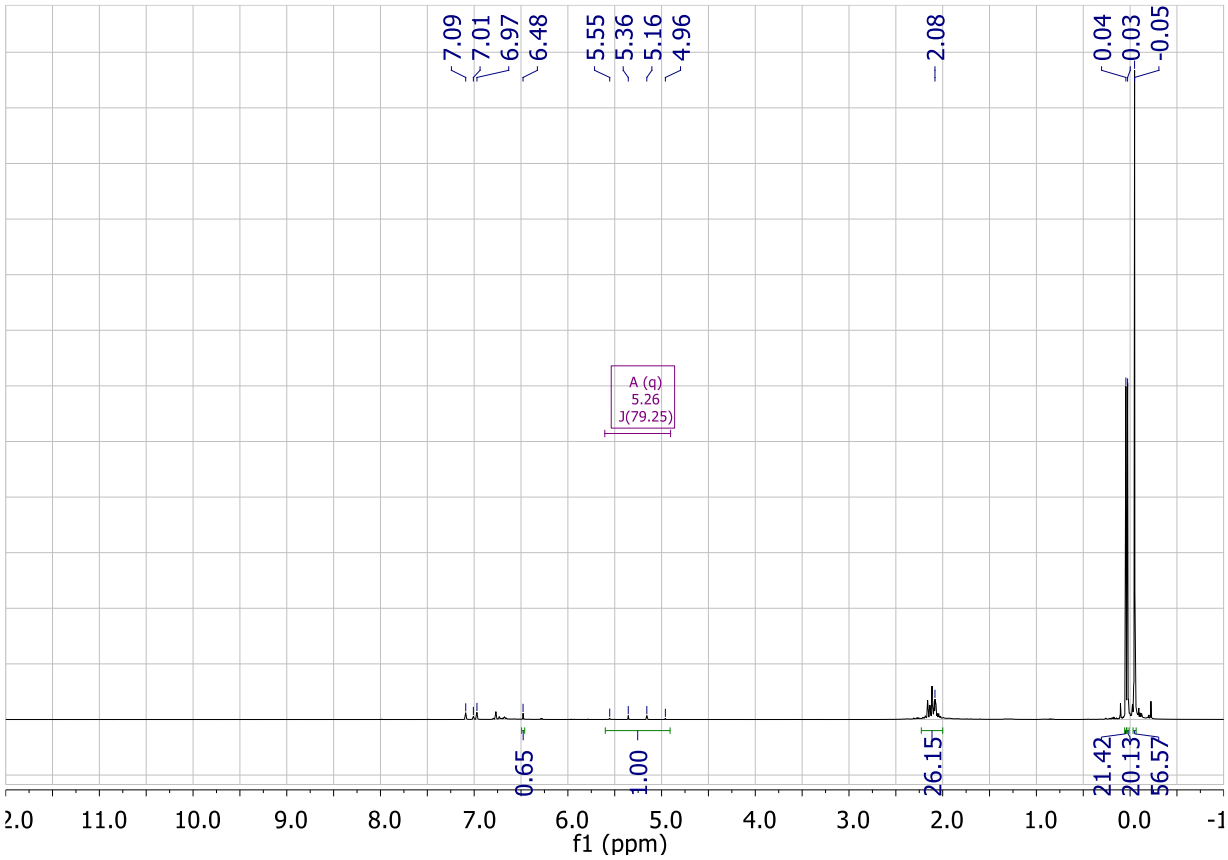
IMes (30 mg) in DMSO-d_6 (0.4 mL) Under PDMS (9,000 g·mol^{-1}, 0.3 mL) (DMF Standard) After 20 Days (^{1}H DMSO-d_6)



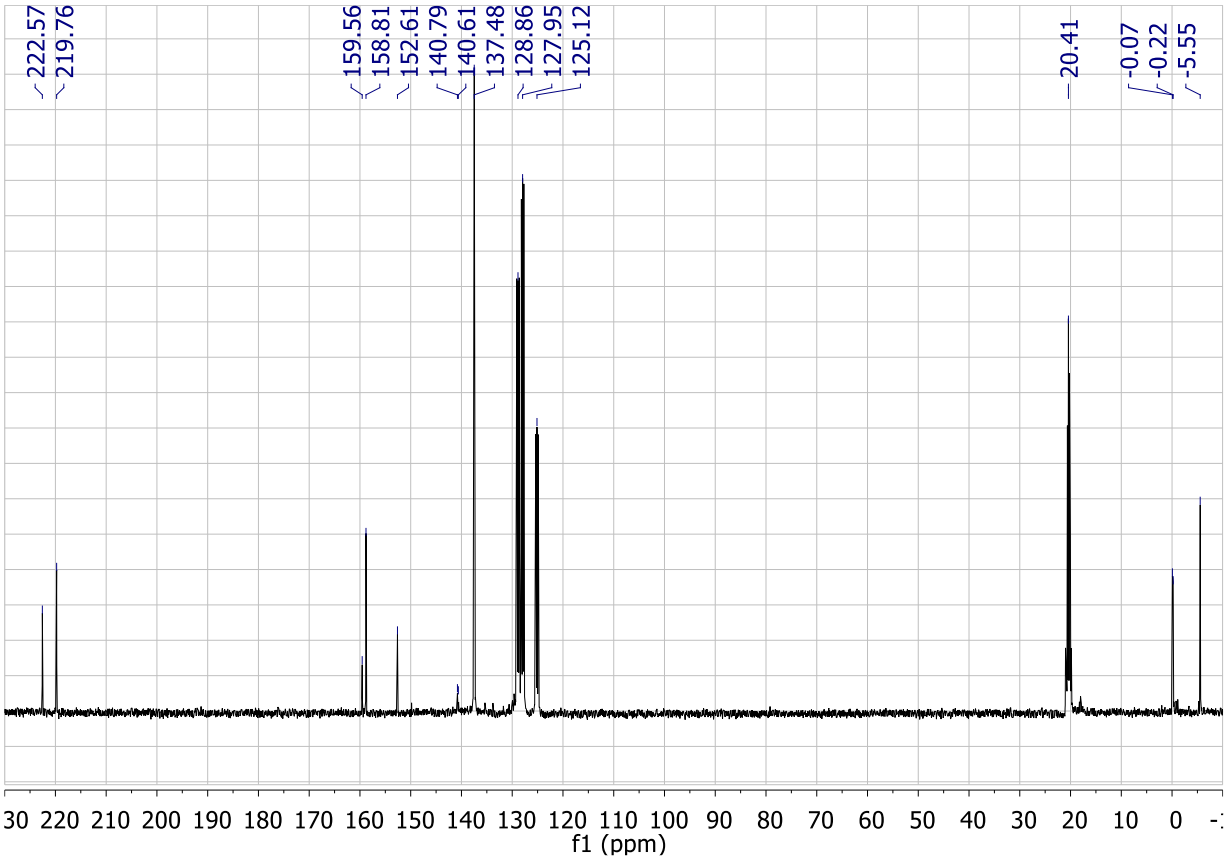
IMes (30 mg) in DMSO-d_6 (0.4 mL) Under PDMS (9,000 g·mol^{-1}, 0.3 mL) (DMF Standard) After 20 Days (^{13}C DMSO-d_6)



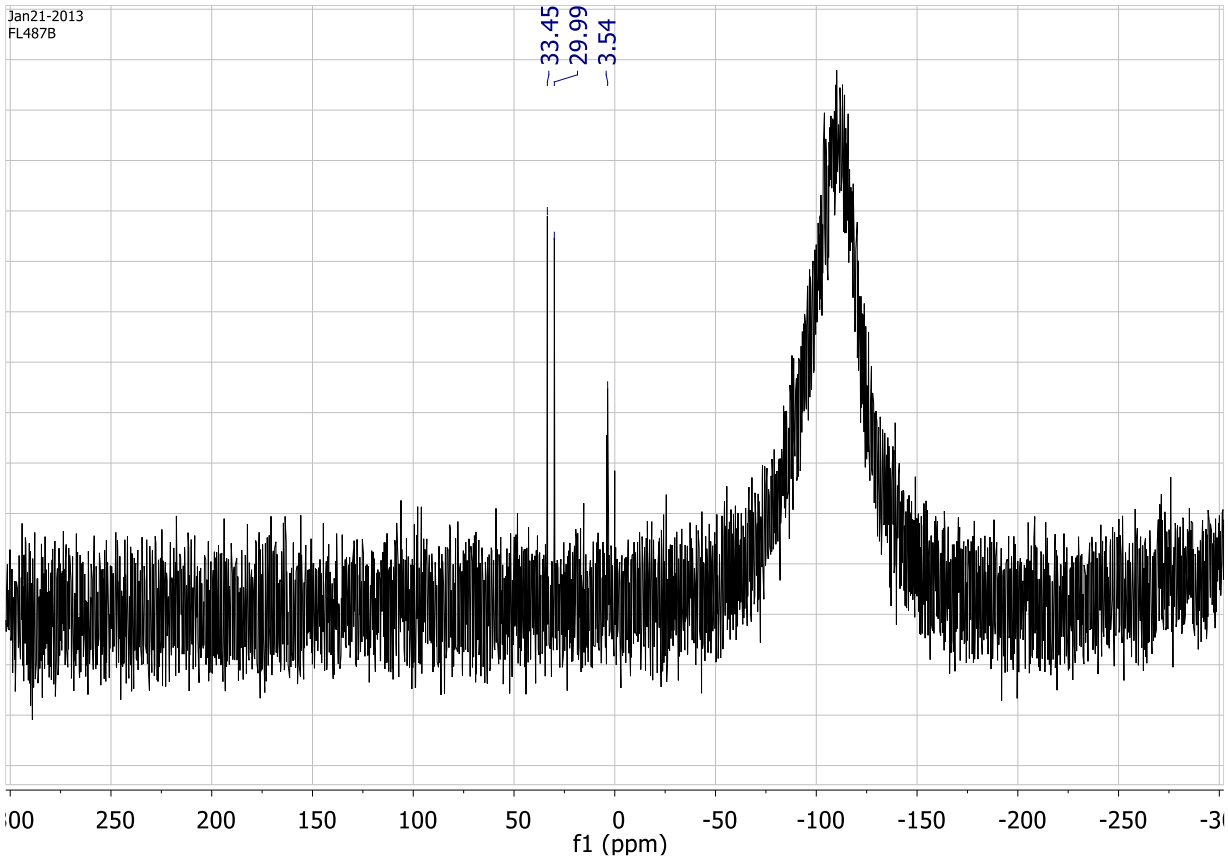
IMes (0.01 mmol) (CF_3)$SiMe_3$ (0.1 mmol) (^{1}H Toluene-d_8)



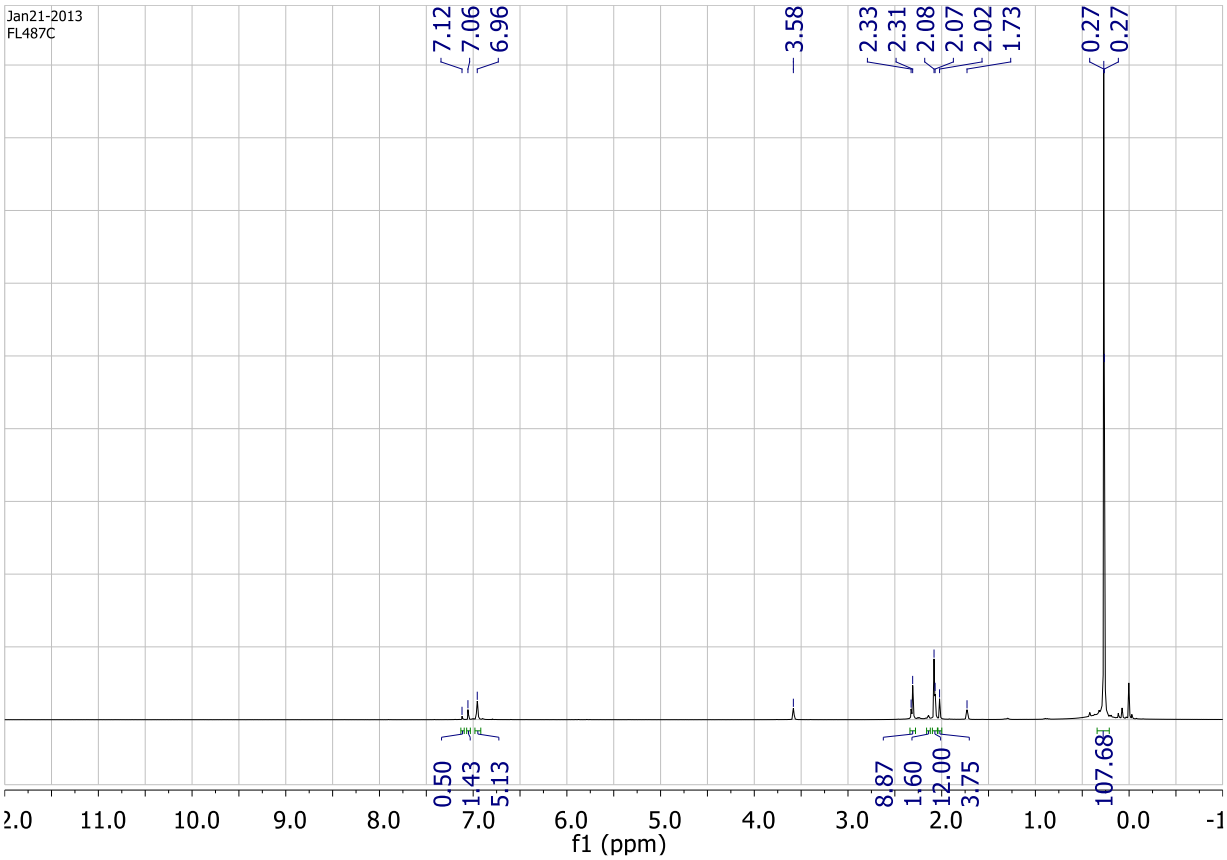
IMes (0.01 mmol) (CF_3)$SiMe_3$ (0.1 mmol) (^{13}C Toluene-d_8)



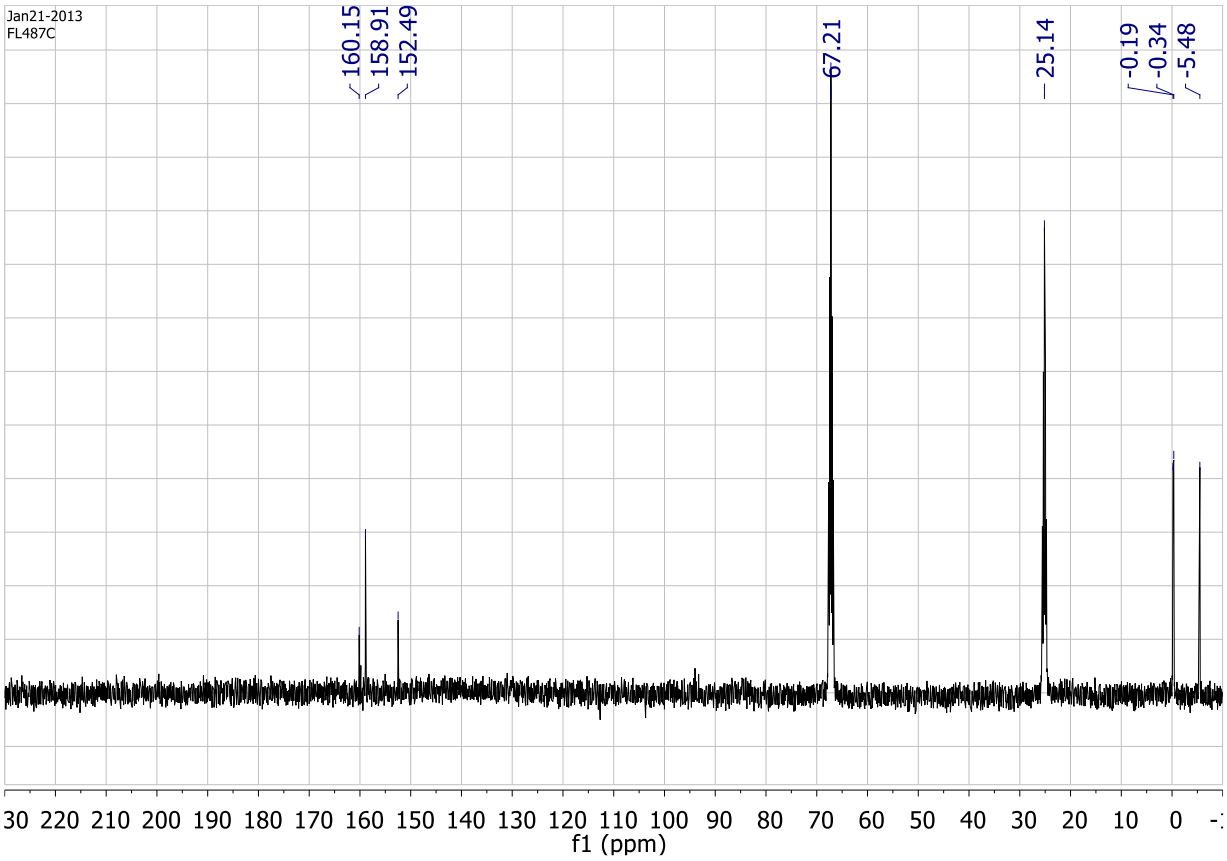
IMes (0.01 mmol) $(CF_3)SiMe_3$ (0.1 mmol) (^{29}Si Toluene-d_8)



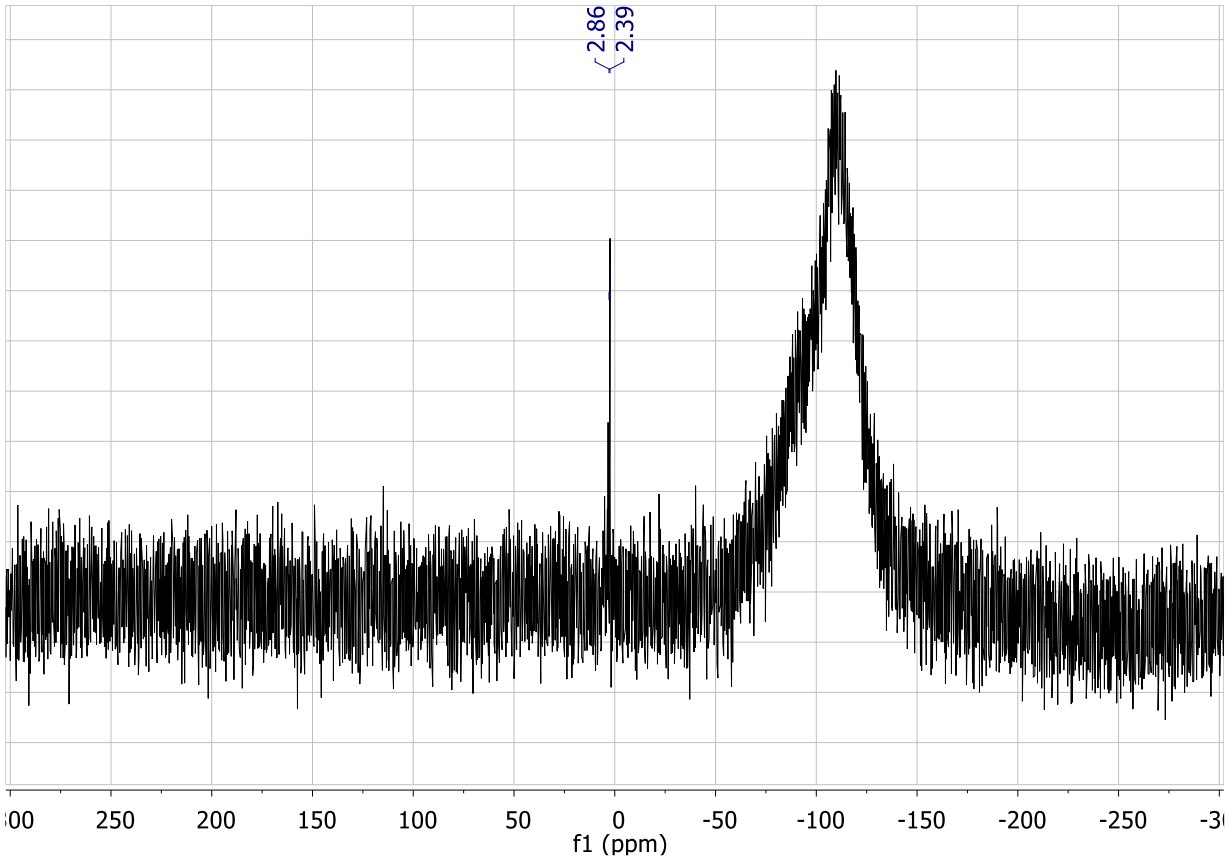
IMes (0.01 mmol) (CF_3)$SiMe_3$ (0.1 mmol) (^{1}H THF-d_8)



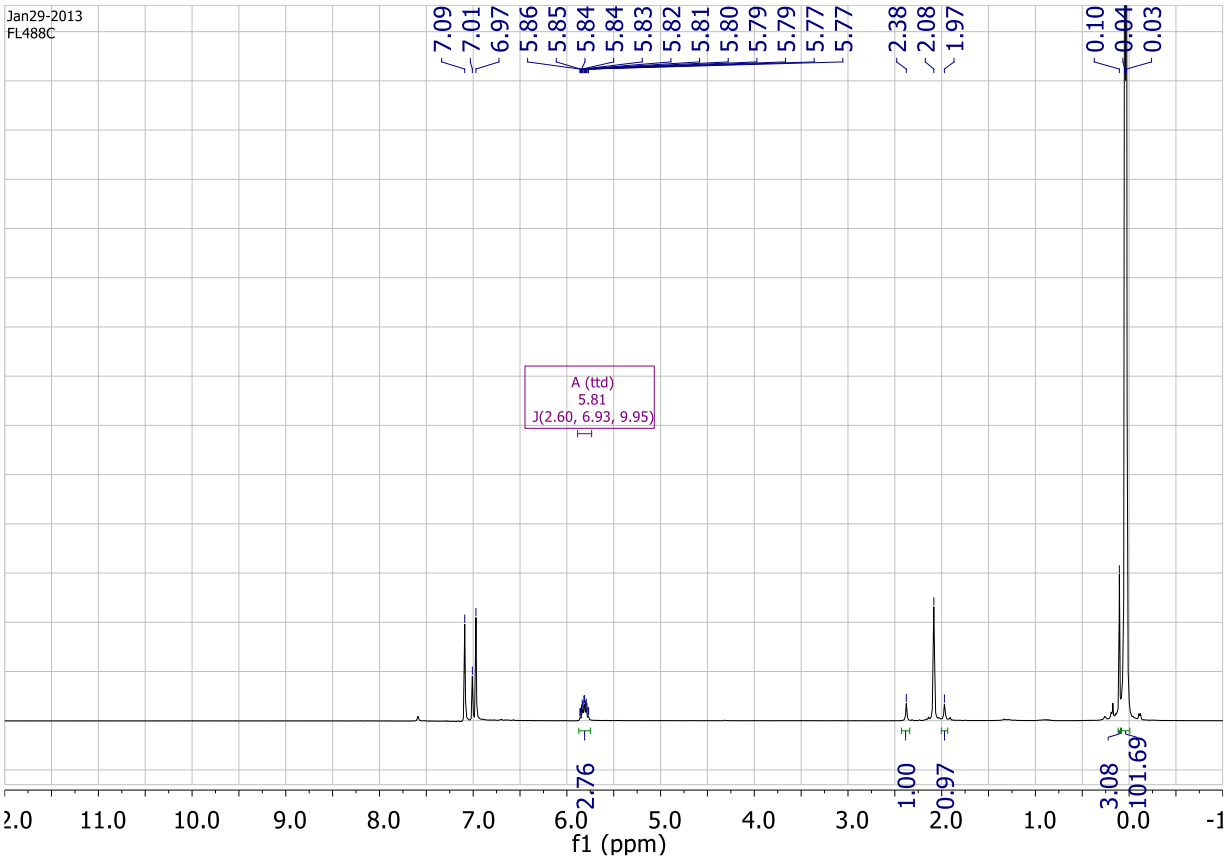
IMes (0.01 mmol) $(CF_3)SiMe_3$ (0.1 mmol) (^{13}C THF-d_8)



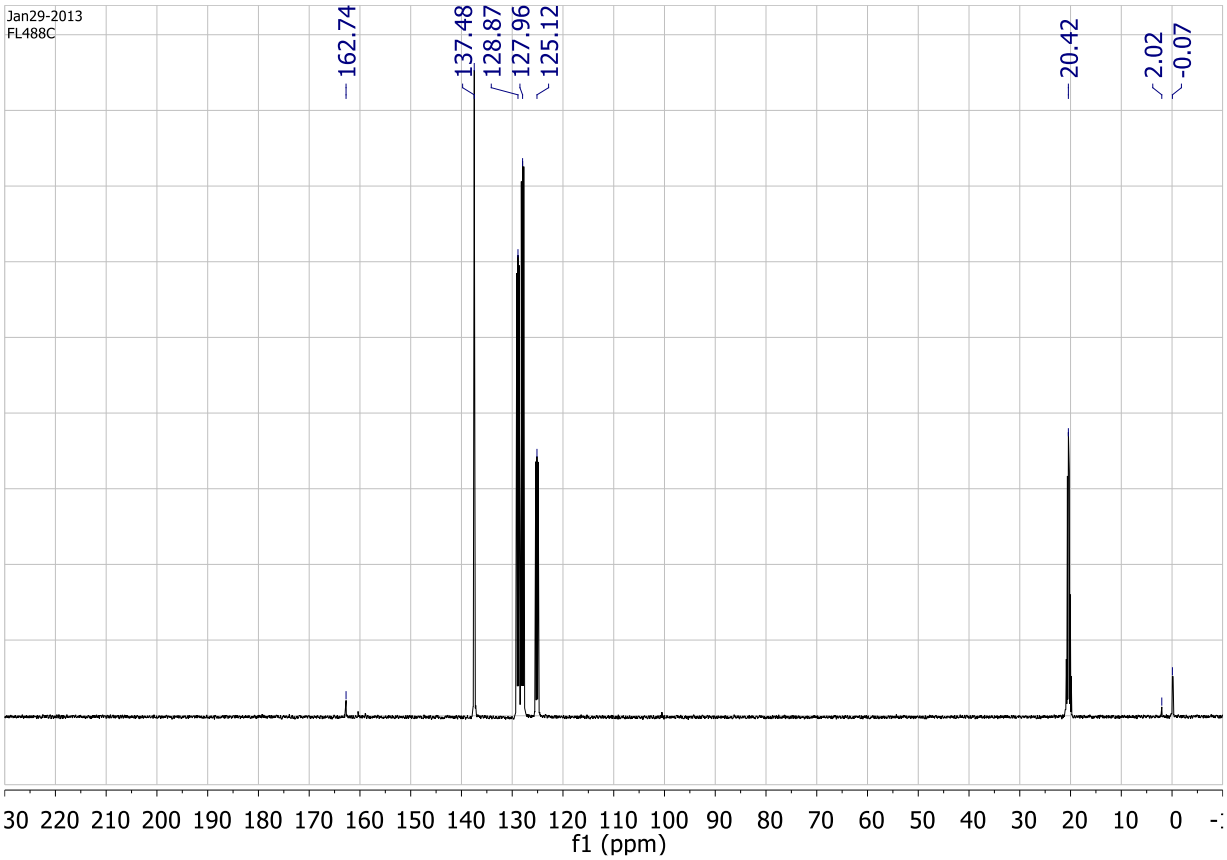
IMes (0.01 mmol) $(CF_3)SiMe_3$ (0.1 mmol) (^{29}Si THF-d_8)



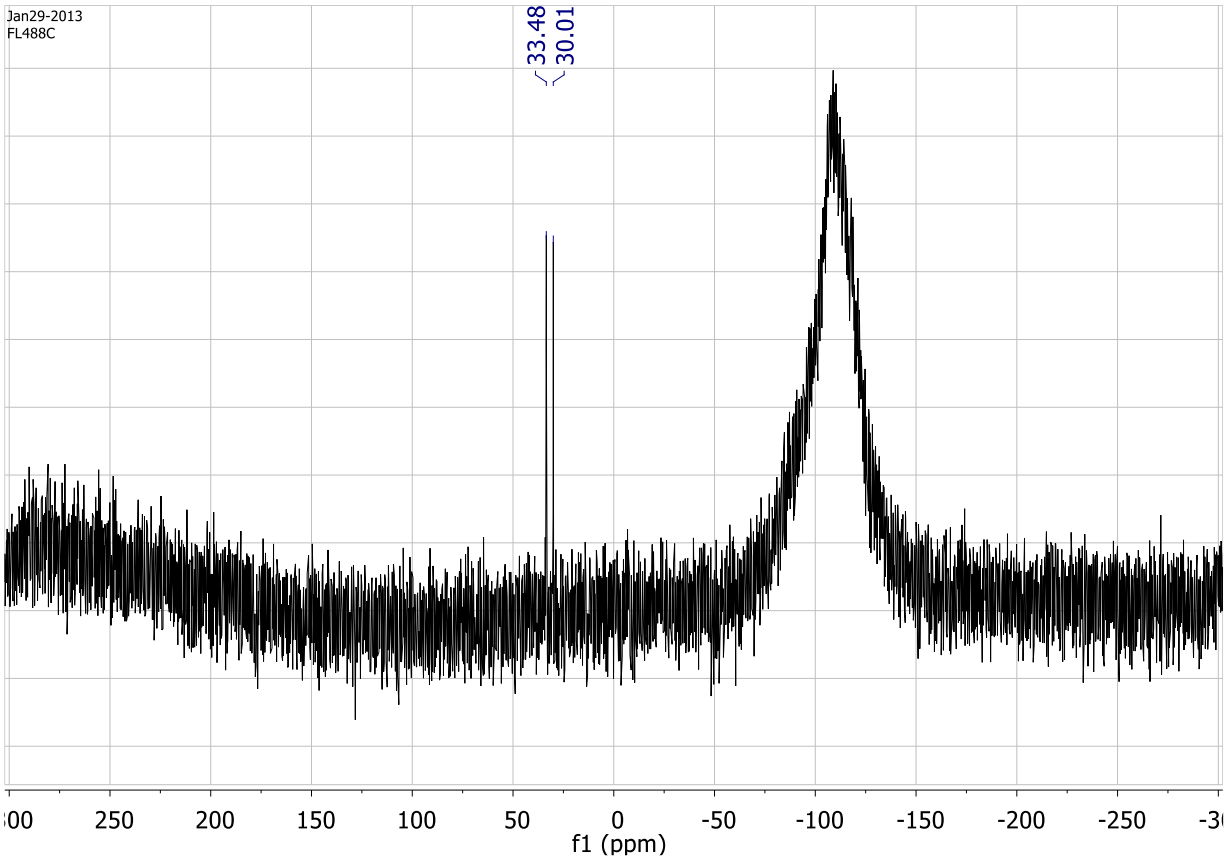
IMes (0.01 mmol) (C_6F_5)$SiMe_3$ (0.05 mmol) (^{1}H Toluene-d_8)



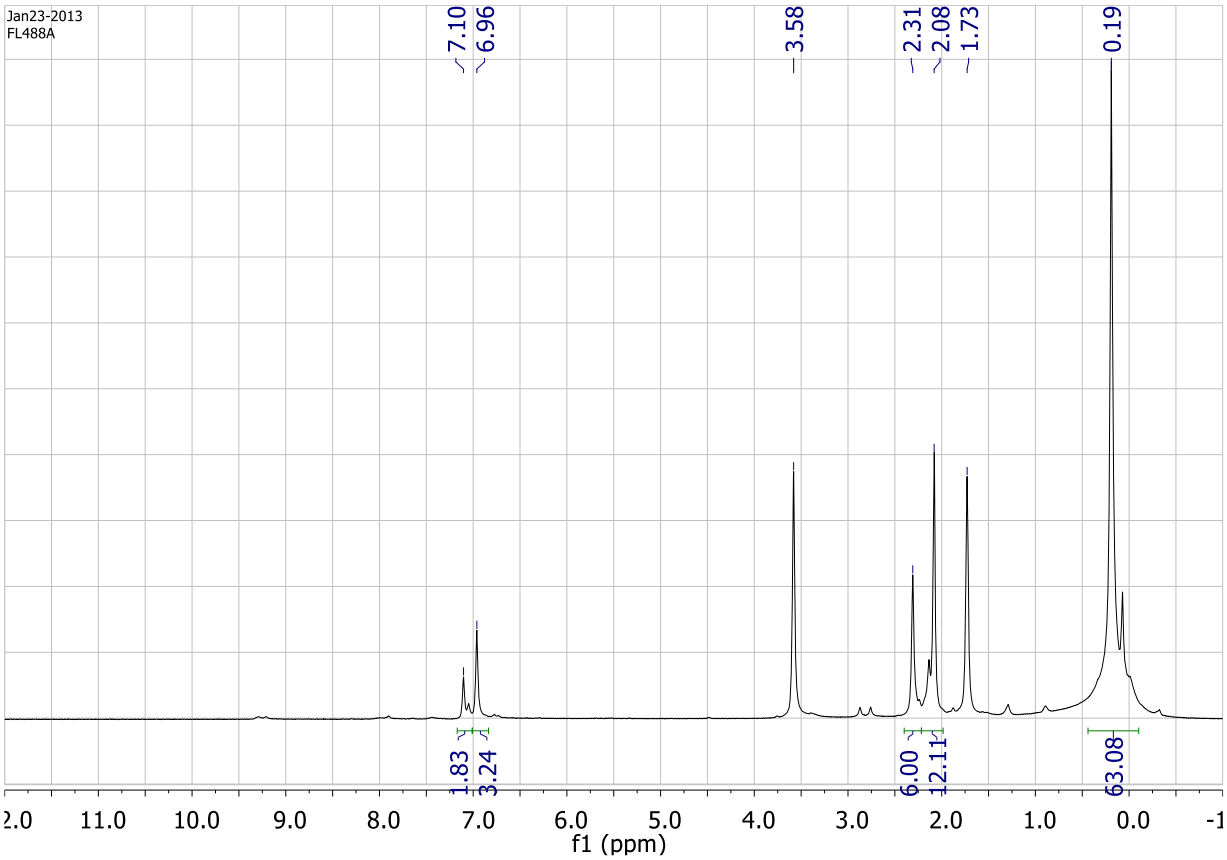
IMes (0.01 mmol) (C_6F_5)$SiMe_3$ (0.05 mmol) (^{13}C Toluene-d_8)



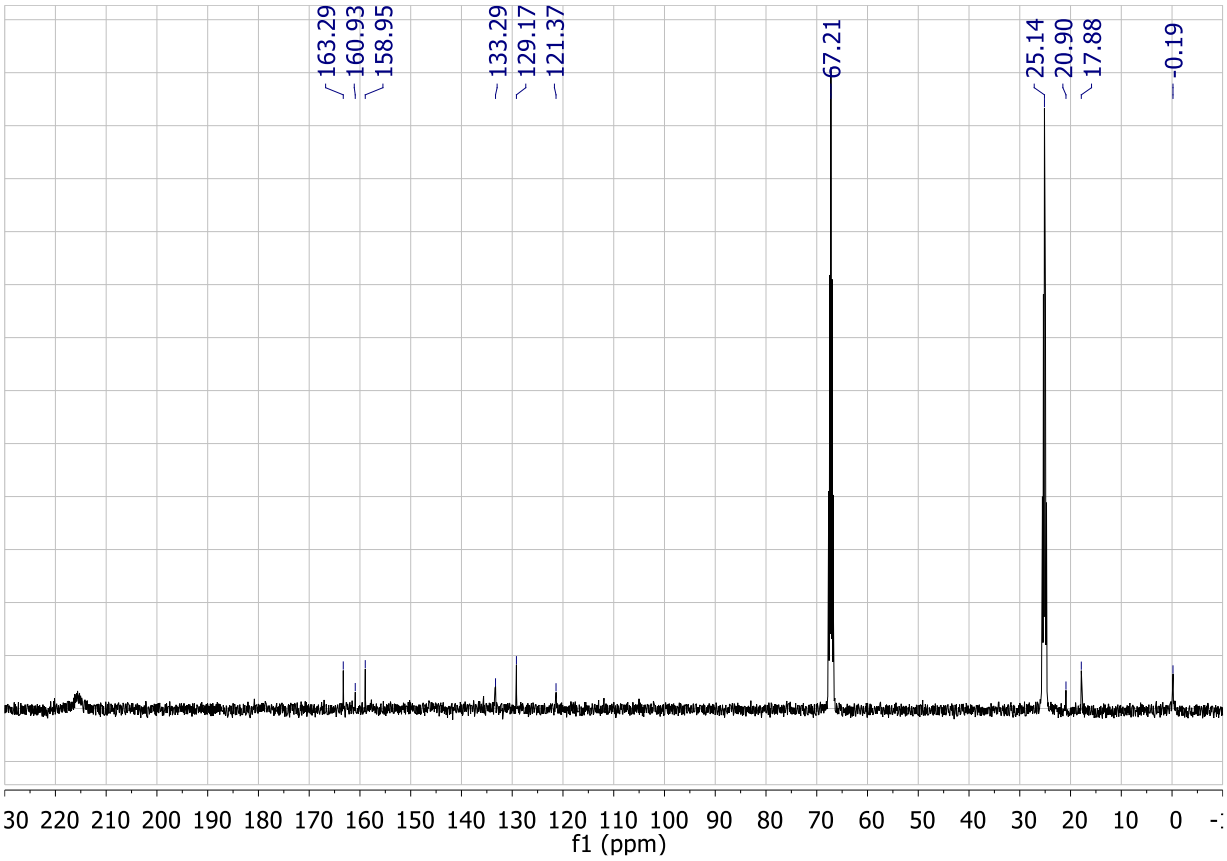
IMes (0.01 mmol) (C_6F_5)$SiMe_3$ (0.05 mmol) (^{29}Si Toluene-d_8)



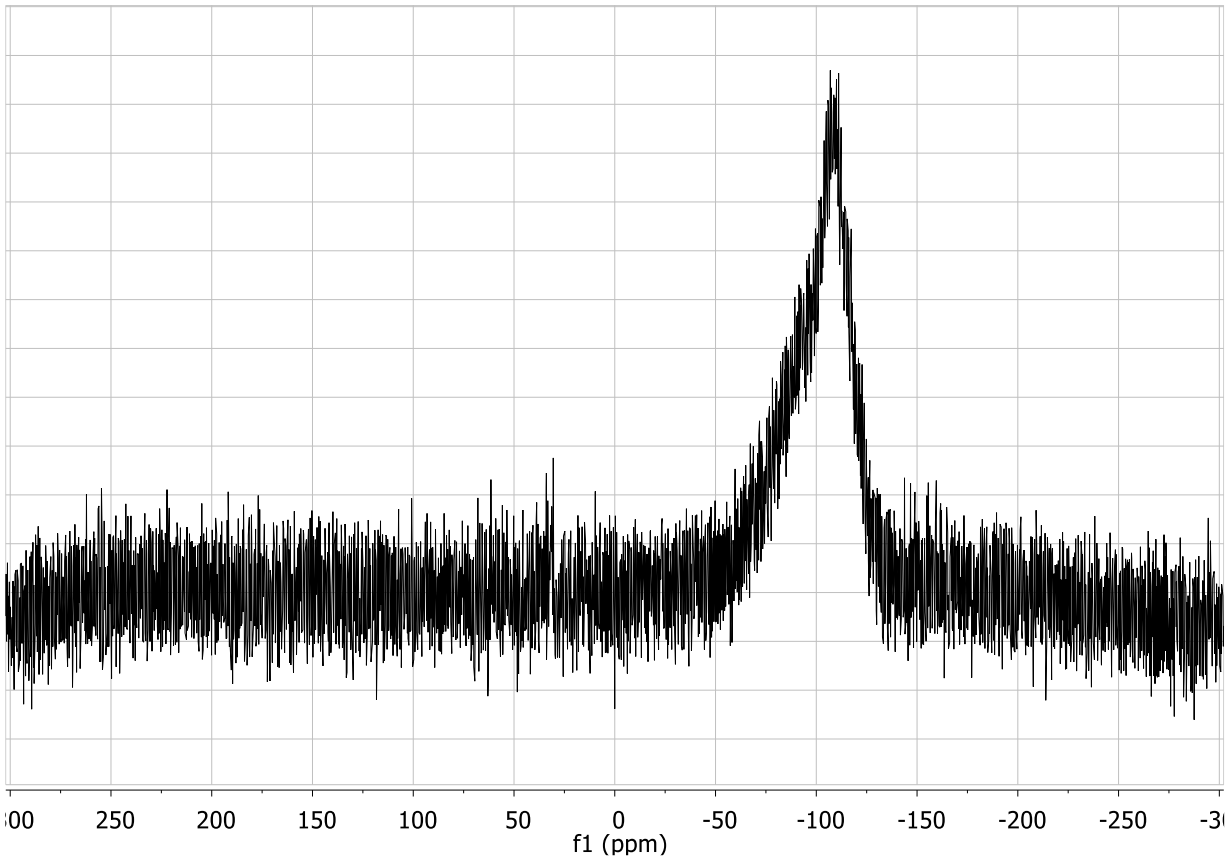
IMes (0.01 mmol) (C_6F_5)$SiMe_3$ (0.1 mmol) (^{1}H THF-d_8)



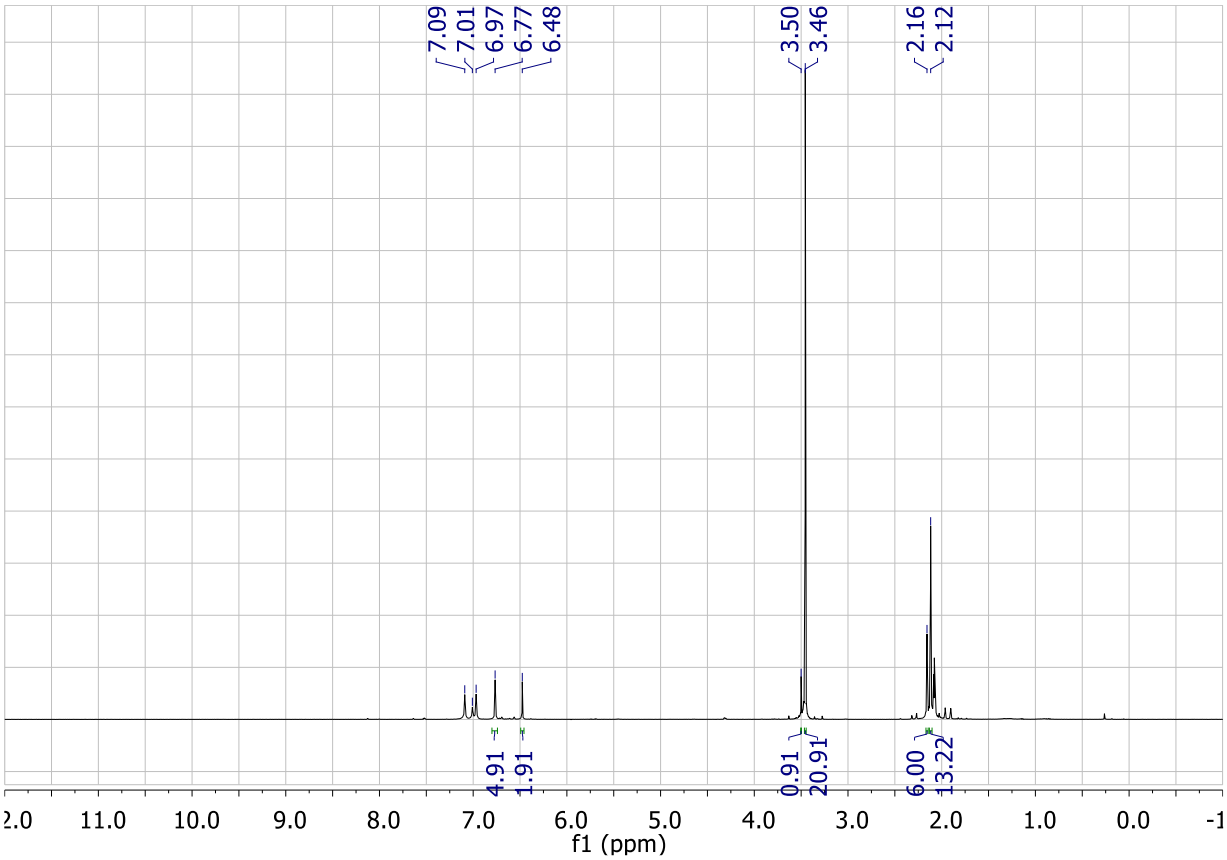
IMes (0.01 mmol) (C_6F_5)$SiMe_3$ (0.1 mmol) (^{13}C THF-d_8)



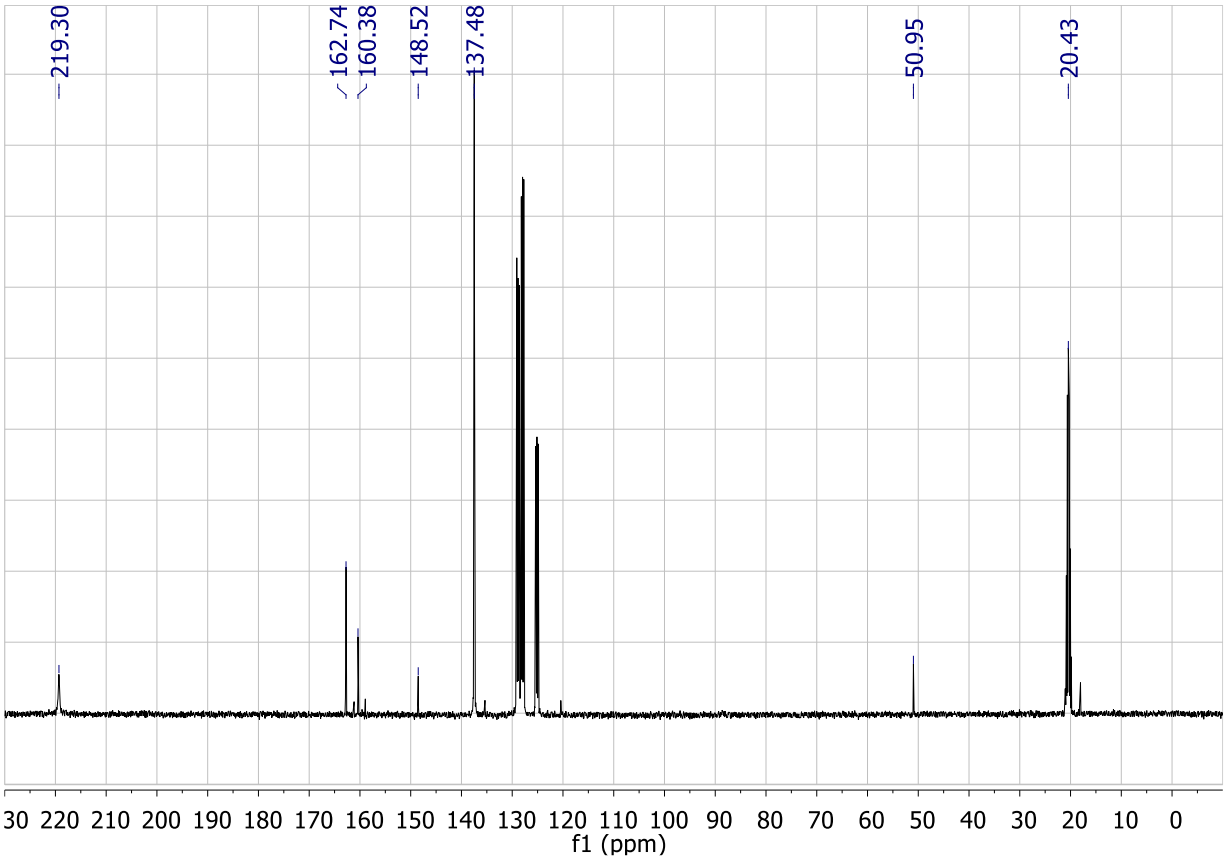
IMes (0.01 mmol) (C_6F_5)$SiMe_3$ (0.1 mmol) (^{29}Si THF-d_8)



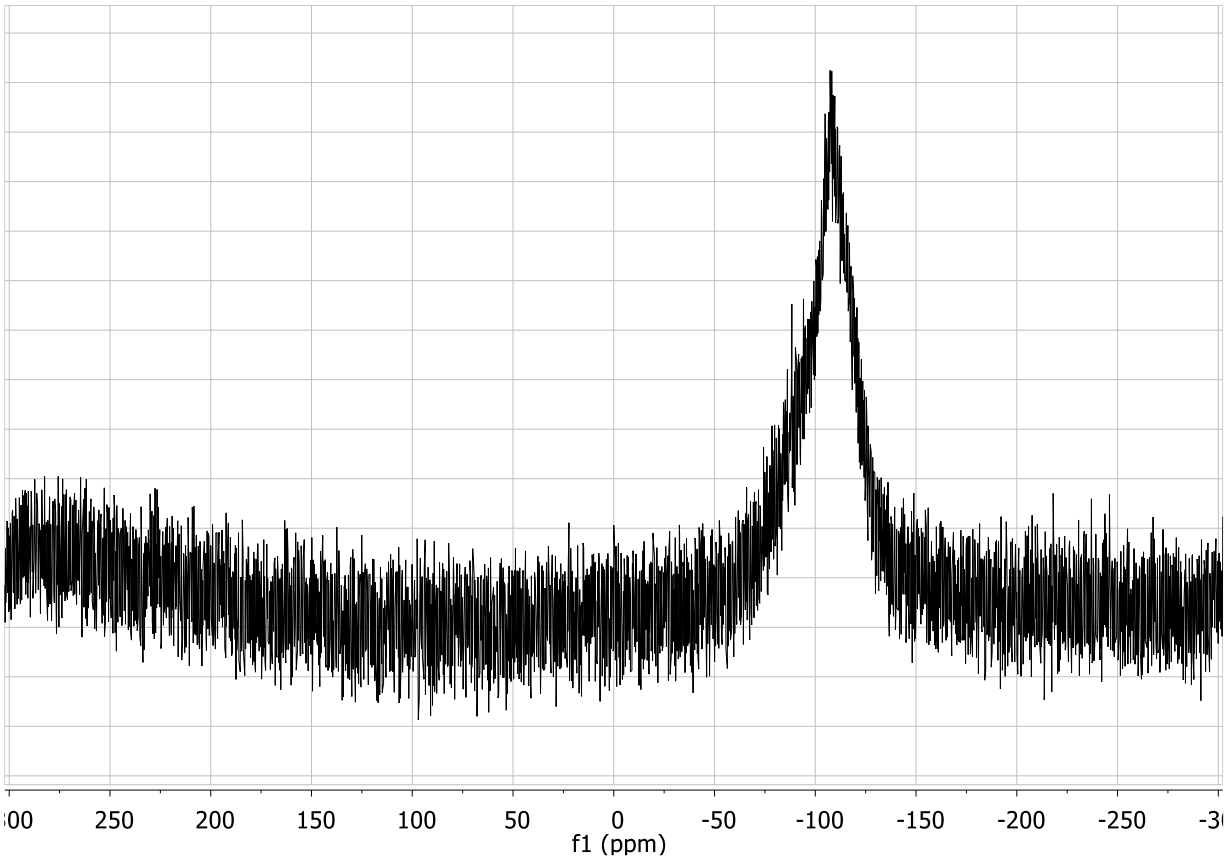
IMes (0.01 mmol) $(C_6F_5)_2Si(OMe)_2$ (0.01 mmol) (^{1}H Toluene-d_8)



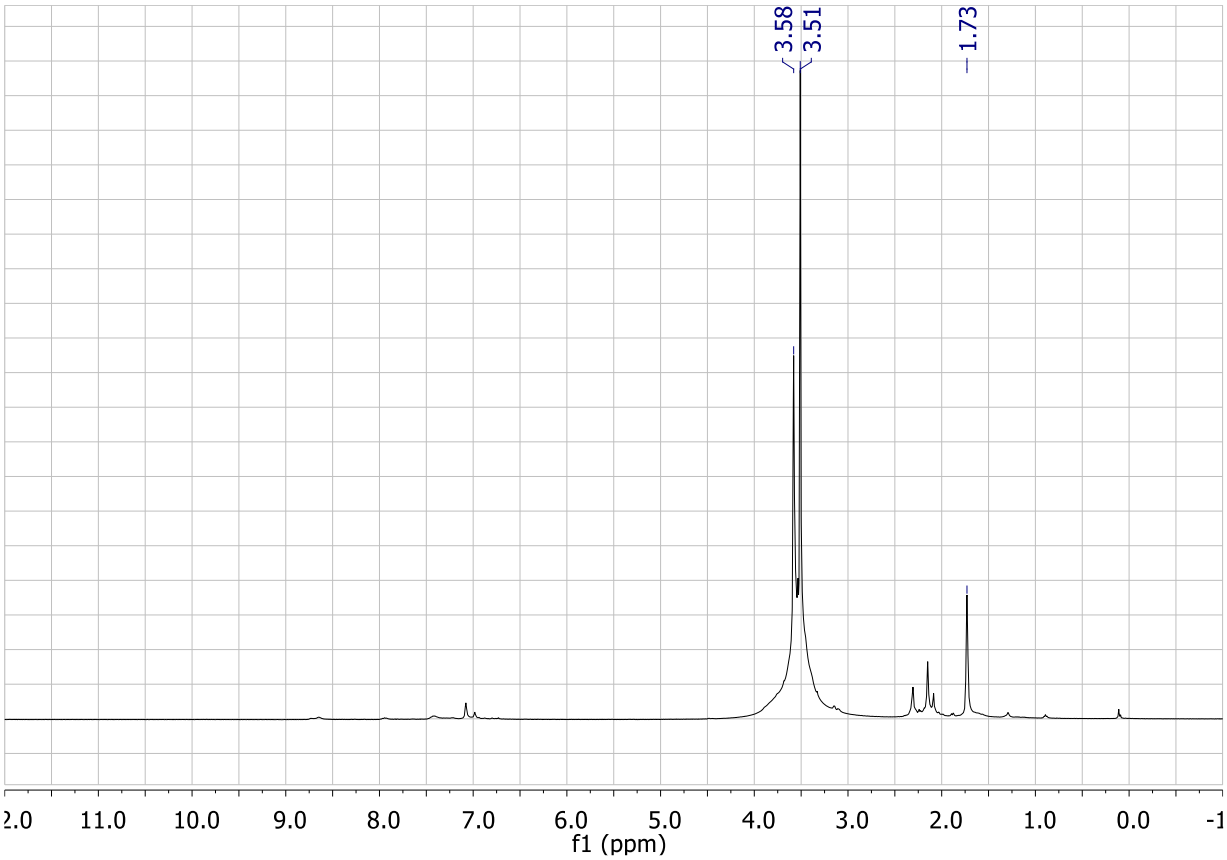
IMes (0.01 mmol) $(C_6F_5)_2Si(OMe)_2$ (0.01 mmol) (^{13}C Toluene-d_8)



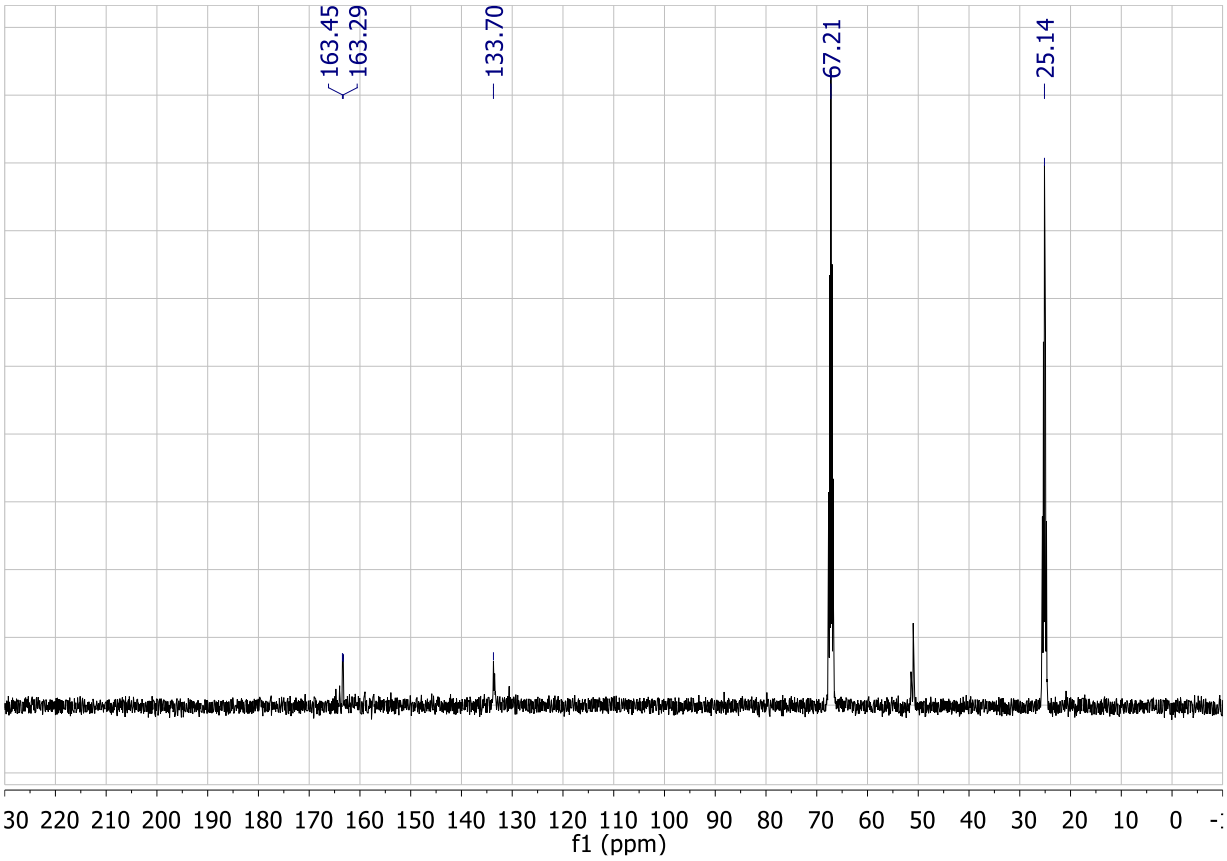
IMes (0.01 mmol) $(C_6F_5)_2Si(OMe)_2$ (0.01 mmol) (^{29}Si Toluene-d_8)



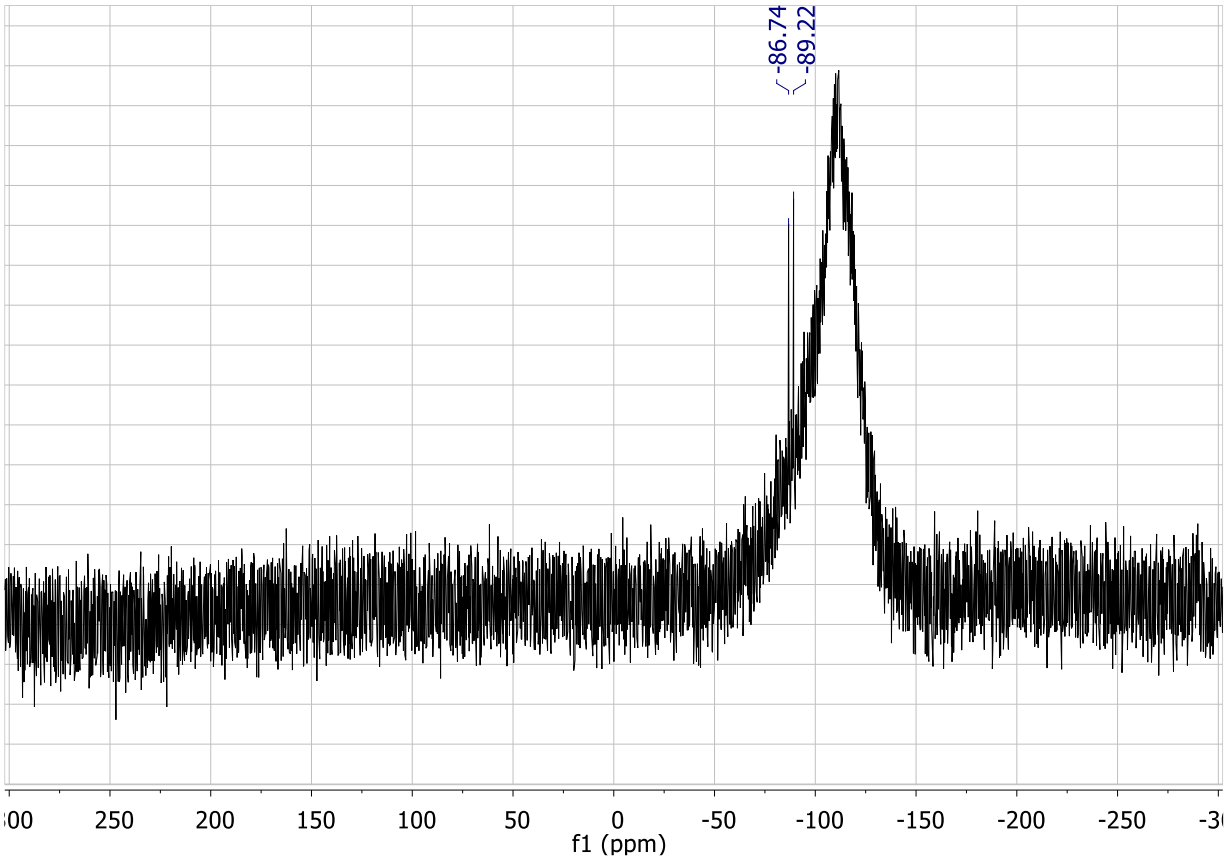
IMes (0.01 mmol) $(C_6F_5)_2Si(OMe)_2$ (0.1 mmol) (^{1}H THF-d_8)



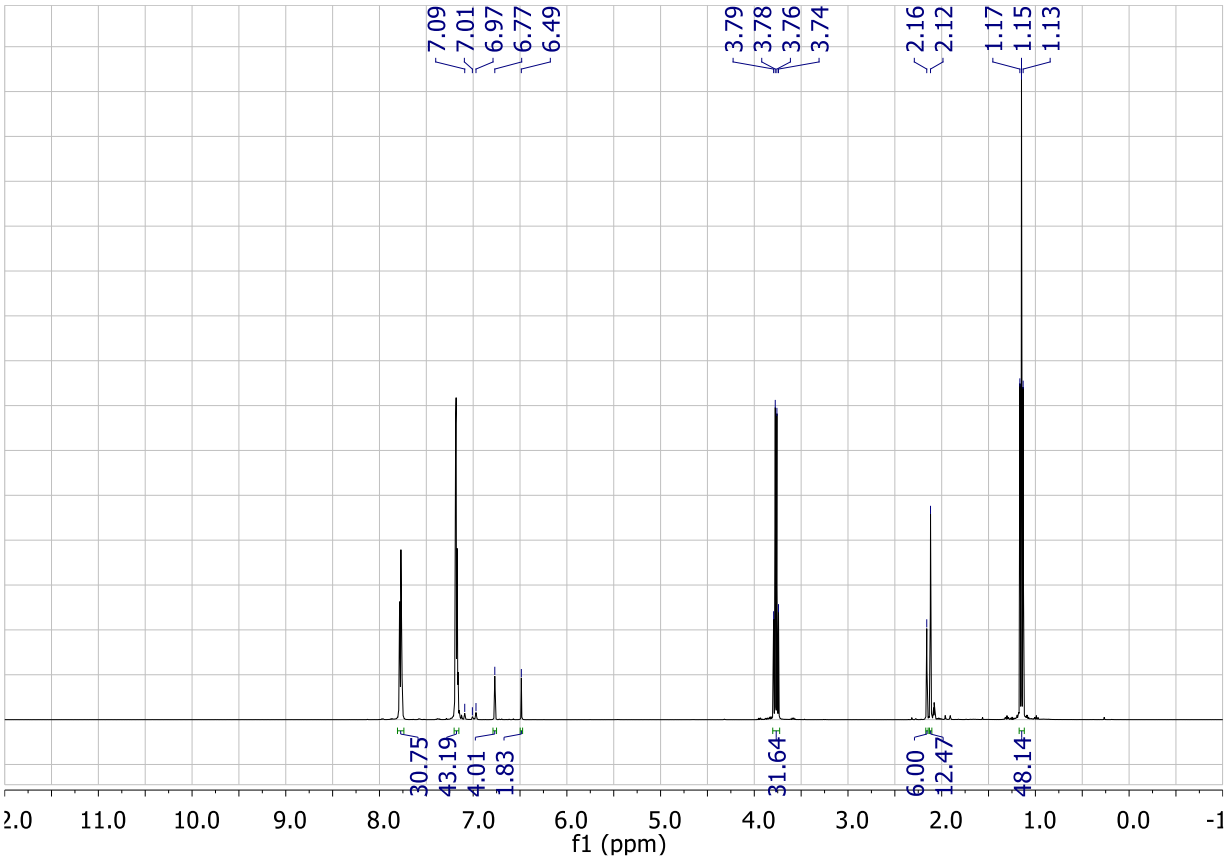
IMes (0.01 mmol) $(C_6F_5)_2Si(OMe)_2$ (0.1 mmol) (^{13}C THF-d_8)



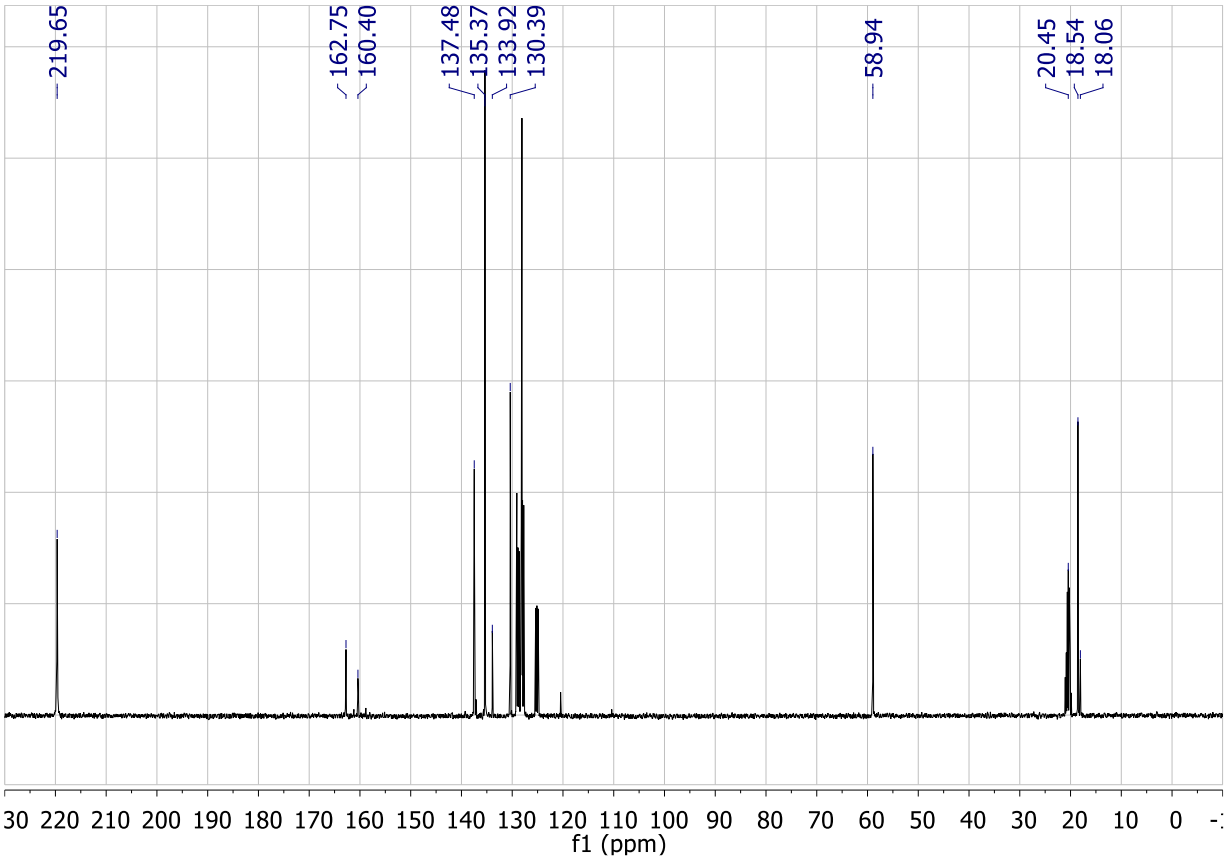
IMes (0.01 mmol) $(C_6F_5)_2Si(OMe)_2$ (0.1 mmol) (^{29}Si THF-d_8)



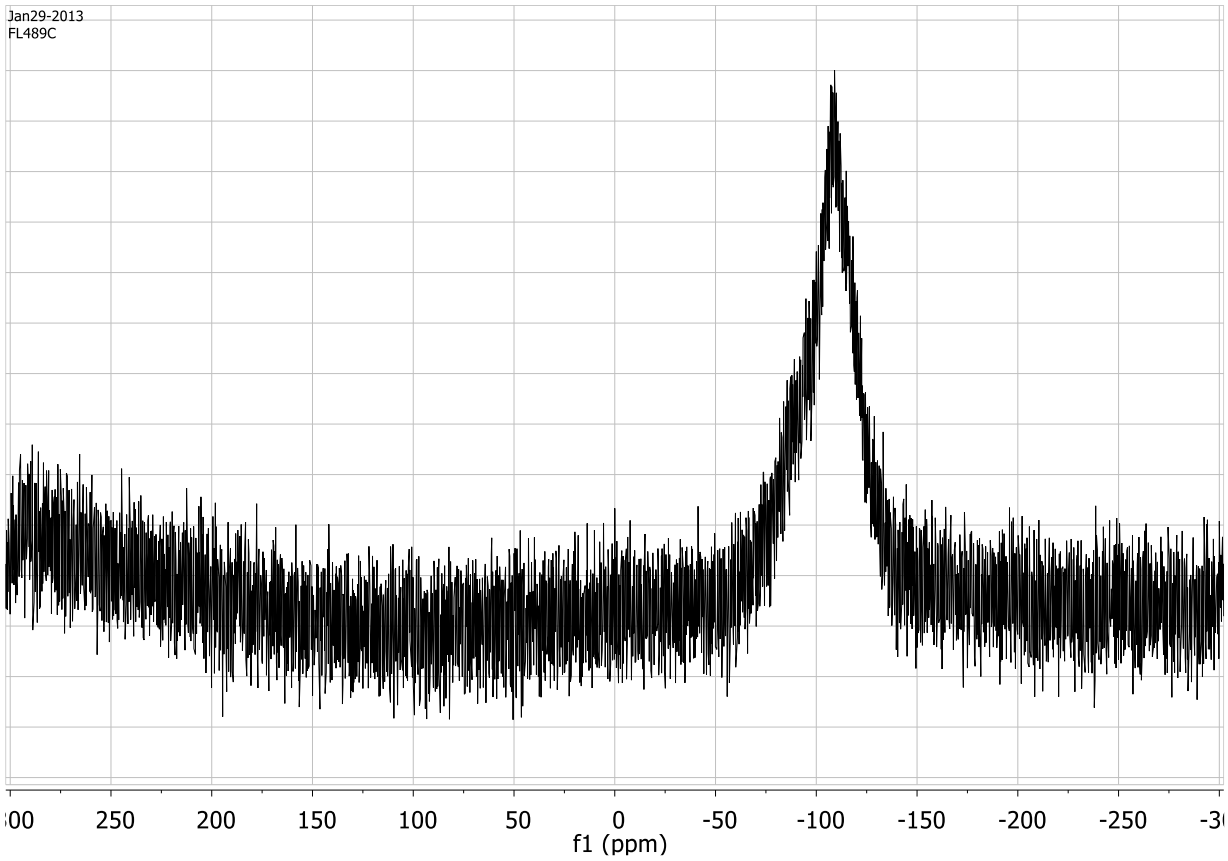
IMes (0.01 mmol) $(EtO)_2SiPh_2$ (0.1 mmol) (^{1}H Toluene-d_8)



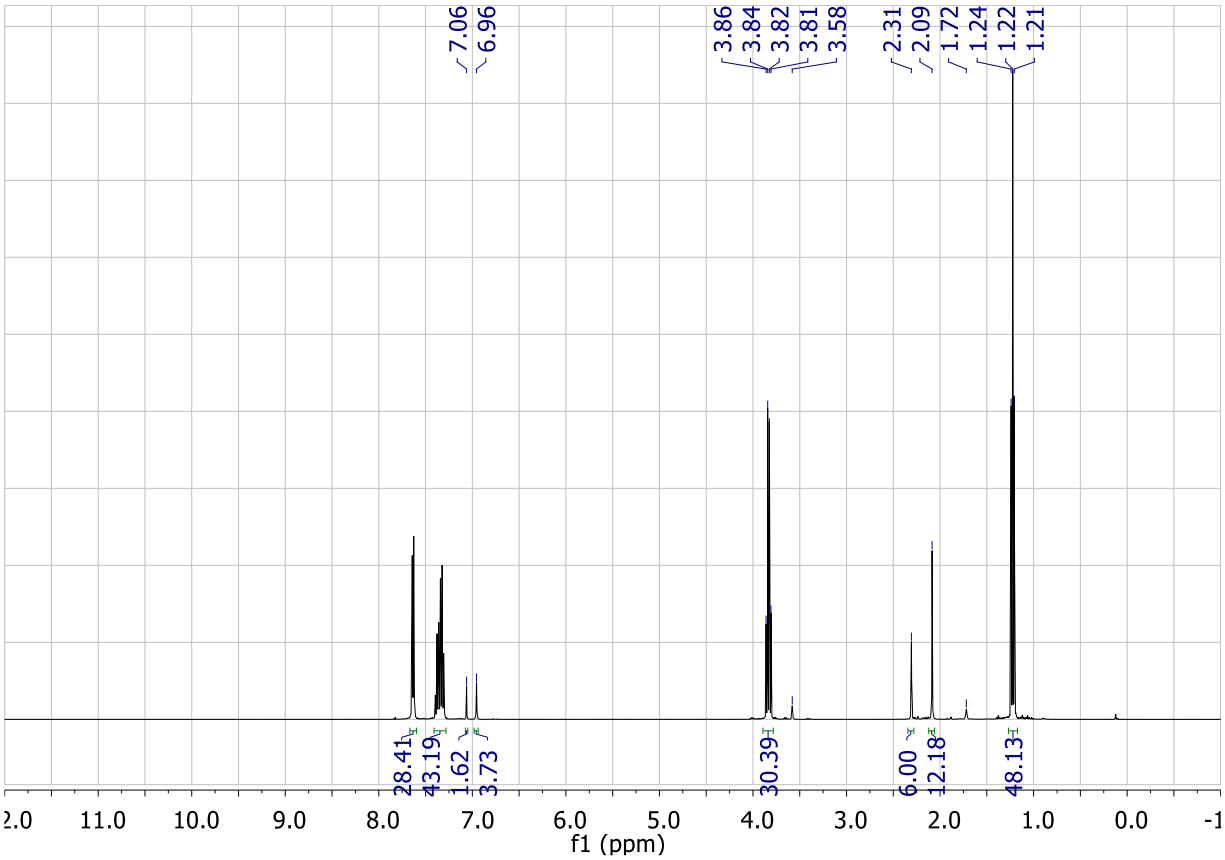
IMes (0.01 mmol) $(EtO)_2SiPh_2$ (0.1 mmol) (^{13}C Toluene-d_8)



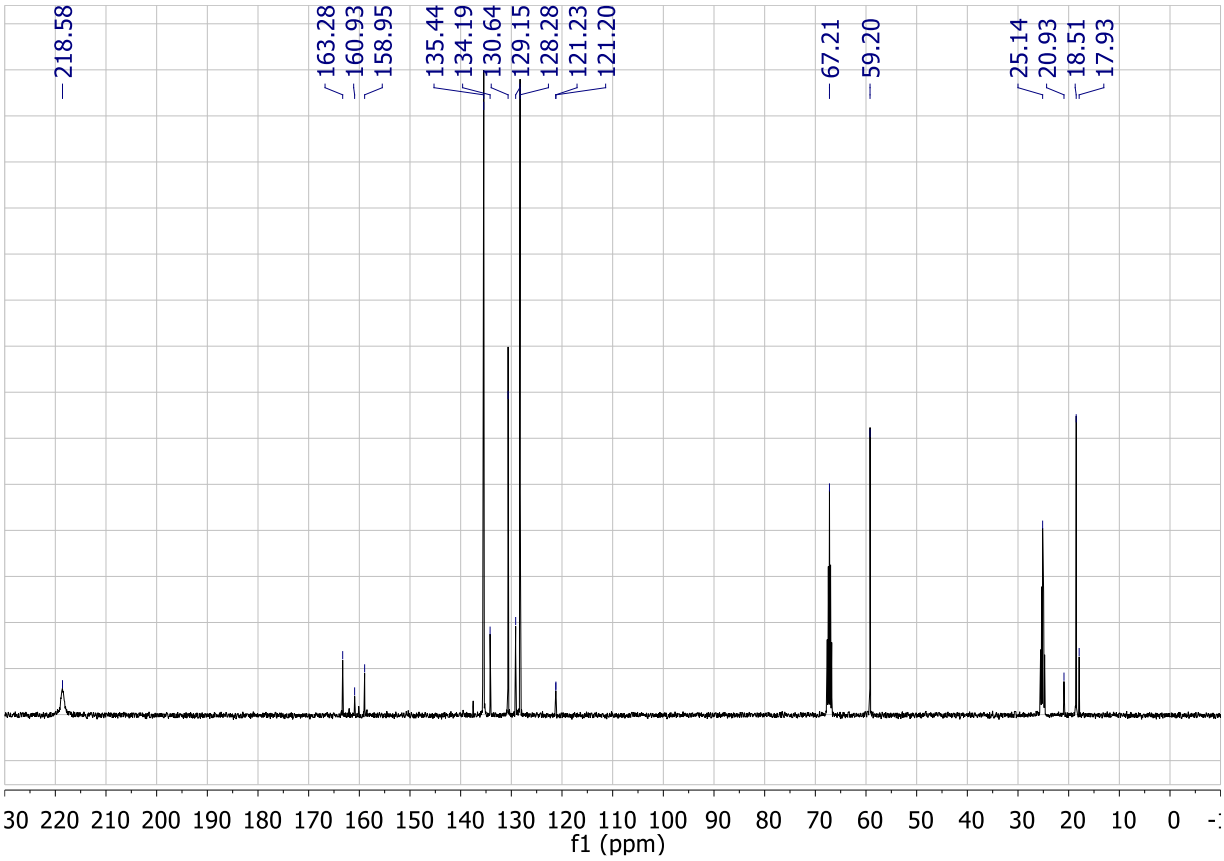
IMes (0.01 mmol) $(EtO)_2SiPh_2$ (0.1 mmol) (^{29}Si Toluene-d_8)



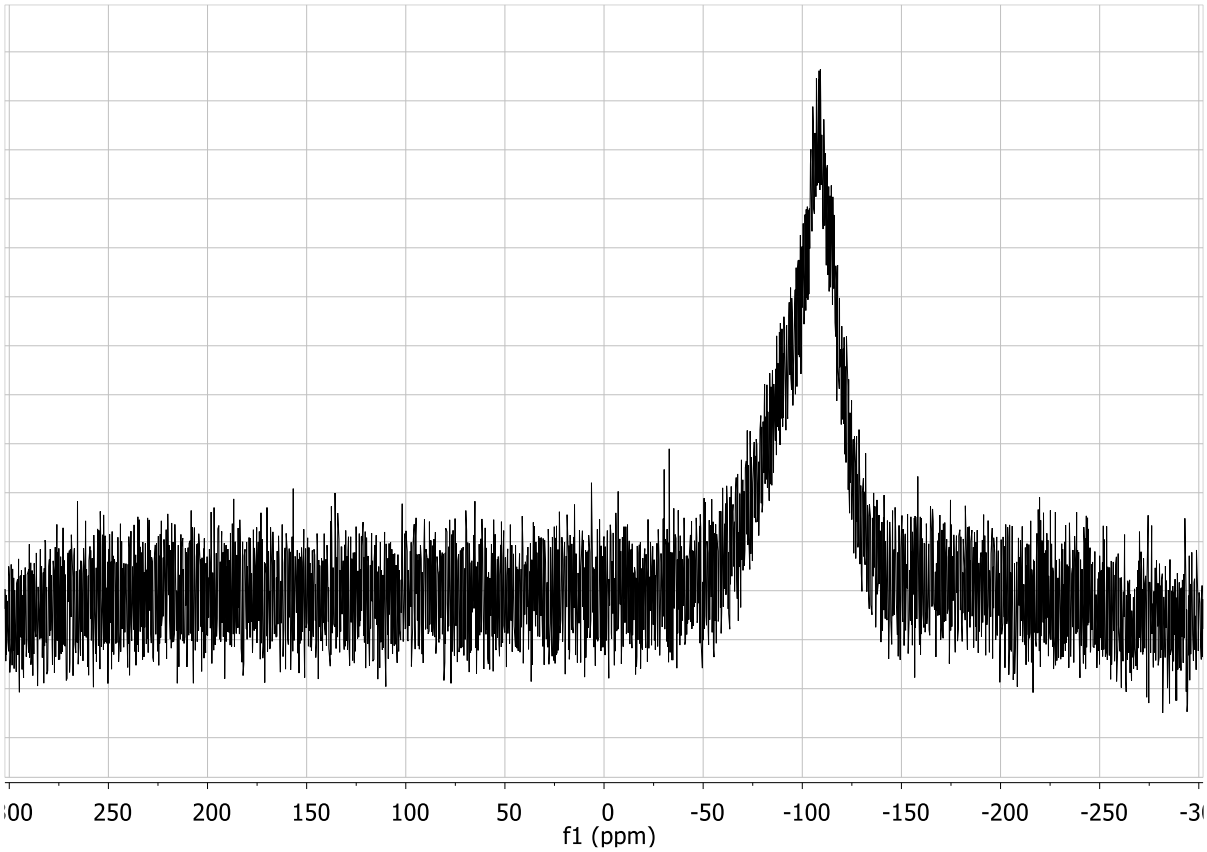
IMes (0.01 mmol) $(EtO)_2SiPh_2$ (0.1 mmol) (^{1}H THF-d_8)



IMes (0.01 mmol) $(EtO)_2SiPh_2$ (0.1 mmol) (^{13}C THF-d_8)

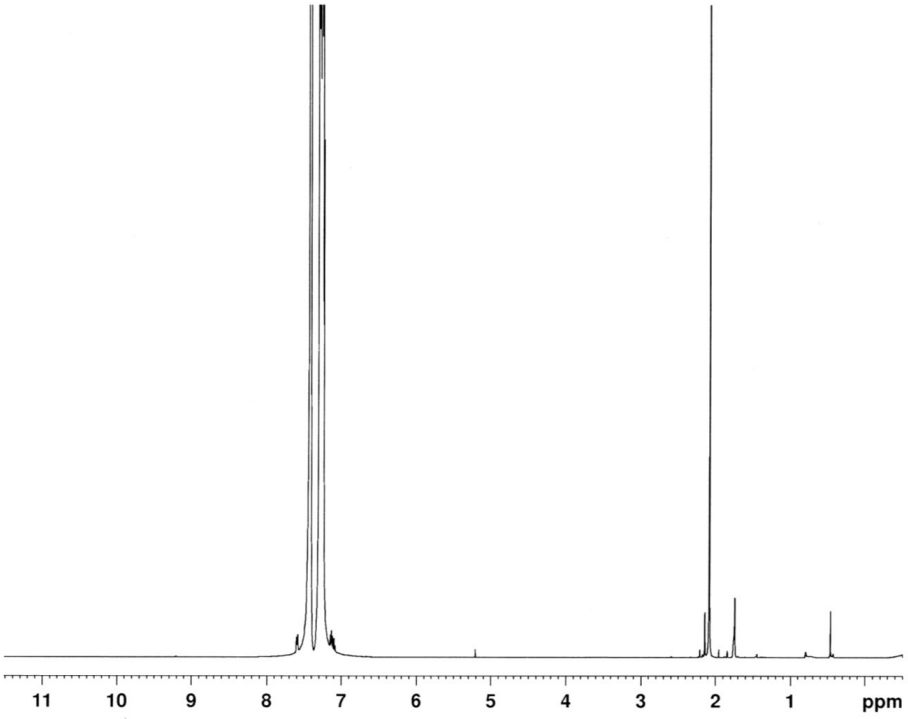


IMes (0.01 mmol) $(EtO)_2SiPh_2$ (0.1 mmol) (^{29}Si THF-d_8)



Me_2ItBu (0.02 mmol) $(C_6F_5)_2SiMe_2$ (0.1 mmol) (^1H C_6H_5Cl/D_2O)

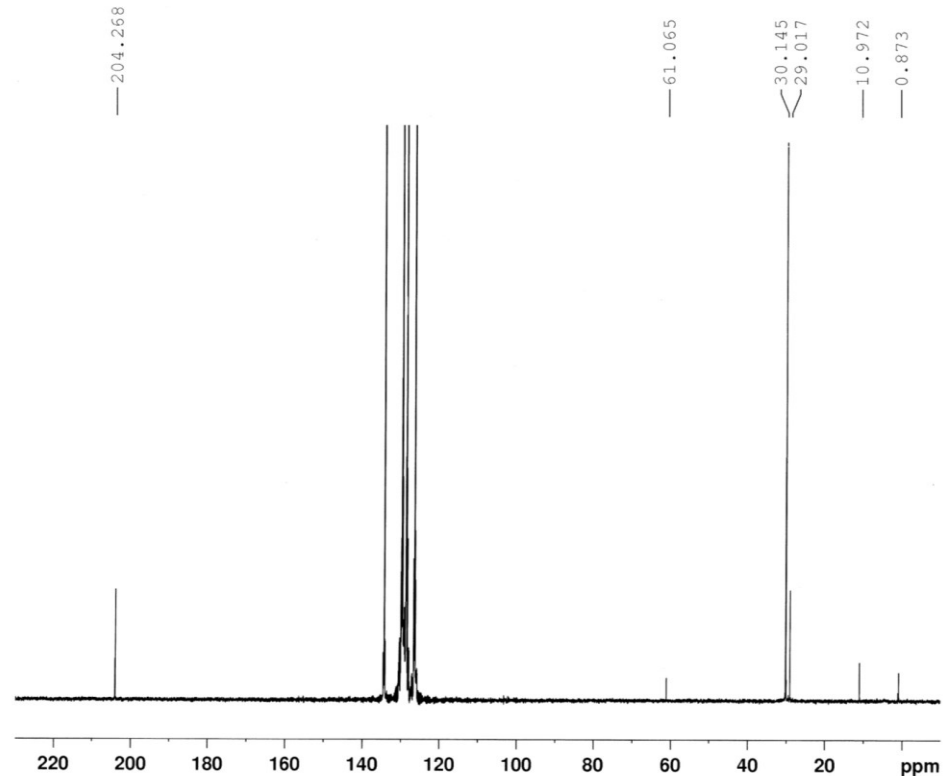
F Lee FL Me2ItBu.Me2Si(C6F5)2 in C6H5Cl/D2O capillary ; 1H spectrum at rt using Av500 ; Jan08-2013/4



NAME	Jan08-2013
EXPNO	4
PROCNO	1
Date_	20130108
Time	16.07
INSTRUM	spect
PROBHD	5 mm PABBO BB-
PULPROG	zg30
TD	32768
SOLVENT	D2O
NS	128
DS	4
SWH	6009.615 Hz
FIDRES	0.183399 Hz
AQ	2.7263477 sec
RG	7.12
DW	83.200 usec
DE	6.00 usec
TE	298.0 K
D1	2.00000000 sec
TD0	1
======== CHANNEL f1 ========	
NUC1	1H
P1	12.70 usec
PL1	1.00 dB
PL1W	20.75072861 W
SFO1	500.1325006 MHz
SI	32768
SF	500.1297471 MHz
WDW	no
SSB	0
LB	0.00 Hz
GB	0
PC	1.00

Me_2ItBu (0.02 mmol) $(C_6F_5)_2SiMe_2$ (0.1 mmol) (^{13}C C_6H_5Cl/D_2O)

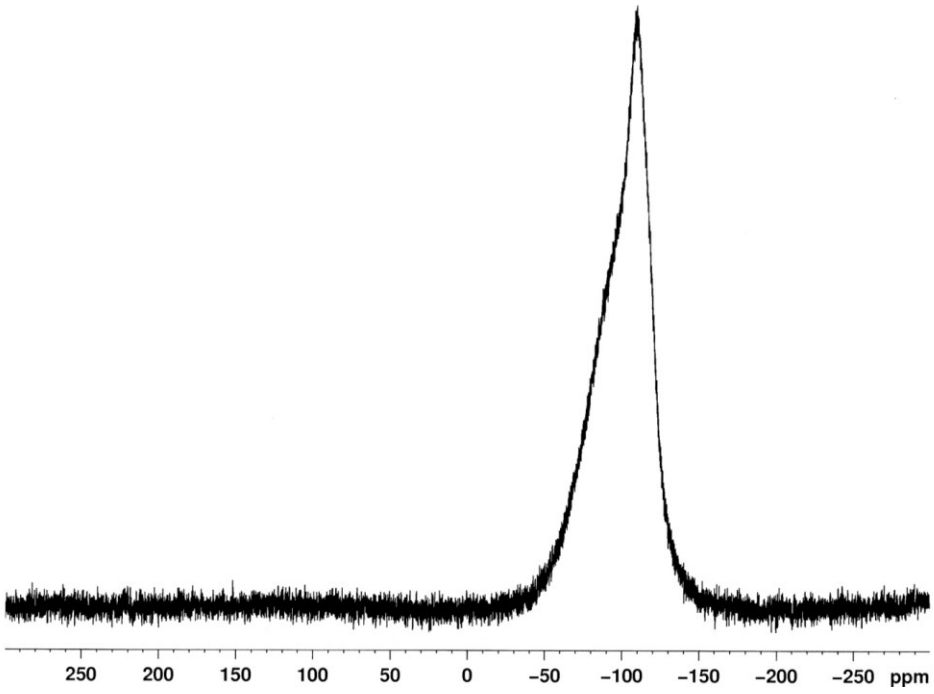
F Lee FL Me2ItBu.Me2Si(C6F5)2 in C6H5Cl/D2O capillary ; 13C{1H} spectrum at rt using Av500 ; Jan08-2013/5



NAME	Jan08-2013
EXPNO	5
PROCNO	1
Date_	20130109
Time	10.00
INSTRUM	spect
PROBHD	5 mm PABBO BB-
PULPROG	zgpg30
TD	32768
SOLVENT	D2O
NS	3267
DS	4
SWH	35714.285 Hz
FIDRES	1.089913 Hz
AQ	0.4588020 sec
RG	2050
DW	14.000 usec
DE	12.00 usec
TE	298.0 K
D1	1.00000000 sec
D11	0.03000000 sec
TD0	1
======== CHANNEL f1 ========	
NUC1	13C
P1	9.70 usec
PL1	1.50 dB
PL1W	23.82894325 W
SFO1	125.7703648 MHz
======== CHANNEL f2 ========	
CPDPRG2	waltz16
NUC2	1H
PCPD2	100.00 usec
PL2	1.00 dB
PL12	18.59 dB
PL13	20.37 dB
PL2W	20.75072861 W
PL12W	0.36143759 W
PL13W	0.23990166 W
SFO2	500.1325006 MHz
SI	32768
SF	125.7577388 MHz
WDW	EM
SSB	0
LB	2.00 Hz
GB	0
PC	1.00

Me_2ItBu (0.02 mmol) $(C_6F_5)_2SiMe_2$ (0.1 mmol) (^{29}Si C_6H_5Cl/D_2O)

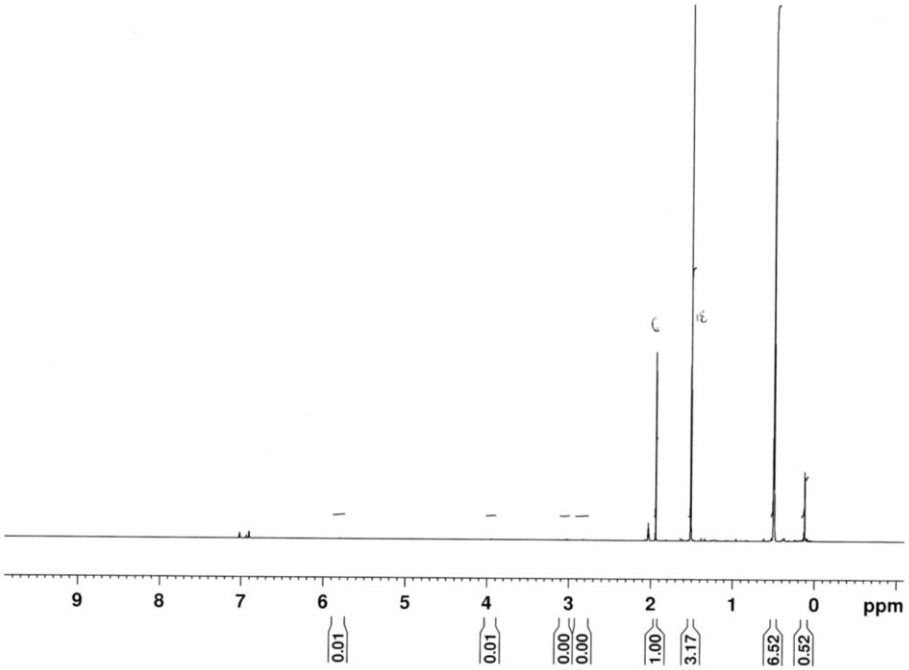
F Lee FL Me2ItBu.Me2Si(C6F5)2 in C6H5Cl/D2O capillary ; 29Si{1H} inverse-gated spectrum at rt using Av50C
Jan08-2013/6 acquired overnight.



NAME	Jan08-2013
EXPNO	6
PROCNO	1
Date_	20130108
Time	16.10
INSTRUM	spect
PROBHD	5 mm PABBO BB-
PULPROG	zgig
TD	65536
SOLVENT	D2O
NS	4111
DS	0
SWH	59523.809 Hz
FIDRES	0.908261 Hz
AQ	0.5505524 sec
RG	1440
DW	8.400 usec
DE	12.00 usec
TE	298.0 K
D1	15.00000000 sec
D11	0.03000000 sec
TD0	1
======== CHANNEL f1 ========	
NUC1	29Si
P1	8.25 usec
PL1	3.00 dB
SFO1	99.3617620 MHz
======== CHANNEL f2 ========	
CPDPRG2	waltz16
NUC2	1H
PCPD2	100.00 usec
PL2	1.00 dB
PL12	18.59 dB
PL2W	20.75072861 W
PL12W	0.36143759 W
SFO2	500.1325010 MHz
SI	32768
SF	99.3617568 MHz
WDW	EM
SSB	0
LB	5.00 Hz
GB	0
PC	1.00

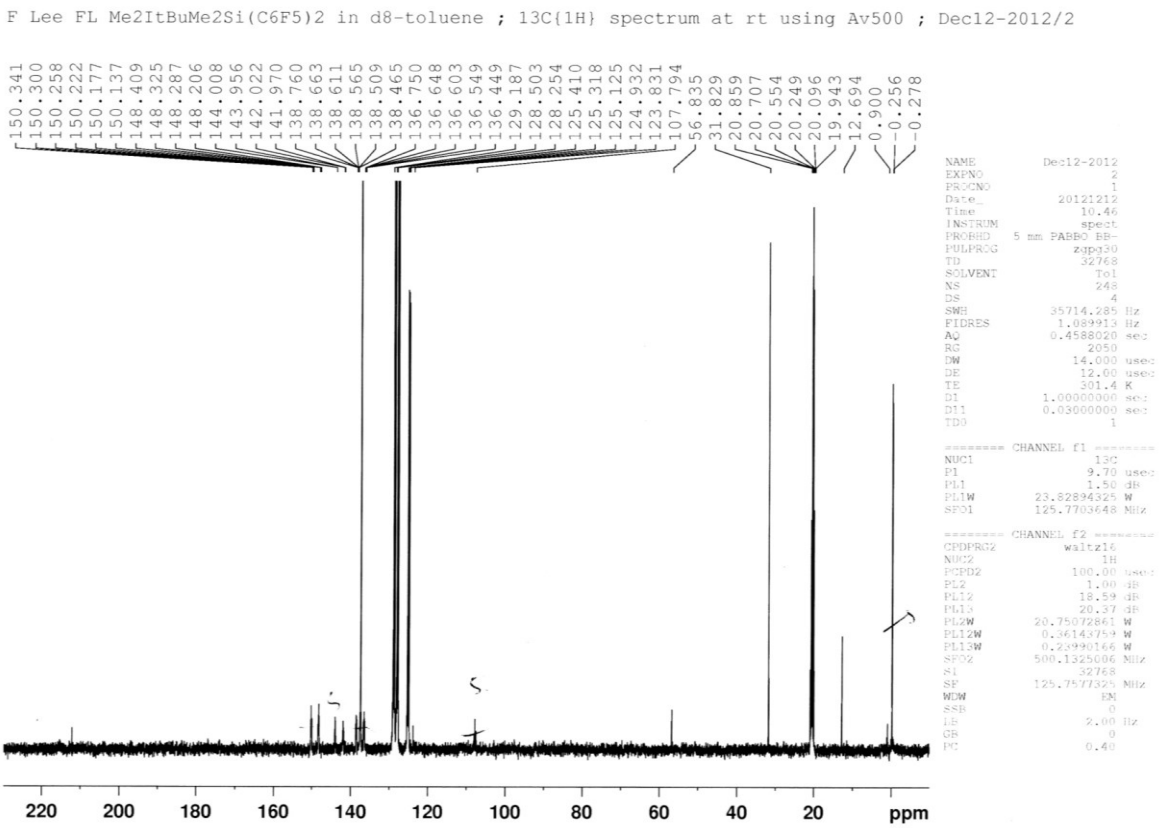
Me_2ItBu (0.02 mmol) $(C_6F_5)_2SiMe_2$ (0.1 mmol) (^{1}H Toluene-d_8)

F Lee FL Me2ItBuMe2Si(C6F5)2 in d8-toluene ; 1H spectrum at rt using Av500 ; Dec12-2012/1



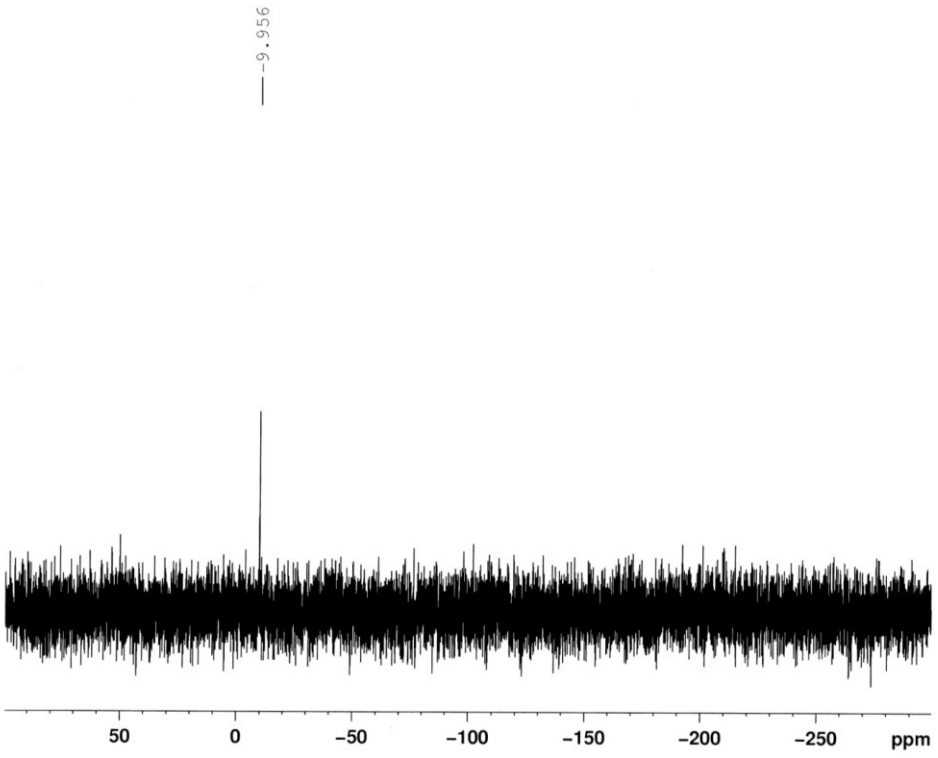
NAME	Dec12-2012
EXPNO	1
PROCNO	1
Date_	20121212
Time	10.43
INSTRUM	spect
PROBHD	5 mm PABBO BB-
PULPROG	zg30
TD	32768
SOLVENT	Tol
NS	16
DS	4
SWH	5498.534 Hz
FIDRES	0.167802 Hz
AQ	2.9797535 sec
RG	114
DW	90.933 usec
DE	6.00 usec
TE	301.3 K
D1	1.00000000 sec
TD0	1
======== CHANNEL f1 ========	
NUC1	1H
P1	12.70 usec
PL1	1.00 dB
PL1W	20.75072861 W
SFO1	500.1322506 MHz
SI	32768
SF	500.1300491 MHz
WDW	no
SSB	0
LB	0.00 Hz
GB	0
PC	1.40

Me_2ItBu (0.02 mmol) $(C_6F_5)_2SiMe_2$ (0.1 mmol) (^{13}C Toluene-d_8)



Me_2ItBu (0.02 mmol) $(C_6F_5)_2SiMe_2$ (0.1 mmol) (^{29}Si Toluene-d_8)

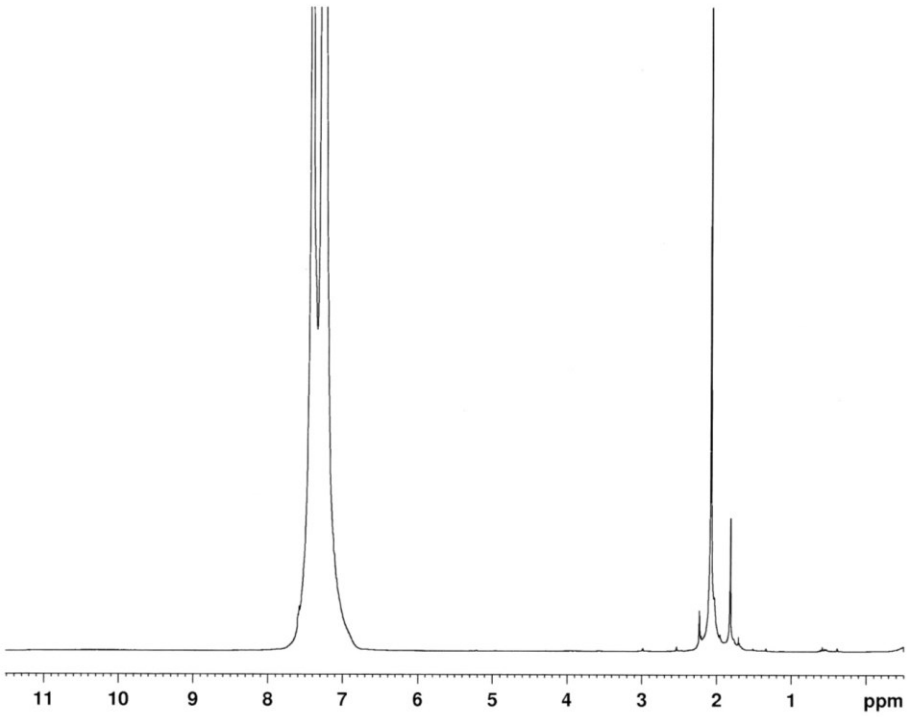
F Lee FL Me2ItBuMe2Si(C6F5)2 in d8-toluene ; 29Si{1H} inverse-gated spectrum at rt using Av500
Dec12-2012/3



NAME	Dec12-2012
EXPNO	3
PROCNO	1
Date_	20121212
Time	11.04
INSTRUM	spect
PROBHD	5 mm PABBO BB-
PULPROG	zgig
TD	65536
SOLVENT	Tol
NS	106
DS	0
SWH	39682.539 Hz
FIDRES	0.605507 Hz
AQ	0.8258036 sec
RG	1620
DW	12.600 usec
DE	12.00 usec
TE	298.9 K
D1	15.00000000 sec
D11	0.03000000 sec
TD0	1
======== CHANNEL f1 ========	
NUC1	29Si
P1	8.25 usec
PL1	3.00 dB
SFO1	99.3518258 MHz
======== CHANNEL f2 ========	
CPDPRG2	waltz16
NUC2	1H
PCPD2	100.00 usec
PL2	1.00 dB
PL12	18.59 dB
PL2W	20.75072861 W
PL12W	0.36143759 W
SFO2	500.1325010 MHz
SI	32768
SF	99.3617568 MHz
WDW	EM
SSB	0
LB	2.00 Hz
GB	0
PC	1.00

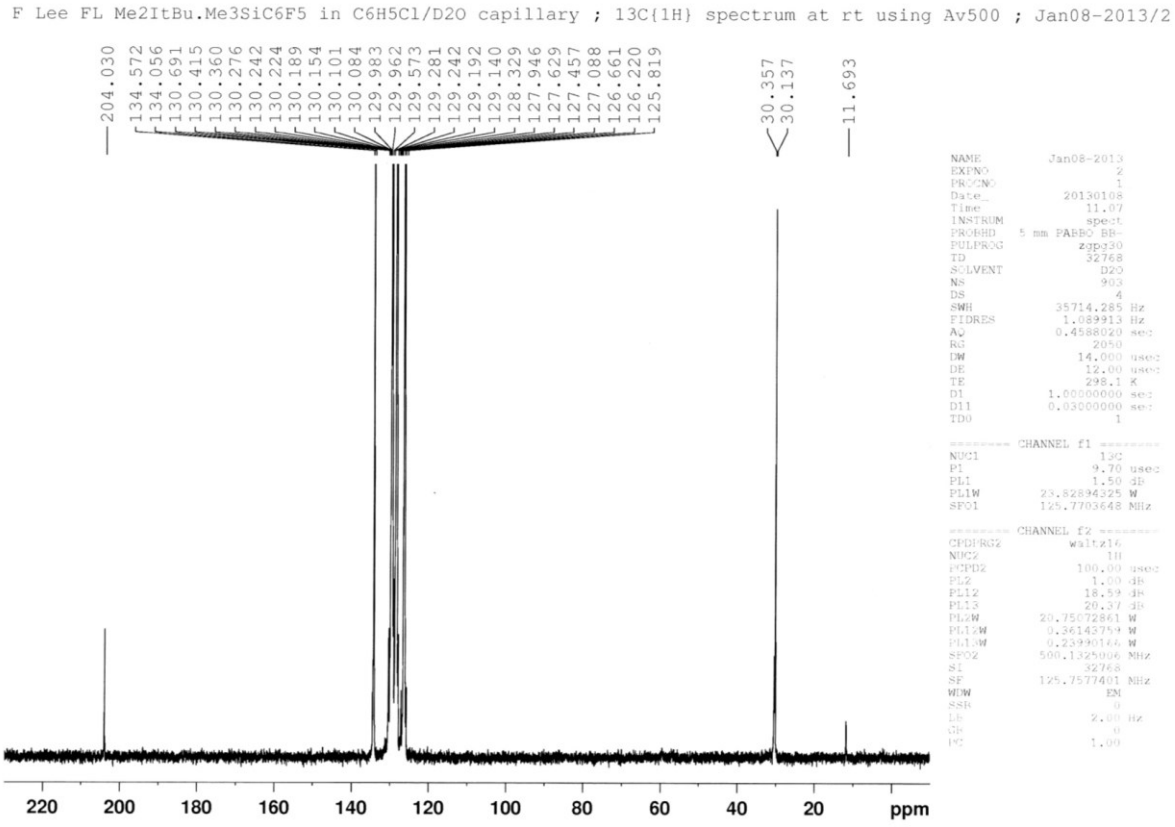
Me_2ItBu (0.02 mmol) $(C_6F_5)SiMe_3$ (0.1 mmol) (^1H C_6H_5Cl/D_2O)

F Lee FL Me2ItBu.Me3SiC6F5 in C6H5Cl/D2O capillary ; 1H spectrum at rt using Av500 ; Jan08-2013/1



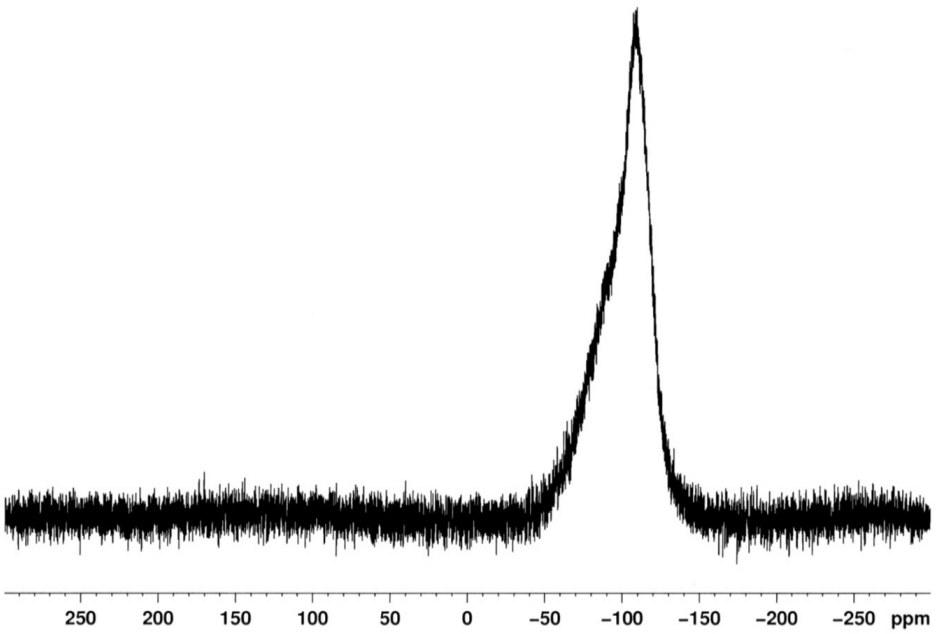
NAME	Jan08-2013
EXPNO	1
PROCNO	1
Date_	20130108
Time	11.04
INSTRUM	spect
PROBHD	5 mm PABBO BB-
PULPROG	zg30
TD	32768
SOLVENT	D2O
NS	248
DS	4
SWH	6009.615 Hz
FIDRES	0.183399 Hz
AQ	2.7263477 sec
RG	7.12
DW	83.200 usec
DE	6.00 usec
TE	298.0 K
D1	2.00000000 sec
TD0	1
======== CHANNEL f1 ========	
NUC1	1H
P1	12.70 usec
PL1	1.00 dB
PL1W	20.75072861 W
SFO1	500.1325006 MHz
SI	32768
SF	500.1297471 MHz
WDW	no
SSB	0
LB	0.00 Hz
GB	0
PC	1.00

Me_2ItBu (0.02 mmol) $(C_6F_5)SiMe_3$ (0.1 mmol) (^{13}C C_6H_5Cl/D_2O)



Me_2ItBu (0.02 mmol) $(C_6F_5)SiMe_3$ (0.1 mmol) (^{29}Si C_6H_5Cl/D_2O)

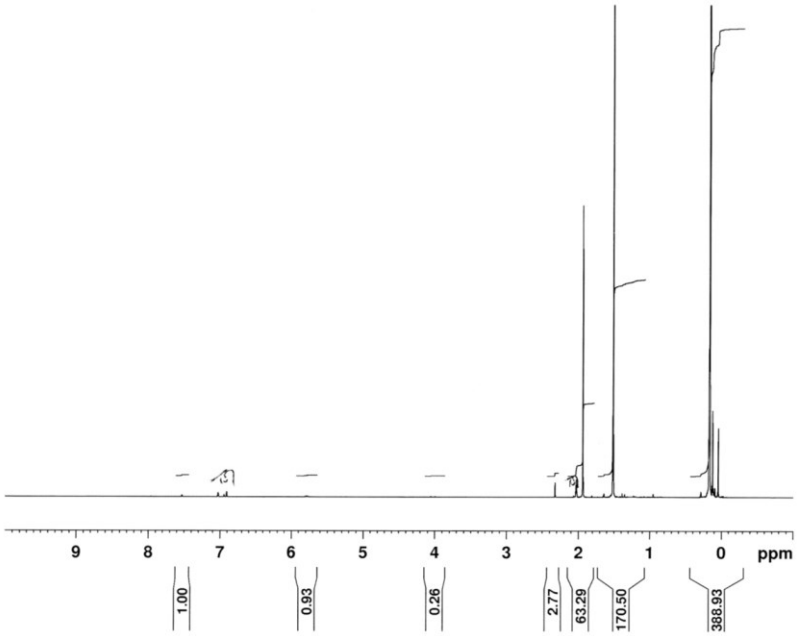
F Lee FL Me2ItBu.Me3SiC6F5 in C6H5Cl/D2O capillary ; 29Si{1H} inverse-gated spectrum at rt using Av500 Jan08-2013/3



NAME	Jan08-2013
EXPNO	3
PROCNO	1
Date_	20130108
Time	11.48
INSTRUM	spect
PROBHD	5 mm PABBO BB-
PULPROG	zgig
TD	65536
SOLVENT	D2O
NS	940
DS	0
SWH	59523.809 Hz
FIDRES	0.908261 Hz
AQ	0.5505524 sec
RG	1440
DW	8.400 usec
DE	12.00 usec
TE	298.0 K
D1	15.00000000 sec
D11	0.03000000 sec
TD0	1
======== CHANNEL f1 ========	
NUC1	29Si
P1	8.25 usec
PL1	3.00 dB
SFO1	99.3617620 MHz
======== CHANNEL f2 ========	
CPDPRG2	waltz16
NUC2	1H
PCPD2	100.00 usec
PL2	1.00 dB
PL12	18.59 dB
PL2W	20.75072861 W
PL12W	0.36143759 W
SFO2	500.1325010 MHz
SI	32768
SF	99.3617568 MHz
WDW	EM
SSB	0
LB	5.00 Hz
GB	0
PC	1.00

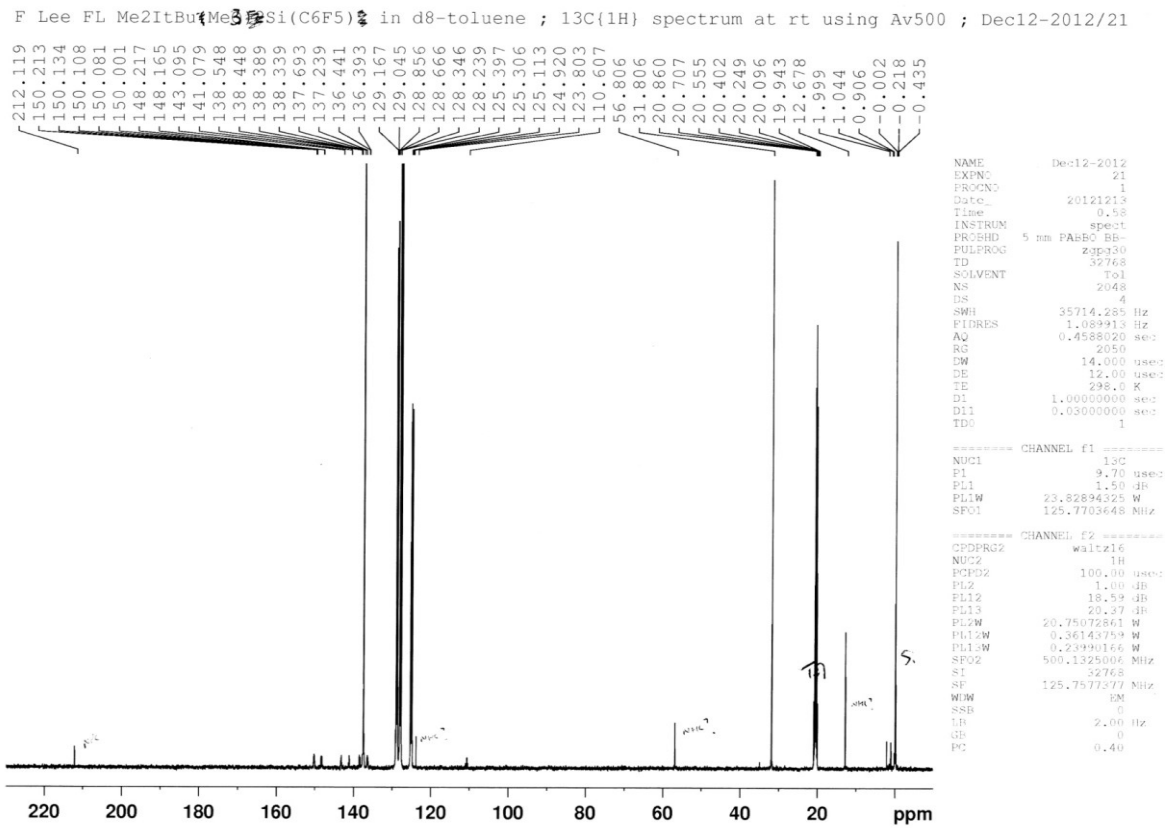
Me_2ItBu (0.02 mmol) $(C_6F_5)SiMe_3$ (0.1 mmol) (^{1}H Toluene-d_8)

F Lee FL Me2ItBu(Me3)2Si(C6F5)2 in d8-toluene ; 1H spectrum at rt using Av500 ; Dec12-2012/20



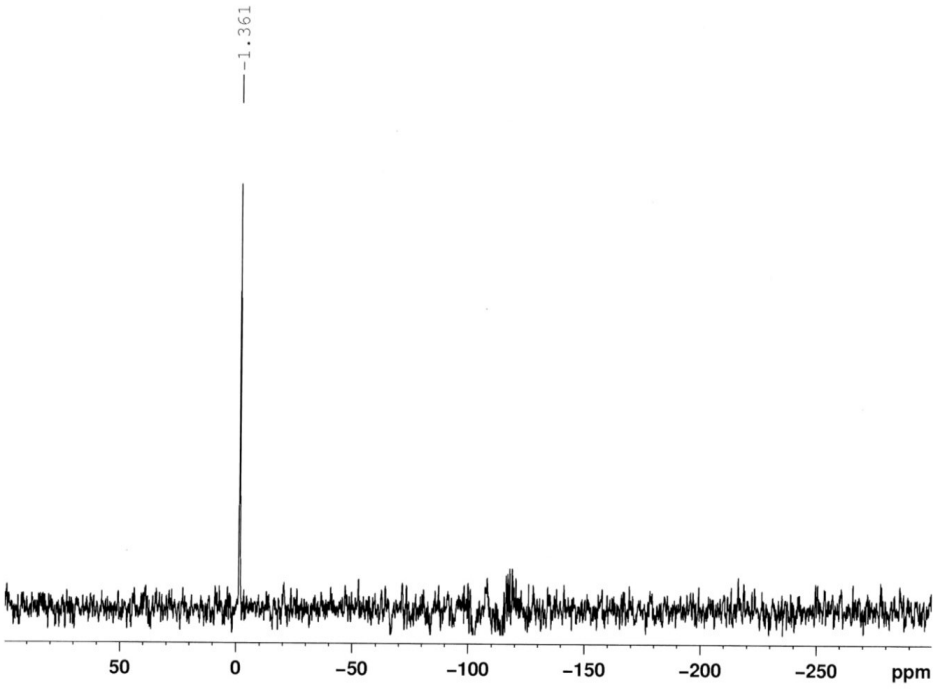
NAME	Dec12-2012
EXPNO	20
PROCNO	1
Date_	20121213
Time	0.04
INSTRUM	spect
PROBHD	5 mm PABBO BB-
PULPROG	zg30
TD	32768
SOLVENT	Tol
NS	64
DS	2
SWH	9014.423 Hz
FIDRES	0.275098 Hz
AQ	1.8175818 sec
RG	90.5
DW	55.467 usec
DE	6.00 usec
TE	298.0 K
D1	1.00000000 sec
TD0	1
======== CHANNEL f1 ========	
NUC1	1H
P1	12.70 usec
PL1	1.00 dB
PL1W	20.75072861 W
SFO1	500.1335009 MHz
SI	32768
SF	500.1300493 MHz
WDW	EM
SSB	0
LB	0.30 Hz
GB	0
PC	1.00

Me_2*t*Bu (0.02 mmol) (C_6F_5)$SiMe_3$ (0.1 mmol) (^{13}C Toluene-d_8)



Me_2ItBu (0.02 mmol) $(C_6F_5)SiMe_3$ (0.1 mmol) (^{29}Si Toluene-d_8)

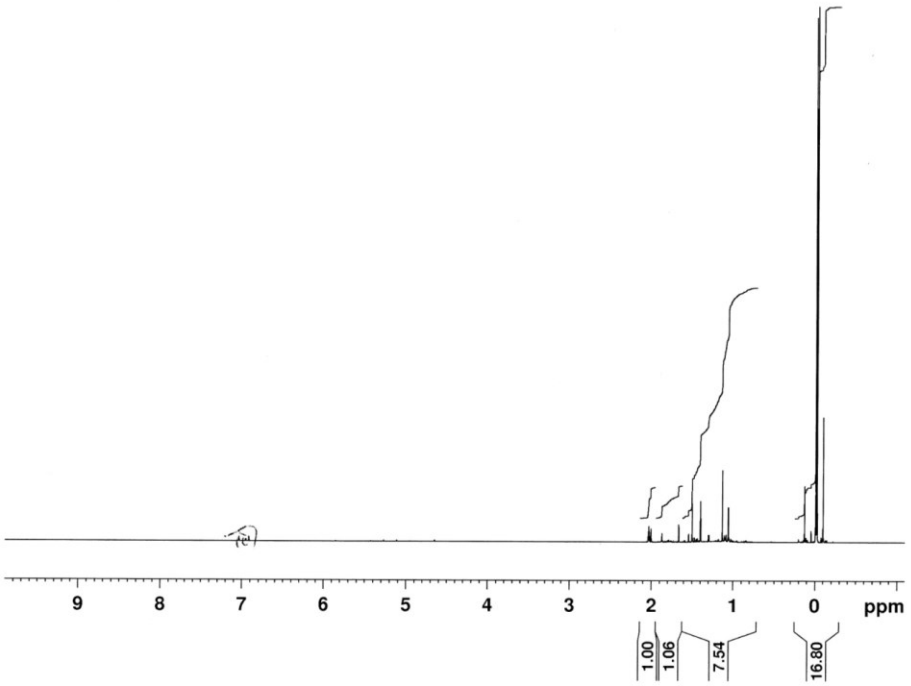
F Lee FL Me2ItBu Me3 Si(C6F5) in d8-toluene ; 29Si{1H} inverse-gated spectrum at rt using Av500
Dec12-2012/22



NAME	Dec12-2012
EXPNO	22
PROCNO	1
Date_	20121213
Time	2.45
INSTRUM	spect
PROBHD	5 mm PABBO BB-
PULPROG	zgig
TD	65536
SOLVENT	Tol
NS	800
DS	0
SWH	39682.539 Hz
FIDRES	0.605507 Hz
AQ	0.8258036 sec
RG	1620
DW	12.600 usec
DE	11.00 usec
TE	298.0 K
D1	15.00000000 sec
D11	0.03000000 sec
TD0	1
======== CHANNEL f1 ========	
NUC1	29Si
P1	8.25 usec
PL1	3.00 dB
SFO1	99.3519258 MHz
======== CHANNEL f2 ========	
CPDPRG2	waltz16
NUC2	1H
PCPD2	100.00 usec
PL2	1.00 dB
PL12	18.59 dB
PL2W	20.75072861 W
PL12W	0.36143759 W
SFO2	500.1325010 MHz
SI	32768
SF	99.3617568 MHz
WDW	EM
SSB	0
LB	20.00 Hz
GB	0
PC	1.00

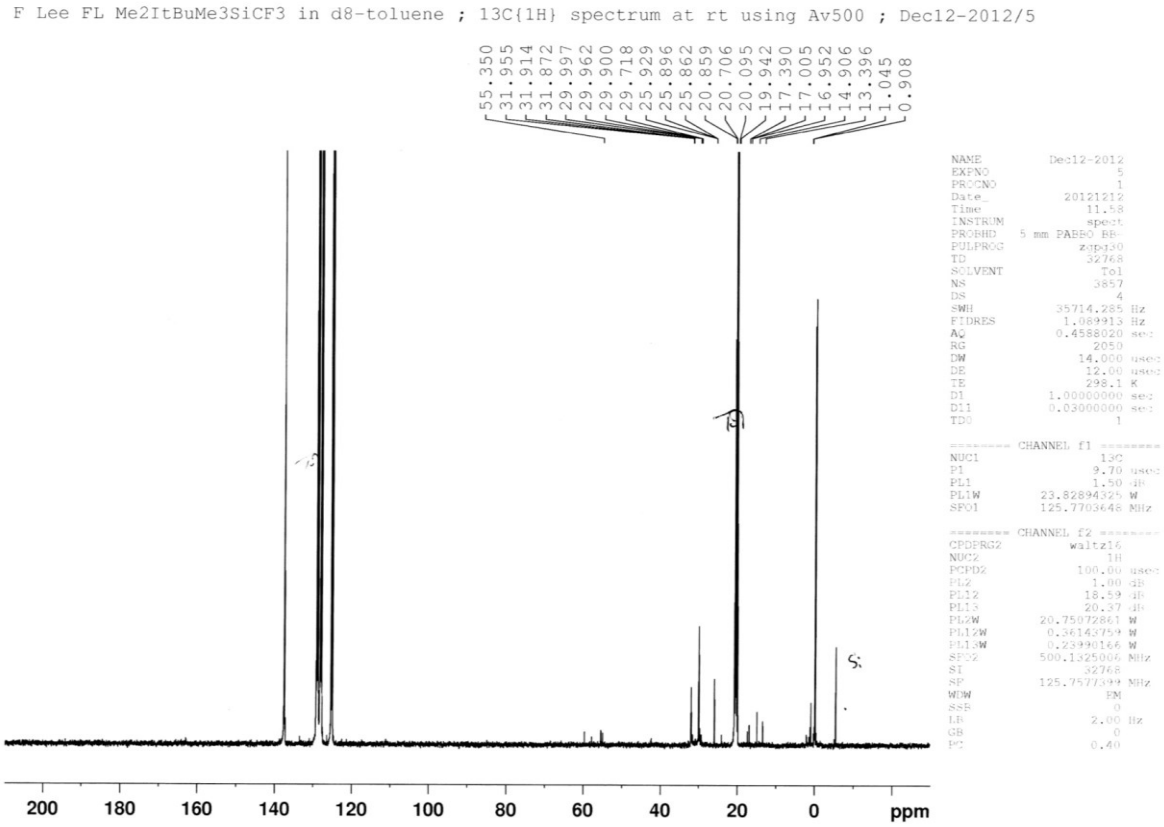
Me_2ItBu (0.02 mmol) $(CF_3)SiMe_3$ (0.1 mmol) (^{1}H Toluene-d_8)

F Lee FL Me2ItBuMe3SiCF3 in d8-toluene ; 1H spectrum at rt using Av500 ; Dec12-2012/4



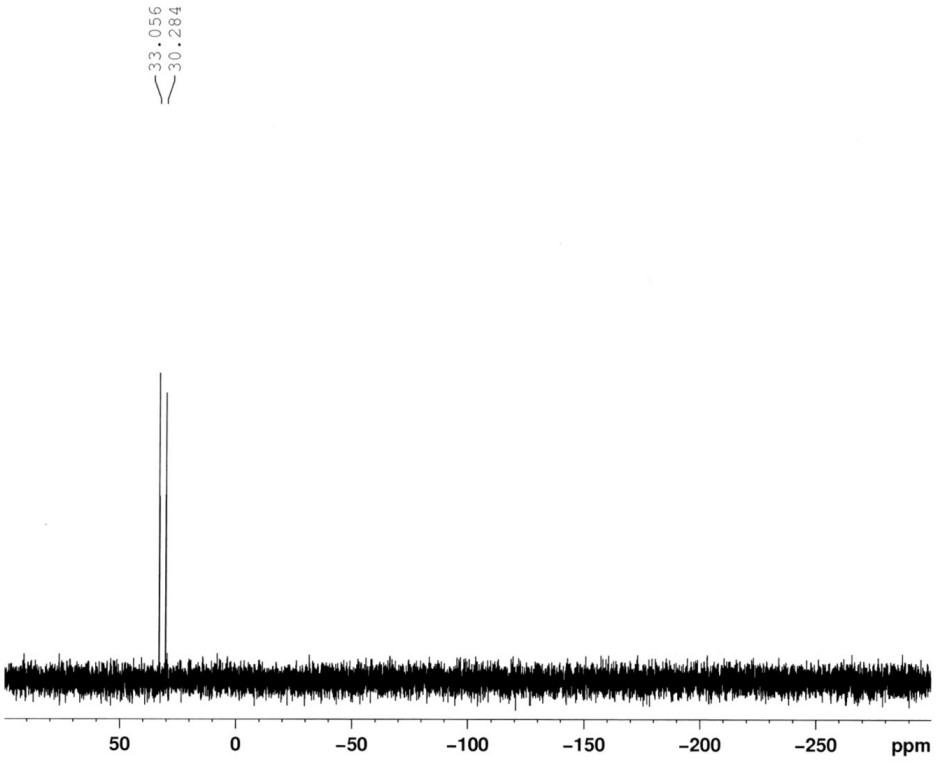
NAME	Dec12-2012
EXPNO	4
PROCNO	1
Date_	20121212
Time	11.30
INSTRUM	spect
PROBHD	5 mm PABBO BB-
PULPROG	zg30
TD	32768
SOLVENT	Tol
NS	16
DS	4
SWH	5498.534 Hz
FIDRES	0.167802 Hz
AQ	2.9797535 sec
RG	114
DW	90.933 usec
DE	6.00 usec
TE	298.0 K
D1	1.00000000 sec
TD0	1
======== CHANNEL f1 ========	
NUC1	1H
P1	12.70 usec
PL1	1.00 dB
PL1W	20.75072861 W
SFO1	500.1322506 MHz
SI	32768
SF	500.1300494 MHz
WDW	no
SSB	0
LB	0.00 Hz
GB	0
PC	1.40

Me_2ItBu (0.02 mmol) $(CF_3)SiMe_3$ (0.1 mmol) (^{13}C Toluene-d_8)



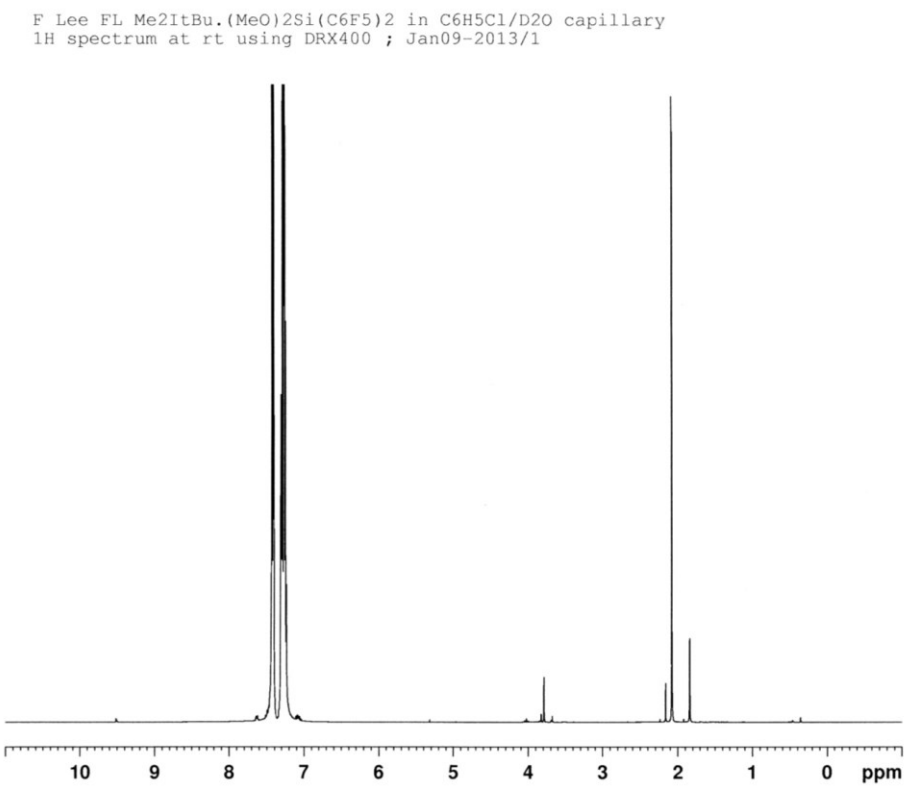
Me_2ItBu (0.02 mmol) $(CF_3)SiMe_3$ (0.1 mmol) (^{29}Si Toluene-d_8)

F Lee FL Me2ItBuMe3SiCF3 in d8-toluene ; 29Si{1H} inverse-gated spectrum at rt using Av500 Dec12-2012/6



NAME	Dec12-2012	
EXPNO	6	
PROCNO	1	
Date_	20121212	
Time	11.53	
INSTRUM	spect	
PROBHD	5 mm PABBO BB-	
PULPROG	zg1g	
TD	65536	
SOLVENT	Tol	
NS	86	
DS	0	
SWH	39682.539	Hz
FIDRES	0.605507	Hz
AQ	0.8258036	sec
RG	1620	
DW	12.600	usec
DE	12.00	usec
TE	298.0	K
D1	15.00000000	sec
D11	0.03000000	sec
TD0	1	
======== CHANNEL f1 ========		
NUC1	29Si	
P1	8.25	usec
PL1	3.00	dB
SFO1	99.3518258	MHz
======== CHANNEL f2 ========		
CPDPRG2	waltz16	
NUC2	1H	
PCPD2	100.00	usec
PL2	1.00	dB
PL12	18.59	dB
PL2W	20.75072861	W
PL12W	0.36143759	W
SFO2	500.1325010	MHz
SI	32768	
SF	99.3617568	MHz
WDW	EM	
SSB	0	
LB	2.00	Hz
GB	0	
PC	1.00	

Me_2ItBu (0.02 mmol) $(C_6F_5)_2Si(OMe)_2$ (0.1 mmol) (^1H C_6H_5Cl/D_2O)



DRX-400

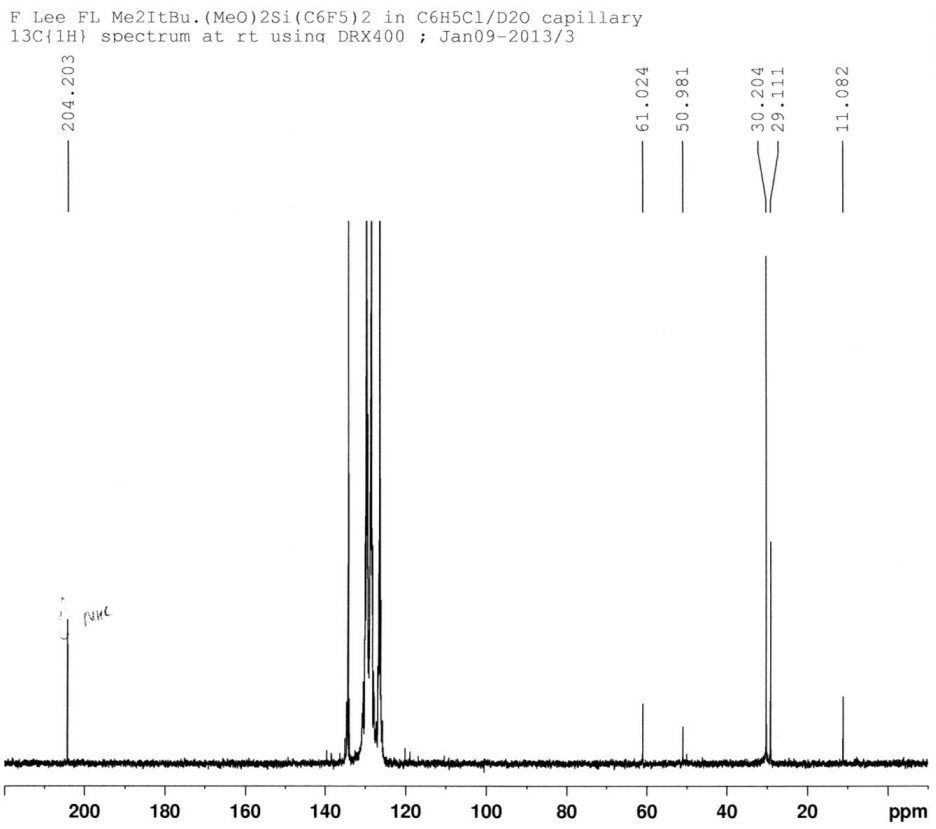
Current Data Parameters
NAME Jan09-2013
EXPNO 1
PROCNO 1

F2 - Acquisition Parameters
Date_ 20130109
Time 18.45
INSTRUM spect
PROBHD 5 mm BBO BB-1H
PULPROG zg30
TD 32768
SOLVENT D2O
NS 128
DS 4
SWH 5592.841 Hz
FIDRES 0.170680 Hz
AQ 2.9295092 sec
RG 14.3
DW 89.400 usec
DE 6.00 usec
TE 300.0 K
D1 2.00000000 sec
TD0 1

======== CHANNEL f1 ========
NUC1 1H
P1 12.00 usec
PL1 0.00 dB
SFO1 400.1320007 MHz

F2 - Processing parameters
SI 32768
SF 400.1297505 MHz
WDW no
SSB 0
LB 0.00 Hz
GB 0
PC 1.00

Me_2ItBu (0.02 mmol) $(C_6F_5)_2Si(OMe)_2$ (0.1 mmol) (^{13}C C_6H_5Cl/D_2O)



DRX-400

Current Data Parameters
NAME Jan09-2013
EXPNO 3
PROCNO 1

F2 - Acquisition Parameters
Date_ 20130110
Time 10.05
INSTRUM spect
PROBHD 5 mm BBO BB-1H
PULPROG zgpg30
TD 32768
SOLVENT CDCl3
NS 1992
DS 4
SWH 28248.588 Hz
FIDRES 0.862078 Hz
AQ 0.5800436 sec
RG 9195.2
DW 17.700 usec
DE 6.00 usec
TE 353.0 K
D1 1.00000000 sec
d11 0.03000000 sec
DELTA 0.89999998 sec
TD0 30

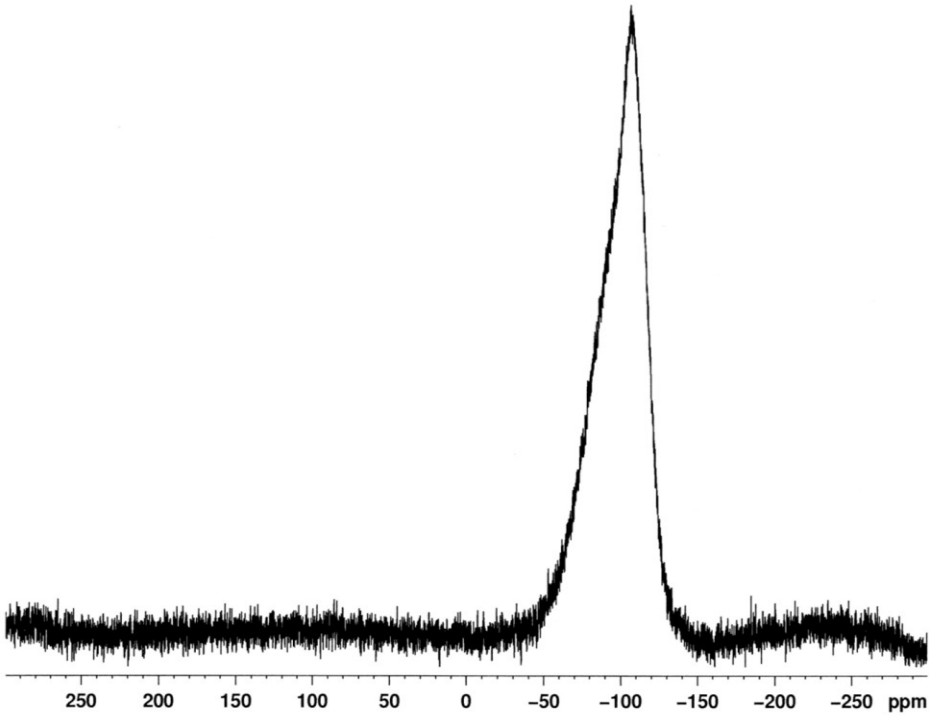
======== CHANNEL f1 ========
NUC1 13C
P1 7.00 usec
PL1 0.00 dB
SFO1 100.6228303 MHz

======== CHANNEL f2 ========
CPDPRG2 waltz16
NUC2 1H
PCPD2 85.00 usec
PL2 0.00 dB
PL12 17.80 dB
PL13 17.80 dB
SFO2 400.1316005 MHz

F2 - Processing parameters
SI 32768
SF 100.6127177 MHz
WDW EM
SSB 0
LB 2.00 Hz
GB 0
PC 1.40

Me_2ItBu (0.02 mmol) $(C_6F_5)_2Si(OMe)_2$ (0.1 mmol) (^{29}Si C_6H_5Cl/D_2O)

F Lee FL Me2ItBu.(MeO)2Si(C6F5)2 in C6H5Cl/D2O capillary ; acquired overnight 29Si{1H} inverse-gated spectrum at rt using DRX400 ; Jan09-2013/2



Current Data Parameters

NAME	Jan09-2013
EXPNO	2
PROCNO	1

F2 - Acquisition Parameters

Date_	20130109
Time	18.57
INSTRUM	spect
PROBHD	5 mm BBO BB-1H
PULPROG	zgig
TD	65536
SOLVENT	C6D6
NS	3472
DS	2
SWH	47619.047 Hz
FIDRES	0.726609 Hz
AQ	0.6881780 sec
RG	2298.8
DW	10.500 usec
DE	6.00 usec
TE	298.0 K
D1	15.00000000 sec
d11	0.03000000 sec
TD0	1

======== CHANNEL f1 ========

NUC1	29Si
P1	9.70 usec
PL1	0.00 dB
SFO1	79.4945750 MHz

======== CHANNEL f2 ========

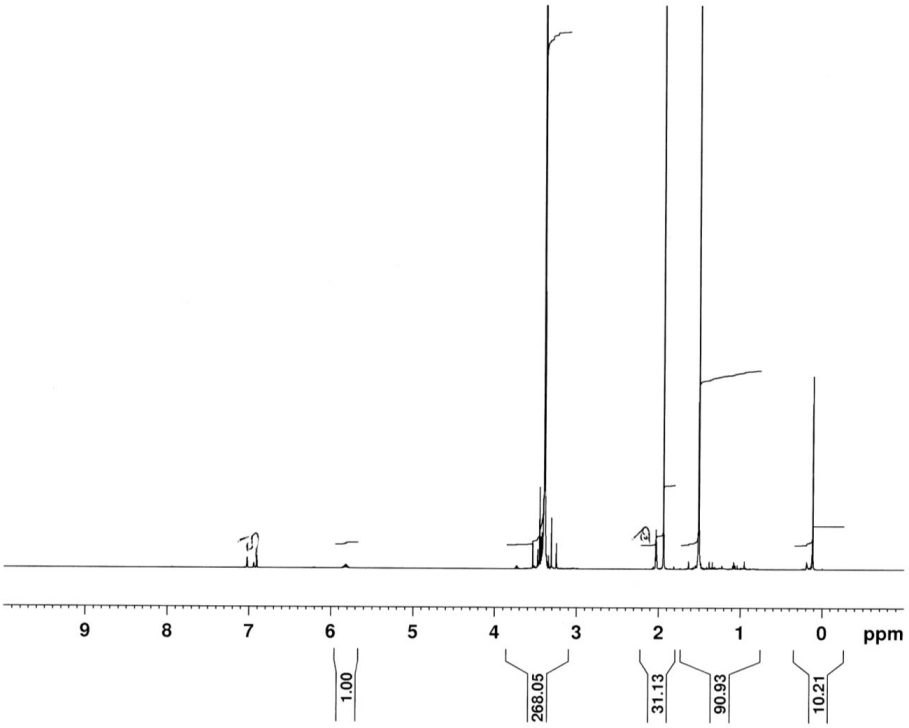
CPDPRG2	waltz16
NUC2	1H
PCPD2	85.00 usec
PL2	0.00 dB
PL12	17.80 dB
SFO2	400.1316000 MHz

F2 - Processing parameters

SI	65536
SF	79.4945712 MHz
WDW	EM
SSB	0
LB	5.00 Hz
GB	0
PC	1.40

Me_2ItBu (0.02 mmol) $(C_6F_5)_2Si(OMe)_2$ (0.1 mmol) (^{1}H Toluene-d_8)

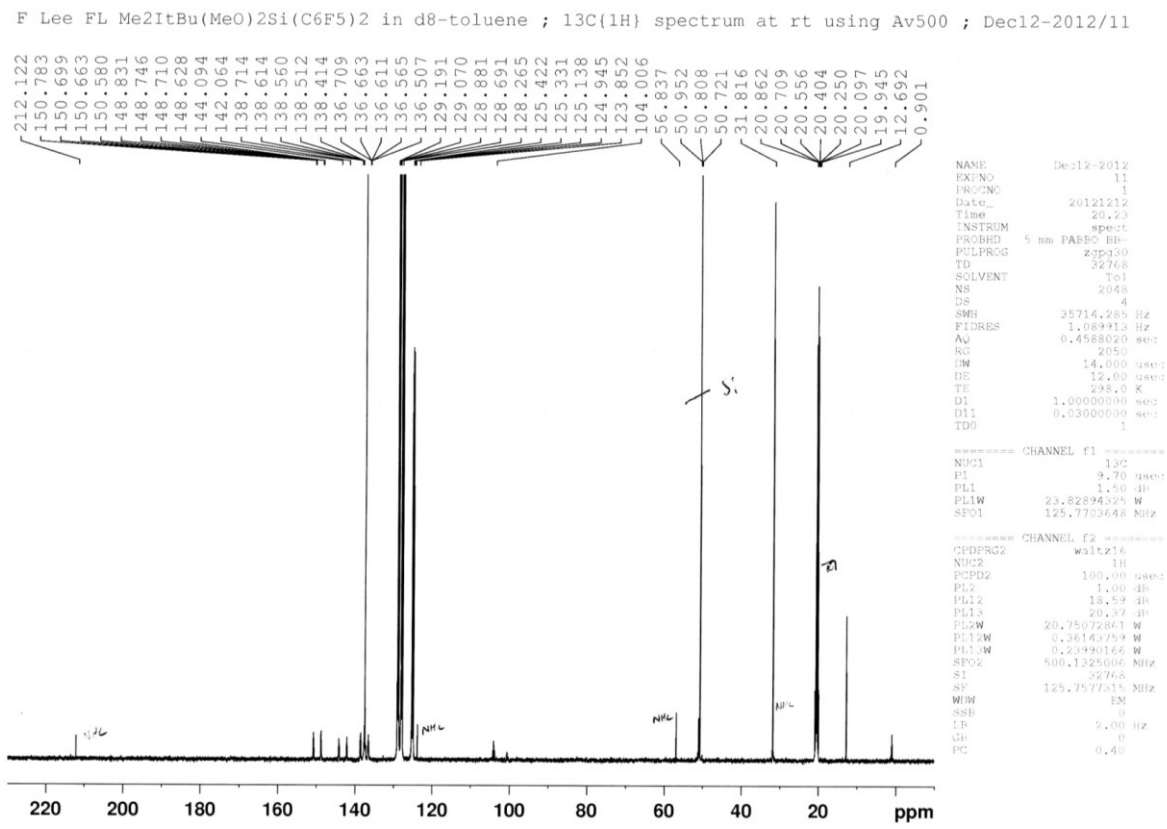
F Lee FL Me2ItBu(MeO)2Si(C6F5)2 in d8-toluene ; 1H spectrum at rt using Av500 ; Dec12-2012/10




```
NAME            Dec12-2012
EXPNO                   10
PROCNO                   1
Date_           20121212
Time                19.29
INSTRUM              spect
PROBHD    5 mm PABBO BB-
PULPROG              zg30
TD                  32768
SOLVENT               Tol
NS                     64
DS                      2
SWH              9014.423 Hz
FIDRES           0.275098 Hz
AQ               1.8175818 sec
RG                   71.8
DW                 55.467 usec
DE                  6.00 usec
TE                298.0 K
D1             1.00000000 sec
TD0                     1

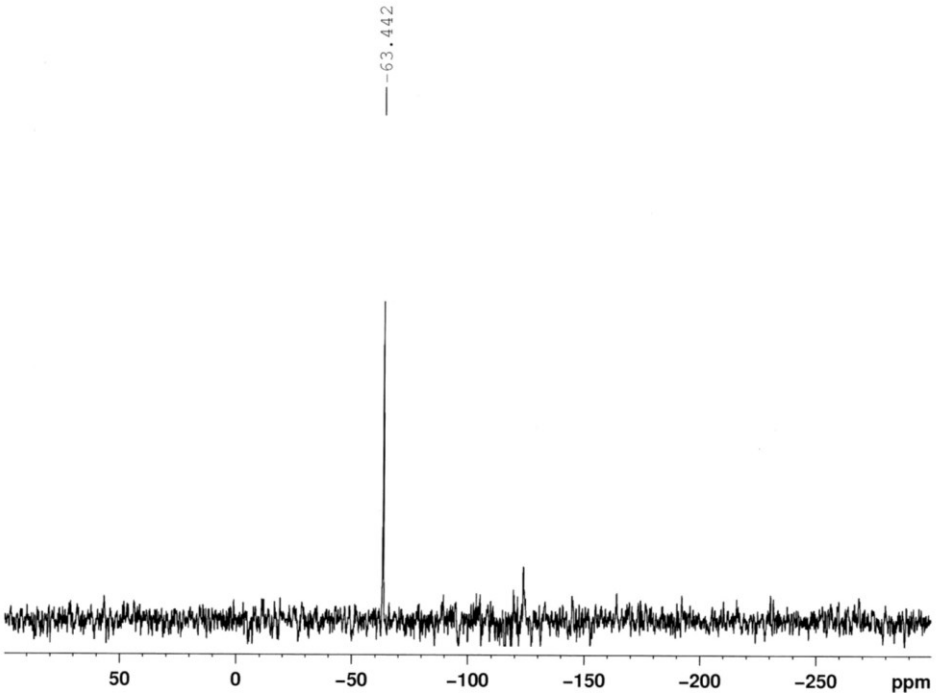
======== CHANNEL f1 ========
NUC1                   1H
P1                  12.70 usec
PL1                  1.00 dB
PL1W          20.75072861 W
SFO1          500.1335009 MHz
SI                  32768
SF            500.1300492 MHz
WDW                    EM
SSB                     0
LB                   0.30 Hz
GB                      0
PC                   1.00
```

Me_2ItBu (0.02 mmol) $(C_6F_5)_2Si(OMe)_2$ (0.1 mmol) (^{13}C Toluene-d_8)



Me_2ItBu (0.02 mmol) $(C_6F_5)_2Si(OMe)_2$ (0.1 mmol) (^{29}Si Toluene-d_8)

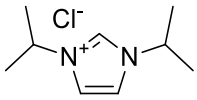
F Lee FL Me2ItBu(MeO)2Si(C6F5)2 in d8-toluene ; 29Si{1H} inverse-gated spectrum at rt using Av500
Dec12-2012/12



NAME	Dec12-2012
EXPNO	12
PROCNO	1
Date_	20121212
Time	22.11
INSTRUM	spect
PROBHD	5 mm PABBO BB-
PULPROG	zgig
TD	65536
SOLVENT	Tol
NS	800
DS	0
SWH	39682.539 Hz
FIDRES	0.605507 Hz
AQ	0.8258036 sec
RG	1440
DW	12.600 usec
DE	12.00 usec
TE	298.0 K
D1	15.00000000 sec
D11	0.03000000 sec
TD0	1
======== CHANNEL f1 ========	
NUC1	29Si
P1	8.25 usec
PL1	3.00 dB
SFO1	99.3518258 MHz
======== CHANNEL f2 ========	
CPDPRG2	waltz16
NUC2	1H
PCPD2	100.00 usec
PL2	1.00 dB
PL12	18.59 dB
PL2W	20.75072861 W
PL12W	0.36143759 W
SFO2	500.1325010 MHz
SI	32768
SF	99.3617568 MHz
WDW	EM
SSB	0
LB	20.00 Hz
GB	0
PC	1.00

Appendix C: Failed Procedures

1,3-Bis(*iso*propyl)imidazolium chloride:[15f]



4·HCl R = *i*Pr

To a solution of paraformaldehyde (0.90 g, 30 mmol) in toluene (5 mL), isopropyl amine (2.6 mL, 30 mmol) was added under stirring such that the temperature of the reaction mixture did not exceed 40 °C. The suspension was stirred for a further 10 minutes. The reaction mixture was then cooled to 3 °C in an ice-bath and a further equivalent of isopropyl amine (2.6 mL, 30 mmol) was added in a slow steady stream. Hydrochloric acid (6 N in H_2O, 5 mL, 30 mmol) was added dropwise such that the temperature of the suspension did not exceed 20 °C. The suspension was removed from the ice-bath and warmed to room temperature. Glyoxal (40 wt% in water, 3.5 mL, 30 mmol) was added and the suspension was stirred for 1 hour. Toluene (4.5 mL) was added and water was removed under Dean-Stark azeotropic distillation. An orange suspension formed which turned dark brown under reflux. The suspension was concentrated *in vacuo* to yield a dark brown solid. The solid was washed with acetonitrile with decolourising carbon and filtered through Celite. Acetonitrile was removed *in vacuo*. ^{1}H NMR analysis of the crude did not identify the product.

Me_2I*t*Bu·$SiCl_4$:

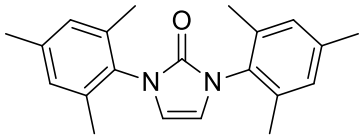


110

To a stirred solution of Me_2I*t*Bu (1 mmol) in hexane (5 mL) at −78 °C, $SiCl_4$ (1.2 mmol, 0.15 mL) was added. On warming to r.t., a white precipitate formed immediately. Removal of excess solvent and

$SiCl_4$ under reduced pressure afforded a white solid. NMR spectra of this solid in CD_2Cl_2 were not consistent with those of the expected product.

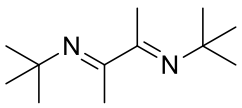
1,3-Bis(2,4,6-trimethylphenyl)-4,5-dihydroimidazol-2-one:



113

Based on a literature procedure reported by Watanabe and co-workers,[122] *N,N'*-Bis(mesityl)urea (148 mg, 0.5 mmol), ethan-1,2-diol (56 µL, 1 mmol), and $RuCl_2(PPh_3)_3$ (38 mg, 0.04 mmol) in THF (2 mL) was refluxed under an inert atmosphere at 180 °C overnight. The title compound could not be identified by ^{1}H NMR analysis of the crude product.

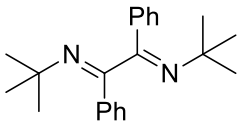
1,4-Bis(*tert*-butyl)-2,3-dimethyl-1,4-diazabutadiene:[136]



122

$TiCl_4$ (11 mL, 100 mmol) was added dropwise to a stirred solution of *tert*-butyl amine (16.8 mL, 160 mmol) in DCM (30mL) at 0 °C. Butan-2,3-dione (1.8 mL, 20 mmol) was added dropwise and a dark precipitate formed immediately. The solution was warmed to r.t. overnight. The reaction was quenched with water and filtered. The aqueous layer was decanted and extracted with DCM. Organic layers were combined and dried over $MgSO_4$. The title compound could not be identified by ^{1}H NMR analysis of the crude product.

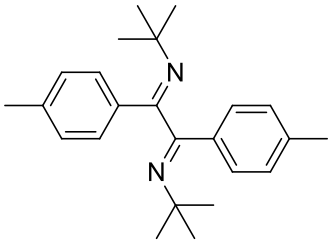
1,4-Bis(*tert*-butyl)-2,3-diphenyl-1,4-diazabutadiene:[136]



123

$TiCl_4$ (1 M in DCM, 100 mL, 100 mmol) was added dropwise to a stirred solution of *tert*-butyl amine (4.2 mL, 40 mmol) in DCM (10mL) at 0 °C. Benzil (4.20 g, 20 mmol) was added dropwise. The solution was warmed to r.t. overnight. The reaction was quenched with water and filtered. The aqueous layer was decanted and extracted with DCM. Organic layers were combined, dried over $MgSO_4$, and concentrated *in vacuo*. The title compound could not be identified by ^1H NMR analysis of the crude product.

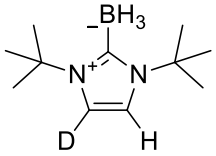
1,4-Bis(*tert*-butyl)-2,3-di-(*p*-tolyl)-1,4-diazabutadiene:[136]



124

$TiCl_4$ (1 M in DCM, 10 mL, 10 mmol) was added dropwise to a stirred solution of *tert*-butyl amine (0.42 mL, 4 mmol) in DCM (5mL) at 0 °C. 1,2-di-*p*-Tolyethan-1,2-dione(0.48 g, 2 mmol) was added dropwise. The solution was warmed to r.t. overnight. The reaction was quenched with water and filtered. The aqueous layer was decanted and extracted with DCM. Organic layers were combined, dried over $MgSO_4$, and concentrated *in vacuo*. The title compound could not be identified by ^1H NMR analysis of the crude product.

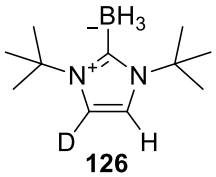
(1,3-di-*tert*-butyl-4-deutero-1H-imidazol-3-ium-2-yl)trihydroborate:



126

Based on a literature procedure reported by Curran and co-workers,[30] *n*-BuLi (2.5 M in hexanes, 0.44 mL, 1.1 mmol) was added dropwise to a stirred solution of I*t*Bu-BH_3 (19.4 mg, 1 mmol) in THF (1 mL) at −78 °C. After 1 h, the reaction was quenched with D_2O. Purification of the reaction mixture by flash column chromatography with DCM yielded starting material only and no deuterium was incorporated as observed by ^{1}H NMR spectroscopy.

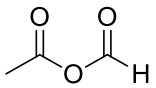
(1,3-di-*tert*-butyl-4-deutero-1H-imidazol-3-ium-2-yl)trihydroborate:



126

n-BuLi (2.5 M in hexanes, 0.40 mL, 1 mmol) was added dropwise to a stirred solution of di*iso*propylamine (0.16 mL, 1.1 mmol) in THF (2 mL) at −78 °C. The reaction mixture was warmed to r.t. and stirred for a further 1 hour, prior to being cooled to −78 °C. The solution was transferred *via* syringe to a stirred solution of I*t*Bu-BH_3 (20 mg, 1 mmol) in THF (1 mL) at −78 °C. After 1 h, the reaction was quenched with D_2O. No deuterium was incorporated in the crude product by ^{1}H NMR spectroscopy. Quenching with MeI led to the return of starting material only.

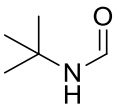
Formyl Actetate from Acetyl Chloride:[138]



133

To a stirred solution of sodium formate (25 g, 368 mmol) in Et_2O (20 mL), acetyl chloride (25 mL, 350 mmol) was added dropwise such that the temperature did not exceed 27 °C. The reaction mixture was stirred at r.t. overnight. Et_2O was removed with a nitrogen purge and the crude product diluted in THF (20 mL). The title compound could not be identified by ^1H NMR analysis of the crude product.

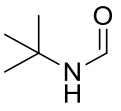
***N*-(*tert*-butyl)formamide from Formic Acid:**[140]



135

A mixture of *tert*-butyl amine (0.28 mL, 2.3 mmol), formic acid (0.3 mL, 7.8 mmol) and $ZnCl_2$ (354mg, 2.6 mmol), was stirred at 70 °C for 1 hour. The reaction mixture was diluted with EtOAc (40 mL), and washed with H_2O (2 x 10 mL), and brine (2 x 10 mL). The organic layer was dried over $MgSO_4$ and concentrated under reduced pressure. The title compound could not be identified by ^1H NMR analysis of the crude product.

***N*-(*tert*-butyl)formamide from Formic Acid:**[141]

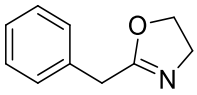


135

A mixture of *tert*-butyl amine (0.53 mL, 0.5 mmol), formic acid (1 mL) and thiamine hydrochloride (33.7mg, 0.1 mmol), was stirred at 80 °C for 40 minutes. The reaction mixture was diluted with EtOAc (20 mL), and washed with aq. HCl (5%), aq. Na_2CO_3 (5%) and brine. The organic layer was dried

over $MgSO_4$ and concentrated under reduced pressure. The title compound could not be identified by ^1H NMR analysis of the crude product.

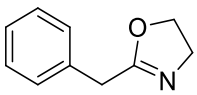
2-Benzyloxazole with PPh_3/DDQ:[180,181]



155

PPh_3 (787 mg, 3 mmol) and DDQ (681 mg, 3 mmol) in DCM (10 mL) were stirred for 5 min during which a dark brown solution formed. *N*-(2-hydroxyethyl)-2-phenylacetamide (358 mg, 2 mmol) was added as a single portion and the mixture stirred overnight. After 15 h, a mustard-yellow solution remained. TLC analysis (30% EtOAc/Hexanes) showed incomplete consumption of starting material. The title compound could not be identified by ^1H NMR analysis of the crude product.

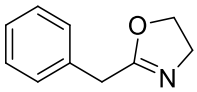
2-Benzyloxazole with PPh_3/DEAD:[55]



155

PPh_3 (787 mg, 3 mmol) and DEAD (372 mg, 3 mmol) in THF (20 mL) were stirred for 5 minutes. *N*-(2-hydroxyethyl)-2-phenylacetamide (358 mg, 2 mmol) was added as a single portion and the mixture stirred overnight. The reaction mixture was poured into 2N NaOH (50 mL) and extracted with DCM (4 x 30 mL). The organic phases were combined and washed with brine. The title compound could not be identified by ^1H NMR analysis of the crude product.

2-Benzyloxazole with $SOCl_2$:[182,183]



155

$SOCl_2$ (0.5 mL, 6.7 mmol) was added dropwise to a stirred solution of *N*-(2-hydroxyethyl)-2-phenylacetamide (179 mg, 1 mmol) in THF or DCM. Volatiles were removed by rotary evaporation. The title compound could not be identified by ^1H NMR analysis of the crude product.